生体時計の分子機構
Molecular Mechanism of Biological Rhythm

研究課題番号　11233101

平成11－14年度科学研究費補助金　特定領域研究

研究成果報告書

1999. 4 － 2003. 3

平成15年3月

研究代表者　　柴 田 重 信
（早稲田大学人間科学部）

はじめに

平成11年度の文部科学省の特定領域研究「生体時計の分子機構」の研究成果を報告する。

本申請書には領域全体の研究目標としては、以下の前文を記載していた。20 世紀宇宙に飛び立った人類は地球を丸ごと外から見るという視点を獲得した。地球上の生命は、巨大な発光体である周期的にエネルギーを得、またそれによる障害から身を守るため体内で時間秩序を形成する機構を進化させてきた。近年の哺乳動物を初めとする多くの生物で時計遺伝子の発見から、体内の時間機構が分子レベルで語られ始めてきた。本プロゼクトにおいて、我々ヒト、哺乳類や各種細胞系を用い、生体における時間生成機構を分子レベルで解明し、ヒトを含む地球上に生息する生物に共通する分子機構を探索する。ヒトの疾病と関連する時間機構のゲノムレベルでの解析も今回の目標である。これらの生体内時間機構の分子レベルでの基礎的研究により、生命のリズムに沿った21世紀の近未来の生活や新しい医学を日本より発信することを目指す。

本研究課題の成果を取りまとめるに当たり、上述した研究目標の体内時計の分子基盤の解明においては、本研究領域は多大な貢献をした。実際新規な時計遺伝子の発見にも寄与した。また、時計遺伝子の働きを解明し、実際に生体の多くの機能に結びつくことも明らかにしてきた。生体レベルのみならず、視交叉上核を始めとして細胞レベルで時計の分子機構を解明する研究も精力的になされた。また、ヒトの睡眠相後退や非24時間睡眠覚醒リズムなどの疾病と時計遺伝子の変異との関連性を調べた研究も、すでに成果を得ている。時計遺伝子の発見により、薬物投与のタイミングを適正化する時間薬理の概念も実体を伴って医学に浸透するようになった。さらに本研究領域で得られた成果は、特許出願や、個々の班研究で述べられているように、新聞等のメディアを通して、広く世間に公表する努力を行ってきた。

また、本研究領域では、一般の研究者や大学院学生等にも公開した平成13と14年に領域班会議を開催した。そのときのプログラムを添付する。

以下に、総括班、個々の研究班ごとに研究成果を記載する。

平成１２年１０月２７日

学術審議会科学研究費分科会審査第一部会
生物系小委員会主査　　豊島　久真男

特定領域研究　研究経過ヒアリング結果について

研究領域名「生体時計の分子機構」

本年９月２０日に行われました審査第一部会生物系小委員会における特定領域研究研究経過ヒアリングの結果、貴殿が領域代表である上記研究領域について以下のとおり評価されました。

評価結果：Ａ　（現行のまま推進すればよい）

また、次のような意見がありましたので、お知らせします。
今後の研究の発展を期待しております。

（意見）
生体時計の分子機構について関連遺伝子のクローニングから発現機序まで焦点を絞って研究が進められており、領域代表者の問題意識が明確で順調に成果が出ている。
このまま研究を推進することにより大きな成果が期待できるが、組織間の連携がやや不十分かと思われるので今後その点についての検討を希望する。研究組織構成の変更は問題ないと考える。

平成12年度特定領域研究B「生体時計の分子機構」
領域班会議プログラム

日時：平成１３年３月１日（木）、２日（金）
場所：神戸大学医学部神緑会館（神戸市中央区楠町7-5-1：神戸大学医学部内）

平成１３年３月１日（木）

１：００　ご挨拶　　岡村均（神戸大学）
　　特定研究B「生体時計の分子機構」のねらい、評価について
１：３０　岡村均（神戸大学）
　　生物時計遺伝子によるリズム発振分子機構の解析
２：００　本間研一（北海道大学）
　　視交叉上核神経細胞におけるサーカディアンリズムの発現とPAS関連時計遺伝子
２：３０　柴田重信（早稲田大学）
　　時計遺伝子による体内時計生理機構の解析
３：００　福永浩司（熊本大学）
　　時計遺伝子産物のリン酸化に関わる分子素過程の解明
３：３０　海老澤尚（埼玉医科大学）
　　ヒトの概日リズム障害を伴う疾患における生体時計関連遺伝子の解析及び治療法の開発

［４：００ー４：３０　休憩（多目的ホール横の会議室）］

４：３０　吉岡亨（早稲田大学）
　　視交叉上核ニューロンのCaシグナリング
５：００　森山芳則（岡山大学）
　　メラトニン出力系と興奮性アミノ酸
５：３０　滝口正樹（千葉大学）
　　微量mRNA増幅法を用いたマウス視交叉上核のDNAマイクロアレイ解析

６：００　中原大一郎（浜松医科大学）
マイクロダイアリシスによるラット松果体メラトニンリズムの長期測定法
６：３０　懇親会（多目的ホール横の会議室）

平成１３年３月２日（金）

９：００　近藤孝男（名古屋大学）
kai 時計遺伝子の分子遺伝学的解析による概日振動発生機構の解明
９：３０　深田吉孝（東京大学）
体内時計の光位相同調とメラトニン出力系の調節メカニズム
１０：００　海老原史樹文（名古屋大学）
鳥類における時計遺伝子の発現

［１０：３０−１１：００　休憩］

１１：００　重吉康史（近畿大学）
視交叉上核における乖離現象と再同調過程の解明
１１：３０　池田正明（埼玉医科大学）
BMAL2 の発現と機能の解析：BMAL2 は時計関連遺伝子か？
１２：００　総括討論：岡村

１３：００−１５：００　計画班員会議（福永、本間、柴田、海老澤、近藤、深田、岡村：書記、山口、八木田、西村）

参加者名

［発表者］
本間さと、本間研一（北海道大学大学院）
深田吉孝、岡野俊行（東京大学大学院）
吉岡亨（早稲田大学人間科学部）
柴田重信（早稲田大学人間科学部）

計画班員会議

日時：平成１４年２月２７日（水）　午後　２：００－７：００
場所：ペアーレ神戸（〒650-0004　神戸市中央区中山手通７丁目３－１８）

参加者名

領域代表：岡村　均（神戸大学大学院）
計画班員：
本間研一（北海道大学大学院）
深田吉孝（東京大学大学院）
柴田重信（早稲田大学人間科学部）
近藤孝男（名古屋大学大学院）
福永浩司（熊本大学医学部）
海老澤尚（埼玉医科大学医学部）
深田吉孝（東京大学大学院）
岡村　均（神戸大学大学院）
評価者：
井上慎一（山口大学理学部）
助言者：
本間さと（北海道大学大学院）
岡野俊行（東京大学大学院）
書記：
八木田和弘（神戸大学大学院）
増渕悟（神戸大学大学院）
石田佳毅（神戸大学大学院）
吉田一子、小池千佳子（神戸大学大学院医学系研究科）

全体会議

日時：平成１４年２月２８日（木）　午前　９：００ー午後５：００

参加者名

［発表者］

本間さと（北海道大学大学院）
本間研一（北海道大学大学院）
井上慎一（山口大学理学部）
深田吉孝（東京大学大学院）
柴田重信（早稲田大学人間科学部）
岩崎秀雄（名古屋大学大学院）
福永浩司（熊本大学医学部）
海老澤尚（埼玉医科大学医学部）
池田正明（埼玉医科大学医学部）
森山芳則（岡山大学薬学部）
滝口正樹（千葉大学医学部）
重吉康史（近畿大学医学部）
八木田和弘（神戸大学大学院）
藤堂　剛（京都大学大学院）
磯島康史（大阪大学蛋白質研究所）
飯郷雅之（聖マリアンナ医科大学）

［特別講演・ゲスト］

Cheng Chi Lee (Molecular Genetics, Baylor College of Medicine)

［書記］

山口　瞬（神戸大学大学院）
西村正高（神戸大学大学院）
八木田和弘（神戸大学大学院）
増渕　悟（神戸大学大学院）
石田佳毅（神戸大学大学院）

平成１３年度科学研究費特定領域研究（B）

生体時計の分子機構計画班員会議

日時：平成１４年２月２７日（水）　午後　２：００－７：００）

場所：　ペアーレ神戸　（神戸市中央区中山手通７丁目3-18）

２：００　ご挨拶　　岡村　均（神戸大学）

特定研究B「生体時計の分子機構」のねらい、評価について

２：２０　柴田重信（早稲田大学）

時計遺伝子による体内時計生理機構の解析

３：００　本間研一（北海道大学）

視交叉上核神経細胞におけるサーカディアンリズムの発現とPAS関連時計遺伝子

３：４０　福永浩司（熊本大学）

時計遺伝子産物のリン酸化に関わる分子素過程の解明

４：２０　海老澤尚（埼玉医科大学）

ヒトの概日リズム障害を伴う疾患における生体時計関連遺伝子の解析及び治療法の開発

[４：２０-５：００　休憩]

５：００　近藤孝男（名古屋大学）

kai時計遺伝子の分子遺伝学的解析による概日振動発生機構の解明

５：４０　深田吉孝（東京大学）

体内時計の光位相同調とメラトニン出力系の調節メカニズム

６：２０　岡村均（神戸大学）

生物時計遺伝子によるリズム発振分子機構の解析

７：００ー懇親会

平成１３年度科学研究費特定領域研究（B）

生体時計の分子機構

Symposium on Molecular Mechanism of Biological Clock

日時：　平成１４年２月２８日（木）　午前９時～午後４時

場所：　ペアーレ神戸
〒650-0004 神戸市中央区中山手通７丁目 3-18　（Tel.078-362-7878）

9:00　ごあいさつ　岡村　均　（神戸大学）

9:05　本間研一（北海道大学）
「視交叉上核神経細胞におけるサーカディアンリズムの発現とPAS 関連時計遺伝子」

9:25　井上慎一（山口大学）
「視交叉上核における Per1, Per2 の免疫組織化学」

9:45　福永浩司（熊本大学）
「概日時計光同調における CaM キナーゼの役割」

10:05　重吉康史（近畿大学）
「視交叉上核の同期と非同期」

10:25-10:40　休憩

10:40　藤堂剛（京都大学）
「クリプトクロームの構造と機能」

11:00　深田吉孝（東京大学）
「G 蛋白質共役受容体による光位相シフトと MAPK リン酸化の概日リズム」

11:20　磯島康史（大阪大学）
「体内時計機構における蛋白質のリン酸化の役割」

11:40　八木田和弘（神戸大学）

「体内時計機構における蛋白質の核－細胞質間輸送と turn-over 調節」

13:00　特別講演

Cheng Chi Lee

(Molecular Genetics, Baylor Collage of Medicine, Heuston, TX)

14:20　池田正明（埼玉医科大学）

「生物時計発振機構における"Inter-activating Loop"」

14.40　飯郷雅之（聖マリアンナ医科大学）

「光受容細胞における生物時計分子機構の解析」

15:00　岩崎秀雄（名古屋大学）

「シアノバクテリアの Kai 時計蛋白質の生化学的解析」

15:20　森山芳則（岡山大学）

「Catalytic switch of serotonin N-acetyltransferase」

15:40-15:55　休憩

15:55　海老澤尚（埼玉医科大学）

「概日リズム障害の遺伝子解析」

16:15　滝口正樹（千葉大学）

「マウス概日リズムの cDNA マイクロアレイ解析」

16:35　柴田重信（早稲田大学）

「体内時計機構におけるセロトニン神経の役割」

16:55　閉会

17:00　懇親会

総括班

総括班「生体時計の分子機構」は、計画班員としての、岡村均（神戸大学；98-99)、本間研一（北海道大学；98)、柴田重信（早稲田大・；98）とともに、井上慎一（山口大学；98-99)、海老原史樹文（名古屋大学；98-99)、中原大一郎（浜松医大； 98-99)、井端泰彦（京都府立医大；98-99)、吉岡亨（早稲田大学；98-99)、重吉康史（近畿大学；98-99)、小林正樹（東北工業大学；99）という独自の参加者を得ていた。単独参加者の研究成果のみを述べると、井上は、時計発振蛋白質である mPER1 を強制発現させたトランスジェニックマウスがリズム周期の延長を起こすことを発見し、無リズムマウスである mCry1mCry2 ダブルノックアウトマウスの視交叉上核を破壊した後に、正常マウスの視交叉上核の脳移植を行うと行動リズムが回復をすることを見出した（Current Biology, in press)。海老原は行動リズムが分離する SC 突然変異異常マウスを発見し、時計遺伝子発現リズムの異常を視交叉上核外で報告し（J. Comp Physiol., 1999)、現在単離を試みている。中原は、ラット松果体の細胞外液から約２ヶ月もの長期にわたって連続的にメラトニンを採取し、その変動を測定する系を初めて確立し、現在この系を用いて、各種明暗条件の影響、メトアンフェタミンの効果などについて検索した。井端は、早期発現遺伝子 zif268 が、光同調時の下垂体ホルモン調節因子産生細胞に発現することを発見し、光入力によるホルモン変動の神経機構の一端を解明した（Eur. J. Neurosci., 1999)。吉岡は、SCN の主なレセプターはムスカリン性 Ach 受容体であることはすでに分かっていたがその経路で活性化される PLCβ のサブタイプが分からなかったことに興味を持ち、PLCβ4 ノックアウトマウスを用い、この PLCβ のサブタイプが β1 であることを確立した（Neuroreport, 2000)。重吉は、視交叉上核の differential mRNA display 法を用いて、lot1 遺伝子を単離し、この転写因子は網膜線維が視交叉上核にシナプス形成をするときにのみ発現することを示した（J. Neurosci. 1999)。小林は、生体極微弱発光の画像計測および量子的解析法の研究を応用した極微弱光検出技術を新しく開発し（J. Neurosci. Meth. 1999)、光ファイバープローブによる遺伝子発現のリアルタイム - in vivo 計測システムの研究開発を岡村・柴田と共同でおこなった（Current Biology, 2000)。

2000 年以降は、各研究代表者８名と、生体リズム研究の権威である永井克也（大阪大学蛋白質研究所長)、井上慎一（山口大学時間学研究所所長）に参加いただいて、実験の総括を行った。

2000－2002 年にかけて、２度の総括班会議を開催し、研究の進捗状況の報告ならびに情報交換を行った。また本会議体をリエゾンオフィスとしての機能、すなわちそれぞれの班での共同研究の活性化や、種々の遺伝子改変動物、プローブ等の共同利用化を促進する場としての機能を果たした。2003 年に最後の総括班会議を開き、班長は４年間の研究成果の取りまとめと、自己評価さらに、将来へ残された問題点などを報告した。これに対して特に評価員の方々から、本研究領域の全体的な評価ならびに個々の班組織の評価を行っていただき、非常に研究が進捗しているし、社会への貢献も多大であるという評価を受けた。

領域内における研究組織

研究組織

この研究は、以下の研究組織によって構成される。

1．総括班「生物時計の分子機構」(研究代表者：柴田重信（早稲田大学))

2．A01：生物時計遺伝子によるリズム発振分子機構の解析（研究代表者：岡村均（神戸大学)）平成11－13年度

3．A02：時計遺伝子産物のリン酸化に関わる分子素過程の解析（研究代表者：福永浩司（東北大学)）平成11－14年度

4．A03：視交叉上核神経細胞におけるサーカディアンリズムの発現とPAS関連時計遺伝子（研究代表者：本間研一（北海道大学)）平成11年度－14年度

5．A04：時計遺伝子のよる体内時計生理機構の解析（研究代表者：柴田重信（早稲田大学))平成11－14年度

6．A05：ヒトの概日リズム障害を伴う疾患における生体時計関連遺伝子の解析および治療法の開発（研究代表者：海老澤尚（埼玉医科大学)）平成11－14年度

7．A06：kai時計遺伝子の分子遺伝学的解析による概日振動発生機構の解明（研究代表者：近藤孝男（名古屋大学)）平成11－14年度

8．A07：体内時計の光位相同調とメラトニン出力系の調節メカニズム（研究代表者：深田吉孝（東京大学)）平成11－14年度

研究経費

平成１１年度	１３４，８００千円
平成１２年度	１２７，５００千円
平成１３年度	１０９，２００千円
平成１４年度	７２，５００千円

領域内の研究の進展状況とこれまでの主な研究成果

1)時計遺伝子のよるリズム発振分子機構の解析(研究代表者:岡村均(神戸大学))

研究代表者： 岡村均 （神戸大学大学院医学系研究科脳科学講座分子脳科学分野）

Ⅰ．研究目的

生命が存在し続けるには、外部環境への適応が必須である。サーカディアンリズム機構は、地球上に現れた生命が、地球の自転により起こる昼夜変化に適応するため獲得した形質であり、哺乳類も例外ではない。たとえば、睡眠覚醒、体温、メラトニンやコルチゾールなどのホルモン分泌が代表的なものである。哺乳類においては、他種にもましてこの体内の時間機構を司る生物時計（Biological Clock）が発達しているが、この事には、サーカディアンリズム発振と環境の明暗周期への同調機構に特化したきわめて精妙な、小さくはあるが非常に多数のニューロンからなる核が脳内に出現したことと大いに関係がある。この一対の核は左右の視神経が交叉する視交叉の直上にあるので視交叉上核と呼ばれる。我々は、1997-1998 年哺乳類の時計遺伝子の同定にたずさわり、この特定領域研究「生体時計の分子機構」を通じて、一貫して時計発振機構を遺伝子・分子レベルで明らかにしようとしてきた。

Ⅱ．研究成果と概要

時計発振の分子メカニズムは、遺伝子レベル、細胞レベル、組織レベル、行動レベルで追求する必要がある。そこで、以下のように、生体リズムの分子機構の研究を進めた。

（１）時計遺伝子の転写制御機構

時計遺伝子は如何にしてリズムを発振するのか？時計遺伝子の発振機構で注目されるのは、転写から行動まで、シアノバクテリアから哺乳類まで、地球上の生物で共通する法則があることである。それは、時計遺伝子が転写・翻訳後産生された時計蛋白質が、自分自身の転写制御を抑制するというオートフィードバックループによる発振分子機構である。哺乳類で見ると、発振の中心となる振動子は、*Per1* と *Per2* の２つの遺伝子である。*Per1, Per2* の転写は、bHLH-PAS 蛋白である CLOCK と BMAL1 のヘテロダイマーが *Per1, Per2* のプロモーターの E-box にポジティブ因子として結合して促進される。続いて、*Per1*、*Per2* の転写によって産生された *Per1* mRNA, *Per2* mRNA から、PER1 蛋白質、PER2 蛋白質ができる。これが、細胞質から核の中へ入って CRY 蛋白と結合して、ポジティブ因子の転写を押さえる。これでループが閉じ、転写減少に続く PER1、PER2 蛋白減少にともなう抑制効果の減少により、*Per1, Per2* 時計遺伝子の転写が再開される。我々は *mPer1* promoter の構造と機能を詳細に解析し、２つの転写開始点がある事を初めて報告し、転写制御能力を確定し、多

くの転写因子が制御することも示した（Current Biology, 2000）。

（２）mCry1/mCry2 ダブルノックアウトマウスという無時計マウスモデルの発見

時計のネガティブフィードバックループを構成すると考えられる強力な新規時計遺伝子 mCry1/mCry2 ノックアウトマウスを用いて、これらマウスの視交叉上核では *mPer1*, *mPer2* のサーカディアン振動が全く止まっていることを示した。ちなみに、末梢時計のある肝臓や網膜でも *mPer1*, *mPer2* の振動は止まっており、これらのマウスでは、中枢末梢とも全身の時計が止まっていることを示した。

（３）時計蛋白による転写制御は PER と CRY の核内における動的制御

単純なフィードバックループでは、リズム発現は説明できても、「なぜ２４時間なのか？」という疑問には答えられない。サーカディアン振動を起こすには、抑制因子の産生から抑制までの過程の時間のずれが必須であり、このずれの長さによって周期が決定される。もっと考えれば、「抑制因子の産生から抑制までの過程の時間のずれ」を作りさえすれば、時計遺伝子の転写リズムは必ずしも必要でないのではないか？我々は、３つの PER のうち NLS 構造を持つ mPER3 が、mPER1 または mPER2 とダイマー形成し、核移行を促進する事を解明した（Genes Develop., 2000）。これまでは CRY が核移行促進蛋白と言われていたが、Cry-double knock out 細胞での我々の検索で、否定された。

哺乳類でも、時計蛋白質、特にループの抑制系を構成する PER1, PER2, CRY1, CRY2 の蛋白質レベルの制御が主役となる。まず初めは、リン酸化による分解制御である。まず、できた PER1, PER2 蛋白質モノマーは、細胞質中に存在する caseine kinase Iε (CKIε)によりリン酸化され、リン酸化された PER1, PER2 は分解される。従って、転写のはじめの段階では、mRNA はできても、蛋白質は次々に分解されて、いっこうに貯まらないという状態が続く。ところが、*Per1, Per2* の転写は刻々と増大し、PER1, PER2 蛋白質もたくさんできてくると、CKIεは一日中一定であるので、蛋白質をリン酸化し分解しきれない状態となる。分解されなかった PER1 と PER2 は、PER3 等とダイマー形成し、自身の NLS（nuclear localization signal）を利用して、核内に移行する。ここで、第二の抑制遅延機構が存在する。それは、PER2 蛋白内の NES（nuclear export signal）による制御であり、核内から細胞外に PER2 蛋白は排出される。この NLS-NES によるシャトリング機構により PER1, PER2 蛋白質の核内濃度は調節される（EMBO J., 2002）。

この核、細胞質間の行きつ戻りつの現象は、核蛋白 CRY1, CRY2 の出現により打ち破られる。CRY1,CRY2 の核内出現は厳密に時間によりコントロールされているが、これが核内に多量になると、PER2 と結合し、安定な PER2-CRY1 及び PER2-CRY2 複合体を形成し、これがポジティブ因子に結合して引き剥がし、*Per1, Per2* の転写を阻害する。これで時計発振のフィードバックループが閉じると考えられる。この PER2, CRY1, CRY2 による抑制を解除するのが、ユビキチン・プロテアゾームによる分解である。この抑制因子の分解により、転写は再開される。蛋白レベルの制御が、どのタイミングで時計のサーカディアン振動に

影響を与えるかは、今後の重要な検討課題である。

（4）時計のコア・フィードバックループのアウトプット経路

時計のコア振動体からの時計シグナルは、多くの遺伝子（clock controlled genes: ccg）を制御し、その時間的発現をコントロールする。この ccg が想定されているよりもはるかに多く少なくとも数百の遺伝子にのぼることは、最近のジーンチップ解析から明らかである。では、どのようにして、コア・ループのシグナルがこれら遺伝子のリズムを引き起こすのであろうか？

まず、E-box を介する制御がある。先ほど述べた *Per1, Per2* 遺伝子の転写を促進するのと同様の CLOCK/BMAL1 ヘテロダイマーが vasopressin などのプロモーターの部位にある E-box に結合する。もう一つの制御を今回我々が見つけた。それは、転写促進因子である PAR 蛋白質群（HLF, TEF, DBP）と転写抑制因子である E4BP4 とが同じ DNA 結合部位で競合して行う制御である。PAR 蛋白質は昼間に発現し転写を促進するが（Mol. Cell Biol., 2000）、E4BP4 は夜に発現し、転写を抑制する（Genes Develop., 2001）。この研究は、従来言われていた E-box 以外の部位も転写に関与する事を示した初めての例であり、時計発振の新しい転写制御系として注目される。これにより、アルブミン、cholesterol 7α hydroxylase、ドーパ脱炭酸酵素などの遺伝子が転写制御されると考えられる（Genes Cells, 2002）。また、この経路は時計遺伝子の発振の増幅にも用いられ、*Per1* のコア・ループ転写も促進・抑制される。最近、*Per1*、*Per2* 遺伝子と逆位相にすなわち、夜に発現する *BMAL1* 遺伝子発現に RevErbα という時計遺伝子制御下にある抑制因子が関与することが明らかとなった（J. Neurosci. Res., 2002）。

（5）転写リズムから行動リズムへ

前述の遺伝子の転写・増幅によるリズム発振のメカニズムは、他に並ぶもののないユニークな性質であるが、サーカディアンリズムのさらに驚くべき特質は、遺伝子の転写リズムが、ほぼ完璧な形で行動リズムに反映している事である。具体的に述べると、リズムセンターである視交叉上核の各細胞におけるごく少数の遺伝子で構成されるコア・ループによる遺伝子レベルの時計発振が、視交叉上核という神経核レベルで同期・増幅され、全脳に伝播し、ついには行動・ホルモン分泌など個体レベルのサーカディアンリズムを生み出す。発振は視交叉上核の各細胞であるが、振動の増幅・伝達機構は脳機能の効率性・特殊性が生かされていると言える。

遺伝子から行動まで同じ現象を追うことができる事は生体リズムの重要な特質で、同じレベルの追求が可能な脳や生体機能はほとんど無いと言ってよい。我々は、発光遺伝子導入トランスジェニックマウス（時計遺伝子プロモーターが活性化するとホタル発光遺伝子 luciferase が発現し、投与した luciferin 基質によって光るマウス）を作成した。生体外での視交叉上核における遺伝子活動をスライス培養で検出することに成功した（Current Biology, 2001）。また、生体レベルで、普通に活動している発光遺伝子導入トランスジェニックマウ

スの視交叉上核に微小光ファイバーを挿入し、連続的に数日間時計遺伝子発現をリアルタイムで検出する事に成功した（Nature, 2001）。この研究は、自由行動下での脳機能遺伝子をリアルタイムで検出した初めての研究で、睡眠覚醒など広く高次脳機能に関与する遺伝子の解析に有望なシステムである。今後、細胞内の遺伝子振動がいかにしてトータルとしての脳・生体機能である行動にまで至るかを解析する有力な実験系として、サーカディアンリズムの研究に用いられて行くであろう。

（６）全身の時計細胞

最近、時計遺伝子が全身の大部分の細胞に発現する事、しかもその多くはリズミックに発現している事が明らかとなった。さらに驚くべき事に、クローン化した線維芽細胞に血清処置を行うと、*Per1, Per2, dbp* などが、少なくとも数周期にわたって約２４時間周期の振動を起こす事が報告された。大動脈でも時計遺伝子のサーカディアン振動が見られ、また、培養血管平滑筋細胞では、アンギオテンシン誘導性のリズムが認められた（Circulation, 2001）。我々は、線維芽細胞系での発振リズムが、視交叉上核と同じ時計遺伝子のコア・フィードバックループからなる事を証明した（Science, 2002）。Rat1 線維芽細胞系を用いた研究で、Endothelin1 でリズム誘導をし、サーカディアン振動を打ち立て、mRNA と蛋白発現の数時間に及ぶ乖離、無リズムマウス（Cry1/Cry2-doubleKO）、短周期マウス（Cry1-KO）、長周期マウス（Cry2-KO）で、行動リズムと全く相関したリズムが認められ、時計遺伝子の分子機構の解明に、セルラインを用いた細胞生物学が適応できることを証明した。この数日続く線維芽細胞のリズムは、視交叉上核と全く同じ時計遺伝子のコア・フィードバックループの仕組みによることを見つけたことは、大変驚きであった。というのは、従来視床下部の視交叉上核にしかないと言われていた生体時計が、末梢臓器にもある事を示しているからである。視交叉上核の時計は先に述べたようにせいぜい一万個だが、全身の細胞にあるすると数兆個の時計があると言える。ただし、この末梢の時計はせいぜい２－３周期で止まってしまい、視交叉上核のようにほぼ永久に振動し続けるというわけではない。この差が何によるかは現在のところ明らかでない。いずれにせよ、哺乳類の時計機構は、光によって外界の明暗周期と同調した視交叉上核からの時刻信号が、神経・液性因子の形で出て、脳内の他の神経核にある細胞時計に伝わり、さらに下位の末梢の細胞時計が制御されるという視交叉上核を頂点とする階層的な時計機構モデルが考えられる。

Ⅲ．分析から統合へ：時計研究は２１世紀のライフサイエンスを切り開く

２０世紀のサイエンスは、多くの生理現象を分析的手法でずたずたに解体した。他分野に遅れて、ようやく２０世紀末にその構成物質が解明された生体リズムの特質は、ごく少数の遺伝子でその発振の原型が構成されるという事である。このシンプルなシステムは、さらに大きな特質を持つ。それは、遺伝子、細胞、局所回路（組織）、器官系、個体、その全てのレベルで、同じ、リズムという現象が現れ、その全てが測定可能であることである。

従って、サーカディアンリズムの研究は、細胞内の遺伝子振動がいかにしてトータルとしての行動にまで至るかを解析する生体機能のインテグレーションメカニズムを探る有力な系では無かろうか。具体的には、サーカディアンシステムは、リズムセンターである視交叉上核の各細胞における遺伝子レベルの発振が、視交叉上核という神経核レベルで同期・増幅された発振につながり、全脳に伝播し、ついには行動・ホルモン分泌など個体レベルに至るシステムである。発振は視交叉上核の各細胞であるが、振動の増幅・伝達機構・修飾は脳機能の効率性・特殊性が生かされている。この分野においては、分子生物学の生物学への導入により、２０世紀後半に勃興し、現在も圧倒的な勢いで進展している網羅的な分子生物学的発見が、リズムという現象を利用して統合に向かう非常に有力な２１世紀の研究分野になる予感がする。現在では、生体リズム研究は、遺伝子転写機構のみならず、核・細胞質相関機構、細胞内情報伝達機構、物理的・化学的細胞間認識機構、神経回路機構、全身の生理統合機構を、リズムという生理学的現象で統括検証するという、稀有な研究分野に成長しつつある。時計遺伝子の発見により普遍的な時計振動発振機構の存在が確認された生体リズム研究は、細部の分析的な研究でずたずたにされた生理現象の理解を、もう一度総合再生させようとするライフサイエンスの前衛的な研究分野の一つとして再生しようとしている。

参考文献

1 Ibata Y, Okamura H, Tanaka M, Tamada Y, Hayashi S, Iijima N, Matsuda T, Takamatsu T, Hisa Y, Shigeyoshi Y, Amata F: Functional morphology of the suprachiasmatic nucleus. ***Front. Neuroendocrinol.***, 20:241-268, 1999.

2 Yan L, Takekida S, Shigeyoshi Y, Okamura H: *Per1* and *Per2* gene expression in the rat suprachiasmatic nucleus: circadian profile and the compartment-specific response to light. ***Neuroscience***, 94:141-150, 1999.

3 Maebayashi Y, Shigeyoshi Y, Takumi T, Okamura H: A putative transcription factor with seven zinc-finger motif identified in the developing suprachiasmatic nucleus by the differential display-PCR method. ***J. Neurosci.*** , 19:10176-10183, 1999.

4 Okamura H, Miyake S, Sumi Y, Yamaguchi S, Yasui A, Muijtjens M, Hoeijmakers JHJ, van der Horst GTJ: Photic induction of mPer1 and mPer2 in Cry-deficient mice lacking a biological clock. ***Science***, 286:2531-2534, 1999.

5 Yan L, Miyake S, Okamura H: Distribution and circadian expression of *dbp* in SCN and extra-SCN areas in the mouse brain. ***J. Neurosci. Res.*** 59:291-295, 2000.

6 Yagita K, Okamura H: Forskolin induces circadian gene expression of *rPer1*, *rPer2* and *dbp* in mammalian rat-1 fibroblasts. ***FEBS Lett.*** 465:79-82, 2000.

7 Yagita K, Yamaguchi S, Tamanini F, van der Horst GTJ, Hoeijmakers JHJ, Yasui A, Loros JJ, Dunlap JC, Okamura H: Dimerization and nuclear entry of mPER proteins in mammalian cells. ***Genes Develop.*** 14:1353-1363, 2000.

8 Yamaguchi S, Mitsui S, Yan L, Yagita K, Miyake S, Okamura H: Role of DBP in the circadian oscillatory mechanism. ***Mol. Cell. Biol.*** 20:4773-4781, 2000.

9 Yamaguchi S, Mitsui S, Miyake S, Yan L, Onishi H, Yagita K, Suzuki M, Shibata S, Kobayashi K, Okamura H: The 5' upstream region of *mPer1* gene contains two promoters and is responsible for circadian oscillation. ***Current Biology*** 10: 873-876, 2000.

10 Horikawa K, Yokota S, Fuji K, Akiyama M, Moriya T, Okamura H, Shibata S: Non-photic entrainment by 5-HT1A/7 receptor agonists accompanying with reduction of *Per1* and *Per2* expression. ***J. Neurosci.*** 20: 5867-5873, 2000.

11 Miyake S, Sumi Y, Yan Y, Takekida S, Fukuyama T, Ishida Y, Yamaguchi S, Yagita S, Okamura H: Phase-dependent responses of *Per1* and *Per2* genes to a light-stimulus in the suprachiasmatic nucleus of the rat. ***Neurosci. Lett.*** 294: 41-44, 2000.

12 Nakagawa T, Ukai K, Ohyama T, Gomita Y, Okamura H: Effects of chronic administration of sibutramine on body weight, food intake and motor activity in neonatally monosodium glutamate-treated obese female rats: Relationship of antiobesity effect with monoamines. ***Exper. Animals***,, 49: 239-249, 2000.

13 Moriya T, Takahashi S, Ikeda M, Suzuki-Yamashita K, Asai M, Kadotani H, Okamura H, Yoshioka T, Shibata S: N-methyl-D-aspartate receptor subtype 2C is not involved in circadian oscillation or photoic entrainment of the biological clock in mice. ***J. Neurosci. Res.,*** 61: 663-673, 2000.

14 Takekida S, Maywood E, Hastings M, Okamura H: Differential adrenergic regulation of the circadian expression of the clock genes *Period1* and *Period2* in the rat pineal gland. ***Eur. J. Neurosci.***, 12: 4557-4551, 2000.

15 Okamura H, Yamaguchi S, Yagita K, Ishida Y, Matsuo T, Yan L: Circadian oscillation of mammalian Period genes. In Zeitgebers, entrainment and masking of the circadian system. Edited by K. Honma and S. Honma, Hokkaido University Press, Sapporo, 2001, pp89-100.

16 Taguchi K, Okura R, Yagita K, Ishida Y, Onishi H, Shigeyoshi Y, Yamaguchi S, Nishimura M, Masubuchi S, Okamura H: Different circadian expression profiles of clock genes in the mouse suprachiasmatic nucleus. ***Biomed. Res.*** 22, 125-131, 2001.

17 Nakamura T, Shigeyoshi Y, Maebayashi Y, Yamaguchi S, Yagita K, Okamura H: Different developmental profiles of the expression of preprosomatostatin and preprotachykinin-A mRNAs in rat SCN neurons. ***Dev. Brain Res.,*** 127: 81-86, 2001.

18 Yamaguchi S, Kobayashi M, Mitsui S, Ishida Y, van der Horst GTJ, Suzuki M, Shibata S, Okamura H: Real time monitoring of clock gene expression in the living mouse. ***Nature,*** 409: 684, 2001.

19 Yamamoto S, Shigeyoshi Y, Ishida Y, Fukuyama T, Yamaguchi S, Yagita K, Moriya Y, Shibata S, Yakashima N, Okamura H: Expression of the *Per1* gene in the hamster: Brain atlas and circadian characteristics in the suprachiasmatic Nucleus. ***J. Comp. Neurol.,*** 430, 518-532, 2001.

20 Wakamatsu H, Takahashi S, Moriya T, Inouye S-IT, Okamura H, Akiyama M, Shibata S: Additive effect of mPer1 and 2 antisense oligonucleotides on light-induced phase shift. ***Neuroreport,*** 12,127-131, 2001.

21 Sugano T, Yagita K, Ibata Y, Nagatsu I, Tanaka M, Yamaguchi S, Okamura H: Morphological survey of reserpine-induced tyrosine hydroxylase in brainstem dopaminergic, noradrenergic and adrenergic neurons with special reference to their projection fibers. ***Biomed. Res.***.21, 269-282, 2001.

22 Nakagawa T, Ukai K, Ohyama T, Gomita Y, Okamura H: Effects of sibutramine on the central dopaminergic nervous system in rodents. ***Neurotoxicity Res.*** 3, 235-247, 2001.

23 Ishida Y, Yagita K, Fukuyama T, Nishimura M, Nagano M, Shigeyoshi Y, Yamaguchi S, Komori T, Okamura H: Constitutive expression and delayed light response of caseine kinase e and d mRNAs in the mouse suprachiasmatic nucleus. ***J. Neurosci. Res.***, 64, 612-616, 2001.

24 Nishiyama K, Yagita K, Yamaguchi S, Kitamura S, Matsuo T, Uno T, Tanaka M, Hisa Y, Ibata Y, Okamura H: Tyrosine hydroxylase and NADPH-diaphorase in the rat nodose ganglion: Colocalization and central projection. ***Acta Histochem. Cytochem.***, 34, 135-141, 2001.

25 Bodnar I, Okamura H, Toth BE, Vecsernyes M, Halasz B, Nagy GM: Effect of neonatal treatment with monosodium glutamate on dopaminergic and L-DOPAergic neurons of the medial basal hypothalamus and on prolactin and MSH secretion of rats. ***Brain Res. Bull.***, 55, 767-774, 2001.

26 Mitsui S, Yamaguchi S, Matsuo T, Ishida Y, Okamura H: Antagonistic role of E4BP4 and PAR proteins in the circadian oscillatory mechanism. ***Genes Develop.***, 15, 995-1006, 2001.

27 Yagita K, Tamanini F, van der Horst GTJ, Okamura H: Molecular mechanisms of the biological clock in Cultured fibroblasts. ***Science***, 292, 278-292, 2001.

28 Nonaka H, Emoto N, Ikeda K, Fukuya H, Saifur RM, Raharjo SB, Yagita K, Okamura H, Yokoyama M: Angiotensin II induces circadian gene expression of clock genes in cultured vascular smooth muscle cells. ***Circulation,*** 104, 1746-1748, 2001.

29 Asai M, Yamaguchi S, Isejima H, Jounouchi M, Moriya T, Shibata S, Kobayashi M, Okamura H: Visualization of *mPer1* transcription *in vitro* by luciferase mediated bioluminescence: NMDA induces a rapid phase-shift of *mPer1* gene in cultured SCN. ***Current Biology***, 11, 1524-1527, 2001.

30 Onishi H, Yamaguchi S, Yagita K, Ishida Y, Dong X, Kimura H, Jing Z, Ohara H, Okamura H: Rev-erb□ gene expression in the mouse brain with special emphasis on its circadian profiles in the suprachiasmatic nucleus. ***J. Neurosci. Res.***, 68, 551-557, 2002.

31 Maywood E.S, Okamura H, Hastings MH: Opposing actions of neuropeptide Y and light on the expression of circadian clock genes in the mouse suprachiasmatic nuclei. ***Eur. J. Neurosci.***, 15, 216-220, 2002.

32 Ishida Y, Yokoyama C, Inatomi T, Yagita K, Dong X, Yan L, Yamaguchi S, Nagatsu I, Komori T, Kitahama K, Okamura H: Circadian rhythm of aromatic $_{L}$-amino acid decarboxylase in the rat suprachiasmatic nucleus: gene expression and decarboxylating activity in clock oscillating cells. ***Genes Cells***, 7, 447-459, 2002.

33 Shigeyoshi Y, Meyer-Bernstein E, Yagita K, Weili F, Chen Y, Takumi T, Schotland P, Sehgal A, Okamura H: Restoration of circadian behavioral rhythms in a period null *Drosophila* mutant (per^{01}) by mammalian period homologues *mPer1* and *mPer2*. ***Genes Cells***, 7, 163-171, 2002.

34 Sumi Y, Yagita K, Yamaguchi S, Ishida Y, Kuroda Y, Okamura H: Rhythmic expression of ROR□ mRNA in the mice suprachiasmatic nucleus. ***Neurosci. Lett.***, 320, 13-16, 2002.

35 Okamura H, Yamaguchi S, Yagita K: Molecular machinery of the circadian clock in mammals. ***Cell Tissue Res.***, 309, 47-56, 2002.

36 Yagita,K, Tamanini F, Yasuda M, Hoeijmakers JHJ van der Horst GTJ, Okamura H. Nucleocytoplasmic shuttling and mCRY-dependent inhibition of ubiquitylation of the mPER2 clock protein., ***EMBO J.***, 21, 1301-1314, 2002.

37 Mutoh T, Shibata S, Korf HW, Okamura H: Melatonin modulates the light-induced sympathoexcitation and vagal suppression with participation of the SCN in mice. ***J. Physiol.***, in press.

38 Kimura H, Dong X, Yagita K, Okamura H: Brain expression of apurinic/apyrimidinic endonuclease (APE/Ref-1) multifunctional DNA repair enzyme gene in the mouse with special reference to the suprachiasmatic nucleus ***Neuroscience Res.***, in press.

39 Sujino M, Masumoto K, Yamaguchi S, van der Horst GTJ, Okamura H, Inouye S-IT: Suprachiasmatic nucleus grafts restore circadian behavioral rhythms of genetically arrhythmic mice., ***Current Biology***, in press.

40 Terazono H, Mutoh T, Yamaguchi S, Kobayashi M, Akiyama M, Udo R, Ohdo S, Okamura H, Shibata S: Adrenergic regulation of clock gene expression in the mouse liver. ***Proc Natl Acad Sci USA***, in press.

41 岡村　均、重吉康史、内匠透、山口瞬、八木田和弘：哺乳類時計遺伝子 mPer,「細胞のシグナリング Selected Reviews」(西塚泰美、貝淵弘三、丸山敬編)，中山書店，315-324 頁，1999.

42 岡村　均、重吉康史：生物時計の分子機構．細胞工学，18，698-707, 1999.

43 岡村　均、山口瞬：時計遺伝子と哺乳類の時間発振機構，医学のあゆみ，190，259-267，1999.

44 岡村　均：時計遺伝子ーその獲得と機能，Molecular Medicine，36，1092-1101，1999.

45 岡村　均、山口瞬、重吉康史：時計遺伝子からみた哺乳類生物時計ー理解への手引き，Molecular Medicine, 36, 1102-1109, 1999.

46 岡村　均、三宅茂：生体内時計の分子メカニズム，循環器科，46，363-368，1999.

47 重吉康史、岡村　均：視交叉上核の細胞構築,「生物時計の分子生物学」(海老原史樹文，深田吉孝編)，シュプリンガー・フェアラーク東京．159-168 頁，1999.

48 内匠透、岡村　均：体内時計とその遺伝子,「細胞工学別冊　脳を知る」(久野　宗編)，秀潤社，143-152 頁，1999.

49 内匠透，岡村　均：転写因子による生物時計の制御．実験医学，17，372-378，1999.

50 重吉康史、均：生物時計とリミットサイクル，生体の科学，50，162-168，1999.

51 内匠透、重吉康史、岡村　均：生物時計の分子機構．神緑会雑誌，15，93-96, 1999.

52 岡村　均、八木田和弘、山口瞬：時計遺伝子と脳機能，脳 21，3，393-401，2000 .

53 岡村　均、八木田和弘：生物時計発振分子のネガティブフィードバックループ，蛋白質核酸酵素増刊号「神経回路形成と機能発達」，40 ，338-345，2000.

54 岡村　均、山口　瞬、八木田和弘、石田佳毅、譜久山剛、角泰雄：サーカディアンリズムと時計遺伝子，ICU と CCU，24，375-382，2000.

55 岡村　均：時計遺伝子と生理機能，日本未熟児新生児学会雑誌，12，187-191，2000.

56 岡村　均、山口　瞬、八木田和弘、西村正高：生物時計の動きの機構ー哺乳類での知見，脳の科学，22，519-525，2000.

57 八木田和弘、岡村　均：サーカディアンフィードバックループー分子から時へ，実験医学，18，1930-1936，2000.

58 岡村　均：概日リズムの調節機構，現代医療，32，1619-1625，2000.

59 閤　莉莉、岡村　均：哺乳類時計制御の分子機構，Clinical Neuroscience，18，1130-1135，2000.

60 岡村　均：生物時計の分子生物学，心臓，32，979-986，2000.

61 岡村　均：生物時計研究のルネサンス，細胞工学，20，794-799，2001.

62 山口　瞬：哺乳類時計遺伝子の転写制御，細胞工学，20，811-816，2001.

63 八木田和弘：哺乳類培養細胞株を用いた細胞時計の解析，細胞工学，20，817-821，2001

64 岡村　均、閤　莉莉、山口　瞬：ヒトの時計遺伝子，「時間診療学」(田村康二編)，永井書店，9 頁ー15 頁，2001.

65 西村正高、岡村　均：脳・神経研究，「先端バイオ研究の進め方」(辻本豪三、田中利男編)，羊土社，47 頁ー52 頁，2001

66 岡村　均、山口　瞬、閤　莉莉：ヒトの時計遺伝子，「時間診療学」(田村康二編)，永井書店，9-15，2001

67 岡村　均：生物時計研究のルネサンス，細胞工学，20，794-799，2001.

68 西村正高、岡村　均：脳・神経研究，「先端バイオ研究の進め方」(辻本豪三、田中利男編)，羊土社，47 頁ー52 頁，2001.

69 石田佳毅, 岡村　均：生体の時計遺伝子が細胞で振動する機構、検査と技術、29，1415-1418，2001

70 岡村　均：時計遺伝子と睡眠、老年精神医学雑誌，12，1336-1343，2001.

71 西村正高、山口瞬、八木田和弘、岡村　均：哺乳類概日リズムの分子生物学、分子精神医学、1、437-443、2001.

72 岡村　均：脳の時計と細胞の時計：遺伝子から時へ、文部科学教育通信、38，26-29，2001.

73 岡村　均、増渕　悟、市原直征、山口　瞬：時計遺伝子のフィードバックループ，神経研究の進歩，45, 755-762，2001.

74 山口　瞬、哺乳類時計遺伝子の転写制御、細胞工学、20、811-816、2001。

75 八木田和弘、哺乳類培養細胞株を用いた細胞時計の解析、細胞工学、20, 817-821, 2001

Photic Induction of *mPer1* and *mPer2* in *Cry*-Deficient Mice Lacking a Biological Clock

Hitoshi Okamura,[1]* Shigeru Miyake,[1] Yasuo Sumi,[1] Shun Yamaguchi,[1] Akira Yasui,[2] Manja Muijtjens,[3] Jan H. J. Hoeijmakers,[3] Gijsbertus T. J. van der Horst[3]

Mice lacking *mCry1* and *mCry2* are behaviorally arrhythmic. As shown here, cyclic expression of the clock genes *mPer1* and *mPer2* (mammalian *Period* genes 1 and 2) in the suprachiasmatic nucleus and peripheral tissues is abolished and *mPer1* and *mPer2* mRNA levels are constitutively high. These findings indicate that the biological clock is eliminated in the absence of both mCRY1 and mCRY2 (mammalian cryptochromes 1 and 2) and support the idea that mammalian CRY proteins act in the negative limb of the circadian feedback loop. The *mCry* double-mutant mice retain the ability to have *mPer1* and *mPer2* expression induced by a brief light stimulus known to phase-shift the biological clock in wild-type animals. Thus, mCRY1 and mCRY2 are dispensable for light-induced phase shifting of the biological clock.

Many physiological and behavioral systems are controlled by an internal self-sustaining molecular oscillating mechanism with a periodicity of approximately 24 hours, known as the biological clock. The core oscillator consists of an autoregulatory transcription-(post) translation–based feedback loop involving a set of clock genes (*1*). In mammals, as in *Drosophila*, three recently identified *mPer* genes (*mPer1*, *mPer2*, and *mPer3*) are thought to be oscillator genes (*2–4*). Transcription of *mPer1* is driven by the CLOCK/BMAL transcriptional activator complex and in turn is repressed by its own gene product (*5*). To maintain synchrony with the solar day/night cycle, the master clock in the suprachiasmatic nucleus (SCN) of the brain needs to be reset by daily light through receptors in the eye (*6*). In mammals, mCRY1 and mCRY2, members of the light-harvesting cryptochrome/photolyase protein family (*7*), have been proposed as candidate photoreceptors required for light-entrainment of the biological clock (*8*). Mouse mutants lacking *mCry1* show an acceleration of the free-run-

[1]Department of Anatomy and Brain Science, Kobe University School of Medicine, Kobe 650-0017, Japan. [2]Department of Molecular Genetics, Institute of Development, Aging and Cancer, Tohoku University, Sendai 980-8575, Japan. [3]MGC, Department of Cell Biology and Genetics, Erasmus University, Post Office Box 1738, 3000 DR Rotterdam, Netherlands.

*To whom correspondence should be addressed. E-mail: okamurah@kobe-u.ac.jp

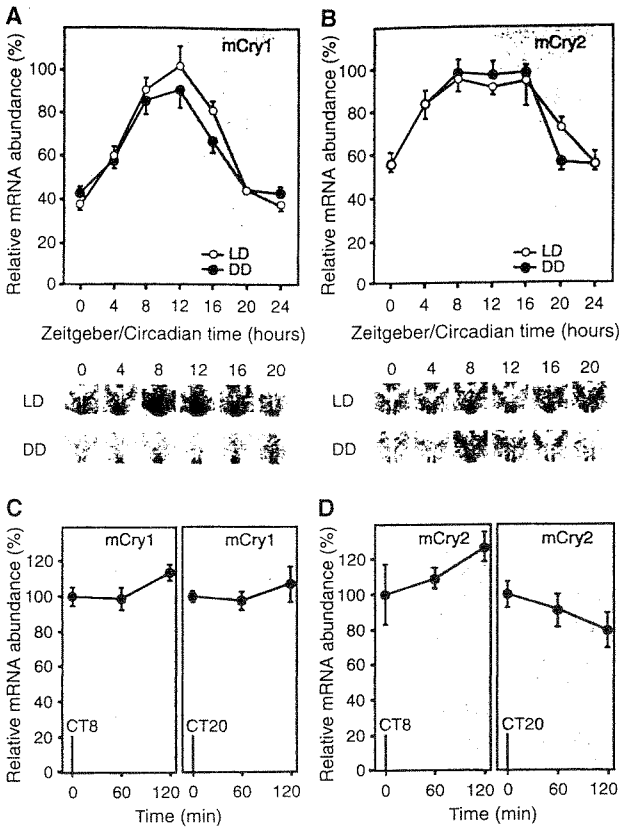

Fig. 1. Expression of *mCry1* and *mCry2* in the suprachiasmatic nucleus (SCN) of wild-type mice. (A and B) Circadian expression of (**A**) *mCry1* and (**B**) *mCry2* mRNA in the SCN in LD 12:12 (open circles) and in DD (closed circles). For each *mCry* gene, the relative RNA abundance was determined by quantitative in situ hybridization, with the value at CT12 adjusted to 100%. Values are expressed as means ± SEM (n = 5). Representative autoradiograms for each time point are shown below the graphs. (C and D) Light-pulse experiments for (**C**) *mCry1* and (**D**) *mCry2*. A 30-min light pulse (600 lux; fluorescent light) delivered at CT8 (left panels) and at CT20 (right panels) does not induce *mCry1* and *mCry2* mRNA. The relative RNA level was measured by quantitative in situ hybridization with the value just before onset of light adjusted to 100%. Values are expressed as means ± SEM (n = 3).

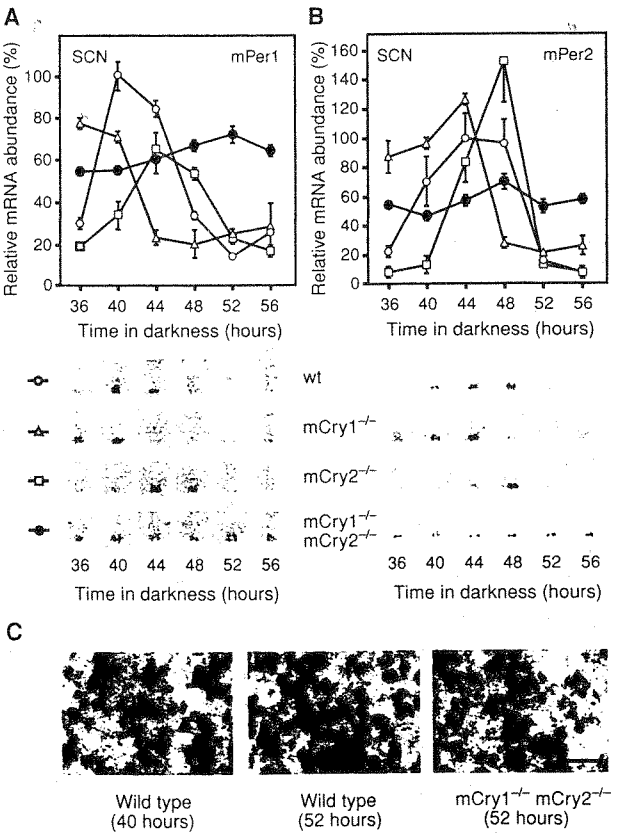

Fig. 2. Expression of *mPer1* and *mPer2* in the SCN of wild-type and *mCry* mutant mice in constant darkness. (A and B) The relative RNA abundance of *mPer1* (**A**) and *mPer2* (**B**) in the SCN of wild-type (open circles), *mCry1*$^{-/-}$ (open triangles), *mCry2*$^{-/-}$ (open squares), and *mCry1*$^{-/-}$*mCry2*$^{-/-}$ (closed circles) mice in constant darkness was determined by quantitative in situ hybridization. The peak values observed in wild-type animals were adjusted to 100%. Values are expressed as means ± SEM (n = 4). Representative autoradiograms are shown below the graphs. Because *mCry1*/*mCry2* double-mutant mice are arrhythmic, we used an environmental time scale (hours in DD) rather than a circadian time (CT) scale. (**C**) Representative examples of *mPer1* mRNA signals (dotted grains) in emulsion-coated sections of the SCN in wild-type and *mCry1*$^{-/-}$ *mCry2*$^{-/-}$ mice. (Left panel) wild-type SCN, 40 hours in darkness (≈CT4; 68 to 80% cells with 10 to 25 grains per cell); (middle panel) wild-type SCN, 52 hours in darkness (≈CT16; <10% cells with 10 to 25 grains per cell); (right panel) *mCry1*$^{-/-}$*mCry2*$^{-/-}$ SCN, 52 hours in darkness (62 to 74% cells with 10 to 25 grains per cell). Bar, 10 μm.

ning clock, as measured by wheel-running activity in constant darkness (*9*), whereas loss of *mCry2* slowed the clock (*9, 10*). Unexpectedly, mice lacking both *mCry* genes completely lack free-running rhythmicity (*9*). Although these results point to an antagonistic clock-adjusting function as well as to an absolute requirement of mCRY proteins for maintenance of circadian rhythmicity, they failed to resolve a possible function of the proteins as circadian photoreceptors and did not elucidate the consequences of mCRY dysfunction at the molecular level. To investigate how mCRY proteins act in the circadian core oscillation mechanism, we examined temporal and light-induced expression profiles of *mCry1*, *mCry2*, *mPer1*, and *mPer2* in the SCN and peripheral tissues of wild-type and *mCry* mutant mice by quantitative in situ hybridization or quantitative polymerase chain reaction (PCR) using real-time TaqMan technology.

Consistent with a possible function as clock gene, mRNA levels of *mCry1* oscillate in a circadian manner in the SCN and skeletal muscle of wild-type mice (*8, 11*). Similarly, *mCry2* expression exhibits a daily rhythm in the skeletal muscle (*11*). In contrast to previous reports (*8, 11*), using a highly sensitive method (*12, 13*), we observed that *mCry2* is rhythmically expressed in the SCN in a manner similar to *mCry1* (Fig. 1, A and B) (*14*). Levels of *mCry2* mRNA peak at the (subjective) day/night transition whether mice were kept under 12-hour light and dark cycles (LD 12:12) or under constant darkness (DD). Expression of the *mCry* genes is not significantly up-regulated by a brief light pulse given during the subjective day (CT8) or night (CT20) (Fig. 1, C and D). This indicates that, unlike *mPer1* and *mPer2* (*3, 15*), *mCry* expression is not directly regulated by light.

Next, we examined the expression profiles of *mPer1* and *mPer2* in entrained wild-type and *Cry* mutant mice (LD 12:12; 2 weeks) starting 36 hours after animals were placed in constant darkness (DD). Both *mPer1* and *mPer2* show a high-amplitude oscillation in the SCN of wild-type animals (Fig. 2, A and B). As expected on the basis of animals' circadian wheel-running behavior (*9*), robust oscillation of *mPer1* and *mPer2* mRNA is maintained in animals mutant for *Cry1* or *Cry2*. On the absolute time scale, consistent with the differences in free-running period length (*9*), *mPer1* and *mPer2* expression peaks earlier in *mCry1* mutant mice (tau = 22.5 hours) and later in *mCry2* mutant mice (tau = 24.6 hours), compared to wild-type animals (tau = 23.8 hours). In marked contrast, *mCry* double-mutant mice fail to show significant *mPer1* and *mPer2* mRNA cycling in the SCN (Fig. 2, A and B); instead, *mPer1* and *mPer2* transcript levels are intermediate to high at all times examined. In addition, we observed a homoge-

neous pattern of *mPer1* labeling in SCN tissue sections of mice deficient in *mCry1* and *mCry2* (Fig. 2C), indicating that transcript levels of *mPer1* are similar in all cells. This suggests that the absence of *mPer1* cycling in double mutants (Fig. 2A) is not due to a synchronization defect.

Because non-SCN tissues also rhythmically express clock genes (*4, 16*), we examined whether oscillation of these putative peripheral clocks was also affected in the absence of CRY. In contrast to wild-type mice, in the retina (Fig. 3A) (*17*) and liver (Fig. 3B) (*18*) of *mCry1/mCry2* double-mutant mice, *mPer1* mRNA no longer cycles and expression is constantly high. Similarly, *mPer2* mRNA did not show a prominent rhythm in retina and liver of *mCry1/mCry2* double-mutant mice (*19*). From the total absence of *mPer1* and *mPer2* oscillation in the SCN and in peripheral tissues, we conclude that the behavioral arrhythmicity observed in *mCry1/mCry2*-deficient mice is the direct consequence of a complete impairment of the molecular clock and that mCRY proteins are indispensable components of the core oscillator. Furthermore, the presence of accelerated and retarded clock oscillation in *mCry1* and *mCry2* single mutants indicates at the molecular level that mCRY1 and mCRY2 have overlapping functions in running the clock and an antagonistic role in determining its pace. The high mRNA levels of *mPer1* and *mPer2* in *mCry1/mCry2*-deficient mice suggest that mCRY proteins negatively affect *mPer* expression. Reppert and co-workers (*11*), as well as other groups (*20, 21*), have shown that whereas mPER and mTIM proteins only have moderate inhibitory effects on CLOCK/BMAL transactivating activity, mCRY1 and mCRY2 can almost completely block transcription from the *mPer1* promoter, which puts the mCRY proteins directly in the negative limb of the circadian feedback loop (*11*). Our findings that, in the absence of mCRY, *mPer1* and *mPer2* appear constitutively expressed at high levels are in agreement with this conclusion.

Circadian photoreceptors in mammals reside in the eye: loss of eyes abolishes photoentraining of the biological clock (*22*). However, rod- and cone-less mice show intact entrainment, indicating that rhodopsins are not involved (*23*). mCRY proteins are likely candidates for the circadian photoreceptors involved in light-entrainment because (i) they belong to the family of blue-light receptors (*7*), (ii) their expression is high in the ganglion cells and inner nuclear layers of the retina (*8*), and (iii) they can exert a clock-adjusting function (*9*) which would be required in the context of effecting a light input into the clock. However, direct proof for the presumed light input function is lacking because, ironically, the absence of a functional clock in *mCry* double-mutant mice precludes analysis of a resetting function by classical phase-shifting experiments. Nevertheless, to investigate a potential mCRY-mediated photoreceptor role, we examined the effect of light pulses on *mPer1* and *mPer2* expression: when light is given early during the subjective night concomitant with phase shifting of the clock, wild-type mice respond with an acute induction of *mPer1* and *mPer2* mRNA (Fig. 4) (*3, 14, 24*). Surprisingly, *mCry* double-mutant mice retained the ability to respond to the brief light pulse with acute induction of *mPer1* and *mPer2* mRNA (Fig. 4). This indicates that the rapid induction of *mPer1* and *mPer2* mRNA by light is still intact in complete absence of mCRY proteins and can occur without a functional clock or core oscillator.

In conclusion, our results show that a complete inactivation of the molecular oscillator driving the biological clock underlies the arrhythmicity observed in *mCry1/mCry2* double-mutant mice. Thus, mCRY1 and mCRY2 are indispensable components of the core oscillator, and *mCry1/mCry2*-deficient mice are, to our knowledge, the first mammals completely lacking a circadian pacemaker. In *mCry1/mCry2* double-mutant mice, the mechanism of light-induced phase shifting by up-regulation of *mPer1* and *mPer2* expression is still intact, which points to the involvement of different transcription regulatory processes for core oscillation and light-mediated phase-shifting. Our data suggest that photoreceptors other than mCRY proteins and rod/cone opsins [for example, mammalian homologs of the recently discovered fish VA-opsin (*25*) or *Xenopus laevis* melanopsin (*26*)] may be responsible for photic entrainment. Although *mPer* transcription repression by mCRY proteins (and thus their function in core oscillation) is light-independent (*20*), we do not completely rule out that mCRY proteins may act as photoreceptor proteins. First, it is possible that phase-shifting is mediated via more than one photoreceptor system, implying functional redundancy. Second, mCRY proteins may be involved in transmitting light inputs to the clock other than those required for phase shifting, such as changes in the length of the day and night, and information on dusk and dawn. Future experiments should shed light on the myste-

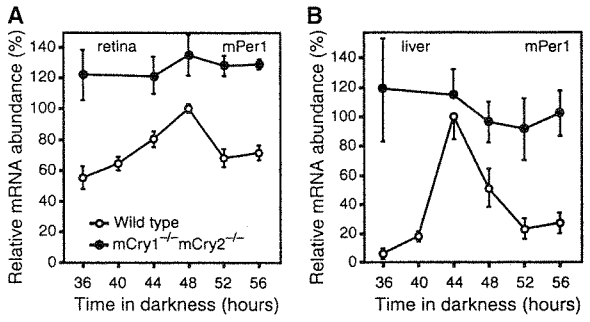

Fig. 3. Expression of *mPer1* in the retina and liver of wild-type and *mCry1*$^{-/-}$*mCry2*$^{-/-}$ mutant mice in constant darkness. (**A**) The relative abundance of *mPer1* mRNA in the retina was determined by quantitative in situ hybridization (five sections per animal; three independent experiments). Values (CT48 was determined as 100%) are expressed as the mean ± SEM. (**B**) The relative abundance of *mPer1* mRNA in the liver was determined by the reverse transcription PCR method with TaqMan technology as described. The calculated expression level of *mPer1* of wild-type at 44 hours divided by that of GAPDH was normalized to 100%. Values are expressed as means ± SEM (n = 3).

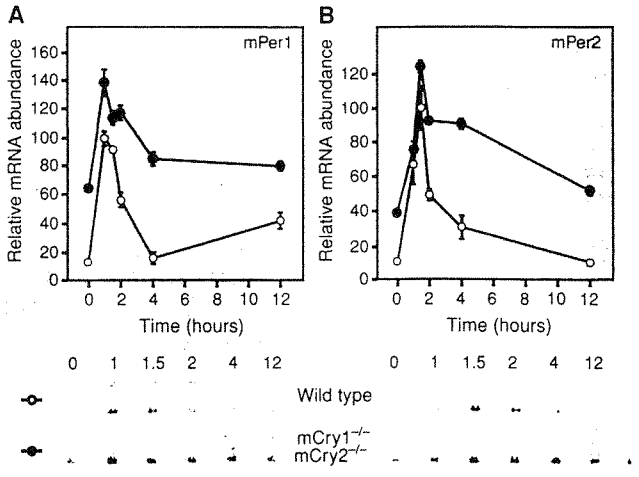

Fig. 4. Light-induced *mPer1* and *mPer2* expression in the SCN of wild-type and *mCry1*$^{-/-}$ *mCry2*$^{-/-}$ mutant mice. A 30-min light pulse (600 lux; fluorescent light) delivered 52 hours after the dark transfer induced (**A**) *mPer1* and (**B**) *mPer2* mRNA in the SCN of wild-type and *mCry1*$^{-/-}$ *mCry2*$^{-/-}$ mutant mice. The relative abundance of *mPer1* mRNA was determined by quantitative in situ hybridization, with the peak induced values of wild-type (1 hour for *mPer1*, 1.5 hour for *mPer2*) adjusted to 100%. Values are expressed as means ± SEM (n = 4). Representative autoradiograms are shown in the lower panels.

rious blue-light receptor properties of mCRY proteins.

Note added in proof: Recently, Vitaterna and colleagues have determined mRNA levels of *mPer1* and *mPer2* in *mCry1/mCry2* double-mutant mice at two time points. In addition, photic induction (measured 30 min after a 1-hour light pulse) was observed for *mPer2* but not for *mPer1* (*27*).

References and Notes

1. J. Dunlap, *Cell* **96**, 271 (1999); S. M. Reppert, *Neuron* **21**, 1 (1998); M. Rosbash *et al.*, *Cold Spring Harbor Symp. Quant. Biol.* **61**, 265 (1996); D. Whitmore, P. Sassone-Corsi, N. S. Foulkes, *Curr. Opin. Neurobiol.* **8**, 635 (1998); L. D. Wilsbacher and J. S. Takahashi, *Curr. Opin. Genet. Dev.* **8**, 595 (1998); M. W. Young, *Annu. Rev. Biochem.* **67**, 135 (1998).
2. H. Tei *et al.*, *Nature* **389**, 512 (1997); Z. S. Sun *et al.*, *Cell* **90**, 1003 (1997).
3. U. Albrecht, Z. S. Sun, G. Eichele, C. C. Lee, *Cell* **91**, 1055 (1997); L. P. Shearman, M. J. Zylka, D. R. Weaver, L. F. Kolakowski Jr., S. M. Reppert, *Neuron* **19**, 1261 (1997); T. Takumi *et al.*, *Genes Cells* **3**, 167 (1998); T. Takumi *et al.*, *EMBO J.* **17**, 4753 (1998).
4. M. J. Zylka, L. P. Shearman, D. R. Weaver, S. M. Reppert, *Neuron* **20**, 1103 (1998).
5. N. Gekakis *et al.*, *Science* **280**, 1564 (1998); A. M. Sangoram *et al.*, *Neuron* **21**, 1101 (1998).
6. R. G. Foster, *Neuron* **20**, 829 (1998).
7. T. Todo *et al.*, *Science* **272**, 109 (1996); P. J. van der Spek *et al.*, *Genomics* **37**, 177 (1996); D. S. Hsu *et al.*, *Biochemistry* **35**, 13871 (1996).
8. Y. Miyamoto and A. Sancar, *Proc. Natl. Acad. Sci. U.S.A.* **95**, 6097 (1998).
9. G. T. J. van der Horst *et al.*, *Nature* **398**, 630 (1999).
10. R. J. Thresher *et al.*, *Science* **282**, 1490 (1999).
11. K. Kume *et al.*, *Cell* **98**, 193 (1999).
12. Wild-type, $Cry1^{-/-}$, $Cry2^{-/-}$, and $Cry1^{-/-}Cry2^{-/-}$ animals (C57B16:Ola 129 hybrid, 8 to 12 weeks old) were individually housed under 12-hour light, 12-hour dark cycles (LD 12:12) and constant temperature. In DD (constant darkness) and light-pulse experiments, animals were kept under LD 12:12 conditions for at least 2 weeks and were used the second day of DD. Animals were exposed to fluorescent light (600 lux for 30 min) and killed at the time points indicated. Because $Cry1^{-/-}Cry2^{-/-}$ animals are arrhythmic, in some of the experiments, we used an absolute time scale rather than a Circadian (CT) or Zeitgeber (ZT) time scale. Circadian expression of *mCry1* and *mCry2* was studied in Balb-c mice (Japan Animal Care, 8 to 10 weeks old).
13. Quantitative in situ hybridizations ("free-floating" method) on serial coronal cryostat sections of the mouse brain (40 μm thick) were performed as described (*15*). Radiolabeled cRNA probes for *mCry1* (1074–1768), *mCry2* (1016–1652), *mPer1* (538–1752), and *mPer2* (1–638) were made with [^{33}P]–uridine triphosphate (New England Nuclear) and a standard protocol for cRNA synthesis. The radioactivity in the SCN of each section on BioMax films (Kodak) or Ilford K5 nuclear track emulsions (Ilford) was analyzed with a microcomputer interfaced to an image analyzer system (MCID, Imaging Research Inc., Ontario, Canada) after conversion into the relative optical densities produced by the [^{14}C]-autoradiographic microscale (Amersham). Data from the SCN were normalized with respect to the signal intensities in an equal area of the corpus callosum. The intensities of the optical density of the sections from the rostral-most to the caudal-most of the SCN (10 sections per brain) were then summed; the sum was considered a measure for the amount of mRNA in this region. Values are expressed as means ± SEM (n as indicated in the text). "Relative mRNA abundance" values are calculated assuming a wild-type peak value as 100%.
14. Using the highly sensitive and quantitative "free-floating" method (*13*), we found a significant difference among six time points in both LD 12:12 [$F(5,48) = 5.20$, $P = 0.023$] and DD [$F(5,48) = 5.20$, $P < 0.001$] conditions (method: one-way ANOVA).
15. Y. Shigeyoshi *et al.*, *Cell* **91**, 1043 (1997).
16. A. Balsalobre, F. Damiola, U. Schibler, *Cell* **93**, 929 (1998).
17. Quantitative in situ hybridizations on eye sections were performed with the thaw-mounted method. Signals were measured in the external granular layer of the retina (five sections per animal; three independent experiments). Values are expressed as the mean ± SEM.
18. Quantitative PCR was performed with real-time TaqMan technology (PE Biosystems) [C. A. Heid *et al.*, *Genome Res.* **6**, 986 (1996)] and analyzed on an ABI PRISM 7700 (Perkin-Elmer) as described [T. Takumi *et al.*, *Genes Cells* **4**, 67 (1999)]. Total RNA was extracted from mouse liver with Trizol (Gibco-BRL) and digested with DNAse RQI (Promega). The primers for *mPer1* are as follows: Forward 5′-CGCCTCCTTGCTACAGGTAC-3′; Reverse, 5′-GGTAGGAACAGCCAGAGGTTTC-3′, and the TaqMan probe, 5′-CAAAGCCAAAGTCCTTCCCTGCCA-3′. As an internal control for the RNA, expression of GAPDH (glyceraldehyde phosphate dehydrogenase) was examined under the same conditions. Ratios of *mPer1* to GAPDH were calculated and normalized. Each value is the mean ± SEM (n = 3).
19. H. Okamura and S. Miyake, data not shown.
20. E. A. Griffin Jr., D. Staknis, C. J. Weitz, *Science* **286**, 768 (1999).
21. mCRY proteins suppress CLOCK/BMAL-mediated transcription from an *mPer1* promoter–luciferase reporter construct in HepG2 cells (S. Yamaguchi and H. Okamura, unpublished data).
22. T. Roenneberg and R. G. Foster, *Photochem. Photobiol.* **66**, 549 (1997).
23. M. S. Freedman *et al.*, *Science* **284**, 502 (1999); R. J. Lucas, M. S. Freedman, M. Muñoz, J.-M. Garcia-Fernández, R. G. Foster, *Science* **284**, 505 (1999).
24. Fifty-two hours after initiation of DD exposure (this corresponds to CT16 for wild-type animals), wild-type and *mCry1/mCry2* double-mutant mice were exposed to a brief fluorescent light stimulus (600 lux for 30 min). Animals were killed 60, 90, and 120 min, and 4 and 12 hours after the initiation of the light exposure.
25. B. G. Soni and R. G. Foster, *FEBS Lett.* **406**, 279 (1997).
26. I. Provencio, G. Jang, W. J. de Grip, W. P. Hayes, M. D. Rollag, *Proc. Natl. Acad. Sci. U.S.A.* **95**, 340 (1998).
27. M. H. Vitaterna *et al.*, *Proc. Natl. Acad. Sci. U.S.A.* **96**, 12114 (1999).

28. We thank T. Takumi, K. Ohata, S. Takekida, H. Onishi, and K. Yagita for support. Supported in part by grants from the Special Coordination Funds of the Science and Technology Agency of Japan; Human Frontier Science; the Louis Jeantet Foundation; the Grant-in-Aid for the Scientific Research on Priority Areas of the Ministry of Education, Science, Sports and Culture of Japan; the Ministry of Welfare of Japan; SRF; and by a Spinoza premium of the Netherlands Organization for Scientific Research (NWO).

22 September 1999; accepted 17 November 1999

Molecular Mechanisms of the Biological Clock in Cultured Fibroblasts

Kazuhiro Yagita,[1] Filippo Tamanini,[2] Gijsbertus T. J. van der Horst,[2] Hitoshi Okamura[1]*

In mammals, the central circadian pacemaker resides in the hypothalamic suprachiasmatic nucleus (SCN), but circadian oscillators also exist in peripheral tissues. Here, using wild-type and *cryptochrome* (*mCry*)–deficient cell lines derived from *mCry* mutant mice, we show that the peripheral oscillator in cultured fibroblasts is identical to the oscillator in the SCN in (i) temporal expression profiles of all known clock genes, (ii) the phase of the various mRNA rhythms (i.e., antiphase oscillation of *Bmal1* and *mPer* genes), (iii) the delay between maximum mRNA levels and appearance of nuclear mPER1 and mPER2 protein, (iv) the inability to produce oscillations in the absence of functional *mCry* genes, and (v) the control of period length by mCRY proteins.

In the mouse, the core oscillator of the master circadian clock in the SCN is composed of interacting positive and negative transcription-translation feedback loops (*1–3*), which involve three homologs of the *Drosophila* gene *period* (*mPer1*, *mPer2*, and *mPer3*), two cryptochrome genes (*mCry1* and *mCry2*), and the transcriptional activator genes *Clock* and *Bmal1* (*1, 2, 4*). A key step in this feedback loop is the shutdown of CLOCK- and BMAL1-driven transcription by mCRY proteins (*4*). To keep pace with the solar day-night cycle, the master clock can be entrained by light received through photoreceptors in the retina (*5*). Molecular oscillators also exist in peripheral tissues, where they cycle with a 6- to 8-hour delay with respect to the central pacemaker (*6–8*). In contrast to *Drosophila* and zebrafish, mammalian peripheral clocks do not directly respond to light but are synchronized by the SCN by neuronal and/or humoral signals (*9*). In vitro, brief treatment of cultured cells with various compounds [serum, forskolin, 12-*O*-tetradecanoylphorbol 13-acetate (TPA), adenosine 3′,5′-monophosphate (cAMP), or dexamethasone] induces rhythmic expression of the clock genes *Per1*, *Per2*, and *Cry1* and the circadian transcription factor gene *dbp* for two to three cycles (*6, 10–12*).

To investigate whether the molecular makeup of the peripheral oscillator in cultured fibroblasts resembles that of the core oscillator in the SCN, we determined the expression profiles of all known clock genes in cultured rat-1 fibroblasts over a period of 3 days (*13*). To trigger the oscillations, we used the vasocontracting peptide endothelin-1 (ET-1) (*14*), which activates the protein kinase C–mitogen-activated protein kinase cascade and cAMP response element–binding protein (CREB) phosphorylation (*15*). This treatment induces a rapid, robust increase in *Per1* and *Per2* gene expression, followed by a sharp reduction in corresponding mRNA levels and subsequent synchronous cycling of *Per1*, *Per2*, *Per3*, and *dbp* mRNAs (Fig. 1) (*16, 17*). Also, robust cycling of *Bmal1* mRNA was observed, with mRNA levels accumulating antiphase to *Per* and *dbp* mRNA cycles. *Clock* mRNA levels were constant at all time points examined. In addition, *Cry1* expression showed rhythmicity, peaking 4 to 8 hours after *Per* mRNAs (*16*). These data demonstrate that ET-1 can induce circadian gene expression in cultured rat-1 cells and that the temporal expression patterns of *Per*, *Bmal1*, *Cry1*, and *dbp* genes (all rhythmically expressed) as well as the *Clock* gene (constitutively expressed) match those in the SCN (*1, 18*). Casein kinase Iε (*CKIε*) and *Cry2* genes did not show apparent rhythmic expression in rat-1 cells, a finding consistent with the observation that in the SCN *CKIε* is constitutively expressed (*19*) and cycling of mouse *Cry2* is weak (*18*) or not detectable (*20*).

Next, we analyzed by immunocytochemistry the PER1 and PER2 protein expression profiles in these cells. Nuclear staining occurred 26 to 28 hours after treatment, indicating that mPER1 and mPER2 protein cycles follow the rhythm of *Per1* and *Per2* mRNA expression with a 4- to 8-hour delay (Fig. 2), as in the SCN (*21*). In addition, pronounced PER1 and PER2 nuclear staining was found 1.5 hours after ET-1 treatment (Fig. 2) (*22*), suggesting that ET-1 causes rapid synthesis of PER1 and PER2 and translocation of these proteins into the nucleus. This nuclear PER2 may up-regulate *Bmal1* expression and down-regulate *Per* gene expression 4 hours after ET-1 treatment (Fig. 1)

[1]Division of Molecular Brain Science, Department of Brain Sciences, Kobe University Graduate School of Medicine, Chuo-ku, Kobe 650-0017, Japan. [2]Center for Biomedical Genetics, Department of Cell Biology and Genetics, Erasmus University, Post Office Box 1738, 3000 DR, Rotterdam, Netherlands.

*To whom correspondence should be addressed. E-mail: okamurah@kobe-u.ac.jp

(*16*). The latter effect may also involve the CRY proteins.

We next used spontaneously immortalized (mutant) mouse embryonic fibroblasts (MEFs) from wild-type and *mCry1*$^{-/-}$*mCry2*$^{-/-}$ mice to test the role of *mCry* genes in the fibroblast clock (*23, 24*). Treatment of wild-type MEFs with ET-1 resulted in a temporary induction of *mPer1* gene expression within 1 hour, followed by synchronous cycling of *mPer1* and *dbp* mRNA (Fig. 3A) (*17*). Four hours after stimulation, increased *Bmal1* mRNA levels were observed (Fig. 3A), which most likely requires synthesis and nuclear translocation of the mPER2 protein and subsequent rhythmic expression of *Bmal1* mRNA antiphase to *mPer1* and *dbp*. Thus, as in rat-1 cells, ET-1 can induce circadian gene expression in MEFs. In marked contrast, ET-1 treatment of *mCry1*$^{-/-}$ *mCry2*$^{-/-}$ MEFs did not result in rhythmic expression of *mPer1*, *Bmal1*, or *dbp* genes (Fig. 3, B and C). Instead, as in the SCN, *mCry1*$^{-/-}$ *mCry2*$^{-/-}$ MEFs showed continuously accumulating *mPer1* mRNA and low levels of *Bmal1* mRNA, respectively. The absence of mCRY proteins also resulted in constant high expression of the *dbp* gene. Because *mCry1*$^{-/-}$ *mCry2*$^{-/-}$ MEFs express *ET-A receptor* mRNA (*25*), the lack of rhythmic gene expression in these cells is unlikely to result from improper activation of signal transduction pathways, but rather is caused by the absence of mCRY proteins. Interestingly, *mCry1*$^{-/-}$*mCry2*$^{-/-}$ cells retain the ability to respond to ET-1 treatment or a serum shock with instantaneous induction of *mPer1* and *mPer2* gene expression (*16*). Thus, as in the SCN and peripheral tissues in intact animals, *mCry* genes are indispensable for generation of molecular rhythm in stimulated cultured mouse fibroblasts.

To investigate whether the periodicity of peripheral clocks is an intrinsic property of the peripheral oscillator or whether it is instigated by cues from the SCN, we have measured temporal expression patterns of the *dbp* gene in immortalized MEFs from *mCry1* and *mCry2* single-mutant mice, known for their short (τ = 22.5 hours) and long (τ = 24.6 hours) free-running periodicity of locomotor activity, respectively (*18, 20, 23*). The periodicity of *dbp* mRNA oscillation in *mCry1*$^{-/-}$ MEFs, although weak, is about 2 to 4 hours shorter than in *mCry2*$^{-/-}$ MEFs (Fig. 3, D and E). This indicates that mCRY-mediated control over the pace of biological clockwork is not restricted to the central pacemaker in the SCN, but holds for circadian oscillators in any mammalian tissue.

Finally, we measured DBP protein oscillation patterns in serum shock–stimulated MEFs. Robust oscillation of nuclearly localized DBP was observed in wild-type and *mCry2*$^{-/-}$ MEFs (Fig. 4) (*26*). In *mCry1*$^{-/-}$ cells, nuclear DBP levels remained high after a brief initial nadir. This finding not only confirms the unexpected pattern of *dbp* gene expression in these cells but also emphasizes the weakness of *mCry2*-mediated oscillations. As expected on the basis of constant high levels of *dbp* mRNA, nuclei of *mCry1*$^{-/-}$ *mCry2*$^{-/-}$ cells were positive at any time. For

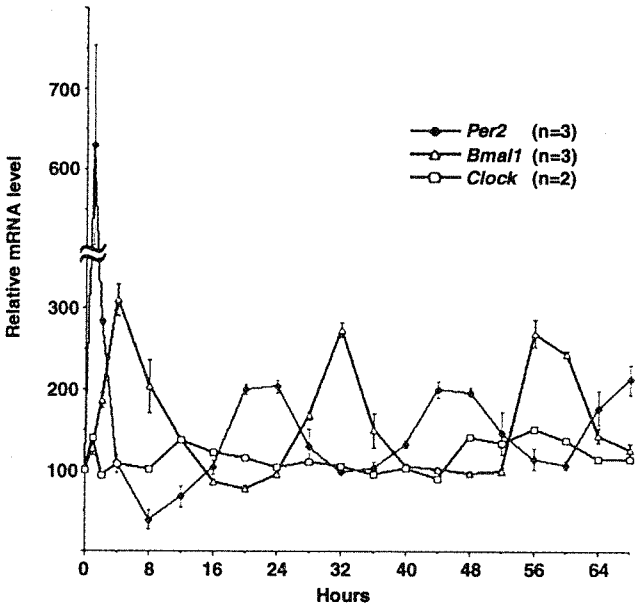

Fig. 1. Temporal expression profiles of clock genes in rat-1 fibroblasts after ET-1 treatment: Quantification of temporal changes in *Per2*, *Bmal1*, and *Clock* mRNAs. Basal levels of each mRNA (at time point 0) were arbitrarily set to 100. Results shown are means ± SEM; *n* = number of experiments.

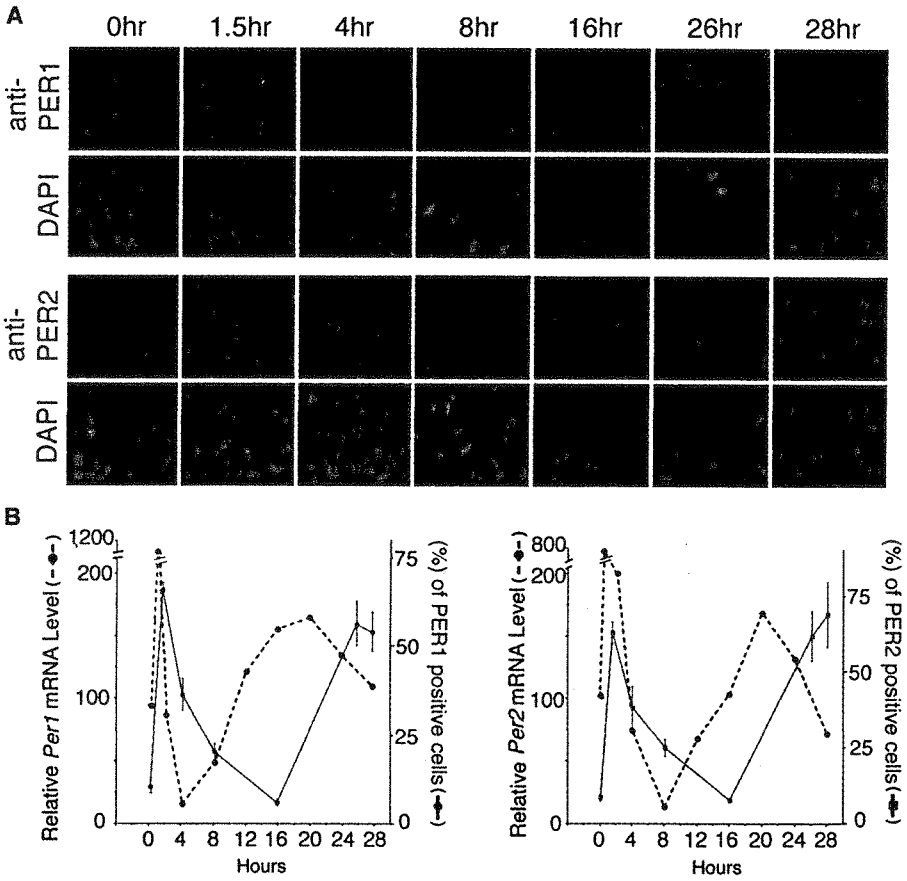

Fig. 2. Temporal PER1 and PER2 protein expression profiles in ET-1–treated rat-1 fibroblasts and comparison with corresponding mRNA expression profiles. (**A**) Immunofluorescence showing accumulation of PER1 and PER2 proteins in nuclei of ET-1–treated rat-1 fibroblasts. (**B**) Percentages of cells positive for antibodies to PER1 and PER2 (counted in 100 to 200 DAPI-stained nuclei) at the indicated times. For comparison, relative mRNA levels of *Per1* and *Per2* are shown as broken lines. Results shown are means ± SEM (three independent experiments).

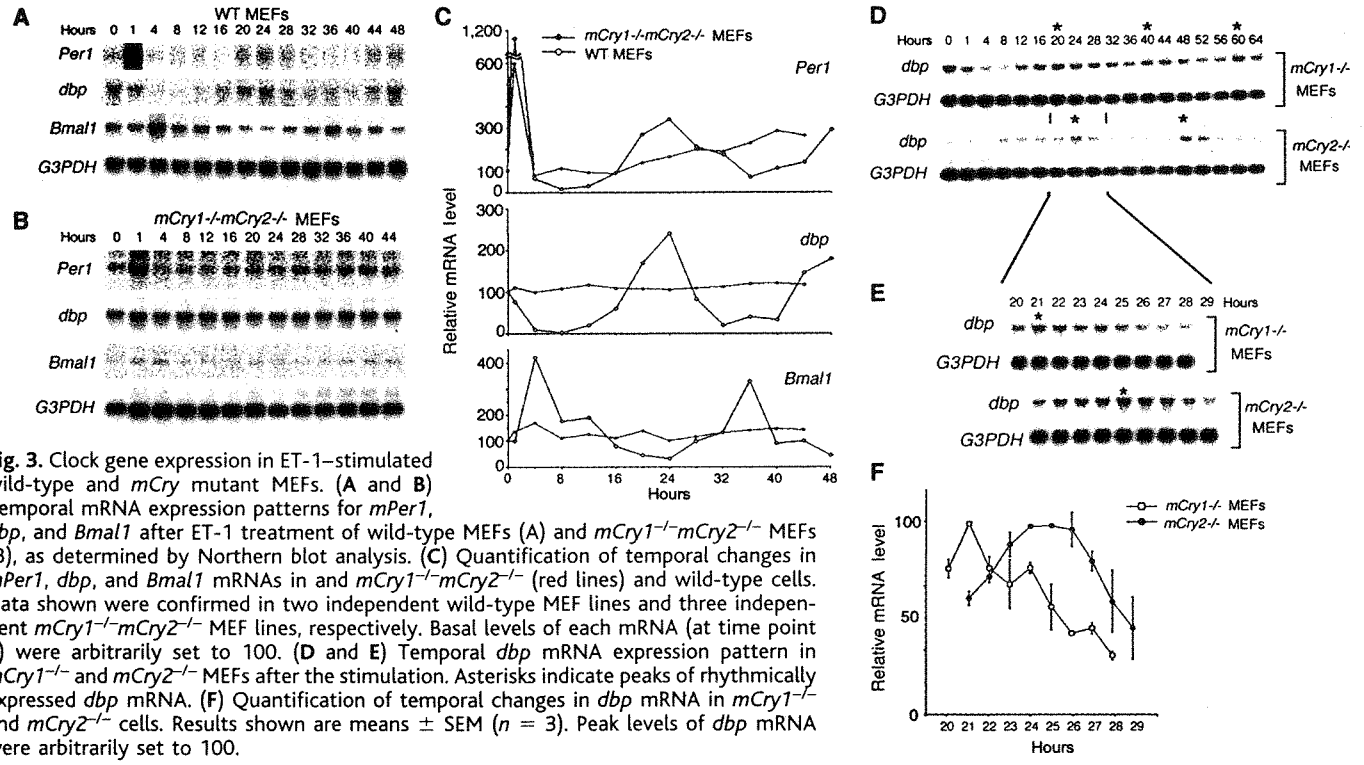

Fig. 3. Clock gene expression in ET-1–stimulated wild-type and *mCry* mutant MEFs. (**A** and **B**) Temporal mRNA expression patterns for *mPer1*, *dbp*, and *Bmal1* after ET-1 treatment of wild-type MEFs (A) and $mCry1^{-/-}mCry2^{-/-}$ MEFs (B), as determined by Northern blot analysis. (**C**) Quantification of temporal changes in *mPer1*, *dbp*, and *Bmal1* mRNAs in and $mCry1^{-/-}mCry2^{-/-}$ (red lines) and wild-type cells. Data shown were confirmed in two independent wild-type MEF lines and three independent $mCry1^{-/-}mCry2^{-/-}$ MEF lines, respectively. Basal levels of each mRNA (at time point 0) were arbitrarily set to 100. (**D** and **E**) Temporal *dbp* mRNA expression pattern in $mCry1^{-/-}$ and $mCry2^{-/-}$ MEFs after the stimulation. Asterisks indicate peaks of rhythmically expressed *dbp* mRNA. (**F**) Quantification of temporal changes in *dbp* mRNA in $mCry1^{-/-}$ and $mCry2^{-/-}$ cells. Results shown are means ± SEM (n = 3). Peak levels of *dbp* mRNA were arbitrarily set to 100.

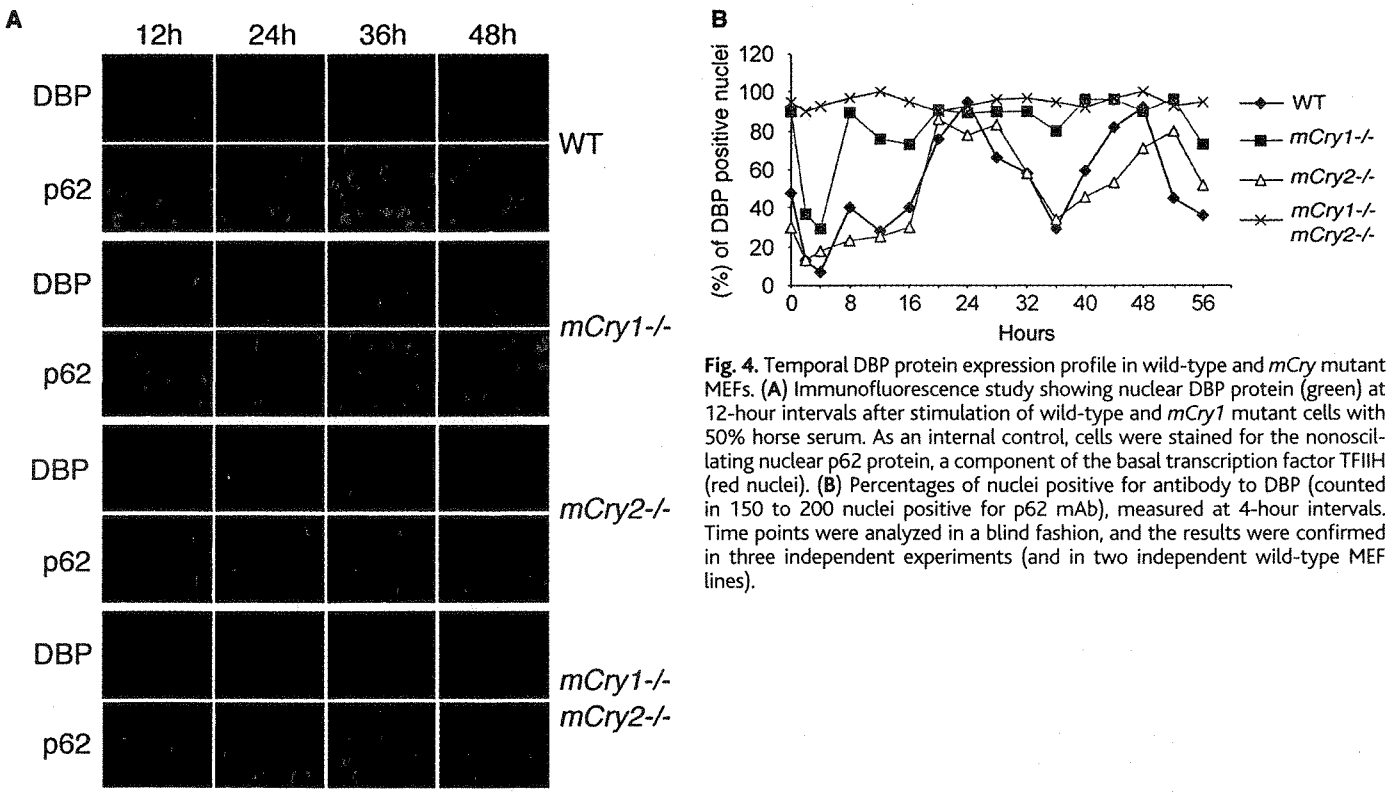

Fig. 4. Temporal DBP protein expression profile in wild-type and *mCry* mutant MEFs. (**A**) Immunofluorescence study showing nuclear DBP protein (green) at 12-hour intervals after stimulation of wild-type and *mCry1* mutant cells with 50% horse serum. As an internal control, cells were stained for the nonoscillating nuclear p62 protein, a component of the basal transcription factor TFIIH (red nuclei). (**B**) Percentages of nuclei positive for antibody to DBP (counted in 150 to 200 nuclei positive for p62 mAb), measured at 4-hour intervals. Time points were analyzed in a blind fashion, and the results were confirmed in three independent experiments (and in two independent wild-type MEF lines).

all cell lines tested, the appearance of nuclear DBP largely coincided with the (ET-1–mediated) *dbp* mRNA expression profile. These findings suggest that, as in the SCN, DBP is rapidly synthesized and translocated into the nucleus (*27*).

Taken together, our data indicate that the molecular makeup of the peripheral circadian oscillator in cultured fibroblasts is similar to that of the master oscillator in the SCN. The same set of circadian genes is assembled into positive and negative transcription-translation feedback loops. The mRNA expression profiles for these circadian genes display an "SCN-like" temporal expression profile as well as phase relationship, and, at least for mPER1, mPER2, and DBP, the delay between onset of transcription and nuclear ap-

pearance of the corresponding gene product is comparable to that in the SCN. Moreover, the homozygous inactivation of one or both *mCry* genes—known to accelerate, retard, or even abolish the biological clock in the SCN (*18, 20, 23*)—affects the peripheral oscillator to a similar extent. Thus, the peripheral oscillator in immortalized cultured fibroblasts constitutes a bona fide in vitro model for the molecular oscillator in the SCN, and could potentially allow the use of skin fibroblasts as a means of identifying clock gene defects in patients with circadian disorders.

Although peripheral clocks in the intact mouse possess some degree of autonomy, as is evident from the uncoupling of entrainment of peripheral and master clocks by glucocorticoid administration or restricted feeding (*6–8*), they differ from the master clock in the SCN in one important aspect. Unlike in cultured SCN slices, rhythmic clock gene expression in cultured peripheral organs/tissues and fibroblasts is dampened after a number of days (*9*). Because, as we have shown, the molecular makeup of the core oscillator of master and peripheral clocks is identical, the mechanism that allows the master clock to keep on ticking remains to be identified.

References and Notes

1. J. Dunlap, *Cell* **96**, 271 (1999).
2. M. W. Young, *Science* **288**, 451 (2000).
3. N. Cermakian, P. Sassone-Corsi, *Nature Rev. Mol. Cell Biol.* **1**, 59 (2000).
4. L. P. Shearman *et al.*, *Science* **288**, 1013 (2000).
5. R. G. Foster, *Neuron* **20**, 829 (1998).
6. A. Balsalobre *et al.*, *Science* **289**, 2344 (2000).
7. F. Damiola *et al.*, *Genes Dev.* **14**, 2950 (2000).
8. K. A. Stokkan *et al.*, *Science* **291**, 490 (2001).
9. S. Yamazaki *et al.*, *Science* **288**, 682 (2000).
10. A. Balsalobre, F. Damiola, U. Schibler, *Cell* **93**, 929 (1998).
11. K. Yagita and H. Okamura, *FEBS Lett.* **465**, 79 (2000).
12. M. Akashi and E. Nishida, *Genes Dev.* **14**, 645 (2000).
13. Rat-1 fibroblasts were cultured as described (*10*). Before stimulation, cells were cultured for 3 to 4 days in medium containing 5% fetal bovine serum. Cells were stimulated by brief treatment (2 hours) with medium containing either endothelin-1 (final concentration 30 nM, Sigma), after which medium was replaced by serum-free Dulbecco's modified Eagle's medium (Nacalai Tesque, Kyoto, Japan).
14. M. Yanagisawa *et al.*, *Nature* **332**, 411 (1988).
15. T. Kuwaki *et al.*, *Prog. Neurobiol.* **51**, 545 (1997).
16. See *Science* Online (www.sciencemag.org/cgi/content/full/292/5515/278/DC1).
17. Northern blot analysis was performed as described (*11*). Probes of *Per1*, *Per2*, and *dbp* were prepared as described (*11*). For *Clock* and *Bmal1*, full-length cDNAs of *hClock* and *hBmal1* (*27*) were digested by Xba I and Sma I, respectively. Fragments of *hClock* (base pairs 364 to 1084 of *hClock* cDNA) and *hBmal1* (base pairs 687 to 1506 of *hBmal1* cDNA) were used for the templates. G3PDH (Clontech) was used as a control. Probes were labeled with [^{32}P]deoxycytidine triphosphate using a TaKaRa random primer labeling kit (TaKaRa, Tokyo, Japan). Hybridization was performed at 42°C for 16 hours, and membranes were washed twice in 0.2× SSC/0.1% SDS at 60°C for 30 min. Membranes were exposed to an imaging plate and analyzed by BAS 5000 (Fuji Film, Tokyo, Japan). For rehybridization purposes, old probes were removed by treatment of membranes with a preheated (80°C) solution containing 1% SDS/0.1× SSC for 3 min.
18. H. Okamura *et al.*, *Science* **286**, 2531 (1999).
19. Y. Ishida *et al.*, *J. Neurosci. Res.*, in press.
20. M. H. Vitaterna *et al.*, *Proc. Natl. Acad. Sci. U.S.A.* **96**, 12114 (1999).
21. M. D. Field *et al.*, *Neuron* **25**, 437 (2000).
22. Immunofluorescence was performed as described (*28*). Rabbit polyclonal antibodies to mPER1 (*28*) (affinity purified, 1:200) and mPER2 (affinity purified, 1:200; ADI, San Antonio, TX) were used as primary antibodies. Cy3-conjugated antibody to rabbit IgG (1:2000; Amersham) was used as a secondary antibody. Nuclear staining was performed with 4′,6′-diamidino-2-phenylindole (DAPI).
23. G. T. J. van der Horst *et al.*, *Nature* **398**, 627 (1999).
24. Spontaneously immortalized MEFs from *mCry1*$^{-/-}$, *mCry2*$^{-/-}$, and *mCry1*$^{-/-}$*mCry2*$^{-/-}$ mice were cultured as described (*28*). Stimulation procedures using ET-1 (final concentration 30 nM) or 50% horse serum (Gibco BRL) were as described (*14*).
25. K. Yagita, F. Tamanini, G. T. J. van der Horst, H. Okamura, data not shown.
26. Immunofluorescence was performed as described (*28*). Rabbit polyclonal antibody to DBP (1:2500) and p62 mouse monoclonal antibody (mAb; 1:3000) were used as primary antibodies. Fluorescein isothiocyanate–conjugated antibody to rabbit IgG (1:2000; Amersham) and Cy3-conjugated antibody to mouse IgG (1:800; Jackson ImmunoResearch) were used as secondary antibodies.
27. S. Yamaguchi *et al.*, *Mol. Cell. Biol.* **20**, 4773 (2000).
28. K. Yagita *et al.*, *Genes Dev.* **14**, 1353 (2000).

29. We thank U. Schibler, J. Ripperger, and J. M. Egly for antibodies, and M. Yasuda for technical support. Supported in part by grants from the Special Coordination Funds of the Science and Technology Agency of Japan, a Grant-in-Aid for Scientific Research on Priority Areas of the Ministry of Education, Science, Sports and Culture of Japan, Ministry of Welfare of Japan, Mitsubishi Foundation, and a Spinoza premium from the Netherlands Organization for Scientific Research.

2 February 2001; accepted 15 March 2001

International weekly journal of science
nature

View of a mouse clock gene ticking

Shun Yamaguchi*[1], Masaki Kobayashi*[2], Shigeru Mitsui*[1], Yoshiki Ishida*[1]
Gijsbertus T. J. Van der Horst*[3], Misako Suzuki*[4],
Shigenobu Shibata*[5], Hitoshi Okamura*[1]

*[1]Department of Anatomy and Brain Science, Kobe University Scool of Medicine,
Kobe 650-0017, Japan e-mail: okamura@kobe-u.ac.jp
*[2]Department of Electronics, Tohoku Insitute of Technology, Sendai 982-8577, Japan
*[3]MGC, Department of Cell Biology and Genetics, Erasmus University,
PO Box 1738, 3000 DR, Rotterdam, The Netherlands
*[4]Institute of Molecular Embryology and Genetics, Center for Animal Resources and Development,
Kumamoto University School of Medicine, Kumamoto 862-0976, Japan
*[5]Department of Pharmacology and Brain Science, School of Human Sciences,
Waseda University, Tokorozawa 359-1192, Japan

Reprinted from Nature, Vol. 409, No. 6821, pp. 684, 8 February 2001

Gene expression

View of a mouse clock gene ticking

Circadian clocks consist of an ingenious autoregulatory feedback loop whereby the cyclically expressed products of the clock gene are able to inhibit their own expression[1]. Here we follow the rhythmic expression of the clock gene *mPer1* in the brain of a living mouse. This model system enables real-time gene expression to be monitored in the intact brain under physiological conditions.

We have previously produced transgenic mice carrying a luciferase (*luc*) reporter gene under the control of the promoter of the oscillating clock gene *mPer1* (refs 2, 3). Using a two-dimensional photon-counting camera, we were able to detect a day–night variation in luciferase-mediated bioluminescence in the suprachiasmatic nucleus (SCN)[3], the mammalian brain's circadian centre[4], in fresh brain slices from these *mPer1–luc* mice.

We inserted a polymer optical fibre (500 μm in diameter; 0.5 numerical aperture) just above the SCN of a *mPer1–luc* transgenic mouse using a stereotaxic frame; the other end of the optical fibre was connected to a photomultiplier tube operating as part of a photon-counting apparatus (Fig. 1a). As luciferase requires a substrate for light emission, we continuously infused luciferin dissolved in artificial cerebrospinal fluid through a lateral ventricle. The substrate concentration in the cerebrospinal fluid, sampled from the contralateral ventricle, reached a plateau at about 1.3 mM within 3 hours and remained more or less constant.

With this system, we continuously recorded light emission from the SCN of the transgenic mice *in vivo* under constant darkness. The luminescence showed a clear circadian fluctuation (Fig. 1b), with a 1.5- to 2.5-fold amplitude and peaks and troughs at circadian time (CT) 4–6 and CT15–20, respectively (where CT0 is subjective dawn and CT12 is subjective dusk).

This temporal profile of bioluminescence strikingly resembles the expression profile of native *mPer1* messenger RNA. The phase lag between transcription of luciferase mRNA and the production of luminescence was only 0–2 h. The circadian period calculated from the intervals between bioluminescence peaks was about 24 h, which is close to the period of locomotor activity of this transgenic mouse line (24.0 ± 0.05 h; $n = 7$).

To confirm that this fluctuation in luminescence represents an endogenous oscillation, we recorded the luminescence from two groups of mice housed for at least two weeks under alternating 12-hour light–dark cycles, with lights on at either 7:00 h (LD-entrained mice) or 19:00 h (DL-entrained mice). Both groups were hooked up to the monitoring system at 14:00 h and the luminescence emitted was recorded under constant darkness. As expected, the luminescence recorded from LD-entrained mice oscillated in the opposite phase to that of DL-entrained animals (Fig. 1c).

Capturing the effect from a luciferase reporter transgene with optical-fibre-mediated photon-counting technology offers a way to measure real-time gene expression profiles in the intact brain under physiological conditions.To our knowledge, this is the first time that a ticking clock gene has been monitored in a living mammal. Real-time optical imaging of gene expression, in combination with real-time measurement of electrophysiological, metabolic and behavioural parameters, should advance the study of mammalian brain function.

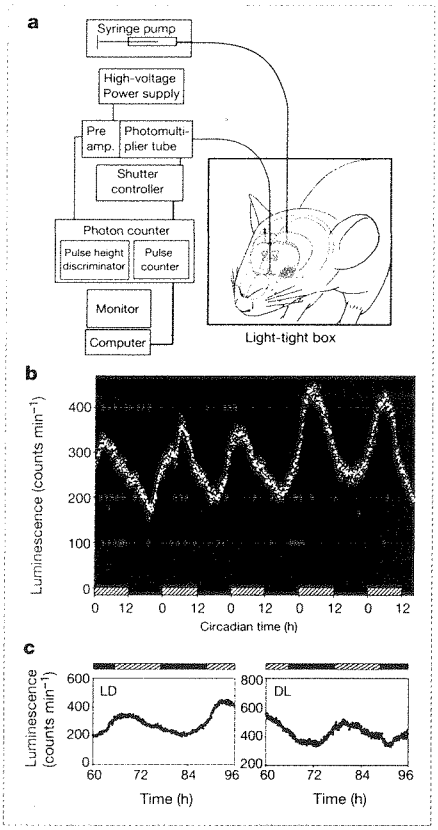

Figure 1 *In vivo* monitoring of bioluminescence from the suprachiasmatic nucleus (SCN). **a,** Experimental set-up. Bioluminescence is detected under constant darkness conditions by means of an optical fibre inserted above the SCN and connected to a photon-counting apparatus with a photomultiplier tube. Luciferin solution (10 mM in artificial cerebrospinal fluid) is infused continuously at 15 μl h^{-1} by a syringe pump. **b,** Circadian fluctuation of luminescence in the SCN of a representative *mPer1–luc* transgenic mouse previously housed under a 12-h light/12-h dark cycle. Each dot represents the average of luminescence counts collected over 5 min. Hatched and black bars along the *x*-axis represent subjective day and subjective night, respectively. **c,** Comparison of the phase of luminescence recorded from left, LD-entrained, and right, DL-entrained mice (see text for details of terminology). Time indicated is time since the start of monitoring. Bars and dots as in **b**.

Shun Yamaguchi*, Masaki Kobayashi†, Shigeru Mitsui*, Yoshiki Ishida*, Gijsbertus T. J. van der Horst‡, Misao Suzuki§, Shigenobu Shibata||, Hitoshi Okamura*

**Department of Anatomy and Brain Science, Kobe University School of Medicine, Kobe 650-0017, Japan*
e-mail: okamurah@kobe-u.ac.jp
†Department of Electronics, Tohoku Institute of Technology, Sendai 982-8577, Japan
‡MGC, Department of Cell Biology and Genetics, Erasmus University, PO Box 1738, 3000 DR Rotterdam, The Netherlands
§Institute of Molecular Embryology and Genetics, Center for Animal Resources and Development, Kumamoto University School of Medicine, Kumamoto 862-0976, Japan
||Department of Pharmacology and Brain Science, School of Human Sciences, Waseda University, Tokorozawa 359-1192, Japan

1. Dunlap, J. C. *Cell* **96,** 271–290 (1999).
2. Tei, H. *Nature* **389,** 512–516 (1997).
3. Yamaguchi, S. *et al. Curr. Biol.* **10,** 873–876 (2000).
4. Rusak, B. *J. Comp. Physiol.* **118,** 145–164 (1977).

Nature Japan K.K., MG Ichigaya Bldg., 19-1 Haraikatamachi, Shinjuku-ku, Tokyo 162-0841 Tel 03-3267-8751 Fax 03-3267-8746

Antagonistic role of E4BP4 and PAR proteins in the circadian oscillatory mechanism

Shigeru Mitsui,[1,3] Shun Yamaguchi,[1,3] Takuya Matsuo,[1,2] Yoshiki Ishida,[1] and Hitoshi Okamura[1,4]

[1]Department of Anatomy and Brain Science, Kobe University School of Medicine, Chuo-ku, Kobe 650-0017, Japan; [2]Department of Physics, Informatics and Biology, Yamaguchi University, Yamaguchi 753-8512, Japan

E4BP4, a basic leucine zipper transcription factor, contains a DNA-binding domain closely related to DBP, HLF, and TEF, which are PAR proteins. Here, we show that the phase of *e4bp4* mRNA rhythm is opposite to that of the *dbp*, *hlf*, and *tef* rhythms in the suprachiasmatic nucleus (SCN), the mammalian circadian center, and the liver. The protein levels of E4BP4 and DBP also fluctuate in almost the opposite phase. Moreover, all PAR proteins activate, whereas E4BP4 suppresses, the transcriptional activity of the reporter gene containing a common binding sequence in transcriptional assays in vitro. An electrophoretic mobility shift assay demonstrated that E4BP4 is not able to dimerize with the PAR proteins, but is able to compete for the same binding sites with them. Furthermore, we showed sustained low *e4bp4* and high *dbp* mRNA levels in *mCry*-deficient mice. These results indicate that the E4BP4 and PAR proteins are paired components of a reciprocating mechanism wherein E4BP4 suppresses the transcription of target genes during the time of day when E4BP4 is abundant, and the PAR proteins activate them at another time of day. E4BP4 and the PAR proteins may switch back and forth between the on-off conditions of the target genes.

[*Key Words*: E4BP4; PAR domain; circadian rhythm; suprachiasmatic nucleus; basic leucine zipper transcription factor; active repressor]

Received December 13, 2000; revised version accepted February 14, 2001.

Circadian (~24-h) rhythms are endogenous rhythms that are observed in a wide range of life forms. The molecular dissection of these endogenous oscillatory mechanisms has advanced using cyanobacteria (Iwasaki and Kondo 2000), *Neurospora* (Dunlap 1999), *Drosophila* (Young 2000), and mice (King and Takahashi 2000) as models. In all four species, the core oscillator consists of a self-sustaining transcriptional and translational feedback loop in which cyclically expressed clock gene products negatively regulate their own expression (for review, see Dunlap 1999).

In mice, the core feedback loop is thought to be composed of a positive element, the CLOCK/BMAL1 heterodimer, and many negative elements including mPER1, mPER2, mPER3, mCRY1, and mCRY2 (Gekakis et al. 1998; Jin et al. 1999; Kume et al. 1999; Okamura et al. 1999). The transcription of the *mPer1* gene, of which regulation has been well analyzed, was shown to be activated by the binding of the CLOCK-BMAL1 complex to E-boxes (CACGTG) in the promoter region of the *mPer1* gene (Gekakis et al. 1998; Yamaguchi et al. 2000a), and this activation was specifically inhibited by mPER1, mPER2, mPER3, mCRY1, and mCRY2 (Jin et al. 1999; Kume et al. 1999).

In this system, all proteins, except mCRY1 and mCRY2, are called PAS proteins, because they all possess PAS (Per-Arnt-Sim) domains that are protein–protein interaction domains and function in various biological pathways (Huang et al. 1993; Lindebro et al. 1995). The importance of this domain in the circadian feedback loop is suggested by the fact that homozygous *mPer2* mutant mice, of which the *mPer2* gene encodes the protein lacking the PAS domain, show significant differences in circadian locomotor activity, and altered expression levels of *mPer1* and *mPer2* in the suprachiasmatic nucleus (SCN), the mammalian circadian center (Zheng et al. 1999).

Subsequently, the light-harvesting cryptochrome/photolyase family proteins, mCRY1 and mCRY2, also were shown to be essential components of the circadian clock feedback loop. Mice lacking *mCry1* and *mCry2* are behaviorally arrhythmic in constant dark (DD) conditions (van der Horst et al. 1999), and their *mPer1* and *mPer2* mRNA levels are constitutively high in the SCN (Okamura et al. 1999). mCRY1 and mCRY2 have structural similarities to DNA repair enzymes called photolyases, but they lack DNA repair activity (Todo et al. 1996; Ko-

[3]These authors contributed equally to this work.
[4]Corresponding author.
E-MAIL okamurah@kobe-u.ac.jp; FAX 81-78-382-5341.
Article and publication are at www.genesdev.org/cgi/doi/10.1101/gad.873501.

bayashi et al. 1998). Moreover, although they also contain a region similar to plant blue-light receptors (cryptochromes), they were shown to act as light-independent inhibitors of CLOCK/BMAL1 (Griffin et al. 1999).

We reported recently that DBP (named for the albumin gene D-site binding protein), a member of another transcription factor family, is closely linked to the core circadian clockwork in mammals (Yamaguchi et al. 2000b). DBP belongs to the PAR (proline and acidic amino acid–rich) basic leucine zipper transcription factor family, along with hepatic leukemia factor (HLF) and thyrotroph embryonic factor (TEF). The transcript levels of *dbp* are highly rhythmic in the SCN, even in DD conditions, with an amplitude comparable to that of *mPer1* (Lopez-Molina et al. 1997; Yan et al. 2000). It has been proposed that this circadian *dbp* transcription is regulated directly by CLOCK/BMAL1-mediated activation and mPERs- and mCRYs-mediated suppression through E-box motifs located in the introns of the *dbp* gene (Ripperger et al. 2000; Yamaguchi et al. 2000b). Moreover, DBP can activate the *mPer1* promoter in transcriptional assays in vitro, and is expressed at the right time to activate *mPer1* transcription in the SCN in vivo (Yamaguchi et al. 2000b). Thus, the cyclical activity of DBP may feed back onto the central clock mechanism.

Interestingly, in the *Drosophila* clock, a transcription factor VRI, which is structurally related to mammalian DBP, is required for a functional *Drosophila* clock (Blau and Young 1999). VRI is expressed in pacemaker cells of *Drosophila* and its RNA levels oscillate with a circadian rhythm via the regulation of the core-clock components, including dCLOCK and dBMAL1. The gene dosage of *vri* affects the period of circadian locomotor activity (Blau and Young 1999). Thus, it resembles mammalian *dbp* in many aspects. However, VRI apparently lacks a PAR domain, although it shows strong homology in its DNA-binding domain to DBP (George and Terracol 1997). The PAR domain is a well-conserved region of DBP and two other mammalian transcription factors, HLF and TEF, and has been shown to act as an activation domain at least in the case of DBP (Lamprecht and Mueller 1999).

In mammals, one basic leucine zipper transcription factor, which has a DNA-binding domain closely related to that of DBP, HLF, or TEF, but lacks a PAR domain, has been found. In fact, this transcription factor, E4BP4 (also called NFIL3), contains the most homologous basic leucine zipper domain to VRI. E4BP4 was isolated as an adenovirus E4 promoter ATF site binding protein (Cowell et al. 1992) and a human interleukin-3 promoter binding protein (Zhang et al. 1995), and has been studied mainly in relation to the hematopoietic system (Ikushima et al. 1997; Kuribara et al. 1999).

To investigate the possible role of E4BP4 in the circadian oscillatory mechanism in mammals, and the possible interactions between the E4BP4 and PAR proteins (DBP, HLF, and TEF), we examined the expression profiles of their mRNAs and proteins. Among the four structurally related transcription factors, *dbp*, *hlf*, and *tef* mRNAs showed similar peak and trough times, but only *e4bp4* mRNA fluctuated in almost the opposite phase in both the SCN and liver. The protein levels of E4BP4 and DBP also fluctuated in almost the opposite phase. Moreover, here, we demonstrate that all PAR proteins activate, whereas E4BP4 suppresses, the transcriptional activity of the reporter gene containing a common binding sequence in transcriptional assays in vitro. These observations suggest that the E4BP4 and PAR proteins complement each other well in regulating the circadian oscillatory mechanism.

Results

Transcripts of the E4BP4 and PAR transcription factor family oscillate in almost the opposite phase in the SCN

We first examined the distribution of *e4bp4* mRNA in the mouse brain using in situ hybridization. The expression of *e4bp4* was high in the SCN, hippocampus, gyrus dentatus, and piriform cortex, and moderate in the internal granular layer of olfactory bulb, dorsomedial hypothalamic nucleus, pontine nuclei, and the granular layer of cerebellum (Fig. 1A). Expression of *e4bp4* was low in other brain regions. These hybridization signals were specific, because hybridization with a sense (control) probe showed no signals in brain sections (data not shown).

Next, we examined the temporal expression profile of *e4bp4* mRNA in the SCN, the mammalian circadian center, with quantitative in-situ hybridization (Fig. 1B,C). In 12-h light:12h dark (LD) cycles, *e4bp4* mRNA displayed a clear diurnal rhythm in the SCN showing a 1.7-fold amplitude with a peak at ZT16 (ZT, Zeitgeber time in LD-conditions; ZT0 is light-on and ZT12 is light-off) and a trough at ZT8 ($P < 0.001$). Under DD conditions, the rhythm of *e4bp4* mRNA was clear, with a peak at circadian time (CT) 12 (where CT0 is subjective dawn and CT12 is subjective dusk) and a trough at CT4 ($P < 0.001$) (Fig. 1B,C).

To compare the expression profile of *e4bp4* with that of structurally related genes, we performed quantitative in-situ hybridization of the PAR transcription factors (*hlf*, *tef*, and *dbp*) in the SCN in DD conditions. The peak expression level of *dbp* mRNA was the highest and that of *tef* mRNA was the lowest of the three (see inserted pictures in Fig. 2). Interestingly, all three mRNAs showed the same expression profile, with a peak at CT4 and a trough at CT16–20 ($P < 0.001$, respectively; Fig. 2). The peak-trough ratio of *dbp* was the highest of three (for *hlf*, *tef*, and *dbp*, 2.3-, 2.3-, and 7.0-fold, respectively). In conclusion, *e4bp4* mRNA fluctuates in almost the opposite phase to the structurally related PAR gene mRNAs (*hlf*, *tef*, and *dbp*) in the SCN.

E4BP4 and DBP proteins also fluctuate in almost the opposite phase in the SCN

Next, we examined E4BP4 protein expression in the SCN with immunocytochemistry using anti-E4BP4 se-

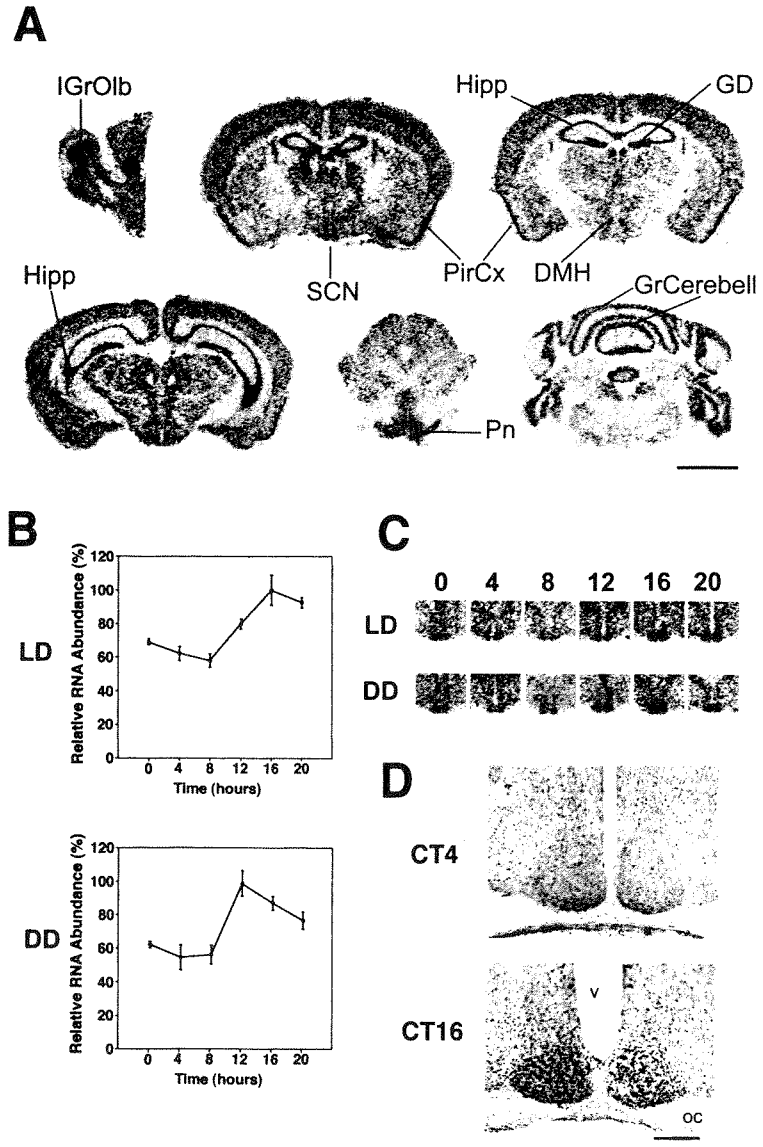

Figure 1. Spatial and temporal expression profiles of the *e4bp4* mRNA and E4BP4 proteins. (*A*) Distribution of *e4bp4* mRNA in the mouse brain. IGrOlb, internal granular layer of the olfactory bulb; SCN, suprachiasmatic nucleus; Hipp, hippocampus; GD, gyrus dentatus; PirCx, piriform cortex; DMH, dorsomedial hypothalamic nucleus; Pn, pontine nuclei; GrCerebell, granular layer of the cerebellar cortex. Scale bar, 3 mm. (*B*) Rhythmic expression of *e4bp4* mRNA in the SCN. Quantitative analysis of *e4bp4* mRNA expressed in the SCN in LD and DD conditions. Relative *e4bp4* mRNA abundance was determined by quantitative in-situ hybridization using isotope-labeled probes, with the mean peak values adjusted to 100 ($n = 5$, means ± SEM). (*C*) Representative in-situ hybridization autoradiographs showing *e4bp4* mRNA in the SCN at various time points under LD and DD conditions. Numbers on the top indicate Zeitgeber (LD) or circadian (DD) times. (*D*) Circadian expression of E4BP4 immunoreactivity in the SCN at CT4 and CT16. OC, optic chiasma; v, third ventricle. Scale bar, 400 μm.

rum (Fig. 1D). Strong E4BP4 immunoreactivity was observed in the nuclei in the majority of the SCN cells (>80%) sampled at night (ZT14, ZT16, and ZT20) in LD conditions and at subjective night (CT12, CT16, and CT20) in DD conditions. This immunoreactivity was specific, because preincubation with an affinity-purified E4BP4 antigen completely abolished the signals (data not shown). In contrast, the SCN sampled at daytime (ZT4, ZT6) in LD conditions, and at subjective daytime (CT4), contained only a few and weakly stained E4BP4-immunoreactive nuclei (Fig. 1D). The similarity between the temporal expression profile of the E4BP4 protein and the

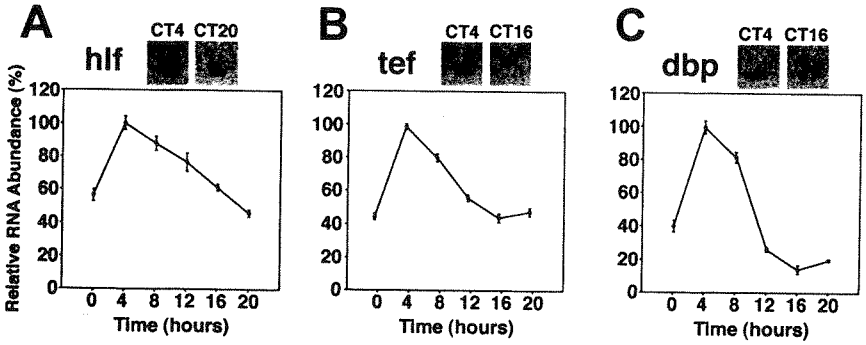

Figure 2. Circadian expression of *hlf*, *tef*, and *dbp* mRNAs in the SCN. Quantitative in-situ hybridization analyses of *hlf*, *tef*, and *dbp* mRNAs in the SCN in DD conditions are shown. Values are means ± SEM (n = 5). The mean peak values are adjusted to 100. Representative photomicrographs are shown at the top.

e4bp4 mRNA suggests the rapid translation and nuclear accumulation of E4BP4, compared with the mPER1 protein, which was delayed by about 6 h relative to *mPer1* mRNA (Field et al. 2000). Moreover, the expression profiles of E4BP4 proteins obviously are different from those of DBP proteins in the SCN we reported previously (Yamaguchi et al. 2000b). Because DBP proteins accumulate in the subjective morning peaking at CT6 in the SCN, the E4BP4 proteins were found to oscillate in almost the opposite phase, as in the case of their transcripts.

An opposite phase relationship also is observed in the liver

Because non-SCN tissues also rhythmically express various genes for which transcription oscillates in the SCN (Falvey et al. 1995; Fonjallaz et al. 1996; Zylka et al. 1998), we examined the temporal expression profile of *e4bp4* mRNA in the liver of DD-housed mice.

Northern blot analysis showed that a 1.9-kb transcript was detectable at all times examined, but its abundance displayed a clear rhythm with a maximum at CT22 and a minimum at CT9 (Fig. 3A,B). In contrast, *dbp*, *hlf* (both 2.6-kb and 4.5-kb transcripts), and *tef* mRNAs cycle in almost opposite phases peaking at the end of subjective day, although the peak time of *dbp* mRNA was slightly earlier than the others (Fig. 3A,B). Therefore, the phase difference between *e4bp4* and PAR family mRNAs in the SCN is conserved in the liver, although the phase of each gene expression in the liver is 5–10 h later than that in the SCN.

We next examined the temporal expression profiles of the E4BP4 and DBP proteins in the liver. Nuclear extracts were prepared from the livers of DD-housed mice and fractionated by SDS-polyacrylamide gel electrophoresis. Immunoblot analysis with anti-E4BP4 serum revealed a single band of ~55 kD, in accordance with the predicted mass of 53 kD (Fig. 3C). The abundance of E4BP4 protein varied, with high levels between CT22 and CT4, and low levels between CT12 and CT20 (Fig. 3C,D). Therefore, the E4BP4 protein was abundant in the liver at about subjective dawn, the same as *e4bp4* mRNA.

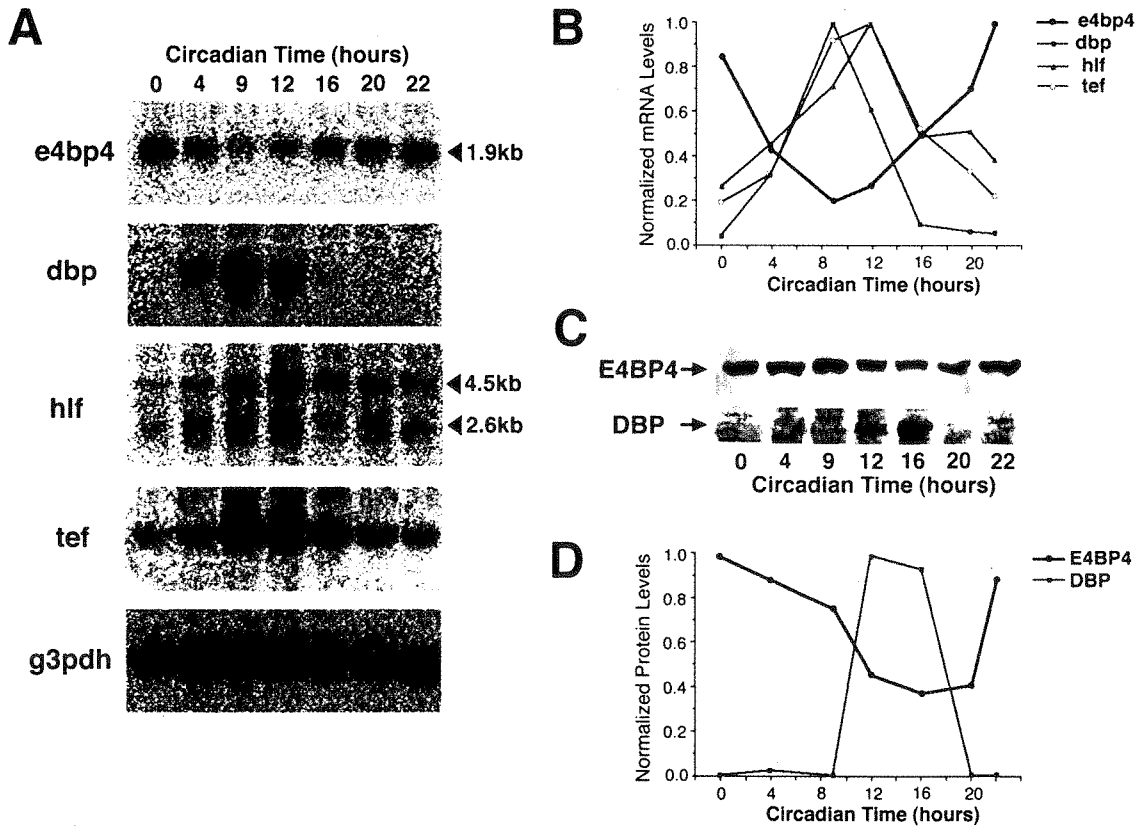

Figure 3. Circadian accumulation of *e4bp4*, *dbp*, *hlf*, and *tef* mRNAs in the mouse liver. (*A*) Northern blot analysis of the total RNAs (10 μg) isolated from the liver of DD-housed mice at different time points. The sizes of *e4bp4* and *hlf* mRNAs are shown on the right. No significant variation in the amounts of loaded mRNA was detected by hybridization with a glyceraldehyde-3-phosphate dehydrogenase (*g3pdh*) cDNA probe. (*B*) Rhythmic expression of *e4bp4* (black) is plotted in comparison with *dbp* (red), *hlf* (blue), and *tef* (green). The *hlf* mRNA levels represent the sum of the quantitated radioactivities of 4.5-kb and 2.6-kb transcripts. Normalized mRNA levels are shown with each peak value adjusted to 1.0. (*C*) Western blot analysis of liver nuclear extracts prepared from DD-housed mice, with anti-E4BP4 antiserum (upper panel) and anti-DBP antiserum (lower panel). (*D*) Rhythmic expression of E4BP4 (black) is plotted in comparison with DBP (red). Protein levels were determined by Western blot analysis in (*C*). The peak values are adjusted to 1.0.

When the liver samples were probed using an antiserum to DBP, the highest protein levels were observed only between CT12 and CT16 (Fig 3C,D), consistent with previous reports by Schibler and coworkers (Fonjallaz et al. 1996; Lopez-Molina et al. 1997). Thus, E4BP4 and DBP proteins also fluctuate in almost the opposite phase in the liver, as in the SCN.

All PAR proteins activate, whereas E4BP4 suppresses the mPer1 promoter through the same sequence

The optimal binding motif for E4BP4, RT(G/T)AYG TAAY (where R is a purine and Y is a pyrimidine), and those for the three PAR proteins are almost identical (Drolet et al. 1991; Cowell et al. 1992; Falvey et al. 1996; Hunger et al. 1996). We showed previously that the *mPer1* promoter contains a DBP-binding sequence, AT TATGCAAC (9 of 10 bases are identical to the optimal binding motif), through which DBP is able to activate the *mPer1* promoter, at least in transient transfection analysis (Yamaguchi et al. 2000b). In this study, we examined the effects of E4BP4, HLF, and TEF on the *mPer1* promoter. A 1.3-kbp fragment of the 5′-flanking region of the *mPer1* gene containing an endogenous promoter and the DBP-binding site was subcloned into a promoterless reporter vector for use in transcriptional analysis in HepG2 cells.

The transcriptional activity of the *mPer1* promoter was suppressed in a dose-dependent manner by increasing amounts of the transfected-E4BP4 expression vector (Fig. 4A). In contrast, the HLF- and TEF- expression vectors, as well as the DBP-expression vector, activated the *mPer1* promoter (Fig. 4A).

We next tested for possible interactions between the E4BP4 and PAR proteins. The 1.3-kbp *mPer1* promoter was cotransfected with E4BP4 expression plasmids and each of the PAR proteins expression plasmids. E4BP4 not only suppressed basal promoter activity (74.2% [$P < 0.001$]), but also significantly reduced the DBP-, HLF-, and TEF-mediated transcriptions (45.2% [$P < 0.001$], 22.0% [$P < 0.005$], and 55.4% [$P < 0.001$], respectively) (Fig. 4B).

To test whether the DBP-binding site actually is responsible for these transcriptional regulations, we examined the transcriptional activity of a construct in which three copies of a 20-bp sequence centered on the DBP-binding site (ATTATGCAAC) were linked in tandem and subcloned into a reporter vector containing the herpes simplex virus thymidine kinase (HSV-TK) minimal promoter. Again, DBP, HLF, and TEF produced a substantial increase in transcriptional activity (19.3-fold [$P < 0.001$], 8.5-fold [$P < 0.001$], and 8.1-fold [$P < 0.001$], respectively) and E4BP4 reduced the basal transcriptional activity (61.8% [$P < 0.001$]; Fig. 4C). Each of the PAR protein- (DBP, HLF, and TEF) induced transcriptions also was reduced (71.3% [$P < 0.001$], 84.6% [$P < 0.001$], and 46.4% [$P < 0.001$], respectively) by the coexpression of E4BP4 (Fig. 4C). Similar results were obtained when an optimal binding motif for all four proteins, ATTACGTAAC, was used as the reporter construct (data not shown). Moreover, when the three DBP-binding sites were mutated, the transcriptional activity of the reporter construct was not affected significantly by the expression of DBP, HLF, TEF, or E4BP4 (data not shown).

Therefore, we conclude that E4BP4 and all PAR proteins are able to suppress and activate transcriptional activity, respectively, through the same sequence and that E4BP4 is able to reduce the PAR protein-induced transcriptions in HepG2 cells. Taken together with the inverse expression profiles of E4BP4 and DBP in vivo, this indicates that E4BP4 suppresses transcription of the target genes during the time of day when E4BP4 is abundant, and DBP activates them, possibly in cooperation with HLF and TEF, at another time of day. These regulations may increase the oscillation amplitudes of the target genes.

E4BP4 competes for the same binding site with the PAR proteins, but does not heterodimerize with them

Although it is known that different PAR family members are able to homodimerize and heterodimerize (Fonjallaz et al. 1996), and that E4BP4 is able to homodimerize (Cowell et al. 1992), the interactions between E4BP4 and PAR proteins are unknown. Moreover, it is uncertain whether the affinities of the four transcription factors for a common recognition site are close enough to compete for the same binding site with each other. To elucidate the mechanism of the antagonistic regulation of PAR proteins and E4BP4 on the same sequence, we performed electrophoretic mobility shift assays (EMSA) with a ^{32}P-radiolabeled probe encompassing a sequence responsible for such transcriptional regulation. As expected, each of the in-vitro translated E4BP4, DBP, HLF, and TEF proteins generated single strong bands resulting from complex formation with the probe (Fig. 5). To compare the binding affinities of E4BP4 and PAR proteins for the probe quantitatively, we performed EMSAs, titrating the amount of a radiolabeled probe against a constant amount of protein (Fig. 5). After the radioactivity of the bound and free forms was measured, the dissociation constants (*Kd*) were determined by Scatchard plots (Fig. 5). The *Kd*s for binding of E4BP4, DBP, HLF, and TEF to the probe were 2.1, 1.3, 4.0, and 2.8 nM, respectively.

Because the four examined proteins showed similar relative affinities to the probe, we reasoned that the PAR proteins bound to the probe may be displaced by E4BP4 in a competitive fashion. To confirm this possibility, we synthesized each protein in a separate reaction and combined a constant amount of each PAR protein, and increasing amounts of E4BP4, prior to a mobility shift assay. Because the mobility of the full-length E4BP4-probe complex was similar to those of the complexes generated by DBP, HLF, and TEF, we used a truncated E4BP4 protein, which yielded a more rapidly migrating complex. This protein retained the basic and leucine zipper domains (amino acids 65–250) and had an affinity for the probe ($Kd = 2.8$ nM) comparable to that of full-length E4BP4.

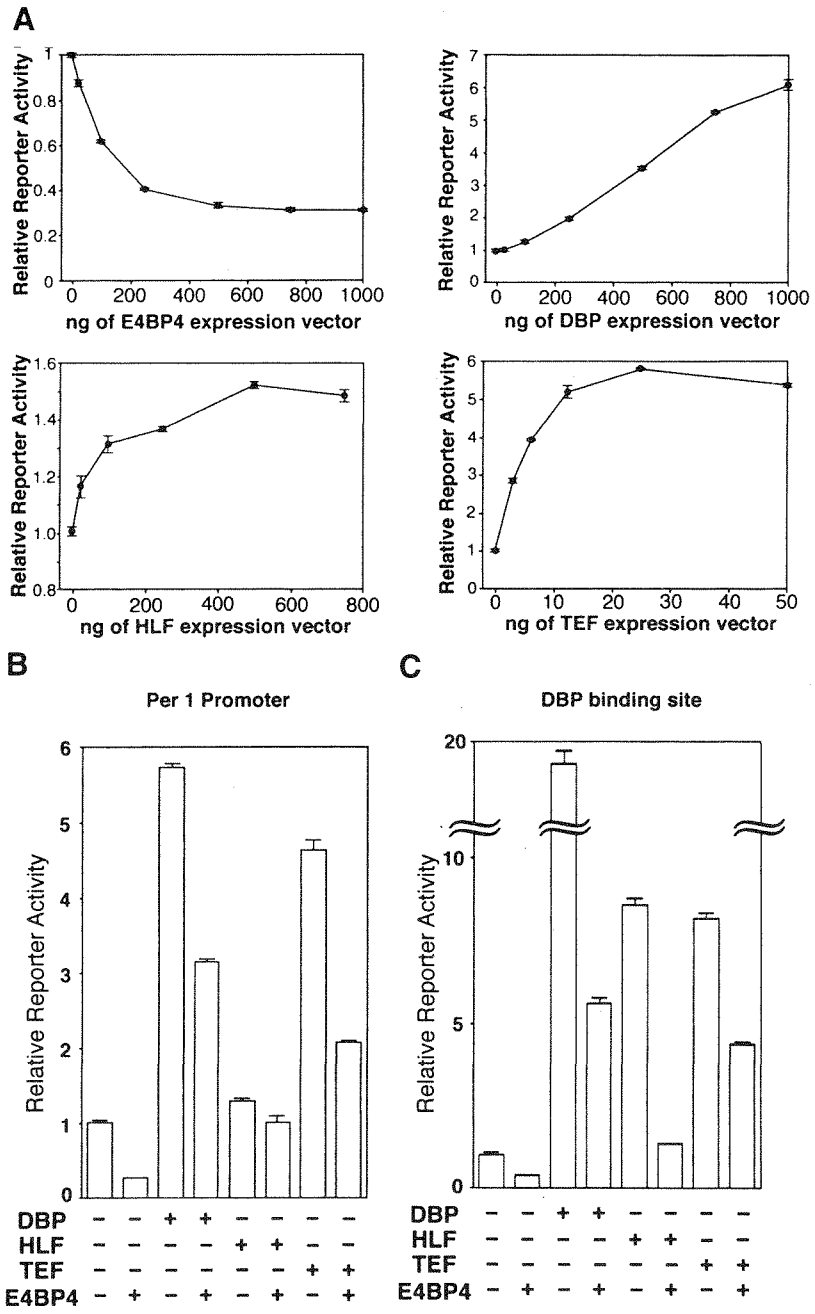

Figure 4. Transcriptional regulation by E4BP4 and PAR proteins. (*A*) Transcriptional regulation of the *mPer1* promoter by E4BP4 and each PAR protein alone. A reporter plasmid (10 ng) containing a 1.3-kbp *mPer1* promoter including the DBP-binding site, and increasing doses of each expression plasmid, were cotransfected. Each value is the mean ± SEM of triplicate results for a single assay. A similar pattern of activation or suppression was reproduced in another experiment. (*B*) Transcriptional regulation of the *mPer1* promoter by the coexpression of E4BP4 and each PAR protein. Presence (+) or absence (−) of DBP-, HLF-, TEF-, and E4BP4-expression plasmids (1000, 500, 25, and 1000 ng, respectively) is noted. (*C*) Transcriptional regulation of an HSV-TK-driven reporter plasmid containing a DBP-binding site derived from the *mPer1* promoter. The presence (+) or absence (−) of DBP-, HLF-, TEF-, and E4BP4-expression plasmids (500, 100, 5, and 500 ng, respectively) is noted. The total amount (1 μg) of expression plasmids per well was adjusted by adding a pcDNA3 plasmid. (*B*,*C*) Each value is the mean ± SEM of three replicates for a single assay. The results shown are representative of at least three independent experiments.

The complexes yielded by DBP, HLF, and TEF diminished clearly with increasing amounts of the complexes generated by the truncated E4BP4 (Fig. 6A). No additional band with intermediate mobility representing the heterodimer formation of the PAR proteins and the truncated E4BP4 was detectable (Fig. 6A). This also was the case when each PAR protein and E4BP4 was synthesized simultaneously in the same reaction mixture by combining the DNA templates prior to the transcription and translation in vitro (Fig. 6B). Conversely, the cotranslation of long- and short-E4BP4 resulted in an additional band demonstrating their dimerization as expected (Fig. 6B). These data suggest that E4BP4 is not able to dimerize with DBP, HLF, and TEF, but is able to compete for the same binding site with them. Therefore, the antagonistic regulation of the PAR and E4BP4 proteins in transcriptional assays may be explained by this competitive mechanism.

e4bp4 *and* dbp *mRNA levels are inversely regulated in* mCry*-deficient mice*

We demonstrated that the transcript levels of the *e4bp4* and PAR transcription factor family, and the protein lev-

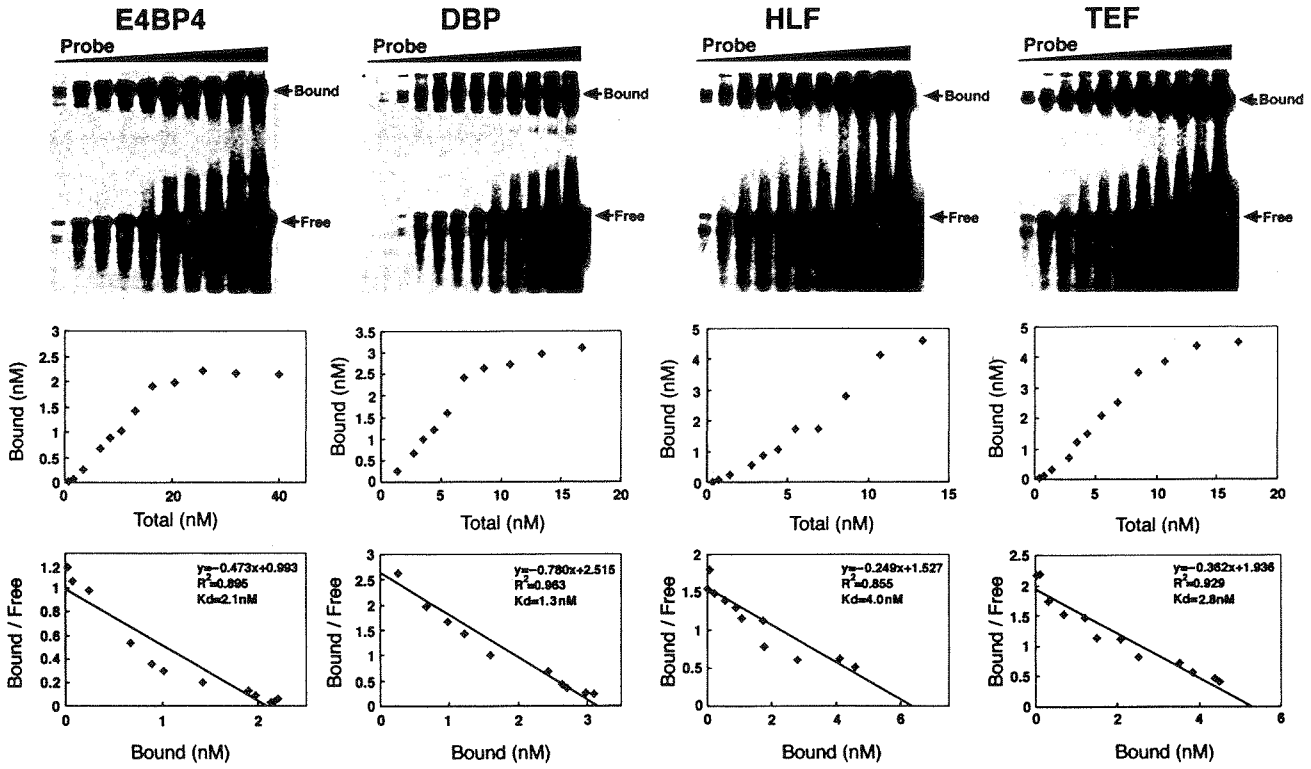

Figure 5. Relative affinities of E4BP4 and the three PAR proteins for an optimal binding site (ATTACGTAAC). A constant amount of protein was incubated with increasing amounts of a radiolabeled probe. After gel electrophoresis and autoradiography (*top* panels), the radioactive bands corresponding to the bound and free forms were quantitated. The concentration of the bound probe was plotted against the total input probe to show saturation curves (*middle* panels). These data also were plotted by the method of Scatchard to determine the *Kd* values (*bottom* panels). The slope of the best-fit line is equal to $-1/Kd$. The correlation coefficients (R^2) are indicated in the *bottom* panels.

els of E4BP4 and at least DBP, oscillate in almost the opposite phase in the SCN and liver. Moreover, E4BP4 and PAR proteins were shown to have suppressing and activating functions on the same sequence, respectively. These findings indicate that the E4BP4 and PAR proteins complement each other well in regulating target genes, and that they are the paired components of a reciprocating mechanism.

To investigate relationships with the putative core oscillation mechanism, we examined the temporal expression profiles of *e4bp4* and *dbp* in the SCN and liver of mice lacking both the *mCry1* and *mCry2* genes. These mutant mice completely lack free-running rhythmicity in constant darkness (van der Horst et al. 1999). In wild-type control animals, the typical circadian variation in *e4bp4* mRNA levels in the SCN was observed with low levels at CT4 (40 h after animals were placed in DD) and high levels at CT12 (48 h in DD) (1.7-fold, $P < 0.001$) (Fig. 7A). In contrast, *e4bp4* mRNA levels were low at both times in *mCry*-deficient mice (Fig. 7A).

We then examined *dbp* mRNA levels in the SCN of *mCry* double-mutant mice. In marked contrast, *mCry* double-mutant mice showed high *dbp* mRNA levels in the SCN (Fig. 7A). This finding is consistent with the proposed regulatory mechanism for the transcription of the *dbp* gene: The CLOCK/BMAL1 heterodimer activates, whereas mCRYs mainly suppresses, the transcription of the *dbp* gene through the E-box motifs (Ripperger et al. 2000; Yamaguchi et al. 2000b).

Sustained low *e4bp4* and high *dbp* mRNA levels also were observed in the liver of *mCry*-deficient mice (Fig. 7B). Therefore, these results indicate that both *e4bp4* and *dbp* are regulated directly or indirectly by the core oscillatory mechanism including CLOCK/BMAL1, mPERs, and mCRYs, maintaining an inverse relationship.

Discussion

On the basis of our results, we propose two working models that can explain the relationship between the *e4bp4* gene and the putative core feedback loop including CLOCK/BMAL1, mPERs, and mCRYs (Fig. 8A,B).

In the model shown in Figure 8A, the *e4bp4* gene is regulated by an unidentified transcriptional repressor (X) that is regulated by CLOCK/BMAL1 and the negative elements, mPERs and mCRYs, as in the case of the *dbp*, *hlf*, and *tef* genes. When X mRNA is translated rapidly and the produced X protein accumulates in the nuclei of the SCN cells with little delay and depresses expression

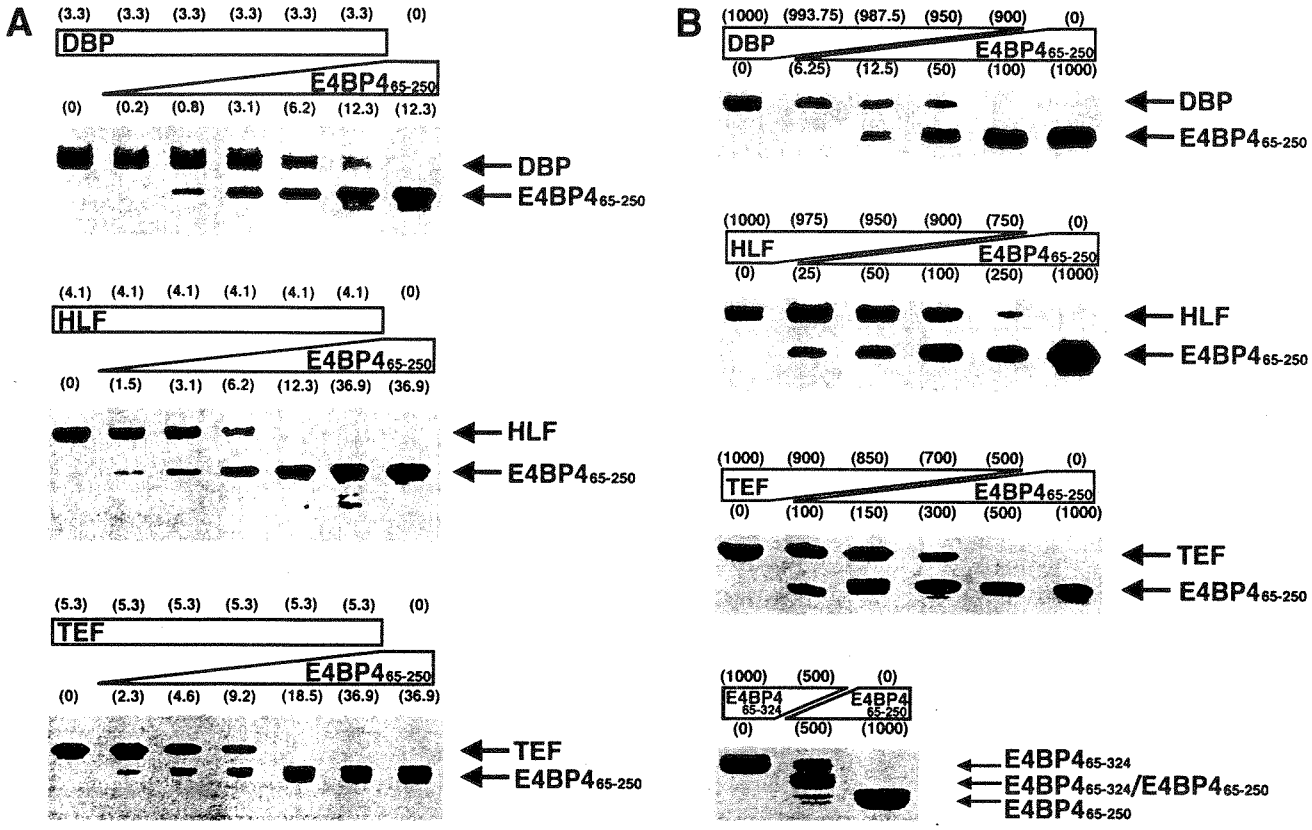

Figure 6. E4BP4 competes for the same binding sequence with PAR proteins. (*A*) E4BP4 and PAR proteins were synthesized in separate reactions prior to combining them. A constant amount of each PAR protein, increasing amounts of E4BP4, and the probe (1 ng) were incubated for 15 min at 30°C before loading the mixture on to the gel. The concentration of input protein (nM) in each reaction was determined by Scatchard plots, as shown in Figure 5 and indicated in parentheses. Each arrow indicates the position of the complex generated by each transcription factor. (*B*) E4BP4 and PAR proteins were synthesized simultaneously in the same reaction mixture before incubation with 1 ng of the probe. Excess amounts of each PAR-protein or long-E4BP4 (65–324) expression plasmids (shown in the left-hand part of the figure), and excess amounts of short-E4BP4 (65–250) expression plasmid (right-hand part of the figure) were combined prior to the transcription and translation in vitro. The amounts of the used expression vectors (ng) are indicated in parentheses. The positions of the complex generated by each transcription factor alone, and the heterodimeric complex formed between long and short E4BP4 are indicated by the arrows.

of *e4bp4*, the phase of the *e4bp4* rhythm thus is expected to be opposite to that of the *dbp*, *hlf*, and *tef* rhythms. Rapidly translated E4BP4 suppresses the transcriptions of target genes during the time of day when E4BP4 is abundant, and the PAR proteins activate them at another time of day. Thereby, the E4BP4 and PAR proteins increase the amplitude of the rhythmically expressed transcript levels of the target genes (Fig. 8A).

In the model in Figure 8B, the *e4bp4* gene is regulated by an unidentified repressor (Y) that is indirectly regulated by CLOCK/BMAL1, mPERs, and mCRYs via DBP-, HLF-, or TEF-mediated regulation. Besides our two models, it also is conceivable that the rhythmic expression of the *e4bp4* gene is controlled by the cycling presence of an unidentified positive element that drives the rhythmic expression of the *bmal1* gene, depending on mPER2 (Shearman et al. 2000). It is noteworthy that in all three models, the existence of an unidentified activator or repressor is indicated.

In the liver, albumin, cholesterol 7α hydroxylase, and cytochrome P450 (*Cyp2c6*, *Cyp2a4*, and *Cyp2a5*) genes are thought to be candidates for the target genes of the PAR proteins (Falvey et al. 1996; Lavery et al. 1999). Conversely, the interleukin 3 gene is thought to be a target of E4BP4 in T lymphocytes (Zhang et al. 1995). The consensus-binding site for E4BP4 and the PAR proteins is different from the CLOCK/BMAL1 E-box binding site. Therefore, E4BP4 and the PAR proteins potentially could regulate a set of output genes that do not also possess an E-box. Moreover, as we have demonstrated, E4BP4 and the PAR proteins regulated the transcriptional activity of the *mPer1* promoter in a transcriptional assay in vitro. Thus, the cyclic activities of E4BP4 and the PAR proteins may feed back onto the central clock mechanism.

E4BP4 was shown to behave as an active transcriptional repressor that directly suppressed the transcriptional activities of genes whose promoters it bound (Cowell and Hurst 1994). This active repression is mainly because of a small transferable repression domain of 65 amino acids in the C-terminal half of the protein (Cowell and Hurst 1994). In the case of DBP, on

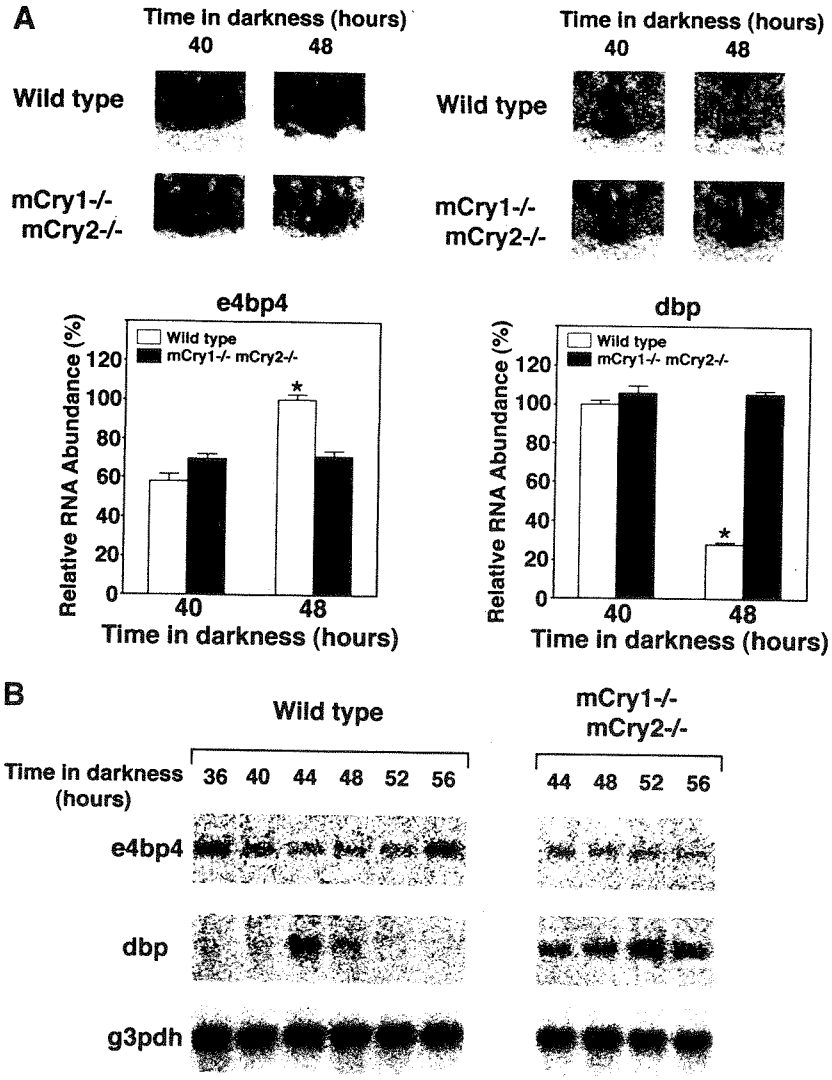

Figure 7. Expression of *e4bp4* and *dbp* in wild-type and $mCry1^{-/-}mCry2^{-/-}$ mice. (*A*) Expression levels of *e4bp4* and *dbp* in the SCN of wild-type (open bars) and *mCry*-deficient (solid bars) mice in constant darkness were determined by quantitative in-situ hybridization. The mean peak values of the wild-type mice were adjusted to 100%. Values are expressed as means ± SEM ($n = 3$). Representative autoradiographs are shown at the top. Because *mCry*-deficient mice are arrhythmic, we used an environmental time scale (hours in DD) rather than a circadian time scale. *, significant differences in wild-type mice, $P < 0.001$; there was no significant difference in $mCry1^{-/-}mCry2^{-/-}$ mice. (*B*) Temporal expression profiles of *e4bp4* and *dbp* in the liver of wild-type and $mCry1^{-/-}mCry2^{-/-}$ mice. Northern blots of the total RNAs (10 μg) prepared from the livers of DD-housed mice are shown. *g3pdh* was used as a control.

the other hand, the PAR (proline and acidic amino acid-rich) domain, which resides amino-terminal to the basic region, has been shown to act as an activation domain (Lamprecht and Mueller 1999). Some other examples of the combination of activator and active repressor that bind the same site are found in genes controlling segmentation during early *Drosophila* development (e.g., Fushi tarazu and Engrailed). It has been proposed that competition between an activator and repressor is not only required, but also is sufficient to establish all-or-none switches in gene expression (Rossi et al. 2000). E4BP4 and the PAR proteins may switch back and forth between the on-off conditions.

The *Drosophila* transcription factor VRI contains a DNA-binding domain closely related to mammalian E4BP4, but lacks a PAR domain. It therefore is comparable to E4BP4. Recently, VRI was shown to be required for a functional *Drosophila* clock: Reducing *vri* gene dosage caused period shortening and elimination of the normal *vri* cycle generated long-period rhythms or arrhythmicity (Blau and Young 1999). Therefore, this family of transcription factors may have an important role in circadian clocks in both *Drosophila* and mammals. However, as we have shown, the phase of the *e4bp4* oscillation was opposite that of the *mPer1*, *mPer2*, and *mPer3* rhythms (Tei et al. 1997; Takumi et al. 1998a,b), which are regulated directly by CLOCK/BMAL1 (Gekakis et al. 1998; Jin et al. 1999). On the other hand, the cycling of *vri* mRNA in *Drosophila* is regulated directly by dCLOCK/dBMAL1, and *vri* mRNA thereby oscillates with the same phase as *per* mRNA in adult heads (Blau and Young 1999). Thus, there may be a difference in the way E4BP4 and VRI are utilized in the mammalian/*Drosophila* clocks.

In summary, our data indicate that E4BP4 and the PAR proteins are paired components of an oscillatory mechanism. This mechanism may be found throughout much of the animal kingdom.

Materials and methods

Animals

Male BALB/c mice (Japan Animal Company, Japan) purchased 5 wk postpartum were exposed to 2 to 4 wk of complete light

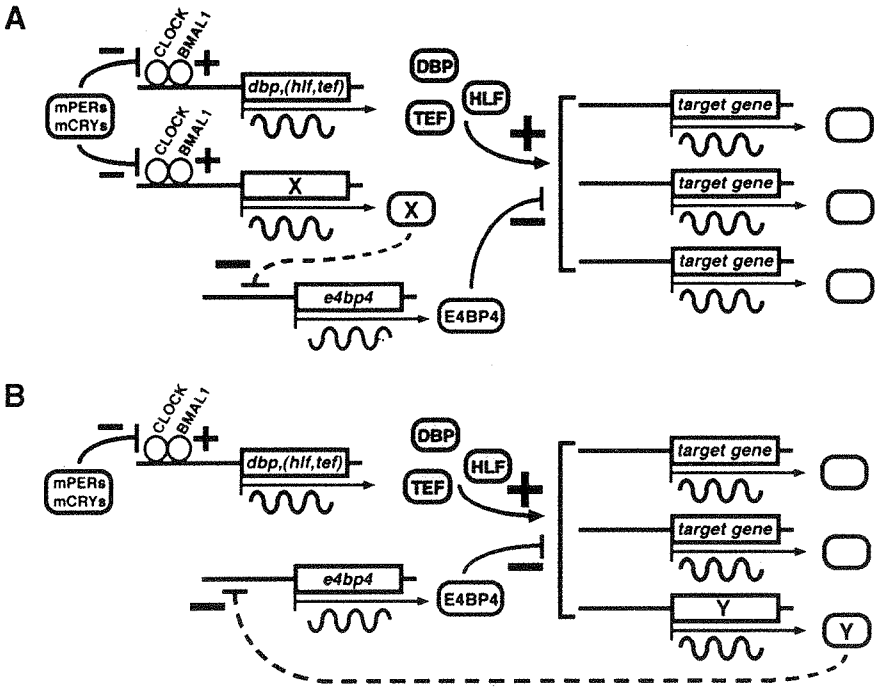

Figure 8. Models of the role of E4BP4 and the PAR proteins, and the regulation of the *e4bp4* gene. (*A*) The *e4bp4* gene is regulated by an unidentified transcriptional repressor (X) that is activated (+) by CLOCK/BMAL1 and suppressed (−) by mPERs and mCRYs, as is the case with the *dbp*, *hlf*, and *tef* genes. DBP, HLF, and TEF activate, whereas E4BP4 suppresses the transcriptions of target genes at different times of day. This regulation increases the amplitude of the oscillation of the target genes. (*B*) The *e4bp4* gene is regulated by an unidentified repressor (Y) that is regulated by DBP, HLF, TEF, and E4BP4 itself.

(fluorescent light, 300 lux)-dark (LD) cycles and then kept in complete darkness for 2 d (DD) as a continuation of the dark phase of the last LD cycle. Wild-type and *mCry1*$^{-/-}$*mCry2*$^{-/-}$ animals (C57Bl6:Ola 129 hybrid, 8 to 12 wk old) generously provided by Dr. G.T.J. van der Horst (Erasmus University), were housed in the same way. The experimental protocol of the current research was approved by the Committee for Animal Research at Kobe University School of Medicine.

Quantitative in-situ hybridization

In-situ hybridization histochemistry using free-floating sections was performed according to a method detailed previously (Shigeyoshi et al. 1997; Yamaguchi et al. 2000b). We used ^{33}P-radiolabeled complementary RNA probes for mouse *e4bp4* (nucleotide residues 194–793; GenBank accession no. U83148), mouse *dbp* (595–1100; U29762), mouse *hlf* (corresponding to nucleotide residues 20–543 of rat *hlf*; S79820), and mouse *tef* (corresponding to nucleotide residues 4–471 of rat *tef*; S58745). All fragments for templates were obtained by reverse transcription-PCR and sequenced to verify their identity and orientation. No specific hybridization signals were observed when sense cRNA probes were used. The radioactivity of each SCN on BioMax film (Kodak) was analyzed using a microcomputer interfaced to an image-analyzing system after conversion into the relative optical density; the 10 sections of the SCN then were summed. For statistical analysis, one-way analysis of variance (ANOVA) followed by Scheffe's multiple comparisons or a two-sample *t* test was applied.

Northern blot analysis

Northern blot analysis was performed as described (Yamaguchi and Nakanishi 1998). Ten micrograms of the total RNAs extracted from the livers of the DD-housed mice sacrificed at various circadian times were analyzed. As templates for the generation of radiolabeled probes, an 812-bp fragment of the 5′-portion of the coding region of mouse *dbp*, a 543-bp *Bgl*II–*Nru*I fragment of human *hlf*, a 622-bp fragment of the 5′-portion of the coding region of rat *tef*, and a 600-bp *Eco*RI–*Nco*I fragment of mouse *e4bp4* cDNA were used. The radioactivity of each band was quantitated with a microcomputer-coupled image-processing system (BAS5000, Fujifilm).

Western blot analysis

Nuclear proteins were extracted from the livers of the DD-housed mice as described previously (Yamaguchi et al. 2000b). For quantification of the nuclear proteins, a bicinchoninic acid (BCA) protein assay reagent kit (Pierce) was used. Forty micrograms of nuclear extracts were mixed with a 3× SDS sample buffer (375 mM Tris-HCl at pH 6.8, 6% SDS, 30% glycerol, 10% 2-mercaptoethanol) and boiled for 3 min. Each sample was fractionated on a 10% SDS-polyacrylamide gel and transferred to a polyvinylidene difluoride membrane (Immunoblot-P membrane, ATTO, Japan). Immunoblotting was performed with a polyclonal rabbit anti-E4BP4 antiserum (No.60, 1:5000), which was kindly provided by Dr. T. Inaba (Jichi Medical School), or anti-DBP antiserum (1:2000) (Yamaguchi et al. 2000b), as a primary antibody. Horseradish peroxidase-conjugated anti-rabbit immunoglobulin (1:5000, Amersham) was used in combination with enhanced chemiluminescence (NEN) to detect proteins. The relative protein level of each band was determined with the aid of a LAS1000 analyzer (Fujifilm).

Immunocytochemistry

Under deep ether anesthesia, LD- and DD-housed male BALB/c mice were perfused with saline, followed by a fixative (2% paraformaldehyde and 0.2% picric acid in a 0.1 M phosphate buffer), and then postfixed with the same fixative for 2 h. Thirty-micrometer sections were cut in a cryostat and processed for free-floating immunohistochemistry using anti-E4BP4 antiserum (1:2000) as described previously (Yagita et al. 2000). After an application of biotinylated anti-rabbit IgG (1:1000, Vector), sections were incubated with avidin-biotin-peroxidase (1:1000, Vector) and visualized with diaminobenzidine (DAB).

Transcriptional assay

Transfection and luciferase assays were carried out as described previously (Yamaguchi et al. 2000b). Unless otherwise specified, ca. 6.0×10^5 HepG2 cells per well in six-well plates were transfected with 2 μg (total) of expression plasmids with the indicated inserts in pcDNA3 (Invitrogen), 10 ng of a reporter plasmid, and 1 ng of an internal control plasmid using Lipofect-Amine Plus reagent (GIBCO). The total amount of DNA per well was adjusted by adding pcDNA3. After 48 h, cells were extracted with 200 μL of passive lysis buffer (Promega), and 20 μL of the extracts were taken for assays of firefly luciferase and *Renilla* luciferase.

A reporter construct containing the *mPer1* promoter was made by ligating a 1.3-kbp fragment of the 5′-flanking region of the *mPer1* gene to the *Renilla* luciferase reporter gene (1212-bp *Hin*dIII–*Xba*I fragment of the pRL-TK vector, Promega) and the simian virus 40 polyadenylation signal. A reporter construct, in which three copies of a 20-bp sequence centered on a DBP-binding site were linked in tandem, was made by inserting annealed oligonucleotides (top strand, 5′-GATCTCTGGCATTATGCAACCCGCCCTGGCATTATGCAACCCGCCCTGGCATTATGCAACCCGCCA-3′; bottom strand, 5′-GATCTGGCGGGTTGCATAATGCCAGGGCGGGTTGCATAATGCCAGGGCGGGTTGCATAATGCCAGA-3′ [binding sites are underlined]) into the *Bgl*II site of the pRL-TK vector (Yamaguchi et al. 2000b).

For the construction of expression plasmids, the total coding regions of mouse *dbp* (GenBank accession no. U29762), human *hlf* (M95585), rat *tef* (S58745), and mouse *e4bp4* (U83148) were obtained by reverse transcription-PCR and subcloned into pcDNA3. All coding regions were used after confirming their sequences. For statistical analysis, a two-sample *t* test was applied.

Electrophoretic mobility shift assay

A double stranded oligonucleotide (top strand, 5′-GCCCGCTACATATTACGTAACAAGCGTTCGC-3′; bottom strand, 5′-GGCGAACGCTTGTTACGTAATATGTAGCGGG-3′) containing a consensus binding sequence for the PAR and E4BP4 proteins was radiolabeled using the Klenow enzyme and [α-^{32}P]dCTP, and used as a probe.

All proteins used in this assay were synthesized by coupled transcription-translation in vitro (TNT T7 Quick Coupled Transcription/Translation System, Promega). For construction of full-length E4BP4, DBP, HLF, and TEF expression plasmids, the total coding regions were ligated into pcDNA3 containing a C-terminal Flag tag (Yagita et al. 2000). For the long (amino acids 65–324) and short (65–250) form E4BP4, the coding regions were supplied with a nucleotide sequence, 5′-GCCACCATG-3′ (Kozak sequence and a first methionine encoding ATG), at the 5′ ends, which then was subcloned into pcDNA3 containing either a C-terminal Flag or an HA tag. All constructs were made using PCR and verified by sequence analysis. Coupled transcription/translation reactions were performed according to the manufacturer's instructions with 1 μg of template DNAs and a 90-min incubation time. To confirm that a protein of the correct size was produced, Western blot analysis with anti-Flag M2 (Sigma) or an anti-HA monoclonal (Boehringer) antibody was carried out.

Binding reactions with the indicated amounts of the labeled probe and the synthesized proteins were performed in a reaction buffer (8 mM HEPES at pH 7.9, 40 mM KCl, 0.4 mM $MgCl_2$, 6.8% glycerol, 0.1 μg/μL bovine serum albumin, 0.8 mM dithiothreitol, 0.2 mM phenylmethylsulfonyl fluoride, and 0.1 μg/μL poly dI-dC; Amersham) at 30°C for 15 min. The resulting products were loaded on an 8% nondenaturing 1× TBE (Tris-borate/EDTA electrophoresis buffer) polyacrylamide gel, and electrophoresed at 150 V. The radioactivity of each band was quantitated as described for the Northern blotting experiments.

Acknowledgments

The authors thank Kazuhiro Yagita and Hiromi Isejima for performing immunocytochemistry and Western blotting. This work was supported in part by grants from the Special Coordination Funds of the Science and Technology Agency of Japan, the Grants-in-Aid for the Scientific Research on Priority Areas of the Ministry of Education, Science, Sports, and Culture of Japan and Mitsubishi Foundation.

The publication costs of this article were defrayed in part by payment of page charges. This article must therefore be hereby marked "advertisement" in accordance with 18 USC section 1734 solely to indicate this fact.

References

Blau, J. and Young, M.W. 1999. Cycling vrille expression is required for a functional *Drosophila* clock. *Cell* **99:** 661–671.

Cowell, I.G., Skinner, A., and Hurst, H.C. 1992. Transcriptional repression by a novel member of the bZIP family of transcription factors. *Mol. Cell. Biol.* **12:** 3070–3077.

Cowell, I.G. and Hurst, H.C. 1994. Transcriptional repression by the human bZIP factor E4BP4: Definition of a minimal repression domain. *Nucleic Acids Res.* **22:** 59–65.

Drolet, D.W., Scully, K.M., Simmons, D.M., Wegner, M., Chu, K., Swanson, L.W., and Rosenfeld, M.G. 1991. TEF, a transcription factor expressed specifically in the anterior pituitary during embryogenesis, defines a new class of leucine zipper proteins. *Genes & Dev.* **5:** 1739–1753.

Dunlap, J.C. 1999. Molecular bases for circadian clocks. *Cell* **96:** 271–290.

Falvey, E., Fleury-Olela, F., and Schibler, U. 1995. The rat hepatic leukemia factor (HLF) gene encodes two transcriptional activators with distinct circadian rhythms, tissue distributions and target preferences. *EMBO J.* **14:** 4307–4317.

Falvey, E., Marcacci, L., and Schibler, U. 1996. DNA-binding specificity of PAR and C/EBP leucine zipper proteins: A single amino acid substitution in the C/EBP DNA-binding domain confers PAR-like specificity to C/EBP. *Biol. Chem.* **377:** 797–809.

Field, M.D., Maywood, E.S., O'Brien, J.A., Weaver, D.R., Reppert, S.M., and Hastings, M.H. 2000. Analysis of clock proteins in mouse SCN demonstrates phylogenetic divergence of the circadian clockwork and resetting mechanisms. *Neuron* **25:** 437–447.

Fonjallaz, P., Ossipow, V., Wanner, G., and Schibler, U. 1996. The two PAR leucine zipper proteins, TEF and DBP, display similar circadian and tissue-specific expression, but have different target promoter preferences. *EMBO J.* **15:** 351–362.

Gekakis, N., Staknis, D., Nguyen, H.B., Davis, F.C., Wilsbacher, L.D., King, D.P., Takahashi, J.S., and Weitz, C.J. 1998. Role of the CLOCK protein in the mammalian circadian mechanism. *Science* **280:** 1564–1569.

George, H. and Terracol, R. 1997. The vrille gene of *Drosophila* is a maternal enhancer of decapentaplegic and encodes a new member of the bZIP family of transcription factors. *Genetics* **146:** 1345–1363.

Griffin, E.A. Jr., Staknis, D., and Weitz, C.J. 1999. Light-independent role of CRY1 and CRY2 in the mammalian circadian clock. *Science* **286:** 768–771.

Huang, Z.J., Edery, I., and Rosbash, M. 1993. PAS is a dimeriza-

tion domain common to *Drosophila* period and several transcription factors. *Nature* **364:** 259–262.

Hunger, S.P., Li, S., Fall, M.Z., Naumovski, L., and Cleary, M.L. 1996. The proto-oncogene HLF and the related basic leucine zipper protein TEF display highly similar DNA-binding and transcriptional regulatory properties. *Blood* **87:** 4607–4617.

Ikushima, S., Inukai, T., Inaba, T., Nimer, S.D., Cleveland, J.L., and Look, A.T. 1997. Pivotal role for the NFIL3/E4BP4 transcription factor in interleukin 3-mediated survival of pro-B lymphocytes. *Proc. Natl. Acad. Sci.***94:** 2609–2614.

Iwasaki, H. and Kondo, T. 2000. The current state and problems of circadian clock studies in cyanobacteria. *Plant Cell. Physiol.* **41:** 1013–1020.

Jin, X., Shearman, L.P., Weaver, D.R., Zylka, M.J., de Vries, G.J., and Reppert, S.M. 1999. A molecular mechanism regulating rhythmic output from the suprachiasmatic circadian clock. *Cell* **96:** 57–68.

King, D.P. and Takahashi, J.S. 2000. Molecular genetics of circadian rhythms in mammals. *Annu. Rev. Neurosci.* **23:** 713–742.

Kobayashi, K., Kanno, S., Smit, B., van der Horst, G.T.J., Takao, M., and Yasui, A. 1998. Characterization of photolyase/blue-light receptor homologs in mouse and human cells. *Nucleic Acids Res.* **26:** 5086–5092.

Kume, K., Zylka, M.J., Sriram, S., Shearman, L.P., Weaver, D.R., Jin, X., Maywood, E.S., Hastings, M.H., and Reppert, S.M. 1999. mCRY1 and mCRY2 are essential components of the negative limb of the circadian clock feedback loop. *Cell* **98:** 193–205.

Kuribara, R., Kinoshita, T., Miyajima, A., Shinjyo, T., Yoshihara, T., Inukai, T., Ozawa, K., Look, A.T., and Inaba, T. 1999. Two distinct interleukin-3-mediated signal pathways, Ras-NFIL3 (E4BP4) and Bcl-xL, regulate the survival of murine pro-B lymphocytes. *Mol. Cell. Biol.* **19:** 2754–2762.

Lamprecht, C. and Mueller, C.R. 1999. D-site binding protein transactivation requires the proline- and acid-rich domain and involves the coactivator p300. *J. Biol. Chem.* **274:** 17643–17648.

Lavery, D.J., Lopez-Molina, L., Margueron, R., Fleury-Olela, F., Conquet, F., Schibler, U., and Bonfils, C. 1999. Circadian expression of the steroid 15 α-hydroxylase (Cyp2a4) and coumarin 7-hydroxylase (Cyp2a5) genes in mouse liver is regulated by the PAR leucine zipper transcription factor DBP. *Mol. Cell. Biol.* **19:** 6488–6499.

Lindebro, M.C., Poellinger, L., and Whitelaw, M.L. 1995. Protein-protein interaction via PAS domains: Role of the PAS domain in positive and negative regulation of the bHLH/PAS dioxin receptor-Arnt transcription factor complex. *EMBO J.* **14:** 3528–3539.

Lopez-Molina, L., Conquet, F., Dubois-Dauphin, M., and Schibler, U. 1997. The DBP gene is expressed according to a circadian rhythm in the suprachiasmatic nucleus and influences circadian behavior. *EMBO J.* **16:** 6762–6771.

Okamura, H., Miyake, S., Sumi, Y., Yamaguchi, S., Yasui, A., Muijtjens, M., Hoeijmakers, J.H.J., and van der Horst, G.T.J. 1999. Photic induction of mPer1 and mPer2 in Cry-deficient mice lacking a biological clock. *Science* **286:** 2531–2534.

Ripperger, J.A., Shearman, L.P., Reppert, S.M., and Schibler, U. 2000. CLOCK, an essential pacemaker component, controls expression of the circadian transcription factor DBP. *Genes & Dev.* **14:** 679–689.

Rossi, F.M., Kringstein, A.M., Spicher, A., Guicherit, O.M., and Blau, H.M. 2000. Transcriptional control: Rheostat converted to on/off switch. *Mol. Cell* **6:** 723–728.

Shearman, L.P., Sriram, S., Weaver, D.R., Maywood, E.S., Chaves, I., Zheng, B., Kume, K., Lee, C.C., van der Horst, G.T.J., Hastings, M.H., et al. 2000. Interacting molecular loops in the mammalian circadian clock. *Science* **288:** 1013–1019.

Shigeyoshi, Y., Taguchi, K., Yamamoto, S., Takekida, S., Yan, L., Tei, H., Moriya, T., Shibata, S., Loros, J.J., Dunlap, J.C., et al. 1997. Light-induced resetting of a mammalian circadian clock is associated with rapid induction of the mPer1 transcript. *Cell* **91:** 1043–1053.

Takumi, T., Matsubara, C., Shigeyoshi, Y., Taguchi, K., Yagita, K., Maebayashi, Y., Sakakida, Y., Okumura, K., Takashima, N., and Okamura, H. 1998a. A new mammalian period gene predominantly expressed in the suprachiasmatic nucleus. *Genes Cells* **3:** 167–176.

Takumi, T., Taguchi, K., Miyake, S., Sakakida, Y., Takashima, N., Matsubara, C., Maebayashi, Y., Okumura, K., Takekida, S., Yamamoto, S., et al. 1998b. A light-independent oscillatory gene mPer3 in mouse SCN and OVLT. *EMBO J.* **17:** 4753–4759.

Tei, H., Okamura, H., Shigeyoshi, Y., Fukuhara, C., Ozawa, R., Hirose, M., and Sakaki, Y. 1997. Circadian oscillation of a mammalian homologue of the *Drosophila* period gene. *Nature* **389:** 512–516.

Todo, T., Ryo, H., Yamamoto, K., Toh, H., Inui, T., Ayaki, H., Nomura, T., and Ikenaga, M. 1996. Similarity among the *Drosophila* (6–4) photolyase, a human photolyase homolog, and the DNA photolyase-blue-light photoreceptor family. *Science* **272:** 109–112.

van der Horst, G.T.J., Muijtjens, M., Kobayashi, K., Takano, R., Kanno, S., Takao, M., de Wit, J., Verkerk, A., Eker, A.P., van Leenen, D., et al. 1999. Mammalian Cry1 and Cry2 are essential for maintenance of circadian rhythms. *Nature* **398:** 627–630.

Yagita, K., Yamaguchi, S., Tamanini, F., van der Horst, G.T.J., Hoeijmakers, J.H.J., Yasui, A., Loros, J.J., Dunlap, J.C., and Okamura, H. 2000. Dimerization and nuclear entry of mPER proteins in mammalian cells. *Genes & Dev.* **14:** 1353–1363.

Yamaguchi, S. and Nakanishi, S. 1998. Regional expression and regulation of alternative forms of mRNAs derived from two distinct transcription initiation sites of the rat mGluR5 gene. *J. Neurochem.* **71:** 60–68.

Yamaguchi, S., Mitsui, S., Miyake, S., Yan, L., Onishi, H., Yagita, K., Suzuki, M., Shibata, S., Kobayashi, M., and Okamura, H. 2000a. The 5′ upstream region of mPer1 gene contains two promoters and is responsible for circadian oscillation. *Curr. Biol.* **10:** 873–876.

Yamaguchi, S., Mitsui, S., Yan, L., Yagita, K., Miyake, S., and Okamura, H. 2000b. Role of DBP in the circadian oscillatory mechanism. *Mol. Cell. Biol.* **20:** 4773–4781.

Yan, L., Miyake, S., and Okamura, H. 2000. Distribution and circadian expression of dbp in SCN and extra-SCN areas in the mouse brain. *J. Neurosci. Res.* **59:** 291–295.

Young, M.W. 2000. Life's 24-hour clock: Molecular control of circadian rhythms in animal cells. *Trends Biochem. Sci.* **25:** 601–606.

Zhang, W., Zhang, J., Kornuc, M., Kwan, K., Frank, R., and Nimer, S.D. 1995. Molecular cloning and characterization of NF-IL3A, a transcriptional activator of the human interleukin-3 promoter. *Mol. Cell. Biol.* **15:** 6055–6063.

Zheng, B., Larkin, D.W., Albrecht, U., Sun, Z.S., Sage, M., Eichele, G., Lee, C.C., and Bradley, A. 1999. The mPer2 gene encodes a functional component of the mammalian circadian clock. *Nature* **400:** 169–173.

Zylka, M.J., Shearman, L.P., Weaver, D.R., and Reppert, S.M. 1998. Three period homologs in mammals: Differential light responses in the suprachiasmatic circadian clock and oscillating transcripts outside of brain. *Neuron* **20:** 1103–1110.

Dimerization and nuclear entry of mPER proteins in mammalian cells

Kazuhiro Yagita,[1] Shun Yamaguchi,[1] Filippo Tamanini,[2] Gijsbertus T.J. van der Horst,[2] Jan H.J. Hoeijmakers,[2] Akira Yasui,[3] Jennifer J. Loros,[4] Jay C. Dunlap,[4] and Hitoshi Okamura[1,5]

[1]Department of Anatomy and Brain Science, Kobe University School of Medicine, Chuoku, Kobe 650-0017, Japan; [2]MGC, Department of Cell Biology and Genetics, Erasmus University, 3000 DR, Rotterdam, The Netherlands; [3]Department of Molecular Genetics, Institute of Development, Aging, and Cancer, Tohoku University, Sendai 980-8575, Japan; [4]Department of Biochemistry, Dartmouth Medical School, Hanover, New Hampshire 03755 USA

Nuclear entry of circadian oscillatory gene products is a key step for the generation of a 24-hr cycle of the biological clock. We have examined nuclear import of clock proteins of the mammalian *period* gene family and the effect of serum shock, which induces a synchronous clock in cultured cells. Previously, mCRY1 and mCRY2 have been found to complex with PER proteins leading to nuclear import. Here we report that nuclear translocation of mPER1 and mPER2 (1) involves physical interactions with mPER3, (2) is accelerated by serum treatment, and (3) still occurs in *mCry1/mCry2* double-deficient cells lacking a functional biological clock. Moreover, nuclear localization of endogenous mPER1 was observed in cultured *mCry1/mCry2* double-deficient cells as well as in the liver and the suprachiasmatic nuclei (SCN) of *mCry1/mCry2* double-mutant mice. This indicates that nuclear translocation of at least mPER1 also can occur under physiological conditions (i.e., in the intact mouse) in the absence of any CRY protein. The mPER3 amino acid sequence predicts the presence of a cytoplasmic localization domain (CLD) and a nuclear localization signal (NLS). Deletion analysis suggests that the interplay of the CLD and NLS proposed to regulate nuclear entry of PER in *Drosophila* is conserved in mammals, but with the novel twist that mPER3 can act as the dimerizing partner.

[*Key Words*: Circadian rhythm; mPER; nuclear entry; cytoplasmic localization domain; mCRY]

Received December 20,1999; revised version accepted April 12, 2000.

Evidence accumulates that many organisms share a common oscillatory mechanism driving their circadian rhythms. This biological clock is comprised of a feedback loop in which cyclically expressed clock gene products negatively regulate their own expression with an approximate 24-hr periodicity (Hastings 1997; Whitmore et al. 1998; Dunlap 1999). In the eukaryotic circadian model systems of *Drosophila* and *Neurospora*, nuclear entry of these oscillatory gene products preparatory to down-regulation of their own transcription constitutes one of the key steps in the control of the clock (e.g., Luo et al. 1998; for review, see Young 1998; Dunlap 1999). In *Drosophila* the product of the *period* (PER) gene oscillates in a circadian manner and appears to be essential for clock functioning. In mammals, three homologs have been identified, *mPer1*, *mPer2*, and *mPer3* (Albrecht et al. 1997; Shearman et al. 1997; Sun et al. 1997; Tei et al. 1997; Takumi et al. 1998a,b; Zylka et al. 1998b). The transcript levels of all three genes oscillate in the suprachiasmatic nucleus (SCN) of the brain, the location of the master clock, as well as in peripheral tissues. Even in cultured cells, induction and subsequent rhythmic expression of *mPer1* and *mPer2* mRNA can be achieved by brief treatment with high levels of serum that either induce or synchronize individual cellular oscillators (Balsalobre et al. 1998).

Remarkably, available evidence suggests that the crucial regulatory step of nuclear entry of PER proteins is mediated differently in different organisms. In *Drosophila*, nuclear translocation of PER is triggered by the concealment of its cytoplasmic retention domain (cytoplasmic localization domain or CLD) by heterodimerization with TIMELESS (TIM) (Vosshall et al. 1994; Saez and Young 1996). The CLD region is preserved in mammalian PER proteins, but a functional role has not been established. In mammals, two homologs of plant cryptochromes (mCRY1 and mCRY2), members of the light-harvesting photolyase family (Hsu et al. 1996; Todo et al. 1996; van der Spek et al. 1996), have been reported recently to complex with mPER proteins and accomplish nuclear translocation, whereas heterodimerization of mPER members with each other also exerted some effect (Kume et al. 1999).

In the present study, we have explored the role of mPER proteins and the effect of serum shock on their nuclear relocation in COS7 cells. We report that nuclear

[5]Corresponding author.
E-MAIL okamurah@kobe-u.ac.jp; FAX 81 78 382 5341.

entry can be accomplished by serum shock-induced heterodimerization of mPER1 and mPER2 with mPER3. In view of the role of mCRY1 and mCRY2 in translocation of mPER proteins into the nucleus (Kume et al. 1999), we also examined nuclear entry of mPER1 in cultured cells derived from *mCry1/mCry2* double-deficient mice (van der Horst et al. 1999). We find that even in the absence of mCRY proteins, mPER1 translocates to the nucleus in a mPER3-dependent manner after serum shock in vitro. Also, we observed a clear nuclear localization of endogenous mPER1 in the SCN and liver of *mCry1/mCry2* double-deficient mice. These findings establish a mCRY-independent route for nuclear translocation of mPER1 under physiological conditions.

Results

Serum shock stimulates heterodimerization of mPER proteins in COS7 cells

Epitope-tagged *mPer* genes were transfected in various combinations into COS7 cells, and the physical interactions between the encoded proteins were analyzed by immunoprecipitation. As brief exposure to high concentrations of horse serum (50%) has been shown to trigger *mPer* oscillation in cultured cells and induce clock functioning (Balsalobre et al. 1998); we also studied the effect of a serum shock on transiently expressed epitope-tagged mPER protein behavior. Following culture in serum-free medium for 12 hr but prior to serum shock, the amount of heterodimerized mPER proteins was very low (Fig. 1). A serum shock did not significantly change the amount of any mPER protein. However, 30 min after treatment, physical interactions of mPER1–mPER2, mPER1–mPER3, and mPER2–mPER3 had remarkably increased (Fig. 1A–C). In addition, we found strong homodimerization of mPER2 and weak homodimerization of mPER3, independent of the serum shock (Fig. 1D). Homodimerization of mPER1 was not detected under the conditions tested (Fig. 1D). Thus, we conclude that a serum shock significantly accelerates heterodimerization of mPER proteins in all combinations with no increase of homodimerization.

Serum shock promotes nuclear entry of mPER1–mPER3 and mPER2–mPER3 heterodimers

The fate of the heterodimerized mPERs in terms of subcellular localization was examined by immunofluorescence in COS7 cells transfected with Flag, Myc, or HA epitope-tagged *mPer* cDNAs. Figure 2 shows representative examples of immunostained single- and double-transfected cells with and without serum shock, as well as the ratio between cells with nuclear or cytoplasmic mPER staining. mPER1 or mPER2 alone showed predominantly cytoplasmic localization (Fig. 2A–F), whereas coexpression with *mPer2* slightly enhanced the number of cells with nuclear mPER1 (Fig. 2G–I). The distribution patterns of mPER1 and mPER2 did not substantially alter after a serum shock. In cells transfected with *mPer3*–Myc, mPER3 was localized mostly in the cytoplasm (95%), and its subcellular localization was not altered after the serum shock (93%) (data not shown). When cells were cotransfected with combinations of *mPer1/mPer3* or *mPer2/mPer3* cDNA, a small increase in the number of cells with nuclear mPER1 and mPER2 was observed (Fig. 2J–O). Remarkably, after brief exposure to high serum, most cells show nuclear localization of the mPER1-HA and mPER2-Flag fusion proteins (75%–80%) (Fig. 2J–O). Thus, a serum shock promotes

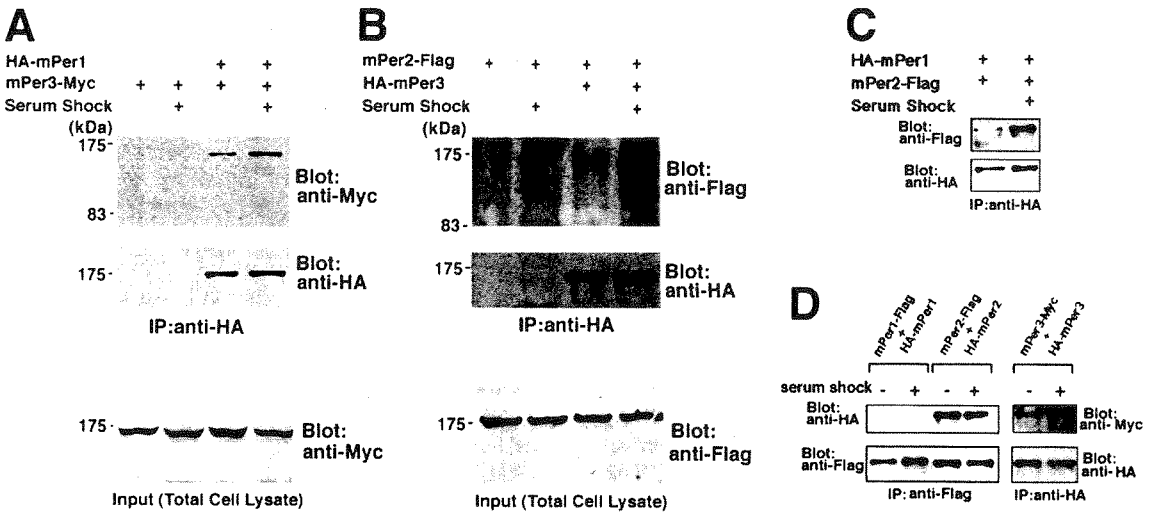

Figure 1. Physical interaction of mPER proteins after serum shock. Heterodimerization detected by the immunoprecipitation in combinations mPER1–mPER3, (*A*), mPER2–mPER3, (*B*) and mPER1–mPER2. (*C*) Treatment with high concentrations of horse serum accelerates the heterodimerizations among mPERs in all combinations. No change was noted in the amount of mPER3-Myc (*A*, *bottom*) and mPER2-Flag (*B*, *bottom*) in total cell lysates showing that serum shock does not increase the amount of expressed proteins. (*D*) Homodimerization detected by immunoprecipitation. mPER2 and mPER3 form homodimers, but mPER1 does not homodimerize to a significant degree; serum shock has no effects on homodimerization.

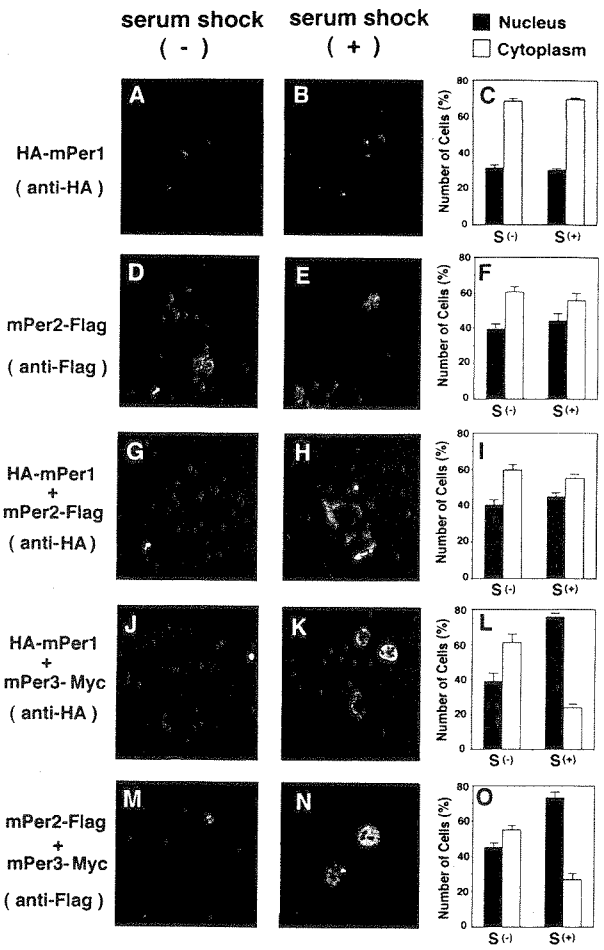

Figure 2. Subcellular localization of heterodimerized mPER proteins. COS7 cells were transfected with HA-*mPer1*, (*A–C*), and *mPer2*-Flag (*D,E,F*); or cotransfected with HA-*mPer1* and *mPer2*-Flag (*G,H,I*), HA-*mPer1* and *mPer3*-His (*J,K,L*), and *mPer2*-Flag, and *mPer3*-His (*M,N,O*). Before (*A,D,G,J,M*) or 30 min after serum shock (*B,E,H,K,N*), cells were fixed and immunostained with anti-HA or anti-Flag M2 antibodies as indicated at *left*. Quantitative analyses are shown at *right* of each condition (*C,F,I,L,O*). Percentage of cells with predominant nuclear (N) and cytoplasmic (C) staining were determined as described. Three to five independent experiments were performed for each condition and one-hundred immunofluorescent cells from each cover glass were counted; means are shown +S.E.M.

nuclear translocation of mPER1 and mPER2 proteins in COS7 cells only when mPER3 is available as a partner. On the basis of the immunoprecipitation and cellular localization data, we hypothesize that serum shock-induced heterodimerization of mPER3 with either mPER1 or mPER2 promotes nuclear entry of these clock proteins.

The mPER3 protein has a functional CLD and NLS

In *Drosophila*, the translocation of PER into the nucleus is triggered by a rapid increase in heterodimerization between PER and TIM (Young 1998). Within PER and TIM, a nuclear localization signal (NLS) and CLD have been noted (Vosshall et al. 1994; Saez and Young 1996). Recently, sequences similar to the *Drosophila* CLD (amino acids 330–389 of mPER3) and NLS (residues 726–734) (Takumi et al. 1998b) were discerned in mPER3. In contrast, the deduced amino acid sequences of mPER1 and mPER2 do not show a typical single basic NLS, although mPER2 has sequences reminiscent of a bipartite basic NLS (Shearman et al. 1997). The absence of clearly distinguishable NLS sequences suggests that the strong serum-stimulated nuclear entry of mPER1 and mPER2 might be dependent on interactions with another protein(s). The data of Figure 2 suggest that mPER3 could fulfill this role.

To examine this possibility and to determine whether the putative NLS and CLD of mPER3 are functional, we have generated the following panel of green fluorescent protein (GFP)–mPER3 fusion constructs as follows: (1) mPER3 (total), which contains the total sequence of mPER3 (1–1115 amino acids); (2) mPER3 (ΔCLD), which lacks amino acids 324–394 including the entire CLD region; (3) mPER3 (228–1077), which includes PAS-B, CLD, and NLS; (4) mPER3 (324–1077), which contains the CLD and NLS; (5) mPER3 (542–1077), which includes only the NLS (Fig. 3A). When expressed in COS7 cells, Western blot analysis using anti-GFP antibodies revealed single protein bands of the expected size (Fig. 3B). In the absence of a serum-shock mPER3 (total)–GFP fusion protein was expressed mainly in the cytoplasm and rarely located in the nucleus. The cytosolic-dominant distribution pattern was even more prominent for GFP–mPER3 fusion proteins [mPER3 (228–1077) and mPER3 (324–1077)] lacking one or more PAS domains but still containing the CLD and NLS (Fig. 3C). In contrast, a further size reduction of the amino-terminal half of mPER3, skipping the CLD, but retaining the NLS, [mPER3 (542–1077)] results in strong nuclear staining in >95% of the cells (Fig. 3C). Interestingly, a mPER3–GFP fusion protein lacking only the CLD portion [mPER3 (ΔCLD)] also showed clear nuclear staining in 40% of the cells (Fig. 3D). This result suggests that deletion of the CLD promotes entry of the mPER3–GFP protein into the nucleus. The weaker effect of mPER3 (ΔCLD) compared with mPER3 (542–1077) might result from interactions with other (endogenous) proteins via PAS-A and PAS-B domains. These data demonstrate that mPER3 has both a functional CLD and NLS and that, as is the case in *Drosophila* PER or TIM (Saez and Young 1996), the CLD is dominant to the NLS in dictating subcellular localization.

mPER3 lacking the NLS fails to promote nuclear entry of mPER1 and mPER2

To further characterize the carboxy-terminal half of mPER3 containing the NLS, we made a truncated, Myc-tagged version [mPER3 (1–542); see Fig. 4A] and examined the effect of this deletion on serum shock-induced heterodimerization with, and nuclear localization of mPER1 and mPER2. Although heterodimerization with mPER1 after serum shock was unaffected by the deletion (Fig. 4B), truncated mPER3 almost completely abolished nuclear entry of mPER1/mPER3 heterodimers as evident

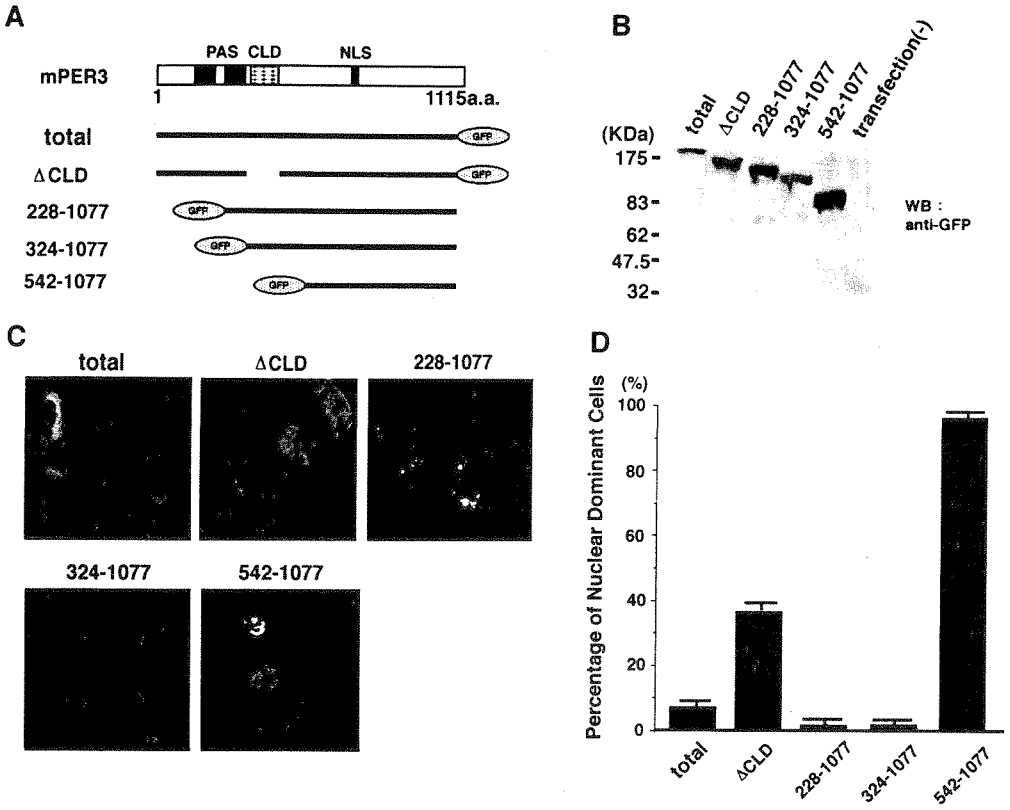

Figure 3. CLD and NLS of mPER3 protein. Three truncated mutants of mPER3 fused with GFP were expressed in COS7 cells. (*A*) Schematic diagrams of the five constructs; (1) mPER3 (total), (2) mPER3 (ΔCLD), (3) mPER3 (228–1077) containing PAS-B, CLD, and NLS, (4) mPER3 (324–1077) containing CLD and NLS, and (5) mPER3 (542-1077) containing NLS and carboxy-terminal portion. (*B*) GFP fusion proteins analyzed by immunoblot confirmed the expression of expected GFP fusion proteins. (*C*) Example photos demonstrating the subcellular localization of each construct. GFP fusion proteins containing both the CLD and NLS [mPER3 (228–1077) and mPER3 (542–1077)] were localized only in the cytoplasm. Deletion of only the CLD region of mPER3 (ΔCLD) greatly increased the nuclear signals. (*D*) Summary of deletion study using truncated mutants of mPER3. Each bar indicates the percentage of cells expressing GFP-fusion proteins with predominant nuclear staining. All data were mean (+S.E.M.) in three independent experiments. In each experiment, 10 fields containing ~200 cells altogether were examined.

from the reduced percentage of cells with nuclear staining (Fig. 4C). Similar results were obtained when Myc-tagged mPER3 (1–542) was replaced by a GFP-tagged version (data not shown). Analogous to the results for mPER1, truncated mPER3 (1–542) also retained the ability to heterodimerize with mPER2 after a serum shock (Fig. 4B). However, the effect of mPER3 truncation on mPER2 nuclear entry was weak compared with its effect on mPER1 (Fig. 4D). It is possible that this moderate effect on mPER2 nuclear localization is related to the putative bipartite basic NLS located in mPER2 (Shearman et al. 1997) that might retain some capacity for nuclear localization. In conclusion, these results demonstrate that the carboxy-terminal half of mPER3 has the capacity to strongly promote nuclear translocation of mPER1/mPER3 dimers and, to a lesser extent, mPER2/mPER3 dimers.

We also studied mPER3-dependent nuclear localization in rat-1 fibroblasts, known to produce a molecular rhythm following serum-shock (Balsalobre et al. 1998). Although in comparison to COS7 cells, rat-1 cells show higher levels of nuclear mPER1 and mPER2 after a single transfection with *mPer1* and *mPer2* cDNA, respectively, coexpression with *mPer3* cDNA significantly increases nuclear localization of mPER1 and mPER2 (Fig. 5). Coexpression of mPER3 (1–542), lacking the NLS, again failed to stimulate nuclear localization of mPER1 and mPER2 (Fig. 5). Thus, mPER3-mediated mPER1 and mPER2 nuclear translocation appears not to be a COS7 cell-specific property, but rather might constitute a common phenomenon in various types of cells.

Nuclear entry of mPER1 in the absence of mCRY proteins

The above experiments strongly suggest that serum shock-induced nuclear translocation of mPER1 and mPER2 is promoted by heterodimerization with mPER3, but do not exclude the possibility that endogenous proteins in COS7 cells also mediate nuclear entry. In a recent study, Kume et al. (1999) demonstrated that mammalian CRY proteins are implicated in nuclear entry of mPER, but they also showed that mPER cellular localization is influenced by PER–PER heterodimerization.

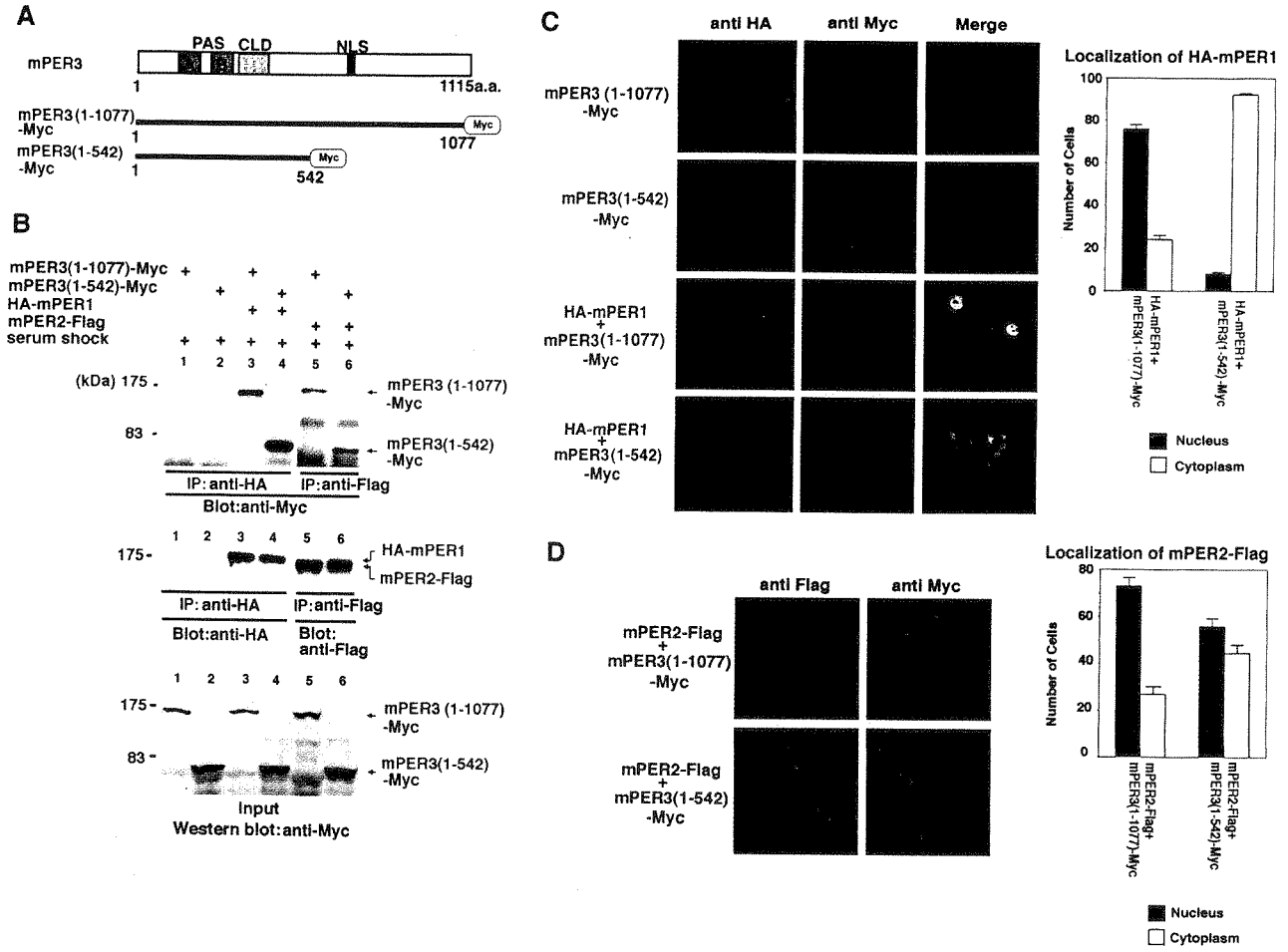

Figure 4. Nuclear entry of a truncation mutant of mPER3 protein lacking the carboxy-terminal half containing the NLS. (*A*) Schematic diagrams of two mPER3-Myc constructs. (*B*) Immunoprecipitation showing that both mPER3 (1–1077)-Myc and mPER3 (1–542)-Myc associate with mPER1 and mPER2 protein. (*C*) Double-label immunofluorescence of cells coexpressing mPER3 (1–1077)-Myc and HA-mPER1, or mPER3 (1–542)-Myc and HA-mPER1. Although mPER1 coexpressed with mPER3 (1–1077) showed nuclear localization, truncated mPER3 (1–542)-Myc failed to allow nuclear entry of coexpressed mPER1 protein. Expression of only mPER3 (1–1077)-Myc or mPER3 (1–542)-Myc in COS7 cells revealed positive cytoplasmic staining to anti-Myc and no immunoreactivity against anti-HA antisera. Serum shock was performed in every case. Cell counts shown at *right* represent the mean of three independent experiments, and error bars indicate the S.E.M. One-hundred stained cells were observed and counted in each experiment. (*D*) Immunofluorescence of mPER3 (1–542)-Myc coexpressed with mPER2. mPER3 (1–542)-Myc also failed to promote nuclear entry of mPER2, but its effect on mPER2 was much weaker than that seen for mPER1. As above, serum shock was performed for all experiments. Results of cell counts represent the mean of three independent experiments, and error bars indicate the S.E.M. One-hundred stained cells were observed and counted in each experiment.

To further examine the role of mCRY and mPER3 proteins in mPER1 nuclear translocation, we investigated the subcellular localization of mPER1 in mCRY-deficient mouse embryonic fibroblasts (MEFs) derived from *mCry1/mCry2* double-mutant mouse embryos (van der Horst et al. 1999).

First, we confirmed by Northern blot analysis that intact *mCry1* and *mCry2* mRNAs were not detectable in these cells (Fig. 6A). Next, *mCry1*, *hCry2*, HA-tagged *mPer1*, and Myc-tagged *mPer3* cDNAs were transfected in various combinations and subcellular localization was analyzed following a serum shock. Representative confocal micrographs (Fig. 6B, right) showed nuclear localization of exogenous mPER1 in the absence of endogenous mCRY in 45% of HA-*mPer1* singly transfected cells (Fig. 6B, graph). Moreover, the percentage of mPER1 nuclear-stained cells was not significantly increased after coexpression with mCRY1, hCRY2, or a combination of the two. In contrast, coexpression with mPER3 dramatically promoted nuclear translocation of mPER1 (89% of nuclei are stained) (Fig. 6B, graph). Coexpression of mPER3 lacking the NLS [mPER3 (1–542)] with mPER1 not only failed to allow nuclear import, but instead promoted cytosolic localization of mPER1 (Fig. 6B, graph). As a control, we also analyzed mPER3-mediated import of mPER1 in wild-type MEFs containing endogenous mCRY proteins after serum shock. Comparable with the findings with *mCry1/mCry2* double-deficient cells, 48% of the wild-type cells transfected with *mPer1* show nuclear staining (Fig. 6C), whereas coexpression with

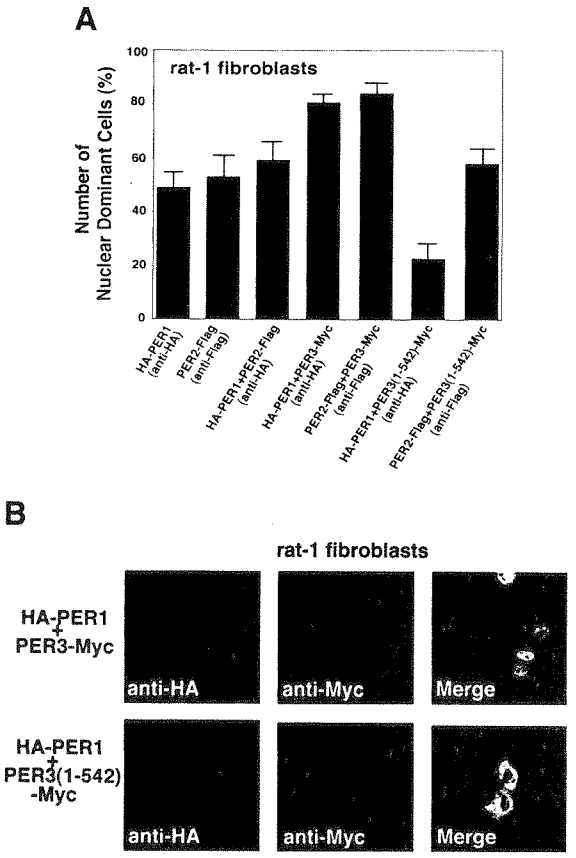

Figure 5. Immunofluorescent study of subcellular localization of mPERs in rat-1 fibroblasts. (*A*) The graph shows the percentages of cells in which expressed mPER proteins show a predominantly nuclear distribution after serum shock. Coexpression with mPER3 significantly increases the ratio of mPER1 or mPER2 cells with a predominant nuclear staining, and coexpression with truncated mPER3 [mPER3 (1–542)] lacking the NLS significantly reduced the nuclear localization of mPER1. (*B*) Confocal images showing transfected cells with HA-mPER1/mPER3-Myc coexpression and HA-mPER1/mPER3 (1–542)-Myc coexpression. As shown in *A*, nuclear localization of expressed mPER1 was strongly enhanced by coexpression of mPER3 protein.

mPER3 significantly promoted nuclear translocation of mPER1 (87%) and truncated mPER3 (1–542) prevented it (19.5%) (Fig. 6C). These results show that under the conditions tested, nuclear localization of mPER1 does not involve mCRY proteins and further support the hypothesis that mPER3 plays a prominent role in nuclear translocation of mPER1 after serum shock.

Nuclear localization of endogenous mPER1 protein in peripheral and central clock tissues of mCry1/mCry2 *double-mutant mice*

In the previous sections, in vitro evidence was obtained for nuclear localization of exogenously expressed mPER1 in *mCry1/mCry2* double-deficient cells. To determine whether these results reflect the in vivo situation, we determined the expression and cellular localization of endogenous mPER1 protein in cells and tissues of wild-type and *mCry1/mCry2* double-mutant mice using immunohistochemistry. In cultured embryonic fibroblasts, endogenous mPER1 was localized predominantly in the nucleus in both wild-type and *mCry1/mCry2* double-mutant-derived cells (Fig. 7A,B). In the liver of wild-type mice, mPER1 could not be detected at ZT12, whereas a clear nuclear staining occurred at ZT24, which is indicative for the presence of a diurnal rhythm (Fig. 7C,E). In hepatocytes of *mCry1/mCry2* double-deficient mice, endogenous mPER1 protein is constitutively expressed in the nucleus (Fig. 7D,F). Next, we examined the expression and localization of mPER1 protein in the SCN (the site of the master oscillator) of wild-type and *mCry1/mCry2* double-mutant mice. In accordance with the literature (Hastings et al. 1999), we find in the SCN of wild-type mice high expression and nuclear localization of mPER1 at CT12–16 (see also Fig. 8A) and very low expression at CT2–6 (data not shown). In the SCN of *mCry1/mCry2* double-mutant mice, mPER1 protein is expressed at a level comparable with that in wild-type mice at CT12–16 (Fig. 8B). In the absence of mCRY proteins, mPER1 protein can still be found in the nucleus (Fig. 8A,B, high magnification). These data clearly show that mCRY-independent nuclear translocation of mPER1 protein also occurs in the intact animal and are entirely consistent with the results of the cellular transfection studies.

Discussion

Nuclear translocation of oscillator gene products is an essential step for the generation of a circadian negative feedback loop. Particularly, this nuclear entry step is considered to play a key role for determining the ~24 hr period. In *Drosophila*, massive nuclear entry of PER occurs at about ZT18 (Young 1998) mediated by complexation with the TIM protein. In mammals, the circadian oscillator involves the products of three oscillator genes (*mPer1*, *mPer2*, and *mPer3*) (Albrecht et al. 1997; Shearman et al. 1997; Shigeyoshi et al. 1997; Sun et al. 1997; Tei et al. 1997; Takumi et al. 1998a,b; Zylka et al. 1998b). In the present study we show that in cultured COS7 cells constitutively expressing *mPer* cDNAs, mPER1 and mPER2 are predominantly localized in the cytoplasm. Similar results have been reported for NIH-3T3 cells (Kume et al. 1999). However, when COS7 cells are exposed to high levels of serum, a condition known to initiate rhythmic expression of *rPer1* and *rPer2* in cultured rat-1 cells (Balsalobre et al. 1998), mPER3 is shown to promote nuclear translocation, particularly of mPER1, and to a lesser extent of mPER2. This process appears to be coupled to a strong increase in heterodimerization of mPER proteins in all possible combinations (mPER1/mPER2, mPER1/mPER3, mPER2/mPER3). Because *Drosophila* PER can interact with each other through the PAS domains (Huang et al. 1995), interactions between mPER proteins may also involve these evolutionary highly conserved domains. The serum shock did not randomly facilitate mPER–mPER interactions, because mPER homodimers were detected at comparable levels

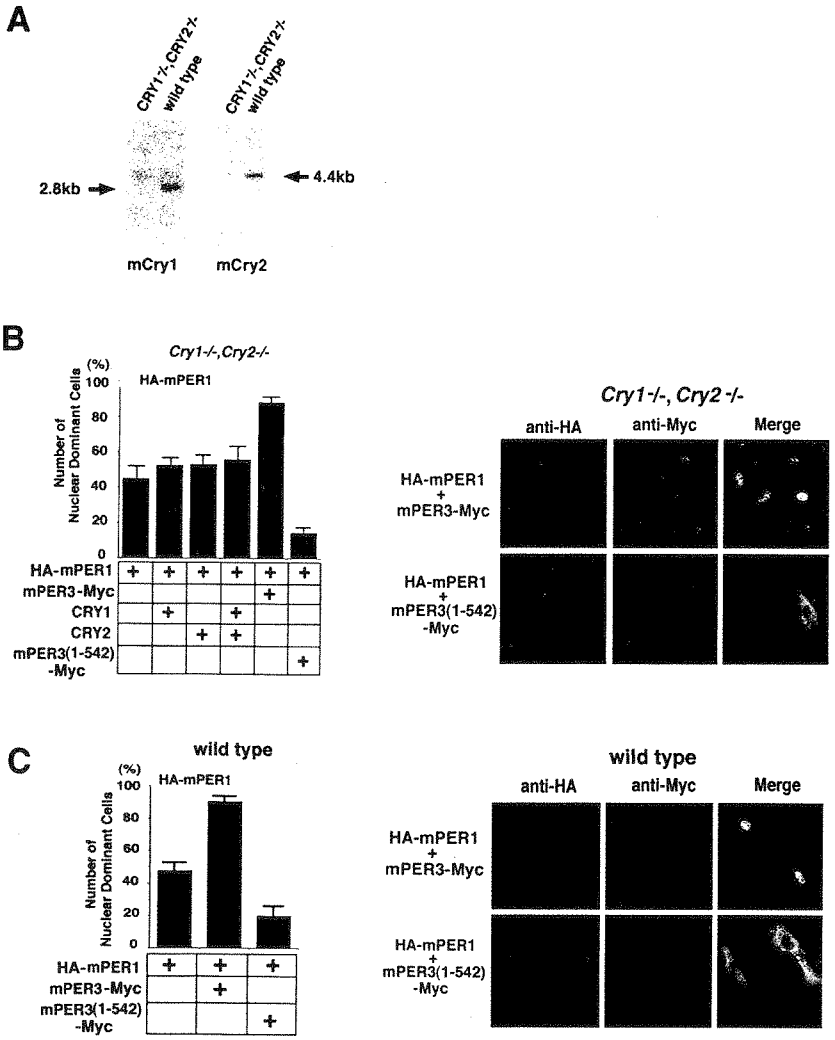

Figure 6. Nuclear entry of mPER1/mPER3 in *mCry1/mCry2* double knockout cells. The effect of mPER3 on nuclear entry of mPER1 was investigated in *mCry1mCry2* double knockout cells. (*A*) Northern blot analysis of *mCry1* (*left*) and *mCry2* (*right*) MEFs from *mCry1/mCry2* double knockout mouse and wild type. In the *mCry1/mCry2* double knockout cells, no signals are seen at the appropriate molecular weight. (*B*) Analysis of nuclear translocation of mPER1 in *mCry1/mCry2* double knockout cells after coexpression of mPER3, CRY1, CRY2, and/or mPER3 (1–542). The percentage of nuclear-positive cells is shown in the bar graph. About one-half of the cells (45%) show nuclear localization by single HA-mPER1 expression, perhaps due to partnering with endogenous proteins. Although transfection of CRY1/2 did not affect the nuclear entry of mPER1, cotransfection of mPER3 markedly increased nuclear entry of mPER1. Truncated mPER3 lacking the carboxy-terminal half including the NLS prevented the nuclear accumulation of mPER1. Confocal laser microscopic images are presented at *right*. (*C*) Control nuclear translocation experiments in MEFs originating from wild-type mice expressing endogenous *mCry1* and *mCry2*. Note the very similar nuclear localization in all combinations in *C*, suggesting that mCRY proteins are not essential for nuclear translocation of mPER1. All results are the mean (+S.E.M.) of three independent experiments in *B* and *C*.

before and after serum treatment. These data suggest that association with mPER3 forms a critical step in the nuclear translocation of mPER1 and mPER2. Accordingly, the rhythmic expression of *rPer1* and *rPer2* after serum shock observed by Balsalobre et al. (1998), starting with a brief, rapid induction followed by suppression of these clock genes, can be explained by rPER3 complex formation and nuclear translocation of rPER1 and rPER2. Recently, mPER1 and mPER3 were shown to coprecipitate from mouse SCN homogenates (Field et al., 2000), indicating that physical interactions between these proteins also occur under physiological conditions. Treatment of rat-1 cells with high concentrations of serum activate MAP kinases and CREB (Yagita and Okamura 2000). It is tentative to speculate that activation of cell signaling pathways may ultimately lead to phosphorylation of mPER proteins, which in turn may facilitate the interaction and subsequent nuclear entry of mPER proteins. It is noteworthy that in *Drosophila*, phosphorylation of dPER is essential for association with dTIM and nuclear translocation of the dPER/dTIM complex (Price et al. 1998).

mPER3 contains sequences similar to the CLD and NLS of *Drosophila* PER (Takumi et al. 1998b; Zylka et al. 1998b). In mPER1 and mPER2, the CLD is conserved, but these proteins do not possess a typical single basic NLS, although mPER2 may have a bipartite NLS (Shearman et al. 1997). Here we show both structural and functional conservation of the CLD and confirmed the dominance of the CLD over NLS activity in cellular localization of mPER3, as seen in *Drosophila* PER and TIM (Saez and Young 1996). According to the fly model for CLD function, PER and TIM associate to mask the CLD of PER, allowing TIM to escort PER into the nucleus (Vosshall et al. 1994; Saez and Young 1996). By analogy, we propose that in mammals, heterodimerization of mPER1/mPER3 or mPER2/mPER3 masks the CLD of each partner, allowing the NLS of mPER3 to direct the heterodimers to the nucleus.

The role of mammalian TIM in the nuclear transportation step of mPER proteins is unknown. In *Drosophila*, the subcellular localization of the TIM protein is regulated in a time-dependent fashion, but in mammalian SCN cells, mTIM is predominantly in the nucleus and

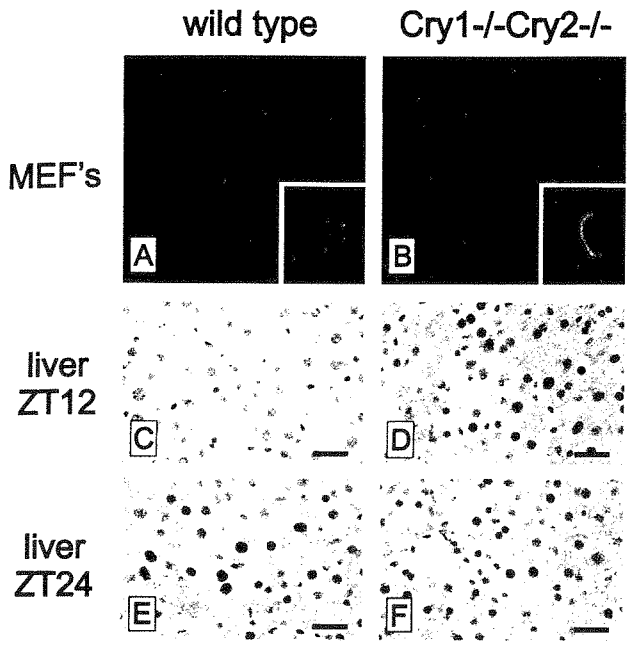

Figure 7. Nuclear localization of endogenous mPER1 in MEF's and liver of wild-type and *mCry1/mCry2* double-mutant mice. Representative examples of immunofluorescent staining of mPER1 in wild-type (*A*) and *mCry1/mCry2* double-mutant (*B*) MEFs (*Insets*) Hoechst stained nuclei. Immunohistochemical detection of mPER1 in the liver of a wild-type mouse at ZT12 (*C*), a *mCry1/mCry2* double-mutant mouse at ZT12 (*D*), a wild-type mouse at ZT24 (*E*), and a *mCry1/mCry2* double-mutant mouse at ZT24 (*F*). Animals were kept under LD conditions (12:12 hr). Bars in *C–F* 25 μm.

does not exhibit circadian rhythmicity (Hastings et al. 1999). Analogously, COS7 cells used in the present study constitutively express significant levels of endogenous *mTim* mRNA, even in the absence of a serum shock

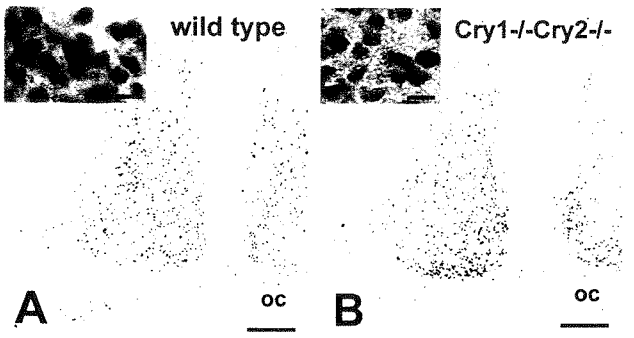

Figure 8. Immunohistochemistry for endogenous mPER1 in the SCN of wild-type and *mCry1/mCry2* double knockout mice. mPER1-immunoreactivity is found in neurons of the suprachiasmatic nucleus in both wild-type (*A*) and *mCry1/mCry2* double-deficient (*B*) mice at ZT14. Note the absence of significant differences in immunoreactivity between wild-type and *mCry1/mCry2* double knockout mice. Each high-magnification photograph shows that endogenous mPER1 is present in the nucleus of SCN cells in both wild-type (*A*) and *mCry1/mCry2*-deficient (*B*) mice. Bars, 100 μm for low-power micrographs, and 10 μm for high-power micrographs.

(data not shown). mPER3-dependent nuclear translocation seems not to correlate with the level of *mTim* expression, because *mTim* mRNA levels are high in COS7 and wild-type embryonic fibroblasts, but low in rat-1 cells and mCry1/mCry2 double knockout embryonic fibroblasts (data not shown).

According to the basic model for the molecular mechanism of the circadian pacemaker, mPER proteins—when in the nucleus—repress CLOCK/BMAL-mediated transcriptional activation of various clock genes (for review, see Reppert 1998; Dunlap 1999). Although mPER proteins inhibit transcription from *mPer1*- or *vasopressin*-promoter driven luciferase reporter constructs, repression is rarely complete (e.g., Sangoram et al. 1998; Zylka et al. 1998a; data not shown), indicating that additional factors are required to completely suppress CLOCK/BMAL function. Recently, mCRY1 and mCRY2, members of the light-harvesting cryptochrome/photolyase protein family (Hsu et al. 1996; Todo et al. 1996; van der Spek et al. 1996), were shown to be indispensable components of the molecular oscillator as mice with inactivated *mCry1* and *mCry2* genes completely lacking a biological clock (Okamura et al. 1999; van der Horst et al. 1999; Vitaterna et al. 1999). Subsequently, Kume et al. (1999) found that mCRY proteins strongly inhibit *mPer1* and *vasopressin* promoter-driven luciferase expression in NIH-3T3 cells and that they act as dimerization partners for translocation of mPER1, mPER2, and mPER3 into the nucleus. However, heterodimerization of mPER by itself was reported to affect cellular localization also. Our findings extend the significance of mPER–mPER interactions for nuclear translocation: mPER3 promotes the nuclear entry of mPER1 and mPER2. The pronounced nuclear localization of exogenous mPER1 in the mCRY-deficient MEFs after serum shock indicates that mPER3 can also accomplish nuclear entry of mPER1 without the help of mCRY proteins. Remarkably, under our experimental conditions, overexpression of mCRY1 or hCRY2 or both in *mCry1/mCry2* double-mutant cells did not increase the mPER1-nuclear entry. In contrast, mPER3 transfection enhances mPER1 nuclear import in mCRY-deficient cells, whereas NLS-deleted mPER3 transfection markedly decreased the nuclear localization. Thus, it appears that there may be more than one route for mPER protein import into the nucleus. Moreover, immunocytochemical analysis using anti-mPER1-specific antisera revealed that endogenous mPER1 also localized in the nucleus in cultured *mCry1/mCry2* double-mutant cells, indicating that mCRY-independent nuclear translocation of exogenous mPER1 is not merely an artifact in cellular transfection studies. Importantly, we also demonstrated mCRY-independent nuclear localization of endogenous mPER1 in SCN and liver of *mCry1/mCry2* double-mutant mice and thus is likely to be of physiological importance.

The absence of an effect of mCRY proteins on mPER subcellular localization when coexpressed in the *mCry1/mCry2* double-deficient cells may be explained in various ways. First, we have used a serum shock, known to stimulate rhythmic expression of clock genes in cultured cells, which may involve additional or different factors

for nuclear translocation of clock gene products. Second, different cell lines and different conditions were used. The COS7 cells used here are exceptional because they hardly express any endogenous *mPer* genes, virtually no *mCry2*, and moderate levels of *mCry1* transcripts (K. Yagita and H. Okamura, unpubl.). In contrast, most other frequently used cell lines including rat-1 and NIH-3T3 fibroblasts highly express all endogenous *mPer* genes and NIH-3T3 cells and also highly express both *mCry* genes (K. Yagita and H. Okamura, unpubl.). As discussed above, it is conceivable that these differences in endogenous mPER and mCRY protein levels have an effect on the exogenous proteins. The nuclear localization of mPER1 in mCRY-deficient cells and tissues shows that the mCRY proteins are not indispensable for nuclear translocation of mPER1. Although mCRY proteins are very strong transcription suppressors of *mPer1* in NIH-3T3 cells (Griffin et al. 1999; Kume et al. 1999) and in HepG2 cells (Yamaguchi et al., 2000), their role in nuclear migration of other clock proteins needs further exploration.

In conclusion, we have shown that there may be more than one route for mPER proteins to reach the nucleus. In addition to mCRY-mediated nuclear migration of mPERs, our data are consistent with a model in which nuclear entry is driven by masking of the CLD of mPER proteins through heterodimer formation of mPER3 with mPER1 or mPER2. In this scenario, the roles of the CLD and NLS in nuclear entry of clock components as described in *Drosophila* would be conserved in mammals, but the part played by TIM as the dimerizing partner for mPER1 and mPER2 might be taken over by mPER3.

Materials and methods

Plasmids

For construction of *mPer1*-Flag in a mammalian expression vector, the primers used were as follows, 5′-AAGCTTCCAGACATGAGTGGTCCCCTAGAAG-3′, 5′-GAATTCGCTGGTGCTGTTTTCTTCTGCAGGTAAAGC-3′. For construction of *mPer2*-Flag, nucleotides 1–3740 (codon 1–1207) were digested from a full-length cDNA of *mPer2* by use of *Not*I and *Cla*I, and this fragment was subcloned into the pcDNA3–Flag vector. Nucleotides 1–3465 (codon 1–1077) of *mPer3* were isolated from a full-length cDNA of *mPer3* by use of *Not*I and *Bam*HI and were subcloned into pcDNA3.1–Myc/His vector (Invitrogen). HA-*mPer1*, HA-*mPer2*, and HA-*mPer3* constructions were gifts from Dr. T. Kishimoto (Sumitomo Electric Industries). Total coding regions of *mPer1*, *mPer2*, and *mPer3* were cloned by PCR by use of an HA epitope sequence fused in 5′ primers, and subcloned into pTargeT vector (Promega).

For the construction of mPER3 (1–542)–Myc, total *mPer3* cDNA cloned into pGEM-T Easy (Promega) was digested by *Not*I and *Kpn*I, and cloned into pcDNA3.1–Myc/His vector.

The total coding region of *mCry1* was obtained by RT–PCR and cloned into pcDNA3 vector (Invitrogen). The plasmid containing the partial human *Cry2* was generously provided by Takahiro Nagase (KAZUSA DNA Research Institute). As the KIAA0658 gene lacks the 5′ end of the human *Cry2*-coding region, the further upstream 5′ fragment was obtained by PCR according to an EST clone (accession no. AL040215). The total coding region of human *Cry2* was cloned into pcDNA3 vector.

Cell culture, transfection, and serum shock

COS7 cells were grown in DMEM supplemented with 10% FBS (GIBCO BRL) and penicillin–streptomycin (GIBCO BRL). MEF's were established from day 13.5 *mCry1/mCry2* double-knockout and wild-type mouse embryos. Cells were grown in the DMEM containing 10% FCS at 37°C under 5% CO_2. Cells were transfected with Lipofectamine-Plus (GIBCO BRL). Two and one-half hours after transfection, the medium was replaced with 5 ml of DMEM with 10% FCS. After 12 hr, medium was replaced with serum-free DMEM and incubated for 12 hr. Thirty minutes before harvest, cells were treated with DMEM containing 50% horse serum.

Immunoprecipitation and immunoblot

Cells were plated into 60-mm plates at 2×10^5 cells 24 hr prior to transfection. Cells in each plate were transfected with 2 μg (total) of DNA.

Immunoprecipitation was performed 24 hr after transfection by use of whole-cell lysates harvested with 0.2 ml of lysis buffer [50 mM Tris-HCl at pH 7.5, 150 mM NaCl, 1% NP 40, 50 mM NaF, 100 μM sodium vanadate, and complete mini-protease inhibitors (Boehringer)]. Total cell lysate was kept on ice for 1 hr and centrifuged at top speed for 10 min at 4°C, 10 μl of total-cell extract was used for each Western blot analysis. The supernatant was transferred to a fresh microtube and anti-Flag M2 (Kodak) or anti-HA antibodies (Boehringer) were added and incubated 4 hr at 4°C with mild agitation. After adding 30 μl of Protein-G Agarose equilibrated with lysis buffer, beads were collected (15,000 rpm, 20 sec) and washed twice with wash buffer (20 mM Tris-HCl at pH 7.5, 500 mM NaCl, 0.1% NP-40, 0.05% sodium deoxycholate). After removing the supernatant completely, 8 μl of 3 × SDS sample buffer was added and samples were boiled for 5 min. Immunoprecipitated samples were separated on 7% SDS–polyacrylamide gel, and transferred to polyvinylidene difluoride (PVDF) membranes. Immunoblotting was performed with anti-Flag M2 (Kodak, 500× dilution), anti-Myc (9E10; Santa Cruz, 5000× dilution), or anti-HA (Boehringer, 2000× dilution) antisera. Chemiluminescence was performed by use of Renaissance Western blot reagent plus (NEN, cat. no. NEL105).

GFP fusion proteins

The total coding region of *mPer3* was cloned into pEGFP-N2 vector (Clontech). For construction of deletion mutants of mPER3 fused with GFP proteins, total *mPer3* cDNA was digested by *Bam*HI or *Dra*I/*Bam*HI or *Kpn*I/*Bam*HI. *Bam*HI fragment (amino acids 228–1077), *Dra*I–*Bam*HI fragment (amino acids 324–1077), and *Kpn*I–*Bam*HI fragment (amino acids 542–1077) were cloned into pEGFP-C vectors (Clontech). For the clone mPER3 (ΔCLD), the total coding region of *mPer3* was digested with *Dra*I and *Nco*I, and then the PCR fragment encoding amino acids 395–476 was ligated in. This construct was cloned into the pEGFP-N2 vector.

COS7 cells were plated onto 60-mm plates at 2×10^5 cells 24 hr prior to the transfection. Cells transfected with indicated constructs were cultured for 24 hr after the transfection. Cells were harvested with 0.2 ml of lysis buffer. Total-cell lysates were prepared as described above. One hundred microliters of 3× SDS sample buffer was added and samples were boiled for 5 min. Ten microliters of samples were separated on 7% SDS–polyacrylamide gel, and transferred to a PVDF membrane. Immunoblotting was performed as described with anti-GFP (Clontech, 200× dilution), and detected by chemiluminescence.

Northern blot analysis

MEFs derived from both *mCry1/2* double knock out and wild type were harvested in the TRIzol regent (GIBCO BRL). Ten micrograms of extracted total RNA was electrophoresed in a 1.2% agarose gel containing 2% formaldehyde. RNAs were transferred to Biodyne Nylon Membrane (Pall BioSupport, NY) and hybridized with probes. For probes, 730–1479 bp of *mCry1* and 397–810 bp of *mCry2* were used for templates. Probes were incubated with membranes at 42°C overnight, washed twice in 0.2× SSC/0.1% SDS at 60°C for 30 min, exposed to Imaging Plates, and analyzed by BAS 5000 (Fuji Film, Tokyo, Japan).

Antisera against mPER1

Polyclonal rabbit antibodies against mPER1 (code no. RY354) were raised using a synthetic peptide (GSSGNESNGPESRGAS-QRC) corresponding to amino acids 51–68 of the deduced amino acid sequence of *mPer1* cDNA (Tei et al. 1997) and containing a carboxy-terminal cysteine residue for conjugation to keyhole limpet hemocyanin for immunization. Immunizations were performed using Freund's complete adjuvant for primary injection and Freund's incomplete adjuvant for boosts (given at 2-week intervals). Rabbits were bled from the marginal vein at 10 days after the fourth immunization. Peptide synthesis and subsequent immunization protocols were conducted at Yanaihara Institute (Fujinomiya, Japan). This antiserum was checked by immunoblots of nuclear extracts of mouse brain and the mPER1, mPER2, and mPER3 expression plasmids transfected with COS7 cells. In the mouse brain and mPER1-expressing COS7 cells, we detected a single band corresponding to the predicted molecular weight. Positive signals were not detected in mPER2 and mPER3-expressing COS7 cells. This antiserum was used for the SCN analysis.

The anti-mPER1 antiserum (Field et al. 1999; Hastings et al. 1999) used for MEFs and liver tissues was kindly provided by Dr. S.M. Reppert (Massachusetts General Hospital, Boston, MA).

Immunofluorescence of cultured cells

COS7 cells were grown on 24 × 24-mm cover glasses and transfected with 1 μg (total) of DNA by using of Lipofectamine-Plus (GIBCO BRL). Transfected cells were cultured in DMEM containing 10% FBS (12 hr) and then serum-free DMEM (12 hr). Serum shock was performed as described for indicated samples before fixation. Transfected cells were fixed in 4% paraformaldehyde in 0.1 M phosphate buffer. Fixed cells were permeabilized by 0.2% Triton-X in 0.1 M PBS for 5 min, and incubated with primary antibodies (anti-Flag M2 500×, anti-HA 1000×; for 16 hr at 4°C). After washing in PBS, FITC-conjugated anti-mouse IgG (Jackson Immuno Research) and/or Cy3-conjugated anti-rat IgG (Amersham) were used as the secondary antibodies in 1-hr incubations at room temperature. Cells were then washed and mounted with glycerol on a cover glass. Cells were observed by confocal laser microscopy (Bio-Rad).

Subcellular localization was assayed by examining immunoreactive cells that were classified into two groups, either cytoplasm dominant (C) in which the intensity of cytoplasmic staining was stronger than that in nucleus or the reverse (N nucleus dominant). We performed the above calculation in all 100 cells examined three to five times in each independent experiment.

Wild-type and *mCry1/mCry2* double-mutant MEFs were cultured in DMEM/F10 with 10% FCS and seeded on glass coverslips 2 days before the immunohistochemistry. Cells were fixed in 0.1 M PBS containing 3% paraformaldehyde for 7 min, followed by a permeabilization step in 100% methanol for 20 min. After incubation with anti-mPER1 antibodies (16 hr, 4°C, 1:2000 dilution), washing, incubation with a secondary fluorescein-conjugated anti-rabbit antibody (1:100 dilution; DAKO) and washing, cells were analyzed under a fluorescence microscope. All steps, except incubation with anti-mPER1 antibodies, were performed at room temperature. Nuclei were counterstained with Hoechst solution at a dilution of 1:2000.

Immunohistochemistry of liver and brain

Animals were housed under 12-hr bright white light:12-hr dark condition. Zeitgeber time (ZT) was defined relative to lights on (ZT0) and lights off (ZT12). Animal experiments were performed under the approval of the Committee for Animal Research at Kobe University School of Medicine and the Animal Care and Use Committee at the Erasmus University Rotterdam.

For analysis of the liver, animals were decapitated at ZT12 and ZT24. Livers were immediately perfused with 0.1 M PBS, followed by overnight fixation in 4% paraformaldehyde, and dehydrated. After dehydration, samples were embedded in paraffin and cut into 7-μm sections. Endogenous peroxidase was inhibited by hydrogen peroxide-sodium azide treatment (0.6% H_2O_2 and 0.125% sodium azide in PBS for 30 min). Endogenous biotin was blocked by subsequent incubation with avidin and biotin (10 min each; biotin blocking system, DAKO). Sections were incubated with a primary rabbit anti-mPER1 antibody (1:2000 dilution), followed by a secondary biotin-conjugated anti-rabbit antibody (1:500). After extensive washing, the mPER1 immunoreactivity was visualized using streptavidin-conjugated peroxidase (Zymed), followed by a DAB (diaminbenzidine chromogen) reaction. Nuclei were counterstained with hematoxilin for 30 sec.

For the SCN, animals were perfused with saline, followed by a fixative (2% paraformaldehyde and 0.2% picric acid in 0.1 M phosphate buffer) under deep ether anesthesia at ZT14, and then post-fixed with the same fixative for 2 hr, then 30-μm-thick sections were cut in a cryostat and processed for free-floating immunohistochemistry as described previously (Yagita et al. 1994). After an application of biotinylated anti-rabbit IgG (1:500), sections were incubated with avidin-biotin-peroxidase (1:500, Vector) and visualized with DAB. After immunoreaction, SCN sections were mounted onto chrome alum/gelatin-coated slides, dehydrated through a graded series of ethanol, and mounted with Entellan.

Acknowledgments

We thank Y. Takahashi (Kobe University) for technical advice, M. Muijtjens (Erasmus University) for establishing the MEF lines, Dr. S.M. Reppert (Massachusetts General Hospital, Boston, MA) for kindly providing mPER1 antibodies for analyses of liver and cultural MEFs, T. Kishimoto (Sumitomo Electric Industries) for donating HA-tagged *mPer1*, *mPer2*, and *mPer3*, Y. Minami (Kobe University) for donating the Flag-fused pcDNA3 vector, and Y. Shigeyoshi (Kinki University) for discussion. This work was supported by research grants to H.O. from the Special Coordination Funds of the Japanese Science and Technology Agency, the Grant-in-Aid for the Scientific Research on Priority Areas of the Ministry of Education, Science, Sports, and Culture of Japan, Mitsubishi Foundation, SRF and Uehara Memorial Foundation, to J.J.L. from the National Science Foundation (MCB-9307299), to J.C.D. and J.J.L. from the National Institute of Health (R01-MH 44651), to J.C.D. from the National Institute of Health (R37-GM 34985 and K05-MH01186), to J.H.J.H. and G.T.J.vd.H. from the Dutch cancer society. J.H.J.H. is recipient of the SPINOZA award of the Dutch Science Foundation.

The publication costs of this article were defrayed in part by payment of page charges. This article must therefore be hereby marked "advertisement" in accordance with 18 USC section 1734 solely to indicate this fact.

References

Albrecht, U., Z.S. Sun, G. Eichele, and C.C. Lee. 1997. A differential response of two putative mammalian circadian regulators, *mPer1* and *mPer2*, to light. *Cell* **91:** 1055–1064.

Balsalobre, A., F. Damiola, and U. Schibler. 1998. A serum shock induces circadian gene expression in mammalian tissue culture cells. *Cell* **93:** 929–937.

Dunlap, J.C. 1999. Molecular bases for circadian clocks. *Cell* **96:** 271–290.

Field, M.D., E.S. Maywood, J.A. O'brien, D.R. Weaver, S.M. Reppert, and M.H. Hastings. 2000. Analysis of clock proteins in mouse SCN demonstrates phylogenic divergence of the circadian clockwork and resetting mechanisms. *Neuron* **25:** 437–447.

Griffin, E.A., Jr., D. Staknis, and C.J. Weitz. 1999. Light-independent role of CRY1 and CRY2 in the mammalian circadian clock. *Science* **286:** 768–771.

Hastings, M.H. 1997. Central clocking. *Trends Neurosci.* **20:** 459–464.

Hastings, M.H., M.D. Field, E.S. Maywood, D.R. Weaver, and S.M. Reppert. 1999. Differential regulation of mPER1 and mTIM proteins in the mouse suprachiasmatic nuclei: New insights into a core clock mechanism. *J. Neurosci.* **11:** 1–7.

Hsu, D.S., X. Zhao, S. Zhao, A. Kazantsev, R.-P. Wang, T. Toda, Y.-F. Wei, and A. Sancar. 1996. Putative human blue-light photoreceptors hCRY1 and hCRY2 are flavoproteins. *Biochemistry* **35:** 13871–13877.

Huang, Z.J., K.D. Curtin, and M. Rosbash. 1995. PER protein interactions and temperature compensation of a circadian clock in *Drosophila*. *Science* **267:** 1169–1172.

Kume, K., M.J. Zylka, S. Sriram, L.P. Shearman, D.R. Weaver, X. Jin, E.S. Maywood, M.H. Hastings, and S.M. Reppert. 1999. mCRY1 and mCRY2 are essential components of the negative limb of the circadian clock feedback loop. *Cell* **98:** 193–205.

Luo, C., J.J. Loros, and J.C. Dunlap. 1998. Nuclear localization is required for function of the essential clock protein FRQ. *EMBO J.* **17:** 1228–1235.

Okamura, H., S. Miyake, Y. Sumi, S. Yamaguchi, A. Yasui, M. Muijtjens, J.H.J. Hoeijmakers, and G.T.J. van der Horst. 1999. Photic induction of *mPer1* and *mPer2* in *Cry*-deficient mice lacking a biological clock. *Science* **286:** 2531–2534.

Price, J.L., J. Blau, A. Rothenfluh, M. Abodeely, B. Kloss, and M.W. Young. 1998. Double-time is a new Drosophila clock gene that regulates PERIOD protein accumulation. *Cell* **94:** 83–96.

Reppert, S.M. 1998. A clockwork explosion *Neuron* **21:** 1–4.

Saez, L. and M.W. Young. 1996. Regulation of nuclear entry of the drosophila clock proteins period and timeless. *Neuron* **17:** 911–920.

Sangoram, A.M., L. Saez, M.P. Antoch, N. Gekakis, D. Staknis, A. Whiteley, E.M. Fruechte, M.H. Vitaterna, K. Shimomura, D.P. King et al. 1998. Mammalian circadian autoregulatory loop: A timeless ortholog and *mPer1* interact and negatively regulate CLOCK-BMAL1-induced transcription. *Neuron* **21:** 1101–1113.

Shearman, L.P., M.J. Zylka, D.R. Weaver, L.F.J. Kolakowski, and S.M. Reppert. 1997. Two period homologs: Circadian expression and photic regulation in the suprachiasmatic nuclei. *Neuron* **19:** 1261–1269.

Shigeyoshi, Y., K. Taguchi, S. Yamamoto, S. Takekida, L. Yan, H. Tei, T. Moriya, S. Shibata, J.J. Loros, J.C. Dunlap et al. 1997. Light-induced resetting of a mammalian circadian clock is associated with rapid induction of the *mPer1* transcript. *Cell* **91:** 1043–1053.

Sun, Z.S., U. Albrecht, O. Zhuchenko, J. Bailey, G. Eichele, and C.C. Lee. 1997. RIGUI, a putative mammalian ortholog of the *Drosophila period* gene. *Cell* **90:** 1003–1011.

Takumi, T., C. Matsubara, Y. Shigeyoshi, K. Taguchi, K. Yagita, Y. Maebayashi, Y. Sakakida, K. Okumura, N. Takashima, and H. Okamura. 1998a. A new mammalian period gene predominantly expressed in the suprachiasmatic nucleus. *Genes Cells* **3:** 167–176.

Takumi, T., K. Taguchi, S. Miyake, Y. Sakakida, N. Takashima, C. Matsubara, Y. Maebayashi, K. Okumura, S. Takekida, S. Yamamoto et al. 1998b. A light independent oscillatory gene *mPer3* in mouse SCN and OVLT. *EMBO J.* **17:** 4753–4759.

Takumi, T., Y. Nagamine, S. Miyake, C. Matsubara, K. Taguchi, S. Takekida, Y. Sakakida, K. Nishikawa, T. Kishimoto, S. Niwa et al. 1999. A mammalian ortholog of *Drosophila timeless*, highly expressed in SCN and retina, forms a complex with mPER1. *Genes Cells* **4:** 67–75.

Tei, H., H. Okamura, Y. Shigeyoshi, C. Fukuhara, R. Ozawa, M. Hirose, and Y. Sakaki. 1997. Circadian oscillation of a mammalian homologue of the *Drosophila period* gene. *Nature* **389:** 512–516.

Todo, T., H. Ryo, K. Yamamoto, H. Toh, T. Inui, H. Ayaki, T. Nomura, and M. Ikenaga. 1996. Similarity among the drosophila (6-4)photolyase, a human photolyase homolog, and the DNA photolyase-blue-light photoreceptor family. *Science* **272:** 109–112.

van der Horst, G.T.J., M. Muijtjens, K. Kobayashi, R. Takano, S.-I. Kanno, M. Takao, J.D. Wit, A. Verkerk, A.P.M. Eker, D.V. Leenen et al. 1999. Mammalian *Cry1* and *Cry2* are essential for maintenance of circadian rhythms. *Nature* **398:** 627–630.

van der Spek, P.J., K. Kobayashi, D. Bootsma, M. Takao, A.P.M. Eker, and A. Yasui. 1996. Cloning, tissue expression, and mapping of a human photolyase homolog with similarity to plant blue-light receptors. *Genomics* **37:** 177–182.

Vitaterna, M.H., C.P. Selby, T. Todo, H. Niwa, C. Thompson, E.M. Fruechte, K. Hitomi, R.J. Thresher, T. Ishikawa, J. Miyazaki et al. 1999. Differential regulation of mammalian period genes and circadian rhythmicity by cryptochromes 1 and 2. *Proc. Natl. Acad. Sci.* **96:**12114–12119

Vosshall, L.B., J.L. Price, A. Sehgal, L. Saez, and M.W. Young. 1994. Block in nuclear localization of *period* protein by a second clock mutation, *timeless*. *Science* **263:** 1606–1609.

Whitmore, D., P. Sassone-Corsi, and N.S. Foulkes. 1998. PASting together the mammalian clock. *Curr. Opin. Neurosci.* **8:** 635–641.

Yagita, K. and H. Okamura. 2000. Forskolin induces circadian gene expression of *rPer1*, *rPer2* and *dbp* in mammalian rat-1 fibroblasts. *FEBS Lett.* **465:** 79–82.

Yagita, K., H. Okamura, and Y. Ibata. 1994. Rehydration process from salt-loading: Recovery of vasopressin and its coexisting galanin, dynorphin and tyrosine hydroxylase immunoreactivities in the supraoptic and paraventricular nuclei. *Brain Res.* **667:** 13–23.

Yamaguchi, S., S. Mitsui, L. Yan, K. Yagita, S. Miyake, and H. Okamura. 2000. Role of DBP in the Circadian Oscillatory Mechanism. *Mol. Cell. Biol.* (in press).

Young, M.W. 1998. The molecular control of circadian behavioral rhythms and their entrainment in *Drosophila*. *Annu. Rev. Biochem.* **67:** 135–152.

Zylka, M.J., L.P. Shearman, J.D. Levine, X. Jin, D.R. Weaver, and S.M. Reppert. 1998a. Molecular analysis of mammalian *timeless*. *Neuron* **21:** 1115–1122.

Zylka, M.J., L.P. Shearman, D.R. Weaver, and S.M. Reppert. 1998b. Three period homolog in mammals: Differential light responses in the suprachiasmatic circadian clock and oscillating transcripts outside of brain. *Neuron* **20:** 1103–1110.

MOLECULAR AND CELLULAR BIOLOGY, July 2000, p. 4773–4781 Vol. 20, No. 13
0270-7306/00/$04.00+0

Role of DBP in the Circadian Oscillatory Mechanism

SHUN YAMAGUCHI, SHIGERU MITSUI, LILY YAN, KAZUHIRO YAGITA, SHIGERU MIYAKE, AND HITOSHI OKAMURA*

Department of Anatomy and Brain Science, Kobe University School of Medicine, Kobe 650-0017, Japan

Received 10 January 2000/Returned for modification 3 March 2000/Accepted 20 March 2000

Transcript levels of DBP, a member of the PAR leucine zipper transcription factor family, exhibit a robust rhythm in suprachiasmatic nuclei, the mammalian circadian center. Here we report that DBP is able to activate the promoter of a putative clock oscillating gene, *mPer1*, by directly binding to the *mPer1* promoter. The *mPer1* promoter is cooperatively activated by DBP and CLOCK-BMAL1. On the other hand, *dbp* transcription is activated by CLOCK-BMAL1 through E-boxes and inhibited by the mPER and mCRY proteins, as is the case for *mPer1*. Thus, a clock-controlled *dbp* gene may play an important role in central clock oscillation.

Most eukaryotes and some prokaryotes have circadian (~24-h) rhythms governed by endogenous oscillators that control daily rhythms in physiology and behavior. Recent molecular dissections in cyanobacteria, *Neurospora*, *Drosophila*, and mice have revealed that oscillations in the transcription of specific clock genes play a central role in the generation of circadian rhythms and that negative feedback loops, in which certain gene products suppress their own transcription, form central elements of the mechanism of the circadian oscillator conserved across species (5, 17).

In mammals, the suprachiasmatic nucleus (SCN) is known as the anatomical locus of a dominant mammalian pacemaker for circadian behavior and hormonal rhythms (16, 21). Following the initial discovery of *mPer1* in the SCN (31) (Sun et al. reported the same gene, *RIGUI*, independently [28]), the first mammalian homologue of the *Drosophila* clock gene *per* (4, 13), many noticed that this gene is one of three genes of the mammalian *period* gene family; *Per2* (1, 26, 29) and *Per3* (30, 36) are also abundantly expressed in neurons of the SCN.

Among mammalian *per* homologues, evidence has accumulated that at least *mPer1* is a component constituting the central oscillatory mechanism. First, transcripts of *mPer1* show a very robust rhythm in the SCN in mice (28, 31) and rats (35), even in extended constant dark (DD) conditions (27). Second, the auto-negative feedback loop seems to be closed for the *mPer1* gene, as with the *Drosophila per* gene product PER, which negatively regulates the expression of its own gene (*per*) (11). The transcription of *mPer1* was shown to be activated by the binding of the CLOCK-BMAL1 complex to the E-boxes (CACGTG) in the promoter region of the *mPer1* gene (9), and this activation is specifically inhibited by PER1 protein and other negative elements, including PER2, PER3, TIM, CRY1, and CRY2 (14, 18, 23, 24). Third and perhaps more important is the finding that *mPer1* expression parallels the behavioral rhythm (27). *mPer1* is rapidly induced by light in a time-of-day and tissue-specific manner that correlates well with the resetting behavior of the overt rhythm in locomotor activity. Moreover, the photic thresholds and dose responses for the two processes are quantitatively very similar, and each shows reciprocity between light intensity and duration (27).

Besides the clock genes constituting this core oscillatory loop, a transcription factor, DBP (named for albumin gene D-site binding protein), is expressed in the SCN with clear rhythm in light-dark (LD) and DD conditions (20). We recently found that DBP is endogenously highly rhythmic, with an amplitude comparable to that of *mPer1*, and its expression is not influenced by environmental light (34). Short-duration light exposure does not alter the *dbp* mRNA levels at any circadian time. DBP belongs to the PAR leucine zipper transcription factor family, which includes thyrotroph embryonic factor (TEF) and hepatic leukemia factor (HLF), and is known to increase the transcription of several genes in the liver (22). Although DBP knockout mice are still rhythmic, they display significant differences in circadian locomotor activity. However, DBP protein is not required for the circadian expression of its own gene (20). Although these findings had previously been interpreted to suggest that DBP is located downstream of the clock, in the present study we present evidence that DBP functions upstream of the clock. During the analysis of the *mPer1* promoter region, we noticed that the nucleotide sequence located between −28 and −37 of the *mPer1* gene (+1 indicates the transcription initiation site) shows homology with the consensus DBP-binding sequence. Here we demonstrate that DBP directly binds to the *mPer1* promoter and thereby increases transcription. Furthermore, we show that DBP protein can be detected in the nuclei of pacemaker cells in the SCN concomitantly with a rise in *mPer1* RNA levels. We also show that *dbp* transcription is regulated by CLOCK-BMAL1 and PER/CRY as well as *mPer1*. Therefore, a clock-controlled *dbp* gene may play an important role in the central oscillatory mechanism.

MATERIALS AND METHODS

Genomic library screening and 5′-RACE analysis of *mPer1* gene. A mouse genomic λ phage library (Stratagene) was screened with a ^{32}P-labeled probe derived from the 5′ portion of the *mPer1* cDNA (encoding nucleotide residues 26 to 551 of *RIGUI* [GenBank accession number AF022992]) by PCR. Approximately 1.6×10^6 phage clones were screened as previously described (33), and 18 hybridization-positive clones were isolated. The overlapping regions of the independent clones were found to have an identical restriction map. Four representative clones were subcloned and subjected to further analysis. The entire 12.8-kbp region upstream of the 3′ end of exon 2 was sequenced.

To identify the transcription initiation site of the *mPer1* gene, 5′-RACE (rapid amplification of cDNA ends) analysis using a 5′-Full RACE core set (TaKaRa, Tokyo, Japan) was carried out according to the manufacturer's instructions. Total RNA (5 μg) prepared from the hypothalamus of mice sacrified at circadian time (CT) 4 (where CT0 is subjective dawn and CT12 is subjective dusk) was used for reverse transcription with 200 pmol of 5′-phosphorylated primer R1 (5′-ATGAGTTCTTTCTGG-3′, complementary to 641 to 627 of *RIGUI*) representing the 5′ portion of the *mPer1* coding region. Since this 5′-RACE analysis was carried out using inverse PCR, the cDNAs were circularized or

* Corresponding author. Mailing address: Department of Anatomy and Brain Science, Kobe University School of Medicine, 7-5-1 Kusunoki-cho, Chuo-ku, Kobe 650-0017, Japan. Phone: (81) 78 382 5340. Fax: (81) 78 382 5341. E-mail: okamurah@kobe-u.ac.jp.

concatenated with each other by T4 RNA ligase and then used as a template. Primer R2 (5′-GTCCTGCTCTGAGCTCGCACTCAGG-3′, complementary to nucleotide residues 576 to 552 of *RIGUI*) and primer F1 (5′-AACCCATCTAC CAGTGGCTGCAGCA-3′, residues 577 to 601 of *RIGUI*), both representing the further 5′ upstream portion of the *mPer1* coding region, were used for the first PCR (25 cycles of 94°C for 30 s, 65°C for 30 s, and 68°C for 30 s). Primer R3 (5′-AGGCTGTAGGCAATGGAGCTGCTGG-3′, complementary to nucleotide residues 551 to 527 of *RIGUI*) and primer F2 (5′-GTGAACAGTCAGCT CGAGCCAGGAC-3′, residues 602 to 626 of *RIGUI*) were employed for the second nested PCR (27 cycles of 94°C for 30 s, 65°C for 30 s, and 68°C for 30 s). The resultant products were electrophoresed on a 0.8% SeaKem GTG agarose gel (FMC Corp.). The specific 5′-RACE product of approximately 550 bp was extracted from the gel and subcloned into pCR2.1-TOPO (Invitrogen) for sequence determination.

Transcriptional assay. HepG2 cells were grown in Dulbecco's modified Eagle's medium (Nacalai Tesque, Kyoto, Japan) supplemented with 10% fetal bovine serum (Sigma). Cells were plated at ca. 6.0×10^5 cells per well in six-well plates 24 h before transfection. Cells were transfected with LipofectAmine-Plus reagent (Gibco; LipofectAmine, 8 μl; Plus reagent, 6 μl) according to the manufacturer's instructions. Unless otherwise noted, cells in each well were transfected with 1 μg (total) of expression plasmids with the indicated inserts in pcDNA3 (Invitrogen), 10 ng of reporter plasmids, and 0.01 to 0.1 ng of internal control plasmids. The total amount of DNA per well was adjusted by adding pcDNA3 vector. After 48 h, cells in each well were extracted with 200 μl of passive lysis buffer (Promega), and 20 μl of the extracts was taken for assays of firefly luciferase and *Renilla* luciferase by luminometry. For statistical analysis, a two-sample *t* test was applied.

For the transcriptional assay of the *mPer1* gene, reporter constructs and internal control plasmid were made as follows. A 1.3-kbp fragment derived from the 5′-flanking region of the *mPer1* gene (−1296 to +32; +1 indicates the transcription initiation site) was ligated to the *Renilla* luciferase reporter gene (1,212-bp *Hin*dIII-*Xba*I fragment of the pRL-TK vector [Promega]) and the simian virus 40 (SV40) polyadenylation signal (3,092-bp *Xba*I-*Mlu*I fragment of the pGL3-Basic vector [Promega]). PCR-based mutagenesis was used to construct the reporter plasmid containing the same 1.3-kb fragment of the *mPer1* promoter with the DBP-binding site mutated to TCGCCATGGC.

A 60-bp construct in which three copies of a 20-bp sequence centered on the DBP-binding site were linked in tandem was made by annealing oligonucleotides 5′-GATCTCTGGCATTATGCAACCCGCCCTGGCATTATGCAACCCGCC CTGGCATTATGCAACCCGCCA-3′ and 5′-GATCTGGCGGGTTGCATAA TGCCAGGGCGGGTTGCATAATGCCAGGGCGGGTTGCATAATGCC AGA-3′ (binding sites are underlined). The annealed oligonucleotides were inserted into the *Bgl*II site of the pRL-TK vector. A 60-bp construct in which three DBP-binding sites were mutated was constructed with oligonucleotides 5′-GATCTCTGGCTCACCCGGCTCCGCCCTGGCTCACCCGGCTCCG CCCTGGCTCACCCGGCTCCGCCA-3′ and 5′-GATCTGGCGGAGCCGGG TGAGCCAGGGCGGAGCCGGGTGAGCCAGGGCGGAGCCGGGTGAG CCAGA-3′ (mutated binding sites are underlined). These annealed oligonucleotides were also subcloned into the *Bgl*II site of the pRL-TK vector.

As the firefly luciferase gene of the pGL3-luciferase vectors (Promega) contains a sequence with 9 of 10 bases identical to the DBP consensus sequence (and is activated by transfection of DBP), we made the following internal control plasmid and used a small amount (0.01 to 0.02 ng). The sequence 5′-GTTATG TAAA-3′ 1,204 nucleotide residues downstream from the translation initiation site was altered to 5′-GCTATGTGAA-3′ without changing the deduced amino acid sequence, and then the coding region was ligated to a 3,132-bp *Xba*I-*Nhe*I fragment derived from vector pRL-CMV (Promega), allowing expression from the cytomegalovirus (CMV) promoter.

For transcriptional assay of the *dbp* gene, reporter plasmids were made as follows. A 300-bp fragment containing the two E-boxes derived from the second intron of the mouse *dbp* gene (GenBank accession number U29762; nucleotide residues 2900 to 3200) was amplified from genomic DNA by PCR and subcloned into the pGL3-promoter vector (Promega). PCR-based mutagenesis was used to construct the reporter plasmids containing mutated E-boxes. The upstream and downstream E-boxes were replaced with TCGCTC and GCTAGT, respectively. The pRL-CMV vector (Promega) was used as an internal control for transcriptional assay of the *dbp* gene. The sequences of all reporter constructs were confirmed.

Expression constructs were made as follows. The coding regions of mouse *dbp* (GenBank accession number U29762), *mPer1* (AB002108), *mPer2* (AF035830), *mPer3* (AB013605), *mTim* (AB019001), *mCry1* (AB000777), and human *BMAL1b* (AB000813) were obtained by reverse transcription-PCR and used after confirming their sequences. The plasmids containing the human *Clock* (AB002332; KIAA0334 gene) and partial human *Cry2* (AB014558; KIAA0658 gene) were generously provided by Takahiro Nagase, KAZUSA DNA Research Institute. As the KIAA0658 gene lacks the 5′ end of the human *Cry2* coding region, an upstream 13-bp fragment was added by PCR according to the sequence of an expressed sequence tag (EST) clone (accession number AL040215). All coding regions were ligated into the pcDNA3 vector.

Gel shift assay. A double-stranded oligonucleotide (top strand, 5′-GGCAGG GCCTGGCATTATGCAACCCGCCTCC-3′; bottom strand, 5′-GGGAGGCG GGTTGCATAATGCCAGGCCCTGC-3′) including the DBP-responsive site derived from the *mPer1* promoter with its flanking sequences, was labeled at both ends with Klenow enzyme in the presence of [α-^{32}P]dCTP and used as a probe. The AP2 consensus binding probe was labeled in the same way using an annealed oligonucleotide (top strand, 5′-GGTGGAAAGTCCCCAGGCTGTGAATCC-3′; bottom strand, 5′-GGGATTCACAGCCTGGGGACTTTCCAC-3′). Nuclear extracts were prepared as described (25), and 8 μg was incubated with a radiolabeled probe. For the control experiment, 30 ng of human AP2 (Promega) was added. Binding reactions and electrophoresis were performed as described before (15). Competitors containing the PAR protein recognition sequence or the mutated sequence were made by annealing the oligonucleotides 5′-GTTCT TGGTTACGTAATCTCCAATGGTTCTT-3′ (top strand) and 5′-AAGAACC ATTGGAGATTACGTAACCAAGAAC-3′ (bottom strand) and 5′-GTTCTTG TCGCCATGGCCTCCAATGGTTCTT-3′ (top strand) and 5′-AAGAACCAT TGGAGGCCATGGCGACAAGAAC-3′ (bottom strand), respectively. For the supershift assays, 0.25 μl of DBP antiserum was added to DNA-protein complexes, and the incubation was continued for 15 min on ice.

Quantitative in situ hybridization using radiolabeled probes. (i) Animals. Male BALB/c mice (Japan Animal Company, Osaka, Japan) purchased 5 weeks postpartum were exposed to 2 to 4 weeks of complete light (fluorescent light, 300 lux)-dark (LD) cycles and then kept in complete darkness for 2 days as a continuation of the dark phase of the last LD cycle. The expression profiles of *mPer1* and *dbp* mRNA were examined in the second dark-dark (DD) cycle every 2 h ($n = 5$ at each time point) starting at CT0. The experimental protocol of the current research was approved by the Committee for Animal Research at Kobe University School of Medicine.

(ii) In situ hybridization. In situ hybridization histochemistry using the free-floating sections was performed according to the method detailed previously (2, 27). We used ^{33}P-radiolabeled complementary RNA (cRNA) probes for *mPer1* and *dbp* for the present in situ hybridization studies (27, 34). The radioactivity of each SCN on BioMax film (Kodak) was analyzed using a microcomputer interfaced to an image-analyzing system after conversion into the relative optical densities produced by the [^{14}C]acrylic standards. The intensities of the optical density of the 10 sections of the SCN were then summed. The results are expressed as means ± standard error of the mean (SEM). For statistical analysis, one-way analysis of variance (ANOVA) followed by Sheffe's multiple comparisons were applied. The peak value was adjusted to 100 (CT4 for *dbp*, and CT6 for *mPer1*), and relative RNA abundance was used.

Immunocytochemistry of DBP. (i) Antiserum to DBP. The total coding region of mouse *dbp* was subcloned into vector pGEX6P-1 (Pharmacia). The full length of DBP fused with glutathione-*S*-transferase (GST) was expressed in *Escherichia coli* and purified through a glutathione-Sepharose 4B column (Pharmacia). New Zealand White rabbits received a subcutaneous injection of purified antigen containing 50% Freund's complete adjuvant. The animals were boosted three times with purified antigen containing 50% Freund's incomplete adjuvant at 2-week intervals. Two weeks after the last injection, blood was collected. To remove antibodies which cross-react with other PAR proteins, antiserum was incubated with HLF-GST fusion protein bound to glutathione-Sepharose 4B. Antibodies were checked by Western blots of nuclear extracts of mouse liver and DBP expression plasmid-transfected HepG2 cells. In both cases, we detected a single band lying at a relative molecular mass of approximately 46 kDa, corresponding to the size reported previously (8).

(ii) Immunocytochemistry. Under deep ether anesthesia, DD-housed male BALB/c mice were examined for DBP expression in the second DD cycle every 2 h ($n = 4$ at each time point) starting at CT0.

Immunocytochemistry of DBP was performed using the avidin-peroxidase method as described previously (2). Immunoreactions were visualized with diaminobenzidine (DAB). The specificity was confirmed by dilution tests and absorption tests; 10 μg of purified antigen expressed in *E. coli* completely abolished the positive reaction. Quantitative analysis was performed in DBP-immunoreactive sections at each time point. We counted the number of immunoreactive nuclei in three sections in the middle portion of the SCN. We repeated the examination in four animals. Statistical analysis of the data was done by one-way ANOVA followed by Scheffe's multiple comparisons.

Double-labeling histochemical method for *mPer1* and *dbp*. To find out if cells express both *mPer1* and *dbp*, we used two double-labeling histochemical methods. Colocalization of two types of mRNAs was detected by double-labeling in situ hybridization using [^{35}S]CTP (New England Nuclear)-labeled *dbp* probe and digoxigenin-labeled *mPer1* probe in CT6 animals ($n = 3$). We made digoxigenin-labeled antisense *mPer1* cRNA probes using digoxigenin-UTP (Boehringer, Mannheim, Germany) following the manufacturer's instructions. Tissue preparation, prehybridization, hybridization, and posthybridization washing were the same as for isotope probe hybridization except that we used 20-μm-thick sections. For digoxigenin-labeled probes, sections were processed for immunocytochemistry with the nucleic acid detection kit (Boehringer).

We also tried to detect DBP protein and *mPer1* mRNA in single cells by double-labeling immunocytochemistry and in situ hybridization. Tissue fixation was performed at CT6 ($n = 3$) as for the in situ hybridization described above. The sections were processed for immunocytochemistry of DBP as described above. After the brown DAB reaction, sections were processed for prehybridization, hybridization, and posthybridization washes as described above. Perikaryal digoxigenin-labeled *mPer1* mRNA signals were stained blue with the nucleic acid detection kit (Boehringer).

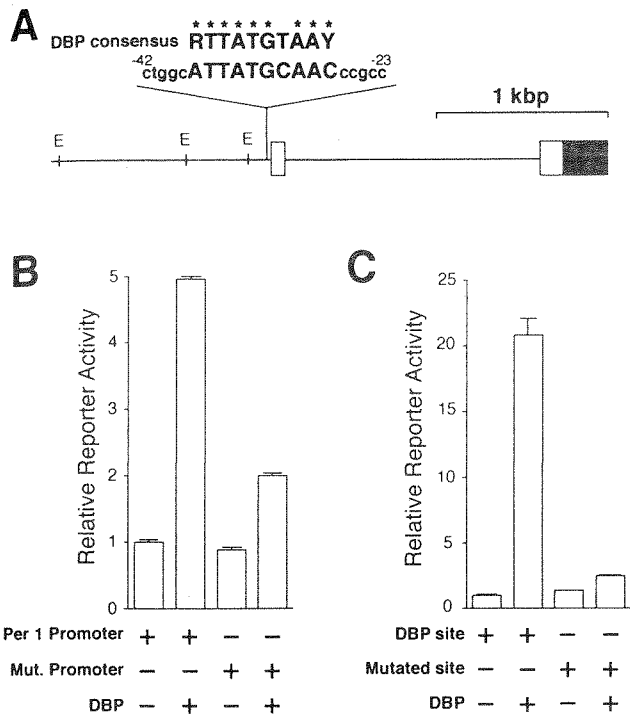

FIG. 1. Transcriptional regulation of the *mPer1* promoter by DBP. (A) A long vertical line indicates the site that matches the consensus DBP-binding sequence in the 5′-flanking region of the *mPer1* gene. The sequence of that site and 5 bp of flanking sequence (lowercase letters) on each side and the consensus DBP-binding sequence (R, purine; Y, pyrimidine) are noted (identical bases are shown by asterisks). The numbers of the nucleotide residues indicate the distance from the transcription start site. The solid and open boxes show the protein-coding region and the 5′ untranslated region, respectively. The locations of the E-box sites (E) are also indicated by short vertical lines. (B) Transcriptional activation of the reporter plasmid including the *mPer1* promoter. Reporter plasmids containing a 1.3-kbp fragment including the putative DBP-binding site (ATTATGCAAC) (Per1 promoter) or a mutated site (TCGCCATGGC) (Mut. promoter) were used for the transcriptional assay. (C) Transcriptional activation of an HSV-TK-driven reporter plasmid containing the putative DBP-binding site. A 60-bp construct in which three copies of either the putative DBP-binding site (DBP site) or a mutated site (TCACCCGGCT) (Mutated site) and flanking sequence were linked in tandem was subcloned into the HSV-TK-driven reporter plasmid. (B and C) Presence (+) or absence (−) of reporter and DBP expression plasmids (750 ng) is noted. Each value is the mean + SEM of three replicates for a single assay. The results shown are representative of at least three independent experiments.

Characterization of the *mPer1* antisense probe (nucleotide positions 538 to 1752) and *dbp* antisense probe (595 to 1100) used in this study was precisely described in previous reports (27, 34). The specificities of these probes were confirmed by RNase-digested sections and competition experiments.

RESULTS

DBP activates *mPer1* promoter. Since the nucleotide sequence located between −28 and −37 in the *mPer1* gene shows homology with the consensus DBP-binding sequence (Fig. 1A) (9 of 10 bases match), we tested the ability of DBP to drive *mPer1* transcription through the putative DBP-binding site. A 1.3-kbp fragment of the 5′-flanking region of the *mPer1* gene containing the endogenous promoter including this potential site was subcloned into a promoterless reporter vector for use in transcriptional analysis in HepG2 cells. Acting through this promoter, DBP produced an increase in transcriptional activity (5.0-fold; $P < 0.001$) (Fig. 1B); this activation was dependent on the putative DBP-binding site, because mutation of this site reduced the transcriptional activation by DBP from 5.0-fold to 2.0-fold (Fig. 1B). To confirm that this putative binding site is actually responsive to DBP, we next examined the transcriptional activity of a construct in which three copies of a 20-bp sequence centered on that site were linked in tandem and subcloned into a reporter vector containing the herpes simplex virus thymidine kinase (HSV-TK) minimal promoter. DBP produced a substantial activation through this tandem repeat (20.8-fold; $P < 0.001$) (Fig. 1C), and this activation was reduced from 20.8-fold to 2.5-fold when the three putative DBP-binding sites were mutated (Fig. 1C). Thus, we conclude that DBP is able to activate the *mPer1* promoter through this site in vitro.

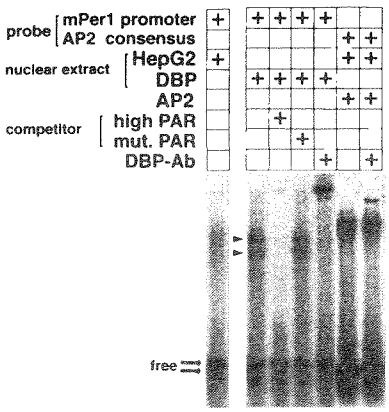

FIG. 2. Binding of DBP to the *mPer1* promoter. Gel shift assays with a probe encompassing the putative DBP-binding site derived from the *mPer1* promoter were performed. Nuclear extracts from untransfected (HepG2) or DBP expression plasmid-transfected (DBP) HepG2 cells were incubated with the probe. For the competition experiment, a 100-fold excess of a double-stranded oligonucleotide containing the PAR protein recognition sequence GTTACGTAAT (high PAR) or containing the mutated sequence TCGCCATGGC (mut.PAR) was added. For the supershift experiment, 0.25 μl of DBP antiserum was added. The complex of human AP2 and an AP2 consensus binding probe was not affected by adding the DBP antiserum. The presence (+) of each probe, nuclear extract, AP2, competitor, and anti-DBP antibody is noted. Arrowheads indicate two bands representing complexes of DBP and the probe. Thick arrows point to the locations of the free probes.

DBP directly binds to *mPer1* promoter. The optimal core binding motif for DBP, RTTATGTAAY (where R is a purine and Y is a pyrimidine), is known to be bound by the other members of the PAR and C/EBP families of basic leucine zipper proteins (7). Thus, we used a gel shift assay to examine whether transcriptional activation by DBP is due to direct binding of DBP to the *mPer1* promoter or to indirect mechanisms, including other regulatory proteins. When a radiolabeled 32-bp probe encompassing the putative DBP-binding site was incubated with nuclear extract from untransfected HepG2 cells, only weak smeared bands corresponding to endogenous proteins were observed (Fig. 2). In contrast, nuclear extracts from cells transfected with the DBP expression vector gave rise to two intense bands. These intense bands were abolished by a 100-fold excess of an unlabeled competitor containing PAR protein high-affinity sequence; on the other hand, they were not affected by a 100-fold excess of competitor containing a mutated sequence (Fig. 2). Thus, these intense bands represent specific protein-DNA complexes.

To characterize the proteins involved in the protein-DNA complexes, DBP antiserum was added to the binding reaction for the nuclear extract from the DBP-expressing cells. The resultant protein-DNA complexes showed a supershifted band, and the two intense bands previously observed were diminished (Fig. 2). This is a specific effect of the antiserum with

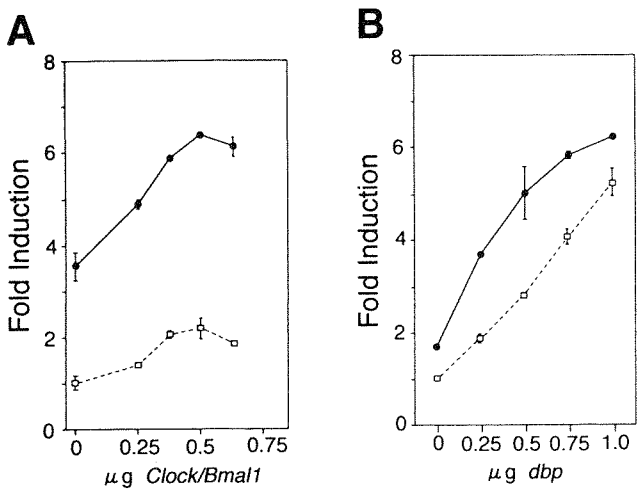

FIG. 3. Transcriptional activation of the *mPer1* promoter by DBP and CLOCK-BMAL1. (A) Dose-response curve of CLOCK-BMAL1-mediated transcriptional activation in the presence and absence of DBP. The reporter plasmid which contains the 1.3-kbp *mPer1* promoter, including the three E-boxes and the DBP-responsive site, was used. Increasing doses of CLOCK and BMAL1 expression plasmids were transfected with (solid line) or without (dashed line) 750 ng of DBP expression plasmid. The total amount of DNA (2 μg) per well was adjusted by adding pcDNA3 vector. (B) Dose-response curve of DBP-mediated transcriptional activation in the presence and absence of CLOCK-BMAL1. Increasing doses of DBP expression plasmid were transfected with (solid line) or without (dashed line) 500 ng each of CLOCK and BMAL1 expression plasmids. (A and B) Each value is the mean ± SEM of duplicate for a single assay. A similar pattern of activation was reproduced in another experiment.

DBP, since a complex of AP2 transcription factor with its consensus binding probe was not affected by adding DBP antiserum (Fig. 2). Thus, the two intense bands contain the DBP proteins. Although DBP can form heterodimers with HLF and TEF (8), the endogenous expression levels of these proteins in HepG2 cells are low (data not shown). Therefore, each of the intense bands may represent different posttranslational modifications or proteolytic products.

Taken together with the ability of DBP to drive *mPer1* in the transcriptional assay, it is suggested that DBP positively regulates *mPer1* gene expression by directly binding to the *mPer1* promoter.

DBP and CLOCK-BMAL1 cooperatively activate the *mPer1* promoter. Since the CLOCK-BMAL1 complex is already known to activate transcription through E-boxes in the *mPer1* promoter (9), we next tested for a possible interaction with DBP. The 1.3-kbp *mPer1* promoter reporter plasmid includes the three E-boxes and the DBP-responsive site (Fig. 1A), and it was cotransfected with CLOCK, BMAL1, and DBP expression plasmids.

The *mPer1* promoter responded in a dose-dependent manner to increasing amounts of transfected CLOCK and BMAL1 expression vectors in the absence of the DBP expression vector (Fig. 3A). The small increase in transcriptional activity (maximum 2.3-fold; $P < 0.01$) that we observed might be due to the HepG2 cells used in this assay, since a more substantial increase was observed when other cell lines, such as NIH 3T3 cells, were used (data not shown). Coexpressing DBP at any dose of CLOCK and BMAL1 expression plasmids further increased the transcriptional activation (maximum 6.6-fold; $P < 0.001$) (Fig. 3A). This response is additive rather than synergistic, because the activation induced by both DBP and CLOCK-BMAL1 is close to the sum of the effects of each working alone.

This additive effect is also observed at any dose of DBP expression plasmid when 0.5 μg each of CLOCK and BMAL1 expression plasmids were cotransfected (Fig. 3B). These observations indicate that DBP and CLOCK-BMAL1 cooperatively activate the *mPer1* transcription in an additive fashion.

Circadian expression of DBP is in phase with the transcription of *mPer1* in the SCN. *mPer1* transcripts exhibit a striking circadian oscillation in the SCN, peaking during the subjective morning (31). If DBP protein increases the transcription of *mPer1* in the SCN, as indicated by the transcriptional assay for the *mPer1* promoter, DBP protein should be expressed in advance of or at least in phase with *mPer1* transcription in the SCN. To test this hypothesis, we examined the precise circadian profiles in the mouse SCN of *dbp* mRNA and DBP protein and compared them to that of *mPer1* mRNA.

For detecting circadian changes in mRNA in the SCN, we adopted a well-established quantitative in situ hybridization with free-floating sections and examined DD-housed mice perfused for fixation every 2 h (27) (Fig. 4A). *dbp* mRNA levels were highest in the subjective morning at CT4 (CT0, subjective light on; CT12, subjective light off) and lowest in the subjective early night (CT18) ($P < 0.001$). The amplitude of this oscillation under DD conditions was over 10-fold.

Next, DBP protein expression was examined in the SCN by immunocytochemistry using anti-DBP serum (Fig. 4B). Analysis of the brains of mice sampled at CT6 showed DBP only in the nuclei (not cytoplasm) in the SCN (Fig. 4B, inset) as in other brain regions, including caudate-putamen and piriform cortex (data not shown). This characteristic of DBP nuclear antigenicity has already been reported in hepatocytes (22). The majority of SCN cells (>80%) appeared to be immunoreactive for the antigen tested, and the immunoreactivity is specific, being completely blocked by preincubation with affinity-purified DBP antigen (data not shown). In contrast, the SCN sampled at CT20 contained only a few weakly stained DBP-immunoreactive nuclei. Quantitative analysis of the number of immunoreactive nuclei in the SCN sampled at 2-h intervals over 24 h in DD showed a clear circadian variation (Fig. 4B). The abundance of proteins was low at subjective dawn (CT0) and rapidly increased to the highest level at CT6, and subsequently there was a progressive decline during subjective afternoon, producing trough levels in the subjective night ($P < 0.001$). In contrast, expression of DBP in other areas did not exhibit appreciable circadian variation (data not shown), consistent with the constitutive expression of mPER1 proteins in regions of the brain other than the SCN (12).

Thus, in the SCN, we found that the peak time of *dbp* mRNA accumulation was CT4 and that of DBP protein was CT6, and the time lag between the two was about 2 h. This is consistent with prior observations in the liver, where the appearance of *dbp* mRNA precedes DBP protein by about 2 h (6). The rapid translation and nuclear accumulation of DBP contrast strikingly with mPER1, which accumulates with a delay of about 6 h (12).

Next we compared the circadian profile of DBP protein with that of *mPer1* mRNA, which showed a peak at CT6 and a trough at CT20. Strikingly, the profiles of DBP protein accumulation and *mPer1* mRNA are the same (Fig. 4A and B). These data indicate that DBP is expressed at the right time to activate *mPer1* transcription in the SCN.

To test whether *dbp* and *mPer1* are coexpressed in the same cells within the SCN, we performed double-labeling in situ hybridization experiments on the SCN at CT6, when levels of both *dbp* and *mPer1* are high. We used an isotope-labeled *dbp* probe, which results in silver grains, and a digoxigenin-labeled *mPer1* probe, which gives a purple reaction product. In the

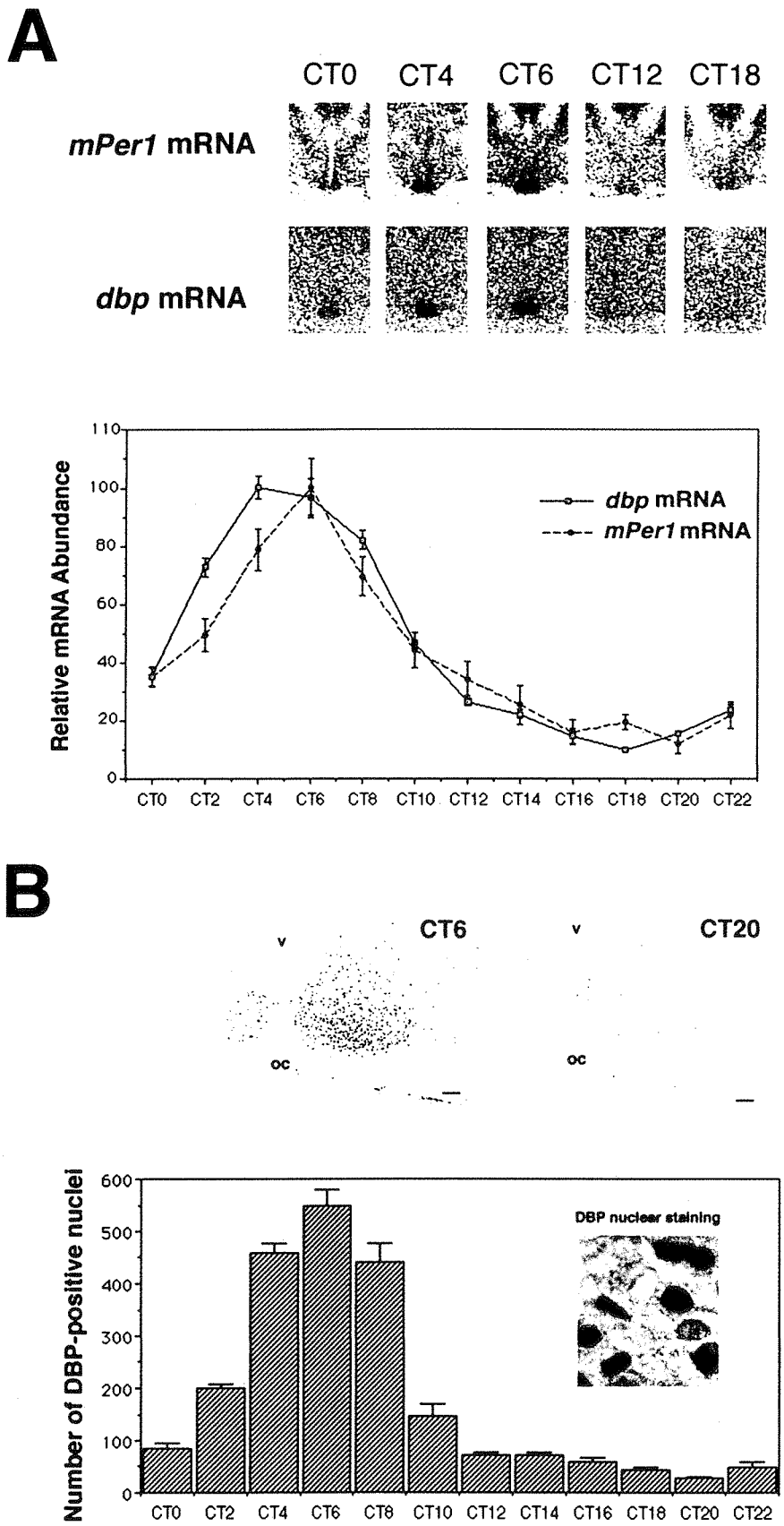

FIG. 4. Circadian expression of *dbp* and *mPer1* mRNA and DBP protein in the SCN. (A) Quantitative analysis of *dbp* (open square with blue line) and *mPer1* (solid circle with dotted black line) mRNA expressed in the SCN in DD conditions (n = 5, mean ± SEM). Relative *dbp* and *mPer1* mRNA abundance was determined by quantitative in situ hybridization using isotope-labeled probes with the mean peak values adjusted to 100. Representative in situ hybridization autoradiograms at specific time points are shown on the top panels. (B) Circadian expression of DBP immunoreactivity in the SCN. The photomicrographs show immunoreactivity at CT6 and CT20. Cell counts of SCN nuclei staining positive for DBP (per section) are shown. Values are means + SEM for four animals. oc, optic chiasma; v, third ventricle. Bar, 70 μm.

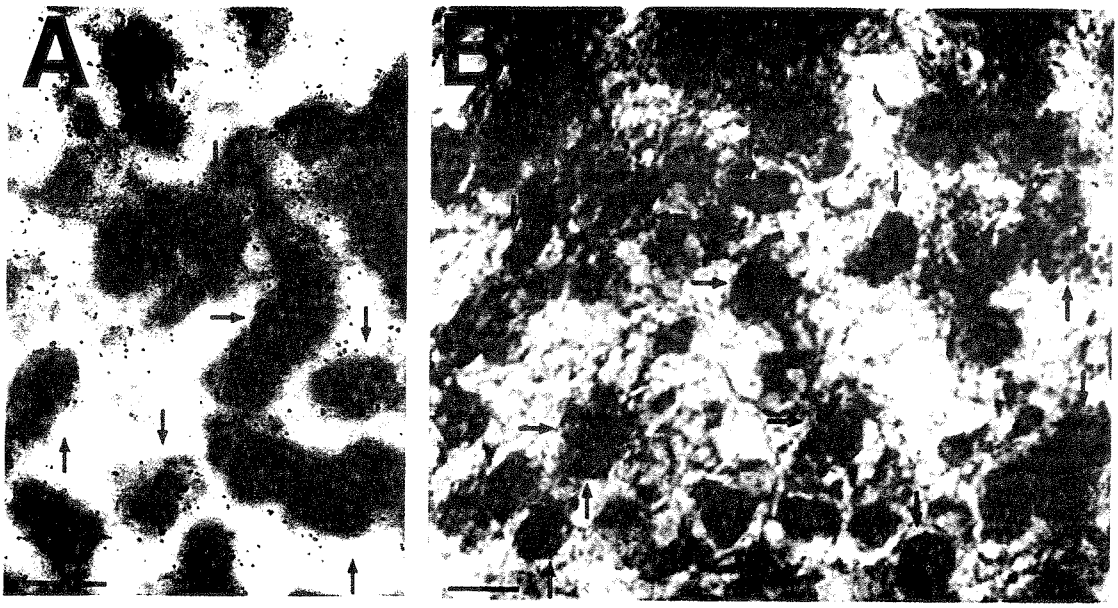

FIG. 5. Coexpression of *dbp* transcripts and DBP proteins with *mPer1* transcripts. (A) Double-labeling in situ hybridization using digoxigenin-labeled *mPer1* probe and isotope-labeled *dbp* probe. Note that most cells express both *mPer1* (purple) and *dbp* (silver grains) mRNAs. (B) Double labeling of *mPer1* in situ hybridization and DBP protein immunocytochemistry. Note that the blue stain of digoxigenin-labeled *mPer1* mRNA in the thin cytoplasm surrounds the brown-stained DBP protein localized in the nucleus. Arrows indicate representative double-labeled cells. All SCN sections were sampled at CT6. Bar, 10 μm.

SCN, most *mPer1* mRNA-positive cells also gave *dbp* mRNA-positive signals (Fig. 5A). This coexpression was confirmed by double-labeling using *mPer1* in situ hybridization and DBP protein immunocytochemistry. By this combination, we found that the cytoplasmic blue stain of digoxigenin-labeled *mPer1* mRNA surrounded the nuclear brown-stained DBP protein in many SCN cells (Fig. 5B). These findings demonstrate that DBP and *mPer1* are coexpressed in the majority of SCN cells. The results therefore show that DBP is expressed in the same cells as *mPer1* in the SCN and at the right time to participate in *mPer1* transcription. This adds in vivo relevance to our transcriptional and DNA-binding studies. We propose that DBP may accelerate *mPer1* transcription and contribute to the central oscillatory mechanism in SCN cells.

***dbp* transcription is activated by CLOCK-BMAL1 and suppressed by CRY1, CRY2, and mPER3.** The above findings suggest that rhythmic expression of *dbp* plays an important role in regulating the amplitude of the *mPer1* transcript rhythm. How then is the cyclic expression of *dbp* regulated? Circadian expression profiles indicate that transcription of *dbp* occurs with a similar phase to *mPer1*, although *dbp* is slightly earlier. Since *mPer1* transcription is known to be activated by the CLOCK-BMAL1 heterodimer through E-boxes (CACGTG) and suppressed by mPER1, mPER2, mPER3, mTIM, CRY1, and CRY2 (9, 14, 18, 23, 24), in the following experiments we examined the possibility that similar transcriptional regulation occurs for *dbp* gene transcription. The mouse *dbp* gene is composed of four exons, and data from mice lacking exons 1 to 4 has shown that this region is essential for the circadian expression of its own gene in the SCN (20). We found two E-boxes in the second intron, ~2.5 kbp downstream from the DBP transcription initiation site (Fig. 6A).

A 300-bp fragment centered on these E-boxes was subcloned into a reporter vector containing the SV40 promoter for use in transcriptional analysis in HepG2 cells. We found that CLOCK and BMAL1 together produced a large increase in transcriptional activity through this region (7.7-fold; $P < 0.001$) (Fig. 6B). Only a negligible increase was detected when either CLOCK or BMAL1 was examined alone. CLOCK-BMAL1 heterodimers apparently act through the E-box elements, because when both E-boxes were mutated, this activation was completely abolished. Unexpectedly, this CLOCK-BMAL1 activation was mainly dependent on the upstream E-box, because mutation of this site reduced the activation by CLOCK-BMAL1 from 7.7-fold to 1.5-fold, while mutation of the downstream E-box resulted in a small reduction (4.6-fold) (Fig. 6B). Interestingly, when compared to the reported sequence of the human *dbp* gene, the upstream E-box and the surrounding sequence are seen to be well conserved, but the downstream E box was replaced (CACGTG to GACGTG) in the human genome.

Although the E-boxes are located within an intron, they are thought to act as an enhancer which functions regardless of direction or location. In fact, in both cases when the fragment was inserted in the reverse 5′-to-3′ direction immediately upstream of the SV40 promoter or in the native 5′-to-3′ direction immediately downstream of the luciferase reporter gene, CLOCK-BMAL1 produced a large increase in transcriptional activity (10.1-fold [$P < 0.001$] and 8.8-fold [$P < 0.001$], respectively). Thus, the data indicate that CLOCK-BMAL1 has the ability to regulate DBP transcription through the E-boxes.

To investigate the negative elements which may contribute to DBP regulation, we examined whether mPER, mTIM, or CRY could individually inhibit CLOCK-BMAL1-induced transcription. Among them, mPER3 significantly reduced (24.3%; $P < 0.001$) and CRY1 and CRY2 completely abolished CLOCK-BMAL1-mediated transcription (Fig. 6C). Any possible combination of mPERs and mTIM expression plasmids did not inhibit more effectively than when they were transfected alone (data not shown). These results do not exclude the possibility that mPERs and mTIM are important for negative regulation, because endogenous expression of these genes is observed in the cell lines used (data not shown). Although the precise interactions among negative elements requires further analysis, the data imply that the

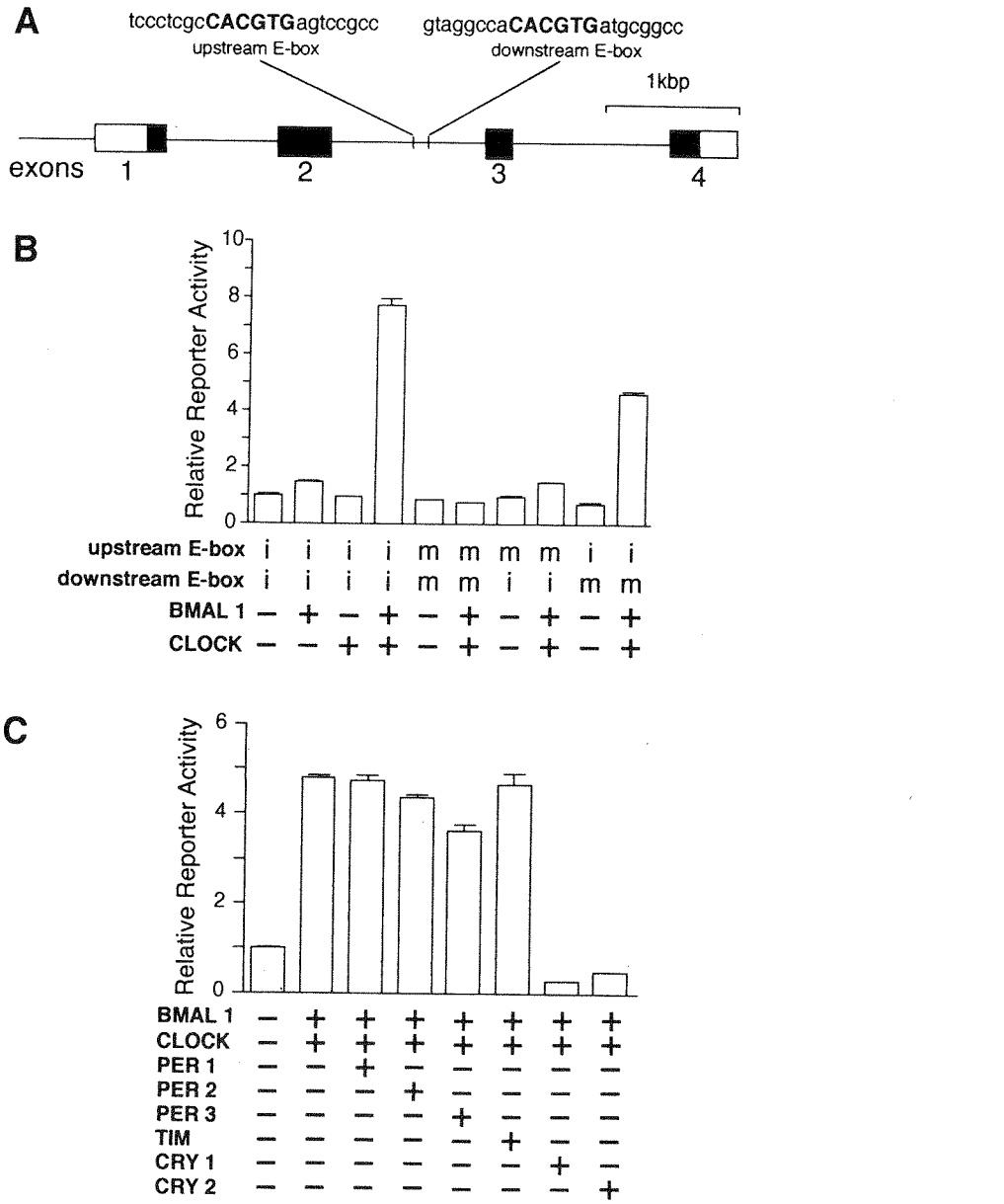

FIG. 6. Transcriptional regulation of the mouse *dbp* gene by clock genes. (A) Structure of the mouse *dbp* gene and locations of the E-box sites. The solid and open boxes show the protein-coding region and the 5′ and 3′ untranslated regions, respectively. The locations of the E-box sites are indicated by vertical lines, and the sequence of each E-box with 8 bp of flanking sequence (lowercase letters) on each side is shown at the top. (B) Transactivation from the E-box sites by CLOCK-BMAL1 heterodimer. For transcriptional analysis, an SV40-driven reporter containing a 300-bp fragment derived from the mouse *dbp* gene centered on the two E-boxes was constructed and used (2.5 ng). The fragment was inserted immediately upstream of the SV40 promoter in the native 5′-to-3′ direction. Reporter plasmids in which one or two E-boxes were mutated were also constructed and used. Intact (i) or mutated (m) E-box of each reporter plasmid is shown, and 500 ng each of expression plasmids was used. (C) Negative regulation of CLOCK-BMAL1-induced transcription. The reporter plasmid (5 ng) containing the 300-bp fragment with the intact E-boxes was used. The amounts of the expression plasmids used were 750 ng for BMAL1 and CLOCK; 125 ng for PER1, PER2, PER3, and mTIM; and 50 ng for CRY1 and CRY2. The total amount (2 μg) of DNA was adjusted by adding pcDNA3 vector. (B and C) Presence (+) or absence (−) of the expression plasmids is shown. Each value is the mean + SEM of three replicates for a single assay. The results shown are representative of at least three independent experiments.

dbp gene is regulated by central clock components, including CLOCK-BMAL1 and PER3, CRY1, and CRY2.

DISCUSSION

Molecular dissection of the mammalian clock oscillating system has been advanced using *Drosophila* as a model, because many genes structurally homologous to *Drosophila* clock genes are found in mammals. The first and most completely characterized clock gene in the animal kingdom is the *Drosophila per* gene. Three mammalian structural homologues were isolated from mouse and human (1, 25, 27, 29, 30), and among them *mPer1*, the first identified mouse *period* gene, attracted intense attention because it resembled the *Drosophila per* gene in many aspects (5). Transcription of *mPer1* is activated by binding of the CLOCK-BMAL1 heterocomplex, both of which are basic helix-loop-helix (bHLH)-PAS proteins, to the E-boxes in the promoter region of *mPer1*. The negative limb of the feedback

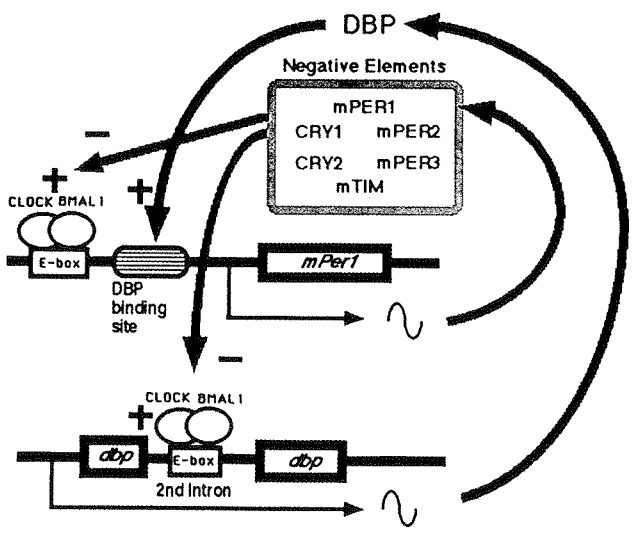

FIG. 7. Schematic representation of the role of DBP in the circadian oscillatory mechanism of the SCN. In addition to the negative autoregulatory feedback loop of *mPer1*, a DBP-mediated loop exists. As DBP protein positively regulates the *mPer1* promoter, DBP amplifies the circadian oscillation of *mPer1* and thereby influences the circadian oscillator.

loop includes mPER1, mPER2, mPER3, CRY1, CRY2, and mTIM, and these are thought to form a multimeric protein complex with CLOCK-BMAL1, similar to the fruit fly PER, TIM, and CLOCK (19), and to suppress transcription.

In the present study, we have integrated the *dbp* gene and DBP protein into this negative feedback loop (Fig. 7). In this model, at the phase of increasing *mPer1* transcription in the subjective morning, when negative elements cease their suppression of CLOCK-BMAL1-induced transactivation, CLOCK-BMAL1 begins to promote the transcription of *mPer1*. At the same time, CLOCK-BMAL1 binds to E-boxes in the second intron of the *dbp* gene and activates *dbp* transcription. Rapidly produced DBP proteins go into the nucleus and directly bind to the DBP-binding site of the *mPer1* promoter. There, DBP cooperatively increases the transcription rate of *mPer1*. During the subjective afternoon, when negative elements strongly suppress the CLOCK-BMAL1-induced transcription, the transcripts of *mPer1* and *dbp* decrease. The decrease in *dbp* transcripts is followed by the immediate decrease in DBP protein. Because *mPer1* is regulated by CLOCK-BMAL1, PER, CRY, and DBP, decreased DBP protein facilitates the decrease in *mPer1* transcripts. Thus, the time-specific appearance and disappearance of DBP may help to increase the amplitude of *mPer1* transcripts.

DBP as well as mTIM, mPER1, mCRY1, and mCRY2 (12, 18) is found in the nucleus of clock-oscillating SCN cells. These genes show time-specific expression in SCN cells except for mTIM, which is constantly expressed at all times examined (12). Interestingly, the peaks of CRY1, CRY2, and mPER1 proteins occur at subjective dusk (CT12) in the SCN (12, 18). However, the circadian expression profile of DBP was completely different from these and showed a peak in the subjective morning (CT6). Since DBP is a positive element and mPER1, mCRY1, and mCRY2 are negative elements, it is possible that these transcription factors are expressed according to their role in *mPer1* transcription and in the clock.

In addition to its role in core clock oscillation, DBP may also be involved in the circadian output system. It was recently shown that circadian oscillation of vasopressin mRNA levels is directly regulated by the central loop of the mammalian clock. The vasopressin gene is activated by CLOCK-BMAL1 heterodimers and repressed by the mPER, mTIM, and mCRY proteins through an E-box in the promoter region (14, 18). Therefore, output genes that may be responsible for changes in the physiology and behavior of the animal can be directly linked to the central clock mechanism. This type of clock gene regulation will fit genes having an E-box. The consensus binding site for DBP is different from the CLOCK-BMAL1 E-box binding site. Therefore, DBP, which is tightly linked to core clock oscillation, could potentially regulate a totally different set of output genes. In fact, DBP activates the transcription of some genes in the liver by directly binding to their promoters, such as the albumin, cholesterol 7α hydroxylase, and cytochrome P450 (CYP2C6) genes (7). Although the target genes in SCN neurons have not been elucidated at present, DBP may diversify the circadian output in the SCN.

Although DBP knockout mice are rhythmic with a slightly shortened period (20), this finding is consistent with the suggestion that DBP is an important component of the circadian clock. However, interpretation of this rhythmicity and short period length should be done with extreme discretion, since DBP is one of the PAR (proline and acidic amino acid-rich) leucine zipper transcription factors, as well as HLF and TEF (8). HLF and TEF may interact with DBP and share the possible binding sites (6). This kind of redundancy and complexity were found in *mCry* genes, composed of *mCry1* and *mCry2*. Although *mCry1 mCry2* double-knockout mice were completely arrhythmic, *mCry1* or *mCry2* single-knockout mice were rhythmic (31). Moreover, *mCry1* and *mCry2* single-knockout mice showed a shorter and longer free-running period, respectively (31), in spite of the indistinguishable actions of mCRY1 and mCRY2 proteins on the *mPer1* promoter (18). Further study of the potential influence of the other PAR leucine zipper transcription factors would thus be interesting.

Recently, the *Drosophila vri* (*vrille*) gene, which showed strong homology in its DNA-binding domain to DBP (10), was demonstrated to also be expressed in pacemaker cells (3). VRI also has a role in circadian locomotor activity: the gene dosage of *vri* affects the period of the circadian rhythm (3). VRI apparently lacks a PAR domain, which is conserved among DBP, HLF, and TEF. However, there is a set of proteins, including mammalian E4BP4, *Drosophila* Giant, and *Caenorhabditis elegans* CES2 (10), that have DNA-binding domains closely related to that of DBP but also lack a PAR domain. Interestingly, the E4BP4, Giant, and CES2 proteins all have the ability to repress transcription. Therefore, VRI may play a suppressive role in the *Drosophila* clock, in contrast to DBP's activating role. Indeed, recent data have shown that continuous *vri* expression decreases PER protein and *tim* mRNA levels (3). It is possible that the activating PAR leucine zipper proteins and the related repressing transcription factors make good complements to each other for regulating the clock.

In summary, our data indicate that DBP is part of the central oscillatory clock in mammals and has an important role in ensuring a precise 24-h rhythm. This finding will provide a new viewpoint for the circadian oscillatory system and suggests that this family of transcription factors may have roles in the clock in many diverse organisms.

ACKNOWLEDGMENTS

We thank K. Taguchi, S. Takekida, Y. Sumi, and H. Onishi for technical assistance; T. Nagase for providing human *Clock* and *Cry2* clones; K. Okubo for donating HepG2 cells; and J. Blau, M. Young, and Y. Shigeyoshi for useful discussions and comments on the manuscript.

This work was supported in part by grants from the Special Coordination Funds of the Science and Technology Agency of Japan, the Grant-in-Aid for the Scientific Research on Priority Areas of the Ministry of Education, Science, Sports and Culture of Japan, Mitsubishi Foundation, and SRF.

REFERENCES

1. **Albrecht, U., Z. S. Sun, G. Eichele, and C. C. Lee.** 1997. A differential response of two putative mammalian circadian regulators, mper1 and mper2, to light. Cell **91**:1055–1064.
2. **Ban, Y., Y. Shigeyoshi, and H. Okamura.** 1997. Development of circadian VIP rhythm in the rat suprachiasmatic nucleus. J. Neurosci. **17**:3920–3931.
3. **Blau, J., and M. W. Young.** 1999. Cycling vrille expression is required for a functional Drosophila clock. Cell **99**:661–671.
4. **Citri, Y., H. V. Colot, A. C. Jacquier, Q. Yu, J. C. Hall, D. Baltimore, and M. Rosbach.** 1987. A family of unusually spliced biologically active transcripts encoded by a *Drosophila* clock gene. Nature **326**:42–47.
5. **Dunlap, J. C.** 1999. Molecular bases for circadian clocks. Cell **96**:271–290.
6. **Falvey, E., F. Fleury-Olela, and U. Schibler.** 1995. The rat hepatic leukemia factor (HLF) gene encodes two transcriptional activators with distinct circadian rhythms, tissue distributions and target preferences. EMBO J. **14**: 4307–4317.
7. **Falvey, E., L. Marcacci, and U. Schibler.** 1996. DNA-binding specificity of PAR and C/EBP leucine zipper proteins: a single amino acid substitution in the C/EBP DNA-binding domain confers PAR-like specificity to C/EBP. Biol. Chem. **377**:797–809.
8. **Fonjallaz, P., V. Ossipow, G. Wanner, and U. Schibler.** 1996. The two PAR leucine zipper proteins, TEF and DBP, display similar circadian and tissue-specific expression, but have different target promoter preferences. EMBO J. **15**:351–362.
9. **Gekakis, N., D. Staknis, H. B. Nguyen, F. C. Davis, L. D. Wilsbacher, D. P. King, J. S. Tahahashi, and C. J. Weitz.** 1998. Role of the CLOCK protein in the mammalian circadian mechanism. Science **280**:1564–1569.
10. **George, H., and R. Terracol.** 1997. The vrille gene of Drosophila is a maternal enhancer of decapentaplegic and encodes a new member of the bZIP family of transcription factors. Genomics **146**:1345–1363.
11. **Hardin, P. E., J. C. Hall, and M. Rosbash.** 1990. Feedback of the drosophila period gene product on circadian cycling of its messenger RNA levels. Nature **343**:536–540.
12. **Hastings, M. H., M. D. Field, E. S. Maywood, D. R. Weaver, and S. M. Reppert.** 1999. Differential regulation of mPER1 and mTIM proteins in the mouse suprachiasmatic nuclei: new insights into a core clock mechanism. J. Neurosci. **11**:1–7.
13. **Jackson, F. R., T. A. Bargiello, S. H. Yun, and M. W. Young.** 1986. Product of per locus of Drosophila shares homology with proteoglycans. Nature **320**:185–188.
14. **Jin, X., L. P. Shearman, D. R. Weaver, M. J. Zylka, G. J. de Vries, and S. M. Reppert.** 1999. A molecular mechanism regulating rhythmic output from the suprachiasmatic nucleus. Cell **96**:57–68.
15. **Kageyama, R., Y. Sasai, and S. Nakanishi.** 1991. Molecular characterization of transcription factors that bind to the cAMP responsive region of the substance P precursor gene: cDNA cloning of a novel C/EBP-related factor. J. Biol. Chem. **266**:15525–15531.
16. **Klein, D. C., R. Y. Moore, and S. M. Reppert.** 1991. Suprachiasmatic nucleus: the mind's clock, p. 467. Oxford University Press, New York, N.Y.
17. **Kondo, T., and M. Ishiura.** 1999. The circadian clocks of plants and cyanobacteria. Trends Plant Sci. **4**:171–176.
18. **Kume, K., M. J. Zylka, S. Sriram, L. P. Shearman, D. H. Weaver, X. Jin, E. Maywood, M. H. Hastings, and S. M. Reppert.** 1999. mCRY1 and mCRY2 are essential components of the negative limb of the circadian clock feedback loop. Cell **98**:193–205.
19. **Lee, C., K. Bae, and I. Edery.** 1998. The Drosophila CLOCK protein undergoes daily rhythms in abundance, phosphorylation, and interactions with the PER-TIM complex. Neuron **21**:857–867.
20. **Lopez-Molina, L., F. Conquet, M. Dubois-Dauphin, and U. Schibler.** 1997. The DBP gene is expressed according to a circadian rhythm in the suprachiasmatic nucleus and influences circadian behavior. EMBO J. **16**:6762–6771.
21. **Moore, R. Y.** 1982. The suprachiasmatic nucleus and the organization of a circadian system. TINS (Trends Neurosci.) **5**:404–407.
22. **Mueller, C. R., P. Maire, and U. Schibler.** 1990. DBP, a liver-enriched transcriptional activator, is expressed late in ontogeny and its tissue specificity is determined posttranscriptionally. Cell **61**:279–291.
23. **Okamura, H., S. Miyake, Y. Sumi, S. Yamaguchi, A. Yasui, M. Muijtjens, J. H. Hoeijmakers, and G. T. van der Horst.** 1999. Photic induction of mPer1 and mPer2 in cry-deficient mice lacking a biological clock. Science **286**:2531–2534.
24. **Sangoram, A. M., L. Saez, M. P. Antoch, N. Gekakis, D. Staknis, A. Whiteley, E. M. Fruechte, M. H. Vitaterna, K. Shimomura, D. P. King, M. W. Young, C. J. Weitz, and J. S. Takahashi.** 1998. Mammalian circadian autoregulatory loop: a timeless ortholog and mPer1 interact and negatively regulate CLOCK-BMAL1-induced transcription. Neuron **21**:1101–1113.
25. **Schreiber, E., P. Matthias, M. Mueller, and W. Schffner.** 1989. Rapid detection of octamer binding proteins with "mini-extracts" prepared from a small number of cells. Nucleic Acids Res. **17**:6419.
26. **Shearman, L. P., M. J. Zylka, D. R. Weaver, L. F. J. Kolakowski, and S. M. Reppert.** 1997. Two period homologs: circadian expression and photic regulation in the suprachiasmatic nuclei. Neuron **19**:1261–1269.
27. **Shigeyoshi, Y., K. Taguchi, S. Yamamoto, S. Takekida, L. Yan, H. Tei, T. Moriya, S. Shibata, J. J. Loros, J. C. Dunlap, and H. Okamura.** 1997. Light-induced resetting of a mammalian circadian clock is associated with rapid induction of the *mPer1* transcript. Cell **91**:1043–1053.
28. **Sun, Z. S., U. Albrecht, O. Zhuchenko, J. Bailey, G. Eichele, and C. C. Lee.** 1997. RIGUI, a putative mammalian ortholog of the Drosophila period gene. Cell **90**:1003–1011.
29. **Takumi, T., C. Matsubara, Y. Shigeyoshi, K. Taguchi, K. Yagita, Y. Maebayashi, Y. Sakakida, K. Okumura, N. Takashima, and H. Okamura.** 1998. A new mammalian period gene predominantly expressed in the suprachiasmatic nucleus. Genes Cells **3**:167–176.
30. **Takumi, T., K. Taguchi, S. Miyake, Y. Sakakida, N. Takashima, C. Matsubara, Y. Maebayashi, K. Okumura, S. Takekida, S. Yamamoto, K. Yagita, L. Yan, M. L. Young, and H. Okamura.** 1998. A light independent oscillatory gene *mPer3* in mouse SCN and OVLT. EMBO J. **17**:4753–4759.
31. **Tei, H., H. Okamura, Y. Shigeyoshi, C. Fukuhara, R. Ozawa, M. Hirose, and Y. Sakaki.** 1997. Circadian oscillation of a mammalian homologue of the *Drosophila period* gene. Nature **389**:512–516.
32. **van der Horst, G. T., M. Muijtjens, K. Kobayashi, R. Takano, S. Kanno, M. Takao, J. de Wit, A. Verkert, A. P. Eker, D. van Leenen, R. Buijs, D. Bootsma, J. H. Hoeijmakers, and A. Yasui.** 1999. Mammalian Cry1 and Cry2 are essential for maintenance of circadian rhythms. Nature **398**:627–630.
33. **Yamaguchi, S., and S. Nakanishi.** 1998. Regional expression and regulation of alternative forms of mRNAs derived from two distinct transcription initiation sites of the rat mGluR5 gene. J. Neurochem. **71**:60–68.
34. **Yan, L., S. Miyake, and H. Okamura.** 1999. Distribution and circadian expression of dbp in SCN and extra-SCN areas in the mouse brain. J. Neurosci. Res., in press.
35. **Yan, L., S. Takekida, Y. Shigeyoshi, and H. Okamura.** 1999. *Per1* and *Per2* gene expression in the rat suprachiasmatic nucleus: circadian profile and the compartment-specific response to light. Neuroscience **94**:141–150.
36. **Zylka, M. J., L. P. Shearman, D. R. Weaver, and S. M. Reppert.** 1998. Three period homolog in mammals: differential light responses in the suprachiasmatic circadian clock and oscillating transcripts outside of brain. Neuron **20**:1103–1110.

extends lifespan in *Caenorhabditis elegans*. *Nature* 2001, **410:**227-230.
20. Rikke B, Murakami S, Johnson TE: **Paralogy and orthology of tyrosine kinases that can extend the life span of *Caenorhabditis elegans*.** *Mol Biol Evol* 2000, **17:**671-683.
21. Lin YJ, Seroude L, Benzer S: **Extended life-span and stress resistance in the *Drosophila* mutant methuselah.** *Science* 1998, **282:**943-946.
22. Service PM, Hutchinson EW, Mackinley MD, Rose MR: **Resistance to environmental stress in *Drosophila melanogaster* selected for postponed senescence.** *Physiol Zool* 1985, **58:**380-389.
23. Pierrou S, Hellquivist M, Samuelsson L, Enerback S, Carlsson P: **Cloning and characterization of seven human forkhead proteins: binding site specificity and DNA bending.** *EMBO J* 1994, **13:**5002-5012.
24. Ailion M, Inoue T, Weaver CI, Holdcraft RW, Thomas JH: **Neurosecretory control of aging in *Caenorhabditis elegans*.** *Proc Natl Acad Sci USA* 1999, **96:**7394-7397.
25. Hsin H, Kenyon C: **Signals from the reproductive system regulate the lifespan of *C. elegans*.** *Nature* 1999, **399:**362-366.
26. Murakami S, Johnson TE: **Regulation of life span in model organisms.** *Curr Genomics*, in press.
27. Sohal RS, Weindruch R: **Oxidative stress, caloric restriction, and aging.** *Science 1996,* **273**: 59-63.
28. Sagan LA: **What is hormesis and why haven't we heard about it before?** *Health Phys* 1987, **52:**521-525.
29. Bauxenbaum H: *Biological Effects of Low-Level Exposure to Chemicals and Radiation.* Ann Arbor, Michigan: Lewis Publications Inc.; 1992.
30. Tatar M, Khazaeri AA, Curtsinger JW: **Chaperoning extended life.** *Nature* 1997, **390:**30.
31. Parks TL, Elia AJ, Dickinson D, Hilliker AJ, Phillips JP, Boulianne GL: **Extension of *Drosophila* lifespan by overexpression of human SOD1 in motorneurons.** *Nat Genet* 1998, **19:**171-174.
32. Migliaccio E, Giorgio M, Mele S, Pelicci G, Reboldi P, Pandolfi PP, *et al.*: **The p66shc adaptor protein controls oxidative stress response and life span in mammals.** *Nature* 1999, **402**:309-313.
33. Fire A, Xu S, Montgomery MK, Kostas SA, Driver SE, Mello CC: Potent and specific genetic interference by double-stranded RNA in *Caenorhabditis elegans*. *Nature* 1998, **391:**806-811.
34. Paradis S, Ailion M, Toker A, Thomas TH, Ruvkun G: A PDK homolog is necessary and sufficient to transduce AGE-1 PI3 kinase signals that regulate diapause in *Caenorhabditis elegans*. *Genes Dev* 1999, **13:**1438-1452.
35. Taub J, Lau JF, Ma C, Hahn JH, Hoque R, Rothblatt J, *et al.*: **A cytosolic catalase is needed to extend adult lifespan in C. elegans *daf-c* and *clk-1* mutants.** *Nature* 1999, **399:**162-166.
36. Clancy DJ, Gems D, Harshman LG, Oldman S, Stocker H, Hafen E, *et al.*: **Extension of life-span by loss of CHICO, a *Drosophila* insulin receptor substrate protein.** *Science* 2001, **292:**104-106.
37. Tatar M, Kopelman A, Epstein D, Tu M-P, Yin C-M, Garofalo RS: **A mutant *Drosophila* insulin receptor homolog that extends life-span and impairs neuroendocrine function.** *Science* 2001, **292:**107-110.
38. Miller RA: **Genetics of increased and retarded aging in mice. *In* The Handbook of the Biology of Aging, 5th edn.** Edited by Masoro EJ, Austad SN. London: Academic Press; 2001:361-387.

Visualization of *mPer1* transcription in vitro: NMDA induces a rapid phase shift of *mPer1* gene in cultured SCN

Makoto Asai*†¥, Shun Yamaguchi*¥, Hiromi Isejima*‡, Masafumi Jonouchi§, Takahiro Moriya†, Shigenobu Shibata†, Masaki Kobayashi¶ and Hitoshi Okamura*

Many physiological and behavioral phenomena are controlled by an internal, self-sustaining oscillator with a periodicity of approximately 24 hr. In mammals, the principal oscillator resides in the suprachiasmatic nucleus (SCN). A light pulse during the subjective night causes a phase shift of the circadian rhythm via direct glutamatergic retinal afferents to the SCN [1]. Along with the accepted theoretical models of the clock, it is suggested that behavioral resetting of mammals is completed within 2 hr [2]; however, the molecular mechanism has not been elucidated. Here, we show the real-time image of the transcription of the circadian-clock gene *mPer1* in the cultured SCN by using the transgenic mice that carry a luciferase reporter gene under the control of the *mPer1* promoter [3]. The real-time image demonstrates that the *mPer1* promoter activity oscillates robustly in a circadian manner and that this promoter activity is reset rapidly (within 2–3 hr) when a phase shift occurs.

Addresses: *Division of Molecular Brain Science, Department of Brain Sciences, Kobe University Graduate School of Medicine, Chuo-ku, Kobe 650-0017, Japan. †Department of Pharmacology and Brain Science, School of Human Sciences, Waseda University, Tokorozawa 359-1192, Japan. ‡Department of Physics, Informatics, and Biology, Yamaguchi University, Yamaguchi 753-8512, Japan. §Division of Biology, Japan Lab Animals Company, Osaka 561-0802, Japan. ¶Department of Electronics, Tohoku Institute of Technology, Sendai 982-8577, Japan.

Correspondence: Hitoshi Okamura
E-mail: okamurah@kobe-u.ac.jp

¥These authors contributed equally to this work.

Received: **20 June 2001**
Revised: **30 July 2001**
Accepted: **20 August 2001**

Published: **2 October 2001**

Current Biology 2001, 11:1524–1527

0960-9822/01/$ – see front matter

Results and discussion

The luminescence from the suprachiasmatic nucleus (SCN) was considerably higher than that from the remaining outside region, thereby allowing the direct assessment of the *mPer1* gene's transcriptional activity only in the master clock, SCN (Figure 1a). The luminescence from the SCN cultures showed robust circadian oscillations with an amplitude (peak/trough ratio = 6.39 ± 0.35, mean ± SEM; n = 26; Figure 1b) comparable to that of the *mPer1* mRNA in vivo [4]. The luminescence gradually decreased in amplitude after several cycles but was recovered to the initial level by changing the culture medium (Figure 1b). With no changing of the culture medium, the peak intervals of the bioluminescence from a single culture showed no significant variation within at least four cycles. The average periods of the individual cultures were very close (95% of the mean values fell within 25.05 ± 0.61 hr, n = 20). We were able to monitor the clear and stable circadian rhythm of the *mPer1* gene transcription for more than 60 days by exchanging the medium every 4 days.

To respond rapidly to the changes in gene expression, a genetic reporter must have a short half-life within the biological system [5]. To assess the functional half-life of the luciferase proteins in this system, we inhibited protein synthesis by applying cycloheximide (10 μg/ml) to the culture medium. The luminescence decayed with a half-life of 1.4 hr. Considering the rapid turnover of the luciferase protein and the robust oscillation of the luminescence, this system seems to be suitable for monitoring the transcriptional dynamics of the *mPer1* gene in real time.

The key role of *mPer1* in the entrainment was speculated from the evidence that the application of *mPer1* antisense oligonucleotides blocked the light-induced phase shifts of the behavioral rhythm [6, 7]. To address the question of how rapidly the transcriptional activity of the *mPer1* gene is reset by a light pulse, we applied *N*-methyl-D-aspartate (NMDA) (as a counterpart of a light pulse in vitro [8]) to the SCN cultures at various time points. We chose the application of 30 μM NMDA for 30 min since we observed no or weak effects at 5 μM and 10 μM, and a toxic effect at 60 μM (data not shown).

When NMDA was applied at 6 hr after the peak point of the luminescence (in the decreasing phase), the next peak was significantly phase delayed in comparison to the control medium (NMDA, −1.94 ± 0.18 hr, n = 6; control, −0.23 ± 0.04 hr, n = 3; negative and positive values represent phase delays and phase advances, respectively; $p < 0.01$, Student's t test; Figure 2a,b). These findings were compatible with our previous study in vivo demon-

Figure 1

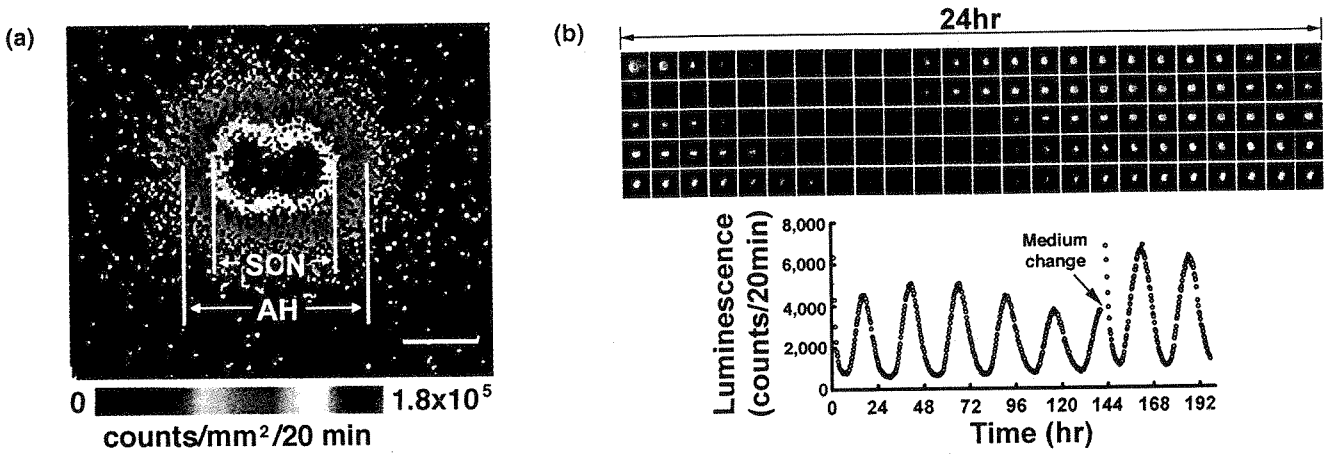

Continuous recording of bioluminescence in the culture of the suprachiasmatic nucleus (SCN) from the *mPer1-luc* transgenic mice. **(a)** High-power image of the bioluminescence in a SCN culture. During the measurement, 1 mM luciferin was added to the medium. Note that the SCN occupies the majority of the slice, and the surrounding anterior hypothalamic area (AH) is thin. The scale bar represents 500 μm. **(b)** Circadian fluctuation of bioluminescence in a SCN culture. The upper panels show the images integrated the bioluminescence for 20 min. The images are lined every three images (every 60 min) for 5 days. In the lower graph, each circle represents the total intensity of luminescence counted for 20 min. An arrow indicates the change of the culture medium.

strating the next peak in *mPer1* transcript levels following the light pulse is delayed by 2 hr as compared to the controls that did not receive light, although the immediate response of the bioluminescence to the NMDA application is quite little compared to the induced level of *mPer1* mRNA by light [4]. When NMDA was applied at 12 hr after the peak (in the trough phase of the luminescence), the phase was advanced (NMDA, 0.86 ± 0.10 hr, n = 3; control, 0.32 ± 0.09 hr, n = 3; $p < 0.05$) (Figure 2c,d). These responses were specific since the simultaneous application of 25 μM D-2-amino-5-phosphonovalerate (D-APV), an antagonist for NMDA receptor, abolished the effects completely (Figure 2e). Figure 3 shows the NMDA-induced phase shifts at various time points. Data were normalized to the circadian time calculated from the peak intervals of the bioluminescence, and the phase shifts were expressed as degrees of arc (see Figure 3 legend) to clarify the phase-response relationship. The direction and the magnitude of the NMDA-induced phase shifts were dependent on the circadian phase. The applications at 4.2–7.2 circadian hr after the peak caused phase delays, and the applications at 9.8–12.7 circadian hr caused phase advances. The contour of the phase-response curve corresponds well with the light-induced phase shifts of the locomotor activity in vivo [9].

To define how rapidly the resetting occurred in this system, we overlaid the wave form of the NMDA-treated cycle on that of the preceding cycle (Figure 4). When NMDA was applied at 6 hr after the peak, the wave form shifted right for 2–3 hr within 2 hr after the NMDA treatment (Figure 4a). The similar rapid right shifts (within 2 hr) were observed at the other time points of the delay part (4.2–7.2 circadian hr after the peak) of Figure 3 (data not shown). The application of NMDA at 12 hr after the peak shifted the graph to the left for about 1 hr within 2–3 hr after the NMDA treatment (Figure 4b). Similar rapidity of the phase shifts was observed at the other time points of the advance part (9.8–12.7 circadian hr after the peak) of Figure 3 (data not shown). Therefore, in cases both of phase delays and of phase advances, the phase shift of the bioluminescence was completed within 2–3 hr. This suggests that the resetting of the *mPer1* promoter's transcriptional activity has similar rapidity. By using a 2 pulse light paradigm, accepted theoretical models for the resetting and entraining of all circadian clocks, including those of mammals, hold that, unlike the overt rhythms driven by them (which take several days to reset), the biological oscillators themselves can be reset rapidly [10, 11]. This model was clearly established in the present study by the demonstration that the resetting occurs rapidly in the core oscillator based on a transcription-(post)translation feedback loop of a set of clock genes. The real-time imaging system in vitro together with the monitoring system in vivo [12, 13] will be useful for the elucidation of the transcriptional events of the clock genes in the circadian oscillatory mechanism.

Materials and methods

SCN culture

The neonatal (4- to 7-day-old) transgenic mice [3] maintained under the light-dark cycle (light for 12 hr, dark for 12 hr) were anesthetized with ether, and the brains were quickly removed. The coronal brain slices (400 μm thick), which contained the paired SCN, were made with a tissue chopper, and the brain slices were dissected carefully to minimize

Figure 2

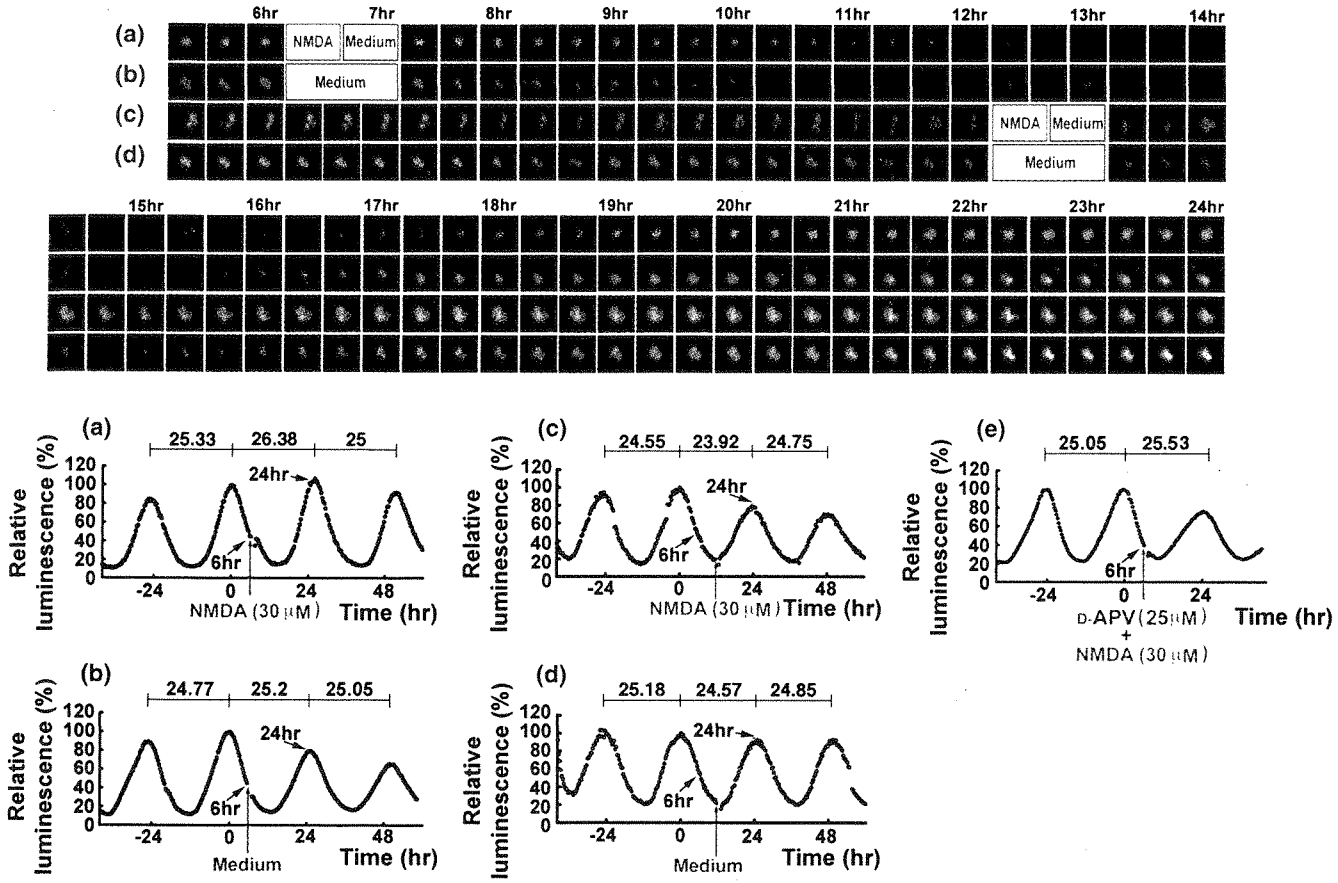

NMDA-induced phase shifts of luminescence. The application of NMDA induced the phase shifts of luminescence phase dependently. The images of the representative results are shown in the upper panels. The corresponding graphs are shown below defining the peak values (time 0) as 100%. **(a)** Exposure to NMDA at 6 hr after the peak of the luminescence induced a phase delay. **(c)** NMDA applied at 12 hr after the peak induced a phase advance. The exposure to the control medium without NMDA at **(b)** 6 hr and **(d)** 12 hr after the peak did not change the phase. **(e)** Simultaneous application of 25 μM D-APV completely abolished the NMDA-induced phase shift.

the outside regions of the SCN under a stereomicroscope. The SCN explants (approximately 0.7 mm long and 0.7 mm wide) were maintained on a membrane (Millicell-CM, Millipore, Bedford, Massachusetts, USA) dipped into a culture medium (50% minimum essential medium, 25% Hank's balanced salt solution, 25% horse serum, 36 mM glucose, and penicillin/streptomycin) at 35°C. The SCN cultures were incubated at least for a week, and bioluminescence recordings were started.

Bioluminescence recording

The SCN cultures were maintained in a sealed 35 mm petri dish with 1 ml of the culture medium containing 1 mM luciferin at 36°C. The bioluminescence from the SCN cultures was measured by a two-dimensional photon-counting camera (Imaging Photon Detector IPD 418, Photek, East Sussex, United Kingdom). An IBM PC-type computer that interfaced to a two-dimensional photon-counting camera that continuously recorded data integrated the bioluminescence for 20 min.

Drug application

In the experiment of NMDA-induced phase shifts, the SCN cultures were transferred to the control medium (50% minimal essential medium, 50% Hank's balanced salt solution, 36 mM glucose, and penicillin/streptomycin) with or without NMDA (30 μM) for 30 min at 36°C and were then washed with the control medium (three times) for 30 min at 36°C. After the wash, the SCN cultures were returned to the original culture medium. The application of NMDA (30 μM) with D-APV (25 μM) was performed on the same schedule. In the inhibition of protein synthesis, cycloheximide (10 μg/ml) was added to the culture medium.

Acknowledgements

Dr. Keiko Tominaga is acknowledged for the introduction of SCN slice culture. We thank Chikako Koike for assistance with manuscript preparation. This work was supported in part by grants from the Special Coordination Funds of the Science and Technology Agency of Japan; the Grant in Aid for the Scientific Research on Priority Areas of the Ministry of Education, Science, Sports, and Culture of Japan.

References

1. Moore RY: **The suprachiasmatic nucleus and the circadian timing system.** In *Suprachiasmatic Nucleus: The Mind's Clock.* Edited by Klein DC, Moore RY, Reppert SM. New York: Oxford University Press; 1991:13-15.
2. Best JD, Maywood ES, Smith KL, Hastings MH: **Rapid resetting of the mammalian circadian clock.** *J Neurosci* 1999, **19:**828-835.
3. Yamaguchi S, Mitsui S, Miyake S, Yan L, Onishi H, Yagita K, *et al.*: **The 5′ upstream region of *mPer1* gene contains two**

Figure 3

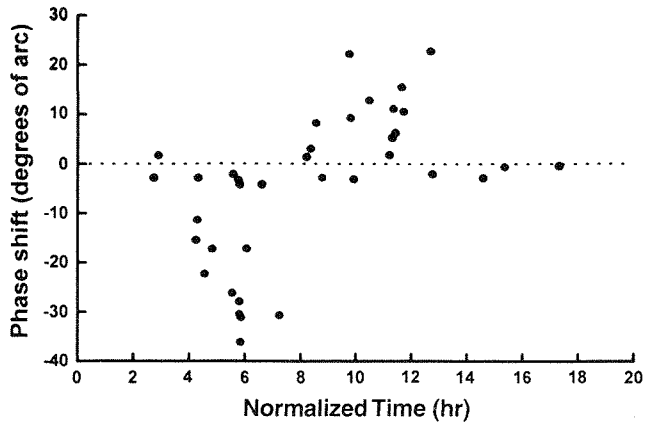

Direction and magnitude of phase shifts for NMDA treatment of the SCN culture. The *x* axis represents circadian hours (1 hr = free-running period/24 hr) from the peak point. The *y* axis represents phase shifts normalized into degrees of arc by multiplying each shift in hr by the factor 360°/free-running period [9, 10]. Blue dots represent the control group, and red dots represent the NMDA-treated group. The contour of the phase response was virtually the same as that obtained when the half-maximal points were used as reference points.

Figure 4

Wave form of the NMDA-treated cycle (red squares) and the preceding cycle (blue squares). The trough value of each cycle is defined as 0%. The decreasing phase (between the preceding peak and the trough) and the increasing phase (between the trough and the next peak) are shown, defining the preceding peak as 100% and the next peak as 100%, respectively. Each value is the mean ± SEM (n = 3). Application of NMDA **(a)** at 6 hr after the peak induced a phase delay and **(b)** at 12 hr after the peak induced a phase advance. Note that the phase shift of the bioluminescence is completed within 2–3 hr in both cases.

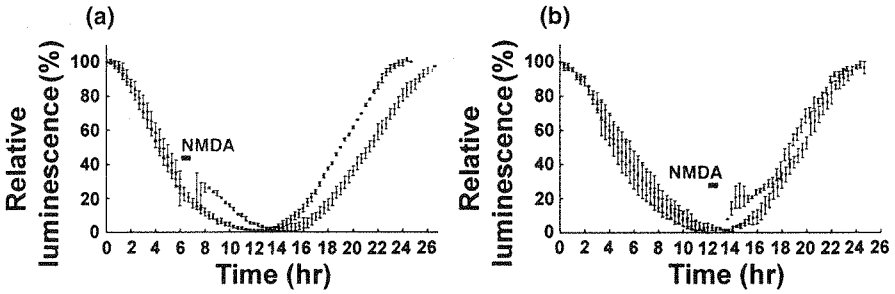

promoters and is responsible for circadian oscillation. *Curr Biol* 2000, **10:**873-876.

4. Shigeyoshi Y, Taguchi K, Yamamoto S, Takekida S, Yan L, Tei H, *et al.*: **Light-induced resetting of a mammalian circadian clock is associated with rapid induction of the *mPer1* transcript.** *Cell* 1997, **91:**1043-1053.
5. Wood KV: **Marker proteins for gene expression.** *Curr Opin Biotechnol* 1995, **6:**50-58.
6. Akiyama M, Kouzu Y, Takahashi S, Wakamatsu H, Moriya T, Maetani M, *et al.*: **Inhibition of light- or glutamate-induced *mPer1* expression represses the phase shifts into the mouse circadian locomotor and suprachiasmatic firing rhythms.** *J Neurosci* 1999, **19:**1115-1121.
7. Wakamatsu H, Takahashi S, Moriya T, Inouye ST, Okamura H, Akiyama M, *et al.*: **Additive effect of *mPer1* and *mPer2* antisense oligonucleotides on light-induced phase shift.** *Neuroreport* 2001, **12:**127-131.
8. Shibata S, Watanabe A, Hamada T, Ono M, Watanabe S: **N-methyl-D-aspartate induces phase shifts in circadian rhythm of neuronal activity of rat SCN in vitro.** *Am J Physiol* 1994, **267:**R360-364.
9. Schwartz WJ, Zimmerman P: **Circadian timekeeping in BALB/c and C57BL/6 inbred mouse strains.** *J Neurosci* 1990, **10:**3685-3694.
10. Pittendrigh CS: **Temporal organization: reflections of a Darwinian clock-watcher.** *Annu Rev Physiol* 1993, **55:**16-54.
11. Pittendrigh CS: **Circadian oscillations in cells and the circadian organization of multicellular systems.** In *The Neurosciences. Third Study Program.* Edited by Schmitt FO, Worden FG. Cambridge, Massachusetts: The MIT Press; 1974:437-458.
12. Yamaguchi S, Kobayashi M, Mitsui S, Ishida Y, van der Horst GT, Suzuki M, *et al.*: **View of a mouse clock gene ticking.** *Nature* 2001, **409:**684.
13. Yamazaki S, Numano R, Abe M, Hida A, Takahashi R, Ueda M, *et al.*: **Resetting central and peripheral circadian oscillators in transgenic rats.** *Science* 2000, **288:**682-685.

When more means less: neural activity related to unsuccessful memory encoding

Leun J. Otten and Michael D. Rugg

The neural correlates of memory encoding have been studied by contrasting neural activity elicited by items at the time of learning according to whether they were later remembered or forgotten [1]. Previous studies have focused on regions where neural activity is greater for subsequently remembered items [2–8]. Here, we describe regions where activity is greater for subsequently *forgotten* items. In two experiments that employed the same incidental learning task, activity in an overlapping set of cortical regions (posterior cingulate, inferior and medial parietal, and dorsolateral prefrontal) was associated with failure on a subsequent memory test.

Address: Institute of Cognitive Neuroscience and Department of Psychology, University College London, London WC1N 3AR, United Kingdom.

Correspondence: Leun J. Otten
E-mail: l.otten@ucl.ac.uk

Received: **23 July 2001**
Revised: **20 August 2001**
Accepted: **20 August 2001**

Published: **2 October 2001**

Current Biology 2001, 11:1528–1530

0960-9822/01/$ – see front matter

Results and discussion

With the advent of event-related fMRI, it has become possible to identify the neural correlates of the encoding of individual items into memory [1]. Neural activity is measured while volunteers study a sequence of items, after which each volunteer's memory for the items is tested. Activity elicited by the items at the time of study is then contrasted according to whether they were remembered or forgotten in the subsequent memory test. Differences between the activity elicited by subsequently remembered and subsequently forgotten items are taken as putative neural correlates of memory encoding. Using this approach, studies have identified a role for inferior frontal and medial temporal regions in the encoding of words into memory [2–8]. With one exception [8], these studies have only described regions that showed greater activity for subsequently remembered relative to subsequently forgotten items. However, the subsequent memory procedure permits detection of any region where activity is associated with later memory performance, and there is no a priori reason to suppose that the relationship between neural activity and successful encoding will invariably be a positive one. To gain a full understanding of the neural basis of memory encoding, it is arguably as important to identify processes that impair effective memory encoding as it is to characterize those that facilitate it. Here we describe data from two experiments that formed the basis of previous reports [6, 7] of regions where greater activity was associated with subsequent memory. In the analysis presented below, the focus was on regions demonstrating the inverse relationship. We took advantage of the fact that the two experiments each included as one of their experimental conditions the same incidental study task.

A number of native English-speaking volunteers (15 in experiment 1 [6] and 17 in experiment 2 [7]; mean ages of 26 and 25 years, respectively; 6 men in each case) gave written consent to participate in the two experiments, which were approved by the joint Medical Ethics Committee of the National Hospital for Neurology and Neurosurgery and the Institute of Neurology. The experiments consisted of two phases: an incidental study phase during which scanning took place, followed by a memory test performed outside the scanner after a delay of 15–20 min. During the study period, the volunteers viewed 280 critical words (4–9 letters, 1–30 occurrences per million) presented one at a time for 300 ms every 4–5 s. Each word was preceded by a cue, which indicated the type of decision that had to be made about the upcoming word. In both experiments, one of the cues indicated that the decision should be based on semantic properties of the word (whether or not the upcoming word was animate). Volunteers indicated their decision by pressing one of two buttons. During the test, all the studied words were presented again along with words not seen before in the experiment. For each word, volunteers decided whether or not they had seen the word during the study period and indicated whether they were confident or nonconfident about their decision.

A 2T Siemens VISION system was used to acquire both T1 anatomical volume images and T2*-weighted echoplanar images with blood oxygenation level-dependent contrast. Each echoplanar image comprised 31 axial slices, each 2 mm thick, acquired continuously during the study phase (TR of about 2.9 s). The processing of the image time series was as described previously [6, 7] and, along with the subsequent statistical analyses, was accomplished using Statistical Parametric Mapping (SPM99; www.fil.ion.ucl.ac.uk/spm/spm99.html). Item-related BOLD responses

The 5′ upstream region of *mPer1* gene contains two promoters and is responsible for circadian oscillation

S. Yamaguchi*, S. Mitsui*, S. Miyake*, L. Yan*, H. Onishi*, K. Yagita*, M. Suzuki†, S. Shibata‡, M. Kobayashi§ and H. Okamura*

The *mPer1* gene is assumed to be a key molecule in the regulation and functioning of the mammalian circadian clock, which is based on the oscillation generated by a transcription–(post)translation feedback loop of a set of clock genes [1]. Robust circadian oscillation and acute light-elicited induction of *mPer1* mRNA expression have been observed in the suprachiasmatic nucleus (SCN), the mammalian circadian center [2,3]. To investigate the mechanism underlying the complex regulation of *mPer1* expression, we isolated and characterized the 5′ upstream region of the *mPer1* gene. Unexpectedly, we identified two promoters, each followed by alternative first exons of *mPer1*. Consistent with the presence of multiple E-boxes in the promoters, exon-specific *in situ* hybridization of the SCN established that both promoters function in circadian oscillation and in light-induction of *mPer1* expression. Transgenic mice carrying the 5′ upstream region of the *mPer1* gene fused to the luciferase gene demonstrated that a DNA fragment carrying both promoter regions is sufficient to elicit striking circadian oscillation in the SCN and responsiveness to light. Moreover, luminescence in the SCN accurately mirrored the *mPer1* transcriptional activity. These transgenic mice will be very useful for monitoring clock-specific *mPer1* expression in intact organisms and to follow the circadian clock in real time.

Addresses: *Department of Anatomy and Brain Science, Kobe University School of Medicine, Kobe, Japan. †Institute of Molecular Embryology and Genetics, Center for Animal Resources and Development, Kumamoto University School of Medicine, Kumamoto, Japan. ‡Department of Pharmacology and Brain Science, School of Human Sciences, Waseda University, Tokorozawa, Japan. §Department of Electronics, Tohoku Institute of Technology, Sendai, Japan.

Correspondence: H. Okamura
E-mail: okamurah@kobe-u.ac.jp

Received: **2 May 2000**
Revised: **30 May 2000**
Accepted: **30 May 2000**

Published: **30 June 2000**

Current Biology 2000, 10:873–876

0960-9822/00/$ – see front matter

Results and discussion

To investigate the structural organization of the 5′ region of the *mPer1* gene, we identified the 5′ extreme sequence of *mPer1* mRNA by screening a mouse brain cDNA library (Figure 1). Twelve clones were isolated and these sequences were compared with the *mPer1* genomic sequence. Five clones contained a novel extreme 5′ sequence (exon 1A) that was connected to the exon 2 sequence. The other seven clones possessed the exon 1B

Figure 1

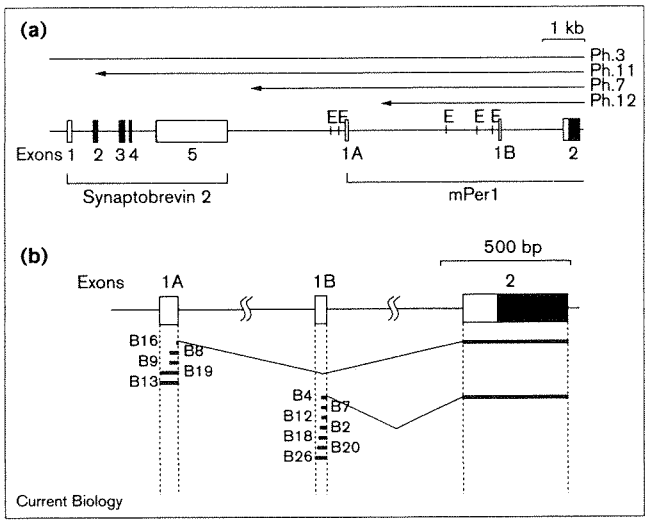

Structural organization of the 5′ region of the *mPer1* gene. **(a)** Exon/intron arrangements of the 5′ region of the *mPer1* gene. Four representative cloned genomic DNAs containing the *mPer1* gene (Ph.3, Ph.7, Ph.11 and Ph.12) were aligned according to restriction mapping and sequence determination. The closed and open boxes show protein-coding regions and the 5′- and 3′-untranslated regions, respectively. E, E-boxes. **(b)** Structures of cloned cDNAs containing 5′-upstream sequences of *mPer1*. A mouse (C57Bl/6J) brain cDNA plasmid library (SuperScript Mouse Brain cDNA Library, Gibco BRL) was subjected to the following serial PCRs: in the first PCR (30 cycles; 94°C for 1 min, 55°C for 1 min, 72°C for 1 min), the 5′ primer used was SP6 (5′-AGCTATTTAGGTGACACTATAG-3′) which corresponded to the vector sequence flanking the multiple cloning site, whereas the 3′ primer used was R1 (5′-GTCCTGCTCTGAGCTCG-CACTCAGG-3′, complementary to nucleotide residues 576–552 of *m-rigui*) which represented the exon 3 sequence. Then, a nested PCR (20 cycles; 94°C for 1 min, 55°C for 1 min, 72°C for 1 min) was performed with the use of SP6 nested primer (5′-TGCAGGTACCGG-TCCGGAATTC-3′) and R2 (5′-AGGCTGTAGGCAATGGAGCTGCT-GG-3′, complementary to nucleotide residues 551–527 of *m-rigui*) which represented an upstream sequence of exon 3. The locations of exons are indicated by open boxes (the 5′ untranslated region) and solid box (the protein-coding region). The sequences contained in individual cDNA clones are indicated below the exon structures by thick lines. The names of the cDNA clones are shown on the left. The intron sequences removed by splicing are shown by connective lines.

Figure 2

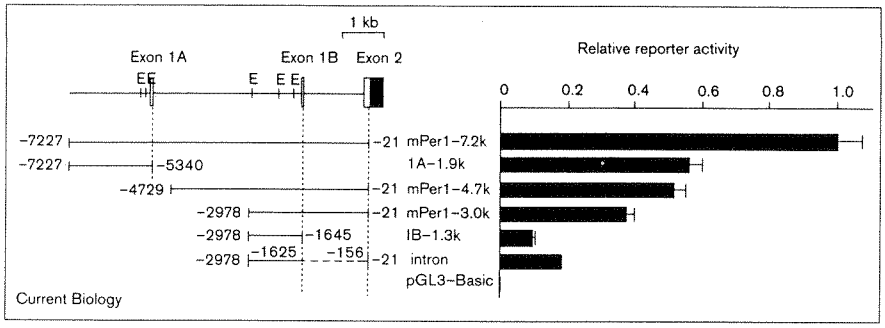

Deletion analysis of the *mPer1* promoter. Luciferase reporter plasmid containing either various lengths of the *mPer1* promoter or no promoter (pGL3-Basic) was transfected into NIH3T3 cells and luciferase assay was performed as described [9]. The number of moles of reporter constructs corresponding to 10 ng of the mPer1-7.2k reporter construct were transfected with 0.5 ng of pRL-CMV, a *Renilla* luciferase internal control plasmid (Promega). The total amount (1 μg) of the transfected DNA was also adjusted by adding pBluescript II plasmid (Stratagene). The sequences contained in individual reporter plasmids are indicated by lines below the exon structures shown as Figure 1a. The nucleotide residues of the 5′ and 3′ ends of the *mPer1* promoter used are numbered relative to the translation initiation (+1). The luciferase activity of each promoter was measured relative to that of mPer1-7.2k. Each value is the mean ± SEM of three replicates for a single assay. The results shown are representative of at least three independent experiments.

sequence corresponding to the 5′ portion of the *mPer1* cDNA reported previously (nucleotide residues 33–92 of *m-rigui*, as Sun *et al.* refer to *mPer1* gene [4]). Thus, this rescreening of the mouse cDNA library revealed that the 5′ extreme sequences of the *mPer1* mRNA start from two alternative first exons, which are then spliced out to form mature mRNAs containing the common exon 2 sequence. The 5′ extreme sequence of *m-rigui* (residues 1–32; GenBank accession number AF022992) was not found in the 12.8 kb upstream region of the *mPer1* gene and none of the cloned cDNAs containing the 5′ upstream sequence of *mPer1* possessed this sequence. The 5′ extreme sequence of *m-rigui* may be unique to specific mouse strains or an artifact of the cloning procedure. The nucleotide sequence of the 5′ region of the *mPer1* gene also revealed that *synaptobrevin 2* gene, encoding a small integral membrane protein specific to the synaptic vesicles in neurons, is located ~2.8 kb upstream from exon 1A of the *mPer1* gene (Figure 1a). Thus, this result suggested that our isolated genomic clones are sufficient to cover the *mPer1* promoter region.

To demonstrate that promoters exist upstream of each of the two exons and to examine the regions that regulate the activity, we analyzed the promoter activity of the *mPer1* gene using a transient transfection method. Various lengths of the 5′ region of the *mPer1* gene were subcloned into a promoterless reporter vector (pGL3-Basic) for transcriptional analysis in NIH3T3 cells. Figure 2 shows that the longest genomic DNA fragment (mPer1-7.2 k) that spanned the preceding region of exon 1A to the untranslated region of exon 2 demonstrated the highest transcriptional activity. Deletion of the 5′ extreme region including exon 1A (mPer1-4.7 k) showed moderately reduced promoter activity (48.8%, $p < 0.001$). Consistent with the results of the cDNA recloning, the 1.9 kb preceding region of exon 1A (1A-1.9 k) had a relatively high promoter activity (Figure 2). The 1.3 kb upstream region of exon 1B (1B-1.3 k) also had some promoter activity (Figure 2). Thus, we conclude that two functional promoters are located in the 5′ region of the *mPer1* gene. Moreover, a deletion of the 3′ flanking region of exon 1A (mPer1-3.0 k) or most of the intron between exon 1B and exon 2 (Δintron) led to a reduction in activity (27.3%, $p < 0.001$ and 50.0%, $p < 0.001$, respectively; Figure 2). These results suggest that *mPer1* expression is controlled by several regulatory regions.

To define which first exon is used in circadian oscillation and in light induction *in vivo*, we performed quantitative *in situ* hybridization analysis using the probes specific to exon 1A and exon 1B. Both mRNAs, containing either the exon 1A-containing sequence or the exon 1B-containing sequence, were expressed in the SCN at CT4 (CT, circadian time in constant dark condition; CT0 is subjective dawn and CT12 is subjective dusk), whereas little of either mRNA was expressed at CT16 (2.9-fold, $p < 0.001$ and 3.4-fold, $p < 0.001$, respectively; Figure 3a–c). Remarkably, a brief light pulse (600 lux, 30 minutes) delivered from CT15 to CT15.5 induced both mRNAs in the SCN (4.5-fold, $p < 0.001$ and 5.2-fold, $p < 0.001$, respectively; Figure 3a–c). These results suggest that both first exons are functional and both promoters are important not only in circadian oscillation but also in light induction.

It has been proposed that the cyclic expression of the *mPer1* mRNA in the SCN is generated by activation of the Clock–Bmal1 heterodimer through three E-boxes (CACGTG) in the 5′ flanking region of exon 1B [5], and by suppression of mPer1, mPer2, mPer3, mTim, Cry1 and Cry2 [6–8]. However, there are two E-boxes in the flanking region of exon 1A (Figure 1a), and these are also responsive to the Clock–Bmal1 heterodimer in transcriptional assays *in vitro* (S. Yamaguchi and H. Okamura, unpublished observations). Thus, not only the three E-boxes preceding exon 1B but also the two E-boxes preceding exon 1A may

contribute to the cyclic expression of *mPer1* mRNA. Many potential enhancers and regulatory DNA elements other than these E-boxes are also positioned in the flanking regions of exon 1A and 1B (see GenBank accession number AF223952). The sequence of up to 1830 bp determined for the 5′ flanking region of exon 1A contains three cyclic AMP-responsive elements (CREs), two AP-1 binding motifs, one proline and acidic amino acid-rich (PAR) protein binding motif, and one Egr-1 binding motif. In the sequence between exon 1A and exon 1B, there are one CRE, two AP-1, one AP-3 [13] and one PAR protein binding motif. Some of these motifs may contribute to the circadian oscillation or the light induction of the *mPer1* mRNAs.

To investigate whether or not the *mPer1* promoter region we identified is functional *in vivo*, we generated transgenic mice carrying the *mPer1* promoter–luciferase reporter gene. Based upon our characterization of the 5′ region of the *mPer1* gene, the 7.2 kb *mPer1* promoter-luciferase construct (mPer1-7.2k in Figure 2) was chosen as a transgene. Eight independent transgenic lines were obtained. From these lines, three lines were characterized in detail. Lines A3, B4 and D17 possessed 2, 18 and 12 copies, respectively, of the luciferase gene in the genomic DNA (data not shown). The regional distribution of luciferase mRNA in the brain was first examined by *in situ* hybridization analysis. Although D17 showed the highest expression level, all three lines exhibited a similar spatial expression pattern; expression levels were high in the SCN, and moderate in the cerebral cortex, hippocampus, thalamic nuclei and cerebellar cortex (data not shown). This expression profile resembles the reported distribution of *mPer1* mRNA in the brain [2].

We then examined the circadian expression profile of the luciferase mRNA of the D17 line in the SCN by quantitative *in situ* hybridization. Under extended constant dark conditions, the expression was very high at CT4, moderate at CT8 and CT12, and very low between CT16 and CT0 (Figure 4a). This temporal expression profile is very similar to that of *mPer1* mRNA [3]. The A3 and B4 lines also expressed high levels of luciferase mRNA in the SCN during subjective morning and low levels during subjective night (data not shown). Thus, we conclude that the 7.2 kb DNA fragment containing the two promoter regions is sufficient for the robust circadian oscillations in the SCN. We next investigated the response of the luciferase mRNA to light. When D17 transgenic mice were exposed to 30 minutes of light between CT15 and CT 15.5, the luciferase mRNA was significantly induced (4.7-fold, $p < 0.001$; Figure 4b). This suggests that the 7.2 kb DNA contains the light-responsive elements. However, the magnitude of the luciferase mRNA induction was lower than that of the native *mPer1* mRNA [3]. Therefore, further regulatory regions may function in light induction.

Figure 3

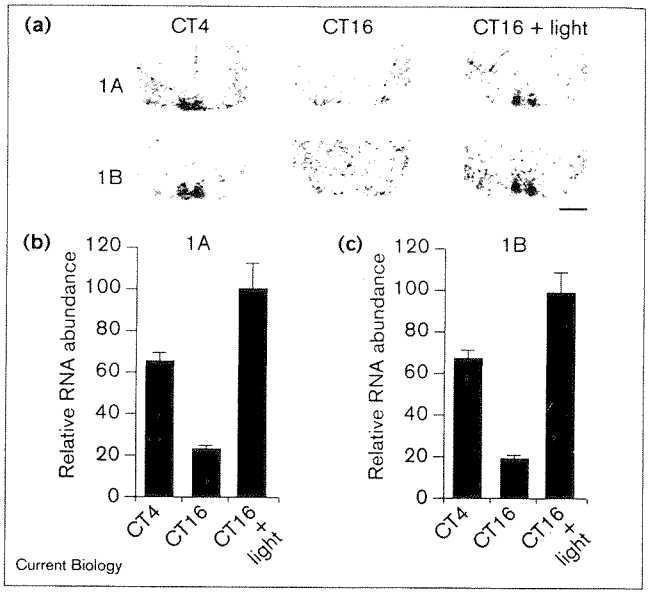

Expression of mRNAs containing exons 1A and 1B in mouse SCN. **(a)** Representative autoradiograms of *in situ* hybridization. For light induction experiments, mice were exposed to an incandescent light stimulus (600 lux, 30 min) at CT15 in the second DD cycle and sacrificed 60 min after the initiation of light exposure ($n = 5$ at each time point). Hybridization was performed by using oligonucleotide probes complementary to the 1A and 1B-containing mRNAs; 5′-AGTTCCGAGCGCACGTAGACTCCAAATTTCTT-3′ (32 mer), 5′-CTGGCCGTTCGAGCGCCCTCCATCCGCTTGCCGTTT-3′ (36 mer), respectively. The hybridization signal of each probe was completely abolished by an 1,000× excess of the same cold probe but was not blocked by an excess of the alternative cold probe. The scale bar represents 1 mm. **(b,c)** Quantitative analysis of the 1A and 1B mRNAs. Values were determined by quantitative *in situ* hybridization using isotope-labelled probes with the mean peak value of light-treated CT16 adjusted to 100. Values are expressed as means ± SEM ($n = 5$).

To examine the ability of the *mPer1* promoter–luciferase transgenic mice to monitor rhythmic changes in *mPer1* transcriptional activity by using bioluminescence, we imaged the bioluminescence from coronal brain slices containing the paired SCN with a two-dimensional photon-counting camera. The brain slices prepared from transgenic mice housed under 12 hour light:12 hour dark (LD) cycles, were placed immediately in phosphate-buffered saline with 1 mM luciferin. The spatial distribution pattern of the luminescence was very similar to that of the luciferase mRNAs (data not shown). The luminescence from the SCN showed a clear day–night variation (Figure 4c), although brain regions other than the SCN did not show appreciable differences of light emission by this imaging method. In the SCN, the signal level of luminescence was high between ZT4 and ZT9 but low between ZT18 and ZT0 (ZT, Zeitgeber time in LD condition; ZT0 = light on, ZT12 = light off; Figure 4c). Slices prepared from mice housed under constant dark conditions also showed a similar result (data not shown). Since the *mPer1* mRNA

Figure 4

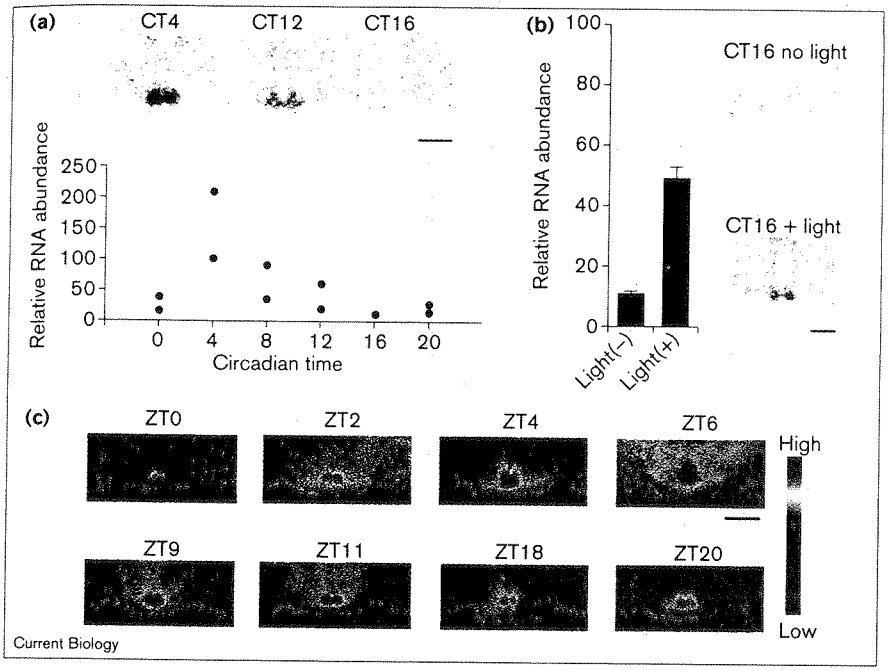

Expression of luciferase mRNA and bioluminescence in the SCN of transgenic mice carrying the *mPer1* promoter-luciferase gene (Line D17). **(a)** Quantitative *in situ* hybridization of the luciferase mRNA of the transgenic mice in the SCN with a ^{33}P-UTP-labelled cRNA probe. A single point represents the summation of signals of 10 sections from a single mouse. Two mice were used at each time point. Representative autoradiograms are shown on the top. **(b)** The effect of a light pulse on luciferase mRNA in the SCN of D17 mice. A 30 min light pulse was delivered as in Figure 3. In (b,c) the RNA levels are expressed relative to the mean value at CT16 (10). Values are expressed as means ± SEM ($n = 4$). **(c)** Day–night change of light emission from the SCN of D17 mice. Images displayed with pseudocolor represent accumulated photocounts. 500 μm coronal brain slices cut in the middle of the SCN were placed immediately in phosphate-buffered saline with 1 mM luciferin and recorded by the two-dimensional photon-counting camera (Imaging Photon Detector IPD 418, Photek) for 10 min at 25°C. The scale bars represent 1 mm.

shows a peak at ZT4–8 and a trough at ZT16–20 [3], the light emission from the SCN accurately mirrored the *mPer1* gene transcriptional activity. Therefore, the *mPer1* promoter–luciferase transgenic mice are useful to investigate the *mPer1* mRNA regulation in real time.

In conclusion, the novel findings of our study are as follows: first, there are two alternative splice forms of *mPer1*, one containing a previously unknown first exon; second, each of the alternative first exons (1A and 1B) is associated with its own predicted promoter, and the new promoter associated with exon 1A contains copies of the E-box element thought to be involved in regulation of the *mPer1* transcription, as was previously shown for the promoter now referred to as that associated with exon 1B; third, both forms of *mPer1* message are regulated in the SCN in a circadian manner, and both are induced in the SCN by light during subjective night; fourth, the 7.2 kb fragment including both promoters is sufficient to confer circadian regulation and light-responsiveness on a reporter gene *in vivo* in transgenic mice; and fifth, since the luminescence from the SCN accurately mirrors the *mPer1* gene transcriptional activity, the transgenic mice are instrumental for monitoring the *mPer1* mRNA regulation in real-time. These results will pave the way for monitoring the changes of the clock gene expression in living mice in real time.

Acknowledgements

We thank Y. Sumi, T. Fukuyama, Y. Ishida and S. Kitamura for assistance. This work was supported in part by grants from the Special Coordination Funds of the Science and Technology Agency of Japan, the Grant-in-Aid for the Scientific Research on Priority Areas of the Ministry of Education, Science, Sports and Culture of Japan, and Mitsubishi Foundation.

References

1. Dunlap JC: **Molecular bases for circadian clocks.** *Cell* 1999, **96**:271-290.
2. Tei H, Okamura H, Shigeyoshi Y, Fukuhara C, Ozawa R, Hirose M, *et al.*: **Circadian oscillation of a mammalian homologue of the *Drosophila period* gene.** *Nature* 1997, **389**:512-516.
3. Shigeyoshi Y, Taguchi K, Yamamoto S, Takekida S, Yan L, Tei H, *et al.*: **Light-induced resetting of a mammalian circadian clock is associated with rapid induction of the *mPer1* transcript.** *Cell* 1997, **91**:1043-1053.
4. Sun ZS, Albrecht U, Zhuchenko O, Bailey J, Eichele G, Lee CC: **RIGUI, a putative mammalian ortholog of the *Drosophila* period gene.** *Cell* 1997, **90**:1003-1011.
5. Gekakis N, Staknis D, Nguyen HB, Davis FC, Wilsbacher LD, King DP, *et al.*: **Role of the CLOCK protein in the mammalian circadian mechanism.** *Science* 1998, **280**:1564-1569.
6. Sangoram AM, Saez L, Antoch MP, Gekakis N, Staknis D, Whiteley A, *et al.*: **Mammalian circadian autoregulatory loop: a timeless ortholog and *mPer1* interact and negatively regulate CLOCK-BMAL1-induced transcription.** *Neuron* 1998, **21**:1101-1113.
7. Jin X, Shearman LP, Weaver DR, Zylka MJ, de Vries GJ, Reppert SM: **A molecular mechanism regulating rhythmic output from the suprachiasmatic nucleus.** *Cell* 1999, **96**:57-68.
8. Kume K, Zylka MJ, Sriram S, Shearman LP, Weaver DH, Jin X, *et al.*: **mCRY1 and mCRY2 are essential components of the negative limb of the circadian clock feedback loop.** *Cell* 1999, **98**:193-205.
9. Yamaguchi S, Mitsui S, Yan L, Yagita K, Miyake S, Okamura H: **Role of DBP in the circadian oscillatory mechanism.** *Mol Cell Biol* 2000, **20**:4773-4781.

讀賣新聞

THE YOMIURI SHIMBUN

5月7日 日曜日
2000年(平成12年)

発行所
読売新聞大阪本社
大阪市北区野崎町5-9
郵便番号 530-8551
電話(06)6361-1111

第17014号 (旧刊)©読売新聞大阪本社2000年

森首相が帰国

森首相は六日午後、七月の沖縄サミット（主要国首脳会議）に参加する米欧露七か国の訪問を終え、政府専用機で羽田空港に到着した。

（3、5、8面に関連記事）

光る「体内時計」

マウスで画像化 神戸大など成功

ホタル遺伝子組み入れ ▼ ▼ ▼ 目覚めて動くと青白く

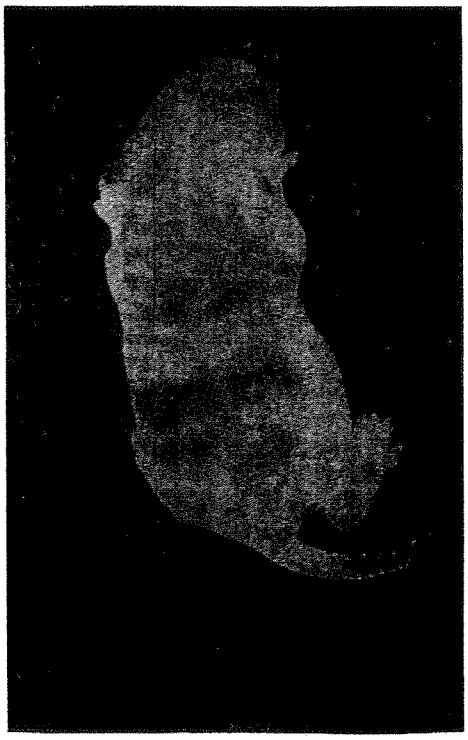

体内時計が活性化し青白く光るマウス（岡村均・神戸大教授提供）

目覚めると全身が光るマウスを作ることに、神戸大などの研究チームが六日までに成功し、画像にとらえた。生物には遺伝子の働きにより一日周期の生活リズムを刻む「体内時計」があり、この働きが活発になると全身が光る。遺伝子組み換えの技術を使い、ほ乳類としては世界で初めて体内時計の遺伝子の働きを刻一刻と見えるようにした。ナゾの多い体内時計の仕組み解明につながる画期的な成果で、米国で十日に始まる全米生体リズム学会で発表する。

ほ乳類は、脳の視床下部に体内時計の中枢があり、この「時計遺伝子」が作り出すたんぱく質の量が変化するのに応じて、遺伝子の働きを活性化させるスイッチが入ったり切れたりする仕組みを持ち、生活リズムを作り出している。

それに対応して、血圧や心拍数、陣痛の始まりやすさ、ホルモン濃度などが変動する。海外旅行などで起きる「時差ボケ」も、この体内時計と移動距離のズレを反映している。

その複雑で巧妙な仕掛けの解明には、動物の細胞単体を調べる研究だけでは不十分。時間の経過に沿って遺伝子の活動が変化する様子を、生きたままで確認できる研究手法の開発が急がれていた。

岡村均・神戸大医学部教授らは一九九七年、マウスの時計遺伝子を発見。その遺伝子に、ホタルの発光遺伝子を組み込んだマウスを作製。生まれて一週間後に暗室に入れ、超高感度の電荷結合素子（CCD）カメラで撮影した。

マウスは夜行性のため、行動が盛んな夜間には全身の皮膚が青白く光り、脳の中枢にある時計が出す指令に従って、体の各組織が同じリズムで同調した。寝ているときが多い昼間は、発光はほとんどなかった。

脳に光ファイバーを通し、遺伝子の活動の様子を生きたまま直接、連続的に記録できる装置も、柴田重信・早稲田大教授、小林正樹・東北工業大助教授と共同開発している。赤外線センサーで行動を記録することも可能で、岡村教授は、「生命現象を時間軸に沿って解析する新しい道が開けた。体内時計の全容解明に迫りたい」と話している。

◇

光るマウスの写真は、読売ニュース・ストリーム（http://www.yomiuri.co.jp/stream/）でも、見ることができる。

読売新聞
2000年5月7日(日)
朝刊
(1面)

神戸新聞

2001年4月13(金)

朝刊

皮膚細胞にも「体内時計」

睡眠、胃腸障害の遺伝子検査も可能に

ほぼ二十四時間周期の体内のリズムを制御している体内時計の遺伝子が、皮膚などの組織細胞内にも存在し、脳内の「親時計」と同調して働いていることを、神戸大医学部の岡村均教授（分子脳科学）らがオランダの研究者と共同で、マウスを使って突き止め、十三日発行の米科学誌サイエンスで発表した。

神大・岡村教授ら発見

脳内の中枢と連動

時計遺伝子の仕組みはほ乳類でほぼ共通するため、人にも同じ仕組みがあるとみられる。体内時計の異常で起きるとみられる睡眠障害や胃腸障害など、さまざまなリズム障害を皮膚細胞の遺伝子検査でも診断できると期待される。

ほ乳類では、左右の視神経が交差する脳の視床下部内の視交叉（しこうさ）上核という部分で「ピリオド」や「クロック」などの複数の時計遺伝子が確認されており、ここが体内時計の中枢と考えられている。

岡村教授らはマウスの皮膚の結合組織の線維芽細胞にも、これらと同じ時計遺伝子群があることを発見。

時計遺伝子によりつくられるタンパク質が一定量を超えると、逆にその生成が抑制されるという計時の仕組みも同じで、しかも脳内の親時計と連動して働いていることを確認した。

岡村教授は「今後は、親時計が末端の時計をどのように制御しているかを明らかにするのが課題。そして時計がなぜ一つではなく末端にもあるのかについても研究したい」としている。

日本経済新聞

2001年 4月13日(金)

朝刊

皮膚細胞にも「体内時計」

神戸大学がマウス実験

脳で約二十四時間のリズムを刻む「体内時計」の働きが、皮膚など末端の組織にもあることを神戸大学の研究チームがマウスの細胞を使った実験で突き止めた。体内時計の仕組みはほ乳類でほぼ共通のため、人間も同様の仕組みを持つとみられる。極端な睡眠障害など体内時計の異常による病気の診断や、治療薬開発の手がかりになる。

研究は岡村均医学系研究科教授らがオランダのエラスムス大学と共同で実施、十三日発行の米科学誌「サイエンス」に発表した。これまでに脳の視交叉（こうさ）上核と呼ばれる場所に体内時計の役割の細胞が存在、細胞内では十個近い遺伝子が協調して働いていることがわかっている。

岡村教授らはマウスの皮膚にある線維芽細胞に注目。複数の遺伝子が働くパターンを時間を追って調べたところ、脳内の「時計遺伝子」と同じ動きをしていることがわかった。岡村教授は「脳の親時計が何らかの仕組みで体内の子時計を制御しているのでは」とみている。

神戸新聞 2001年 4月26日(木)
朝刊(1面)

1 4版 (明治31年2月12日第3種郵便物認可) 神戸 亲

経済財政相 竹
文部科学相 遠

副大臣の人事 閣僚意向尊重

山崎幹事長

自民党の山崎拓幹事長は二十六日午前の記者会見で、組閣に伴う副大臣と政務官の人事について、再任か交代かの判断は閣僚の考えを尊重するとの方針を示した。

入閣予想顔触れ

これまでに固まった新内閣閣僚は次の通り (敬称略)

総務	片山虎
文部科学	遠山敦
厚生労働	坂口
国土交通	扇 千
環境	川口順
官房	福田康
金融	柳沢伯
経済財政	竹中平

ポスト調整中

田中真紀子、尾身幸

た。

長引く不況克服に向けた景気対策が新内閣の最大の課題。このため小泉氏は「構造改革なくして景気回復なし」をスローガンに経済、財政、社会保障、行政などの構造改

日銀は二十六日、今後一年程度にわたる国内経

日銀2001年経済見通

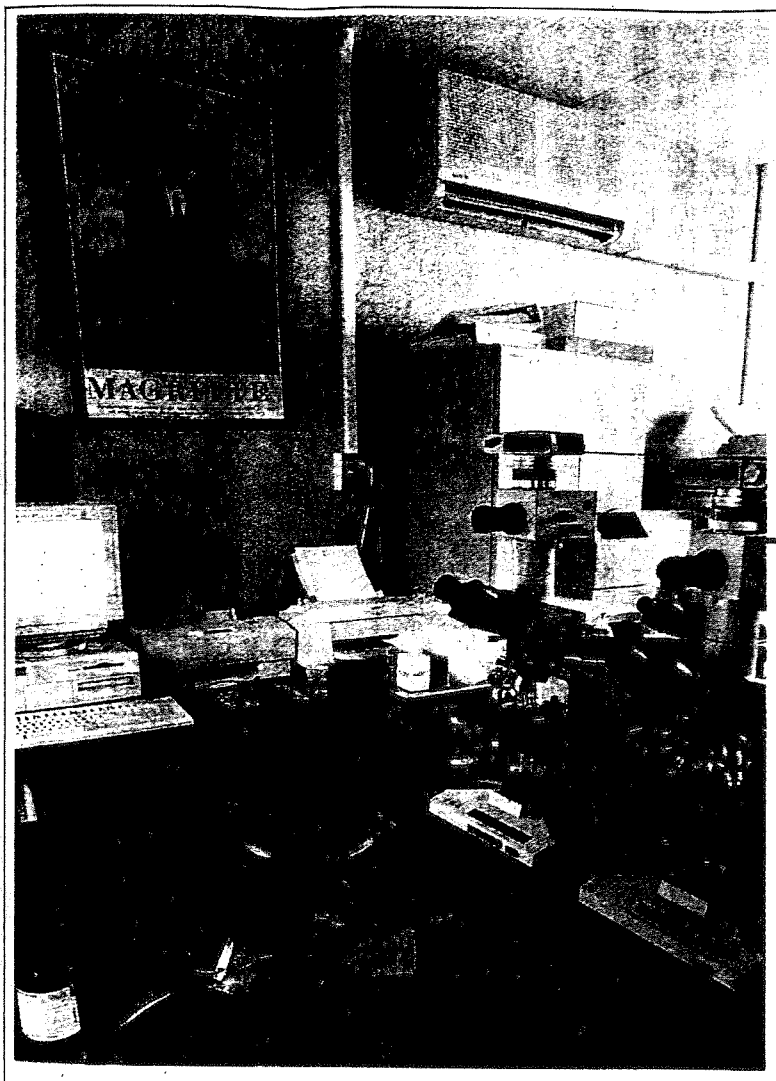

あの人の仕事場 6

体内時計の解読に挑む

神戸大大学院教授 岡村均さん

おかむら・ひとし 1952年生まれ。仏留学などを経て、95年から神大教授。分子脳科学専攻。大津市在住。

医学部の研究室には、絵がかかる。前に、DNA解析の機器、顕微鏡が並ぶ。

世界的な「体内時計」の専門家。論文は科学誌ネイチャーなどを飾る。地球上のほぼすべての生き物は約二十四時間周期のリズムを刻む。その遺伝子を解き明かせないか？ 関心はそこにある。

小さな実験室がいくつも。目につくのは、絵。壁にも天井にも。書棚には自ら描いた赤と黒の渦巻き模様の紙片。体内時計の司令塔がある脳細胞のイメージという。

二十世紀の科学は、すべてを細分化して追究してきた。「今世紀はそれが統合へ向かう」。だから重要なのは部分ではなく全体のイメージ。「絵」のように。

生命のリズムの解読は、深遠な世界にある。

写真・三浦拓也
文・磯辺康子

随時掲載します

神戸新聞 2001年2月9日(金) 夕刊

生きたマウスの体内時計遺伝子観察

神大医学部 岡村教授ら

脳に光ファイバー直結

マウスの脳に光ファイバーを通して、生物の体内時計をつかさどる時計遺伝子の活動を記録することに、神戸大学医学部の岡村均教授、山口勝助手らのチームが成功した。ほ乳類の遺伝子活動を生きたまま直接記録できたのは世界で初めて。九日までに、英科学誌ネイチャーに発表した。岡村教授は「遺伝子の働きをありのまま観察できる画期的な方法」としており、今後進められる脳機能や神経細胞の解析・研究にも弾みを与えそうだ。

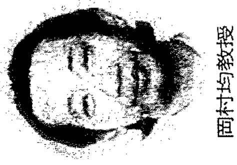

岡村均教授

24時間周期の「活動」「休息」確認

体内時計は、睡眠など生物の生活に大きく関与し、海外旅行の際に「時差ボケ」を引き起こすことでも知られる。ほ乳類は、脳内の視床下部にある体内時計を中心に、体内のすべての細胞が時計を刻んでいる。

岡村教授らは、一九九七年、ヒトやマウスなどほ乳類の時計遺伝子を発見。昼は活動、夜は休息、という約二十四時間周期のリズムを持っていることを突きとめた。

さらに今回、マウスの時計遺伝子を一部組み換えることで、活動の変化に応じて光を発するように設定。脳内の視床下部付近に、直径〇・五ミリの光ファイバーを差し込んで、時計遺伝子の発光リズムの記録に成功した。

記録では、光はおよそ十二時間ごとに強弱を繰り返し、時計遺伝子が活動と休息を二十四時間の周期で行っていることが、あらためて確認された。

従来、ほ乳類の遺伝子活動の記録、研究は、体から遺伝子を切り離して行われてきたが、今回、生きたマウスの遺伝子活動をそのまま同時に記録できたことで、今後の遺伝子研究が大きく前進する可能性が出てきた。

今回の研究は、神大、東北工業大、早稲田大の合同チームで行った。

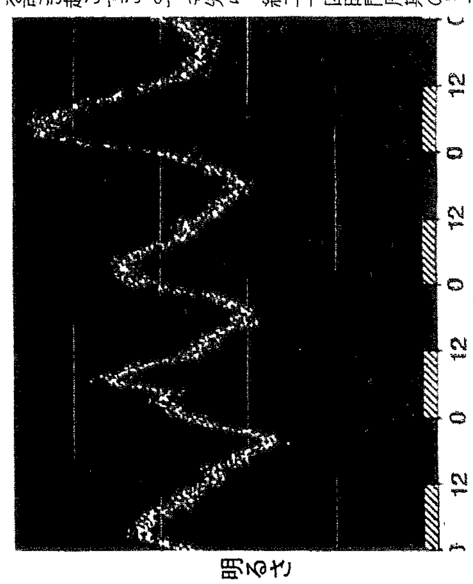

時計遺伝子の発光状況を記録したグラフ。12時間おきに、強弱を繰り返しているのがわかる（岡村均教授提供）

元経営者も認否留保

「起訴事実の特定不十分」

大阪ミナミぼったくり

大阪・ミナミの風俗店「ドリームランド」で男性客が睡眠導入剤を飲まされ薬物中毒死した事件で、傷害致死などの罪に問われた元経営者の今井和子(四三)ら三被告の初公判が九日、大阪地裁（岡田信裁判長）であり、罪状認否で三人の弁護人は「起訴事実の特定が不十分」と認否を留保した。

起訴状によると、今井被告とホステス二人は昨年十月二十五日深夜、大阪市中央区の同店で、客の姫路市、自営業三浦秋敏さん＝当時(四九)＝に睡眠導入剤入りのアルコール飲料を飲ませてこん睡状態にし、上着のポケットから現金五万円を抜き取った。

さらに、髙被告ら三人に店外に運ばせて路上に放置し、アルコールと睡眠導入剤の相乗効果による薬物中毒で死亡させた。

……こん睡状態のこの男性を店外に運び路上に放置して死なせたとして、保護責任者遺棄致死罪に問われた店長高善哲被告(三五)ら三人も、六日の初公判で認否を……

だんじり部屋 短銃4丁隠す

大阪で男を逮捕

……は九日までに、神社敷地内のだんじり部屋に短銃などを隠していたとして、銃刀法違反の現行犯で、大阪府阪南市貝掛、……八二、建築業武輪俊夫容疑者(五二)を逮捕、短銃四丁と実弾百三十四発を押収した。

調べによると、武輪容疑者は自動式短銃三丁と回転式短銃一丁、実弾百三十四発を木箱や段ボールに入れて隠していた疑い。

同課が情報を得て、七日にだんじり部屋など大阪府内十七カ所を捜索。短銃が見つかったこの部屋のかぎを保管していた武輪容疑者が「預かっていた」と認めたため、現行犯逮捕した。

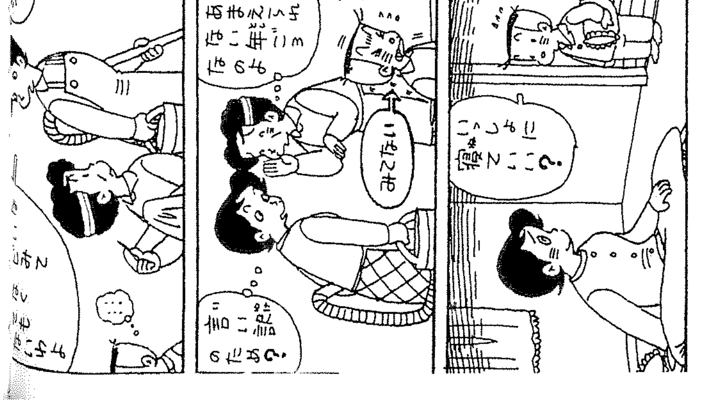

朝日新聞
2001年4月13日(金)
朝刊

応ぜず
する権利主張

日、「人道主義の配慮から乗員の出国は許したが、事件はまだ終わっていない。中国には米側の責任を追及する権利がある」と主張した。国連総会議長との会談で説明した。

体内時計、皮膚にも
神戸大で確認
全身に分布、「主時計」の脳で同調

睡眠などの生活リズムを約1日周期で刻む「体内時計」が、脳内だけでなく皮膚などの細胞にもあることを、神戸大学の岡村均教授、八木田和弘助手らのグループが動物実験で突き止めた。13日発行の米科学誌サイエンスに発表する。

ほ乳類の体内時計は、脳内の「視交叉（こうさ）上核」という場所にあることが知られている。ラットとマウスを使った実験で、体内時計のリズムを作り出す9種類の「時計遺伝子」が、脳内だけでなく、全身に分布する「線維芽細胞」の中でも働いていることが分かった。

時計遺伝子の一部の働きを止めたマウスは、脳内と線維芽細胞の両方で体内時計のリズムが狂うことも確認された。

岡村さんらは、体内時計は全身に広く分布していて、脳内の「主時計」がそれらを同調させている、とみている。

こうした遺伝子はヒトを含むほ乳類で共通。線維芽細胞は皮膚にもある。睡眠障害に悩む患者の皮膚を分析すれば、遺伝子の異常が原因のタイプかどうかを見分けられ、治療に役立てられそうという。

ひと

アルゼンチンの博物館に常設展示室ができた写真家
藤原（ふじわら）幸一（こういち）さん

ニュージーランドの山中、泥だらけで木の根を乗り越えて来るフィヨルドランドペンギンと出くわした。ペンギンの獣道に足を踏み入れていた。

「南極を主な繁殖地にするペンギンは2種だけ。多くは森で子育てをします」

開発で街ができ、海岸から線路や道路を渡り森に行く。交通事故にも遭う。人家の床下や古タイヤに巣作りをするペンギンもいる。

廃油にまみれたり、漁網にかかったり。ガラパゴス諸島では異常気象で激減した。野生動物が置かれた過酷な状況を写真で訴える。

美しい緑の牧場も、もとはすみかの原生林だった。ペンギンが片隅の木立でたちすくむ姿もとらえた。「彼らの目には荒涼とした風景に映るでしょう」

干拓前の秋田・八郎潟を見て育った。海やサンゴ礁に魅せられ、沖縄の大学、豪の大学院で海洋生物学を学び、博士号を取った。豪の海岸でペンギンを初めて見て「アイドルの素質がある」とのめり込んだ。「まず『可愛い』で関心を持ってくれればいいと思っているんです。次に環境問題に目を向けて欲しい」

3月、南極の玄関口であるアルゼンチン最南端の博物館に常設展示室ができた。ペンギン関係の展示品がなく、請われて作品を提供。全18種を収めた写真集「ペンギンたちの旅・病める南極海」も出した。

1年のうち半年は撮影で海外に出かけ、うち1カ月はテント生活。大荒れの南極海で危険と隣り合わせることもある。「交通事情、汚れた空気。東京にいるときの方が危険ですよ」

文　黒沢　大陸
写真　近藤　悦朗

「人の写真？ 撮りますよ。生活のために必要です」。46歳。

【ソウル12日＝箱田哲也】韓国政府は12日、日本の歴史教科書問題を政府全体で協議するため設置した「日本歴史教科書わい曲対策班」の初会合を開き、問題の教科書の再修正を要求することを確認した。

出席者によると、前日に金大中大統領が「善処を求める」という表現で事実上の再修正を初めて日本に求めたことを受け「わい曲部分の分析作業が終わり次第、政府として再修正を要求することを決めた。日本が再修正に応じなかった場合の対応策も協議したが、結論は出なかったという。

タイ紙社説
韓国に理解

【バンコク12日＝木村文】タイの代表的な英字紙「ネーション」は12日付の社説で日本の歴史教科書問題を取り上げ、「戦後50年をすぎても、日本とアジア諸国の関係は敵意を乗り越えていない」と指摘した。

同紙は、駐日大使を帰国させた韓国の対応について「驚くべきことではない」と理解を示した。

北＝田村宏嗣
ン＝杉本宏

の世論や議会の対中強硬論が台湾の追い風になる」が、議員の多くは「この11日間で損なわれた信頼をうかがっている。共和党の台湾派は対中めている。中国が増強しているミ 研究員は指摘している。ブッシュ政権もイージ

2）遺伝子産物のリン酸化に関わる分子素過程の解明（研究代表者：福永浩司（東北大学））

研究代表者：　福永浩司　（東北大学大学院薬学研究科）
研究分担者：　滝口正樹　（千葉大学大学院医学研究院）
　　森山芳則　（岡山大学薬学部）

Ⅰ．研究成果

視交叉上核における概日リズム発現には Per 蛋白質発現のネガティブ・フィードバック機構が関与している。網膜からの光刺激は網膜視床下部路のグルタミン酸神経を介して視交叉上核の内在性概日時計を外界の明暗サイクルに同調させる刻。この光同調には視交叉上核の腹外側部ニューロンにおける CaM キナーゼ II 、 MAP キナーゼの活性化反応が関与すると考えられているが実験的証拠は得られていない。本研究では福永は視交叉上核における光依存性同調の分子機構を解析し、動物個体と視交叉上核スライス標本を用いて、Per 1 遺伝子発現に関与する CaM キナーゼ II の作用機序を明らかにした。滝口はマウス視交叉上核、肝臓から cDNA ライブラリーを構築して、マイクロアレイの作成および解析を行い、新たな概日リズム遺伝子を探索した。概日リズムの出力系として松果体のメラトニンがある。森山はメラトニン合成酵素 serotonin-N-acetyltransferase (NAT) のレドックススイッチによる調節機構を見出した。

（1）光依存性同調と Per 1 遺伝子発現の CaM キナーゼ II による調節機構

視交叉上核の腹外側部の vasoactive intestinal peptide (VIP) 神経は網膜視床下部路のグルタミン酸神経によって支配されている。光刺激によって終末より放出されたグルタミン酸は NMDA 受容体を活性化して細胞内カルシウム上昇を引き起こす。続いて CaM キナーゼ II 、 MAP キナーゼが活性化される。光依存性同調機構には時計遺伝子 Per 1、Per 2 の発現が関与しているがこれらの時計遺伝子誘導のおけるカルシウムの作用機構は不明であった。主観的暗期に光照射すると視交叉上核腹外側部で CaM キナーゼ II 、MAP キナーゼが活性化される (Yokota et al., 2001)。脳室内にこれらのプロテインキナーゼの阻害剤を投与して、Per 1、Per 2 発現に対する効果を調べると、 CaM キナーゼ II の阻害剤は完全に抑制した。しかし、 MAP キナーゼ阻害剤は効果を示さなかった。主観的暗期の初期に光照射したハムスターで行動位相後退に及ぼす影響を調べた。Per 1、Per 2 遺伝子誘導と同様に、 CaM キナーゼ II 阻害剤のみが有意に位相後退を阻害した。これらの結果は、ハムスターの光依存性同調機構には主に、 CaM キナーゼ II が関与していることを示唆している。

CaM キナーゼ II はどのようにして Per 1、Per 2 遺伝子を誘導するのかについて検討した。VIP 神経における Per 1、Per 2 遺伝子の誘導には NMDA 受容体の活性化反応が関与している。Storm らは cAMP キナーゼ、MAP キナーゼの活性化反応に伴う

cAMP-responsive element binding protein (CREB) のリン酸化反応の重要性を示唆している (Obrietan et al. J. Biol. Chem., 274,17748-17756, 1999)。NMDA 受容体からのカルシウム上昇に伴う CaM キナーゼ II の活性化反応と CaM キナーゼ阻害剤、 KN93 の Per 1、Per 2 遺伝子誘導の阻害を考えるとむしろ、 CaM キナーゼ II あるいは CaM キナーゼ IV の関与が示唆される。ラット視交叉上核腹外側部でのこれらのキナーゼの発現を調べると、 CaM キナーゼ II の 4 つのアイソフォームのうちデルタ型が主に発現していた (Nomura et al., 2003)。脳の他の部位でのアルファ型とベータ型の発現とは対照的である。一方、 CaM キナーゼ IV はほとんど発現していない。 CaM キナーゼ IV は海馬においては CREB のリン酸化反応を介して記憶形成に関与するキナーゼであるが、視交叉上核腹外側部での CREB のリン酸化反応には関与していない。

視神経を保持した視交叉上核スライス標本を用いて、視神経刺激による視交叉上核腹外側部でのリン酸化反応について調べた。100 Hz、1 秒という高頻度刺激によって CaM キナーゼ II 、 MAP キナーゼの活性化反応と CREB のリン酸化反応が上昇した (Fukunaga et al., 2001)。阻害剤の効果から、CREB のリン酸化反応には主に、 MAP キナーゼが関与していると考えられる。海馬同様に、100 Hz、1 秒という高頻度刺激によって興奮性シナプス電位の長期増強 (LTP) が誘導された。この LTP の誘導は NMDA 受容体と CaM キナーゼ II の活性化反応に依存していた。しかし、視交叉上核での LTP の機能的役割は不明でる。面白いことに、光非依存性同調因子であるメラトニンを処理すると、視神経刺激による CaM キナーゼ II の活性化反応が選択的に阻害された。メラトニン受容体を介するシグナルは CaM キナーゼ II を阻害することが明らかとなった。セロトニン、ニューロペプチド Y などの光非依存性同調因子も同様に視交叉上核において CaM キナーゼ II 活性を阻害することから、光非依存性同調機構にも CaM キナーゼ II が関与すると考えられる。

つぎに、マウス Per 1 遺伝子の 7.2 K のプロモーターをルシフェラーゼ遺伝子につないだレポーター遺伝子を用いて CaM キナーゼ II 反応エレメントを解析した。恒常的活性型の CaM キナーゼ II、CaM キナーゼ IV、cAMP キナーゼと MAP キナーゼの上流である MEK の活性型と Per 1 プロモーターのルシフェラーゼレポーター遺伝子を神経芽腫細胞に導入してプロモーター活性を測定した。 MAP キナーゼと CaM キナーゼ II がプロモーター活性を上昇させのに対して、 CaM キナーゼ IV と cAMP キナーゼは効果を示さなかった (Nomura et al., 2003)。マウス Per 1 遺伝子の 1.8 K 上流のプロモーターを用いた Sassone-Corci らの結果では cAMP キナーゼと MAP キナーゼによって強い誘導が起こること、CREB 結合部位の重要性が確認されている (Travnickova-Bendova et al., PNAS, 99, 7728-7733, 2002)。しかし、カルシウム反応エレメントの存在は確認されていない。これらの結果の違いは用いたプロモーターの長さと細胞の違いによるものである。しかし、in vitro における Per 1 遺伝子の誘導は CaM キナーゼ II 阻害剤で抑制されこと、Per 1 プロモーターの全長を用いた場合に CaM キナーゼ II に対する反応が見られることから、 CaM キナーゼ II 反応エレメントの重要性が示唆される。さらに、プロモー

ターの切断、変異を用いた解析から、 Exon 1B の上流にある DBP 結合部位のすぐ上流にある GAGGGG エレメントが CaM キナーゼ II 反応に重要なエレメントであることが解った。このエレメントは SP-1 の DNA 結合部位に類似しており、 CaM キナーゼ II と SP-1 との相互作用が示唆される。しかし、DBP による Per 1 プロモーターの活性化反応も CaM キナーゼ II によって促進されることから、 CaM キナーゼ II は SP-1 に加えて DBP とも相互作用して Per 1 の遺伝子誘導を引き起こすと考えられる。しかし、詳細な転写活性化機構は不明である。さらに、 MAP キナーゼ、cAMP キナーゼ、 CaM キナーゼ II の Per 1 誘導の効果が細胞種で異なることから、視交叉上核 VIP ニューロンでの解析が必要である。

（2）マウス肝臓および視交叉上核における概日遺伝子の cDNA マイクロアレイ解析

血液凝固線維素原であるフィブリノーゲンは (Aα)2(Bβ)2γ2 のサブユニット構造をとり、各サブユニットの遺伝子はヒトおよびマウスの染色体上でクラスターを形成する。CT6 および CT18 におけるマウス肝臓より抽出した poly(A)+ RNA を用いて、約 2,300 種類のマウス肝臓 cDNA をスポットした自家製チップによるマイクロアレイ解析を行なった。アレイ解析の結果、最も変動の大きい 6 種類の遺伝子について、経時的にノザン解析を行なったところ、3β-HSD と Gabarapl1 が明期に、Spot14、Hspa8、Hspa5、Hsp84-1 が暗期に一峰性に発現の高い概日変動を示した。一方、フィブリノーゲンのサブユニットである Aα，Bβ，γの遺伝子の発現は明期、暗期両方においてピークを示す二峰性を示し、また，互いに同期していた。これは(Aα)2(Bβ)2(γ)2 の 6 量体の化学量論的維持に効果的と考えられた。また、Clock 変異マウスではリズムが消失しており、フィブリノーゲン遺伝子の二峰性発現が時計遺伝子の制御下にあることが明らかとなった。さらに、フィブリノーゲン遺伝子クラスターの塩基配列を検索したところ、多数の概日転写因子の結合部位様配列が認められた。つぎに、視交叉上核において光刺激に応答して発現の変動する遺伝子を検索した。独自に開発した全 cDNA/cRNA の増幅方法を用いて、マウス視交叉上核の cDNA ライブラリーを構築した。約千クローンの 5'端配列を決定したところ 750 種類の遺伝子に分類された。これに海馬由来 cDNA を加えた 3,200 種類の cDNA を搭載したマイクロアレイを作成した。光刺激後 2 時間、6 時間の視交叉上核および対照同核から、やはり cDNA/cRNA 増幅法を用いてセンス鎖 cRNA を増幅し、これを用いてアレイ解析を行い、候補遺伝子について RT-PCR を用いて発現変動を解析中である。

（3）松果体におけるメラトニン合成制御機構に関する研究

松果体は概日リズム変換器である。視交叉上核からの生物時計シグナルをメラトニンという液性情報に変換し、体内に行き渡らせている。メラトニンの合成は概日リズムと共に振動しており、その合成・分泌と分解は厳密に制御されている。その制御の中心となるのはメラトニン合成の律速酵素 serotonin-N acetyltransferase (NAT)である。これまで、交感神経入力により NAT 合成が亢進する調節機構がよく研究されていた。私たちは本研究に

おいてNAT活性の調節機構を解析し、以下の2つの成果を得た。すなわち、(1)グルタミン酸を伝達物質とする新しいNAT制御系が存在することを見出した。(2) NAT自身が内在するレドックス制御系を見出した。以下にその概要を記す。

松果体細胞はメラトニンの内分泌細胞としての属性の他にグルタミン酸作動性細胞としての属性も備えている。我々は、松果体細胞に発現しているイオン型グルタミン酸受容体・代謝型グルタミン酸受容体を全て同定し、その機能を明らかにした。これらの受容体はメラトニン合成抑制の入力系として機能している。次に、松果体細胞がグルタミン酸を放出する機構の概要を解明した。グルタミン酸は synaptic-like microvesicle (SLMVs) の中に vesicular glutamate transporter 1 と 2 を介して蓄積された後、開口放出される。SLMVs の内部 pH や構成因子を明らかにした。同様に、松果体細胞がグルタミン酸を再吸収する機構を解明した。

NATは転写レベルで活性が調節されていると考えられている。酵素レベルでの調節機構はよくわかっていない。我々はNATのCys61とCys177間のSS結合がスイッチとなり活性が調節されていることを見出した。この機構がNAT調節において中心的な役割を果たしていることを明らかにしつつある。

参考文献

福永浩司

K. Fukunaga, D. Muller, M. Ohmitsu, E. Bakó, A.A. DePaoli-Roach and E. Miyamoto: Decreased protein phosphatase 2A activity in hippocampal long-term potentiation. *J. Neurochem.*, 74, 807-817 (2000)

J. Kasahara, K. Fukunaga and E. Miyamoto: Activation of Ca^{2+}/calmodulin-dependent protein kinase IV in cultured rat hippocampal neurons. *J. Neurosci. Res.*, 59, 594-600 (2000))

H. Kanasaki, K. Fukunaga, K. Takahashi, K. Miyazaki and E. Miyamoto: Involvement of p38 mitogen-activated protein kinase activation in bromocriptine-induced apoptosis in rat pituitary GH3 cells. *Biol. Reprod.*, 62, 1486-1494 (2000)

Y. Takeuchi, H. Yamamoto, K. Fukunaga, T. Miyakawa and E. Miyamoto: Identification of the isoforms of Ca^{2+}/calmodulin-dependent protein kinase II in rat astrocytes and their subcellular localization. *J. Neurochem.*, 74, 2557-2567 (2000)

H. Tabuchi, H. Yamamoto, K. Matsumoto, K. Ebihara, Y. Takeuchi, K. Fukunaga, H. Hiraoka, Y. Sasaki, M. Shichiri and E. Miyamoto: Regulation of insulin secretion by overexpression of Ca^{2+}/calmodulin-dependent protein kinase II in insulinoma MIN6 cells. *Endocrinology*, 141, 2350-2360 (2000)

I. Munir, K. Fukunaga, H. Kanasaki, K. Miyazaki, T. Ohba, H. Okamura and E. Miyamoto: Expression of cyclo-oxygenase 2 by prostaglandin E_2 in human endometrial adenocarcinoma cell line HEC-1B. *Biol. Reprod.*, 63, 933-941 (2000)

T. Moriya, Y. Kouzu, S. Shibata, H. Kadotani, K. Fukunaga, E. Miyamoto and T. Yoshioka: Close linkage between calcium/calmodulin kinase II α/β and NMDA-2A receptors in the

lateral amygdala and significance for retrieval of auditory fear conditioning. *Eur. J. Neurosci.*, **12**, 3307-3314 (2000)

Q. Zhang, S. Yoshida, K. Sakai, J. Liu and K. Fukunaga: Changes of free fatty acids and acyl-coas in rat brain hippocampal slice with tetraethylammonium-induced long-term potentiation. *Biochem. Biophys. Res. Commun.*, 267, 208-212 (2000)

K. Fukunaga and E. Miyamoto: A working model of CaM kinase II activity in hippocampal long-term potentiation and memory. Neurosci. Res., 38, 3-17 (2000)

福永浩司，宮本英七：海馬における神経活動依存性シナプス伝達効率の調節．蛋白質 核酸 酵素，増刊「神経回路形成と機能発達」(編集：津本忠治，村上富士夫，小幡邦彦，吉岡 亨，川合述史)，**45**，474-482 (2000)

T. Yonehara, H. Kanasaki, H. Yamamoto, K. Fukunaga, K. Miyazaki and E. Miyamoto: Involvement of mitogen-activated protein kinase in cyclic adenosine 3',5'-monophosphate-induced hormone gene expression in rat pituitary GH_3 cells. *Endocrinology*, 142, 2811-2819, (2001)

S.-I. Yokota, M. Yamamoto, T. Moriya, M. Akiyama, K. Fukunaga, E. Miyamoto and S. Shibata: Involvement of calcium-calmodulin protein kinase but not of mitogen-activated protein kinase in light-induced phase delay and Per gene expression in the suprachiasmatic nucleus of hamster. *J. Neurochem.*, 77, 618-627 (2001)

J. Kasahara, K. Fukunaga and E. Miyamoto: Activation of calcium/calmodulin-dependent protein kinase IV in long-term potentiation in the rat hippocampal CA1 region. *J. Biol. Chem.*, 276, 24044-24050 (2001)

E. Miyamoto, J. Liu, K. Fukunaga and D. Muller: Involvement of CaM kinase II and mitogen-activated protein kinase in hippocampal long-term potentiation. Neuroscientific Basis of Dementia (eds.: C. Tanaka, P.L. McGeer, Y. Ihara), pp. 49-57 (2001), Birkhäuser Verlag, Basel, Switzerland

M. Morioka, K. Fukunaga, Y. Kai, T. Todaka, S. Yano, J. Hamada, E. Miyamoto and Y. Ushio: Intravenously injected FK506 failed to inhibit hippocampal calcineurin. *Biochem. Biophys. Res. Commun.*, 286, 802-806 (2001)

福永浩司：長期増強と CaM キナーゼ. Clinical Neuroscience vol. 20 618-619, 中外医学社 (2002)

H. Kanasaki, T. Yonehara, H. Yamamoto, Y. Takeuchi, K. Fukunaga, K. Takahashi, K. Miyazaki and E. Miyamoto: Differential regulation of pituitary hormone secretion and gene expression by thyrotropin-releasing hormone. A role for mitogen-activated protein kinase signaling cascade in rat pituitary GH3 cells. *Biol. Reproduction*, 67, 107-113 (2002)

Y. Takeuchi, K. Fukunaga and E. Miyamoto: Activation of Ca^{2+}/calmodulin-dependent protein kinase II and brain-derived neurotrophic factor gene expression by stimulation of dopamine D2 receptor in transfected NG108-15 cells. *J. Neurochem.* 82, 316-328 (2002))

A. Uezu, K. Fukunaga, J. Kasahara and E. Miyamoto: Activation of Ca^{2+}/calmodulin-dependent protein kinase I in cultured rat hippocampal neurons. *J.*

Neurochem. 82, 585-593 (2002)

Y. Takeuchi, E. Miyamoto and K. Fukunaga: Analysis on the promoter region of exon IV-BDNF in NG108-15 cells. *J. Neurochem.* 83, 67-79 (2002)

Y. Takeuchi, E. Miyamoto and K. Fukunaga: Activation of the rat dopamine D2 receptor promoter by mitogen-activated protein kinase and Ca^{2+}/calmodulin-dependent protein kinase II pathways. *J. Neurochem.* 83, 784-796 (2002)

K. Fukunaga, K. Horikawa, S. Shibata, Y. Takeuchi and E. Miyamoto: Ca^{2+}/calmodulin-dependent protein kinase II-dependent long-term potentiation in the rat suprachiasmatic nucleus and its inhibition by melatonin. *J. Neurosci. Res.* 70, 799-807 (2002)

K. Fukunaga, J. Kasahara and E. Miyamoto: In: Recent Research Developments in Neurochemistry (ed.: S.G. Pandalai), Differential role of CaM kinases II and IV activities in neuronal plasticity and memory. Vol. 5, 143-158 Research Signpost, Kerala, India (2002)

H. Kanasaki, T. Yonehara, Y. Yamada, K. Takahashi, K. Hata, R. Fujiwaki, H. Yamamoto, Y. Takeuchi, K. Fukunaga, E. Miyamoto and K. Miyazaki: Regulation of gonadotropin α subunit gene expression by dopamine D_2 receptor agonist in clonal mouse gonadotroph □T3-1 cells. *Biol. Reproduction* 67, 1218-1224 (2002)

X.-L. Li, S. Aou, Y. Oomura, N. Hori, K. Fukunaga and T. Hori: Impairment of long-term potentiation and spatial memory in leptin receptor-deficient rodents. *Neuroscience* 113, 607-615 (2002)

K. Nomura, Y. Takeuchi, S. Yamaguchi, H. Okamura and K. Fukunaga: Involvement of calcium/calmodulin-dependent protein kinase II in the induction of mPer1. *J. Neurosci. Res.* in press (2003)

Y. Takeuchi and K. Fukunaga: Differential regulationof NF-κB, SRE and CRE by dopamine D1 and D2 receptors in transfected NG108-15 cells. *J. Neurochem.* in press (2003)

H. Nishimura, H. Sakagami, A. Uezu, K. Fukunaga, M. Wananabe and H. Kondo: Cloning, characterization, and expression of two alternatively splicing isoforms of Ca^{2+}/calmodulin-dependent protein kinase Iα in the brain. *J. Neurochem.* in press (2003)

Y. Takeuchi and K. Fukunaga: Differential subcellular localiztion of two dopamine D2 receptor isoforms in transfected NG108-15 cells. J. Neurochem. in press (2003)

滝口正樹

K. Sugahara, T. Sadohara, M. Sugita, K. Iyama and M. Takiguchi: Differential expression of CCAAT enhancer binding protein family in rat alveolar epithelial cell proliferation and in acute lung injury. *Cell Tissue Res.* 297, 261-270 (1999)

O. Braissant, P. Honegger, M. Loup, K. Iwase, M. Takiguchi and C. Bachmann: Hyperammonemia: regulation of argininosuccinate synthetase and argininosuccinate lyase genes in aggregating cell cultures of fetal rat brain. *Neurosci. Lett.* 266, 89-92 (1999)

W.-Y. Zhang, M. Takiguchi, Y. Koshiyama, T. Gotoh, A. Nagasaki, K. Iwase, K. Yamamoto,

H. Takeshima, A. Negi and M. Mori: Expression of citrulline-nitric oxide cycle in lipopolysaccharide and cytokine-stimulated rat astroglioma C6 cells. *Brain Res.* 849, 78-84 (1999)

K. Yanai, K. Hirota, K. Taniguchi-Yanai, Y. Shigematsu, Y. Shimamoto, T. Saito, S. Chowdhury, M. Takiguchi, M. Arakawa, Y. Nibu, F. Sugiyama, K. Yagami and A. Fukamizu,: Regulated expression of human angiotensinogen gene by hepatocyte nuclear factor 4 and chicken ovalbumin upstream promoter-transcription factor. *J. Biol. Chem.* 274, 34605-34612 (1999)

K. Iwase, K. Miyanaka, A. Shimizu, A. Nagasaki, T. Gotoh, M. Mori and M. Takiguchi: Induction of endothelial nitric-oxide synthase in rat brain astrocytes by systemic lipopolysaccharide treatment. *J. Biol. Chem.* 275, 11929-11933 (2000)

S. Oyadomari, F. Matsuno, S. Chowdhury, T. Kimura, K. Iwase, E. Araki, M. Shichiri, M. Mori and M. Takiguchi: The gene for hepatocyte nuclear factor (HNF)-4α is activated by glucocorticoids and glucagon, and repressed by insulin in rat liver. *FEBS Lett.* 478, 141-146 (2000)

T. Hiwasa, M. Nakata, M. Nakata, S. Ohno, M. Maki, K. Suzuki and M. Takiguchi: Regulation of transformed state by calpastatin via PKCε in NIH3T3 mouse fibroblasts. *Biochem. Biophys. Res. Commun.* 290, 510-517 (2002)

S. Oyadomari, K. Takeda, M. Takiguchi, T. Gotoh, M. Matsumoto, I. Wada, S. Akira, E. Araki and M. Mori: Nitric oxide-induced apoptosis in pancreatic β cells is mediated by the endoplasmic reticulum stress pathway. *Proc. Natl. Acad. Sci. USA* 98, 10845-10850 (2001)

K. Sugahara, K. I. Iyama, T. Kimura, K. Sano, G. J. Darlington, T. Akiba and M. Takiguchi: Mice lacking CCAAT/enhancer-binding protein-α show hyperproliferation of alveolar type II cells and increased surfactant protein mRNAs. *Cell Tissue Res.* 306, 57-63 (2001)

T. Kimura, S. Chowdhury, T. Tanaka, A. Shimizu, K. Iwase, S. Oyadomari, T. Gotoh, H. Matsuzaki, M. Mori, S. Akira and M. Takiguchi: CCAAT/enhancer-binding protein α is required for activation of genes for ornithine cycle enzymes by glucocorticoids and glucagon in primary-cultured hepatocytes. *FEBS Lett.* 494, 105-111 (2001)

T. Akiba, N. Kuroiwa, Y. A. Shimizu, K. Iwase, T. Hiwasa, H. Yokoe, H. Kubosawa, R. Kageyama, G. J. Dahrington, M. Mori, H. Tanzawa and M. Takiguchi: Expression and regulation of the gene for arginase I in mouse salivary glands: requirement of CCAAT/enhancer-binding protein α for the expression in the parotid gland. *J. Biochem.* 132, 621-7 (2002)

T. Hiwasa, H. Shimada, T. Ochiai, T. L. Liu, Y. Yuasa, M. Takiguchi and M. Ohkoshi: Decrease in growth factor receptors after treatment with serine protease inhibitor ONO-3403. *Int. J. Oncol.* 20, 797-802 (2002)

H. Shimada, T. L. Liu, T. Ochiai, T. Shimizu, Y. Haupt, H. Hamada, T. Abe, M. Oka, M. Takiguchi and T. Hiwasa: Facilitation of adenoviral wild-type p53-induced apoptotic cell death by overexpression of p33(ING1) in T.Tn human esophageal carcinoma cells.

Oncogene 21, 1208-1216 (2002)

森山芳則

G. Kawa, A. Yamamoto, T. Yoshimori, K. Muguruma, T. Matsuda and Y. Moriyama: Immunohistochemical localization of V-ATPases in rat spermatids. *Int. J. Androl.*, 23, 278-283 (2000)

M. Hayashi, H. Yamada, T. Mitamura, T. Horii, A. Yamamoto and Y. Moriyama: Vacuolar H^+-ATPase localized in plasma membranes of malaria parasite cells, *Plasmodium falciparum*, is involved in regional acidification of parasitized erythrocytes. *J. Biol. Chem.*, 275(44), 34353-34358 (2000)

M. Takeda, M. Haga, H. Yamada, M. Kinoshita, M. Otsuka, S. Tsuboi and Y. Moriyama: Ionotropic glutamate receptors expressed in human retinoblastoma Y79 cells. *Neurosci. Lett.*, 294 (2), 97-100 (2000)

S. Yatsushiro, M. Hayashi, M. Morita, A. Yamamoto and Y. Moriyama: Glutamate receptor subunit $\delta 2$ is highly expressed in a novel population of glial-like cells in rat pineal glands in culture. *J. Neurochem.*, 75(3), 1115-1122 (2000)

S. Yatsushiro, H. Yamada, M. Hayashi, A. Yamamoto and Y. Moriyama: Ionotropic glutamate receptors microvesicle-mediated exocytosis of L-glutamate in rat pinealocytes. *J. Neurochem.*, 75, 288-297 (2000)

Y. Moriyama, M. Hayashi, H. Yamada, S. Yatsushiro, S. Ishio and A. Yamamoto: Synaptic-like microvesicles, synaptic vesicle counterparts in endocrine cells, are involved in a novel regulatory mechanism for hormonal synthesis and secretion. *J. Exp. Biol.*, 203, 117-125 (2000)

M. Futai, T. Oka, Sun-Wada, Y. Moriyama, H. Kanazawa and Y. Wada : Luminal acidification of diverse organelles by V-ATPase in animal cells. *J. Exp. Biol.* 203, 107-116 (2000)

M. Hayashi, S.Taniguchi, Y. Ishizuka, Hye-Sook Kim, Y.Wataya, A. Yamamoto and Y. Moriyama: A homologue of N-ethylmaleimide-sensitive factor in the malaria parasite, *Plasmodium falciparum*, is exported and localized in vesicular structure in the cytoplasm of infected erythrocyte in the brefeldin A-sensitive pathway. *J. Biol. Chem.* 276, 15249-15255 (2001)

M. Hayashi, M. Otsuka, R. Morimoto, S. Hirota, S. Yatsushiro, J. Takeda, A. Yamamoto and Y. Moriyama: Differentiation-associated Na^+-dependent inorganic phosphate cotransporter (DNPI) is a vesicular glutamate transporter in endocrine glutamatergic systems. *J. Biol. Chem.* 276, 43400-43406 (2001)

S.Nakatsuka, M. Hayashi, A. Muroyama, M. Otsuka, S. Kozaki, H. Yamada and Y. Moriyama: D-Aspartate is stored in secretory granules and released through a Ca^{2+}-dependent pathway in a subset of rat pheochromocytoma PC 12 cells. *J. Biol. Chem.* 276, 26589-26596 (2001)

H. Yamada, M. Otsuka, M. Hayashi, S.Nakatsuka, K. Hamaguchi, A. Yamamoto and Y. Moriyama: Ca^{2+}-dependent exocytosis of L-glutamate by αTC6, clonal mouse pancreatic α cells, *Diabetes*, 50, 1012-1020 (2001)

K. Sakata, T. Yamashita, M. Maeda, Y. Moriyama, S. Shimada and M. Tohyama: Cloning of a lymphatic peptide/histidine transporter, *Biochem. J.* 356,53-60 (2001)

S. Tsuboi, Y. Kotani, K. Ogawa, T. Hatanaka, S. Yatsushiro, M. Otsuka and Y. Moriyama: An intramolecular disulfide bridge as a catalytic switch for serotonin N-acetyltransferase. *J Biol Chem.* 277, 44229-44235 (2002)

M. Hayashi, A. Yamamoto and Y. Moriyama: The internal pH of synaptic-like microvesicles in rat pinealocytes in culture. *J. Neurochem.* 82, 698-704 (2002)

H. Yamada, M. Hayashi, S. Uehara, M. Kinoshita, A. Muroyama, M. Watanabe, K. Takei and Y. Moriyama: Norepinephrine triggers Ca^{2+}-dependent exocytosis of 5-hydroxytryptamine from rat pinealocytes in culture. *J. Neurochem.* 81, 533-540 (2002)

M. Hayashi, M. Otsuka, R. Morimoto, A. Muroyama, M. Uehar, A. Yamamoto and Y. Moriyama: Vesicular inhibitory amino acid transporter is present in glucagon-containing secretory granules in alpha cells of islet of Langerhans. *Diabetes* in press (2003)

Y. Moriyama, M. Hayashi, S. Yatsushiro and A. Yamamoto: Vacuolar proton pumps in malaria parasite cells. *J. Bioenerg. Biomembr.* in press (2003)

M. Hayashi, H. Yamada, S. Uehara, R. Morimoto, A. Muroyama, J. Takeda, A. Yamamoto and Y. Moriyama: Secretory granule-mediated co-secretion of L-glutamate and glucagon triggers a glutamatergic signal transmisson in islets of Langerhans. *J. Biol. Chem.* 278, 1966-1974 (2003)

R. Morimoto, M. Hayashi, S. Yatsushiro, M. Otsuka, A. Yamamoto and Y. Moriyama: Co-expression of vesicular glutamate transporters (VGLUT1 and VGLUT2) and their association with synaptic-like microvesicles in rat pinealocytes. *J. Neurochem.* 84, 382-391 (2003)

高森茂雄、森山芳則　細胞工学　グルタミン酸化学伝達の鍵分子：小胞型グルタミン酸トランスポーター　in press

Journal of Neuroscience Research 70:799–807 (2002)

Ca^{2+}/Calmodulin-Dependent Protein Kinase II-Dependent Long-Term Potentiation in the Rat Suprachiasmatic Nucleus and Its Inhibition by Melatonin

Kohji Fukunaga,[1]* Kazumasa Horikawa,[2] Shigenobu Shibata,[2] Yusuke Takeuchi,[1] and Eishichi Miyamoto[1]

[1]Department of Pharmacology, Kumamoto University School of Medicine, Kumamoto, Japan
[2]Department of Pharmacology Waseda University School of Human Science, Tokorozawa, Japan

We recently reported that Ca^{2+}/calmodulin-dependent protein (CaM) kinase II is involved in light-induced phase delays and *Per* gene induction in the suprachiasmatic nucleus (SCN). To clarify the activation mechanisms of CaM kinase II by glutamate receptor stimulation in the SCN, we documented CaM kinase II activation following induction of long-term potentiation (LTP) in the rat SCN. High-frequency stimulation (100 Hz, 1 sec) applied to the optic nerve resulted in LTP of a postsynaptic field potential in the rat SCN. Unlike LTP in the hippocampal CA1 region, LTP onset in the SCN was slow and partly dependent on *N*-methyl-*D*-aspartate receptor activation. LTP induction in the SCN was completely inhibited by treatment with a nitric oxide synthase inhibitor or with a specific CaM kinase II inhibitor. Immunoblotting analysis using phosphospecific antibodies against autophosphorylated CaM kinase II revealed that LTP induction was accompanied by an increase in autophosphorylation. After high-frequency stimulation, we could visualize activation of CaM kinase II in vasoactive intestinal polypeptide-positive neurons in the SCN by immunohistochemistry. Treatment with cyclosporin A, a calcineurin inhibitor, potentiated LTP induction in the rat SCN. Interestingly, treatment with melatonin totally prevented LTP induction, without changes in basal synaptic transmission. Analyses of phosphorylation of CaM kinase II, mitogen-activated protein kinase, and cAMP-responsive element binding protein revealed that stimulatory and inhibitory effects on CaM kinase II autophosphorylation underlie the effects of cyclosporin A and melatonin, respectively. These results suggest that CaM kinase II plays critical roles in LTP induction in the SCN and that melatonin has inhibitory effects on synaptic plasticity through CaM kinase II.

Key words: CaM kinase II; calcineurin; NOS; LTP; SCN; circadian rhythm

The mammalian suprachiasmatic nucleus (SCN) plays a pivotal role as a primary oscillator in circadian rhythms (King and Takahashi, 2000; Reppert and Weaver, 2001). Entrainment of circadian rhythms to the environmental light/dark cycle is mediated by excitatory input through the direct retinohypothalamic tract. Both *N*-methyl-*D*-aspartate (NMDA) and non-NMDA receptors are involved in mediating photic information in the SCN. In addition, light induces phase shifts through a Ca^{2+}-dependent signaling pathway mediated by NMDA receptor activation, stimulation of nitric oxide synthase (NOS) activity, and production of nitric oxide (NO) during the subjective night (Ding et al., 1994; Shibata et al., 1994; Shirakawa and Moore, 1994; Watanabe et al., 1994). The recent characterization of clock genes, including period genes, has also defined the molecular basis of the circadian clock and entrainment mechanisms. With regard to photic entrainment, brief exposure to light during subjective night results in a large and rapid induction of *mPer1* and *mPer2* expression (Albrecht et al., 1997; Shigeyoshi et al., 1997; Miyake et al., 2000). The expression of *Per* genes is known to play a fundamental role in photic entrainment as well as in oscillator activity in circadian rhythm. However, the signaling cascade involved in the *Per* gene expression following photic stimulation is not fully understood. We recently found that Ca^{2+}/calmodulin-dependent protein kinase (CaM kinase) but not mitogen-activated protein (MAP) kinase was required for light-induced *Per1* gene expression and for light-induced phase delays in the hamster (Yokota et al., 2001).

Contract grant sponsor: Ministry of Education, Science, Sports and Culture of Japan; Contract grant number: 11470025; Contract grant number: 11170244; Contract grant number: 11233205; Contract grant sponsor: Human Frontiers Science Program.

*Correspondence to: Kohji Fukunaga, PhD, Department of Pharmacology, Tohoku University Graduate School of Pharmaceutical Sciences, Aramaki-Aoba, Aoba-ku, Sendai 980-8578, Japan. E-mail: fukunaga@mail.pharm.tohoku.ac.jp

Received 4 April 2002; Revised 10 June 2002; Accepted 18 June 2002

Published online 23 September 2002 in Wiley InterScience (www.interscience.wiley.com). DOI: 10.1002/jnr.10400

These results were consistent with the previous observation that both calmodulin inhibitors and CaM kinase II inhibitors significantly block glutamate-induced phase delay in the rat SCN (Fukushima et al., 1997). Previous workers using general NOS inhibitors have also suggested that NO might be required for photic entrainment of circadian rhythms in the SCN. For example, treatment with NOS inhibitors in vivo blocked light-induced entrainment of behavioral rhythm (Ding et al., 1994; Weber et al., 1995a; Melo et al., 1997). However, no obvious changes in the ability to entrain to the light/dark cycle, phase shift locomotor activity, or free run in constant dark were observed in nNOS knockout mice (Kriegsfeld et al., 1999). These observations suggest that NO is not essential for photic entrainment but rather modulates the process.

High-frequency stimulation (HFS) of the optic nerve has been known to induce long-term potentiation (LTP) in field excitatory postsynaptic potentials (fEPSPs) in the rat SCN (Nishikawa et al., 1995). The expression of LTP in the SCN after HFS to the optic nerve showed a circadian change in light/dark conditions. For example, during subjective day but not subjective night, HFS of the optic nerve produced an LTP formation in the SCN. This observation was in contrast to the lack of obvious circadian changes observed in hippocampal LTP formation (Nishikawa et al., 1995). In addition, electrical stimulation of the optic nerve in early and late subjective night produced a phase delay and advance, respectively, of circadian rhythm of SCN neuronal firing activity (Kim et al., 2001). Although the molecular basis underlying LTP may not be the same as that in the electrical stimulation-induced phase shift, LTP in the SCN is a useful model in vitro with which to investigate intracellular signaling associated with the optic nerve stimulation in the SCN. Furthermore, we report here that calcineurin is expressed in the SCN and that inhibition of its activity by cyclosporin A treatment potentiates LTP induction and also that melatonin inhibits LTP induction by inhibiting CaM kinase II activity in the rat SCN.

MATERIALS AND METHODS

Materials

The following chemicals and materials were obtained from the indicated sources: antiactive MAP kinase (pERK), calmidazolium (R24517), and L-NAME from Sigma (St. Louis, MO); D-AP5 from Tocris (Langford, United Kingdom); myristoylated AIP, a CaM kinase II inhibitor, and myristoylated PKI amide, a protein kinase A inhibitor, from Biomol (Plymouth Meeting, PA); antivasoactive intestinal polypeptide (VIP) antibody from Santa Cruz Biotechnology (Santa Cruz, CA); and antiphosphorylated cAMP-responsive element binding protein (CREB) from Cell Signaling Technology (Beverly, MA). Antiactive CaM kinase II was prepared as described elsewhere (Liu et al., 1999). Cyclosporin A (Sandimmun) was a kind gift of Sandoz.

Electrophysiology

Electrophysiological experiments were performed basically according to a previous report (Nishikawa et al., 1995). Briefly, male Wistar rats (200–250 g) or male golden hamsters (80–100 g) were housed under a 12:12 hr light/dark cycle (lights on at 0700 hr). Because we wanted to analyze the Ca^{2+}-dependent signaling pathways involved in glutamate-induced phase shifts, we stimulated SCN slices in the early subjective night. To do so, animals were decapitated at zeitgeber time (ZT)10–12 while under ether anesthesia and the brains quickly removed from the skull. Horizontal hypothalamic slices (500 μm thickness) with optic nerves were prepared using a microslicer (DTK-1500; D.S.K. microslicer). The slices were incubated in continuously oxygenized (95% O_2, 5% CO_2) artificial cerebrospinal fluid (ACSF) at room temperature for 1 hr and at 34°C for another 1 hr. After a 2-hr recovery period, a slice was transferred to an interface recording chamber and perfused with ACSF warmed to 34°C. The fEPSP was evoked by a 0.05-Hz test stimulus through a bipolar stimulating electrode placed on the optic nerve and recorded from the ventrolateral portion of the SCN using a glass electrode filled with 3 M NaCl during ZT12–18 as described elsewhere (Nishikawa et al. 1995). The fEPSP was collected at 0.05 Hz and averaged for every 1 min (three traces). The amplitude of the EPSP was automatically recorded by an LTP analyzing system (FAL-3000; Furusawa Laboratory, Saitama, Japan). Before induction of LTP, the strength of optic nerve stimulation was adjusted to obtain a response of about half of the maximal amplitude of population spikes. After observation of a stable response from the SCN over 30 min, HFS (100 Hz for 1sec) was applied to induce LTP. The amplitude of the postsynaptic field potential before HFS was expressed as 100%.

Immunohistochemistry

After electrophysiological experiments, slices were fixed at 4°C overnight in 4% paraformaldehyde and 0.1% glutaraldehyde in 0.1 M phosphate buffer at the indicated time. Fifty-micrometer slices were prepared using the microslicer from 500-μm slices in Tris-buffered saline (TBS) containing 20 mM Tris-HCl, pH 7.5, and 0.15 M NaCl. The thin slices were incubated in TBS containing 0.03% Triton X-100 for 1 hr at room temperature prior to fluorescence immunohistochemistry using tyramide signal amplification (NEN Life Science Products, Inc., Boston, MA), according to the manufacturer's protocol. Antiactive CaM kinase II (rabbit IgG) and anti-VIP (goat IgG) antibodies were used as primary antibody. Bound rabbit IgG was visualized using Alexa 488-conjugated anti-rabbit IgG (Molecular Probes, Inc., Eugene, OR), and bound goat IgG was detected by a combination of biotinylated anti-goat IgG and horseradish peroxidase (HRP)-conjugated streptavidin, followed by treatment with tetramethylrhodamine-tyramide (NEN Life Science Products, Inc.). The sections were analyzed by laser confocal microscopy (FluoView; Olympus, Tokyo, Japan).

Immunoblot Analysis

To measure the activities of CaM kinase II and MAP kinase (ERK) and the phosphorylation of CREB, bilateral SCN were dissected under a microscope 5 min after HFS. The SCN was dissected at the same time from control slices without HFS but with the test stimulation at 0.05 Hz. Each tissue sample was stored in a test tube and kept at −80°C before use. Each frozen

slice was homogenized with a hand homogenizer and sonicated with a Sonifier-250 (Branson, Danbury, CT) at 0°C in 50 μl of the homogenization buffer containing 50 mM Tris-HCl (pH 7.5), 0.5% Triton X-100, 4 mM EGTA, 10 mM EDTA, 0.5 M NaCl, 1 mM Na_3VO_4, 30 mM sodium pyrophosphate, 50 mM NaF, 50 μg/ml leupeptin, 25 μg/ml pepstatin A, 50 μg/ml trypsin inhibitor, and 1 mM dithiothreitol (DTT). Insoluble materials were removed by a 10-min centrifugation at 15,000*g*. Following determination of protein content in each supernatant fraction using Bradford's solution, each sample containing equivalent amounts (20 μg) of protein was applied to a 10% acrylamide denaturing gel (SDS-PAGE). After electrophoresis, proteins were transferred for 2 hr at 70 V to a polyvinylidene difluoride membrane (Millipore, Bedford, MA). Blotted membranes were incubated for 1 hr in phosphate-buffered saline (PBS) containing 4% dry milk (blocking solution) at room temperature and incubated overnight at 4°C with a 1:500 dilution of antiactive CaM kinase II antibody in blocking solution. After several washes with TBS containing 0.1% Nonidet P-40 (NTBS), the membranes were incubated for 1 hr with HRP-conjugated anti-rabbit antibody (Amersham Pharmacia Biotech, Arlington Heights, IL) diluted 1:5,000. The membranes were then processed with enhanced chemiluminescence (ECL) Western blotting detection reagents (Amersham Pharmacia Biotech). The images were scanned and analyzed semiquantitatively using NIH Image (available at http://rsb.info.nih.gov/nih-image). Similar methods were used for immunoblotting with antiactive MAP kinase (pERK), anti-CaM kinase II, or antiphosphorylated CREB (pCREB).

Statistical Evaluation

The values are means ± SE. Comparison between two experimental groups was made by the unpaired Student's *t*-test. For multiple comparisons, one-way analysis of variance with Sheffe's correction was used, and *P* values of <0.05 were considered to have statistical significance.

RESULTS

Effects of Various Inhibitors on HFS-Induced LTP in the SCN

The induction of LTP in the rat SCN was known to represent circadian changes in which HFS of the optic nerve in the subjective day but not in the subjective night produced LTP in the fEPSP (Nishikawa et al., 1995). To determine the role of Ca^{2+}-dependent signaling pathways in light- and glutamate-induced phase shifts in the subjective night, we stimulated the optic nerve and recorded the fEPSP during the subjective night. Thus we prepared the SCN slices during ZT10–12 for electrophysiological experiments and monitored the fEPSP from the SCN during ZT12–18. Similarly to the case in previous work (Nishikawa et al., 1995), LTP in the rat SCN slowly developed, and maximally increased EPSP was observed 60–90 min after HFS (Fig. 1B). We also observed inhibition of the EPSP immediately after HFS in most of the SCN slices, which was not observed in the previous work (Nishikawa et al., 1995). LTP induction was partially inhibited by

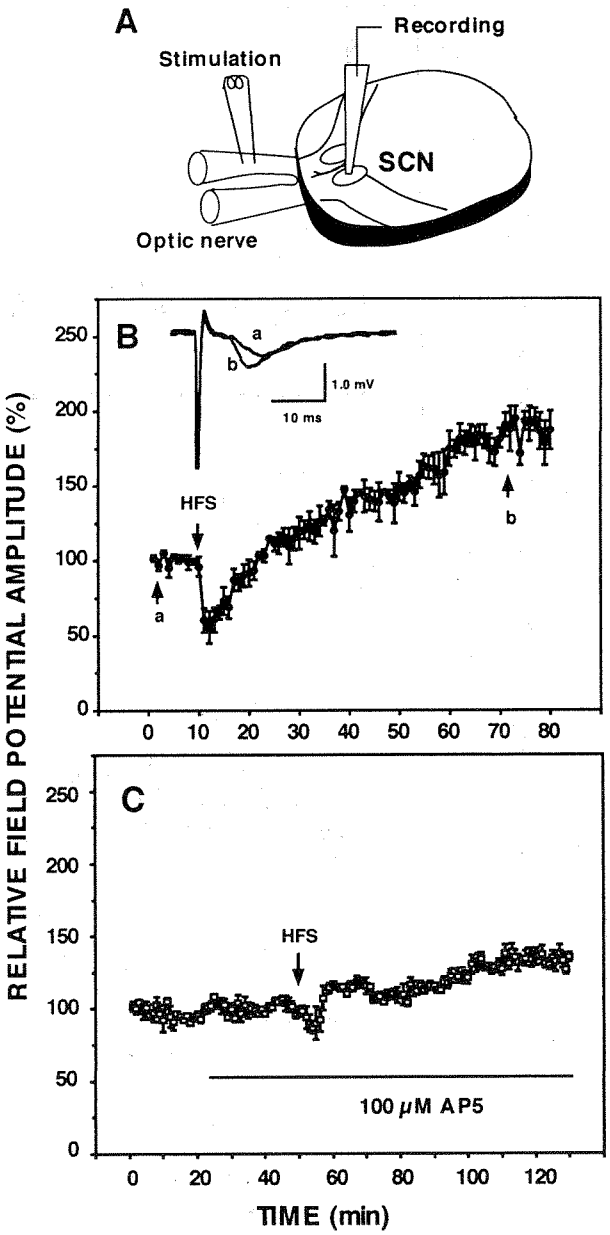

Fig. 1. Expression of LTP in the rat SCN and the effects of AP5. **A:** SCN slices were prepared, and the optic nerve was stimulated to evoke field EPSP (fEPSP). **B,inset:** Representative traces show the postsynaptic fEPSP recorded at the indicated time (arrows a and b). Each trace is an average of three sweeps. Time course of the induction of LTP in the SCN after HFS (100 Hz, 1 sec duration). The averaged fEPSP amplitude at each time point was normalized to the averaged baseline for 10 min before HFS, which is represented as 100% (n = 6). **C:** The slices were treated with 100 μM AP5 before and after HFS (as indicated by the bar; n = 4).

treatment with D-AP5, an NMDA receptor antagonist (Fig. 1C). The evoked EPSP was not blocked by D-AP5 but was totally blocked by treatment with the AMPA receptor antagonist CNQX (data not shown). These ob-

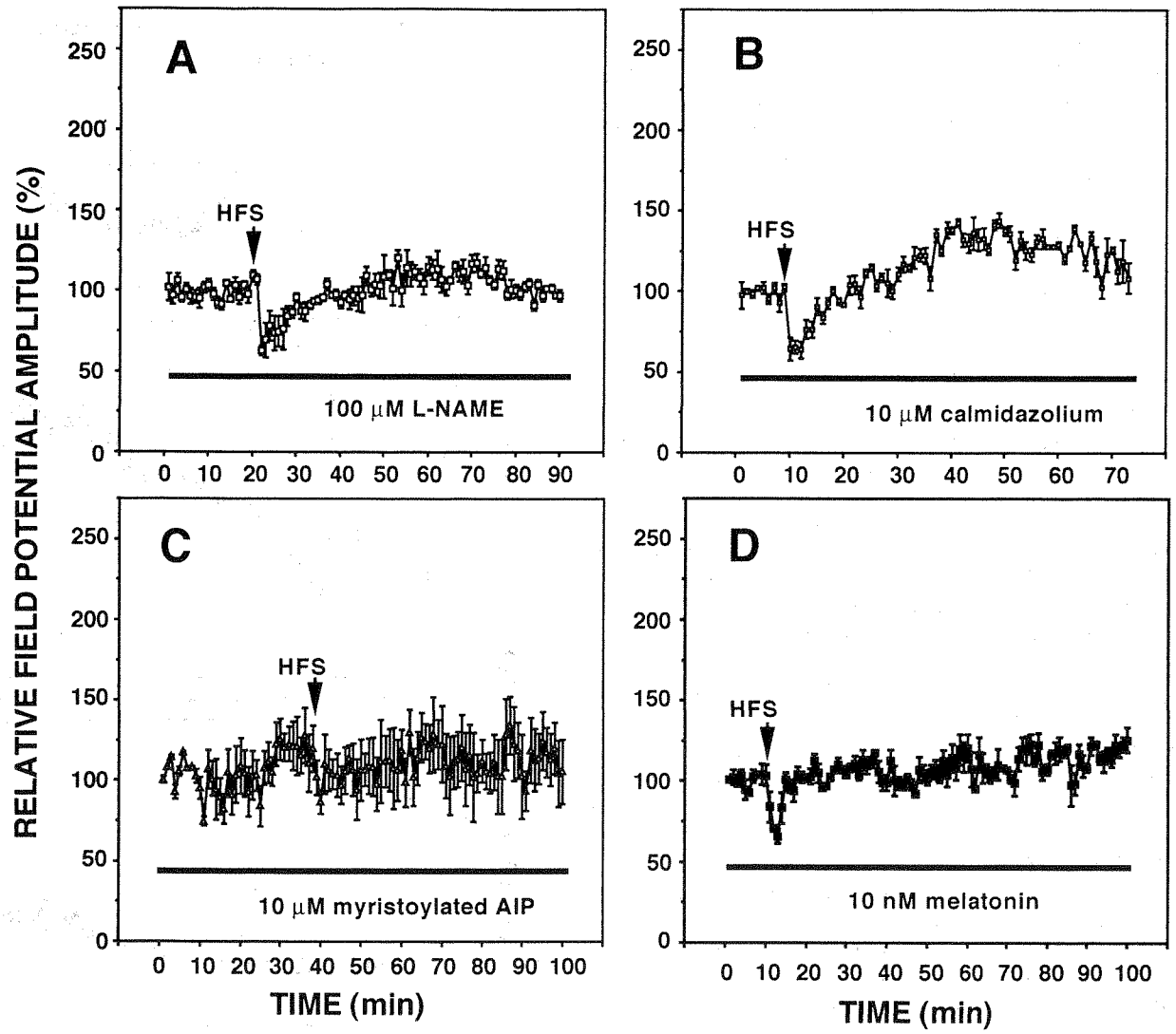

Fig. 2. Effects of L-NAME, calmidazolium, myristoylated AIP, and melatonin on HFS-induced LTP in the rat SCN. Each time point indicates the average of the fEPSP amplitude and is expressed as percentage of the baseline (n = 4). The slices were treated with 100 μM L-NAME (**A**), 10 μM calmidazolium (**B**), 10 μM myristoylated AIP (**C**), or 10 nM melatonin (**D**) before and after HFS. None of these treatments affected basal synaptic neurotransmission.

servations suggest that the evoked EPSP occurred through AMPA receptor ion channels.

To identify the intracellular mechanisms involved in LTP induction in the SCN, we tested several inhibitors of NOS and CaM kinases on LTP induction. We first found that treatment with L-NAME, a potent inhibitor of NOS, completely inhibited LTP induction, without changing an early inhibition of EPSP (Fig. 2A). Treatment with calmidazolium, a calmodulin antagonist, also prevented LTP induction (Fig. 2B). Because LTP induction in the hippocampus requires CaM kinase II activation, we determined the effect of a cell-permeable CaM kinase II inhibitor, myristoylated-AIP, on LTP induction. Treatment with myristoylated AIP did not affect basal synaptic transmission (data not shown) but totally abolished LTP induction (Fig. 2C). Treatment with myristoylated PKI amide, a cell-permeable protein kinase A inhibitor, did not affect LTP induction, as described below (see Fig. 4). Taken together, these findings indicate that CaM kinase II plays a pivotal role in LTP induction in the rat SCN, as it does in hippocampal LTP. We next determined the effect of melatonin, which forms a feedback loop to the SCN from the pineal gland and can affect the biological clock by phase shifting of circadian rhythms. Treatment with 10 nM melatonin had no effect on basal synaptic transmission (see Fig. 4) but totally abolished HFS-induced LTP (Fig. 2D). Thus melatonin may act on CaM kinase II-dependent signals involved in LTP induction, as discussed below.

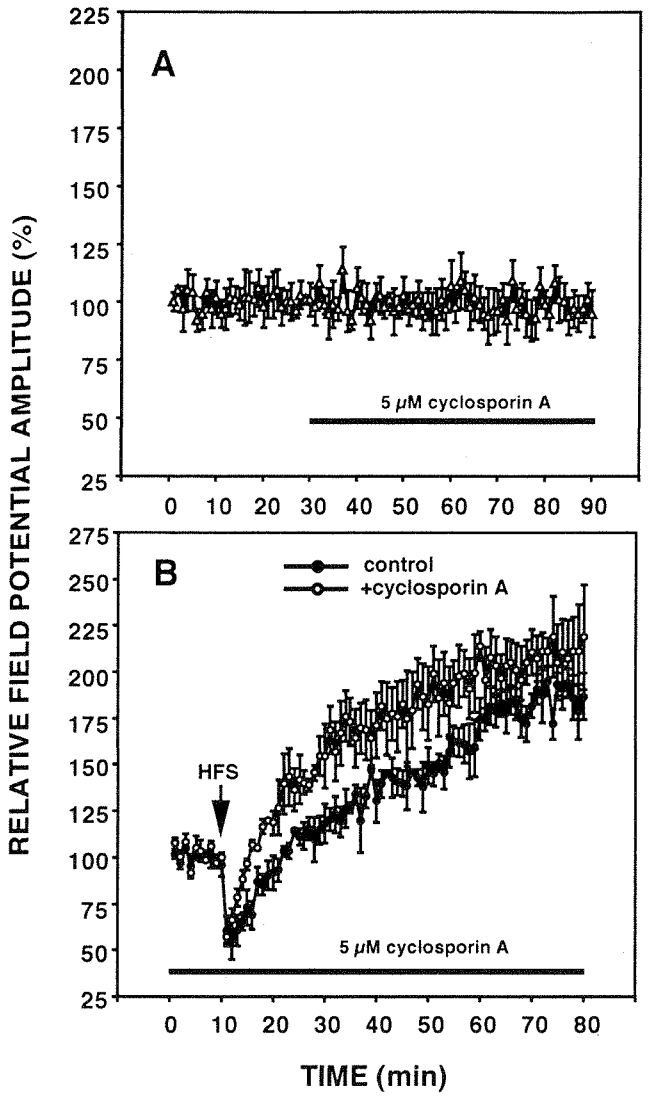

Fig. 3. Effect of cyclosporin A on HFS-induced LTP in the rat SCN. **A:** Effects of 5 μM cyclosporin A on basal synaptic transmission. After a stable baseline was obtained, slices were treated cyclosporin A for 60 min during recording. **B:** After a stable baseline was obtained in the presence of 5 μM cyclosporin A, the slices received HFS at the indicated time. Each trace is an average of three sweeps (means ± SE from four slices).

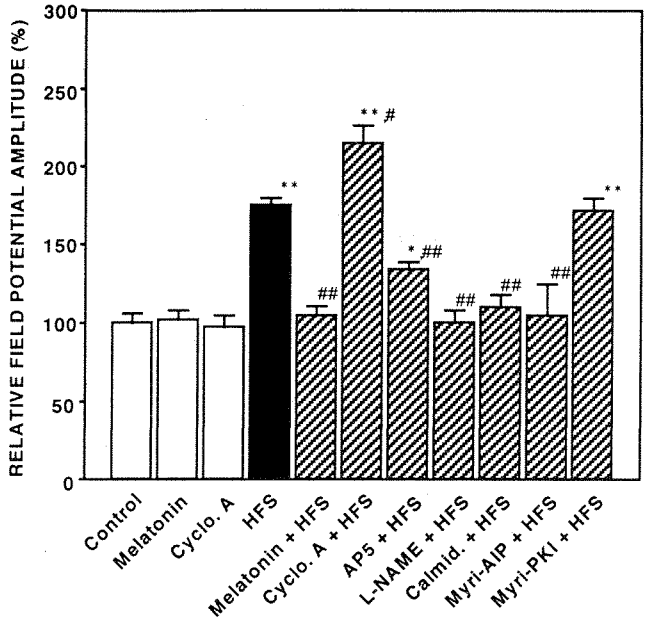

Fig. 4. Summary of effects of various inhibitors and melatonin on basal synaptic transmission and HFS-induced LTP in the rat SCN. Each value indicates percentage changes in fEPSF 60 min after HFS and is normalized by averaged fEPSP amplitude before HFS. Open columns indicate basal synaptic transmission in the presence or absence of drugs. The averaged values of fEPSP between 55 and 65 min was expressed as percentage of fEPSP before application of drugs or HFS (n = 4 in melatonin and cyclosporin A groups). The solid and hatched columns represent fEPSP following HFS without and with drugs, respectively. The fEPSPs at 60 min after HFS were the averaged values between 55 and 65 min after HFS (n = 8 in control and HFS; n = 6 in cyclosporin A, AP5, and melatonin treatments; and n = 4 in L-NAME, calmidazolium, myristoylated AIP, and myristoylated PKI treatments). $*P < 0.05$, $**P < 0.01$ between control and HFS groups. $\#P < 0.05$, $\#\#P < 0.01$ vs. control within each control and HFS group.

Effects of Cyclosporin A on HFS-Induced LTP

Because calcineurin is required for expression of long-term depression (LTD) in the hippocampal CA1 region (Mulkey et al., 1994), we asked whether calcineurin functions in LTP induction in the SCN. Treatment with 5 μM cyclosporin A, a calcineurin inhibitor, significantly potentiated LTP induction, without affecting basal synaptic transmission in the rat SCN (Fig. 3A,B). The effects of various inhibitors and melatonin on basal synaptic transmission and HFS-induced LTP in the rat SCN are summarized in Figure 4. Similarly to melatonin and cyclosporin A treatment, treatment with AP5, L-NAME, calmidazolium, or myristoylated AIP or PKI had no effect on the basal synaptic transmission (data not shown). Two significant observations in the present study were that, in the rat SCN, melatonin completely abolished LTP induction, whereas cyclosporin A significantly potentiated LTP induction.

HFS-Induced Activation of CaM Kinase II in the SCN

To confirm involvement of CaM kinase II following LTP induction, we analyzed autophosphorylation of CaM kinase II 5 min after HFS in cell extracts from control and potentiated slices by immunoblotting with antiphospho-Thr-286 antibody (also known as "antiactive CaM kinase II antibody"). We also determined the effects of cyclosporin A, myristoylated AIP, and melatonin treatment on CaM kinase II autophosphorylation. The antibody used recognizes autophosphorylation of Thr-286/287 in all CaM kinase II isoforms (data not shown). Four major

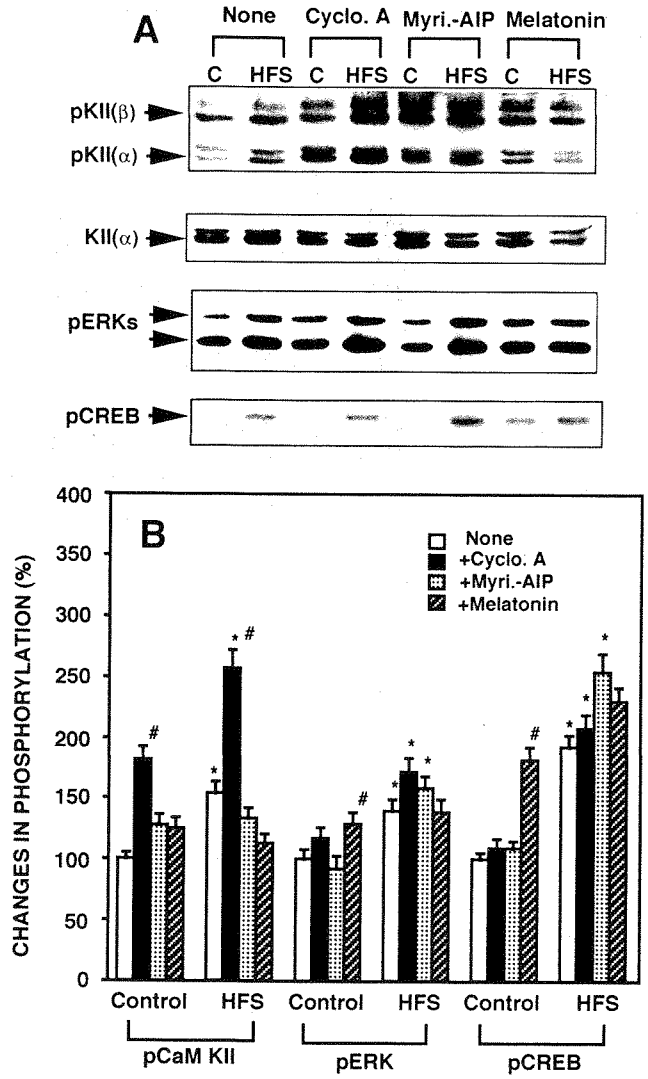

Fig. 5. Effects of cyclosporin A, myristoylated AIP, and melatonin on HFS-induced phosphorylation of CaM kinase II, MAP kinase, and CREB. Slices were treated with 5 μM cyclosporin A, 10 μM myristoylated AIP, and 10 nM melatonin as for Figures 2 and 3. The SCN was dissected 5 min after HFS. Control slices were dissected under the same procedure without HFS. Slices were obtained from six rats in each treatment. **A:** Immunoblotting analysis using antibodies against autophosphorylated CaM kinase II (pKII), CaM kinase IIα (KIIα), phosphorylated MAP kinase (pERKs), and phosphorylated CREB (pCREB) was carried out with extracts from the same slices. **B:** Immunoreactive bands in the autoradiograph were analyzed semiquantitatively using NIH Image and are summarized. $*P < 0.05$ vs. control in each condition. $\#P < 0.05$ vs. control without test drug (none).

immunoreactive proteins of 50–60 kDa in the rat SCN were recognized by the antibody used (Fig. 5A). Among them, a 50-kDa form of CaM kinase IIα was the predominant autophosphorylated product in the SCN following HFS. Other CaM kinase II isoforms of 51, 59, and 60 kDa were less responsive following HFS. Because the CaM kinase IIα antibody recognized the 51-kDa protein in addition to a 50-kDa α subunit, the 51-kDa subunit is possibly the α_B subunit of CaM kinase II previously described (Takeuchi et al., 2000). As shown in Figure 5A, HFS increased autophosphorylation of CaM kinase II at Thr-286 without changing CaM kinase IIα protein levels. Treatment with cyclosporin A alone stimulated CaM kinase II autophosphorylation under basal conditions and further enhanced the autophosphorylation following LTP induction. Consistently with inhibition of LTP induction, myristoylated AIP prevented increased autophosphorylation of CaM kinase II, without affecting basal autophosphorylation. Similarly, melatonin completely eliminated HFS-induced increases in CaM kinase II autophosphorylation (Fig. 5A,B).

To address specificity and relevance of inhibitor effects, we also measured MAP kinase activation and phosphorylation of its downstream target, CREB. As expected, in the SCN, HFS stimulated dual phosphorylation of the activation loop of MAP kinase (ERK), resulting in 42- and 44-kDa products (Fig. 5A,B). However, cyclosporin A did not potentiate phosphorylation of MAP kinase in either control or potentiated slices. Myristoylated AIP had no effect on HFS-induced MAP kinase activation. Interestingly, treatment with melatonin stimulated MAP kinase phosphorylation as well as CREB phosphorylation under the basal conditions but did not potentiate MAP kinase activation and the CREB phosphorylation following HFS. Consistently with our hypothesis, phosphorylation of Ser-133 of CREB was closely associated with MAP kinase activation following LTP induction. Finally, the effects of inhibitors and melatonin on phosphorylation of protein kinases and CREB are summarized in Figure 5B. The immunoblot analysis showed that cyclosporin A significantly potentiated CaM kinase II autophosphorylation and that melatonin inhibited HFS-induced CaM kinase II activation.

We next determined the localization of the active form of CaM kinase II in the rat SCN by immunohistochemistry using the antiactive CaM kinase II antibody. Under basal conditions, modest immunoreactivity against active CaM kinase II was observed primarily in cell bodies, and weak immunoreactivity was seen in dendrites (Fig. 6C). Strong immunoreactivity was evident in dendrites and cell bodies in most VIP-positive neurons 5 min after HFS (Fig. 6D). In cell bodies, modest immunoreactivity was also observed in the nuclei of some neurons following HFS. In the ventral SCN, most active CaM kinase II-immunoreactive neurons were VIP positive, as shown in Figure 6A and B. Thus active CaM kinase II-reactive neurons are possibly innervated by glutamatergic neurons through the retinohypothalamic tract. Increased immunoreactivity against active CaM kinase II was stable for at least 1 hr after HFS (data not shown). Immunoreactivity detected by the conventional CaM kinase II antibody was not changed by HFS (data not shown).

DISCUSSION

We obtained several significant findings regarding the HFS-induced LTP in the rat SCN. As with hippocam-

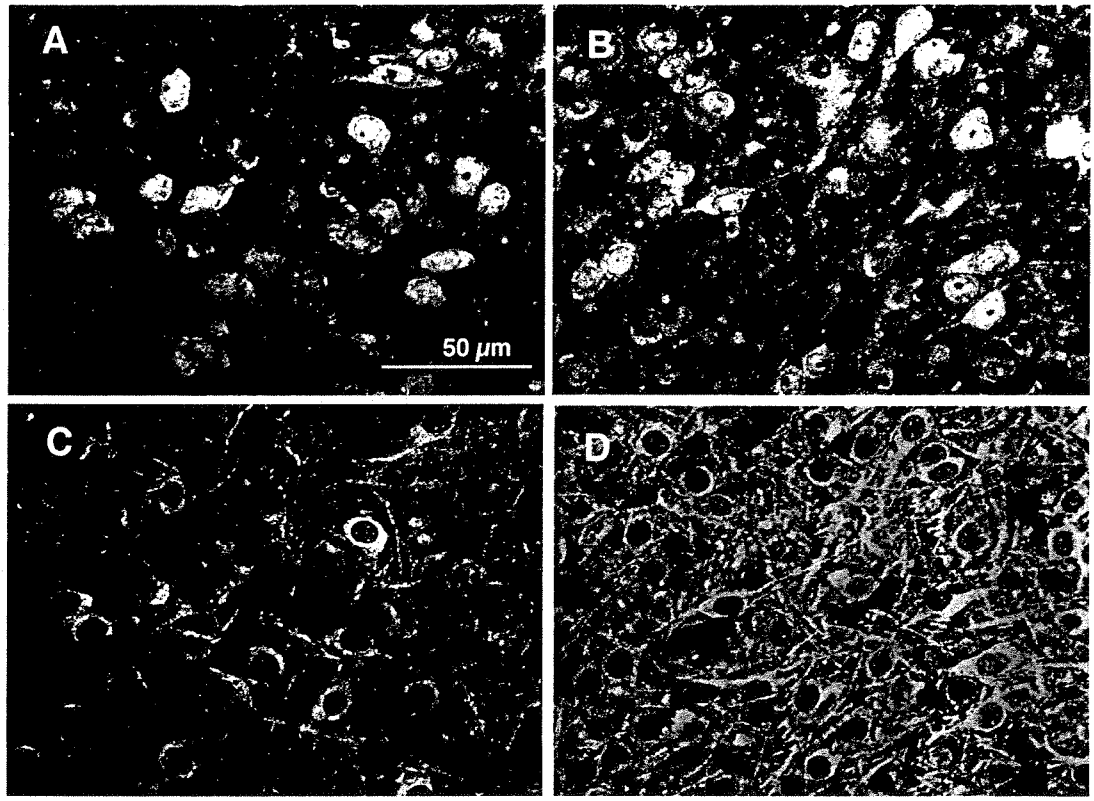

Fig. 6. Confocal images of immunoreactivity against antiactive CaM kinase II antibody. Control (**A,C**) and potentiated (**B,D**) SCN slices were fixed with 4% paraformaldehyde and 0.1% glutaraldehyde. Horizontal sections (50 μm) were made using a microslicer as described in Materials and Methods. The sections were doubly stained with anti-VIP antibody (A,B) and antiactive CaM kinase II antibody (C,D) and visualized using laser confocal microscopy. Images were composed of 10 confocal scans at 1-μm increments in the slices using the same intensity of the laser.

pal LTP, CaM kinase II plays an essential role in the induction of LTP in the SCN. Similarly, the MAP kinase pathway functions as a CREB kinase in the SCN LTP. Calcineurin in the SCN may suppress LTP induction through inhibition of the CaM kinase II pathway but not the MAP kinase pathway. The most interesting finding is that melatonin inhibits LTP induction through elimination of HFS-induced CaM kinase II activation.

Inconsistently with previous observations, in which LTP was hardly induced in the subjective night (Nishikawa et al., 1995), HFS-induced LTP was observed in the subjective night in most of the slices used in the present study. Although we cannot explain this discrepancy, animals were kept under constant dark conditions (DD condition) before preparing SCN slices in the previous study (Nishikawa et al., 1995) but in a 12:12 hr light/dark cycle (LD condition) in the present studies. Chambille (1999) recently reported observing circadian rhythm in immunoreactivity of the AMPA receptor GluR2/3 subunit in the SCN of syrian hamster: Strong immunoreactivity was seen during the subjective day compared with the subjective night in DD conditions, and LD conditions reduced the differences observed between day and night. A free-running procedure such as constant dark is possibly important for elucidating the circadian rhythms in LTP formation (Nishikawa et al., 1995). Because we could obtain stable LTP in the subjective night under our conditions, we tried to define molecular mechanisms underlying the LTP in rat SCN.

During the night, phase-shifting light stimuli evoked release of glutamate from neurons of the retinohypothalamic tract and activated NMDA and non-NMDA receptors. Therefore, the influx of Ca^{2+} activated neuronal NOS (nNOS) to produce NO (Ferreyra et al., 1998). The NO-cGMP signaling plays an essential role in light- and glutamate-induced phase shifting of circadian rhythms (Ding et al., 1994, 1997; Weber et al., 1995a; Mintz et al., 1999). For example, L-NAME, an NOS inhibitor, selectively attenuates phase advances of locomotor rhythms in vivo (Weber et al., 1995a; Melo et al., 1997), and inhibitors of cGMP-dependent protein kinase block light-induced phase advances of circadian rhythms in vivo (Weber et al., 1995b; Mathur et al., 1996). Similarly, CaM kinase inhibitors block the light-induced phase shifting in the circadian rhythm (Golombek and Ralph, 1994; Fukushima et al., 1997). Thus, cGMP-dependent protein ki-.

nase and CaM kinase signaling pathways may mediate light-induced phase shifts in circadian rhythms. In this study, LTP in the SCN was also blocked by treatment with L-NAME or CaM kinase inhibitors. We recently reported that CaM kinase II in vivo was activated by light stimulation (exposure with 300 lux for 15 min) in the hamster SCN (Yokota et al., 2001). The activation occurred predominantly in the ventrolateral SCN. Activation of CaM kinase II but not MAP kinase was correlated with induction of the *Per1* gene (Yokota et al., 2001). Optic nerve stimulation in this study also elicits pronounced activation of CaM kinase II in VIP neurons in the ventrolateral SCN. Although the phenomenon of LTP in the SCN observed here may not be directly associated with mechanisms underlying light-induced phase shifts, HFS-induced LTP is a useful model with which to investigate intracellular signaling following optic nerve stimulation.

Light-induced phase shifting in vivo in locomotor activity is associated with CREB phosphorylation in the SCN (Ginty et al., 1993; Von Gall et al., 1998). Here we show that HFS of the optic nerve consistently enhanced CREB phosphorylation in SCN slices in vitro (Fig. 5). However, myristoylated AIP did not inhibit HFS-induced CREB phosphorylation but blocked LTP induction. Thus, HFS-induced CREB phosphorylation may not occur through activation of CaM kinase II and is not involved in the early phase of LTP induction. MAP kinase was also activated by HFS in the same slices with increased CREB phosphorylation. Correlation between MAP kinase activation and CREB phosphorylation in the profile of effects of myristoylated AIP, cyclosporin A, and melatonin clearly demonstrates that MAP kinase and not CaM kinase II is the upstream kinase that promotes HFS-induced CREB phosphorylation.

Interestingly, treatment with melatonin alone produced increased CREB phosphorylation but failed to potentiate CREB phosphorylation by HFS. Consistently with these results, PACAP-induced CREB phosphorylation has been reported to be inhibited by melatonin treatment in the rat SCN (Kopp et al., 1999). Melatonin is an endogenous substance involved in nonphotic entrainment in the mammalian SCN. Melatonin elicits its effects through binding mt_1 and MT_2 receptors that are coupled to inhibition of adenylate cyclase activity (Reppert et al., 1994). Melatonin also activates calcium signaling pathways though protein kinase C activity (Godson and Reppert, 1997; McArthur et al., 1997). Melatonin-induced MAP kinase activation possibly is due to activation of protein kinase C. In the present study, we were not able to identify the mechanisms underlying the inhibitory effect of melatonin on HFS-induced CaM kinase II activation. Because melatonin inhibits calcium influx through voltage-dependent channels in the hypophysial gonadotrophs (Vanecek and Klein, 1992), melatonin may prevent the increase in the intracellular Ca^{2+} levels following HFS in the SCN. However, Kopp et al. (1999) reported the melatonin had no effects on PACAP-induced calcium influx in the rat SCN. Further experiments are needed to determine whether modulation of CaM kinase II and/or MAP kinase by melatonin is relevant for melatonin-induced entrainment of the biological clock.

Other noteworthy observations in the present study are that cyclosporin A caused potentiation of LTP induction as well as CaM kinase II autophosphorylation. Calcineurin did not directly dephosphorylate autophosphorylated CaM kinase II (Goto et al., 1985). Inhibition of calcineurin by cyclosporin A possibly enhanced phosphorylation of inhibitor 1 and thereby inhibited protein phosphatase 1, as described previously (Mulkey et al., 1994). The inhibition of protein phosphatase 1 may account for the increase in CaM kinase II autophosphorylation. The physiological relevance of calcineurin in the SCN is now under investigation using cyclosporin A in vivo.

In the present work, electrophysiological studies suggest that common mechanisms underlie the elucidation of HFS-induced LTP and light-induced phase shifting in the SCN. We have observed that melatonin blocks CaM kinase II signaling and that the inhibition is correlated with elimination of LTP. Although several endogenous substances, such as neuropeptide Y and serotonin, have been identified as nonphotic stimulants of circadian rhythm, the intracellular mechanisms of the nonphotic entrainment were not clear. Thus, the HFS-induced LTP observed in SCN slices is a useful model for investigating signaling of nonphotic as well as photic entrainment. Our future direction is to determine the intracellular signaling pathways underlying optic nerve stimulation-induced phase shifts and nonphotic entrainment using SCN slices in vitro.

REFERENCES

Albrecht U, Sun ZS, Eichele G, Lee CC. 1997. A differential response of two putative mammalian circadian regulators, mper1 and mper2, to light. Cell 91:1055–1064.

Chambille I. 1999. Circadian rhythm of AMPA receptor GluR 2/3 subunits immunoreactivity in the suprachiasmatic nuclei of Syrian hamster and effects of a light-dark cycle. Brain Res 833:27–38.

Ding JM, Chen D, Weber ET, Faiman LE, Rea MA, Gillette MU. 1994. Resetting the biological clock: mediation of nocturnal circadian shifts by glutamate and NO. Science 266:1713–1717.

Ding JM, Faiman LE, Hurst WJ, Kuriashkina LR, Gillette MU. 1997. Resetting the biological clock: mediation of nocturnal CREB phosphorylation via light, glutamate, and nitric oxide. J Neurosci 17:667–675.

Ferreyra GA, Cammarota MP, Golombek DA. 1998. Photic control of nitric oxide synthase activity in the hamster suprachiasmatic nuclei. Brain Res 797:190–196.

Fukushima T, Shimazoe T, Shibata S, Watanabe A, Ono M, Hamada T, Watanabe S. 1997. The involvement of calmodulin and Ca^{2+}/calmodulin-dependent protein kinase II in the circadian rhythms controlled by the suprachiasmatic nucleus. Neurosci Lett 227:45–48.

Ginty DD, Kornhauser JM, Thompson MA, Bading H, Mayo KE, Takahashi JS, Greenberg ME. 1993. Regulation of CREB phosphorylation in the suprachiasmatic nucleus by light and a circadian clock. Science 260: 238–241.

Godson C, Reppert SM. 1997. The Mel1a melatonin receptor is coupled to parallel signal transduction pathways. Endocrinology 138:397–404.

Golombek DA, Ralph MR. 1994. KN-62, an inhibitor of Ca^{2+}/calmodulin kinase II, attenuates circadian responses to light. Neuroreport 5:1638–1640.

Goto S, Yamamoto H, Fukunaga K, Iwasa T, Matsukado Y, Miyamoto E. 1985. Dephosphorylation of microtubule-associated protein 2, tau factor, and tubulin by calcineurin. J Neurochem 45:276–283.

Kim DY, Kang HC, Shin HC, Lee KJ, Yoon YW, Han HC, Na HS, Hong SK, Kim YI. 2001. Substance p plays a critical role in photic resetting of the circadian pacemaker in the rat hypothalamus. J Neurosci 21:4026–4031.

King DP, Takahashi JS. 2000. Molecular genetics of circadian rhythms in mammals. Annu Rev Neurosci 23:713–742.

Kopp MD, Schomerus C, Dehghani F, Korf H-W, Meissl H. 1999. Pituitary adenylate cyclase-activating polypeptide and melatonin in the suprachiasmatic nucleus: effects on the calcium signal transduction cascade. J Neurosci 19:206–219.

Kriegsfeld LJ, Demas GE, Lee SE Jr, Dawson TM, Dawson VL, Nelson RJ. 1999. Circadian locomotor analysis of male mice lacking the gene for neuronal nitric oxide synthase (nNOS−/−). J Biol Rhythms 14:20–27.

Liu J, Fukunaga K, Yamamoto H, Nishi K, Miyamoto E. 1999. Differential roles of Ca^{2+}/calmodulin-dependent protein kinase II and mitogen-activated protein kinase activation in hippocampal long-term potentiation. J Neurosci 19:8292–8299.

Mathur A, Golombek DA, Ralph MR. 1996. cGMP-dependent protein kinase inhibitors block light-induced phase advances of circadian rhythms in vivo. Am J Physiol 270:R1031–R1036.

McArthur AJ, Hunt AE, Gillette MU. 1997. Melatonin action and signal transduction in the rat suprachiasmatic circadian clock: activation of protein kinase C at dusk and dawn. Endocrinology 138:627–634.

Melo L, Golombek DA, Ralph MR. 1997. Regulation of circadian photic responses by nitric oxide. J Biol Rhythms 12:319–326.

Mintz EM, Marvel CL, Gillespie CF, Price KM, Albers HE. 1999. Activation of NMDA receptors in the suprachiasmatic nucleus produces light-like phase shifts of the circadian clock in vivo. J Neurosci 19:5124–5130.

Miyake S, Sumi Y, Yan L, Takekida S, Fukuyama T, Ishida Y, Yamaguchi S, Yagita K, Okamura H. 2000. Phase-dependent responses of Per1 and Per2 genes to a light-stimulus in the suprachiasmatic nucleus of the rat. Neurosci Lett 294:41–44.

Mulkey RM, Endo S, Shenolikar S, Malenka RC. 1994. Involvement of a calcineurin/inhibitor-1 phosphatase cascade in hippocampal long-term depression. Nature 369:486–488.

Nishikawa Y, Shibata S, Watanabe S. 1995. Circadian changes in long-term potentiation of rat suprachiasmatic field potentials elicited by optic nerve stimulation in vitro. Brain Res 695:158–162.

Reppert SM, Weaver DR. 2001. Molecular analysis of mammalian circadian rhythms. Annu Rev Physiol 63:647–676.

Reppert SM Weaver DR, Ebisawa T. 1994. Cloning and characterization of a mammalian melatonin receptor that mediates reproductive and circadian responses. Neuron 13:1177–1185.

Shibata S, Watanabe A, Hamada T, Ono M, Watanabe S. 1994. N-methyl-D-aspartate induces phase shifts in circadian rhythm of neuronal activity of rat SCN in vitro. Am J Physiol 267:R360–R364.

Shigeyoshi Y, Taguchi K, Yamamoto S, Takekida S, Yan L, Tei H, Moriya T, Shibata S, Loros JJ, Dunlap JC, Okamura H. 1997. Light-induced resetting of a mammalian circadian clock is associated with rapid induction of the mPer1 transcript. Cell 91:1043–1053.

Shirakawa T, Moore RY. 1994. Glutamate shifts the phase of the circadian neuronal firing rhythm in the rat suprachiasmatic nucleus in vitro. Neurosci Lett 178:47–50.

Takeuchi Y, Yamamoto H, Fukunaga K, Miyakawa T, Miyamoto E. 2000. Identification of the isoforms of Ca^{2+}/calmodulin-dependent protein kinase II in rat astrocytes and their subcellular localization. J Neurochem 74:2557–2567

Vanecek J, Klein DC. 1992. Sodium-dependent effects of melatonin on membrane potential of neonatal rat pituitary cells. Endocrinology 131: 939–946.

Von Gall C, Duffield GE, Hastings MH, Kopp MD, Dehghani F, Korf HW, Stehle JH. 1998. CREB in the mouse SCN: a molecular interface coding the phase-adjusting stimuli light, glutamate, PACAP, and melatonin for clockwork access. J Neurosci 18:10389–10397.

Watanabe A, Hamada T, Shibata S, Watanabe S. 1994. Effects of nitric oxide synthase inhibitors on N-methyl-D-aspartate-induced phase delay of circadian rhythm of neuronal activity in the rat suprachiasmatic nucleus in vitro. Brain Res 646:161–164.

Weber ET, Gannon RL, Michel AM, Gillette MU, Rea MA. 1995a. Nitric oxide synthase inhibitor blocks light-induced phase shifts of the circadian activity rhythm, but not c-fos expression in the suprachiasmatic nucleus of the Syrian hamster. Brain Res 692:137–142.

Weber ET, Gannon RL, Rea MA. 1995b. cGMP-dependent protein kinase inhibitor blocks light-induced phase advances of circadian rhythms in vivo. Neurosci Lett 197:227–230.

Yokota S, Yamamoto M, Moriya T, Akiyama M, Fukunaga K, Miyamoto E, Shibata S. 2001. Involvement of calcium-calmodulin protein kinase but not mitogen-activated protein kinase in light-induced phase delays and Per gene expression in the suprachiasmatic nucleus of the hamster. J Neurochem 77:618–627.

THE JOURNAL OF BIOLOGICAL CHEMISTRY
Vol. 278, No. 3, Issue of January 17, pp. 1966–1974, 2003
Printed in U.S.A.

Secretory Granule-mediated Co-secretion of L-Glutamate and Glucagon Triggers Glutamatergic Signal Transmission in Islets of Langerhans*

Received for publication, July 8, 2002, and in revised form, October 21, 2002
Published, JBC Papers in Press, October 31, 2002, DOI 10.1074/jbc.M206758200

Mitsuko Hayashi‡§, Hiroshi Yamada‡¶, Shunsuke Uehara‡, Riyo Morimoto‡, Akiko Muroyama‡, Shouki Yatsushiro‡‖, Jun Takeda, Akitsugu Yamamoto‡‡, and Yoshinori Moriyama‡§§**

*From the ‡Department of Biochemistry, Faculty of Pharmaceutical Sciences, Okayama University, Okayama 700-8530, the **Department of Cell Biology, Institute for Molecular and Cellular Regulation, Gunma University, Maebashi 371-8512, and the ‡‡Department of Physiology, Kansai Medical University, Moriguchi, Osaka 570-8506, Japan*

L-Glutamate is believed to function as an intercellular transmitter in the islets of Langerhans. However, critical issues, *i.e.* where, when and how L-glutamate appears, and what happens upon stimulation of glutamate receptors in the islets, remain unresolved. Vesicular glutamate transporter 2 (VGLUT2), an isoform of the vesicular glutamate transporter essential for neuronal storage of L-glutamate, is expressed in α cells (Hayashi, M., Otsuka, M., Morimoto, R., Hirota, S., Yatsushiro, S., Takeda, J., Yamamoto, A., and Moriyama, Y. (2001) *J. Biol. Chem.* 276, 43400–43406). Here we show that VGLUT2 is specifically localized in glucagon-containing secretory granules but not in synaptic-like microvesicles in αTC6 cells, clonal α cells, and islet α cells. VGLUT1, another VGLUT isoform, is also expressed and localized in secretory granules in α cells. Low glucose conditions triggered co-secretion of stoichiometric amounts of L-glutamate and glucagon from αTC6 cells and isolated islets, which is dependent on temperature and Ca^{2+} and inhibited by phentolamine. Similar co-secretion of L-glutamate and glucagon from islets was observed upon stimulation of β-adrenergic receptors with isoproterenol. Under low glucose conditions, stimulation of glutamate receptors facilitates secretion of γ-aminobutyric acid from MIN6 m9, clonal β cells, and isolated islets. These results indicate that co-secretion of L-glutamate and glucagon from α cells under low glucose conditions triggers GABA secretion from β cells and defines the mode of action of L-glutamate as a regulatory molecule for the endocrine function. To our knowledge, this is the first example of secretory granule-mediated glutamatergic signal transmission.

L-Glutamate is the major excitatory neurotransmitter in the central nervous system and plays important roles in many neuronal processes such as fast synaptic transmission and neuronal plasticity (1, 2). To use L-glutamate as an intercellular signaling molecule, neuronal cells develop the glutamatergic system. Thus, L-glutamate is accumulated in synaptic vesicles through vesicular glutamate transporters (VGLUTs),[1] and is secreted through exocytosis. The released L-glutamate binds to the receptor so as to transmit signals intercellularly. The excess amount of L-glutamate in synaptic cleft is sequestrated through plasma membrane-type glutamate transporter.

Recent evidence has indicated that peripheral non-neuronal tissues also possess the glutamatergic system and use L-glutamate as an intercellular transmitter (3). The islet of Langerhans, a pancreatic miniature organ for the hormones regulating the blood glucose level, is composed of four major types of endocrine cells, *i.e.* insulin-secreting β cells, glucagon-secreting α cells, somatostatin-secreting δ cells, and pancreatic polypeptide-secreting F cells. These islet cells expresses functional glutamate receptors and plasma membrane-type glutamate transporter (4–11), suggesting that L-glutamate functions as an intercellular transmitter in islet. In fact, L-glutamate has been shown to affect secretion of insulin or glucagon from islet cells, isolated islets, or perfused pancreas (4–11). However, the role of L-glutamate as an intercellular chemical transmitter in the islets has been long controversial, mainly because critical issues, *i.e.* where, when, and how L-glutamate appears in the islets and what happens upon stimulation of glutamate receptors in the islets, remain unresolved.

Recent findings indicate that brain-specific Na^+-dependent inorganic phosphate cotransporter (12) and its isoform, differentiation-associated Na^+-dependent inorganic phosphate cotransporter (13), function as VGLUTs and are thus abbreviated as VGLUT1 and VGLUT2, respectively (14–21). These VGLUTs seem to be potential probes for the site of L-glutamate release in peripheral tissues as well as the central nervous system since these transporters are essential for L-glutamate signal output. We have shown that VGLUT2 is expressed in αTC6 cells, clonal α cells, and islet α cells, but not in β or δ cells (18). These results are consistent with the occurrence of Ca^{2+}-dependent exocytosis of L-glutamate from αTC6 cells (22) and suggest that α cells are the sites of L-glutamate signal appearance.

During course of the study, we noticed that the expression and subcellular localization of VGLUTs are of extraordinary

* This study was supported by a grant-in-aid for Scientific Research from the Ministry of Education, Science, Sports, and Culture of Japan, Core Research for Evolutional Science, the Yamanouchi Foundation for Research on Metabolic Disorders, the Takeda Science Foundation, and the Umami Research Foundation. The costs of publication of this article were defrayed in part by the payment of page charges. This article must therefore be hereby marked "*advertisement*" in accordance with 18 U.S.C. Section 1734 solely to indicate this fact.

§ Supported by a Research Fellowship from the Japan Society for the Promotion of Science for Young Scientists.

¶ Present address: Dept. of Neuroscience, Graduate School of Medicine and Dentistry, Okayama University, Okayama 700-8558, Japan.

‖ Supported by a Research Fellowship from the Japan Society for the Promotion of Science for Young Scientists.

§§ To whom correspondence should be addressed. Tel.: 81-86-251-7933; Fax: 81-86-251-7933; Email: moriyama@pheasant.pharm.okayama-u.ac.jp.

[1] The abbreviations used are: VGLUT, vesicular glutamate transporter; MOPS, 4-morpholinepropanesulfonic acid; RT, reverse transcription; DMEM, Dulbecco's modified Eagle's medium; GABA, γ-aminobutyrate; AMPA, (RS)-α-amino-3-hydroxy-5-methyl-4-isoxazolepropionic acid; CNQX, 6-cyano-7-nitroquinoxaline-2,3-dione; SLMV, synaptic-like microvesicles.

significance as to islet physiology. Here we show that both VGLUT1 and VGLUT2 are specifically localized with glucagon-containing secretory granules in αTC6 cells and islet α cells. Low glucose conditions triggers co-secretion of stoichiometric amounts of L-glutamate and glucagon. Stimulation of glutamate receptors in turn facilitates GABA secretion from β cells. These results solve, at least in part, where, when, and how L-glutamate appears in the islets and what happens upon stimulation of glutamate receptors in the islets. Since evidence for a role of GABA as a paracrine signal transmitter in the islet has been reported (23–26), these results also suggest the presence of L-glutamate- and GABA-mediated cross-talk between α and β cells in the islets of Langerhans.

EXPERIMENTAL PROCEDURES

Preparations—Islets of Langerhans were isolated from male Wistar rats at 7–8 postnatal weeks by the collagenase digestion method combined with discontinuous Ficoll gradient centrifugation (27). Islets were then handpicked and suspended in a bicarbonate-buffered Hanks' solution supplemented with 0.2% bovine serum albumin. αTC6 cells were cultured as described (28). MIN6 m9 cells were cultured as described (29).

In some experiments, αTC6 cells (1.0×10^8 cells) were washed with 20 mM MOPS-Tris (pH. 7.0) containing 0.3 M sucrose, 5 mM EDTA, 5 μg/ml leupeptin, and 5 μg/ml pepstatin A and then extensively homogenized. The homogenate was centrifuged at 800 × *g* for 10 min, and the resultant supernatant was centrifuged at 100,000 × *g* for 30 min. The particulate fraction was suspended in the above buffer and applied to a continuous sucrose density gradient (0.4–1.4 M) and centrifuged at 78,000 × *g* for 3.5 h. Then, the supernatant was fractionated in 11 tubes from the bottom, and the glucagon content was determined (see Fig. 1*C*). Crude synaptic vesicles (LP2 fraction) were prepared as described previously (18). To prepare membrane fraction of islets, at least 500 islets were washed, suspended in 2 ml of 20 mM MOPS-Tris (pH 7.0) containing 0.3 M sucrose, 5 mM EDTA, 10 μg/ml pepstatin A and 10 μg/ml leupeptin, and homogenized by hand with a small glass homogenizer. The homogenate was centrifuged at 900 × *g* for 10 min, and the resultant supernatant was centrifuged at 266,000 × *g* for 30 min in a Beckman Optima TLX ultracentrifuge. The pellet was suspended in the same buffer and used for experiments.

Immunohistochemistry and Immunoelectronmicroscopy—Indirect immunofluorescence microscopy was performed as described previously, using an Olympus FV-300 confocal laser microscope (18). For immunoelectronmicroscopy, the LR White embedding immunogold method was used with a slight modification (30). The animals were anesthetized with ether and then perfused intracardially with saline followed by 0.2% glutaraldehyde and 4% paraformaldehyde in 0.1 M phosphate buffer (pH 7.4). Then each pancreas was cut into small pieces, washed with 0.1 M cacodylate buffer (pH 7.4), stained with uranyl acetate for 2 h, dehydrated, and then embedded in LR White for 2 days at −20 °C. Ultra-thin sections on nickel grids were incubated with phosphate-buffered saline containing 2% goat serum and 0.5% bovine serum albumin for 15 min and then treated with a mixture of antibodies against VGLUT2 (50-diluted serum), glucagon (1000-diluted), and insulin (200-diluted) or with a mixture of VGLUT2, glucagon, and somatostatin (25-diluted) for 30 min. In the experiments in Fig. 2*D*, a mixture of antibodies against VGLUT1 (50-diluted serum) and glucagon (1000-diluted) was used. Then the sections were washed and treated with the secondary antibodies conjugated with colloidal gold. Then the sections were washed with 0.1 M cacodylate buffer, postfixed with 5% glutaraldehyde, stained sequentially with uranyl acetate for 30 min and lead citrate for 1 min, and observed under a Hitachi H-7100S electron microscope.

Antibodies—Site-specific rabbit polyclonal antibodies against rat VGLUT2 were raised as described previously (18). For the preparation of anti-VGLUT1 antibodies, DNA fragments encoding G506-S560 were amplified by PCR and cloned into the *Eco*R1 site of expression vector pGEX3X (Amersham Biosciences) to form glutathione *S*-transferase fusion plasmids. After transformation, the glutathione *S*-transferase fusion proteins encoding G506-S560 were purified on a glutathione-Sepharose 4B column (Amersham Biosciences) and then injected into a rabbit with complete adjuvant two times with a 2-week interval. The immunological specificity of the VGLUT1 and VGLUT2 antibodies was proven using VGLUT1 and VGLUT2 expressed in COS7 cells (15, 18). The mouse monoclonal antibodies against synaptophysin and glucagon were from Progen. The rat monoclonal antibodies against L-glutamate were from Dia Sorin Inc. The rat monoclonal antibodies against somatostatin were from Chemi-Con. The guinea pig polyclonal antibodies against insulin were from Biogenesis Ltd. The secondary antibodies conjugated with colloidal gold were obtained from British Biocell International Ltd. Alexa Fluor 568-labeled anti-mouse IgG and Alexa Fluor 488-labeled goat anti-rabbit IgG were from Molecular Probes.

Reverse Transcription Polymerase Chain Reaction (RT-PCR)—Total RNA extracted from isolated islets (1 μg) was transcribed into cDNA in a final volume of 20 μl of a reaction buffer containing 0.2 mM each dNTP, 10 mM dithiothreitol, 25 pmol of random octamers, and 200 units of Moloney murine leukemia virus reverse transcriptase (Amersham Biosciences). After 1 h of incubation at 42 °C, the reaction was terminated by heating at 90 °C for 5 min. For PCR amplification, the 10-fold diluted synthesized cDNA solution was added to the reaction buffer containing 0.6 mM total dNTP (150 μM each dNTP), 25 pmol of primers and 1.5 units of Ampli *Taq*-Gold DNA polymerase (PerkinElmer Life Sciences). Thirty-five temperature cycles were conducted, as follows: denaturation at 94 °C for 30 s, annealing at 54 °C for 30 s, and extension at 72 °C for 1 min. The amplification products were analyzed by polyacrylamide gel electrophoresis. The sequences of the oligonucleotides used as primers were based on the published sequences of a VGLUT1-specific sense primer, 5′-AGTGAAATGGAAGACGAGGTT-3′ (bases 1687–1707) and antisense primer, 5′-TTCGGCACGAGCTTGAAACT-3′ (bases 2002–2021) (12). DNA sequencing was performed by the chain-termination method.

Western Blotting—Samples were denatured with SDS sample buffer containing 1% SDS and 10% β-mercaptoethanol. Then Western analysis was conducted as described (18).

Assay for L-Glutamate Release—Isolated islets (20 pieces per assay) or cultured cells (4.0×10^6 cells/dish) were washed three times with DMEM and then incubated in Ringer's solution containing 10 mM HEPES (pH 7.4), 0.2% bovine serum albumin and glucose at the specified concentrations for 1 h at 37 °C. Then, the islets or cultured cells were transferred to 350 μl of the above Ringer's solution containing glucose at the specified concentrations. At the times indicated, samples (70 μl) were taken and the amount of L-glutamate was determined by high pressure liquid chromatography on a RESOLVE C18 column (3.9 × 150 mm; Waters Ltd.) and fluorescence detection as described previously (22). To determine the total L-glutamate concentration, islets (50 pieces per assay) were vigorously homogenized in a bicarbonate-buffered Hanks' solution in the presence of 6% perchloric acid, sonicated for 5 min, and centrifuged at 25.000 × *g* for 15 min. Then, the supernatant was carefully taken, and its L-glutamate concentration was measured by HPLC, it being found to correspond to 102 ± 13 pmol/islet ($n = 3$).

Assay for GABA Release—Islets (20 pieces/assay) or cultured cells (4.0×10^6 cells/dish) were washed three times with DMEM and then incubated in a Ringer's solution comprising 10 mM HEPES (pH 7.4), 0.2% bovine serum albumin, and glucose at the specified concentrations for 1 h at 37 °C. Then, islets or cells were transferred to 350 μl of a Ringer's solution containing glucose at the specified concentrations. After 30 min of incubation, samples (70 μl) were taken and the amount of GABA was determined by high pressure liquid chromatography on a CAPCELL PAK C18 column (2.0 × 250 mm; Sizeido Co., Ltd.) and amperometric detection (31). When necessary, L-glutamate, AMPA, or kainate at 0.5 mM each or CNQX at 50 μM was also included. In the experiments on MIN6 m9 cells, GABA release was also quantified by measuring radioactive GABA according to Refs. 32 and 33. Both procedures gave essentially the same results. For loading radiolabeled GABA, MIN6 m9 cells (4.0×10^6 cells/dish) were incubated in DMEM containing 0.2% bovine serum albumin, 1 mM aminoxyacetic acid, and 30 nM [^{3}H]GABA (specific activity, 60 Ci/mmol; NEN) for 2 h and then washed with a Ringer's solution containing 16.7 mM glucose. Then the cells were incubated in a Ringer's solution containing glucose at the specified concentrations for 1 h and transferred to 2 ml of the same solution for 30 min as described above. Then the radioactivity in the culture medium and cell lysate was counted.

Intracellular [Ca^{2+}] Measurement and Other Procedures—For the analysis of intracellular [Ca^{2+}], an Argus 20/CA ratio imaging system (Hamamatsu Photonics Co., Hamamatsu, Japan) was used (22). Cells were cultured on a thin glass coverslip precoated with poly-L-lysine (0.12 mm thick and 40 mm in diameter; 8.0×10^5 cells/coverslip). Then the cells were treated with 5 μM Fura-2 AM (Dojindo Co., Kumamoto, Japan) for 50 min at 37 °C and washed twice with the same medium. The cells were perfused with the warmed Ringer's solution or Ca^{2+}-Ringer's solution. Images were continuously taken at 37 °C with a silicon-intensified camera (C2741–08; Hamamatsu

Photonics Co.). The velocity of data acquisition for F334 by F380 images was 4 s at a resolution of 256 × 256 pixels per image. A personal computer with appropriate software (U4469; Hamamatsu Photonics Co.) was used to control the optical equipment and then recording and data analysis. The software enabled subtraction of background fluorescence, pixel-to-pixel division of F334 by F380 images, fitting of the F334/F380 ratios to a $[Ca^{2+}]$ calibration curve prepared separately, and digital averaging of the Ca^{2+} concentration in multiple cells. Glucagon and insulin were quantified with enzyme immunoassay assay kits obtained from Amersham Biosciences and Yanaihara, Inc., according to the manufacturers' manuals.

RESULTS

Localization of VGLUT2 in Glucagon-containing Secretory Granules—αTC6 cells and islet α cells possess at least two kinds of secretory vesicles, glucagon-containing secretory granules and synaptic-like microvesicles (SLMVs) (18). Indirect immunofluorescence microscopy indicated that VGLUT2 is co-localized with glucagon, a marker of secretory granules, but not with synaptophysin, a marker of synaptic vesicles or SLMVs, in αTC6 cells (Fig. 1, *A* and *B*). Consistently, sucrose density gradient centrifugation of the particulate fraction of αTC6 cells separated glucagon (fractions 3–7) and synaptophysin (fractions 7–11), indicating the separation of glucagon-containing secretory granules and SLMVs (Fig. 1*C*). VGLUT2 is distributed similarly to glucagon but not to synaptophysin, which is in contrast with the co-localization of VGLUT2 and synaptophysin in neuronal synaptic vesicles (Fig. 1*C*). In the islets of Langerhans, triple labeling for immunoelectronmicroscopy indicated that 15 nm of gold particles for VGLUT2 were specifically associated with the membranes of secretory granules (Fig. 1, *D* and *E*, and *insets*, *arrowheads*) that had been labeled with 5 nm of gold particles for glucagon (Fig. 1, *D* and *E*, and *insets*, *arrows*). In contrast, essentially no gold particles for VGLUT2 were observed in any organelles, including secretory granules in β or δ cells in the islets (Fig. 1, *D* and *E*, *white arrows*). Quantitatively, the labeling densities for VGLUT2 in glucagon-containing secretory granules, cytoplasm, and nucleus of α cells were 21.13 ± 1.99, 0.35 ± 0.12, and 0.85 ± 0.21 (number of immunogold particles/μm^2, four independent experiments), respectively. The labeling densities less than 0.79 ± 0.13 (number of immunogold particles/μm^2, four independent experiments) were also observed in secretory granules and cytoplasm of β and δ cells. Neither control serum nor antiserum preabsorbed with an antigenic peptide for VGLUT2 gave any specific labeling (data not shown). Taken together, these results demonstrated that VGLUT2 is associated with secretory granules in αTC6 cells and islet α cells.

Expression and Localization of VGLUT1 in Glucagon-containing Secretory Granules—To exclude the possibility of the presence of VGLUT in β and δ cells completely, we next examined the expression and localization of VGLUT1, another VGLUT isoform specifically expressed in neuron (14, 15).

Expression of VGLUT1 in αTC6 cells is under detection limit in our experimental systems (data not shown). However, unexpectedly, expression of the VGLUT1 gene in isolated islets was proven by RT-PCR using a specific DNA probe (Fig. 2*A*). An amplified product with the expected size and nucleotide and deduced amino acid sequences for VGLUT1 was obtained. Western blotting with specific antibodies for VGLUT1 detected a single islet polypeptide exhibiting similar migration to that of neuronal VGLUT1 (Fig. 2*B*) (14, 15). Immunohistochemistry on the frozen sections of islets revealed that VGLUT1 is co-localized with glucagon but not insulin or somatostatin (Fig. 2*C*). Together, these results indicate that VGLUT1 is also expressed in α cells but not in β or δ cells. Expression of VGLUT1 was somewhat heterogeneous among α cells, and some α cells showed intense immunoreactivity in contrast with ubiquitously intense expression of VGLUT2 (18).

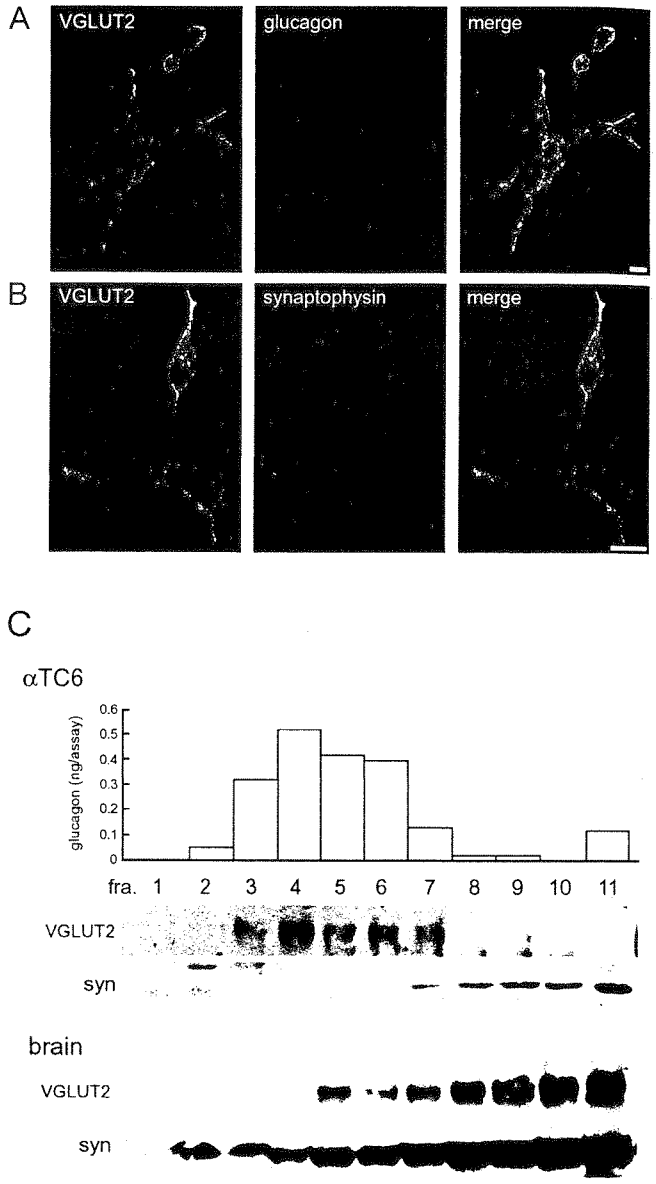

FIG. 1. **VGLUT2 is present in glucagon-containing secretory granules.** *A* and *B*, cultured αTC6 cells were doubly immunostained with a pair of antibodies against VGLUT2 and glucagon (*A*) or VGLUT2 and synaptophysin (*B*) and then observed under a confocal laser microscope. Merged pictures are also shown. *Bar*, 10 μm in *A*, *B*. *C*, subcellular fractionation revealed that VGLUT2 is associated with the secretory granule fraction. Sucrose density gradient of ultracentrifugation of the particulate fraction of αTC6 cells was conducted according to "Experimental Procedures", and the glucagon content in each fractions was determined. Aliquots (40 μl) were also subjected to SDS-polyacrylamide gel electrophoresis, followed by Western blotting with antibodies against VGLUT2 and synaptophysin (*syn*). Crude synaptic vesicles (P2 fraction) were also fractionated as described above, and immunoblotting of each fraction was performed. *D* and *E*, triple gold labeling immunoelectronmicroscopy of islets. *D*, VGLUT2 (15 nm in diameter), insulin (10 nm in diameter), and glucagon (5 nm in diameter). *E*, VGLUT2 (15 nm in diameter), somatostatin (10 nm in diameter), and glucagon (5 nm in diameter). VGLUT2 is associated with secretory granules in α cells, while VGLUT2 is not present in β or δ cells. *Arrowheads* and *arrows* indicate labeling for VGLUT2 and glucagon, respectively. *White arrows* indicate labeling for insulin in β cells and somatostatin in δ cells. *Insets* in *D* and *E*, boxed areas enlarged. *Bar* = 1 μm.

Double labeling for immunoelecronmicroscopy indicated that gold particles for VGLUT1 were specifically associated with the

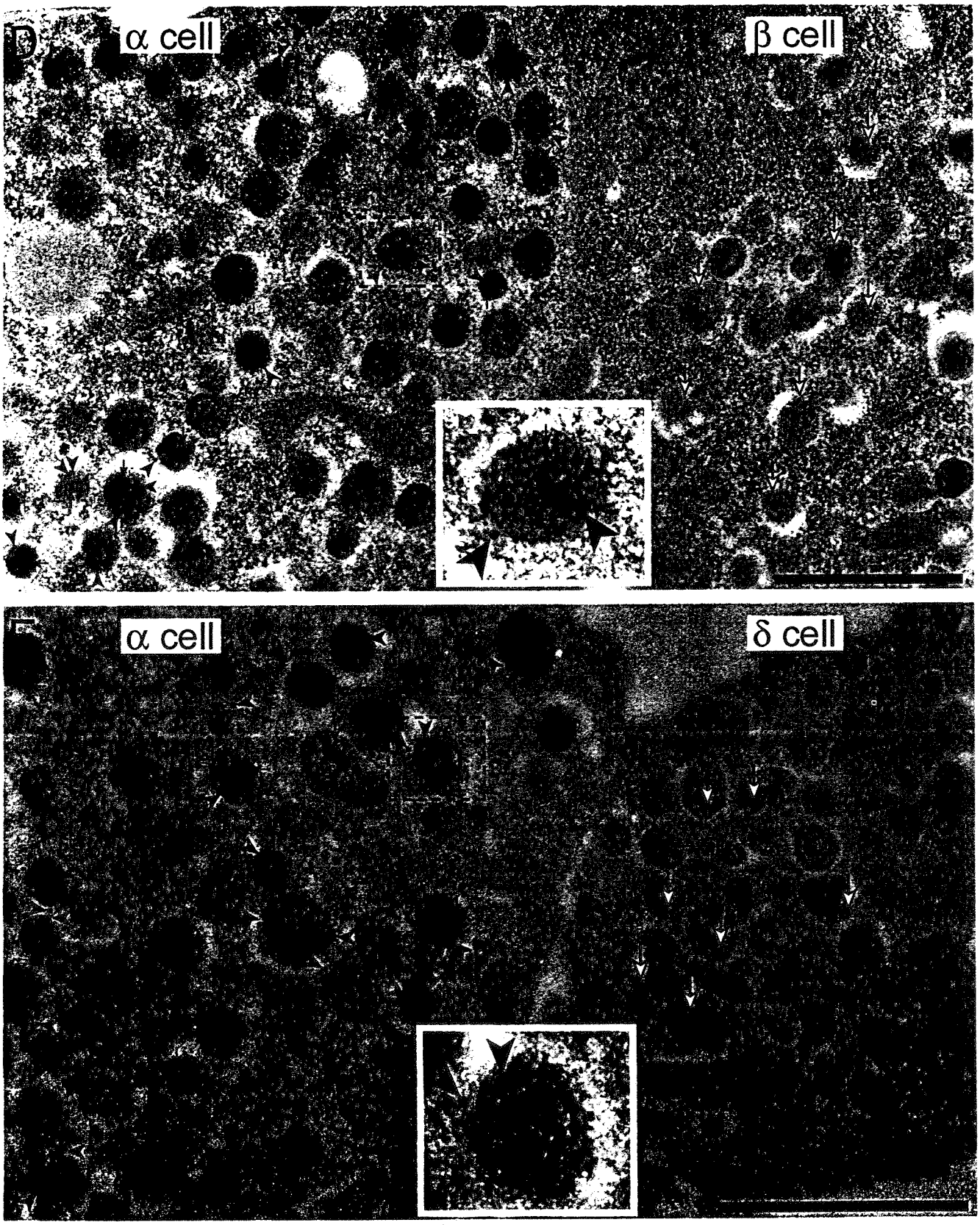

FIG. 1—*continued*

membranes of glucagon-containing secretory granules (Fig. 2*D*). Like localization of VGLUT2 shown in Fig. 1, *D* and *E*, essentially no gold particles for VGLUT1 were observed in any organelles, including secretory granules in β or δ cells in the islets (data not shown). Taken together, it is concluded that both VGLUT1 and VGLUT2 are expressed in islet α cells and only VGLUT2 is expressed in αTC6 cells and that both VGLUTs are specifically localized with glucagon-containing secretory granules.

Co-secretion of L-Glutamate and Glucagon—The specific lo-

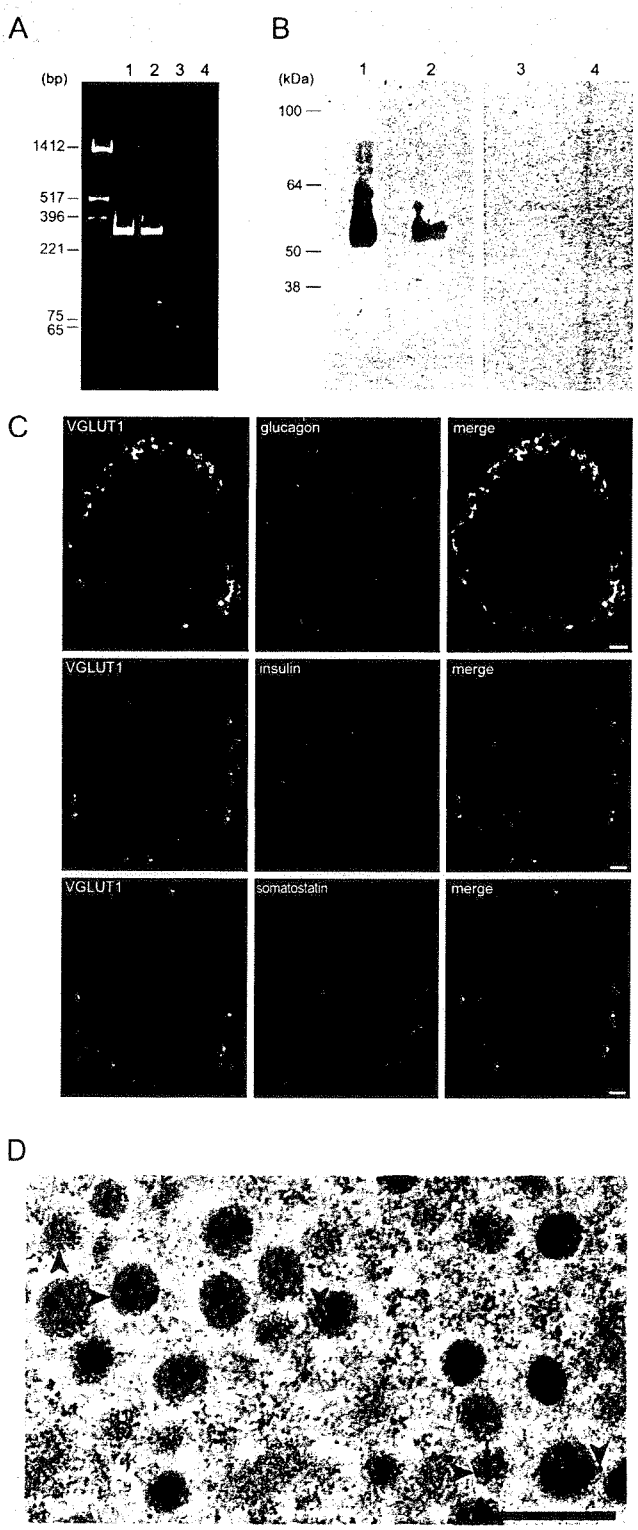

FIG. 2. **Expression and localization of VGLUT1 in islets.** A, expression of the VGLUT1 gene in brain (*lanes 1, 3*) and isolated islets (*lanes 2, 4*) was detected by RT-PCR. No amplified products were obtained without the RT reaction (*lanes 3* and *4*). *B*, Western blotting indicates the presence of VGLUT1 in islets. *Lanes 1* and *3*, crude synaptic vesicles from rat brain (20 μg); *lanes 2* and *4*, islets (30 μg each). In *lanes 3* and *4*, antibodies preabsorbed with antigenic peptides (2 mg) were used. *C*, sections of pancreas were doubly immunostained with antibodies against VGLUT1 and glucagon, VGLUT1 and insulin, or VGLUT1 and somatostatin, and then observed under a confocal laser microscope. Merged pictures are also shown. *Bar* = 20 μm. *D*, double gold labeling immunoelectronmicroscopy of islets. *Arrowheads* and *arrows* indicate labeling for VGLUT1 (15 nm in diameter) and glucagon (5 nm in diameter), respectively. *Bar* = 500 nm.

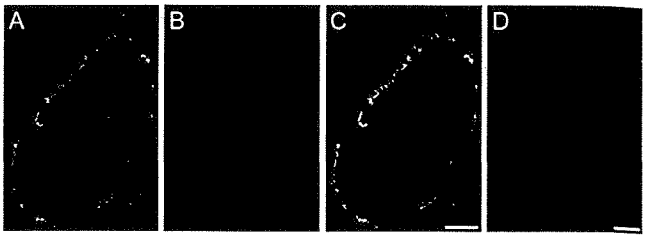

FIG. 3. **Immunological co-localization of L-glutamate and VGLUT2 in the islet.** An islet was immunostained for L-glutamate (*A*) and VGLUT2 (*B*), and then observed under a confocal laser microscope. Merged picture is also shown as *C*. In *D*, antibodies against L-glutamate after incubation with 1 mg/ml bovine serum albumin-L-glutamate for overnight were used. *Bar* = 50 μm.

calization of VGLUTs with glucagon-containing secretory granules means that L-glutamate is co-stored and co-secreted with glucagon from α cells under low glucose conditions. Consistently, the L-glutamate immunoreactivity coincided with that of VGLUT2 in the islets (Fig. 3). The L-glutamate immunoreactivity decreased to the background level when the antibodies preabsorbed with L-glutamate conjugated with bovine serum albumin were used (Fig. 3*D*).

We then investigated whether or not the islets co-secrete L-glutamate with glucagon. To facilitate the secretion of glucagon, islets or αTC6 cells were incubated with 16.7 mM glucose and then transferred to low glucose conditions, *i.e.* 3.3 mM. It was found that appreciable amounts of L-glutamate as well as glucagon were secreted from the islets: 54.3 ± 2.9 pmol L-glutamate per islet at 30 min, corresponding to about 53% of total L-glutamate, was released (Fig. 4*A*, *open circles*). When the islets were transferred to the same glucose conditions at 16.7 mM, about 30% L-glutamate release was observed at 30 min (Fig. 4*A*, *closed circles*). Essentially the same basal level of L-glutamate release was observed when islets were first incubated with 3.3 mM glucose and then transferred to glucose solution at 16.7 mM (data not shown). Thus, L-glutamate release from the islets constitutes the low glucose-stimulated and glucose-independent one. The low glucose-stimulated L-glutamate release disappeared at below 20 °C or in the presence of EGTA, indicating that the low glucose-stimulated L-glutamate release was dependent on Ca^{2+} and temperature (Fig. 4*A*, *open squares*). Phentolamine, which inhibits the exocytosis of glucagon via G_i2-dependent activation of calcineurin (34), inhibited the low glucose-stimulated and Ca^{2+}-dependent L-glutamate secretion in a parallel manner (Fig. 4, *open triangles*). The ratio of the low glucose-stimulated and Ca^{2+}-dependent secretion of L-glutamate and glucagon was always stoichiometric, being 1229 ± 105 (mol/mol, n = 4). Together, these results strongly suggest that the low glucose-stimulated L-glutamate release is due to exocytosis of glucagon-containing secretory granules. In contrast, the glucose-independent L-glutamate release was Ca^{2+}-independent, suggesting that it is due to nonspecific leakage from islet cells.

Low glucose-stimulated and Ca^{2+}-dependent secretion of L-glutamate and glucagon was also observed in αTC6 cells: 2.6 ± 0.3 nmol L-glutamate and 6.8 ± 0.7 ng glucagon per 10^6 cells per hour (n = 6) were secreted. In this case, the L-glutamate released corresponded to about 23% of total L-glutamate, the stoichiometry being 1345 ± 208.

Next, we investigated whether or not isoproterenol at 1 μM triggers L-glutamate secretion from isolated islets since the compound is known to trigger glucagon secretion by way of β-adrenergic receptors on α cells irrespective of glucose conditions (35). As expected, even when the islets were incubated with 16.7 mM glucose condition, isoproterenol triggered the stoichiometric secretion of L-glutamate (35.9 ± 2.3 pmol/islet,

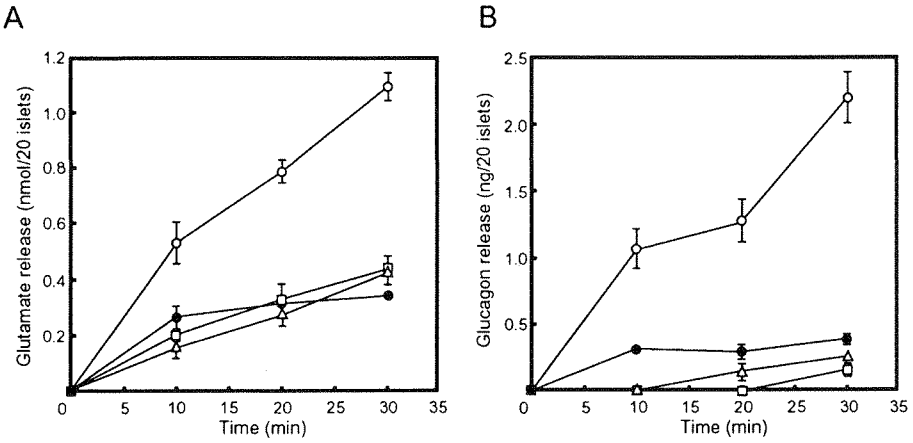

FIG. 4. **Low-glucose conditions trigger co-secretion of L-glutamate and glucagon from islets.** Islets (20 pieces per assay) were incubated in a Ringer's solution containing 16.7 mM glucose for 1 h. Then, the glucose concentration was changed to 3.3 mM (all *open symbols*) or 16.7 mM (*closed circles*). In *open triangles*), islets (20 pieces per assay) were incubated in a Ringer's solution containing 16.7 mM glucose for 1 h. Then, the glucose concentration was changed to 3.3 mM in the presence of 100 μM phentolamine according to Ref. 34. In *open squares*, islets (20 pieces per assay) were incubated in a Ringer's solution containing 16.7 mM glucose for 1 h. Then, the glucose concentration was changed to 3.3 mM in the presence of EGTA. Ca^{2+} in the medium was reduced to 40 nM. Then the medium was sampled at the times indicated, and the concentrations of L-glutamate (*A*) and glucagon (*B*) released from islets were measured. All the results are means ± S.E. (four independent experiments).

n = 4) and glucagon (0.091 ± 0.005 ng/islet, n = 4) at 30 min. The isoproterenol-evoked release of L-glutamate and glucagon was observed irrespective of glucose conditions employed, totally Ca^{2+}-dependent, and inhibited by 91 ± 3 and 95 ± 3% (n = 4), respectively, by propranolol, a β blocker, at 10 μM. Thus, either the low glucose conditions or stimulation of β-adrenergic receptors triggers release of stoichiometric amounts of L-glutamate and glucagon from isolated islets and αTC6 cells.

L-Glutamate Triggers GABA Secretion from β Cells under Low Glucose Conditions—What happens upon stimulation of glutamate receptors in the islets? β cells may receive the glutamate signal since they express glutamate receptors (6–8, 10, 11). It has been shown that β cells store GABA in SLMVs, but not insulin granules (36, 37), and secrete it through a Ca^{2+}-dependent exocytotic pathway (32, 33). We investigated whether or not L-glutamate affects GABA secretion from β cells.

MIN6 m9 cells are subclonal MIN6 β cells that retain glucose-responsive insulin secretion capacity (29). Consistently, the cells could secrete insulin (205 ± 8 ng/10^6 cells at 30 min, four independent experiments) when they were first incubated with 3.3 mM glucose and then transferred to 16.7 mM glucose (Fig. 5). Under other glucose conditions, *e.g.* the cells were first incubated with 16.7 mM glucose and then transferred to 16.7 mM or 3.3 mM glucose or the cells were incubated with 3.3 mM glucose throughout, a decreased level or only a background level of insulin secretion was observed (Fig. 5). MIN6 m9 cells also secrete GABA: on average, 0.62 ± 0.07 nmol of GABA/10^6 cells at 30 min, which corresponds to about 6% of total GABA, was secreted when the cells were first incubated with 16.7 mM glucose and then transferred to 16.7 mM or 3.3 mM glucose, or the cells were incubated with 3.3 mM glucose throughout (Fig. 5). GABA secretion was stimulated about 1.2-fold, when they were first incubated with 3.3 mM glucose and then transferred to 16.7 mM glucose (Fig. 5). Thus, GABA secretion is not significantly dependent on the glucose conditions as compared with insulin secretion, confirming the presence of distinct secretory pathways for insulin and GABA, as shown by the published works (31–33).

It was found that AMPA and kainate as well as L-glutamate at 500 μM (glutamatergic stimulation) each stimulated GABA secretion about 1.5–1.9-fold when the cells were first incubated with 16.7 mM glucose and then transferred to 3.3 mM glucose (Fig. 5). Glutamate-stimulated GABA release was also observed when the cells were incubated with 3.3 mM glucose throughout. Such a stimulatory effect was not observed under high glucose conditions. The glutamatergic stimulation-evoked GABA secretion was blocked by CNQX, a specific antagonist for AMPA-type receptors. Taking 1.1 ± 0.1 nmol/10^6 cells (n = 4) as a 100% control of kainate-stimulated GABA release, the omission of Ca^{2+} upon incubation of the cells with EGTA-AM at 50 μM inhibited the glutamatergic stimulation-evoked GABA release by 93 ± 4.4% (n = 4). Nifedipine, an L-type voltage-gated Ca^{2+} channel blocker, at 20 μM inhibited the kainate-evoked GABA release by 70 ± 11% (n = 4). When Na^+ in the medium was replaced with *N*-methyl-D-glucamine, kainaite-evoked GABA release was blocked by 80 ± 13% (n = 4). In parallel experiments, we measured intracellular [Ca^{2+}] in MIN6 m9 cells under similar conditions to above. Intracellular [Ca^{2+}] in the resting cells amounted to 93 ± 3 nM (n = 62). L-Glutamate, AMPA, and kainate at 500 μM each increased intracellular [Ca^{2+}], which corresponded to 109 ± 9 (n = 6), 117 ± 16 (n = 7), and 132 ± 18 nM (n = 15), respectively. The kainate-evoked increase in intracellular [Ca^{2+}] was blocked upon incubation with EGTA-AM at 50 μM or with nifedipine at 20 μM. Furthermore, replacement of Na^+ in the medium with *N*-methyl-D-glucamine prevented the increase in intracellular [Ca^{2+}] by 88 ± 13% (n = 20). Thus, the glutamatergic stimulation-evoked GABA secretion and increased intracellular [Ca^{2+}] were well correlated, indicating that stimulation of AMPA receptors triggers Ca^{2+}-dependent secretion of GABA under low glucose conditions.

Glutamatergic stimulation-evoked GABA secretion was also observed with the isolated islets (Fig. 6). The islets were first incubated under 16.7 mM glucose conditions and then transferred to 3.3 mM glucose conditions to facilitate the secretion of L-glutamate from α cells as described in the previous section. About 2-fold GABA was released from the islets as compared with the control level, *i.e.* the value obtained for islets with 16.7 mM glucose. The low glucose-responsive GABA release was sensitive to CNQX, suggesting that endogenous L-glutamate from α cells triggers GABA secretion. Exogenous L-glutamate and kainate stimulated the GABA release about 1.1–1.5-fold as compared with the absence of these compounds. CNQX decreased the L-glutamate- and kainate-evoked GABA release to the control levels. Consistent with the results for MIN6 m9 cells, under high glucose conditions, neither GABA secretion

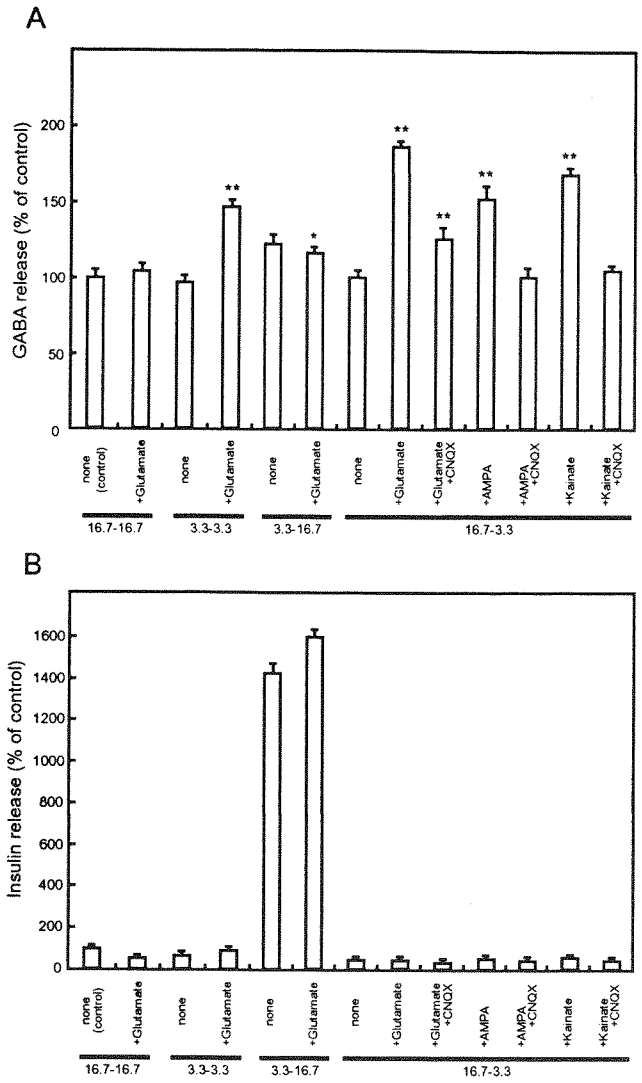

FIG. 5. **Secretion of GABA and insulin from MIN6 m9 cells.** Secretion of GABA (*A*) and insulin (*B*) under different glucose conditions was examined in the presence or absence of L-glutamate or an agonist or antagonist of glutamate receptors. The cells were first incubated with 16.7 or 3.3 mM sucrose and then transferred to 16.7 or 3.3 mM glucose, as specified, in the presence of L-glutamate, AMPA, or kainate at 0.5 mM. After 30 min, GABA and insulin in the medium were determined. In some experiments, CNQX at 50 μM was also included. 100% GABA corresponds to 0.58 ± 0.05 nmol/10^6 cells (n = 4). 100% insulin release corresponds to 14.4 ± 0.6 ng/10^6 cells (n = 4). An *asterisk* indicates that a value is significantly different from the value obtained in a control experiment (none) without an agonist or antagonist under each set of incubation conditions with Student's t test (*, $p < 0.05$; **, $p < 0.01$).

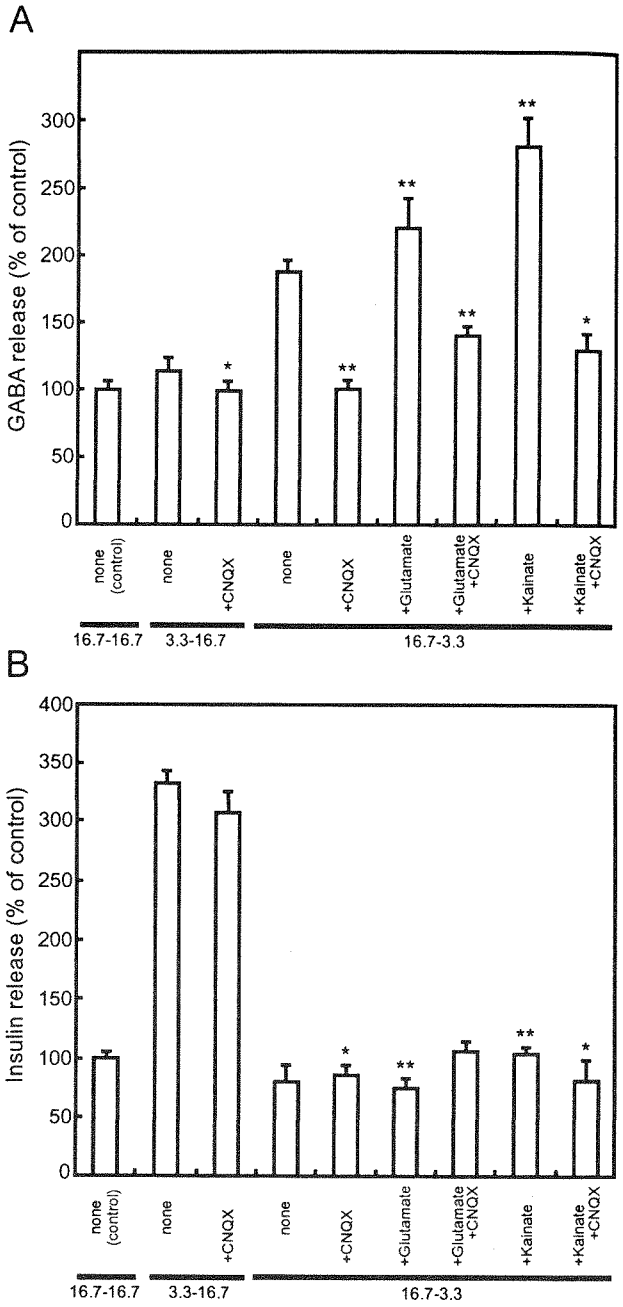

FIG. 6. **Secretion of GABA and insulin from isolated islets.** Isolated islets (20 pieces per assay) were incubated as described in the legend to Fig. 5, and then GABA (*A*) and insulin (*B*) release were quantified. 100% GABA corresponds to 1.3 ± 0.1 nmol/10^6 cells (n = 4). 100% insulin release corresponds to 15.1 ± 0.6 ng/10^6 cells (n = 4). An *asterisk* indicates that a value is significantly different from the value obtained in a control experiment (none) without an agonist or antagonist under each set of incubation conditions with Student's t test (*, $p < 0.05$; **, $p < 0.01$).

nor insulin secretion was stimulated by the addition of either L-glutamate or kainate.

DISCUSSION

In this study, we presented evidence that α cells are glutamatergic in nature and indicated the conditions when and how L-glutamate appears. L-Glutamate is co-stored with glucagon in secretory granules in α cells. Then, the low glucose conditions facilitate secretion of L-glutamate and glucagon so as to trigger the glutamatergic signaling in the islet. In our previous study, we proposed that SLMVs in αTC6 cells are responsible for storage and secretion of L-glutamate (22). However, combined immunohistochemistry and immunoelectronmicroscopy clearly indicate that glucagon-containing secretory granules, but not SLMVs, are the sites for L-glutamate storage in αTC6 cells and islet α cells. These results are consistent with observation by Tong *et al.*, although they did not identify the VGLUT2-positive vesicles as glucagon-containing secretory granules in α cell (11).

We showed that both VGLUT1 and VGLUT2 are specifically localized with glucagon-containing secretory granules in islet α cells. L-Glutamate may be accumulated in glucagon-containing secretory granules by active transport through VGLUTs at the expense of an electrochemical gradient of protons across the membrane, which is established by vacuolar H^+-ATPase. Since apparent difference in transport properties between VGLUT1

and VGLUT2 has not been obtained yet (14–21), the VGLUT isoforms in α cells may be simply responsible for the storage of L-glutamate. Localization of VGLUTs with glucagon-containing secretory granules predicts the mode of L-glutamate signal output. In fact, we next showed that L-glutamate immunoreactivity is co-localized with VGLUT2 (Fig. 3). Moreover, we showed that either low glucose conditions or stimulation of β receptors on α cells actually triggers release of stoichiometric amount of L-glutamate and glucagon with similar Ca^{2+} and temperature dependence and drug sensitivities. Overall, we concluded that L-glutamate is co-stored and co-secreted with glucagon from α cells under low glucose conditions. α cells should be regarded as L-glutamate-secreting endocrine cells.

Several works have reported that L-glutamate or agonists of glutamate receptor stimulate to some extent the secretion of insulin under high glucose conditions in cultured cells, isolated islets, and perfused pancreas (4, 6, 7, 9). Consistently, we observed that L-glutamate slightly stimulates (~10%) insulin secretion from MIN6 m9 cells (Fig. 5*B*). However, the L-glutamate-stimulated insulin secretion might not occur under physiological conditions, since the high glucose conditions do not trigger the L-glutamate signaling (Fig. 4), and therefore, L-glutamate is not expected to become an intercellular transmitter in islets under high glucose conditions.

Another significant finding obtained in the present study is that the L-glutamate signaling triggers GABAergic response in clonal β cells and isolated islets. The released L-glutamate may bind to the corresponding receptors on the islet cells, causing a paracrine or autocrine response (3–11). Islet β cells contain GABA in SLMVs at concentrations comparable level to the central nervous systems (36, 37). Upon depolarization, β cell secretes GABA through Ca^{2+}-dependent exocytosis (32, 33), and the released GABA becomes a paracrine or autocrine transmitter (24–26). However, the mode of action of GABA as an intercellular chemical transmitter, especially the timing for its appearance with the receptor-accessible manner in islet, was less understood. Previous studies on GABA release have been performed after a long incubation period, around a day (31, 38, 39). Under such conditions, amounts of GABA release may reflect the metabolic state of β cells but not directly reflect the rate of GABA secretion through exocytosis of SLMVs. In contrast, depolarization-evoked exocytosis of GABA-containing SLMVs seems to be completed within around 10–20 min (32, 33). We found that L-glutamate, AMPA or kainate stimulates GABA release from clonal β cells and isolated islets. The properties of the GABA secretion, *e.g.* time course, temperature, and Ca^{2+}-dependences and sensitivities to Ca^{2+} channel blockers are similar to those of GABA secretion through depolarization-evoked exocytosis of SLMVs (32, 33). Thus, it is concluded that the L-glutamate triggers GABA secretion through enhanced exocytosis of GABA-containing SLMVs. It is noteworthy that our results indicate for the first time that α cells and β cells communicate together by way of L-glutamate- and GABA-mediated signaling. The glutamatergic signaling and resultant GABAergic signaling cease when the blood glucose concentration increases because of voltage-dependent inhibition of Na^+ channel due to closure of the K^+-ATP channel of α cells (40). Then, the exocytosis of insulin is facilitated through KATP channel-mediated depolarization of β cells (40).

The glutamatergic stimulation-evoked GABA secretion exhibits some unique features as to the mode of L-glutamate signal reception. At first, the glutamatergic signals become effective when the glucose concentration in the medium decreases. This suggests that the ability of glutamate signal input of β cells changes with glucose concentration, and then β cells can receive L-glutamate signals only when α cells secrete L-glutamate. Although we can not explain the molecular mechanism underlying the glucose-dependent change on L-glutamate signal reception at present, one plausible explanation is that AMPA receptors on β cells take on agonist-accessive and -inaccessive forms depending on the glucose concentrations. Another important feature is that the glutamatergic stimulation selectively triggers GABA secretion and does not facilitate exocytosis of insulin granules. Although the exocytosis of GABA-containing SLMVs and insulin granules requires an increase in intracellular $[Ca^{2+}]$ (this study and Refs. 32 and 41), the present results strongly suggest that the exocytosis of these two kinds of secretory vesicles is differently regulated. Recently, synaptotagmins were reported to form a hierarchy of exocytotic Ca^{2+} sensors with distinct Ca^{2+} affinities (42). Furthermore, β cells express various kinds of synaptotagmin isoforms involved or not involved in insulin exocytosis (43–45). It is possible that synaptotagmins and/or the related proteins associated with SLMVs may cause a secretory response distinct to that of insulin granules. Both possibilities are now under investigation in our laboratory.

As to the physiological significance of the glutamatergic and GABAergic signaling in the islets, we propose that these signaling pathways may be involved in negative regulatory mechanism on glucagon secretion, since the secreted GABA in turn binds to GABAA receptors on α cells, causing inhibition of glucagon secretion (25, 26, 46). Consistent with the idea, stimulation of metabotropic glutamate receptor type 8 (mGluR8), a class III receptor, on α cells, strongly inhibited glucagon secretion under the low glucose condition (11). In this case, L-glutamate may function as an autocrine-type chemical transmitter. We predict that L-glutamate also triggers somatostatin secretion since δ cells express AMPA type receptors (8), and somatostatin inhibits glucagon secretion by way of the somatostatin receptors on α cells (47). We are now investigating this possibility in more details.

In conclusion, we solved critical issues, at least partly, *i.e.* where, when, and how L-glutamate appears, and what happen upon stimulation of glutamate receptors in the islets: the low glucose conditions and β adrenergic stimulation trigger L-glutamate secretion, and the released L-glutamate in turn triggers GABA secretion in the isolated islets. We presented the direct evidence that α cells and β cells mutually interact by way of L-glutamate- and GABA-signaling. Although the results obtained *in vitro* assay conditions may not necessary apply to native islet of Langerhans, it is probable that *in vivo* changes of blood glucose concentration directly regulate the glutamatergic signal transmission in the islets.

To our knowledge, this is the first example of secretory granule-mediated glutamatergic chemical transduction. Recently, we showed that D-aspartate is accumulated in secretory granules and secreted from PC12 cells (48). Thus, co-secretion of excitatory amino acids with hormones might be a common feature in endocrine signal transmission.

Acknowledgments—We thank Dr. S. Takamori and Prof. R. Jahn (Max-Plank Institute for Biophysical Chemistry) for providing an expression plasmid for VGLUT1, Prof. S. Seino (Chiba University) and Dr. K. Hamaguchi (Oita University) for their kind supply for MIN6 m9 cells and αTC6 cells, respectively.

REFERENCES

1. Foster, A., and Fagg, G. (1984) *Brain Res.* **319,** 103–276
2. Mayer, M. L., and Westbrook, G. (1997) *Prog. Neurobiol.* **28,** 197–276
3. Moriyama, Y., Hayashi, M., Yamada, H., Yatsushiro, S., Ishio, S., and Yamamoto, A. (2000) *J. Exp. Biol.* **203,** 117–125
4. Bertrand, G., Gross, R., Puech, R., Loubatieres-Mariani, M. M., and Bockaert, J. (1992) *Br. J. Pharmacol.* **106,** 354–359
5. Bertrand, G., Gross, R., Puech, R., Loubatieres-Mariani, M. M., and Bockaert, J. (1993) *Eur. J. Pharmacol.* **237,** 45–50
6. Gonoi, T., Mizuno, N., Inagaki, N., Kuromi, H., Seino, Y., Miyazaki, J., and Seino, S. (1994) *J. Biol. Chem.* **269,** 16989–16992

7. Inagaki, N., Kuromi, H., Gonoi, T., Okamoto, Y., Ishida, H., Seino, Y., Kaneko, T., Inagawa, T., and Seino, S. (1995) *FASEB J.* **9,** 686–691
8. Weaver, C. D., Yao, T. L., Powers, A. C., and Verdoorn, T. A. (1996) *J. Biol. Chem.* **271,** 12977–12984
9. Weaver, C. D., Gundersen, V., and Verdoorn, T. A. (1998) *J. Biol. Chem.* **273,** 1647–1653
10. Brice, N. L., Varadi, A., Ashcroft, S. J., and Molnar, E. (2002) *Diabetologia* **45,** 242–252
11. Tong, Q., Quedraogo, R., and Kirchgessner, A. L. (2002) *Am. J. Physiol. Endocrinol. Metab.* **282,** E1324–E1333
12. Ni, B., Rosteck, P. R., Nadi, N. S., and Paul, S. M. (1994) *Proc. Natl. Acad. Sci. U. S. A.* **91,** 5607–5611
13. Aihara, Y., Mashima, H., Onda, H., Hisano, S., Kasuya, H., Hori, T., Yamada, S., Tomura, H., Yamada, Y., Inoue, Y., Kojima, I., and Takeda, J. (2000) *J. Neurochem.* **74,** 2622–2625
14. Bellocchio, E. E., Reimer, R. J., Fremeau, R. T., and Edwards, R. H. (2000) *Science* **289,** 957–960
15. Takamori, S., Rhee, J. S., Rosenmund, C., and Jahn, R. (2000) *Nature* **407,** 189–194
16. Fremeau, R. T., Troyer, M. D., Pahner, I., Nygaard, G. O., Tran, C. H., Reimer, R. J., Belocchio, E. E., Fortin, D., Storm-Mathisen, J., and Edwards, R. H. (2001) *Neuron* **31,** 247–260
17. Bai, L., Xu, H., Collins, J. F., and Ghishan, F. K. (2001) *J. Biol. Chem.* **276,** 36764–36769
18. Hayashi, M., Otsuka, M., Morimoto, R., Hirota, S., Yatsushiro, S., Takeda, J., Yamamoto, A., and Moriyama, Y. (2001) *J. Biol. Chem.* **276,** 43400–43406
19. Takamori, S., Rhee, J. S., Rosenmund, C., and Jahn, R. (2001) *J. Neurosci.* **21,** RC182
20. Herzog, E., Bellenchi, G. C., Gras, C., Bernard, V., Ravassard, P., Bedet, C., Gasnier, B., Giros, B., and ElMestikaway, S. (2001) *J. Neurosci.* **21,** RC181
21. Varoqui, H., Schafer, M. K-H., Zhu, H., Weihe, E., and Erickson, J. D. (2002) *J. Neurosci.* **22,** 142–155
22. Yamada, H., Otsuka, M., Hayashi, M., Nakatsuka, S., Hamaguchi, K., Yamamoto, A., and Moriyama, Y. (2001) *Diabetes* **50,** 1012–1020
23. Okada, Y., Taniguchi, H., and Shimada, C. (1976) *Science* **194,** 620–622
24. Okada, Y. (1986) in *GABAergic Mechanisms in the Mammalian Periphery* (Erdo, S. L., and Bowery, N. G., eds) pp. 223–240, Raven Press, New York
25. Rorsman, P., Berggren, P. O., Bokvist, K., Ericson, H., Mohler, H., Otenson, V. G., and Smith, P. A. (1989) *Nature* **341,** 233–236
26. Robbins, M. S., Grouse, L. H., Sorenson, R. L., and Elde, R. P. (1981) *Diabetes* **30,** 168–171
27. Gotoh, M., Maki, T., Satomi, S., Porter, J., Bonner-Weir, S., O'Hara, C. J., and Monaco, A. P. (1987) *Transplantation* **43,** 725–730
28. Hamaguchi, K., and Leiter, E. H. (1990) *Diabetes* **39,** 415–425
29. Minami, K., Yano, H., Miki, T., Nagashima, K., Wang, C-Z., Tanaka, H., Miyazaki, J., and Seino, S. (2000) *Am. J. Physiol. Endocrinol. Metab.* **279,** E773–E781
30. Fukui, Y., Yamamoto, A., Masaki, R., Miyauchi, K., and Tashiro, Y. (1992) *J. Histochem. Cytochem.* **40,** 73–82
31. Gaskins, H. R., Baldeon, M. E., Sellassie, L., and Beverly, J. L. (1995) *J. Biol. Chem.* **270,** 30286–30289
32. Ahnert-Hilger, G., Stadtbaumer, A., Strubing, C., Scherubl, H., Schultz, G., Riecken, E.-O., and Wiedenmann, B. (1996) *Gastroenterol.* **110,** 1595–1604
33. Ahnert-Hilger, G., and Wiedenmann, B. (1987) *FEBS Lett.* **314,** 41–44
34. Hoy, M., Bokvist, K., Xiao-Gang, W., Hensen, J., Juhl, K., Berggren, P.-O., Buschard, K., and Gromada, J. (2001) *J. Biol. Chem.* **276,** 924–930
35. Schuit, F. C., and Pipeleers, D. G. (1986) *Science* **232,** 875–877
36. Reetz, A., Solimena, M., Matteoli, M., Folli, F., Takei, K., and De Camilli, P. (1991) *EMBO J.* **10,** 1275–1284
37. Thomas-Reetz, A. C., Hell, J. W., During, M. J., Walch-Solimena, C., Jahn. R., and De Camilli, P. (1993) *Proc. Natl. Acad. Sci. U. S. A.* **90,** 5317–5321
38. Smismans, A., Schuit, F., and Pipeleers, D. (1997) *Diabetologia* **40,** 1411–1415
39. Winnock, F., Ling, Z., Proft, R., Dejonghe, S., Schuit, F., Gorus, F., and Pipeleers, D. (2002) *Am. J. Physiol. Endocrinol. Metab.* **282,** E937–E942
40. Gopel, S. O., Kanno, T., Barg, S., Weng, X. G., Gromada, J., and Rorsman, P. (2000) *J. Physiol.* **528,** 509–520
41. Easom, R. A. (2000) *Semin. Cell Dev. Biol.* **11,** 253–266
42. Sugita, S., Shin, O.-H., Han, W., Lao, Y., and Sudhof, T. C. (2002) *EMBO J.* **21,** 270–280
43. Mizuta, M., Inagaki, N., Nemoto, Y., Matsukura, S., Takahashi, M., and Seino, S. (1994) *J. Biol. Chem.* **269,** 11675–11678
44. Mizuta, M., Kurose, T., Miki, T., Shoji-Kasai, Y., Takahashi, M., Seino, S., and Matsukura, S. (1997) *Diabetes* **46,** 2002–2006
45. Gut, A., Kiraly, C. E., Fukuda, M., Mikoshiba, K., Wollheim, C. B., and Lang, J. (2001) *J. Cell Sci.* **114,** 1709–1716
46. Gilon, P., Bertrand, G., Loubatieres-Mariani, M. M., Remacle, C., and Henquin, J. C. (1991) *Endocrinology* **129,** 2521–2529
47. Gromada, J., Hoy, M., Buschard, K., Salehi, A., and Rorsman, P. (2001) *J. Physiol.* **535,** 519–532
48. Nakatsuka, S., Hayashi, M., Muroyama, A., Otsuka M., Kozaki, S., Yamada, H., and Moriyama, Y. (2001) *J. Biol. Chem.* **276,** 26589–26596

3）視交叉上核神経細胞におけるサーカディアンリズムの発現と PAS 関連時計遺伝子（研究代表者：本間研一（北海道大学））

Ⅰ．研究成果

当研究班では、哺乳動物の生物時計、視交叉上核内におけるリズム発振メカニズムを、PAS 関連遺伝子である時計遺伝子をマーカーに分子、細胞、個体レベルで追求すると共に、サーカディアン機構内での時計遺伝子機能、および時計遺伝子を分子マーカーとした行動リズム発機構の研究を行った。さらに bHLH 転写因子遺伝子 *Dec* が新規時計遺伝子であることを検討した。

1．行動リズムを駆動する振動機構の解析

時計遺伝子は、生物時計の局在する視交叉上核だけでなく、全身の多くの組織臓器において、発現にリズムをもつ。そこで、視交叉上核の中枢時計と視交叉上核外の末梢時計から構成される多振動体階層構造をもつサーカディアン機構を、時計遺伝子を指標に検討し、視交叉上核と行動リズムを駆動する末梢時計機構は乖離しうること、行動に関与する脳内諸部位の中にも行動リズムと乖離した時計遺伝子発現を示す部位があることを明らかにした。

1） メタンフェタミン慢性投与による検討：メタンフェタミンの慢性投与で行動、体温などに発現するフリーランリズムの中枢機構を、*Per1,Per2,Bmal1* を指標に検討し、大脳皮質前頭前野、線条体において時計遺伝子発現リズムが行動リズムと一致すること、一方、視交叉上核時計遺伝子発現とメラトニンリズムは明暗サイクルに同調したままで行動リズムと乖離することを明らかにした。この結果、行動リズムを駆動する末梢時計機構が視交叉上核から乖離して独自リズムを発振すること、サーカディアンリズムの内的脱同調がヒト以外でも生じることが明らかとなった。

2） 行動リズム乖離モデル動物による検討：恒常暗で行動リズムが二成分にスプリットする CS 系マウスを用い、行動リズムと脳内時計遺伝子発現リズムを比較したところ、視交叉上核では、一峰性の明瞭な *Per1,Per2* 発現リズムを示し、左右視交叉上核間にも乖離はみられなかったが、大脳皮質では行動に一致した二峰性を示すことを明らかにした。

3） *Clock* 変異マウスの行動リズム：恒常暗で行動リズムが無周期となる *Clock* 変異では、Clock/Bmal1 による *Per* 遺伝子転写が起こらないため、分子時計が振動停止すると考えられてきた。しかし、メタンフェタミン連続投与では明瞭な行動リズム発現することが明らかとなり、中枢覚醒剤による行動リズム駆動には *Clock* 変異は影響しないことが分かった。

2．視交叉上核におけるリズム発振と多振動体構造

ラット、マウス、*Clock* 変異マウスの視交叉上核をマルチ電極ディッシュ上に培養し、個々の視交叉上核神経細胞の活動リズムを連続記録解析することにより、視交叉上核細胞内リ

ズム発振と神経核内多振動体構造について検討した。

1）視交叉上核神経細胞リズム周期分布とシナプスを介するリズム同期：ラット視交叉上核分散培養では、個々の神経活動リズム周期は20-30時間の広い範囲で正規分布し、シナプスを介してリズム同期する。一方、神経核構造が維持されたスライス培養では個々の神経細胞リズムは22-28時間の間に正規分布し、スライス内では神経細胞活動リズムがほぼ同期していることから、リズム同期には神経核構造維持が重要であることが明らかとなった。

2）視交叉上核内の二振動体：スライス培養では、バゾプレッシンリズムの安定持続とVIPリズムの早期減衰がみられるが、バゾプレッシン神経が局在する背側では、VIPが局在する腹側部位に比べ、サーカディアン振動を示す神経細胞の頻度が高いことが明らかとなり、視交叉上核内部位特異的二振動体の機能的差異が振動細胞密度に依存することが分かった。

3）*Clock* 変異マウスの視交叉上核神経活動リズム：*Clock* 変異マウスの視交叉上核をマルチ電極ディッシュ上で培養したところ、スライス培養では77%の、分散培養では15%の神経細胞に、27.28時間の長周期のサーカディアンリズムが確認された。この結果、*Clock* 変異は細胞内サーカディアン振動を停止しないこと、視交叉上核細胞のすべてが時計細胞ではないことを、神経核構造維持が視交叉上核からのリズム発振に必須であることが明らかとなった。

3．新規時計遺伝子DECの発見とその機能

Clock, Bmal1による*Per*転写促進とPer, Cryによる転写抑制の1サイクルがサーカディアン振動を作り出すという時計遺伝子転写翻訳フィードバックループモデルが、サーカディアン振動の分子メカニズムと考えられている。このコアループに新たな時計遺伝子 *Dec* が加わっていることを明らかにし、さらにコアループと連動した *Dec* ループの存在が示唆された。

1）視交叉上核における *Dec* 発現リズムと光誘導：bHLH型転写因子Dec1とDec2は視交叉上核において、明暗サイクルおよび連続暗下で、主観的明期に発現ピークをもつ明瞭なサーカディアンリズムを示し、視交叉上核以外の脳部位では、主観的暗期にピークをもつリズムを示した。*Dec1* は主観的暗期の光パルスにより発現が誘導されるが、*Dec2* 発現は光パルスに影響されない。光による *Dec1* 誘導は照射開始1時間後にピークをもつため、*Per1* と同様、分子時計機構の光同調に関与する遺伝子であることが強く示唆された。

2） コアループにおけるDecの機能：Dec1, Dec2はE-boxに結合し、下流の遺伝子発現を調節しうる。そこで、Clock/Bmal1によるE-boxを介する *Per1* 発現への影響を、mPer1上流のE-boxを含むレポーターコンストラクトを用い、ルシフェラーゼアッセイにて検討した。その結果、Dec1,Dec2共に用量依存的にClock/Bmal1によるルシフェラーゼ活性上昇を抑制し、抑制程度は従来知られたコアループの抑制因子よりも強力であった。またその作用機序は、E-boxへのClock/Bmal1との競合的結合、およびDec蛋白N末のBmal1蛋白への結合によることが分かった。*Dec* はリズム発振に関わると共に、下流の遺伝子発現

にリズムを作り出す時計の出力因子としても機能しうる。さらに、*Dec*上流にはE-boxが存在するため、*Dec* loop と *Per* loop の連動したフィードバックループの存在が強く示唆される。

参考文献

1. Abe, H. Honma, S., Namihira, M., Ikeda, M. and Honma, K. Phase-dependent induction by light of rat *Clock* gene expression in the suprachiasmatic nucleus. *Mol. Brain Res.* 66: 104-110, 1999.

2. Abe, H., Honma, S., Suzuki, T., Ebihara, S. and Honma, K. Functional diversities of two activity components of circadian rhythm in genetical splitting mice (CS strain). *J. comp. Physiol. A* 184:243-251, 1999

3. Masubuchi, S., Hashimoto, S., Endo, T., Honma, S. and Honma, K. Amplitude reduction of plasma melatonin rhythm in association with an internal desynchronization in a subject with non-24 hour sleep-wake syndrome. *Psychiat. Clin. Neurosci.* 53:249-251,1999.

4. Honma, S. and Honma, K. Light-induced uncoupling of multi-oscillatory circadian system in a diurnal rodent, chipmunk, *Eutamias Asiaticus*. *Am. J. Physiol.* 276:R1390-R1396, 1999.

5. Namihira, M., Honma, S., Abe, H., Tanahashi, Y., Ikeda, M., and Honma, K. Daily variation and light responsiveness of mammalian clock gene *Clock* and its partner gene, *BMAL1*, transcripts in the pineal body and different areas of brain in rats. *Neurosci. Lett.*267:69-72,1999.

6. Yu, W., Ikeda, M., Abe, H., Honma, S., Ebisawa, T., Yamauchi, T., Honma, K., and Nomura, M. Characterization of three splice variants and genomic organization of the mouse BMAL1 gene. *Biochem. Biophys .Res.Comm.* 260:760-767, 1999.

7. Namihira, M., Honma, S., Abe, H., Tanahashi, Y., Ikeda, M., and Honma, K. Circadian rhythm and light responsiveness of mammalian clock gene, *Clock* and *BMAL1*, transcripts in the rat retina.. *Neurosci. Lett.*271:1-4,1999.

8. Shirakawa, S., Honma, S., Katsuno, Y., Oguchi, H. and Honma, K. Synchronization of circadian firing rhythms in cultured rat suprachiasmatic neurons. *Eur. J. Neurosci.*12:2833-2838,2000.

9. Shinohara, K., Honma, S, Katsuno, Y.. and Honma, K. Circadian release of excitatory amino acids in the suprachiasmatic nucleus culture is Ca^{2+}- independent. *Neurosci. Res.* 36:245-250, 2000.

10. Ikeda, M., Yu, W., Hirai, M., Ebisawa, T., Honma, S., Yoshimura, K., Honma, K. and Nomura,M, cDNA cloning of a novel bHLH-PAS transcription factor superfamily gene, BMAL2: Its mRNA expression, subcellular distribution, and chromosomal localization. *Biochem. Biophys. Res. Commun.* 275:493-502, 2000.

11. Masubuchi, S., Honma, S., Abe, H., Ishizaki, K., Namihira, M., Ikeda, M. and Honma,

K. Clock genes outside the suprachiasmatic nucleus involved in manifestation of locomotor activity rhythm in rats. *Eur. J. Neuroscience* 12: 4206-4214, 2000.

12. Honma, S., Shirakawa, S., Namakura, W. and Honma, K., Synaptic communication of cellular oscillations in the rat suprachiasmatic neurons. *Neurosci. Lett.* 294:113-116, 2000.

13. Tanahashi, Y., Ohmiya, Y. Honma, S., Katsuno, Y., Ohta, H., Nakamura, H. and Honma, K. Continuous measurement of targeted promoter activity by a secreted bioluminescence reporter, *Vargula hilgendorfii* luciferase. *Analytica Biochem.*. 289: 260-266, 2001.

14. Namihira, M. Honma, S. Abe, H., Masubuchi, S., Ikeda, M. and Honma, K., Circadian pattern, light responsiveness and localization of *rPer1* and *rPer2* gene expression in the rat retina. *Neuroreport* 12: 471-475, 2001.

15. Abe, H., Honma, S., Namihira, M., Masubuchi, M., Ikeda, M., Ebihara, S. and Honma K. Clock gene expressions in the suprachiasmatic nucleus and other areas of the brain during rhythm splitting in CS mice. *Mol. Brain Res.*87:92-99, 2001.

16. Suzuki,T., Ishikawa, A., Yoshimura, T., Namikawa, T., Abe, H., Honma, S., Honma, K. and Ebihara, S. Quantitative trait locus analysis of abnormal circadian period in CS mice. *Mammalian Genome* 12:272-277, 2001.

17. Shirakawa T., Honma, S., and Honma, K. Multiple oscillators in the suprachiasmatic nucleus. *Chronobiol. Int.* 18:371-387,2001.

18. Nakamura, W., Honma, S., Shirakawa, T., Oguchi, H. and Honma, K. Regional pacemakers composed of multiple oscillator neurons in the rat suprachiasmatic nucleus. *Eur. J. Neurosci.* 14:666-674, 2001.

19. Yoshihara, T., Matsumoto, Y., Katsuno, Y., Honma, S., Oguchi, H., and Honma,K. Liquid meal attenuates meal anticipation in rat adrenocortical activity. *Physiol. Behav.* 74:133-137, 2001.

20. Masubuchi, S., Honma, S., Abe, H., Nakamura, W. and Honma, K.. Circadian activity rhythm in *Clock* mutant mouse by methamphetamine. *Eur. J. Neurosci.*,14: 1177-1180, 2001. |

21. Abe, H., Honma,S., Namihira, M., Masubuchi, S., and Honma,. K. Behavioral rhythm splitting in the CS mouse is related to clock gene expressions outside the suprachiasmatic nucleus. *Eur. J. Neurosci.* 14:1121-1128, 2001.

22. Nakamura, W., Honma, S., Shirakawa, T. and Honma, K. *Clock* mutation lengthens the circadian period without damping rhythms in individual SCN neurons. *Nature Neurosci.* 5:399-400,2002.

23. Ohta, H., Honma,S., Abe, H. and Honma,. K. Effects of nursing mothers on *rPer* and *rPer2* circadian expressions in the neonatal rat suprachiasmatic nuclei vary with developmental stage. *Eur. J. Neurosci.* 15:1953-1960, 2002.

24. Honma,S., Kawamoto,T., Takagi,Y., Fujimoto,K., Sato,F., Noshiro,N., Kato,Y. and

Honma,K. *Dec1* and *Dec2* are regulators of mammalian molecular clock. *Nature* 419:841-844, 2002.

25. Nakao, M., Yamamoto, K., Honma, K., Hashimoto, S., Honma, S., Katayama, N., and Yamamoto, M. A phase dynamics model of human circadian rhythms. *J.Biol. Rhythms.* 17: 476-489,2002.

26. Ohta, H., Honma,S., Abe, H. and Honma,. K. Periodic absence of nursing mothers phase-shifts circadian rhythms of clock genes in the suprachiasmatic nucleus of rat pups. *Eur. J. Neurosci.* 2003 (in press)

27. Ishizaki, K., Honma,S., Katsuno,Y., Abe, H., Masubuchi, S., Namihira,M., and Honma,K. Gene expression of Neuropeptide Y in the nucleus of the solitary tract is activated in rats under restricted daily feeding but not under 48-hour food deprivation. *Eur. J. Neurosci.* 2003 (in press).

28. 近江谷克裕、棚橋祐典、本間さと．生物発光によるホルモン転写活性の連続測定．比較内分泌学会ニュース 92：32-35,1999.

29. 本間さと．視交叉上核ニューロンにおける概日リズム：リズム発現と時計遺伝子．*生体の科学* 50:169-174, 1999

30. 本間さと・本間研一．生物時計の多振動体機構と時計遺伝子．*実験医学（増刊）* 17: 2145-2150, 1999.

31. 本間さと．行動リズムと時計遺伝子機能．*Molecular Medicine* 36: 1136-1141, 1999.

32. 安倍博、本間さと、本間研一．時を刻む遺伝子ー時計遺伝子研究の最前線ー．*脳の科学* 21: 1135-1139, 1999.

33. 本間研一、本間さと．時計遺伝子．*脳の科学* 22：499-503,2000.

34. 本間さと、橋本聡子、増渕　悟、遠藤拓郎、本間研一．ヒトのリズムー環境への同調メカニズム．*脳の科学* 22: 555-561,2000

35. 安倍　博、本間さと、本間研一．体内時計の分子機構．*自律神経* 37:163-168,2000.

36. 本間さと．時計遺伝子と脳のリズム.*神経研究の進歩* 44:868-873,2000.

37. 本間研一．生体リズムと脳．日本 ME 学会雑誌 44:13-20,2000.

38. 本間さと．哺乳動物生物時計の多振動体モデル.*神経研究の進歩* 45:775-782,2001.

39. 本間さと．視交叉上核と生物時計 *Clinical Neuroscience* 19:1132-1134,2001.

40. 本間さと、安倍　博、本間研一．時計遺伝子発現と行動リズム．分子精神医学 1:449-454, 2001.

41. 本間さと、中村　渉、白川哲夫、本間研一．マルチ電極アレイを用いた視交叉上核のリズム発振機構解析．*脳の科学* 25:35-41,2003.

42. 本間さと　第5の時計遺伝子ファミリー*Dec*と生物時計の多重連動フィードバックループ 実験医学 21:497-499,2003

43. 本間さと、本間研一. 概日リズムと時計遺伝子-分子フィードバックループによる細胞内リズム発振メカニズム　医学のあゆみ 204:773-777, 2003.

Nature 419:841-844（Oct.24）2002 に関する記事

体内時計の「歯車役」発見

北大・広大グループ

リズム乱れ調整 5番目の遺伝子

朝目覚め夜眠くなるなどの周期を作る体内時計で、時計の「歯車」役を果たす新たな遺伝子が見つかった。約24時間のリズムを刻む遺伝子として知られているのは四つあるが、これが五つ目。リズムに狂いが生じたときに調整する「歯車」とみられ、時差ぼけ、睡眠障害などの治療法開発に役立つかもしれない。本間研一・北海道大教授、加藤幸夫・広島大教授らのグループが24日付の英科学誌ネイチャーに発表する。

哺乳（ほにゅう）類で見つかっていた時計遺伝子は、ピリオド、クライ、クロック、ビーマル。これらが作り出すたんぱく質が太陽光などによって増減し、1日の周期が生じると考えられている。

本間さんらは、脳の視床下部にある視交叉上核（しこうさじょうかく）で、この4種の働きが活発な場所を調べた。その結果、同じ場所で別のたんぱく質が作られ、これらの遺伝子に作用していることを突き止めた。

別のたんぱく質を作っている遺伝子「デック」は、ピリオドの働きを抑えたり、クロックやビーマルが作るたんぱく質の影響を受けたりしていた。光を感じて働くこともわかった。

朝日新聞　2002年10月24日夕刊

体内時計

チクタク チクタク……に 精密遺伝子

北大助教授ら「五つ目」発見

睡眠や起床など1日24時間のリズムを作り出すために必要な新たな時計遺伝子を、北海道大大学院医学研究科の本間さと助教授（統合生理学）らの研究グループが発見した。人間の体内時計を安定させ、太陽光などの状態に反応して1日のリズムを整える働きがある。睡眠障害などの治療に結びつく可能性があり、24日付の英科学誌「ネイチャー」に発表した。本間助教授によると、1日24時間のリズムは、脳の視床下部にある四つの時計遺伝子の作用で整えられる。しかし人間の体内時計は1日のずれが小さく精密なため、別の時計遺伝子があるとみられていた。

本間助教授らはマウスやラットの実験で、新たに遺伝子「Dec」が体内時計を制御していることを確認した。1日のうち昼ごろに働きのピークが現れ、24時間のリズムを作り出す。太陽光など体外の光の状態に反応しており、真夜中でも人工光をあてると働きが活発になることが分った。本間助教授は「第5時計遺伝子群は、これまで遺伝子群との相互作用で精な体内時計を安定化させるきがあるのではないか」としている。【江口一】

毎日新聞二〇〇二年十月二十四日夕刊

体内時計に関与 2遺伝子を発見

生物の一日のリズムを刻む体内時計の調節に関与している新たな遺伝子を、北海道大と広島大の研究グループが突き止めた。不眠症の治療薬の開発などにつながる可能性がある。

哺乳（ほにゅう）類の場合、体内時計は脳の視交叉（しこうさ）上核という部分にあり、関連する遺伝子はすでに十個ほど見つかっている。今回発見されたのは、「Dec1」と「Dec2」と呼ばれる遺伝子で同じ視交叉上核にあり、体内時計が安定して動くよう助けているらしい。本間研一・北海道大大学院教授は「生物時計は精密な調節の仕組みがあることが分かった」と話している。

読売新聞　2002年11月11日夕刊

European Journal of Neuroscience, Vol. 12, pp. 2833–2838, 2000

Synchronization of circadian firing rhythms in cultured rat suprachiasmatic neurons

Tetsuo Shirakawa,[1] Sato Honma,[2] Yumiko Katsuno,[2] Haruhisa Oguchi[1] and Ken-ichi Honma[2]
[1]Department of Oral Functional Science, Hokkaido University Graduate School of Dental Medicine, Sapporo 060–8586, Japan
[2]Department of Physiology, Hokkaido University Graduate School of Medicine, Sapporo 060–8638, Japan

Keywords: cross-correlation, GABA, multielectrode dish, spontaneous action potential, synapse

Abstract

The circadian clock in mammals is located in the suprachiasmatic nucleus (SCN) which consists of multiple oscillating neurons. Integration of the cellular oscillations is essential for the generation of a single circadian period in the SCN. By using a multielectrode dish (MED), we measured circadian firing rhythms in individual SCN neurons for more than 2 weeks continuously, and examined the involvement of synaptic communication in the synchronization of circadian rhythms. Cross-correlation analysis of spontaneous action potentials revealed that a neuron pair was functionally connected by synapses when their circadian rhythms were synchronized. No correlation was found between the paired neurons whose circadian rhythms were not synchronized. Calcium (Ca^{2+})-dependent synaptic transmission in the cellular communication was indicated by dose-dependent lengthening of an intercellular spike interval and loss of spike correlation with a Ca^{2+} channel blocker. Approximately 60% of the SCN neurons in culture were immunoreactive to antibodies against γ-aminobutyric acid (GABA) or glutamic acid decarboxylase (GAD). Spontaneous firing of all the neurons tested was either increased or decreased by bicuculline, the $GABA_A$ receptor antagonist. These findings indicate that synaptic communication plays a critical role in the synchronization of circadian rhythms in individual SCN neurons and the GABAergic transmission is involved in the synchronization mechanism.

Introduction

The circadian clock in the suprachiasmatic nucleus (SCN) entrains to a 24-h light–dark cycle and regulates the temporal organization of physiological functions (Moore & Eichler, 1972; Stephan & Zucker, 1972). In the absence of external time cues, the SCN generates an endogenous single circadian period *in vivo* (Inouye & Kawamura, 1979). The SCN in rats contains about 8000 neurons (van den Pol, 1980). Recently, single SCN neurons were demonstrated to show circadian firing rhythms with different periods, indicating that many SCN neurons have their own circadian oscillator (Welsh *et al.*, 1995; Liu *et al.*, 1997; Herzog *et al.*, 1998; Honma *et al.*, 1998a). Therefore, the multiple oscillators must be integrated within the SCN to generate a single circadian period.

With respect to the synchronization mechanism of circadian rhythms among individual SCN neurons, calcium spikes, paracrine–hormonal interaction, electrical coupling via gap junctions and ionic interactions have been suggested (Bouskila & Dudek, 1993; van den Pol & Dudek, 1993; Jiang *et al.*, 1997). On the other hand, contribution of synaptic communication to the rhythm synchrony is questioned because day–night variation of SCN metabolic activity is detected prenatally before the initiation of synaptogenesis (Reppert & Schwartz, 1984; Shibata & Moore, 1988). However, the finding does not necessarily deny the role of synaptic transmission in the rhythm synchrony, because individual oscillation in the fetal SCN neurons may be separately entrained by time cues, such as maternal rhythms. The number of synapses in the SCN markedly increases from postnatal day 4 to day 10 and neural networks continue to develop with the extension of dendritic processes (Moore & Bernstein, 1989). In rat brain it is well established that synaptogenesis occurs in a few days and neural networks which can induce synchronized bursting develop progressively (Kamioka *et al.*, 1996; van den Pol *et al.*, 1998). Inhibitory synaptic currents were frequently detected in cultured SCN neurons by whole-cell patch recordings (Welsh *et al.*, 1995), although interaction of spontaneous spike discharge was not confirmed among individually oscillating neurons in this study. Thus, the function of the synaptic communication among SCN neurons is still unknown.

By using a multielectrode dish (MED), we measured circadian firing rhythms in 4–8 neurons simultaneously and demonstrated that individual SCN neurons exhibited robust circadian firing rhythms (Honma *et al.*, 1998a). In the present study, we found pairs of SCN neurons that showed synchronized circadian firing rhythms. Temporal correlation of spontaneous discharges among SCN neurons on a MED was studied by means of cross-correlation analysis (Toyama *et al.*, 1981; Huntsman *et al.*, 1999). The method is noninvasive and enables us to analyse the synaptic mechanism of rhythm synchronization among individual SCN neurons. In addition, properties of the synaptic transmission were examined by using a Ca^{2+} channel blocker and a $GABA_A$ receptor antagonist.

Materials and methods

SCN cell culture

Four-day-old Wistar rats from an inbred colony were anaesthetized by hypothermia and decapitated in the daytime. SCN cells were dissociated as described previously in detail (Honma *et al.*, 1998a,

Correspondence: Dr S. Honma, as above.
E-mail: sathonma@med.hokudai.ac.jp

Received 9 December 1999, revised 11 April 2000, accepted 2 May 2000

1998b) and cultured by plating ~1.0–1.5 × 10^5 vial cells in the central area of a MED. The SCN cells were incubated with 1 mL of culture medium at 37 °C, 5% CO_2 and 95% air with saturating humidity throughout the experiment.

Spike recording

Extracellular action potentials of single neurons were recorded simultaneously by a multichannel recording system (Panasonic, Kyoto, Japan). The MED contains 64 planar embedded microelectrodes (50 × 50 μm in size) which were arranged in an area of 1 mm^2. Recording of spontaneous firing was started at 4–10 days after the start of the culture and continued for 2–15 weeks. Seventy-two dishes were used for the experiments. Neurons (n = 4–8) on the same dish were selected for measurement using the criteria of S/N ratio (> 5.0). Spike discharges were fed through window discriminators (Nihon Koden, Tokyo, Japan) to a microcomputer and the number of spikes was counted every 10 s.

Analysis of circadian rhythm and cross-correlation

Circadian rhythm was analysed using a sequential data array of the mean firing rate over 15 min. The circadian period was calculated over 20–28 h by the chi-square periodogram (Sokolove & Bushell, 1978) using the data of at least five consecutive days. Neurons which had a single and statistically significant circadian period (P < 0.01) were designated as those with circadian oscillation. Cross-correlation was calculated by a micro1401 interface (CED, Cambridge, UK) for spike discharges collected with a multichannel data recorder (TEAC, Tokyo, Japan) at different times of the day. A spike discharge from one of the paired neurons was used as a reference, and the timing of spikes from the other neuron was examined over the range within ± 1 s. This process was repeated until the number of reference spikes exceeded 500 (maximum 2000). A histogram consisting of cumulated spike numbers plotted against time was constructed (cross-correlogram). To detect the excitatory synaptic communication, the resolution limit was set at 100 μs and the inhibitory communication at 1 or 10 ms. An intercellular spike interval (ISI) was obtained from the cross-correlogram of the paired neurons with excitatory communication. The possibility of receording spikes originated from different processes of the same neuron was excluded by confirming that some of the spikes from one electrode occurred independently of those from the other.

Pharmacological treatment

Cadmium chloride ($CdCl_2$; Sigma, St Louis, MO, USA) and bicuculline (RBI, Natick, MA, USA) were dissolved in distilled water and mixed with the culture medium. The volume of the test solution added to the medium was ≤ 5 μL. Increasing doses of the drugs were added every 4–5 min. We judged that the efficiency of the synaptic communication was affected by a pharmacological treatment when a neuron pair showed > 0.2 ms lengthening as well as > 10% increase in the ISI.

Immunohistochemistry

Immunohistochemistry for glutamic acid decarboxylase (GAD) was carried out as follows. The SCN cells cultured on the MED were fixed with 4% paraformaldehyde in 0.1 M phosphate buffer (pH 7.4) for 45 min. After incubating with mouse monoclonal anti-GAD antibody (1 μg/mL; Boehringer Mannheim, Mannheim, Germany) at 4 °C for 40 h, the cells were processed by the standard avidin–biotin–

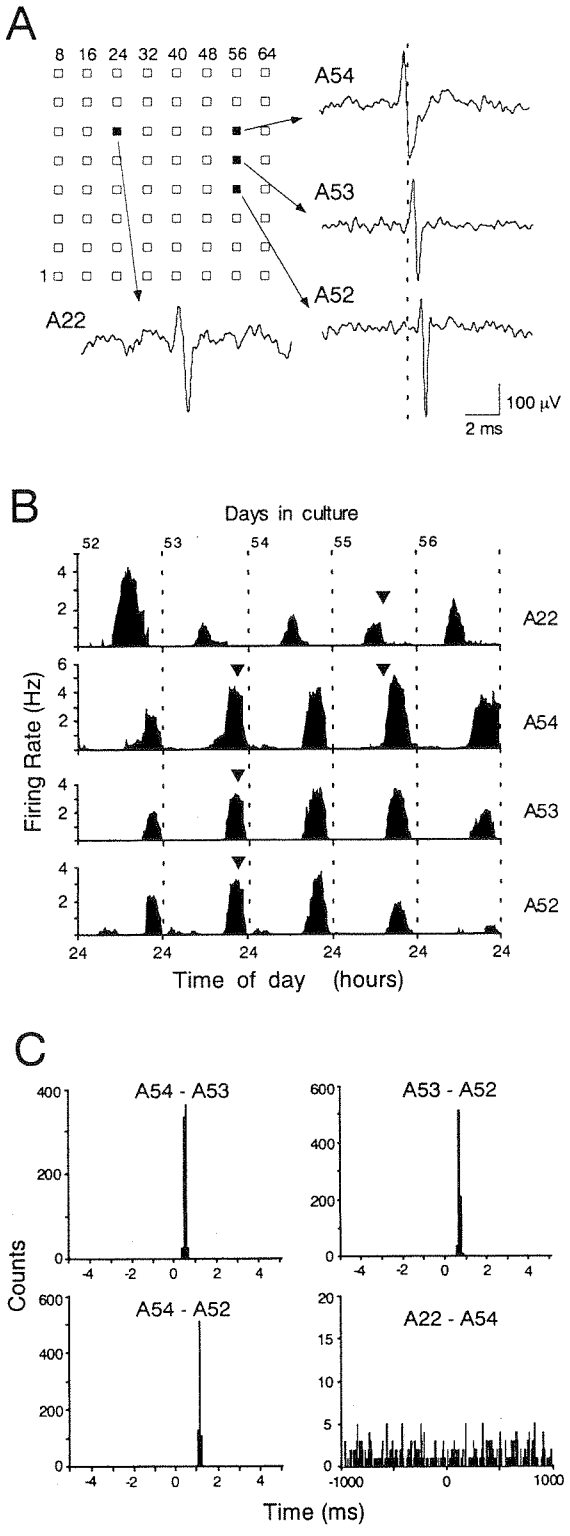

FIG. 1. Spontaneous discharges and circadian variations in firing rate in four neurons on a MED. (A) Diagram of the MED and representative spike waveforms recorded from neurons A54, A53, A52 and A22. The interpolar distances from A54 to A53, to A52, and to A22 were 150, 300, and 600 μm, respectively. (B) Synchronization and desynchronization of circadian firing rhythms in the four neurons. The circadian rhythm is expressed as the mean firing rate (Hz) in 15 min. The triangles in the graph indicate the time when the cross-correlations were analysed. (C) Cross-correlograms. Correlations that indicate excitatory synaptic communications were present between the neurons (A54, A53, A52) whose circadian rhythms were synchronized. The abscissa is the timing of spikes with bins of 100 μs (except for A22–A54) and of 10 ms (A22–A54), and the ordinate is the cumulative number of spikes.

peroxidase method (Vectastain Elite ABC Kit; Vector, Burlingame, CA, USA) using diaminobenzidine tetrahydrochrolide (Dojin, Tokyo, Japan) as a chromogen (Honma *et al.*, 1998b). For GABA immunostaining, the SCN cells cultured on the MED were fixed with 1.75% glutaraldehyde and 2% paraformaldehyde in 0.1 M cacodylate buffer (pH 7.4) for 10 min. After incubating with rabbit polyclonal anti-GABA antibody (1 : 200; Chemicon, Temecula, CA, USA) at 4 °C for 48 h, the cells were processed by the avidin–biotin–peroxidase method as described above.

Results

SCN neurons show synchronized circadian firing rhythms

Spontaneous action potentials in individual SCN neurons became obvious as early as the fourth day in the dissociated cell culture on the MED. Figure 1 shows spontaneous spike discharges and circadian variations in firing rate measured simultaneously in four neurons on the same MED. Three neurons (A52, A53, A54) showed synchronized circadian rhythms with a period of 23.7 h (Fig. 1B). The A22 neuron exhibited the circadian rhythm with a different period (23.0 h), which phase-led the other three by 7 h at the beginning of the recording. Cross-correlograms (Fig. 1C) indicate a unidirectional excitatory communication between A54–A53, A53–A52, and A54–A52. The former neurons (A54, A53, A54) in the three pairs are used as a reference. ISI, an interval between the reference time (0 ms) and the peak in the correlogram, was 0.5 ms (A54–A53), 0.7 ms (A53–A52) and 1.2 ms (A54–A52), respectively. In contrast, there was no correlation in the timing of spikes between A22 and A54 (and between A22 and the others; data not shown), indicating a lack of synaptic communication.

TABLE 1. Relationship between synchronization of circadian firing rhythms and synaptic communication

	Rhythm(+/+)				
	Synchro(+)	Synchro(–)	Rhythm(+/–)	Rhythm(–/–)	Total
Numbers of neuron pairs					
Correlation (+)	45	0	43	50	138
Correlation (–)	0	81	123	140	344
Total	45	81	166	190	482

Numbers of neuron pairs are shown. In total, 264 neurons were examined and, of these, 123 showed circadian firing rhythm throughout the experiment. When the circadian periods of firing rhythms in a paired neurons are identical, the circadian rhythms are regarded as synchronized [synchro(+)]. Rhythm(+/+), both of the neurons showed circadian firing rhythms; rhythm(+/–), one neuron showed a circadian rhythm but the other did not; rhythm(–/–), none of the paired neurons showed a circadian rhythm.

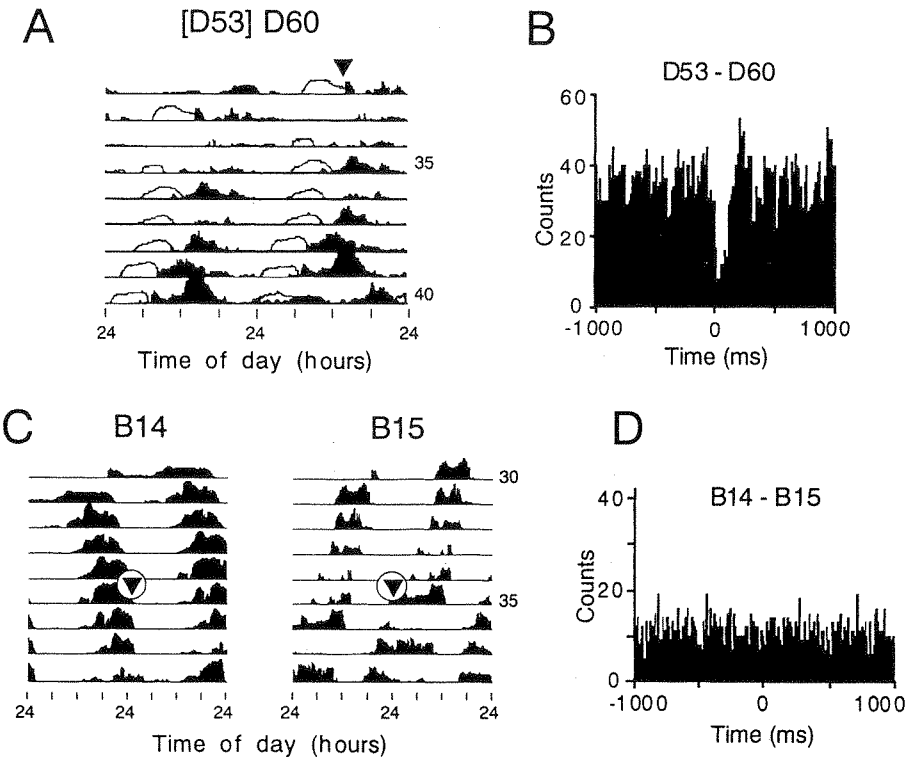

FIG. 2. Circadian firing rhythms of paired neurons and their cross-correlograms. (A) Double-plotted circadian firing rhythms of neurons with inhibitory synaptic communication. These rhythms were synchronized with a phase-lag of about 6 h and the circadian period of both neurons was 23.6 h. The rhythm of D53 (outlines) is superimposed on that of D60. Triangles indicate the time when the cross-correlation was analysed. The numbers at the right side of the graph indicate the number of days in cell culture. The full scale of firing rate, 8 (Hz, D53) and 6 (D60). (B) A cross-correlogram between D53 and D60. Here, D53 exerted a synaptic inhibition on D60. Suppression of the action potentials of D60 was observed from 4 to 140 ms after the reference spikes of D53. The two neurons were located on adjacent electrodes. (C) Double-plotted circadian rhythms of two neurons on the same MED. These rhythms were not synchronized. The circadian period of B14 was 25.2 h and that of B15 was 22.8 h. Triangles in the graph indicate the time when the cross-correlation was analysed. The full scale of firing rate, 7 (B14) and 4 (B15). The two neurons were located on adjacent electrodes. (D) An absence of the cross-correlation in the neuron pair B14 and B15.

Table 1 summarizes the relationship between the synchronization of circadian rhythms and the synaptic communication in 482 neuron pairs. One hundred and twenty-six neuron pairs displayed circadian firing rhythms in both neurons and, of these, 45 showed synchronized circadian rhythms. In the neuron pairs with synchronized circadian rhythms, either excitatory or inhibitory communication was demonstrated without exception. Forty-two pairs had an excitatory communication, and the remaining three displayed an inhibitory communication. In the synchronized neuron pairs with inhibitory communication, neuronal firing was suppressed for 100–140 ms after the reference time (Fig. 2A and B). Interestingly, these neurons showed a large phase-angle difference in the circadian rhythms. In 81 of 126 pairs, circadian rhythms were not synchronized. We did not detect any synaptic communication among these neuron pairs (Fig. 2C and D).

Synaptic delay and neuronal conduction velocity

The ISI of the excitatory communication ranged from 0.1 to 5.0 ms in the neuron pairs with synchronized circadian rhythms. Ten neuron pairs of 42 showed an ISI of <0.3 ms. The relation between the ISI and intercellular distance was analysed in 32 pairs with the ISI of 0.3 ms or longer (Fig. 3). Because neuron pairs can be connected either mono- or polysynaptically, they were divided into two groups according to their ISI (i.e. shorter or longer than 2 ms; Toyama *et al.*, 1981). The ISI was strongly correlated with the distance between the paired neurons in both groups. Neuron pairs on the lower regression line had a synaptic delay of 0.3 ms and a conduction velocity of 0.38 m/s. Neuron pairs on the upper regression line had a synaptic delay of 2.2 ms and a conduction velocity of 0.33 m/s.

Properties of the synaptic communication

The nature of neural communication in the cultured SCN neurons was tested by applying Cd^{2+}, a nonselective Ca^{2+} channel blocker (Müller *et al.*, 1992). Of the 12 synchronized pairs examined, cross-correlation was lost in four pairs at doses of 1 μM Cd^{2+}. Dose-dependent lengthening of the ISI was detected in the remaining eight pairs (Fig. 4). In three of them, the correlation was lost with 50 μM Cd^{2+}. Spontaneous firing rate was changed by Cd^{2+} application in nine of ten neurons tested. Seven neurons showed an increase and two showed a decrease in firing rate with 50 μM Cd^{2+}.

The involvement of neural communication through GABA was investigated. About 60% of the neurons (56.9 ± 1.0%, mean ± SEM, $n=5$) were immunoreactive to antibodies against either GABA or GAD (Fig. 5A). The GAD-immunoreactive axon varicosities were closely associated with dendrites and somata of the other neurons. Bicuculline, a $GABA_A$ receptor antagonist, was added to the medium and the responses of the spontaneously firing neurons ($n=43$) on the MEDs ($n=7$) were examined. The spontaneous firing rate was increased in 36 neurons and decreased in seven at 10 μM, and increased in 40 and decreased in three at 50 μM bicuculline.

The effect of 10–100 μM bicuculline on the spontaneous firing activity was further examined in another 11 neurons consisting of seven pairs with synchronized rhythms. The spontaneous firing was decreased dose-dependently in three and increased in eight neurons. By the application of bicuculline, ISI was either lengthened or abolished in two pairs but was unchanged in the remaining five pairs. In one of the former three neurons, the firing rate was decreased by bicuculline when the spontaneous firing rate was high (active phase), but was increased when the firing rate was low (inactive phase; Fig. 5B and C). Vehicle treatment (5 μL of distilled water) had no effect on the spontaneous firing rate nor on the ISI.

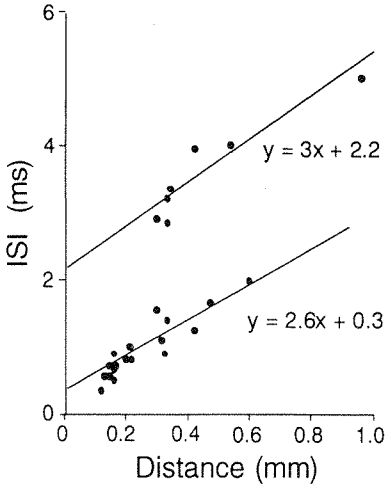

FIG. 3. Relationship of the ISI to the distance between the paired neurons with synchronized circadian rhythms. The oblique lines in the graph indicate the regression lines obtained from two groups of the neuron pairs. Correlation coefficient of the neuron pairs on the lower regression line and the upper regression line was 0.789 ($n=25$, $P<0.0001$) and 0.934 ($n=7$, $P<0.001$), respectively.

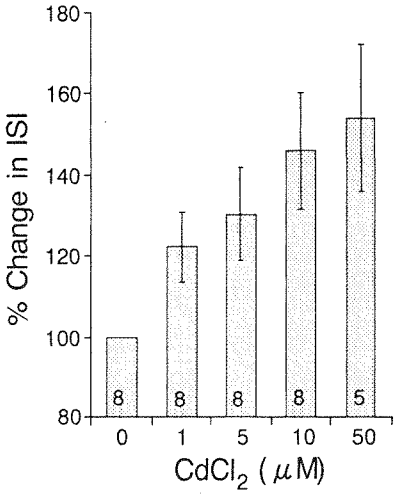

FIG. 4. Dose-dependent lengthening of the ISI by Cd^{2+} ($P<0.002$, one-way ANOVA of repeated measures). The ordinate indicates ISI expressed as percentage of the pretreatment value (mean ± SEM). The number in the column indicates number of neuron pairs analysed.

Discussion

Our data demonstrate that the SCN neurons cultured on the MED were functionally connected by synapses when their circadian rhythms were synchronized. Cross-correlograms indicate a unidirectional communication between the neurons with synchronized circadian rhythms (Fig. 1C). Forty-five neuron pairs of 482 showed synchronized circadian rhythms and exhibited either excitatory or inhibitory communication without exception. We did not detect any synaptic communication among neuron pairs whose circadian rhythms were not synchronized, which is consistent with a previous report by Welsh *et al.* (1995). In their study, however, synchronized circadian rhythms were not observed in any neuron pair, in marked contrast to our findings where in 36% of neuron pairs the circadian rhythms were synchronized.

In the neuron pairs with excitatory communication, Cd^{2+} either lengthened the ISI or abolished the cross-correlation (Fig. 4). Cd^{2+} is

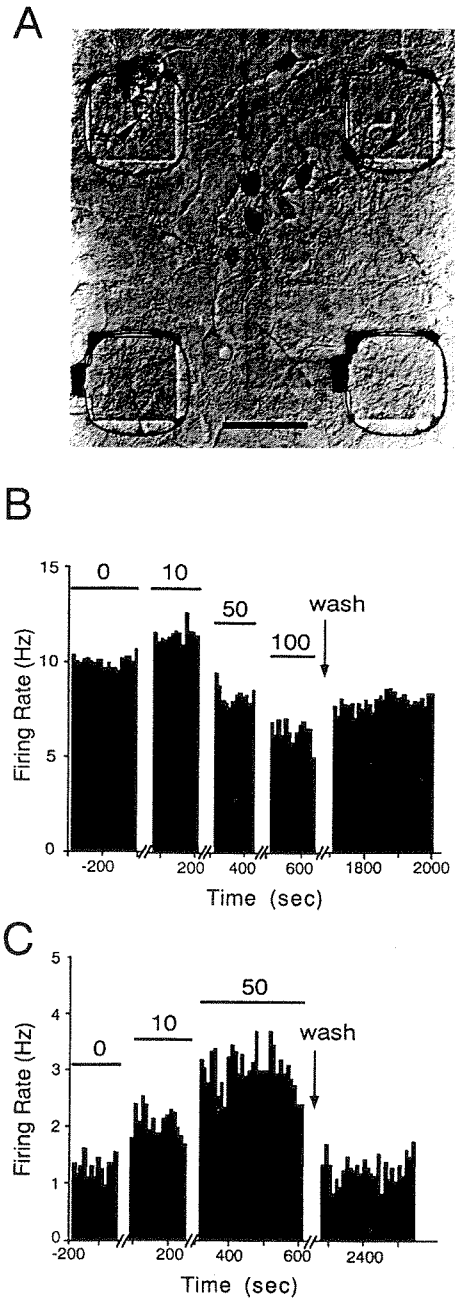

FIG. 5. GAD-immunoreactive neurons and responses of a neuron to bicuculline. (A) Photomicrograph of GAD immunohistochemistry. The SCN neurons on a MED were fixed on the 14th day of culture. Most neurons in the micrograph are GAD-positive. Four electrodes appear as squares located at regular intervals (interpolar distance 150 μm). An arrow and arrowhead indicate GAD-positive and -negative neurons on the electrode, respectively. Scale bar, 50 μm. (B and C) Effects of bicuculline on spontaneous firing activity of a single SCN neuron which showed circadian rhythm. Dose-dependent decrease in the firing rate at the active phase (B) or increase at the inactive phase (C) was observed in the same neuron measured 8 days apart. Concentrations of bicuculline (μM) are indicated above the horizontal bars. Blanks between the firings in these records correspond the time when the MED was offline. The abscissa indicates the time after the start of the bicuculline application.

known to block the voltage-activated Ca^{2+} channels and suppress the synaptic transmission (Müller *et al.*, 1992). The velocity of synaptic transmission was correlated with the Ca^{2+} entry in the presynaptic terminal, and the synaptic delay became longer when the Ca^{2+} entry was decreased (Sabatini & Regehr, 1996). The present result indicates that the intercellular communication is synaptic. In the 42 neuron pairs with synchronized circadian rhythms, the ISI varied from 0.1 to 5 ms. Among them, 10 pairs with the ISI shorter than 0.3 ms were regarded as receiving common inputs (Toyama *et al.*, 1981). In the remaining 32 pairs, the ISI was strongly correlated with the distance between the paired neurons (Fig. 3). The conduction velocity calculated from the ISI and intercellular distance was close to the value previously measured in unmyelinated fibers (0.55 m/s; Lee *et al.*, 1986) in both groups with mono- and polysynaptic connections.

Most SCN neurons contain GABA (Moore & Speh, 1993) which is generally regarded as an inhibitory neurotransmitter (Kim & Dudek, 1992; Strecker *et al.*, 1997; Gribkoff *et al.*, 1999). In the present experiment, about 60% of neurons on the MED were either GABA- or GAD-positive, which was a similar rate to that reported by Welsh *et al.* (1995). Bicuculline increased the spontaneous firing rate in most of the neurons examined, indicating that the GABAergic transmission is primarily inhibitory. On the other hand, as long as the neuron pairs with synchronized rhythms were analysed, more than 90% of the synapses were found to be excitatory. About 80% of the excitatory communications had a short (< 2 ms) ISI and the synaptic delay was calculated to be 0.3 ms. The predominance of excitatory communication may not be explained by excitation through disinhibition of the GABAergic inputs, because the estimated synaptic delay is in the range of monosynaptic communication at physiological temperature (Appenteng *et al.*, 1989; Borst *et al.*, 1995; Sabatini & Regehr, 1996). GABA has been shown to act as an excitatory transmitter (Alger & Nicoll, 1982; Nicoll *et al.*, 1990; Michelson & Wong, 1991; Kaila, 1994; Chen *et al.*, 1996; Wagner *et al.*, 1997). Especially, in the SCN, GABA increased the spontaneous firing rate during the subjective day while decreased it during the subjective night which was explained by shifts in the chloride equilibrium potential (Wagner *et al.*, 1997). Although the findings are not necessarily confirmed (Gribkoff *et al.*, 1999), bicuculline decreased spontaneous firing dose-dependently in some neurons in our culture, indicating that GABA can act as an excitatory neurotransmitter. Furthermore, one neuron decreased its firing rate in response to bicuculline at the active phase while increased it at the inactive phase (Fig. 5B and C). The result indicates that the responsiveness of the neuron to GABA is phase-dependent. Cross-correlation analysis was performed mostly during the active phase which corresponded to the subjective day when GABA was reported to excite SCN neurons (Wagner *et al.*, 1997). Therefore, the apparent discrepancy between the abundance of GABAergic neurons in the SCN and the predominance of excitatory communication in the neuron pairs with synchronized rhythms can be explained at least partly by excitatory transmission through GABA. Other mechanisms mediating excitatory intercellular communication among SCN neurons have been suggested (Bouskila & Dudek, 1993; van den Pol & Dudek, 1993). In the present experiment, ten neuron pairs with synchronized circadian rhythm had very short ISIs of < 0.3 ms. Although they can be regarded as receiving common inputs, possible roles of electrical coupling are not excluded in the cellular communication because coupling through gap junctions has been identified in SCN neurons (Jiang *et al.*, 1997). In addition, glutamatergic synapses, which are generally known to mediate fast excitatory transmission, could be concerned with the mechanism, although glutamatergic neurons have not yet been confirmed in the SCN (Strecker *et al.*, 1997). Further experiments are necessary to clarify this issue.

In conclusion, synaptic communication plays a critical role in the synchronization of circadian rhythms in individual SCN neurons.

GABA, which is demonstrated to act as either an inhibitory or excitatory transmitter, is involved in the synchronization mechanism.

Acknowledgement

This work was supported in part by grants from the Ministry of Education, Science and Culture of Japan (Nos 12557005 and 11557164).

Abbreviations

GAD, glutamic acid decarboxylase; ISI, intercellular spike interval; MED, multielectrode dish; SCN, suprachiasmatic nucleus.

References

Alger, B.E. & Nicoll, R.A. (1982) Pharmacological evidence for two kinds of GABA receptor on rat hippocampal pyramidal cells studied *in vitro*. *J. Physiol. (Lond.)*, **328**, 125–141.

Appenteng, K., Conyers, L. & Moore, J.A. (1989) The monosynaptic excitatory connections of single trigeminal interneurones to the V motor nucleus of the rat. *J. Physiol. (Lond.)*, **417**, 91–104.

Borst, J.G.G., Helmchen, F. & Sakmann, B. (1995) Pre- and postsynaptic whole-cell recordings in the medial nucleus of the trapezoid body of the rat. *J. Physiol. (Lond.)*, **489**, 825–840.

Bouskila, Y. & Dudek, F.E. (1993) Neuronal synchronization without calcium-dependent synaptic transmission in the hypothalamus. *Proc. Natl Acad. Sci. USA*, **90**, 3207–3210.

Chen, G., Trombley, P.Q. & van den Pol, A.N. (1996) Excitatory actions of GABA in developing rat hypothalamic neurones. *J. Physiol. (Lond.)*, **494**, 451–464.

Gribkoff, V.K., Pieschl, R.L., Wisialowski, T.A., Park, W.K., Strecker, G.J., de Jeu, M.T.G., Pennartz, C.M.A. & Dudek, F.E. (1999) A reexamination of the role of GABA in the mammalian suprachiasmatic nucleus. *J. Biol. Rhythms*, **14**, 126–130.

Herzog, E.D., Takahashi, J.S. & Block, G.D. (1998) Clock controls circadian period in isolated suprachiasmatic nucleus neurons. *Nature Neurosci.*, **1**, 708–713.

Honma, S., Shirakawa, T., Katsuno, Y., Namihira, M. & Honma, K. (1998a) Circadian periods of single suprachiasmatic neurons in rats. *Neurosci. Lett.*, **250**, 157–160.

Honma, S., Katsuno, Y., Tanahashi, Y., Abe, H. & Honma, K. (1998b) Circadian rhythms of arginine vasopressin and vasoactive intestinal polypeptide do not depend on cytoarchitecture of dispersed cell culture of rat suprachiasmatic nucleus. *Neuroscience*, **86**, 967–976.

Huntsman, M.M., Porcello, D.M., Homanics, G.E., DeLorey, T.M. & Huguenard, J.R. (1999) Reciprocal inhibitory connections and network synchrony in the mammalian thalamus. *Science*, **283**, 541–543.

Inouye, S.T. & Kawamura, H. (1979) Persistence of circadian rhythmicity in a mammalian hypothalamic 'island' containing the suprachiasmatic nucleus. *Proc. Natl Acad. Sci. USA*, **76**, 5962–5966.

Jiang, Z.G., Yang, Y.-Q. & Allen, C.N. (1997) Tracer and electrical coupling of rat suprachiasmatic nucleus neurons. *Neuroscience*, **77**, 1059–1066.

Kaila, K. (1994) Ionic basis of $GABA_A$ receptor channel function in the nervous system. *Prog. Neurobiol.*, **42**, 489–537.

Kamioka, H., Maeda, E., Jimbo, Y., Robinson, H.P. & Kawana, A. (1996) Spontaneous periodic synchronized bursting during formation of mature patterns of connections in cortical cultures. *Neurosci. Lett.*, **206**, 109–112.

Kim, Y.I. & Dudek, F.E. (1992) Intracellular electrophysiological study of suprachiasmatic nucleus neurons in rodents: inhibitory synaptic mechanisms. *J. Physiol. (Lond.)*, **458**, 247–260.

Lee, K.H., Chung, K., Chung, J.M. & Coggeshall, R.E. (1986) Correlation of cell body size, axon size, and signal conduction velocity for individually labeled dorsal root ganglion cells in the cat. *J. Comp. Neurol.*, **243**, 335–346.

Liu, C., Weaver, D.R., Strogatz, S.H. & Reppert, S.M. (1997) Cellular construction of a circadian clock: period determination in the suprachiasmatic nuclei. *Cell*, **91**, 855–860.

Michelson, H.B. & Wong, R.K.S. (1991) Excitatory synaptic responses mediated by $GABA_A$ receptors in the hippocampus. *Science*, **253**, 1420–1423.

Moore, R.Y. & Eichler, V.B. (1972) Loss of a circadian adrenal corticosterone rhythm following suprachiasmatic lesions in rat. *Brain Res.*, **42**, 201–206.

Moore, R.Y. & Bernstein, M.E. (1989) Synaptogenesis in the rat suprachiasmatic nucleus demonstrated by electron microscopy and synapsin I immunoreactivity. *J. Neurosci.*, **9**, 2151–2162.

Moore, R.Y. & Speh, J.C. (1993) GABA is the principal neurotransmitter of the circadian system. *Neurosci. Lett.*, **150**, 112–116.

Müller, T.H., Misgeld, U. & Swandulla, D. (1992) Ionic currents in cultured rat hypothalamic neurones. *J. Physiol. (Lond.)*, **450**, 341–362.

Nicoll, R.A., Malenka, R.C. & Kauer, J.A. (1990) Functional comparison of neurotransmitter receptor subtypes in mammalian central nervous system. *Physiol. Rev.*, **70**, 513–565.

Reppert, S.M. & Schwartz, W.J. (1984) The suprachiasmatic nuclei of the fetal rat: characterization of a functional circadian clock using ^{14}C-labeled deoxyglucose. *J. Neurosci.*, **4**, 1677–1682.

Sabatini, B.L. & Regehr, W.G. (1996) Timing of neurotransmission at fast synapses in the mammalian brain. *Nature*, **384**, 170–172.

Shibata, S. & Moore, R.Y. (1988) Development of a fetal circadian rhythm after disruption of the maternal circadian system. *Brain Res.*, **469**, 313–317.

Sokolove, P.G. & Bushell, W.N. (1978) The chi square periodogram: its utility for analysis of circadian rhythms. *J. Theor. Biol.*, **72**, 131–160.

Stephan, F.K. & Zucker, I. (1972) Circadian rhythms in drinking behavior and locomotor activity of rats are eliminated by hypothalamic lesions. *Proc. Natl Acad. Sci. USA*, **69**, 1583–1586.

Strecker, G.J., Wuarin, J.-P. & Dudek, F.E. (1997) $GABA_A$-mediated local synaptic pathways connect neurons in the rat suprachiasmatic nucleus. *J. Neurophysiol.*, **78**, 2217–2220.

Toyama, K., Kimura, M. & Tanaka, K. (1981) Cross-correlation analysis of interneuronal connectivity in cat visual cortex. *J. Neurophysiol.*, **46**, 191–201.

van den Pol, A.N. (1980) The hypothalamic suprachiasmatic nucleus of rat: Intrinsic anatomy. *J. Comp. Neurol.*, **191**, 661–702.

van den Pol, A.N. & Dudek, F.E. (1993) Cellular communication in the circadian clock, the suprachiasmatic nucleus. *Neuroscience*, **56**, 793–811.

van den Pol, A.N., Obrietan, K., Belousov, A.B., Yang, Y. & Heller, H.C. (1998) Early synaptogenesis *in vitro*: Role of axon target distance. *J. Comp. Neurol.*, **399**, 541–560.

Wagner, S., Castel, M., Gainer, H. & Yarom, Y. (1997) GABA in the mammalian suprachiasmatic nucleus and its role in diurnal rhythmicity. *Nature*, **387**, 598–603.

Welsh, D.K., Logothetis, D.E., Meister, M. & Reppert, S.M. (1995) Individual neurons dissociated from rat suprachiasmatic nucleus express independently phased circadian firing rhythms. *Neuron*, **14**, 697–706.

European Journal of Neuroscience, Vol. 12, pp. 4206–4214, 2000

Clock genes outside the suprachiasmatic nucleus involved in manifestation of locomotor activity rhythm in rats

Satoru Masubuchi,[1] Sato Honma,[1] Hiroshi Abe,[1] Kouji Ishizaki,[1] Masakazu Namihira,[1] Masaaki Ikeda[2] and Ken-ichi Honma[1]

[1]Department of Physiology, Hokkaido University Graduate School of Medicine, N-15, W-7, Kita-ku, Sapporo 060-8638, Japan
[2]Department of Physiology, Saitama Medical School, Moroyama, Saitama 350-0495, Japan

Keywords: behavioural rhythm, clock genes, internal desynchronization, melatonin rhythm, methamphetamine

Abstract

Chronic treatment of methamphetamine (MAP) in rats desynchronized the locomotor activity rhythm from the light–dark cycle. When the activity rhythm was completely phase-reversed with respect to a light dark-cycle, 24 h profiles were examined for the clock gene (*rPer1*, *rPer2*, *rBMAL1*, *rClock*) expressions in several brain structures by *in situ* hybridization, and for the pineal as well as plasma melatonin levels. In the MAP-treated rats, the *rPer1* expression in the suprachiasmatic nucleus (SCN) showed a robust circadian rhythm which was essentially identical to that in the control rats. Circadian rhythms in pineal as well as plasma melatonin were not changed significantly in the MAP-treated rats. However, robust circadian rhythms in the *rPer1*, *rPer2 and rBMAL1* expressions detected in the caudate-putamen (CPU) and parietal cortex were completely phase-reversed in the MAP-treated rats, compared with those in the control rats, indicating desynchronization from the SCN rhythm. Such desynchronization was not observed in the circadian rhythms of clock gene expression in the nucleus accumbens and cingulate cortex. The circadian *rClock* expression rhythm in the MAP-treated rats was not phase-reversed in the CPU and parietal cortex. These findings indicate that the locomotor activity rhythm in rats is directly driven by the pacemaker outside the SCN, in which *rPer1*, *rPer2 and rBMAL1* in the CPU and parietal cortex are involved.

Introduction

It is well established that the suprachiasmatic nucleus (SCN) in mammals drives the circadian rhythms which entrain to the daily light–dark (LD) cycle (Rusak & Zucker, 1979). However, chronic treatment of methamphetamine (MAP) in drinking water modifies the circadian locomotor rhythm extensively in rats (Honma *et al.*, 1986; Ruis *et al.*, 1990; Honma *et al.*, 1991; Shibata *et al.*, 1994), which ranges from phase-delay shift of the activity band to systematic changes in the phase relationship to the LD cycle (relative coordination). The MAP treatment in the SCN lesioned rats also induces a robust locomotor rhythm in the circadian domain, which does not entrain to the LD cycle and persists for at least several cycles after the termination of MAP treatment, indicating an endogenous nature (Honma *et al.*, 1987). Other stimulants of the central nervous system, such as amphetamine and methylphenidate, have similar effects on rat locomotor rhythm (Ikeda & Chiba, 1982; Honma & Honma, 1992). However, MAP does not seem to affect the circadian pacemaker in the SCN (Honma *et al.*, 1986; Moriya *et al.*, 1996). Therefore various modifications of the circadian locomotor rhythm in the SCN intact rats are thought to be due to an oscillatory interaction between the SCN circadian pacemaker and MAP-induced oscillation at the level of locomotor rhythm expression (Honma *et al.*, 1991). Neither the site nor the mechanism of MAP-induced oscillation is known. The dopaminergic system has been suggested to be involved in the MAP-induced oscillation, as MAP is known to modify the functions of dopaminergic neurons. In addition, haloperidol, a dopamine receptor antagonist, produced phase-dependent phase shifts in the MAP-induced locomotor rhythm (Honma *et al.*, 1995).

Recently, several clock genes were cloned in mammals and demonstrated to be expressed in the SCN in a circadian fashion (Dunlap, 1999). Circadian rhythm in the SCN is considered to be generated by a molecular feedback loop. The loop involves transactivation of a *Per1* gene by a CLOCK-BMAL1 heterodimer and suppression of its transactivation effect by the *Per1* gene product (Gekakis *et al.*, 1998; Sangoram *et al.*, 1998). These clock genes are also periodically expressed in other brain regions as well as in the peripheral tissues (Honma *et al.*, 1998; Oishi *et al.*, 1998; Zylka *et al.*, 1998; Namihira *et al.*, 1999a,b). The gene expression rhythms outside the SCN seem to be driven by the SCN pacemaker, since the bilateral SCN lesions abolished the *rPer2* expression rhythm in certain tissues in rats (Sakamoto *et al.*, 1998). However, in drosophila and zebra fish, the clock gene expression rhythms in peripheral tissues are self-sustaining (Plautz *et al.*, 1997; Whitmore *et al.*, 1998). There is some evidence in mammals that suggests the damping oscillation of clock genes in tissues outside the SCN. Rat-1 fibroblast cells and H35 hepatoma cells became oscillating in *rPer1* and *rPer2* expressions for at least a few cycles by serum shock, which otherwise did not oscillate at all (Balsalobre *et al.*, 1998). Taking these results together, we hypothesize that MAP treatment may induce circadian oscillations in clock gene expression in the dopaminergic system of the brain. The oscillations are closely related to the locomotor activity rhythm but do not depend on the SCN pacemaker. Here we are able to demonstrate the circadian rhythms in the clock genes, *rPer1*, *rPer2* and *rBMAL1*, expressions in the caudate-putamen (CPU) and parietal

Correspondence: Dr Ken-ichi Honma, as above.
E-mail: kenhonma@med.hokudai.ac.jp

Received 29 June 2000, revised 7 September 2000, accepted 18 September 2000

cortex, which desynchronize from the SCN pacemaker, but kept synchrony with the locomotor activity rhythm.

Materials and methods

MAP treatment

Female rats of Wistar strain were used for the MAP treatment (n = 49) and the control (n = 58) experiments. Thirty rats from each group were subjected to the determination of clock gene rhythms by *in situ* hybridization. They were born and raised in animal quarters where environmental conditions were kept constant (light: LD 12 h: 12 h, ≈200 lux; temperature: 22 ± 22 °C; humidity: 60 ± 5%). They were fed commercial rat chow and tap water *ad libitum*. The experiments in this study were performed following the Guide for the Care and Use of Laboratory Animals, Hokkaido University School of Medicine (Hokkaido, Japan).

At the age of 2–3 months, they were transferred to individual cages and locomotor activity was measured. All experiments were carried out under the light–dark cycle. About 1 week later, MAP treatment was started. MAP (Dainippon, Osaka, Japan) was given by dissolving in drinking water at a concentration of 0.01%. The average duration of MAP treatment was 60 days (mean ± SEM, 60.39 ± 4.32). Daily intake of MAP was 3.04 ± 0.11 mg (mean ± SEM).

Measurements of locomotor activity and melatonin

Locomotor activity was continuously monitored by an Animex (Animex III, Shimadzu, Kyoto, Japan), as described previously (Honma *et al.*, 1986; Honma *et al.*, 1991), and analysed using a Chronobiology Kit (Stanford Software Systems, Stanford, CA, USA). When the activity band of MAP-treated rats coincided with the light phase, they were decapitated at one of six different zeitgeber times (ZTs) — 22, 2, 6, 10, 14 and 18 — where ZT 12 was defined as the time of light off. For each animal, the day of decapitation was determined when the activity onset became located around ZT 22. The control rats were decapitated at the same time-points. Decapitation at the dark phase was done with an aid of a red lamp (≈ 0.1 lux). Trunk blood was collected in a heparinized tube and separated plasma was stored at –40 °C until the assay of melatonin. The pineal was quickly removed and stored at –40 °C. The pineal was homogenized with Tris buffer (200 µL, 0.1 mol/L, pH 7.4) and centrifuged (10 000 r.p.m., 17 000 *g* for 30 min). The supernatant was supplied for melatonin assay by radioimmunoassay, as described previously (Honma *et al.*, 1995). The intra- and interassay variances were 6.9% and 6.2%, respectively.

Cloning of rPer1 *and* in situ *hybridization of* rPer1, rPer2, rBMAL1 *and* rClock

rPer1 cDNA was cloned using DNA fragments isolated from Marathon-Ready cDNA (Clontech, Palo Alto, CA, USA). Briefly, 5′ cDNA clones were isolated by PCR using primers designed from the *mPer1* cDNA (Sun *et al.* 1997; Tei *et al.*, 1997). The sequences of the primers were as follows; 5′-TACCAGCCATTCCGCCTAAC-3′; 5′-GGAGCTGAAGCTACACTGAC-3′. The PCR products were cloned using the TA cloning kit (Invitrogen, San Diego, CA, USA). The nucleotide sequence was determined by the fluorescence dye-labelling cycle sequencing system (Amersham Pharmacia Biotech, Uppsala, Sweden) using fluorescein isothiocyanate-labelled primers and an automated DNA sequencer (DSQ1000, Shimadzu, Kyoto, Japan). *In situ* hybridization of *rPer1* mRNA was done according to the protocol described previously (Honma *et al.*, 1998). Antisense 45mer oligonucleotide probe for *rPer1* (5′-CTCTTGTCAGGAGGAATCCGGGGAGCTTCATAACCAGAGTGGATG-3′) was labelled with ^{35}S-dAMP by using ^{35}S-dATP (NEN, Boston, MA, USA) and terminal deoxyribonucleotidyl transferase (GIBCO BRL, Rockeville, MD, USA). Antisense oligonucleotide probes for *rPer2* (complementary to nucleotide residues from 1925 to 1969) (5′-GTGGCCTTCCGGGATGGGATGTTGGCTGGGAACTCGCACTTTCTT-3′) (Sakamoto *et al.*, 1998), *rBMAL1* (complementary to nucleotide residues from 7 to 51) (Honma *et al.*, 1998) and *rClock* (complementary to nucleotide residues from 254 to 298) (Abe *et al.*, 1999) were labelled same as *rPer1*.

After decapitation, the brains (five brains for each ZT) were immediately frozen on a glass plate cooled with dry ice and stored at –80 °C until hybridization. The coronal sections (20 µm thickness) included the SCN (bregma –0.92 mm), parietal cortex and CPU (bregma 1.20 mm), cingulate cortex and nucleus accumbens (NAC) (bregma 2.20 mm) were saved according to the rat brain atlas (Paxinos & Watson, 1986). The sections were incubated in the hybridization buffer containing the radiolabelled antisense probe for 10 h at 42 °C. A high-stringency post-hybridization wash was performed at 55 °C. The sections were air-dried and exposed to hyperfilm β-max (Amersham Pharmacia Biotech, Uppsala, Sweden) for 4 weeks with ^{14}C-acrylic standards. For the negative control, a competitive hybridization was simultaneously performed by adding an overdose of unlabelled probe (0.02 pmol/µL, 20 times higher than the concentration of the labelled probe). The hybridization signals were quantified by the method described previously (Honma *et al.*, 1998). Optical density (OD) at the structure of interest was normalized by subtracting the OD of the firm background (0-value of the ^{14}C-acrylic standard). The amount of mRNA per unit area (kBq/g) was calculated for each rat using four sections (the sum of mRNA in four sections was divided by the total area examined). The areas we measured were determined using the brain atlas (Paxinos & Watson, 1986). These areas are as follows: parietal cortex area 1 (from the second to forth layers), 5.5 mm lateral to the middle line and 3.0 mm lower from the top; CPU, 2.5 mm lateral to the middle and 3.0 mm lower from the top (bregma 1.2 mm; plate 13); NAC, 1.5 mm lateral to the middle and 7.0 mm lower from the top; cingulate cortex, 0.5 mm lateral to the middle and 3.5 mm lower from the top (bregma 2.2 mm; plate 10). The diameters of these areas were approximately 0.24 mm.

Statistical analysis

The 24 h variations of melatonin and mRNA were statistically tested by one-way ANOVA. The effect of MAP on the rhythms were tested by two-way ANOVA. A *post hoc* Bonferonni test was used for the comparison between the values of control and MAP-treated groups at the same time points.

Results

Locomotor activity rhythm

Figure 1 illustrates activity rhythms of three rats treated with MAP in drinking water. The activity onset as well as the offset were phase-delayed relative to the LD cycle, as compared with the controls in the first several weeks. In the later stage, the locomotor rhythms were completely desynchronized from the LD cycle and ran freely with a period longer than 24 h showing signs of relative coordination. The cycle length of the locomotor rhythm immediately before decapitation (between the activity onset on the day before decapitation and that on the day of decapitation) was 25.75 ± 0.26 h (mean ± SEM).

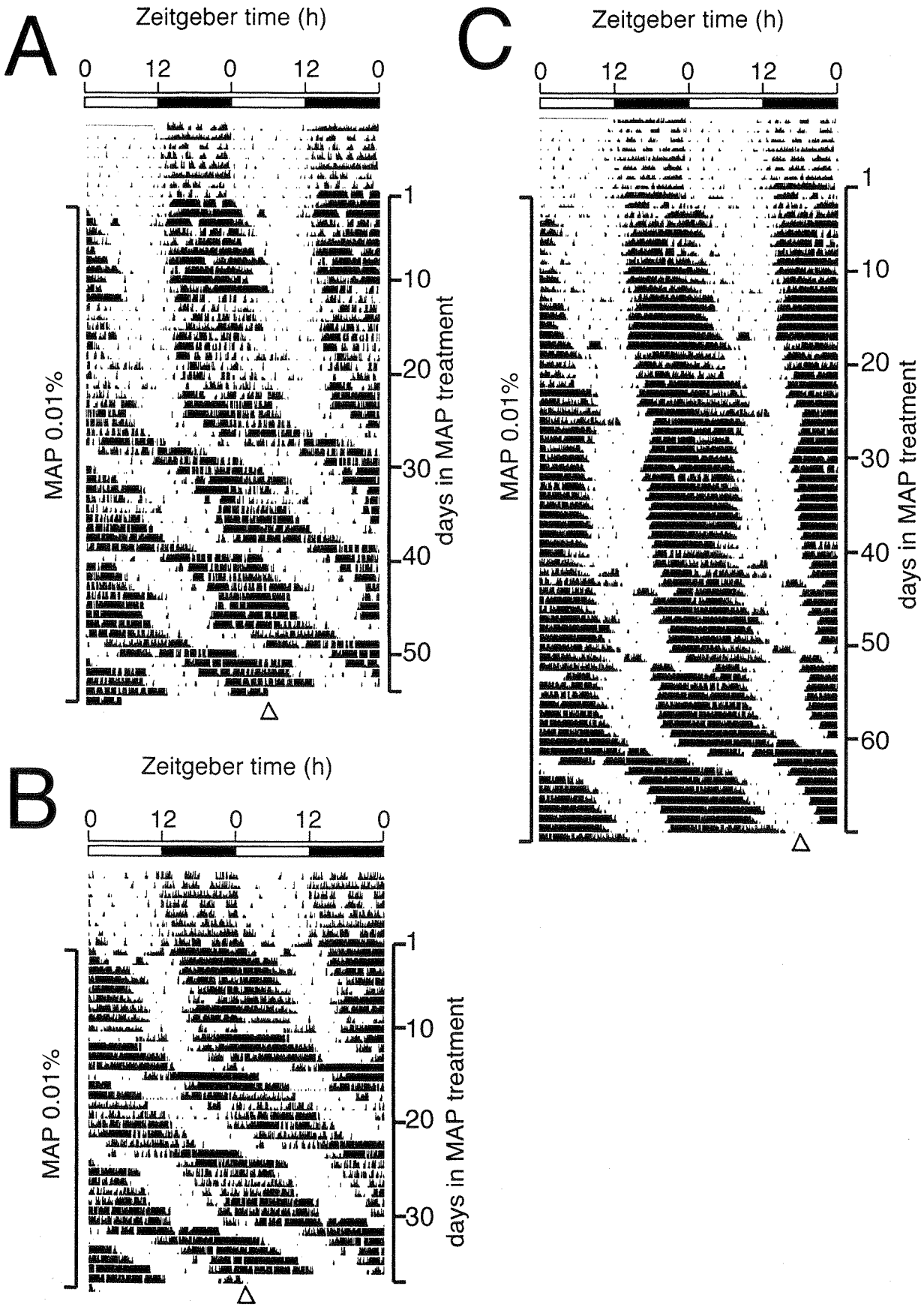

FIG. 1. Double plotted locomotor activity rhythms of MAP-treated rats under the LD cycle. Locomotor activities were expressed in the histogram (counts/min). The horizontal bars at the top of the panels represent the lighting cycle. Open bars represent the light phase and the filled bars, the dark phase. The times of decapitation (A, ZT 6; B, ZT 2; and C, ZT 18) are indicated by triangles.

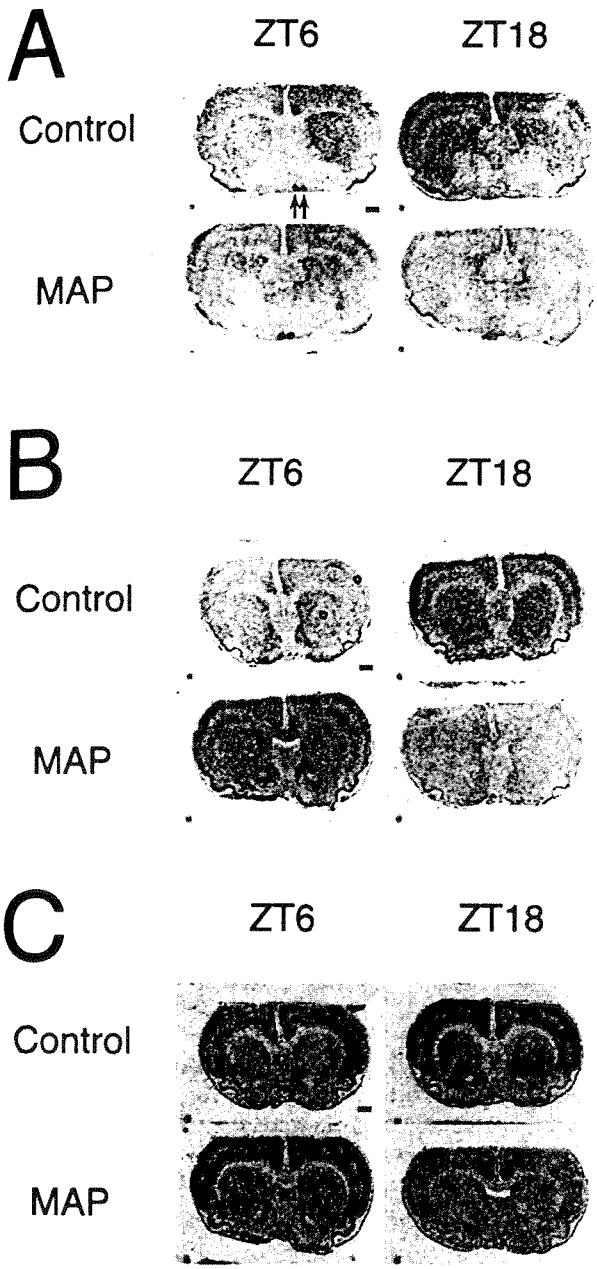

FIG. 2. Representative autoradiographs of *rPer1* and *rPer2* by *in situ* hybridization. (A) At the level of the SCN (arrows) (*rPer1*). (B and C) At the level of the parietal cortex and CPU (B, *rPer1*; C, *rPer2*). Circles in the autoradiograph indicate the sites of hybridization signal measured. Scale bars, 2 mm.

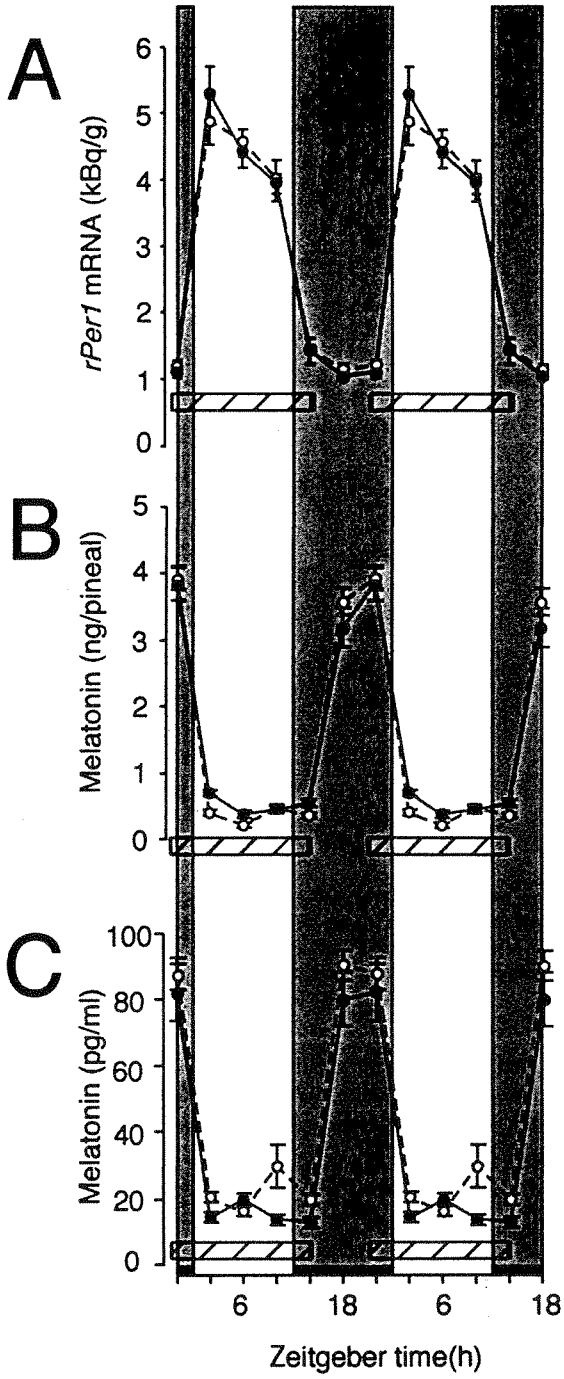

FIG. 3. Circadian rhythms in the SCN *rPer1* mRNA and in pineal and plasma melatonin. Circadian rhythms in *rPer1* mRNA (A), pineal as well as plasma melatonin (B and C) in the MAP-treated (closed circles with solid lines) and in the control rats (open circles with broken lines) (mean ± SEM). The circadian rhythms are illustrated in duplicate. Hatched horizontal bars indicate the mean activity band with SEM of locomotor rhythm in the MAP-treated rats. Dark horizontal bars on the abscissa and shaded areas indicate the dark phase.

The mean activity onset was located at ZT 21.41 ± 0.13 and the offset was at ZT 13.96 ± 0.27 on the day of decapitation.

rPer1 *in the SCN and melatonin rhythms*

The circadian rhythms in the SCN *rPer1* expression and pineal as well as plasma melatonin were demonstrated in Figs 2 and 3. Figure 2A demonstrates representative autoradiographs of SCN *rPer1* mRNA in the MAP-treated and control rats. The *rPer1* expression was robust in the SCN at ZT 6 but not at ZT 18 in both groups.

The *rPer1* expression in the SCN (Fig. 3A) was rhythmic in both groups (one-way ANOVA; $P < 0.0001$). They were high during the light phase and low during the dark phase. The maximum level was five times higher than the minimum level. The melatonin rhythms in the pineal and in plasma (Fig. 3B and C) showed the peaks at the dark phase (one-way ANOVA; $P < 0.0001$). The circadian rhythms in these functions in the

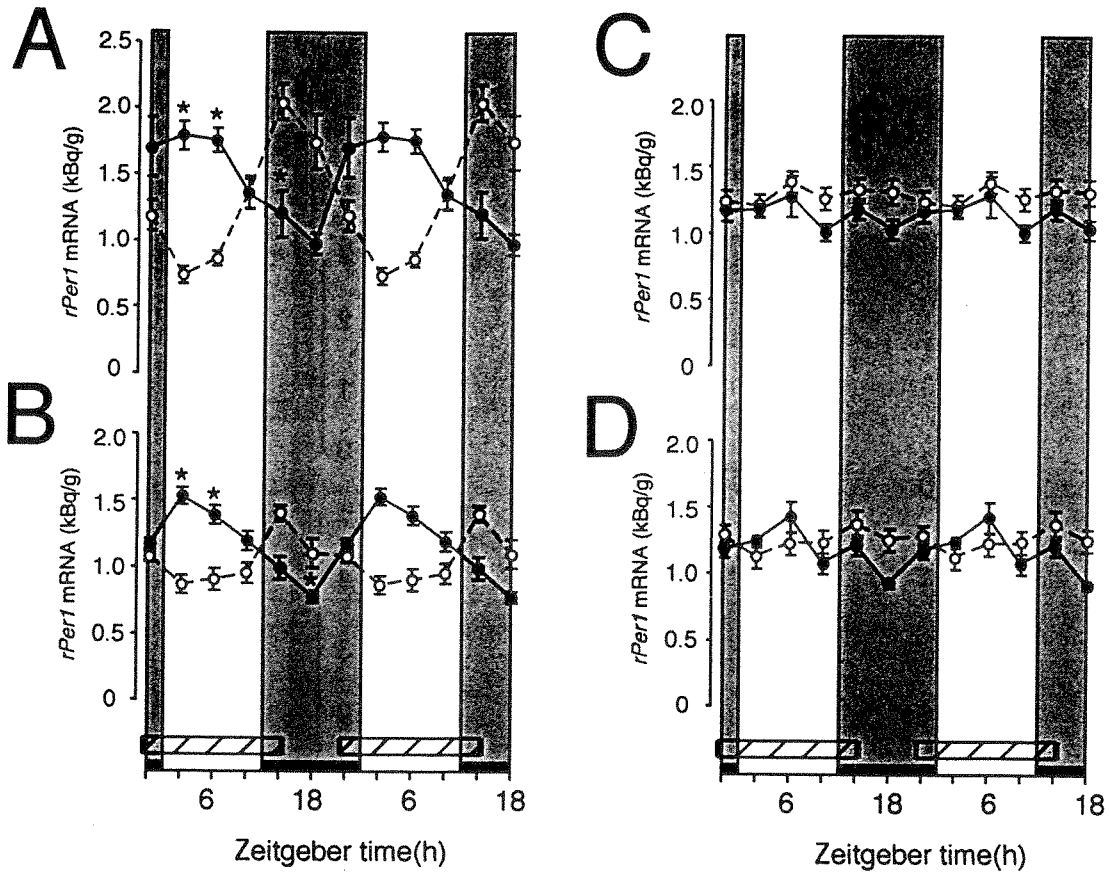

FIG. 4. Circadian *rPer1* expression outside the SCN. Circadian rhythms in *rPer1* mRNA in the parietal cortex (A), CPU (B), NAC (C) and cingulate cortex (D) in MAP-treated (closed circles with solid lines) and control rats (open circles with broken lines) (mean ± SEM). The circadian rhythms are illustrated in duplicate. Hatched horizontal bars indicate the mean activity band with SEM of locomotor rhythm in the MAP-treated rats. Dark horizontal bars on the abscissa and shaded areas indicate the dark phase. *$P < 0.0001$ for MAP-treated vs. control rats.

MAP-treated rats were not significantly different from those in the control (two-way ANOVA: *rPer1*, $P = 0.8031$; pineal melatonin, $P = 0.1830$; plasma melatonin, $P = 0.3948$).

Clock genes outside the SCN

rPer1

Figure 2B demonstrates representative autoradiographs of *rPer1* mRNA in the CPU and parietal cortex. The gene expression in the control rats was much stronger at ZT 18 than at ZT 6, while that in the MAP-treated rats was much stronger at ZT 6 than at ZT 18. As demonstrated in Fig. 4A and B, the *rPer1* expression rhythms were also detected in the parietal cortex and CPU (one-way ANOVA; parietal cortex, $P < 0.0001$ for control, $P = 0.014$ for MAP; CPU, $P = 0.0009$ for control, $P < 0.0001$ for MAP), which were completely phase-reversed by MAP treatment (two-way ANOVA, $P < 0.0001$ in both structures). The *rPer1* expressions were low during the light phase (lowest at ZT 2) and high during the dark phase (highest at ZT 14) in both structures of the control rats, while they were high during the light phase and low during the dark phase in the MAP-treated rats. The phase relationship between the *rPer1* expression and locomotor activity rhythms was not changed by MAP treatment. In contrast, the *rPer1* expression rhythms in the NAC (Fig. 4C) were not prominent for both groups (one-way ANOVA; NAC, $P = 0.7218$ for control, $P = 0.2716$ for MAP). However, the *rPer1* expression rhythm in the cingulate cortex (Fig. 4D) was not detected in the control animals (one-way ANOVA $P = 0.5492$ for control). By MAP treatment, the circadian rhythm became evident in synchrony with the *rPer1* expression rhythms in the parietal cortex and CPU (one-way ANOVA $P = 0.0011$, two-way ANOVA $P = 0.0193$).

rPer2

The *rPer2* expression rhythms were also detected in the parietal cortex and CPU (Figs 2C, and 5A and B) (one-way ANOVA; $P < 0.0001$ for both groups), which were completely phase-reversed in the MAP-treated rats (two-way ANOVA; $P < 0.0001$ for both structures) similar to the *rPer1* expression rhythm. The *rPer2* expressions were low during the light phase (lowest at ZT 6) and high during the dark phase (highest at ZT 14) in the control rats, while they were high during the light phase (highest at ZT 2) and low during the dark phase (lowest at ZT 18) in the MAP-treated rats. The phase relationship of *rPer2* expression rhythm to the locomotor activity rhythm was not altered by MAP treatment.

rBMAL1

The *rBMAL1* expression showed the circadian rhythm in the parietal cortex and CPU (Fig. 5C and D) (one-way ANOVA; parietal cortex; $P = 0.0006$ for control, $P < 0.0001$ for MAP, CPU; $P < 0.0001$ for control, $P < 0.0001$ for MAP). In the control rats, the *rBMAL1*

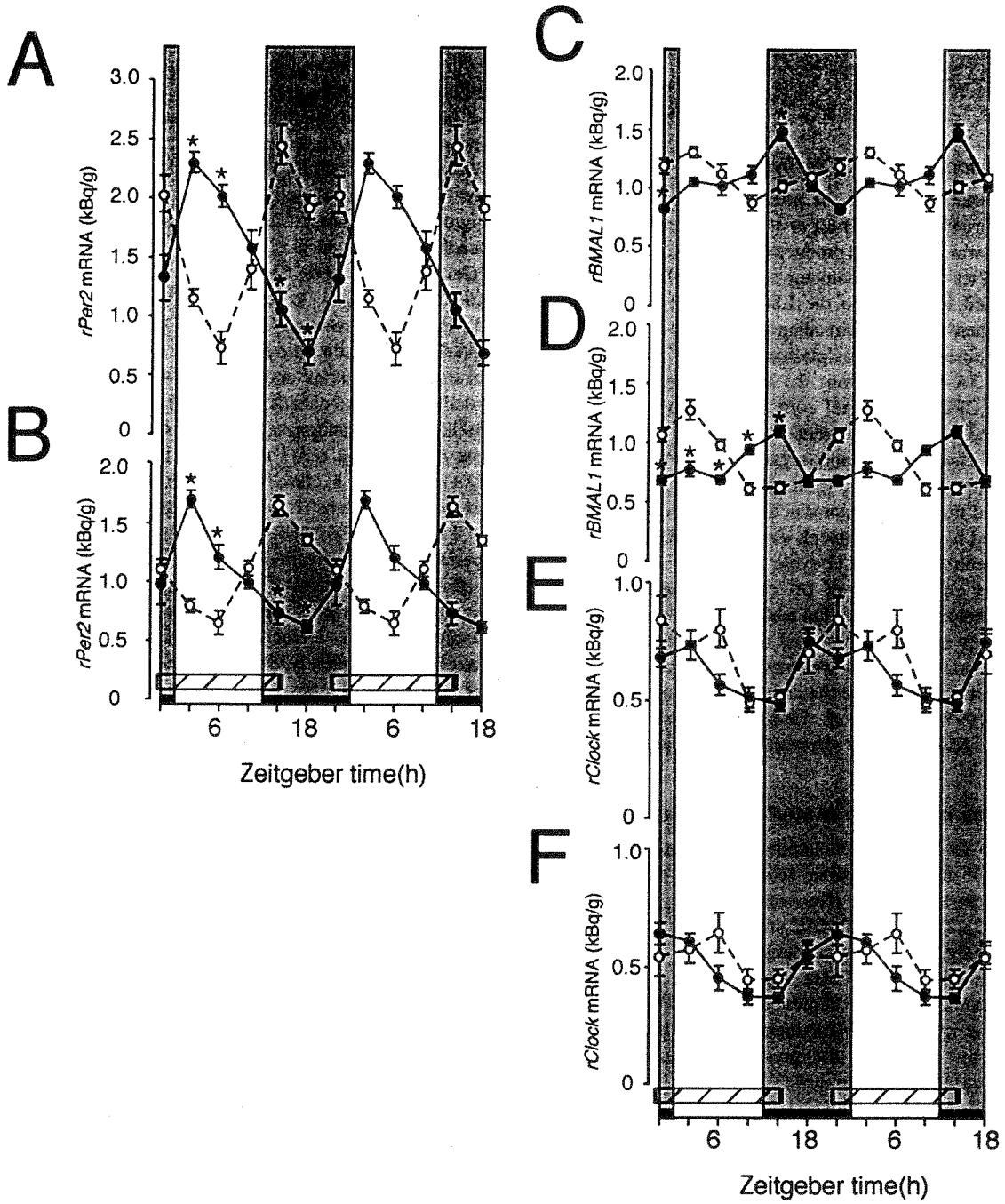

FIG. 5. Circadian *rPer2*, *rBMAL1* and *rClock* expression outside the SCN. Circadian rhythms in *rPer2*, *rBMAL1* and *rClock* mRNA in the parietal cortex (A, C and E) and CPU (B, D and F) in MAP-treated (closed circles with solid lines) and control rats (open circles with broken lines) (mean ± SEM). The circadian rhythms are illustrated in duplicate. Hatched horizontal bars indicate the mean activity band with SEM of locomotor rhythm in the MAP-treated rats. Dark horizontal bars on the abscissa and shaded areas indicate the dark phase. *$P < 0.0001$ for MAP-treated vs. control rats.

expression rhythm was antiphasic to the rhythms in *rPer1* and *rPer2* expressions, which was phase-reversed by MAP treatment (two-way ANOVA; $P < 0.0001$). Therefore, the phase relationship was not changed between the *rBMAL1* and *rPer1* or *rPer2* expression rhythms by MAP treatment. The same is true for the phase relationship between the *rBMAL1* expression and the locomotor activity rhythms. The *rBMAL1* expression always peaked at near the offset of the activity band.

rClock

The circadian rhythm of *rClock* expression was detected in the parietal cortex (Fig. 5E) (one-way ANOVA, $P = 0.0046$) in the control rats, but not in the CPU (Fig. 5F) (one-way ANOVA, $P = 0.2409$). By MAP treatment, *rClock* expression was not changed significantly in the parietal cortex, while they became rhythmic in the CPU (one-way ANOVA; $P < 0.0001$). In contrast to the *rPer1, rPer2 and rBMAL1* rhythms, the *rClock* rhythms in these areas were not phase-reversed

by MAP treatment (two-way ANOVA: parietal cortex, $P = 0.093$; CPU, $P = 0.115$).

Discussion

Desynchronization from the SCN rhythm by MAP treatment

The most interesting finding in the present study was the so-called internal desynchronization (Aschoff *et al.*, 1967; Wever, 1979) in the rat circadian system, which was produced by chronic MAP treatment. In spite of the fact that the locomotor activity rhythm in the MAP-treated rats failed to entrain to the LD cycle and free-ran with a period longer than 24 h, the circadian rhythms in the SCN *rPer1* expression and pineal, as well as plasma melatonin, entrained to the LD cycle (Fig. 3A–C). Moreover, the *rPer1* and *rPer2* expression rhythms in the CPU and parietal cortex were also desynchronized from the LD cycle. This phenomenon has been called as partial entrainment (Aschoff, 1981) and regarded as evidence that two different oscillators are involved in the circadian system. Previously, we demonstrated that the locomotor activity rhythm in the circadian domain appeared by MAP treatment, even in the SCN lesioned rats, which did not entrain to the LD cycle (Honma *et al.*, 1987). This finding suggests an existence of (a) circadian oscillator(s) which drives the locomotor activity rhythm and is located outside the SCN. In the SCN intact rats, MAP modified the expression of locomotor activity rhythm extensively and systematically (Honma *et al.*, 1986), but seemed to have no effect on the circadian pacemaker in the SCN (Honma *et al.*, 1991; Moriya *et al.*, 1996). The present results clearly demonstrate that MAP does not affect the circadian pacemaker in the SCN.

The site and the mechanism of MAP-induced oscillation

MAP is known to affect catecholaminergic neurons and stimulate dopamine (DA) or noradrenaline release from nerve terminals resulting in hyperlocomotion (Kuczenski *et al.*, 1995; Segal & Kuczenski, 1997). The CPU and NAC are heavily innervated, and the neocortex diffusely, by the dopaminergic as well as noradrenergic neurons (Ungerstedt, 1971). These structures are involved in the regulation of locomotor activity (Creese & Iversen, 1975; Kelly *et al.*, 1975; Darracq *et al.*, 1998). MAP increases catecholamines in the synaptic cleft by competing the presynaptic transporters which reuptake the released catecholamines (Wall *et al.*, 1995). Previously, we demonstrated that haloperidol, a DA receptor antagonist, shifted the phase of MAP-induced locomotor rhythm (Honma & Honma, 1995). The effect was dependent on the phase of MAP-induced rhythm where haloperidol was administrated. A phase-response curve for haloperidol was obtained. In this context, it is worth noting that greater responses to MAP in the female dopaminergic system than males have been reported in the CPU (Walker *et al.*, 2000). Female rats were known to be more sensitive to MAP than males for the induction of locomotor activity rhythm (Honma *et al.*, 1986). These findings suggest that the dopaminergic system is involved in the MAP-induced rhythm.

As demonstrated in Fig. 4, the effect of MAP on the circadian *rPer1* expression rhythm is structure specific. The NAC has been considered to be associated with hyperactivity, while the CPU with stereotyped behaviours (Creese & Iversen 1975; Kelly *et al.*, 1975). The *rPer1* expression rhythms were completely phase-reversed in the CPU, but weakly affected in the NAC by MAP treatment, suggesting that it is not the NAC but the CPU that is involved in the expression of circadian locomotor rhythm. The notion is consistent with the findings of recent studies that showed a strong correlation between the DA release and spontaneous locomotor rhythm in the CPU (Paulson & Robinson, 1994) indicating a greater effect of MAP on DA reuptake inhibition in the CPU than in the NAC (Kokoshka *et al.*, 1998). We hypothesize that the CPU and/or parietal cortex is the site of MAP-induced oscillation or the structure closely related to it. In this respect, it is interesting to note that both the *rPer* rhythms and the *rBMAL1* expression rhythms were phase-reversed in these structures by MAP treatment, while the *rClock* rhythms were not changed significantly. *BMAL1*, *Clock* and *Per1* constitute a molecular negative feedback loop, which is believed to generate the circadian rhythm (Gekakis *et al.*, 1998; Sangoram *et al.*, 1998). Furthermore, *Per* and *Clock* are shown to compose interlocking feedback loops in drosophila (Glossop *et al.*, 1999). Our results failed to show an interlocking relationship between the *Clock* and *Per* rhythms, at least in the parietal cortex and CPU. *BMAL1* expression shows circadian oscillation in and outside the SCN (Honma *et al.*, 1998; Oishi *et al.*, 1998), which is antiphasic to the *Per1* expression rhythm. Reversal of the *rBMAL1* and *rPer1* rhythms in the parietal cortex and CPU by MAP suggests a close relationship between *rBMAL1* and *rPer1* expression rhythms (Hardin & Glossop, 1999).

The *rPer1*, *rPer2* and *rBMAL1* expression rhythms in the CPU and parietal cortex covaried with locomotor activity rhythm. MAP enhances the expression of *rPer1* immediately (unpublished observation), which raised the possibility that the 24 h pattern of *rPer1* expression is a direct consequence of MAP intake. But, this possibility is unlikely as neither the daily amounts of *rPer1* and *rPer2* mRNAs nor the difference between the peak and trough levels were changed by MAP treatment. If the gene expressions were a direct consequence of MAP intake, the level of oscillation or controlled by the negative feedback, the amplitude of oscillation would be increased in MAP-treated rats. It is also less likely that the *rPer1* and *rPer2* expression rhythms are not the cause but the result of enhanced locomotor activity. The *rPer1* and *rPer2* expressions were already increased at the beginning of activity onset and gradually decreased even when the locomotor activity was still enhanced by MAP. These patterns of rhythmicity strongly suggest an endogenous nature rather than an exogenously induced origin.

Recently, serum shock was reported to induce a damped oscillation of the *rPer1* and *rPer2* expressions in cultured mammalian cells which otherwise did not oscillate (Balsalobre *et al.*, 1998). The oscillation could appear either by internal synchronization of multiple oscillating cells or by *de novo* generation of circadian oscillation by the clock gene(s). Whatever the mechanism might be, this would be a good model for the master–slave relationship in the hierarchical multi-oscillatory circadian system (Pittendrigh, 1974) and for the MAP-induced oscillation (Fig. 6). The slave oscillator(s) which drives the locomotor rhythm is under the control of SCN master oscillator without MAP treatment, but desynchronized from the SCN pacemaker with MAP treatment.

MAP-treated rat is an animal model for the human circadian system

In the present study, the locomotor activity rhythm in MAP-treated rats was desynchronized from melatonin rhythms. Such an internal desynchronization has not been observed, except in the human circadian system (Aschoff *et al.*, 1967; Wever, 1979). When human subjects were isolated from temporal cues, internal desynchronization occurred between the sleep–wake rhythm and the circadian rhythms in rectal temperature and plasma melatonin. The period of sleep–wake rhythm becomes either extremely longer or shorter than 24 h, while the periods of circadian rhythms remain close to 24 h by internal desynchronization. Two oscillators which drive desynchro-

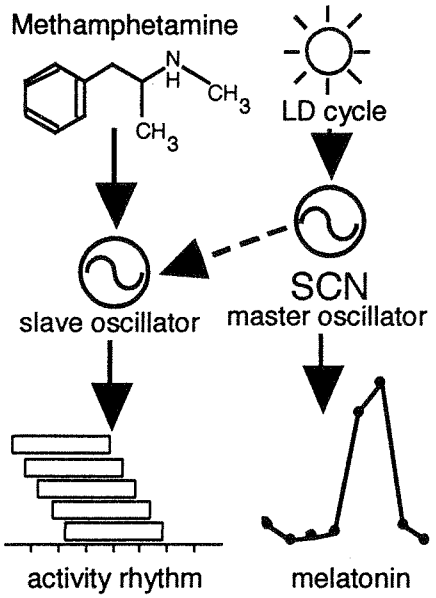

FIG. 6. A master–slave relationship in the hierarchical multi-oscillatory circadian system and a possible site of MAP action. In this model, photic data in the LD cycle reset the SCN pacemaker (master oscillator) that drives the circadian rhythms, as in the pineal melatonin. Without MAP treatment, the slave oscillator that drives the locomotor activity rhythm is regulated by the SCN master oscillator. With MAP treatment, the slave system is released from the master oscillator and begins to free-run with its own period.

nized rhythms have been hypothesized (Wever, 1979). By MAP treatment, at least two different circadian oscillations became evident in different brain structures, the SCN and CPU and/or parietal-cortex. These structures may correspond to the site of assumed oscillators in humans (Wever, 1979). The MAP-induced locomotor rhythm showed similar characteristics to the human sleep–wake rhythm, such as internal desynchronization from the melatonin rhythm, circabidian rhythm (≈ 48 h rhythm) (Honma & Honma, 1988; Honma *et al.*, 1992) and entrainment to nonphotic zeitgebers (Honma *et al.*, 1992; Honma *et al.*, 1994). Therefore, the MAP-treated rats are regarded as an excellent animal model for the human circadian system.

Acknowledgements

The present study was supported in part by grants from the Ministry of Education, Science and Culture of Japan (Nos 10470014 and 11877011). We thank Dr S. Hashimoto for technical advise and Ms. T. Yasuda and Y. Hatagawa for technical assistance.

Abbreviations

CPU, caudate-putamen; LD cycle, light–dark cycle; MAP, methamphetamine; NAC, nucleus accumbens; SCN, suprachiasmatic nucleus.

References

Abe, H., Honma, S., Namihira, M., Tanahashi, Y., Ikeda, M., Yu, W. & Honma, K. (1999) Phase-dependent induction by light of rat Clock gene expression in the suprachiasmatic nucleus. *Brain Res. Mol. Brain. Res.*, **66**, 104–110.

Aschoff, J., Gerecke, U. & Wever, R. (1967) Desynchronization of human circadian rhythms. *Jpn. J. Physiol.*, **17**, 450–457.

Aschoff, J. (1981) Freerunning and entrained circadian rhythms. In Aschoff, J. (ed.), *Handbook of Behavioral Neurobiology*, **Vol. 4** Biological Rhythms. Plenum Press, New York, NY, pp. 81–93

Balsalobre, A., Damiola, F. & Schibler, U.A. (1998) Serum shock induces circadian gene expression in mammalian tissue culture cells. *Cell*, **93**, 929–937.

Creese, I. & Iversen, S.D. (1975) The pharmacological and anatomical substrates of the amphetamine response in the rat. *Brain Res.*, **83**, 419–436.

Darracq, L., Blanc, G., Glowinski, J. & Tassin, J.P. (1998) Importance of the noradrenaline-dopamine coupling in the locomotor activating effects of D-amphetamine. *J. Neurosci.*, **18**, 2729–2739.

Dunlap, J.C. (1999) Molecular bases for circadian clocks. *Cell*, **96**, 271–290.

Gekakis, N., Staknis, D., Nguyen, H.B., Davis, F.C., Wilsbacher, L.D., King, D.P., Takahashi, J.S. & Weitz, C.J. (1998) Role of the CLOCK protein in the mammalian circadian mechanism. *Science*, **280**, 1564–1569.

Glossop, N.R., Lyons, L.C. & Hardin, P.E. (1999) Interlocked feedback loops within the Drosophila circadian oscillator. *Science*, **286**, 766–768.

Hardin, P.E. & Glossop, N.R. (1999) The CRYs of flies and mice. *Science*, **286**, 2460–2461.

Honma, K., Honma, S. & Hiroshige, T. (1986) Disorganization of the rat activity rhythm by chronic treatment with methamphetamine. *Physiol. Behav.*, **38**, 687–695.

Honma, K., Honma, S. & Hiroshige, T. (1987) Activity rhythms in the circadian domain appear in suprachiasmatic nuclei lesioned rats given methamphetamine. *Physiol. Behav.*, **40**, 767–774.

Honma, K. & Honma, S. (1988) Circadian rhythm: its appearance and disappearance in association with a bright light pulse. *Experientia*, **44**, 981–983.

Honma, K., Honma, S., Endo, T., Nakamura, K. & Hashimoto, S. (1994) Social Entrainment of Human Circadian Clock. In Hiroshige, T., Honma, K. (eds), *Evolution of Circadian Clock*. Hokkaido University Press, Sapporo, pp. 247–261

Honma, K., Honma, S., Nakamura, K., Sasaki, M., Endo, T. & Takahashi, T. (1995) Differential effects of bright light and social cues on reentrainment of human circadian rhythms. *Am. J. Physiol.*, **268**, R528–R535.

Honma, S., Honma, K. & Hiroshige, T. (1991) Methamphetamine effects on rat circadian clock depend on actograph. *Physiol. Behav.*, **49**, 787–795.

Honma, S. & Honma, K. (1992) Locomotor rhythms induced by methylphenidate in suprachiasmatic nuclei-lesioned rats. *Neurosci. Lett.*, **137**, 24–28.

Honma, S., Kanematsu, N. & Honma, K. (1992) Entrainment of methamphetamine-induced locomotor activity rhythm to feeding cycles in SCN-lesioned rats. *Physiol. Behav.*, **52**, 843–850.

Honma, S. & Honma, K. (1995) Phase-dependent phase shift of methamphetamine-induced circadian rhythm by haloperidol in SCN-lesioned rats. *Brain Res.*, **674**, 283–290.

Honma, S., Ikeda, M., Abe, H., Tanahashi, Y., Namihira, M., Honma, K. & Nomura, M. (1998) Circadian oscillation of BMAL1, a partner of a mammalian clock gene Clock, in rat suprachiasmatic nucleus. *Biochem. Biophys. Res. Commun.*, **250**, 83–87.

Ikeda, Y. & Chiba, Y. (1982) Effects of psychotropics on circadian motor activity in rats. In Takahashi, R., Halberg, F., Walker, C.A. (eds), *Toward Chronopharmacology*. Pergamon Press, New York, NY, pp. 3–10

Kelly, P.H., Seviour, P.W. & Iversen, S.D. (1975) Amphetamine and apomorphine responses in the rat following 6-OHDA lesions of the nucleus accumbens septi and corpus striatum. *Brain Res.*, **94**, 507–522.

Kokoshka, J.M., Vaughan, R.A., Hanson, G.R. & Fleckenstein, A.E. (1998) Nature of methamphetamine-induced rapid and reversible changes in dopamine transporters. *Eur. J. Pharmacol.*, **361**, 269–275.

Kuczenski, R., Segal, D.S., Cho, A.K. & Melega, W. (1995) Hippocampus norepinephrine, caudate dopamine and serotonin, and behavioral responses to the stereoisomers of amphetamine and methamphetamine. *J. Neurosci.*, **15**, 1308–1317.

Moriya, T., Fukushima, T., Shimazoe, T., Shibata, S. & Watanabe, S. (1996) Chronic administration of methamphetamine does not affect the suprachiasmatic nucleus-operated circadian pacemaker in rats. *Neurosci. Lett.*, **208**, 129–132.

Namihira, M., Honma, S., Abe, H., Tanahashi, Y., Ikeda, M. & Honma, K. (1999a) Circadian rhythms and light responsiveness of mammalian clock gene, Clock and BMAL1, transcripts in the rat retina. *Neurosci. Lett.*, **271**, 1–4.

Namihira, M., Honma, S., Abe, H., Tanahashi, Y., Ikeda, M. & Honma, K. (1999b) Daily variation and light responsiveness of mammalian clock gene, Clock and BMAL1, transcripts in the pineal body and different areas of brain in rats. *Neurosci. Lett.*, **267**, 69–72.

Oishi, K., Sakamoto, K., Okada, T., Nagase, T. & Ishida, N. (1998) Antiphase

circadian expression between BMAL1 and period homologue mRNA in the suprachiasmatic nucleus and peripheral tissues of rats. *Biochem. Biophys. Res. Commun.*, **253**, 199–203.

Paulson, P.E. & Robinson, T.E. (1994) Relationship between circadian changes in spontaneous motor activity and dorsal versus ventral striatal dopamine neurotransmission assessed with on-line microdialysis. *Behav. Neurosci.*, **108**, 624–635.

Paxinos, G. & Watson, C. (1986) *The Rat Brain in Stereotaxic Coordinates*, 2nd edn. Academic Press, San Diego, CA.

Pittendrigh, C.S. (1974) Circadian oscillations in cells and the circadian organization of multicellular systems. In Schmitt, F.O., Worden, F.G. (eds), *The Neurosciences. Third Study Program*. The MIT Press, Cambridge, MA, USA,. pp. 437–458

Plautz, J.D., Kaneko, M., Hall, J.C. & Kay, S.A. (1997) Independent photoreceptive circadian clocks throughout Drosophila. *Science*, **278**, 1632–1635.

Ruis, J.F., Buys, J.P., Cambras, T. & Rietveld, W.J. (1990) Effects of T cycles of light/darkness and periodic forced activity on methamphetamine-induced rhythms in intact and SCN-lesioned rats: explanation by an hourglass-clock model. *Physiol. Behav.*, **47**, 917–929.

Rusak, B. & Zucker, I. (1979) Neural regulation of circadian rhythms. *Physiol. Rev.*, **59**, 449–526.

Sakamoto. K., Nagase, T., Fukui, H., Horikawa, K., Okada, T., Tanaka, H., Sato, K., Miyake, Y., Ohara, O., Kako, K. & Ishida, N. (1998) Multitissue circadian expression of rat period homolog (rPer2) mRNA is governed by the mammalian circadian clock, the suprachiasmatic nucleus in the brain. *J. Biol. Chem.*, **273**, 27039–27042.

Sangoram, A.M., Saez, L., Antoch, M.P., Gekakis, N., Staknis, D., Whiteley, A., Fruechte, E.M., Vitaterna, M.H., Shimomura, K., King, D.P., Young, M.W., Weitz, C.J. & Takahashi, J.S. (1998) Mammalian circadian autoregulatory loop: a timeless ortholog and mPer1 interact and negatively regulate CLOCK-BMAL1-induced transcription. *Neuron*, **21**, 1101–1113.

Segal, D.S. & Kuczenski, R. (1997) Repeated binge exposures to amphetamine and methamphetamine: behavioral and neurochemical characterization. *J. Pharmacol. Exp. Ther.*, **282**, 561–573.

Shibata, S., Minamoto, Y., Ono, M. & Watanabe, S. (1994) Aging impairs methamphetamine-induced free-running and anticipatory locomotor activity rhythms in rats. *Neurosci. Lett.*, **172**, 107–110.

Sun, Z.S., Albrecht, U., Zhuchenko, O., Bailey, J., Eichele, G. & Lee, C.C. (1997) RIGUI, a putative mammalian ortholog of the Drosophila period gene. *Cell*, **90**, 1003–1011.

Tei, H., Okamura, H., Shigeyoshi, Y., Fukuhara, C., Ozawa, R., Hirose, M. & Sakaki, Y. (1997) Circadian oscillation of a mammalian homologue of the Drosophila period gene. *Nature*, **389**, 512–516.

Ungerstedt. U. (1971) Stereotaxic mapping of the monoamine pathways in the rat brain. *Acta. Physiol. Scand. Suppl.*, **367**, 1–48.

Walker, M.B., Rooney, Q.D., Wightman, R.M. & Kuhn, C.M. (2000) Dopamine release and uptake are greater in female than male rat striatum as measured by fast cyclic voltammetry. *Neuroscience*, **95**, 1061–1070.

Wall, S.C., Gu, H. & Rudnick, G. (1995) Biogenic amine flux mediated by cloned transporters stably expressed in cultured cell lines: amphetamine specificity for inhibition and efflux. *Mol. Pharmacol.*, **47**, 544–550.

Wever, R. (1979) *The Circadian System of Man*. Springer-Verlag, New York.

Whitmore, D., Foulkes, N.S., Strahle, U. & Sassone-Corsi, P. (1998) Zebrafish Clock rhythmic expression reveals independent peripheral circadian oscillators. *Nature Neurosci.*, **1**, 701–707.

Zylka, M.J., Shearman, L.P., Weaver, D.R. & Reppert, S.M. (1998) Three period homologs in mammals: differential light responses in the suprachiasmatic circadian clock and oscillating transcripts outside of brain. *Neuron*, **20**, 1103–1110.

Circadian pattern, light responsiveness and localization of *rPer1* and *rPer2* gene expression in the rat retina

Masakazu Namihira, Sato Honma, Hiroshi Abe, Satoru Masubuchi, Masaaki Ikeda[1] and Ken-ichi Honma[CA]

Department of Physiology, Hokkaido University School of Medicine, Sapporo 060-8638; [1]Department of Physiology, Saitama Medical School, Moroyama, Saitama 350-0495, Japan

[CA]Corresponding Author

Received 30 October 2000; accepted 30 November 2000

Circadian expression, light-responsiveness and localization of clock genes, *rPer1* and *rPer2*, were examined in the rat retina under constant darkness. A significant circadian variation was detected in *rPer2* transcript levels with a peak at ZT14, but not in the *rPer1*. A light pulse given after constant darkness of 3 days increased both *rPer1* and *rPer2* expression phase-dependently, while *rPer1* was induced at more times than *rPer2*. A major site of these gene expression within the retina was the inner nuclear layer. These findings indicate that *rPer1* and *rPer2* genes play different roles in the generation and regulation of circadian rhythms in the retina from those in the suprachiasmatic nucleus. *NeuroReport* 12:471–475 © 2001 Lippincott Williams & Wilkins.

Key words: Circadian rhythm; Light; Mammalian clock genes; *Per1*; *Per2*; Rat; Retina

INTRODUCTION

Circadian rhythms in mammals are regulated by the pacemaker located in the suprachiasmatic nucleus (SCN), which oscillates with a periodicity close to 24 h and is capable of entraining to a light–dark cycle (LD) [1]. The light signal which resets the circadian pacemaker is received by the photoreceptors in the retina and conveyed to the SCN through the retinohypothalamic tract [2].

Recently, a mammalian clock gene *Clock* was isolated from the mutant mouse, in which locomotor activity became aperiodic under constant darkness (DD) while rhythmic under LD with a 24 h period [3]. *Clock* encodes a bHLH/PAS type transcription factor and the gene product makes a heterodimer with the product of *BMAL1* which also encodes a bHLH/PAS type transcription factor [4]. The CLOCK/BMAL1 heterodimer was shown to activate the transcription of *Per1* via an E-box in the promoter region of the gene, and the *Per1* product in turn inhibits the transactivation by CLOCK and BMAL1 [4]. This negative feedback loop is thought to be essential for the generation of circadian rhythm [5]. *Clock* and *BMAL1* are expressed in the SCN of mice [4] and rats [6,7]. The expression of *BMAL1* in the SCN depended on the time of day and peaked at the middle of subjective night, while the expression of *Clock* was constant throughout the day [5]. The expression of two *Per* genes, *Per1* and *Per2*, was found to be rhythmic in the SCN [8,9] and peaked at the subjective day. The expression of these *clock* genes in the SCN was enhanced by a brief exposure to light under DD. Light-induced *Per1* and *Per2* expression was phase-dependent and high in the subjective night where the spontaneous expression was low. The expression of *Per1* and *Per2* appears to be related to photic entrainment [8,10]. An antisense oligonucleotide directed against *Per1* was reported to inhibit phase-shifts of behavioral rhythm by light and glutamate [11].

On the other hand, isolated mammalian retinas were shown to contain functional circadian systems that are entrainable to light without the SCN [12]. Since the mammalian retina is necessary for light entrainment but not for generation of the circadian oscillation which drives behavioral and endocrine rhythms, the circadian pacemaker in the retina is assumed to contribute to the fine tuning of light reception [13]. The two *Per* genes were also expressed in the retina [7,8], suggesting that they may play a central role of the retinal circadian oscillation, but the mechanism as well as the site of oscillation are remained to be elucidated.

In this study, in order to have a better understanding of roles of the clock genes, *rPer1* and *rPer2*, in the retina, we examined the 24 h pattern and light responsiveness of these gene expression using Northern blot analysis. We also analyzed the localization of the gene expression by *in situ* hybridization.

MATERIALS AND METHODS

Animals and housing: Male rats of the Wistar strain were used in the present experiment. Animals were taken care according to the Guideline for the Care and Use of Laboratory Animals in Hokkaido University School of Medicine. They were born and reared in our animal quarters where environmental conditions were controlled (lights on 06:00–18:00 h; temperature 24 ± 1°C). The light was supplied by fluorescent tubes, and the intensity of light was ~100 lux at the level of the cage. Three to four animals were housed together in a Plexiglas cage and had free access to food chow and tap water.

Experimental protocols: At the age of 8 weeks, rats were transferred to DD. On the third day of DD, animals were decapitated at six circadian phases ($n = 4–5$ for each phase), namely ZT (Zeitgeber Time) 2, 6, 10, 14, 18 and 22, where ZT 12 equals the time of lights off (18:00 h) in the previous LD cycle. In another series of experiment, rats were exposed to light of 300 lux for 30 min at the six circadian phases mentioned above ($n = 4–5$ for each phase), and decapitated 60 min after the start of light exposure. To determine the time course of light-induced change in the levels of *rPer1* and *rPer2* transcripts, rats were exposed to light of 300 lux for 30 min, and decapitated at different times (15, 30, 60, 90, 120 and 180 min) after lights on. Three animals were used at each time point. Control rats, which were exposed to DD for 3 days but not to the light pulse, were decapitated at the same time of day as the exposed rats. ZT14 was selected for the time course study, where a 30 min light pulse induced the largest phase delay shift in the locomotor activity rhythm in rats [14]. Decapitation was performed under red dim lights (< 0.01 lux). The eyeballs were quickly removed and frozen in a tube with dry ice. The tissues were stored at −80°C until hybridization or Northern blot analysis.

Northern blot analysis: The retinas were carefully removed from the eyeball using forceps and total RNA was isolated from the retina with ISOGEN (Nippon Gene, Tokyo, Japan) and further separated on a 1% agarose/0.7 M formaldehyde gel. Each lane contained 10 μg total retinal RNA. The ^{32}P-labeled random primed probes were generated from rat *rPer2* cDNA fragment (kindly provided by Dr Takahiro Nagase, bases 1–837; GenBank accession number AB016532) for *rPer2* and the PCR-amplified cDNA for *rPer1* (kindly provided by Dr Norio Ishida, described in [7]). The probes were hybridized to blots at 42°C, and the final wash was carried out at 65°C in 0.1 × SSC/0.1% SDS for 15 min twice. Hybridized blots were exposed with intensifying screens to X-ray films for 2 days. Autoradiograms were quantified by using NIH image software on a Macintosh computer. Hybridization signals were normalized in reference to glyceraldehyde-3-phosphate dehydrogenase (rat GAPDH, GenBank accession number M17701) mRNA.

In situ *hybridization:* *In situ* hybridization was performed as described previously [15]. Serial 20 μm sections of the retina were obtained with a cryostat, and placed on a slide glass coated with aminopropyltriethoxysilane (Sigma). Slide glasses were air dried and stored at −80°C until hybridization. Alternative sections were hybridized with either *rPer1* or *rPer2* probe. Antisense 45mer oligonucleotide probes for *rPer1* (complementary to nucleotide residues 254–298) and *rPer2* (to nucleotide residues 1925–1969) were labeled with [^{35}S]dAMP using [^{35}S]dATP (NEN) and terminal deoxyribonucleotidy transferase (BRL). For the negative control, a competitive hybridization was simultaneously performed by adding excess unlabeled probe (0.02 pmol/μl, > 20 times higher than the concentration of the labeled probe). The sections were dipped in nuclear track emulsion, and exposed for 9 weeks at 4°C. The sections were photographed by dark-field microscopy. For the retinal histology, an eye was fixed with Bouin's solution for 4 h and serial sections of a paraffin-embedded eye were stained with hematoxylin–eosin.

For statistical analysis of gene expression, one-way ANOVA with *post-hoc* Bonferroni/Dunn tests and two-way ANOVA with *post-hoc t*-test were used.

RESULTS

Figure 1 demonstrates the 24 h profiles of gene expression by Northern blot analysis. Hybridization signals of *rPer1* and *rPer2* mRNA were detected at about 5.4 kb (Fig. 1a) and 6.2 kb (Fig. 1c), respectively. There was no variation in the hybridization density of *rPer1* mRNA throughout the day (Fig. 1a, upper part), but a significant variation was seen in the hybridization density of *rPer2* mRNA (Fig. 1c, upper part). Quantitative analysis of mRNA revealed a significant variation in the transcript level for *rPer2* (one-way ANOVA; $p < 0.01$, Fig. 1d) but not for *rPer1* (one-way ANOVA, Fig. 1b). The *rPer2* transcription peaked at ZT14, and bottomed at ZT2. The transcript levels at ZT10 and ZT14 were significantly higher than that at ZT2 (*post-hoc* Bonferroni/Dunn tests).

The light responsiveness of *clock* gene expression is demonstrated in Fig. 2 and Fig. 3. A 30 min light pulse significantly increased the transcript levels of *rPer1* and *rPer2* 60 min after the onset of light pulse (two-way ANOVA; $p < 0.01$, Fig. 2). The light-induced increase of *rPer1* transcripts was evident at ZT2, 6, 10, 14 (*post-hoc t*-test) and the increment was about 1.2–1.4 times the pre-pulse level (Fig. 2b). The light-induced increase of *rPer2* transcripts was phase dependent (Fig. 2d) and evident at only ZT2 with an increment of about 1.8 times the pre-pulse level (*t*-test). Results of time-course experiments after the light exposure at ZT14 are demonstrated in Fig. 3. The *rPer1* mRNA level was increased by light (one-way ANOVA, $p < 0.05$) and significantly higher 60 min and 90 min after lights on than the pre-pluse level (*post-hoc* Bonferroni/Dunn; $p < 0.05$, Fig. 3b). The mRNA level declined subsequently and returned to the control level 3 h after lights on. The same light pulse failed to increase the *rPer2* transcript level at ZT14 (Fig. 3d), when compared with the pre-pulse level or with the controls.

To identify the localization of *rPer1* and *rPer2* expression in the rat retina, *in situ* hybridization was carried out (Fig. 4). Before the light pulse (time 0), the *rPer1* mRNA signals were detected strongly in the inner nuclear layer (IN) and less markedly in the outer nuclear layer (ON; upper panels). There was no signal in the ganglion cell layer (GC) and the outer segment layer (OS). By contrast, the *rPer2* mRNA was detected in the IN and GC, but not in the ON

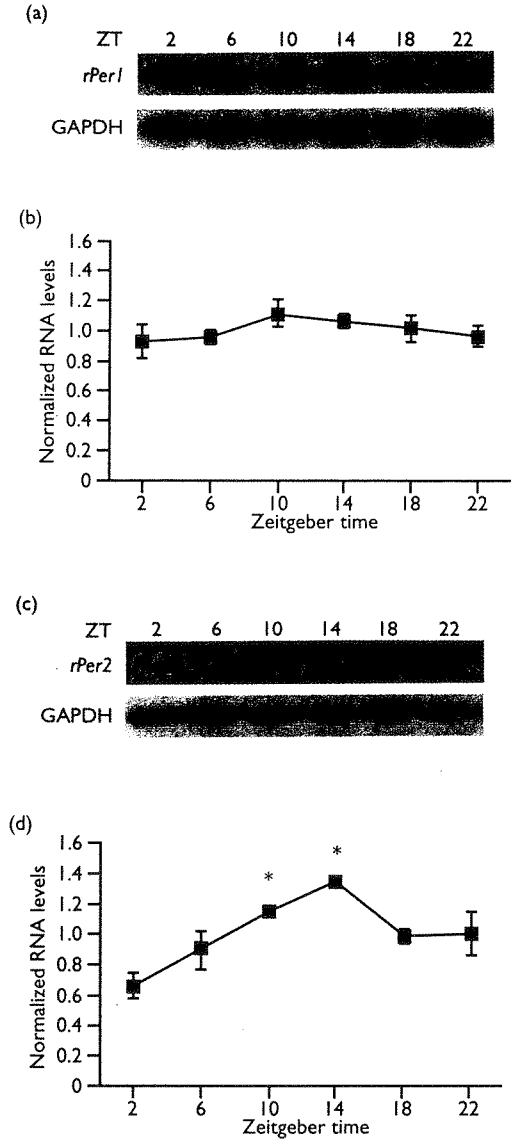

Fig. 1. Twenty-four hour profiles of the expression of *rPer1* (**a,b**) and *rPer2* (**c,d**) in the rat retina. Representative Northern blot analyses of retinal *rPer1* (a), *rPer2* (c) and GAPDH are illustrated in the upper panels. In the lower panels, *rPer1* (b), *rPer2* (d) mRNA levels are expressed in relative to the average value of all samples that is arbitrarily set at 1.0. The values at each time point represent the mean ± s.e.m. of 5 (b) or 4 (d) animals. A significant circadian variation is detected in the *rPer2* transcript level, but not in *rPer1* (d). $^{*}p < 0.01$ *vs* ZT2 (one-way ANOVA, *post-hoc* Bonferroni/Dunn).

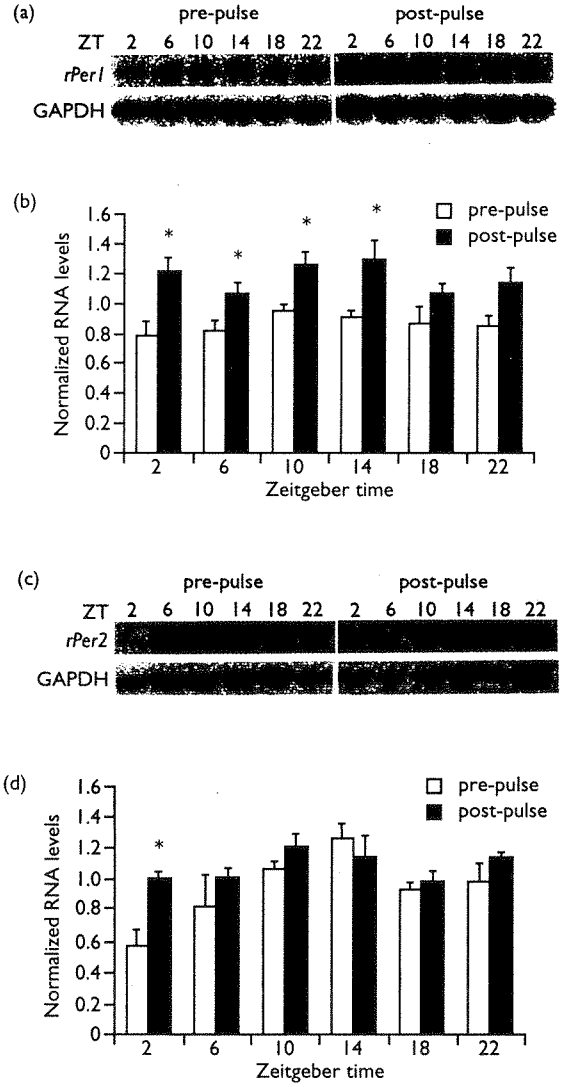

Fig. 2. Light responsiveness of *rPer1* (**a,b**) and *rPer2* (**c,d**) expression in the rat retina. Representative Northern blot analyses of retinal *rPer1* (a), *rPer2* (c) and GAPDH mRNA are illustrated in the upper panels. In the lower panels, *rPer1* (b), *rPer2* (d) mRNA levels are expressed in relative values to the average of all samples that is arbitrarily set at 1.0. Open columns indicate the pre-pulse and filled columns the post-pulse levels, respectively. Each value represents the mean ± s.e.m. of 5 (b) or 4 (d) animals. $^{*}p < 0.05$, *vs* pre-pulse level (Student's *t*-test).

(lower panels). At 60 min after the light pulse, the *rPer1* signals increased in the IN and ON, but the *rPer2* signals were not changed.

DISCUSSION

The present study demonstrates that the expression of *rPer2* underwent a significant circadian variation showing the peak at ZT14, while the level of *rPer1* transcript was constant throughout the day. The *rPer2* expression pattern was similar to, but the *rPer1* expression was quite distinct from those in the SCN [9], where a robust circadian variation was detected in the *rPer1* expression with a peak at the middle of subjective day. A lack of circadian rhythm in the *rPer1* transcript level, however, does not necessarily indicate that *rPer1* in the rat retina is not involved in the generation of circadian rhythm. Because, contributions to the *clock* machinery at the post-transcriptional levels are also possible as demonstrated in tau mutant hamsters [16]. The 24 h pattern of *rPer1* expression in the rat retina is different from that in the mouse. In the mouse, *mPer1* expression showed a circadian rhythm under LD [17] and DD [8,18] with a peak around ZT14, almost 180° out of phase of that in the SCN. The reason for this discrepancy between these reports in mice and the present result in rats is not known. In some of the previous studies [8,17] the

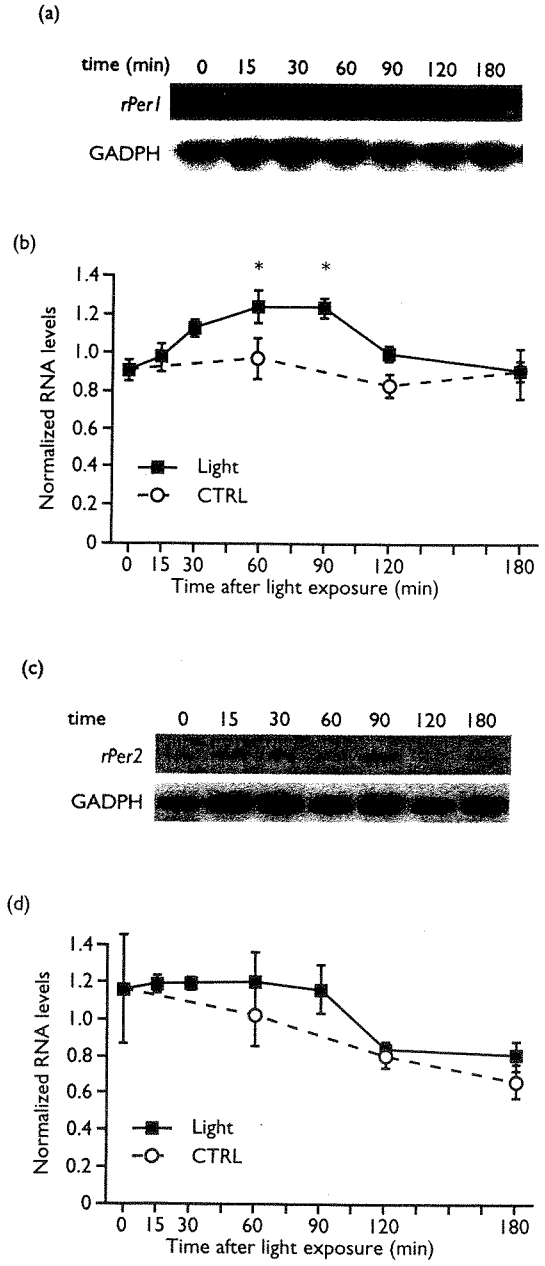

Fig. 3. Time course of *rPer1* (**a,b**) and *rPer2* (**c,d**) expression in the rat retina after light exposure at ZT14. In the upper panels, representative Northern blot analyses of retinal *rPer1* (a), *rPer2* (b) and GAPDH mRNA are illustrated. In the lower panels, *rPer1* (b), *rPer2* (d) mRNA levels are expressed in relative values to the average of all samples arbitrarily set at 1.0. Open circles indicate the results from non-pulse experiments (CTRL) and filled squares light pulse experiments (Light), respectively. Each value represents the mean ± s.e.m. of three animals. * $p < 0.05$ *vs* time 0 (one-way ANOVA, *post-hoc* Bonferroni/Dunn).

whole eyes were used for Northern blot, which were not exactly comparable to the present results in the retina. Interestingly, the amplitude of circadian variation in the *Per1* expression seems to be reduced under DD. It was robust under LD [17] but less marked 2 days after exposure to DD [18]. In the present study, the animals were exposed to DD for 3 days. The 24 h variation in *mPer1* expression might damp out when exposed to DD. A similar damping oscillation has been observed in the 24 h rhythm of a neuropeptide, vasoactive intestinal polypeptide, in the SCN [19]. These findings indicate that *rPer1* and *rPer2* play different roles in the generation of circadian rhythms in the retina from those in the SCN.

The circadian rhythms in the retina are driven by the retinal pacemaker *in vitro* [12] or probably after SCN lesions [13,20], but it is not known whether or not they are regulated solely by their own pacemaker *in vivo*. In the presence of SCN circadian pacemaker, circadin rhythms seem to be controlled dually by the peripheral, if any, as well as the master SCN pacemakers [21]. Roles of *clock* genes in the peripheral pacemakers including the retinal one are not known. We previously demonstrated the circadian expression of *Clock* and *BMAL1* in the rat retina as well as in the SCN [22]. The expression of *BMAL1* was constant throughout the day [22], similar to the *rPer1* expression pattern in the present study, while the expression of *Clock* gene was rhythmic in the retina, distinct from that in the SCN which was arrhythmic. Thus, the rhythmicity of *rPer1* seems to correlate with the rhythmicity of *BMAL1*.

The light-induced *rPer2* expression was observed only at ZT2 where the phase-advance shift of behavioral rhythm was observed by a light pulse. By contrast, the *rPer1* expression was enhanced by light throughout the subjective day (ZT2, 6, 10) and an early part of the subjective night (ZT14). These features of light responsiveness were also distinct from those in the SCN. In the SCN, a brief light pulse increased both the *rPer1* and *rPer2* expression phase-dependently. During the subjective day the light was not effective, while during the subjective night the light increased the gene expression significantly [10,23]. An acute induction of *mPer1* mRNA in the SCN was reported to be necessary for a light-induced phase shift of mouse locomotor rhythm [10,11]. Since the circadian pacemaker in the retina was demonstrated to entrain to LD [12], a light-induced increase in the *rPer1* mRNA in the retina may contribute to a phase shift of the retinal circadian system. However, the light responsive phases for the *rPer1* expression covered the whole subjective day, so that the *rPer1* in the retina may rather be involved in the light perception, especially in the light period. On the other hand, *rPer2* seems to be involved in phase-advance shifts of the pacemaker [14]. Different mechanisms were suggested previously for the phase-advance and delay shifts of the circadian pacemaker for behavioral rhythm [24]. In any case, the present results suggest that *rPer1* and *rPer2* play different roles in the light entrainment of circadian pacemaker in the retina from those in the SCN.

The site of circadian oscillation in the mammalian retina has not been elucidated. As demonstrated in Fig. 4, *rPer1* was expressed predominantly in the IN and slightly in the ON, but not in the GC, and *rPer2* was expressed primarily in the IN and slightly in the GC, but not in the ON. The localization of *rPer1* expression is consistent with the previous report in the mouse [4]. Since *rPer2* expression was rhythmic, the retinal circadian pacemakers is likely to reside in the IN, where the bipolar, amacrine and horizontal cells are located. The amacrine cells in the rat retina contain dopamine and tyrosine hydroxylase which show

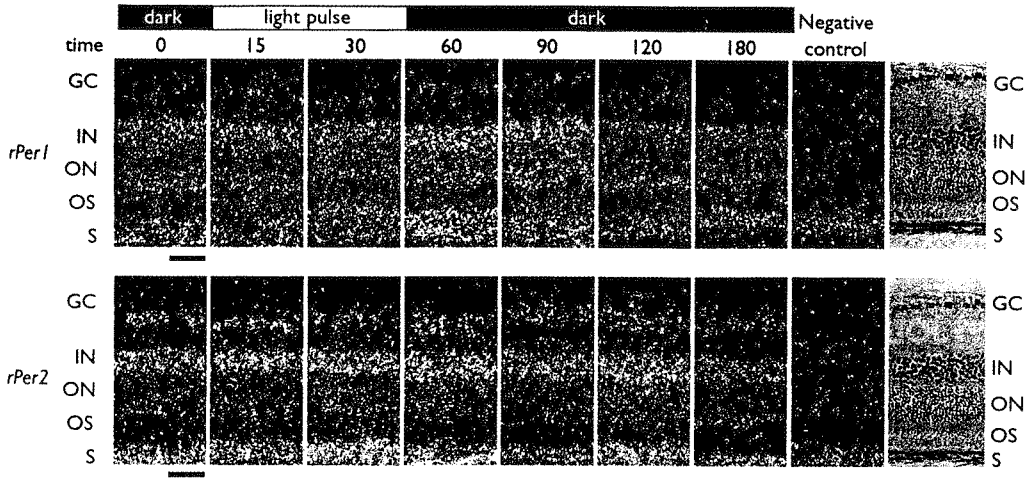

Fig. 4. Localization and light responsiveness of *rPer1* (upper panels) and *rPer2* mRNA signals (lower panels) at ZT14 in the rat retina by *in situ* hybridization. Dark-field micrographs of a rat retina are illustrated along with a time course after the onset of light pulse (300 lux for 30 min). The upper horizontal bar indicates the time of light exposure (open bar) and of a dark period (closed bar). Bars = 50 μm. *rPer1* mRNA signals were detected in the IN and ON, but not in the GC, while *rPer2* mRNA signals were in the IN and GC, but not in the ON. The right panels illustrate respective negative controls (see text) at ZT14, and light micrographs of the retina. OS, outer segments; ON, outer nuclear layer; IN, inner nuclear layer; GC, ganglion cell layer; S, sclera.

circadian rhythms under DD [25]. In pigeons, the melatonin and dopamine rhythms within the retina are mutually regulated [25], suggesting distinct circadian pacemakers driving both rhythms. A similar mutual interaction was recently suggested in the mammalian retina as well [26]. *rPer2* may be involved in the pacemaker responsible for the dopamine rhythm. Alternatively, the *rPer2* expression rhythm in the IN may be driven by the circadian pacemaker in the photoreceptor cells. On the other hand, *rPer1* was slightly and *rPer2* was scarcely expressed in the IN, where the photoreceptor cells are located. These results are rather unexpected and apparently inconsistent with the current idea that the circadian pacemaker is located in the photoreceptor cells [25]. Melatonin and arylalkylamine N-acetyltransferase (AA-NAT), the rate-limiting enzyme for melatonin synthesis, are expressed in the photoreceptor cells of rat retina and showed circadian rhythms [27]. In the rat pineal, the *rPer1* expression closely resembled the AA-NAT gene expression under various light conditions, suggesting that *rPer1* was regulated by the same mechanism which controlled the expression of AA-NAT gene [28]. In the present study, the *rPer1* transcript level in the retina was kept constant around the clock. This does not necessarily indicate a lack of circadian rhythm in *rPer1* expression in the retina. A circadian rhythm of a small amplitude in the IN might be masked by predominant and non-rhythmic expression in the ON.

CONCLUSION

The present results indicate that the mammalian clock genes, *rPer1* and *rPer2*, are expressed intensively in the IN of the rat retina, suggesting an impotant role of the IN in the generation of circadian rhythm in the retina. Circadian patterns and light responsiveness of *rPer1* and *rPer2* expression are distinct from those in the SCN, indicating that these *clock* genes in the retina play different roles in the generation and regulation of circadian rhythms from those in the SCN.

REFERENCES

1. Inouye ST and Kawamura H. *Proc Natl Acad Sci USA* **76**, 5962–5966 (1979).
2. Klein DC and Moore RY. *Brain Res* **174**, 245–262 (1979).
3. Vitaterna MH, King DP, Chang AM *et al. Science* **264**, 719–725 (1994).
4. Gekakis N, Staknis D, Nguyen H *et al. Science* **280**, 1564–1569 (1998).
5. Dunlap JC. *Cell* **96**, 271–290 (1999).
6. Honma S, Ikeda M, Abe H *et al. Biochem Biophys Res Commun* **250**, 83–87 (1998).
7. Oishi K, Sakamoto K, Okada T *et al. Biochem Biophys Res Commun* **253**, 199–203 (1998).
8. Shearman LP, Zylka MJ, Weaver DR *et al. Neuron* **19**, 1261–1269 (1997).
9. Yan L, Takekida S, Shigeyoshi Y *et al. Neuroscience* **94**, 141–150 (1999).
10. Shigeyoshi Y, Taguchi T, Yamamoto S *et al. Cell* **91**, 1043–1053 (1997).
11. Akiyama M, Kouzu Y, Takahashi S *et al. J Neurosci* **19**, 115–1121 (1999).
12. Tosini G and Menaker M. *Science* **272**, 419–421 (1996).
13. Terman M and Terman J. *Ann NY Acad Sci* **453**, 147–161 (1985).
14. Honma K, Honma S and Hiroshige T. *Jpn J Physiol* **35**, 643–658 (1985).
15. Masubuchi S, Honma S, Abe H *et al. Eur J Neurosci* **20**, 4206–4214 (2000)
16. Lowrey PL, Shimomura K, Antoch MP *et al. Science* **288**, 483–491 (2000).
17. Sun ZS, Albrecht U, Zhuchenko O *et al. Cell* **90**, 1003–1011 (1997).
18. Okamura H, Miyake S, Sumi Y *et al. Science* **286**, 2531–2534 (1999).
19. Shinohara K, Tominaga K, Isobe Y *et al. J Neurosci* **13**, 793–800 (1993).
20. Terman JS, Reme CE and Terman M. *Brain Res* **605**, 256–264 (1993).
21. Yamazaki S, Numano R, Abe M *et al. Science* **288**, 682–685 (2000).
22. Namihira M, Honma S, Abe H *et al. Neurosci Lett* **271**, 1–4 (1999).
23. Takumi T, Taguchi K, Miyake S *et al. EMBO J* **17**, 4753–4759 (1998).
24. Ralph MR and Menaker M. *Brain Res* **372**, 405–408 (1986).
25. Cahill GM and Besharse JC. *Prog Retinal Eye Res* **14**, 267–291 (1995).
26. Tosini G and Dirden JC. *Neurosci Lett* **286**, 119–122 (2000).
27. Sakamoto K and Ishida N. *Neurosci Lett* **245**, 113–116 (1998).
28. Fukuhara C, Dirden JC and Tosini G. *Neurosci Lettt* **286**, 167–170 (2000).

Acknowledgements: We thank Drs N. Ishida and T. Nagase for generous provide of *rPer1* and *rPer2* probes and Dr J. Nishihira for technical advise. The present study was supported in part by grants from the Ministry of Education, Science and Culture of Japan (No. 10470014 and 11877011).

Clock mutation lengthens the circadian period without damping rhythms in individual SCN neurons

Wataru Nakamura[1,2], Sato Honma[1], Tetsuo Shirakawa[2] and Ken-ichi Honma[1]

[1] *Department of Physiology, Hokkaido University Graduate School of Medicine, Sapporo 060-8638, Japan*

[2] *Department of Oral Functional Science, Hokkaido University Graduate School of Dentistry, Sapporo 060-8586, Japan*

Correspondence should be addressed to S.H. (sathonma@med.hokudai.ac.jp)

Published online: 15 April 2002, DOI: 10.1038/nn843

Spontaneous discharges of individual neurons in the suprachiasmatic nucleus (SCN) of *Clock* mutant mice were recorded for over 5 days in organotypic slice cultures and dispersed cell cultures using a multi-electrode dish. Circadian rhythms with periods of about 27 hours were detected in 77% of slice cultures and 15% of dispersed cell cultures derived from *Clock/Clock* homozygotes. These findings indicate that the *Clock* mutation lengthens the circadian period but does not abolish the circadian oscillation, and suggest an important role of intercellular communication in the expression of circadian rhythm in the SCN.

The circadian clock in mammals, located in the SCN, regulates the 24-hour profiles of physiology and behavior[1]. The SCN consists of multiple oscillating neurons with different periods, which are mutually coupled to produce the integrated circadian periodicity[2,3]. Mice mutant in the gene *Clock* have altered circadian rhythms[4,5]. Under constant darkness (DD), *Clock*/+ heterozygotes exhibit circadian rhythms in wheel-running behavior, with periods longer than those in wild-type mice (+/+), and *Clock/Clock* homozygotes become arrhythmic[6]. *Clock* is considered a crucial component of the molecular feedback loop that generates the circadian rhythm in the SCN (ref. 7). However, *Clock/Clock* mice often exhibit circadian rhythms in their first several days under DD, with periods of approximately 27 hours[6]. In our colony, 8 of 11 *Clock/Clock* mice showed significant circadian rhythms in wheel-running activity in the first 10 days under DD, with a period of 26.6 ± 0.8 hours (mean ± s.d.) (For experimental details, see **Supplementary Methods** online; all experiments were done following the guidelines for the care and use of laboratory animals of the Hokkaido University Graduate School of Medicine, Hokkaido, Japan.) The circadian rhythms disappeared in the following 10-day period (**Supplementary Fig. 1** online) except in one mouse, which became arrhythmic in the third 10-day period. These results suggest that the role of *Clock* in the circadian system may be different from what has previously been thought.

We assessed circadian firing rhythms of SCN neurons on the recording electrodes of a multi-electrode dish. Slice cultures were prepared from +/+, *Clock*/+ and *Clock/Clock* mice 5–8 days of age, and dispersed cell cultures were prepared from +/+ and *Clock/Clock* mice 2–5 days of age (see **Supplementary Methods**). Among the SCN neurons showing spontaneous discharges, significant circadian rhythms ($P < 0.01$, χ-square periodogram) were detected in 95% (53 of 56) of +/+, 83% (40 of 48) of *Clock*/+ and 77% (36 of 47) of *Clock/Clock* neurons in slice cultures, but in only 46% (28 of 61) of +/+ and 20% (9 of 46) of *Clock/Clock* neurons in dispersed cell cultures. Thus, the percentage of neurons with circadian rhythms was affected not only by genotype but also by culture method ($P < 0.05$, χ-square test for independence).

In the slice cultures (**Supplementary Fig. 2** online), the firing rhythms in *Clock/Clock* slices persisted for more than 5 days and showed a longer circadian period than did those in +/+ and *Clock*/+ slices (**Fig. 1**). One SCN neuron in a *Clock/Clock* slice retained a circadian rhythm for over 60 days in culture, with a circadian period of 26.9 hours. The circadian rhythms were probably not induced by medium exchanges, because no temporal correlation was detected between the times of medium exchange and spontaneous discharges. The maximum firing rate differed from neuron to neuron but was markedly constant in individuals, and did not differ among genotypes. The means of the minimum and maximum firing rates were 1.5 ± 1.4 and 9.2 ± 7.4 spikes/s (mean ± s.d.) in +/+, 1.7 ± 2.5 and 8.0 ± 9.1 in *Clock*/+ and 1.1 ± 1.2 and 6.0 ± 7.4 in *Clock/Clock* slices, respectively. The mean circadian periods were 23.5 ± 0.8 hours (mean ± s.d.) in +/+, 24.8 ± 0.5 hours in *Clock*/+ and 27.2 ± 1.0 hours in *Clock/Clock* slices, respectively (**Fig. 2**). The difference among these was statistically significant ($P < 0.0001$, one-way ANOVA), and each period coincided well with the periods of corresponding behavioral rhythms[6]. However, no significant difference was detected in the amplitude of the firing rhythm. The mean amplitudes were 79.3 ± 16.1% (mean ± s.d.) in +/+, 77.8 ± 14.4% in *Clock*/+ and 77.6 ± 14.4% in *Clock/Clock* slice, respectively.

In the dispersed cell cultures as well, SCN neurons from +/+ and *Clock/Clock* mice showed significant circadian firing rhythms ($P < 0.01$, χ-square periodogram; **Fig. 3**). Some neurons from *Clock/Clock* mice also showed ultradian rhythms,

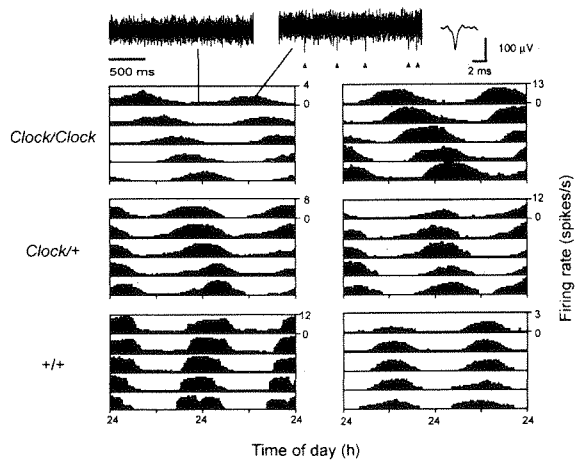

Fig. 1. Representative circadian firing rhythms of SCN neurons from *Clock* mutant and wild-type mice in slice cultures. Above are raw voltage traces of a *Clock/Clock* neuron recorded at the indicated time points and an averaged wave form of ten spikes. Triangles indicate discriminated spikes. The firing rhythm was expressed in a histogram of the mean firing rate in 15 min and double-plotted. The numbers in the right margin of the first lane in each panel were the scales of firing rate. The circadian periods of these firing rhythms were 28.1 h (left) and 28.0 h (right) for *Clock/Clock*, 25.3 h and 24.5 h for *Clock*/+, and 23.3 h and 23.8 h for +/+ neurons, respectively.

with a period of 9.4–11.5 hours; ultradian rhythms were not seen in +/+ neurons. The period of the circadian rhythm in +/+ neurons ranged from 21.4 to 25.9 hours, showing a normal distribution. The mean period was 23.3 ± 1.2 hours (mean ± s.d.). In contrast, the distribution of circadian periods in *Clock/Clock* neurons was bimodal: the periods in the major group (15%, n = 7) ranged from 25.2 to 29.8 hours with a mean of 27.1 ± 1.7 hours, and those in the minor group (4%, n = 2) were 19.2 hours and 19.7 hours. Such a short period has never been seen in the behavioral rhythms of *Clock/Clock* mice in our colony or in the firing rhythms of SCN neurons from +/+ mice. The longer period, however, coincided with the period of the observed behavioral rhythms.

In the present study, the *Clock* mutation lengthened the circadian period, but did not affect rhythm generation itself in individual SCN neurons. These findings challenge a current hypothesis about the role of *Clock* in the molecular clock mechanism[7]. According to this hypothesis, the *Clock* gene product, forming a heterodimer with BMAL1, activates the transcription of *Per* (*Period*) genes. The *Per* gene products, in turn, inhibit transactivation of *Per* by Clock/BMAL1, closing a molecular feedback loop that is considered central to the circadian oscillation. According to this theory, if any of the loop components is lost, the feedback loop will not work and the circadian oscillation may cease. Our results indicate, however, that this is not always the case: the circadian firing rhythm was detected in a higher percentage of slice cultures than dispersed cells, regardless of genotype.

This divergence between theory and our results could be explained at least in part by differences in the intercellular communication of slice and dispersed cell cultures. Cell-to-cell communication is weaker in dispersed cell cultures, where isolated SCN cells are re-organized, than in organotypic slice culture where an intact cell architecture is preserved. Not all rhythmic neurons in the SCN necessarily possess the circadian oscillator[8]. If the population of true oscillating neurons in the SCN is small, the probability of detecting these neurons would be lower in the absence of intercellular communication. The percentage of rhythmic neurons was significantly smaller in *Clock/Clock* than in +/+ cultures, regardless of the culture method, suggesting that the *Clock* mutation somehow weakens the intercellular coupling of circadian rhythms.

A possible cause of this weakened coupling is a lengthening of the circadian period in *Clock/Clock* mutants. In one report, none of 28 firing SCN neurons from *Clock/Clock* dispersed cell cultures showed sustained circadian rhythms[9]. Instead, approximately 50% of *Clock/Clock* cells expressed one or two cycles of near-24-hour periodicity, which was followed by ultradian rhythms with a 4–14-hour period. These findings are not contradictory to our results. A complete loss of intercellular communication would decrease the probability of finding a small number of oscillating neurons. We detected ultradian rhythms in some dispersed *Clock/Clock* cells, but did not see a near-24-hour periodicity. The discrepancy is possibly due to the absence of serum in our culture medium, because the treatment of culture cells with high concentrations of serum is reported to induce near-24-hour rythms in gene expressions[10]. From our results described here, we propose that the uncoupling of population oscillators in *Clock/Clock* leads to a loss of circadian rhythm. Future studies will be needed to test this hypothesis.

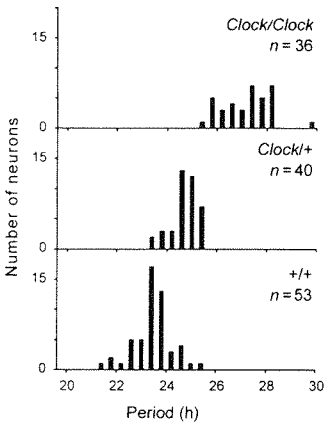

Fig. 2. Distributions of circadian periods in individual SCN neurons for each genotype in the slice culture. The circadian periods were distributed from 25.6 to 29.8 h in *Clock/Clock*, from 23.5 to 25.6 h in *Clock/+* and from 21.5 to 25.6 h in +/+ slices.

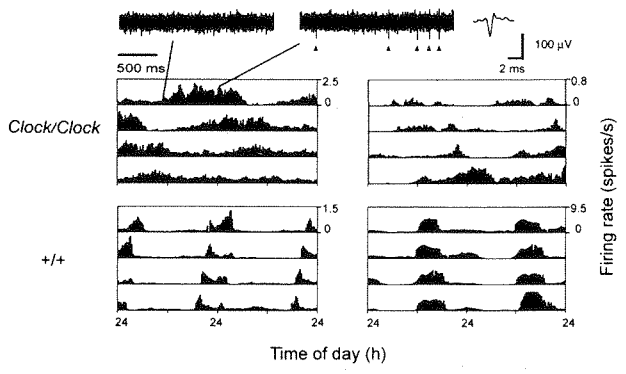

Fig. 3. Representative circadian firing rhythms of SCN neurons from *Clock/Clock* and +/+ mice in the dispersed cell culture. For details, see the legend of Fig. 1. The circadian periods of these firing rhythms were 28.2 h (left) and 26.1 h (right) for *Clock/Clock*, and 23.0 h and 24.5 h for +/+ neurons, respectively.

Note: Supplementary information is available on the Nature Neuroscience website.

Acknowledgements

We thank J. S. Takahashi and N. Ishida for generous gifts of Clock mutant mice, and T. Yasuda for technical assistance. This work was supported in part by a Grant-in-Aid for scientific research from the Ministry of Education, Science, Culture, Sports and Technology of Japan (nos. 11233201 and 12557005).

Competing interests statement

The authors declare that they have no competing financial interests.

RECEIVED 2 JANUARY; ACCEPTED 25 FEBRUARY 2002

1. Klein, D. C., Moore, R. Y. & Reppert, S. M. *The Suprachiasmatic Nucleus: The Mind's Clock* (New York, Oxford Univ. Press, 1991).
2. Welsh, D. K., Logothetis, D. E., Meister, M. & Reppert, S. M. *Neuron* **14**, 697–706 (1995).
3. Honma, S., Shirakawa, T., Katsuno, Y., Namihira, M. & Honma, K. *Neurosci. Lett.* **250**, 157–160 (1998).
4. King, D. P. *et al. Cell* **89**, 641–653 (1997).
5. Antoch, M. P. *et al. Cell* **89**, 655–667 (1997).
6. Vitaterna, M. H. *et al. Science* **264**, 719–725 (1994).
7. King, D. P. & Takahashi, J. S. *Annu. Rev. Neurosci.* **23**, 713–742 (2000).
8. Low-Zeddies, S. S. & Takahashi, J. S. *Cell* **105**, 25–42 (2001).
9. Herzog, E. D., Takahashi, J. S. & Block, G. D. *Nat. Neurosci.* **1**, 708–713 (1998).
10. Balsalobre, A., Damiola, F. & Schibler, U. *Cell* **93**, 929–937 (1998).

Dec1 and *Dec2* are regulators of the mammalian molecular clock

Sato Honma*, Takeshi Kawamoto†, Yumiko Takagi*, Katsumi Fujimoto†, Fuyuki Sato†, Mitsuhide Noshiro†, Yukio Kato† & Ken-ichi Honma*

** Department of Physiology, Hokkaido University Graduate School of Medicine, Sapporo 060-8638, Japan*
† Department of Dental and Medical Biochemistry, Hiroshima University Graduate School of Biomedical Sciences, Hiroshima 734-8553, Japan

The circadian rhythms in mammals are regulated by a pacemaker located in the suprachiasmatic nucleus of the hypothalamus[1,2]. Four clock-gene families have been found to be involved in a transcription–translation feedback loop that generates the circadian rhythm at the intracellular level[3]. The proteins Clock and Bmal1 form a heterodimer which activates the transcription of the *Per* gene from the E-box elements in its promoter region[4,5]. Protein products of *Per* act together with *Cry* proteins to inhibit *Per* transcription[6,7], thus closing the autoregulatory feedback loop. We found that Dec1 and Dec2, basic helix–loop–helix transcription factors, repressed Clock/Bmal1-induced transactivation of the mouse *Per1* promoter through direct protein–protein interactions with Bmal1 and/or competition for E-box elements. *Dec1* and *Dec2* are expressed in the suprachiasmic nucleus in a circadian fashion, with a peak in the subjective day. A brief light pulse induced *Dec1* but not *Dec2* expression in the suprachiasmic nucleus in a phase-dependent manner. *Dec1* and *Dec2* are regulators of the mammalian molecular clock, and form a fifth clock-gene family.

Circadian rhythms are evolutionally conserved from bacteria to humans[8]. All clock genes so far identified in mammals are components of an autoregulatory transcription–translation feedback loop[3]. Gene products of *Clock* and *Bmal1* act as positive components, whereas those of the *Per* and *Cry* genes act as negative ones[4–7]. This molecular feedback loop is widely accepted to be the intracellular machinery for circadian rhythm generation, but the model is insufficient to explain the stability and precision of circadian rhythms in living cells. Interlocked multiple feedback loops are considered as additional components to stabilize the molecular machinery[3,9,10].

DEC1 (*Stra13/Sharp2/BHLHB2*) and *DEC2* (*Sharp1/BHLHB3*) encode basic helix–loop–helix (bHLH) transcription factors related to rat Hes, *Drosophila* Hairy, and Enhancer of split (E(spl))[11–13]. Four of us (T.K., K.F., M.N., and Y.K.) cloned complementary DNA of human *DEC1*[11], a cyclic AMP inducible gene product, in embryonic chondrocytes and cloned cDNAs of *DEC2* in human, mouse and rat, by expressed sequence tag (EST) searching for similar members to *DEC1*[14]. In contrast to other members of Hes/Hairy/E(spl) subgroups, DEC1 and DEC2 lack a carboxy-terminal 'WRPW domain' to which co-repressors bind[11,14]. Circadian expression in peripheral tissues of *Dec1* and *Dec2* (M.N., manuscript in preparation), and reports that related proteins can bind to E-box elements[15,16], prompted us to study the roles of Decs in the mammalian circadian system.

Both Dec1 and Dec2 suppressed Clock/Bmal1-induced activation of *Per1* promoter in a dose-dependent manner as reported by a luciferase assay (Fig. 1a). Firefly reporter plasmid (E54-TK) was constructed by inserting a 5′ flanking region of mouse *Per1* containing 3 E-box elements, CACGTG, upstream of the TK promoter and these were transfected to NIH3T3 cells. The luciferase activity was markedly increased (125-fold) in the presence of *Clock* and *Bmal1* plasmid (50 ng per well). Co-transfection of the same amount of *Dec1* or *Dec2* plasmid suppressed the promoter activity down to 13.3 ± 1.0% (mean ± s.e.) and to 5.9 ± 0.5%, respectively. Even with one-eighth of the amount of plasmid, Dec1 suppressed the promoter activity to 72.5 ± 4.5%, and Dec2, to 14.6 ± 1.1%. The suppressing effects of Dec2 overwhelmed those of Per1, Per2, CRY1 and CRY2 at the same dosage. In our luciferase assay, CRY1 and CRY2 inhibited the promoter activity more strongly than did Per1 or Per2, confirming a previous result[6]. The suppression by Dec1 was comparable to that by CRY1 and CRY2.

Dec1 and Dec2 are not general inhibitors of transcription. Hypoxia inducible factor-1α (HIF-1α) is a bHLH-PAS transcription factor like Clock and Bmal1, and activates transcription of targets such as the erythropoietin gene through hypoxia-response elements (HRE)[17]. We examined the effects of Dec1 or Dec2 cotransfection on a HIF-1α-induced increase of the HRE reporter activity, and found that they did not significantly change the reporter activity (75.3 ± 5.3% and 114.9 ± 9.6%, respectively)—which was increased by HIF-1α (20.4-fold).

Gel retardation assays show that both mouse Dec1 and mouse Dec2 bound to mouse *Per1* proximal E-box elements (Fig. 1b). The binding was specific to an E-box, because excess dose of unlabelled E-box but not mutant E-box inhibited the binding. Thus, Decs may suppress Clock/Bmal1 induced transactivation by competing

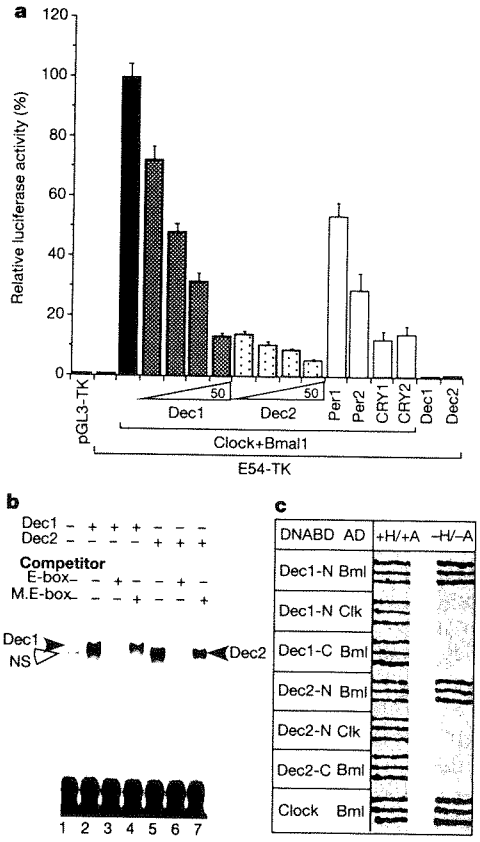

Figure 1 Repression of the Clock/Bmal1-induced E54-TK reporter activity by Dec1 and Dec2, and mechanisms of the repression. **a**, Dose-dependent repression of the Clock/Bmal1-induced E54-TK reporter activity by Dec1 and Dec2, compared with repression by Per1, Per2, CRY1 and CRY2. A relative luciferase activity was calculated as per cent values of the mean luminescence levels of E54-TK with Clock/Bmal1, and expressed in mean ± s.e. Results represent two independent experiments with $n = 4$ of each condition. **b**, Specific binding of Dec1 and Dec2 to the *Per1* proximal E-box by gel retardation assay. Arrow heads, binding bands with Dec1 and Dec2; open arrow head, non-specific band. **c**, Yeast two-hybrid assay showing that N-terminal (-N) but not C-terminal (-C) regions of Dec1 and Dec2 bind to Bmal1(Bml). Clk, Clock; +H/+A, −Leu/−Trp SD plate; −H/−A, −Leu/−Trp/−His/−Ade SD plate.

for E-box binding upstream of mouse *Per1*. Nevertheless, a yeast two-hybrid assay revealed that both Dec1 and Dec2 bound stereospecifically to Bmal1 (Fig. 1c). Dec1 and Dec2 lacking the C-terminal regions were able to bind to Bmal1 as did the full-length Decs, but those lacking the amino terminal failed to bind, suggesting the bHLH is the responsible site. Dec1 and Dec2 with the N-terminal regions did not bind to Clock. In this respect, Decs are different from E4BP4, a basic leucine zipper transcription factor which represses *Per1* transcription by competitively binding to the albumin D-site binding protein (DBP)-binding consensus at the 5′ upstream of *Per1*[18]. Dec1 and Dec2 exert their repressing effects on Clock/Bmal1-induced transactivation through competition for E-boxes with Clock/Bmal1 and/or direct protein–protein interactions with Bmal1.

Dec1 and *Dec2* are expressed in the suprachiasmic nucleus of the hypothalamus (SCN) in a circadian fashion (Fig. 2). Robust circadian rhythms ($P < 0.001$) were detected in both gene expression under continuous darkness (DD) as well as under light–dark conditions (LD) with peaks either early (*Dec1*) or in the middle (*Dec2*) of subjective day (Fig. 2a, b). Different light conditions did not change the circadian profiles. Compared with other brain areas, the hybridization signals in the SCN were weak for *Dec1*, but strong for *Dec2* (Fig. 2c–f).

The circadian rhythms are phase-shifted by a light pulse, which is an important mechanism for the entrainment of the circadian clock to 24-h light–dark environments. Light signals reach the SCN via the retinohypothalamic tract[19], and shift the circadian clock—the amount and direction (advance or delay) of the shift depends on the phase of the light pulse[20]. We examined light responsiveness of *Dec1* and *Dec2* gene expression in rats kept under DD for 3 d and subsequently exposed to a single light pulse of 30 min. *Dec1* and *Dec2* responded differently to the light pulse (Fig. 3). The light pulses given at 20:00, 24:00 and 4:00 significantly increased *Dec1* expression, whereas the same light pulses failed to induce *Dec2* expression. In contrast, the light pulse at 24:00 slightly but significantly decreased *Dec2* expression. Light pulses at other times did not change the level of gene expression for either *Dec1* or *Dec2*. Thus, the light responsiveness of *Dec1* expression was phase-dependent, and corresponded to the light-sensitive portion of a phase response curve[20] (Fig. 3a, c).

The circadian profiles of *Dec1* and *Dec2* expression were also examined in brain structures other than the SCN. Gene expression for *Dec1* and *Dec2* was different in different brain areas (Fig. 2c–f and Fig. 4a, b). *Dec1* was expressed strongly in the cerebral cortex, especially in the fifth layer, thalamus, and superior colliculus. On the other hand, *Dec2* expression was robust in the caudate putamen, pineal gland, and granular cell layer of the cerebellum. Both *Dec1* and *Dec2* were expressed in the olfactory bulb, piriform cortex, hippocampus and hypothalamic nuclei. Significant circadian rhythms were detected in the parietal and piriform cortices for *Dec1*, and in the piriform cortex and caudate putamen for *Dec2* under both LD and DD (Fig. 4c–f). None of them, however, were as robust as in the SCN. The circadian rhythms in these brain areas were almost 180° out of phase to those in the SCN. Phase reversal of the circadian rhythm outside the SCN has been observed in clock genes such as *Per1*, *Per2* and *Bmal1*[21,22] and may be related to behavioural rhythms[22]. Rhythmic expression of *Dec1* and *Dec2* outside the SCN may reflect their roles in the interacting molecular feedback loops of peripheral clocks[23].

Recently, two interacting molecular loops were suggested to be involved in the clock mechanism in mammals[9]. Together with a core feedback loop of *Per* transcription with positive (Clock, Bmal1) and negative components (Per1, Per2, Cry1, Cry2), an additional feed-

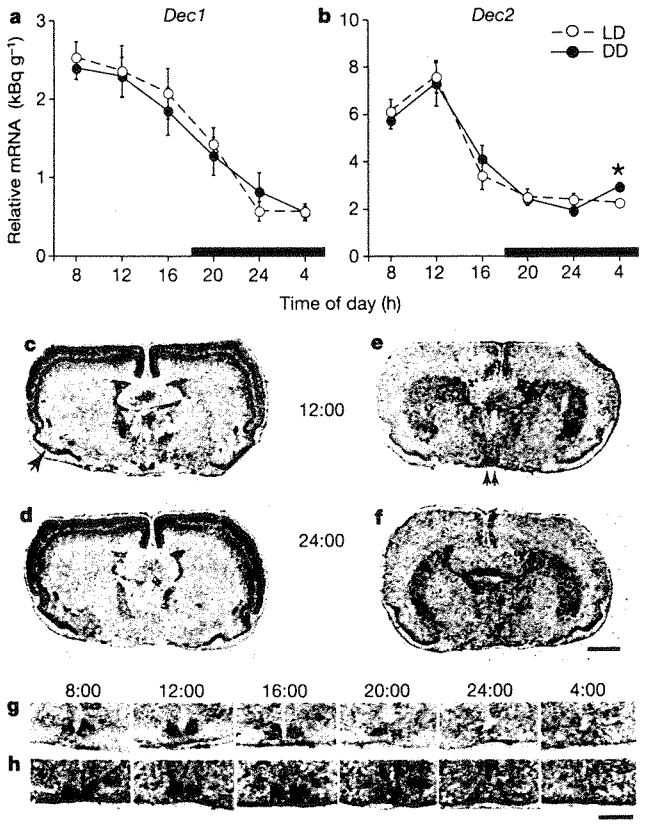

Figure 2 Circadian profiles of *Dec1* and *Dec2* expression in the SCN. *Dec1* (**a**) and *Dec2* (**b**) expression levels under light–dark (LD; open circles) and continuous darkness (DD; filled circles) (mean ± s.e.). Dark horizontal bars on the abscissa, dark period under LD cycle. Asterisk, $P < 0.05$ versus LD (*post hoc* test). Representative autoradiographs show *Dec1* (**c**, **d**) and *Dec2* (**e**, **f**) signals of the coronal brain sections including the SCN on the third day of DD at 12:00 (**c**, **e**) and 24:00 (**d**, **f**). Scale bar (**f**), 2 mm. Sampled areas of the parietal (star) and piriform cortices (an arrow) in **c**, SCN (arrows in **e**), and caudate putamen (star in **f**) are indicated. Higher magnification autoradiographs show *Dec1* (**g**) and *Dec2* (**h**) signals in the SCN at six times of day. Scale bar, 1 mm.

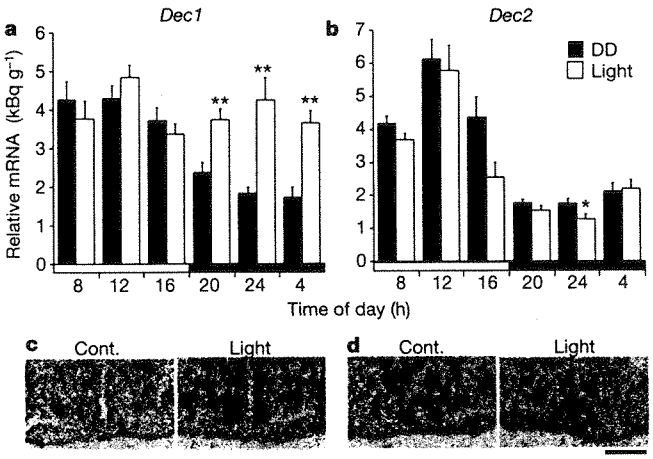

Figure 3 Response of *Dec1* and *Dec2* expression to 30 min light. Circadian variations of the light responsiveness of *Dec1* (**a**) and *Dec2* (**b**) expression in the SCN examined on the third day of DD. White columns, relative mRNA levels at 1 h after the onset of 30-min light pulse. Black columns, levels of control rats without light exposure. Grey and black bars on the abscissa, subjective day and night, respectively. Data are mean ± s.e. of 5 animals. $^{*}P < 0.05$, and $^{**}P < 0.01$ versus control. Representative autoradiographs show *Dec1* (**c**) and *Dec2* (**d**) signals before (Cont.) and 1 h after the light pulse (Light) at 24:00. Scale bar, 1 mm.

Nature Japan K.K., MG Ichigaya Bldg. 19-1 Haraikatamachi, Shinjuku-ku, Tokyo 162-0841 Tel 03-3267-8751 Fax 03-3267-8746

back loop of Bmal1 was suggested to be involved in such a way that *Bmal1* expression was enhanced by Cry1, Cry2 and Per2[9,10]. In the present study, Decs are suggested as strong negative components of the core loop. As Dec expression is up-regulated by Clock/Bmal1 heterodimers (T.K., manuscript in preparation), Decs seem to be important components of an additional autoregulatory feedback loop which interlocks with the core feedback loop of circadian oscillation. Specifically, *Per* proteins activate the production of Bmal1[9,10], which in turn stimulates *Per* and *Dec* transcription. Decs suppress the transactivation of *Per* gene by Clock/Bmal1, thus closing the loop. A physiological role for *Dec* proteins in the molecular clock mechanism is supported by the timing of their expressions in the SCN. High expression in the middle of the subjective day matches the time of maximum Clock/Bmal1 transcriptional activity[24]. A recent study showed that most of the cyclic transcripts were tissue-specific and only a limited number of genes were rhythmically expressed both in the SCN and liver[24], suggesting a key role for these genes in the molecular clock mechanisms. Therefore, rhythmic expression of *Decs* in many peripheral tissues including the liver implies physiological significance (M.N., manuscript in preparation).

A single light pulse enhanced *Dec1* but not *Dec2* expression in a phase-dependent manner, which was similar to *Per1*[25,26]. The light-induced *Dec1* expression is not due to a light-induced increase in Per or Bmal1 proteins but is probably due to a direct action of light. Entraining light signals in mammals are mediated by the retinohypothalamic tract[19], a major neurotransmitter of which is glutamate. Glutamate increases intracellular calcium, which in turn activates cAMP responsive element binding protein (CREB) in the SCN neurons[27]. As happens for *Per1*[28], a binding site for CREB—calcium/cAMP responsive element (CRE)—is found in the upstream promoter region of Dec1[15]. *Per1* and *Dec1* seem to be the doors to the molecular-clock machinery. □

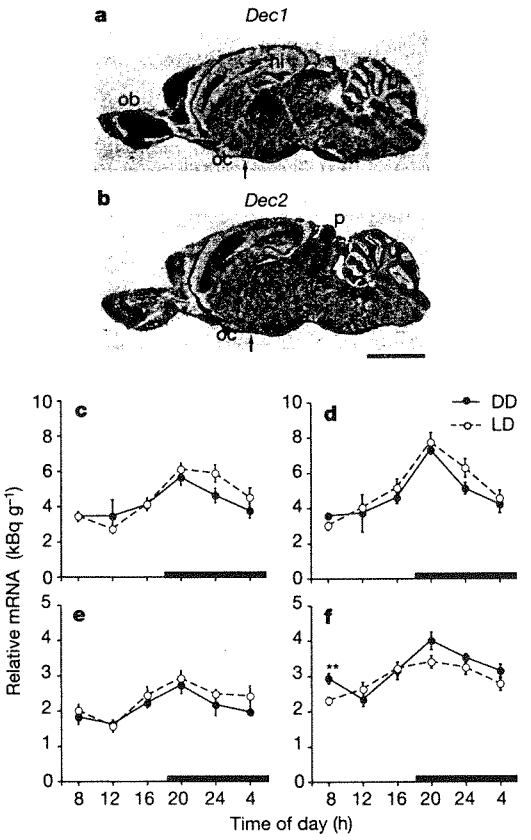

Figure 4 Circadian variation of *Dec1* and *Dec2* expression in the brain structures outside the SCN. Representative autoradiographs of *Dec1* (**a**) and *Dec2* (**b**) *in situ* hybridization in sagittal sections at 12:00 under LD cycle. Scale bar, 5 mm. Arrows indicate the SCN. hi, hippocampus; ob, olfactory bulb; oc, optic chiasm; p, pineal gland; and sc, superior colliculus. Circadian patterns of gene expression in the parietal (**c**) and piriform cortices (**d**) for *Dec1*, and the caudate-putamen (**e**) and piriform cortex (**f**) for *Dec2* under LD (open circles) and DD (filled circles). Dark horizontal bars on the abscissa, dark period under LD cycle. Data are mean ± s.e. of 5 animals. $^{**}P < 0.01$ versus LD (*post hoc* test).

Methods

Transfection and luciferase assay

A firefly reporter plasmid, E54-TK, was constructed by connecting an E54 fragment into the *NheI-XhoI* site upstream of the TK promoter of the pGL3-TK vector[29] (a gift from M. Negishi and T. Sueyoshi). The E54 fragment consisted of three E-boxes within 2.0 kb of the 5′ flanking region of the mouse *Per1* gene with their immediate flanking sequences linked together (TTTAGCCACGTGACAGTGTAAGCACACGTGGGCCCTCAAGT CCACGTGCAGGGA) as reported previously[4]. NIH3T3 cells were plated (3.4×10^4 cells per well) in a 24-well plate 24 h before transfection. Reporter plasmid (E54-TK, 2 ng per well) and mouse *Clock* and mouse *Bmal1b* (each 50 ng per well) expression vectors were transfected with or without one of following vectors; human *DEC1*, mouse *Dec2*, mouse *Per1*, rat *Per2*, human *CRY1* or human *CRY2* (each 50 ng per well) using Lipofectamine PLUS (Gibco-BRL) according to the manufacturer's instruction. In a dose response experiment, DEC1 and Dec2 plasmids were added in doses of 50, 25, 12.5 and 6.125 ng per well. The total concentration of DNA was adjusted to 152.2 ng per well with pcDNA3 (Invitrogen). For the intrinsic standard, 0.2 ng of pRL-SV40 vector (Promega) was transfected to each well. Twenty-four hours after the transfection, cells were lysed with Cell Lysis Buffer (Promega), and renilla and firefly luciferase activities were examined with Dual Reporter Assay Reagent (Promega). Similarly, NIH3T3 cells were transfected with 4 ng of firefly reporter plasmid containing HRE, 50 ng of HIF-1α (provided by L. Poellinger[17]) and 0.2 ng pRL-SV40 vector with or without 50 ng of *Dec1* or *Dec2* plasmid, and relative luciferase activity was measured ($n = 8$).

Expression constructs were made by subcloning full-length coding regions of the following genes into pcDNA3.1 (Invitrogen); mouse *Clock* (AF000998) and mouse *Bmal1b* (AB012601) were obtained by RT–PCR, mouse *Per1* was generously supplied by H. Tei[28], human *CRY1* (D84657), by M. Ikeda, and rat *Per2* (AB016532) and human *CRY2* (AB014558), by T. Nagase. As the AB014558 gene lacks 13 bp at the 5′ end of the human *CRY2* coding region, the fragment was added by PCR according to the sequence of an EST clone (AL 040215).

Gel retardation assay

Mouse Dec1 and Dec2 were translated using the TNT quick coupled transcription/translation system (Promega). The double-stranded oligonucleotides of the *Per1* E-box (5′-cgcgCAAGTCCACGTGCAGGGAtcga-3′) were end-labelled using [^{32}P]dCTP and DNA polymerase Klenow fragment. Synthesized mouse Dec1 or Dec2 was incubated with approximately 30,000 c.p.m. of ^{32}P-labelled probe for 10 min in 10 μl of 10 mM Tris/HCl (pH 8.0), 0.5 mM dithiothreitol, 10% glycerol, 1 μg of poly(dI-dC), 50 mM NaCl and 5 mM $MgCl_2$. In competition experiments, a 200-fold molar excess of unlabelled E-box or mutant E-box (5′-cgcgCAAGTCtcgctcCAGGGAtcga-3′) was added to the reaction mixture. The mixtures were applied to 5% polyacrylamide gel electrophoresis in 12.5 mM Tris-HCl/125 mM glycine/1 mM EDTA buffer.

Yeast two-hybrid assay

cDNAs encoding full-length mouse Bmal1, mouse Clock, human DEC1 and mouse Dec2, and those encoding N-terminal (4–139) and C-terminal (150–412) regions of human DEC1 and N-terminal (1–196) and C-terminal (113–410) regions of mouse Dec2 were cloned with pLP-GADT7AD, pLP-GBKT7DNA-BD, pGADT7AD or pGBKT7DNA-BD vector (Clontech). *Saccharomyces cerevisiae* AH109 was co-transfected with plasmids encoding either GAL4 DNA-BD or GAL4 AD fused protein. The transformants expressing two fused proteins were selected on plates of −Leu/−Trp SD medium. Three independent clones were assayed for transactivation of the HIS3 and ADE2 reporter genes on −Leu/−Trp/−His/−Ade SD plates.

Animal handling and tissue sampling

Male rats of Wistar strain were used at 2–2.5 months old. They were born and reared in our animal quarters, where environmental conditions were controlled (lights on from 06:00–18:00) as described elsewhere[20–22]. In the first experiment, rats were decapitated under LD ($n = 30$) and on the third day in DD ($n = 30$) at 6 times of the day starting from 8:00. In the second experiment, rats ($n = 30$) kept under DD for 3 d were exposed to a light pulse of 300 lux for 30 min from one of six time points as in the first experiment. They were returned to DD and decapitated 1 h after the onset of the light pulse. Control rats ($n = 30$) were decapitated under DD without exposing to light. The brains were quickly removed and frozen as described previously[21,22].

Quantitative *in situ* hybridization

This was performed as described previously[21,22]. Twelve serial sections containing the SCN in each rat were alternatively hybridized with *Dec1* and *Dec2* probes (5′-ACATACAAG CACACGCACGCGCACTCACACACTCACTCTCACACA-3′ and 5′-AAAGGGTAGAG GGTGGGGTGGCAGAAGGGTGAGAAAGGGGCAAAA-3′, respectively) radiolabelled

with ^{35}S-dATP (NEN). In addition, sagittal sections at the level of the SCN were saved in 3 brains obtained at 12:00 under LD. The hybridization signals were analysed using a microcomputer imaging device (Imaging Research). Optical density of the structure of interest was calibrated by converting it to relative signal intensity (kBq g^{-1}) using the ^{14}C-acrylic standards in the same cassette, and normalized by subtracting that of the corpus callosum in the same section as described previously[21].

Statistics

Circadian rhythms were statistically analysed by one-way analysis of variance, ANOVA. Differences between two circadian rhythms were analysed by two-way ANOVA with the Bonfferoni–Dunn *post hoc* test.

Received 11 July; accepted 29 August 2002; doi:10.1038/nature01123.

1. Moore, R. Y. & Eichler, V. B. Loss of a circadian adrenal corticosterone rhythm following suprachiasmatic lesions in the rat. *Brain Res.* **42,** 201–206 (1972).
2. Stephan, F. & Zucker, I. Circadian rhythms in drinking behavior and locomotor activity are eliminated by suprachiasmatic lesions. *Proc. Natl Acad. Sci. USA* **54,** 1521–1527 (1972).
3. Reppert, S. M. & Wever, D. R. Molecular analysis of mammalian circadian rhythms. *Annu. Rev. Physiol.* **63,** 647–676 (2001).
4. Gekakis, N. *et al.* Role of the CLOCK protein in the mammalian circadian mechanism. *Science* **280,** 1564–1569 (1998).
5. Darlington, T. K. *et al.* Closing the circadian loop: CLOCK-induced transcription of its own inhibitors per and tim. *Science* **280,** 1599–1600 (1998).
6. Kume, K. *et al.* mCRY1 and mCRY2 are essential components of the negative limb of the circadian clock feedback loop. *Cell* **98,** 193–205 (1999).
7. Yagita, K. *et al.* Dimerization and nuclear entry of mPER proteins in mammalian cells. *Gene Dev.* **14,** 1353–1363 (2000).
8. Dunlap, J. C. Molecular bases for circadian clocks. *Cell* **96,** 271–290 (1999).
9. Shearman, L. P. *et al.* Interacting molecular loops in the mammalian circadian clock. *Science* **288,** 1013–1019 (2000).
10. Yu, W., Nomura, M. & Ikeda, M. Interacting feedback loop within the mammalian clock: BMAL1 is negatively autoregulated and upregulated by CRY1, CRY2, and PER2. *Biochem. Biophys. Res. Commun.* **290,** 933–941 (2002).
11. Shen, M. *et al.* Molecular characterization of the novel basic helix-loop-helix protein DEC1 expressed in differentiated human embryo chondrocytes. *Biochem. Biophys. Res. Commun.* **236,** 294–298 (1997).
12. Boudjelal, M. *et al.* Overexpression of Stra 13, a novel retinoic acid-inducible gene of the basic helix-loop-helix family, inhibits mesodermal and promotes neuronal differentiation of P19 cells. *Gene Dev.* **11,** 2052–2065 (1997).
13. Rossner, M. J. *et al.* SHARPs: mammalian enhancer-of-split- and hairy-related proteins coupled to neuronal stimulation. *Mol. Cell. Neurosci.* **9,** 460–475 (1997).
14. Fujimoto, K. *et al.* Molecular cloning and characterization of DEC2, a new member of basic helix-loop-helix proteins. *Biochem. Biophys. Res. Commun.* **280,** 164–171 (2001).
15. Teramoto, M. *et al.* Gene structure and chromosomal location of a human bHLH transcriptional factor DEC1·Stra13·SHARP-2/BHLHB2. *J. Biochem. (Tokyo)* **129,** 391–396 (2001).
16. Dear, T. N. *et al.* Identification of interaction partners for the basic-helix-loop-helix protein E47. *Oncogene* **14,** 891–898 (1997).
17. Kallio, P. J. *et al.* Regulation of the hypoxia-inducible transcription factor 1α by the ubiquitin-proteasome pathway. *J. Biol. Chem.* **274,** 6519–6525 (1999).
18. Mitsui, S. *et al.* Antagonistic role of E4BP4 and PAR proteins in the circadian oscillatory mechanism. *Genes Dev.* **15,** 995–1006 (2001).
19. Moore, R. Y. & Card, J. P. Visual pathways and the entrainment of circadian rhythms. *Ann. NY Acad. Sci.* **453,** 123–133 (1985).
20. Honma, K., Honma, S. & Hiroshige, T. Response curve, free-running period, and activity time in circadian locomotor rhythm of rats. *Jpn J. Physiol.* **35,** 643–658 (1985).
21. Honma, S. *et al.* Circadian oscillation of *BMAL1*, a partner of a mammalian clock gene *Clock* in rat suprachiasmatic nucleus. *Biochem. Biophys. Res. Commun.* **250,** 83–87 (1998).
22. Masubuchi, S. *et al.* Clock genes outside the suprachiasmatic nucleus involved in manifestation of locomotor activity rhythm in rats. *Eur. J. Neurosci.* **12,** 4206–4214 (2000).
23. Yamazaki, S. *et al.* Resetting central and peripheral circadian oscillators in transgenic rats. *Science* **288,** 682–685 (2000).
24. Panda, S. *et al.* Coordinated transcription of key pathways in the mouse by the circadian clock. *Cell* **109,** 307–320 (2002).
25. Shigeyoshi, Y. *et al.* Light-induced resetting of a mammalian circadian clock is associated with rapid induction of the *mPer1* transcript. *Cell* **91,** 1043–1053 (1997).
26. Zylka, M. J., Shearman, L. P., Weaver, D. R. & Reppert, S. M. Three period homologs in mammals: different light responses in the suprachiasmatic circadian clock and oscillating transcripts outside of brain. *Neuron* **20,** 1103–1110 (1998).
27. Travnickova-Bendova, Z., Cermakian, N., Reppert, S. M. & Sassone-Corsi, P. Bimodal regulation of mPeriod promoters by CREB-dependent signaling and CLOCK/BMAL1 activity. *Proc. Natl Acad. Sci. USA* **99,** 7728–7733 (2002).
28. Hida, A. *et al.* The human and mouse *Period 1* genes: five well-conserved E-boxes additively contribute the enhancement of *mPer1* transcription. *Genomics* **65,** 224–233 (2000).
29. Sueyoshi, T. *et al.* The repressed nuclear receptor CAR responds to phenobarbital in activating the human CYP2B6 gene. *J. Biol. Chem.* **274,** 6043–6046 (1999).

Acknowledgements This work was supported in part by Grants-in-Aid for Scientific Research and Special Coordination Funds for Promoting Science and Technology from the Ministry of Education, Culture, Sports, Science and Technology, the Japanese Government.

Competing interests statement The authors declare that they have no competing financial interests.

Correspondence and requests for materials should be addressed to S.H. (e-mail: sathonma@med.hokudai.ac.jp).

4）時計遺伝子による体内時計生理機構の解析（研究代表者：柴田重信（早稲田大学））

研究代表者：　柴田重信　（早稲田大学人間科学部　教授）
研究分担者：　守屋孝洋　（学術振興会特別研究員）
秋山正志　（学術振興会特別研究員）
海老原史樹文　（名古屋大学農学研究科）

Ⅰ．研究成果

1．体内時計への光同調に関する研究。

（1）恒明条件下の体内時計遺伝子発現変動

恒明条件下で動物を飼育すると、光は体内時計をリセットするどころか、行動リズムの発振を低下させることが知られている。そこで、このような光条件下で、視交叉上核の Per1、Per2、Per3、BMAL1,Cry1 遺伝子発現リズムを調べた。

その結果、恒明条件下では、行動上のリズム発振は非常に遅くなり、かつリズムの発振強度も低下することが明らかとなった。実際この時、視交叉上核の時計遺伝子発現を調べて見ると、Per2,BMAL1,Cry1 はいずれもリズム性の発振が止まったような状態、つまりmRNA量が中間値を示すようになった。一方、Per1 発現の発振振幅は低下していたが、そのリズム性は保たれていた。したがって、行動上現れる、リズムの発振強度の低下は、Per1 遺伝子の発現リズム低下に起因する可能性が示された。今後、行動リズムの発振が低下し、やがてリズムが消失する過程を明らかにし、行動上のリズム異常を時計遺伝子発現で説明する必要がある。

（2）PACAP による光同調調節。（別刷り添付）

PACAP は視神経の伝達物質としても知られ、光同調に関わる可能性が in vitro の実験系で確かめられている。そこで視交叉上核の時計遺伝子発現に対する PACAP の影響を調べたところ、PACAP は行動上の位相変化を伴って *Per1* 遺伝子発現を増加させた。また、この 2 つの経路（小脳での高 KCl と PACAP、また視交叉上核での光刺激と PACAP）の相互作用を調べてみた所、*Per1* 遺伝子発現には相加や相乗効果は見られず、この 2 つの経路は最終的に 1 つの系として働いている可能性が判明した。すなわち、PACAP は *Per1* 遺伝子の発現調節を補助的制御しているものと考えられた。小脳培養細胞系で *Per1* 遺伝子発現を定常的に観察できる実験系が確立したので、これを使い、末梢の時計遺伝子発現が、PACAP でどのように制御されているかを明らかにすることにした。PACAP による *Per1* 遺伝子発現増大は、PKA を介し、高 KCl 負荷による *Per1* 発現が、CaMKII 系を介するものと異なることを見出した。PACAP は視交叉上核では同調の伝達物質として、小脳では視交叉上核からの信号の入力物質として働いている可能性が強く示唆された。

（3）光同調に対する gastrin-releasing peptide (GRP)の役割解明。（別刷り添付３）

光同調系の実験では視交叉上核に発現している gastrin-releasing peptide (GRP)の役割解

明を行うことを当初の研究目的とした。本研究の遂行には主に GRP 受容体欠損マウスを使用した。当初の研究計画通りに、光照射による視交叉上核内 Per 遺伝子発現、行動の位相変化について調べた。まず GRP のペプチド発現について調べた。その結果光同調入力の終末が豊富に存在する視交叉上核の腹側部の細胞に多数見られた。一方 GRP 受容体の mRNA 発現を調べてみると、視交叉上核の背側部に多いことが判明した。したがって腹側に存在する GRP 神経が光情報を背側部位に伝えている可能性が強く示唆されたので、そのことを時計遺伝子発現で証明するため GRP 受容体欠損マウスを使用した。

まず行動学的に GRP 受容体欠損マウスの明暗条件下ならびに恒暗条件下に活動のリズムを調べた。その結果、GRP 受容体欠損マウスは明暗条件下の 24 時間リズムも恒暗条件下のフリーランリズムもいずれも障害されず、正常マウスと同様であった。このことは光のマスキング作用（光が直接昼活動を低下させ、夜活動をあげる）や体内時計の発振機構には GRP 受容体は関わっていないことが分かった。次に、光のマスキング作用ではなく、同調作用に対する GRP 受容体のかかわりについて調べた。恒暗条件下にフリーランしている動物の行動開始時刻より 2-3 時間後に光を 15 分間照射すると、翌日から行動の開始位相が遅れる（位相後退）。光のこの効果は GRP 受容体欠損マウスでは減弱していることが判明した。この効果は 300 ルックスという高照度光照射時により明瞭に観察された。光同調に GRP 受容体が関わっていることが分かったので、このことをより明確にするため、GRP 受容体拮抗薬の作用を調べた。受容体拮抗薬は受容体欠損マウスと同様に、光同調が減弱することが分かった。光同調が GRP－GRP 受容体を介して起こることがわかったので、そのことをより直接的に確かめる目的で、GRP を脳内に直接投与し行動の位相後退が出現してくるか、またその作用が GRP 受容体欠損マウスでは低下しているか否かを確かめた。その結果、GRP の脳内投与は用量依存的に行動の位相を後退させ、GRP 受容体欠損マウスでは、GRP の高用量投与でも位相になんら影響を及ぼさなかった。

光照射により視交叉上核の *mPer1* と *mPer2* 遺伝子発現は急速に増大することが知られているので、GRP 受容体欠損マウスの視交叉上核における光誘導性 *Per* 遺伝子発現変化を調べた。GRP 受容体欠損動物では光照射による *mPer1* や *mPer2* 遺伝子発現が減弱していることが分かった。また当初考えていたように視交叉上核の亜核で減弱の程度を調べると、GRP 受容体の発現が多い背内側核で減弱が著しいことが分かった。

また、光による行動の位相変位も GRP 受容体欠損動物では減弱していた。以上のように、当初の計画通りに研究を遂行することができた。当初は計画していなかった、光による視交叉上核 FOS タンパクの発現も、GRP 受容体変異マウスでは低下していたことから、この作用は *Per* 遺伝子発現に特異的ではなく、光同調一般が低下することを意味することとなった（図6,7）。つぎに GRP そのものを脳内に投与し *Per* 遺伝子発現がどのように変化するかについて調べた。GRP の投与により、対照マウスではでは背内側の視交叉上核に顕著な *mPer1* や *mPer2* 遺伝子発現の増大が認められた。一方、GRP 受容体欠損マウスでは、上記のような反応が全く認められなかった。本研究から、光同調には GRP を介する *mPer1* や *mPer2* 遺伝子の一過性の発現増大が関わっていることが強く示唆された。

２．給餌性リズム同調に関する研究

（１）給餌性同調時の体内時計遺伝子発現変化。(別刷り添付)

動物に毎日一定時刻餌を与えると、動物は給餌時刻を覚え給餌時刻の 2−3 時間前から活動量が増大するいわゆる予知行動が出現してくる。この行動は視交差上核を破壊しても出現するが約 24 時間の周期の給餌でないと形成できないことから、視交差上核とは異なったある種のサーカディアンリズムであると考えられている。給餌性リズムが形成されたときの大脳皮質や肝臓での時計遺伝子ならびにその下流遺伝子発現を調べた。その結果、給餌制限を行ったマウスの肝臓の mPer1, mPer2 遺伝子発現は、対照マウスの位相が夜間であるのに比較して、昼間に移行した。また、下流遺伝子である CYP7alpha hydoxylase の遺伝子発現リズムも位相が前進することがわかった。この現象は視交差上核を破壊した動物でも観察された。また、大脳皮質、海馬、線条体いずれの脳部位でも肝臓と同様の結果が得られて。

（２）clock ミュータントマウスに対する給餌性同調時の体内時計遺伝子発現変化。(別刷り添付)

clock ミュータント動物は恒暗条件で飼育すると行動リズムの周期が延長し、やがて無周期性を示すようになる。これは視交差上核の体内時計機構が機能を失い行動のリズム性を消失するものと考えられている。そこで、このようにリズムが消失した状態でも給餌性のリズム形成が起こるか否か調べた。その結果、自由摂食の clock ミュータントマウスの心臓では mPer1, mPer1, Bmal1 のいずれの時計遺伝子発現も振幅が増大していた。ところが、給餌制限を加えると、ミュータントマウスでも心臓の時計遺伝子発現は昼間に明瞭なピークを示すようになった。また、その下流遺伝子である Pai-1 遺伝子発現でも昼間にピークが見られるようになった。すなわち、給餌性リズム形成には視交差上核の時計機構は必要でないこと、またそれ以外の場所にも発現している Clock タンパク質は給餌性リズム形成には必要でないこともわかった。

以上の成果を発表論文一覧表に示している。

参考文献

1999 年度(9 報)

1. Akiyama,M., Moriya,T.,Takahashi,S.,Kouzu Y., Wakamatsu,H., and Shibta,S., Inhibition of light-or glutamate-induced mPer1 expression represses the phase shifts into the mouse circadian locomotor and suprachiasmatic firing rhythms. *J.Neurosci.* 1999 19,1115-1121.

2. Hamada T., Kako,T.,Wakamatsu,H.,Shibata,S.,watanabe,S.,Ishida,N., Diurnal reguration of a DNA binding protein to the period repeat sequence in the SCN nuclear extract of rat brain. *Brain Res Mol Brain Res.* 1999 Mar 5;65(2):211-5.

3. Shishido,Y.,Furushiro,M.,Tanabe,S.,Shibata,S.,Hashimoto,S.,Yokokura,T., Effects of prolyl endopeptidase inhibitors and neuropeptides on delayed neuronal death in rats. *Eur J Pharmacol.* 1999 May 14;372(2):135-42.

4. Shishido,Y., Tanaka,T.,Tanabe,S., Furushiro,M., Hashimoto,S., Yokokura,T., Shibata,S., Watanabe,S. ZTTA, a prolyl endopeptidase inhibitor, potentiates the arginine-vasopressin-induced incorporation of C14leucine in rat amygdaloid and cortical slices. *Pharm Res.* 1999 Mar;16(3):463-5.

5. Hamada,T., Yamanouchi,S., Wtanabe,A., Shibata,S., Watanabe,S. Involvement of glutamate release in substanceP-induced phase delays of suprachiasmatic neuron activity rhythm in vitro. *Brain Res.* 1999 Jul 31;836(1-2):190-3.

6. Nikaido T, Moriya T, Takabayashi R, Akiyama M, Shibata S. Sensitization of methamphetamine-induced disorganization of daily locomotor activity rhythm in male rats. Brain Res. 1999 Oct 16;845(1):112-6.

7. Masashi Akiyama, Tomoko Kirihara, Ryouko Shikimoto, Yuko Yoshinobu & Shigenobu Shibata, Modulation of mPer1 gene expression by anxiolytic drugs in mouse cerebellum. *Br J Pharmacol.* 1999 Dec;128(7):1616-22.

8. Wan K, Moriya T, Akiyama M, Takeshima H, Shibata S, Involvement of ryanodine receptor type 3 in dopamine release from the striatum: evidence from mutant mice lacking this receptor. *Biochem Biophys Res Commun.* 1999 Dec 20;266(2):588-92.

9. Shibata S, Asai M, Oshima I, Ikeda M, Yoshioka T. Melatonin normalizes the re-entrainment of senescence accelerated mice (SAM) to a new light-dark cycle. *Adv Exp Med Biol.* 1999 460,261-270.

2000年度(11報)

10. Stork O, Ji F, Kaneko K, Stork S, Yoshinobu Y, Moriya T, Shibata S, Obata K. Postnatal development of a GABA deficit and disturbance of neural functions in mice lacking GAD65. *Brain Res.* 2000 May 19;865(1):45-58.

11. Kouzu,Y., Moriya,T., Takeshima,H., Yoshioka,T., Shibata,S., Mutant mice lacking ryanodine receptor type 3 exhibit deficits of contextual fear conditioning and activation of calcium/calmodulin-dependent protein kinase II in the hippocampus. *Mol Brain Res.* 2000 Mar 10;76(1):142-50.

12. Takahiro Moriya, Yuko Yoshinobu, Yasuko Kouzu, Akira Katoh, Hiroshi Gomi, Masayuki Ikeda, Tohru Yoshioka, Shigeyoshi Itohara and Shigenobu Shibata , The essential role of Glial Fibrillary Acidic Protein (GFAP)-expressing astrocytes in the mouse circadian oscillation under constant lighting condition. *J Neurosci Res.* 2000 60, 212-218.

13. Kazumasa Horikawa, Shin-ichi Yokota, Kazuyuki Fuji, Masashi Akiyama, Takahiro Moriya,Hitoshi Okamura and Shigenobu Shibata. Non-photic entrainment by 5-HT1A/7 receptor agonists accompanying with reduction of Per1 and Per2 expression. *J Neurosci.* 2000 Aug 1;20(15):5867-73.

14. Yamaguchi S, Mitsui S, Miyake S, Yan L, Onishi H, Yagita K, Suzuki M, Shibata S,

Kobayashi M, Okamura H. The 5' upstream region of mPer1 gene contains two promoters and is responsible for circadian oscillation. *Curr Biol.* 2000 Jul 13;10(14):873-6.

15. Ikeda M, Sugiyama T, Suzuki K, Moriya T, Shibata S, Katsuki M, Allen CN, Yoshioka T. PLC beta 4-independent Ca2+ rise via muscarinic receptors in the mouse suprachiasmatic nucleus. *Neuroreport.* 2000 Apr 7;11(5):907-12.

16. T. Moriya, S. Takahashi, M. Ikeda, K. Suzuki-Yamashita, M. Asai, H. Kadotani, H. Okamura, T. Yoshioka and S. Shibata, N-metyl-D-aspartate receptor subtype 2C is not involved in the circadian oscillation or photic entrainment of the biological clock in mice. *J Neurosci Res.* 2000 Sep 15;61(6):663-73.

17. Takahiro Moriya, Yasuko Kouzu, Shigenobu Shibata, Hiroshi Kadotani, , Kohji Fukunaga, Eishichi Miyamoto and Tohru Yoshioka.,Close linkage between Calcium/Calmodulin Kinase II a/ß and NMDA-2A receptors in the lateral amygdala and significance for retrieval of auditory fear conditioning. *Eur J Neurosci.* 2000 Sep;12(9):3307-14.

18. Asai M, Ikeda M, Akiyama M, Oshima I, Shibata S, Administration of melatonin in drinking water promotes the phase advance of light-dark cycle in senescence-accelerated mice, SAMR1 but not SAMP8. *Brain Res.* 2000 Sep 8;876(1-2):220-4.

19. Moriya T., Horikawa K, Akiyama M, Shibata S,. Correlative association between N-Methyl-D-Aspartate (NMDA) Receptor-Mediated Expression of Period Genes in the Suprachiasmatic Nucleus and Phase Shifts in Behavior with Photic Entrainment of Clock in Hamsters. *Mol Pharmacol.* 2000 Dec;58(6):1554-62.

20. Shin-ichi Yokota, Kazumasa Horikawa, Masashi Akiyama, Takahiro Moriya, Shizufumi Ebihara, Takuro Ohta, and Shigenobu Shibata. Inhibitory Action of Brotizolam on Circadian and Light-induced Per1 and Per2 Expression in the Hamster Suprachiasmatic Nucleus. *Br J Pharmacol.* 2000 Dec;131(8):1739-47.

2001 年度(12 報)

21. Wakamatsu, H., Takahashi, S., Moriya, T.,. Inouye, S-I., Okamura, H., Akiyama, M. and Shibata, S. Additive effect of mPer1 and 2 antisense oligonucleotides on light-induced phase shift. *Neuroreport.* 2001 Jan 22;12(1):127-31.

22. Yamaguchi,S., Kobayashi,M., Mitsui,S., Ishida,Y., van der Horst, G.T.J., Suzuki,M., Shibata,S., Okamura H., Real time monitoring of clock gene expression in the living mouse. *Nature.* 2001 409,684.

23. Wakamatsu H., Yoshinobu Y., Aida R., Moriya T., Akiyama M. and Shibata S., Restricted feeding-induced activity rhythm is associated with expression rhythm of mPer1 and mPer2 mRNA in the cerebral cortex and hippocampus but not in the suprachiasmatic nucleus in mice. *Eur J Neurosci.* 2001 Mar;13(6):1190-6.

24. Shimomura H., Moriya T., Sudo M., Wakamatsu H., Akiyama M., Shibata S., Differential Daily Expression of Per1 and Per2 mRNA in the Suprachiasmatic Nucleus

of Fetal and Early Postnatal Mice. *Eur J Neurosci.* 2001 Feb;13(4):687-93.

25. Nikaido T., Akiyama M., Moriya T., and Shibata S., Sensitized Increase of Period Gene Expression in the Mouse Caudate/Putamen Caused by Repeated Injection of Methamphetamine. *Mol Pharmacol.* 2001 Apr;59(4):894-900.

26. Hara R., Wan K., Wakamatsu H., Aida R., Kuriyama K., Moriya T. , Akiyama M. and Shibata S., Restricted feeding entrains circadian clocks in the mouse liver without participation of suprachiasmatic nucleus. *Genes Cells.* 2001 Mar;6(3):269-78.

27. Yokota, S-I., Yamamoto, M., Moriya, T., Akiyama, M., Fukunaga K., Miyamoto, E. and Shibata, S. Involvement of Calcium-calmodulin Protein Kinase but not of Mitogen-activated Protein Kinase in Light-induced Phase Delay and Per Gene Expression in the Suprachiasmatic Nucleus of Hamster. *J Neurochem.* 2001 Apr;77(2):618-27.

28. Yamamoto S, Shigeyoshi Y, Ishida Y, Fukuyama T, Yamaguchi S, Yagita K, Moriya T, Shibata S, Takashima N, Okamura H. Expression of the Per1 gene in the hamster: Brain atlas and circadian characteristics in the suprachiasmatic nucleus. *J Comp Neurol.* 2001 Feb 19;430(4):518-32.

29. Akiyama, M. Minami, Y., Nakajima, T., Moriya, T. and Shibata, S. Calcium and pituitary adenylate cyclase-activating polypeptide induced expression of circadian clock gene mPer1 in the mouse cerebellar granule cell culture. *J Neurochem.* 2001 Aug;78(3):499-508.

30. Takahashi S., Yokota S-I., Hara R., Kobayashi T., Akiyama M., Moriya T., Shibata S. Physical and Inflammatory Stressors Elevate Circadian Clock Gene mPer1 mRNA Levels in the Paraventricular Nucleus of the Mouse. *Endocrinology.* 2001 Nov;142(11):4910-7.

31. Asai M., Yoshinobu Y., Kaneko S., Mori A., Nikaido T., Moriya T., Akiyama M., Shibata S., Circadian profile of Per Gene mRNA expression in the suprachiasmatic nucleus, paraventricular nucleus, and pineal body of aged rats. *J Neurosci Res.* 2001 Dec 15;66(6):1133-9.

32. Asai M., Yamaguchi S., Isejima H., Jonouchi M., Moriya T., Shibata S., Kobayashi M., Okamura H., Visualization of mPer1 transcription in vitro: NMDA induces a rapid phase shift of mPer1 gene in cultured SCN. *Curr Biol.* 2001 Oct 2;11(19):1524-7.

2002 年度(8 報)

33. Aida R., Moriya T., Araki M., Akiyama M., Wada K., Wada E., Shibata S. Gastrin-releasing peptide mediates photic entrainable signals to the dorsal subsets of the suprachiasmatic nucleus via Induction of Period gene in mice. *Mol Pharmacol.* 2002 Jan;61(1):26-34.

34. Nishi M, Hashimoto K, Kuriyama K, Komazaki S, Kano M, Shibata S, Takeshima H. Motor discoordination in mutant mice lacking junctophilin type 3. *Biochem Biophys Res Commun.* 2002 Mar 29;292(2):318-24.

35. Takahashi S, Yoshinobu Y, Aida R, Shimomura H, Akiyama M, Moriya T, Shibata S.

Extended action of MKC-242, a selective 5-HT(1A) receptor agonist, on light-induced Per gene expression in the suprachiasmatic nucleus in mice.
J Neurosci Res. 2002 May 15;68(4):470-8.

36. Minami Y, Furuno K, Akiyama M, Moriya T, Shibata S. Pituitary adenylate cyclase-activating polypeptide produces a phase shift associated with induction of mPer expression in the mouse suprachiasmatic nucleus. *Neuroscience.* 2002;113(1):37-45.

37. Minami Y. Horikawa K, Akiyama M, Shibata S. Restricted feeding induces daily expression of clock genes and Pai-1 mRNA in the heart of Clock mutant mice. *FEBS Lett.* 2002 Aug 28;526(1-3):115-8.

38. Iijima M, Nikaido T, Akiyama M, Moriya T, Shibata S. Methamphetamine-induced, suprachiasmatic nucleus-independent circadian rhythms of activity and mPer gene expression in the striatum of the mouse. *Eur J Neurosci.* 2002 Sep;16(5):921-9.

39. Nisikawa Y, Shimazoe T, Shibata S, WatanabeS. Time-dependent effect of glutamate on long-term potentiation in the suprachiasmatic nucleus of rats. *J Pharmacol.* 2002 Oct;90(2):201-4.

40. Fukunaga K, Horikawa K, Shibata S, Takeuchi Y, Miyamoto E. Ca2+/calmodulin-dependent protein kinase II-dependent long-term potentiation in the rat suprachiasmatic nucleus and its inhibition by melatonin.
J Neurosci Res. 2002 Dec 15;70(6):799-807.

2003年度(2報)

41. Tatsushi Mutoh,Shigenobu Shibata,Horst-Werner Korf,Hiroshi Okamura, Melatonin modulates the light-induced sympathoexcitation and vagal suppression with participation of the suprachiasmitic nucleus in mice. *J Physiol,*547.1,pp.317-332 2003

42. Takahiro Moriyama,Masayuki Ikeda,Koji Teshima,Reiko Hara,Tohru Yoshioka,Charles N.Allen,Shigenobu Shibata, Facilitation of α-amino-3-hydroxy-5-methylisoxazole-4-propionate receptor transmission in the suprachiasmic nucleus by aniracetam enhances photic entrainment of the biological clock in rodents. *J.Neurochem.*in press

総説

1. 柴田重信、心身の開放と脳内物質、体育の科学、49、448-452、1999
2. 堀川和政、柴田重信、体内時計とセロトニン、Molecular Medicine、36、1143-1149、1999.
3. 柴田重信、体内時計の分子基盤研究の競争、日本薬理学雑誌、114、242、1999
4. 柴田重信、体内時計と時間薬理学、 日本薬剤師学会誌、51、1879-1885、1999
5. 柴田重信、体内時計とくすり、脳21、3、101-107、2000
6. 柴田重信、時刻認知と体内時計、脳の科学、22、543-547、2000
7. 守屋孝洋、柴田重信、時計遺伝子とリズム同調、神経研究の進歩、44、874-882、2000
8. 守屋孝洋、柴田重信、視交叉上核における時計のリセティングのシグナル伝達、細胞工学、

20、828-836、2001

9. 秋山正志、柴田重信、光受容分子、臨床検査、45、640-643、2001

10. 秋山正志、柴田重信、視交叉上核と体内時計の同調機構、臨床神経科学、19、55-57、2001

11. 柴田重信、概日リズムの薬理、神経研究の進歩、45、763-774、2001

12. 島田和幸、柴田重信、前村浩二、体内時計と疾患、「現代医療」 Vol.34 No.6 2002. 別刷

0013-7227/01/$03.00/0
Printed in U.S.A.

Endocrinology 142(11):4910–4917

Physical and Inflammatory Stressors Elevate Circadian Clock Gene *mPer1* mRNA Levels in the Paraventricular Nucleus of the Mouse

SATOMI TAKAHASHI, SHIN-ICHI YOKOTA, REIKO HARA, TOMOKO KOBAYASHI, MASASHI AKIYAMA, TAKAHIRO MORIYA, AND SHIGENOBU SHIBATA

Department of Pharmacology and Brain Science (S.T., S.-I.Y., R.H., T.K., M.A., T.M., S.S.) and ARCHS (T.M., S.S.), School of Human Sciences, Waseda University, Tokorozawa, Saitama, Japan 359-1192

Stress induces secretion of corticosterone through activation of the hypothalamic-pituitary-adrenal axis. This corticosterone secretion is thought to be controlled by a circadian clock in the suprachiasmatic nucleus (SCN). The hypothalamic paraventricular nucleus (PVN) receives convergent information from both stress and the circadian clock. Recent reports demonstrate that mammalian orthologs (*Per1*, *Per2*, and *Per3*) of the *Drosophila* clock gene *Period* are expressed in the SCN, PVN, and peripheral tissues. In this experiment, we examined the effect of physical and inflammatory stressors on *mPer* gene expression in the SCN, PVN, and liver. Forced swimming, immobilization, and lipopolysaccharide injection elevated *mPer1* gene expression in the PVN but not in the SCN or liver. A stress-induced increase in *mPer1* expression was observed in the corticotropin-releasing factor-positive cells of the PVN; however, the stressors used in this study did not affect *mPer2* expression in the PVN, SCN, or liver. The present study suggests that a stress-induced disturbance of circadian corticosterone secretion may be associated with the stress-induced expression of *mPer1* mRNA in the PVN. (*Endocrinology* 142: 4910–4917, 2001)

NOT ONLY PHYSICAL stress from forced swimming or immobilization but also inflammatory stress from the injection of lipopolysaccharide (LPS) have been shown to activate the hypothalamic-pituitary-adrenal (HPA) axis (1, 2). Stress-induced secretion of corticotropin-releasing factor (CRF) from the paraventricular nucleus (PVN) of the hypothalamus triggers the synthesis and release of ACTH and, ultimately, glucocorticoids. Thus, CRF participates in the mediation of behavioral responses to stress in mammals (3). In immobilized rats or those receiving LPS injection, a great induction of *fos*-like immunoreactivity in CRF positive cells of the PVN was observed (4, 5), indicating that CRF in the PVN functions as an important neuropeptide mediating stress-induced responses. Several lines of evidence have suggested that the PVN acts as an important relay site for transferring information from the suprachiasmatic nucleus (SCN), a center for the circadian clock, to the pineal body (6). Actually, the PVN receives many different kinds of input from the SCN in the form of vasopressin, glutamate, and γ-aminobutyric acid neurotransmitters, which are thought to convey circadian information (7–9). Interestingly, destruction of the SCN attenuates behavioral rhythms as well as the corticosterone secretion rhythm (10). The results from the above-mentioned studies strongly suggest that the PVN is an important brain site that receives stress-related information as well as information from the circadian clock.

Concerning stress-related information, reports show that basal levels of corticosterone are elevated not only from repeated stress (11, 12) but also from acute, inescapable stress (13). This increase in basal values was especially evident at the diurnal trough of the circadian rhythm and persisted for several days after the stressor was removed. Further, Honma *et al.* (14) reported that destruction of PVN catecholamines suppresses a restricted feeding-associated advance of the corticosterone rhythm in rats. Thus, daily fixed restricted feeding, a form of mild stress, entrains corticosterone rhythm through change in the PVN function.

As for the circadian clock, a recent molecular approach led to the discovery of clock genes such as *Per*, *Clock*, *Bmal1*, and *Cry* that provide a mechanism for the regulation of circadian and seasonal rhythms in mammals (15–17). Although a high expression of *mPer1*, *mPer2*, and *mPer3* (mouse orthologs of the *Dorsophila period* gene) have been observed in the SCN, moderate expression of these genes was also demonstrated in other brain regions such as the cerebral cortex, hippocampus, and PVN and in peripheral tissues such as the liver, heart, and skeletal muscle. To determine whether stress affects circadian activity of the HPA axis through change in the expression of *mPer1* and/or *mPer2* mRNA, we examined the effect of stressors such as forced swimming, immobilization, and LPS on expression of these genes in the PVN and SCN of mice.

In addition, a recent paper reported that glucocorticoid could reset the circadian clock in peripheral tissue such as the liver (18). Therefore, we were further interested in studying how stress can affect liver *mPer* gene expression through corticosterone secretion.

Materials and Methods

Animals

In all experiments, we used 4- to 6-wk-old male *ddY* mice (Takasugi, Saitama, Japan) housed in a 12-h light/12-h dark cycle. All animals were allowed free access to food and water before the start of food-restricted experiments.

Abbreviations: CRF, Corticotropin-releasing factor; HPA, hypothalamic-pituitary-adrenal; LPS, lipopolysaccharide; PB, phosphate buffer; PFA, paraformaldehyde; PVN, paraventricular nucleus; SCN, suprachiasmatic nucleus.

Forced swim test and immobility test procedures

The forced swim protocol described by Porsolt *et al.* (19) was modified for use in the mice experiments. Mice were subjected to a 15-min swim in a cylindrical Plexiglass tank (20 cm in diameter) containing water (25 C) 30 cm in depth and then returned to their home cages. These same mice were then killed 45 or 165 min following the test. Mice in the immobilization group were placed in metal mesh restrainers. After 60 min of immobilization, mice were either immediately killed or returned to their home cages and decapitated 120 min later. Control mice kept in their home cages were killed at the same 60-min time point because *mPer1* expression in the SCN reaches a maximal increase 60 min after light exposure (20).

Telemetry temperature measurement

Under pentobarbital anesthesia, a total of eight mice (three for saline injection, five for LPS injection) were surgically implanted with radiotelemetry transmitters (DSI, St. Paul, MN), which permitted continuous monitoring of core body temperature and activity. After 1 month of recovery from surgery, these animals were injected with the specified drug while the core temperature was monitored.

Sample preparation

Mice were deeply anesthetized with ether and intracardially perfused with saline followed by 0.1 M phosphate buffer (PB) (pH = 7.4) containing 4% paraformaldehyde (PFA). Brains were removed, postfixed in 0.1 M PB containing 4% PFA for 24 h at 4 C, and transferred into 20% sucrose in PB for 72 h at 4 C. Brain slices (40 μm thick) including the PVN and SCN were made using a cryostat (HM505E, Microm, Walldrof, Germany) and were placed in 2× saline sodium citrate until they were processed for hybridization.

In situ hybridization

In situ hybridization was applied to quantify *mPer1* and *mPer2* mRNA expression in the various brain areas. Slices were treated with 1 μg/ml proteinase K in 10 mM Tris-HCl buffer (pH 7.5) containing 10 mM EDTA for 10 min at 37 C, followed by 0.25% acetic anhydride in 0.1 M triethanolamine and 0.9% NaCl for 10 min. The slices were then incubated in the hybridization buffer (60% formamide, 10% dextran sulfate, 10 mM Tris-HCl, pH 7.4, 1 mM EDTA, 0.6 M NaCl, 1× Denhardt's solution (0.02% Ficoll, 0.02% polyvinyl pyrrolidone, 0.02% BSA), 0.2 mg/ml tRNA, 0.25% SDS) containing ^{33}P-labeled cRNA probes for 16 h at 60 C. Radioisotope (α[^{33}P]UTP [PerkinElmer Life Sciences, Inc., Boston, MA])-labeled antisense cRNA probes [*mPer1* (538–1752), *mPer2* (1–638)] (20) were made from restriction enzyme-linearized cDNA templates obtained from Dr. Okamura (Kobe University). After a high-stringency posthybridization wash with 2× saline sodium citrate/50% formamide, slices were treated with RNaseA (10 μg/ml) for 30 min at 37 C. To confirm that the signal intensities fell within the linear range of the detection system, a preliminary experiment was conducted to determine the adequate concentration of each radioisotope-labeled antisense cRNA probe.

The radioactivity of each slice on BioMax MR film (Kodak, New Haven, CT) was analyzed using a microcomputer interface to an image analysis system (MCID, Imaging Research, Inc., Ontario, Canada) after conversion into optical density by ^{14}C-autoradiographic microscales (Amersham Pharmacia Biotech, Little Chalfont, Buckinghamshire, UK) For data analysis, we subtracted the intensities of the optical density in the corpus callosum from those in the SCN and PVN of each section and regarded this value as the net intensity in the SCN and PVN. The intensity values of the sections from the rostral to the caudal part of the SCN and PVN (three to five sections per mouse brain) were then summed. The sum was considered to be a measure of the amount of *mPer1* or *mPer2* mRNA in this region.

Emulsion autoradiography for mPer1 and immunohistochemistry for CRF peptide

After fixation with 4% PFA, slices including the SCN and PVN were processed for immunohistochemistry according to the avidin-biotin-peroxidase complex method. Primary antibody (anti-CRF) (Cambridge Research Biochemical, Cleveland, OH) was diluted to a concentration of 1:5000 in 0.1 M phosphate buffer containing 1% normal goat serum in 0.3% Triton X-100.

For emulsion autoradiography, the same slices were dipped into emulsion (NTB2, Kodak) after hybridization with an *mPer1* probe, after which they were air dried for 3 h and stored in light-tight slide boxes at 4 C for 2 wk. The slides were developed with a D19 developer (Kodak) and then fixed with Fujifix (Fujifilm, Tokyo, Japan). The subnuclear silver grain distribution of each brain slice was examined using an optical microscope.

Statistics

Results are expressed as the mean ± SEM. The significance of differences between groups was determined by a one-way ANOVA followed by Dunnett's test or the *t* test.

Results

Forced swimming-induced mPer1 expression in CRF-positive PVN cells

Fig. 1 shows the emulsion autoradiogram of *mPer1* and CRF-positive cells in the SCN and PVN. During the day, the SCN exhibits high *mPer1* expression in the SCN but not in the PVN (Fig. 1, A and B). Sixty minutes after forced swimming, the expression of *mPer1* increased in the PVN but not in the SCN. To identify the phenotype of *mPer1* mRNA-positive cells in the PVN, we examined *mPer1* induction and CRF expression using the same PVN slices. In this experiment, we used animals pretreated with colchicine (10 mg/kg) 24 h before the forced swim. Pretreatment with colchicine intensified the expression of CRF-positive cells in the PVN (Fig. 1G). If the number of *mPer1* mRNA-labeled dots was at least 2 times higher than that seen in the background anterior hypothalamic area, this cell was identified as being doubly labeled. Interestingly, *mPer1* mRNA and CRF immunoreactivity were colocalized to the same PVN cells (Figs. 1, H and I). Approximately 75% of examined CRF-positive cells co-expressed *mPer1* mRNA using complete series (n = 3) of sections (four to six slices). The *mPer1* signal was not restricted to the CRF-rich zone of the PVN and labeling was seen in other parvocellular compartments.

Forced swimming- and immobilization-induced mPer1 but not mPer2 expression in the PVN

The basal level of *mPer1* and *mPer2* expression was high in the SCN, and forced swimming or immobilization failed to affect *mPer1* or *mPer2* expression in the SCN (Fig. 2, A and B). On the other hand, 60 min after the stressors were presented, there was a strong induction of *mPer1* but not *mPer2* in the PVN, in which basal levels of *mPer1* and *mPer2* were low (Fig. 2, A and B). This increase of *mPer1* in the PVN returned to basal level 3 h after stressor application. Sense control probes for *mPer1* and *mPer2* were used to examine nonspecific binding of these probes to the brain tissue. However, there were no signs of nonspecific binding data (data not shown).

Day/night differences in forced swimming-induced mPer1 expression

To test the hypothesis that the lack of stress-induced *mPer1* expression in the SCN relates to the high level of *mPer1* basal activity, we examined the effect of a stressor on the *mPer1* and

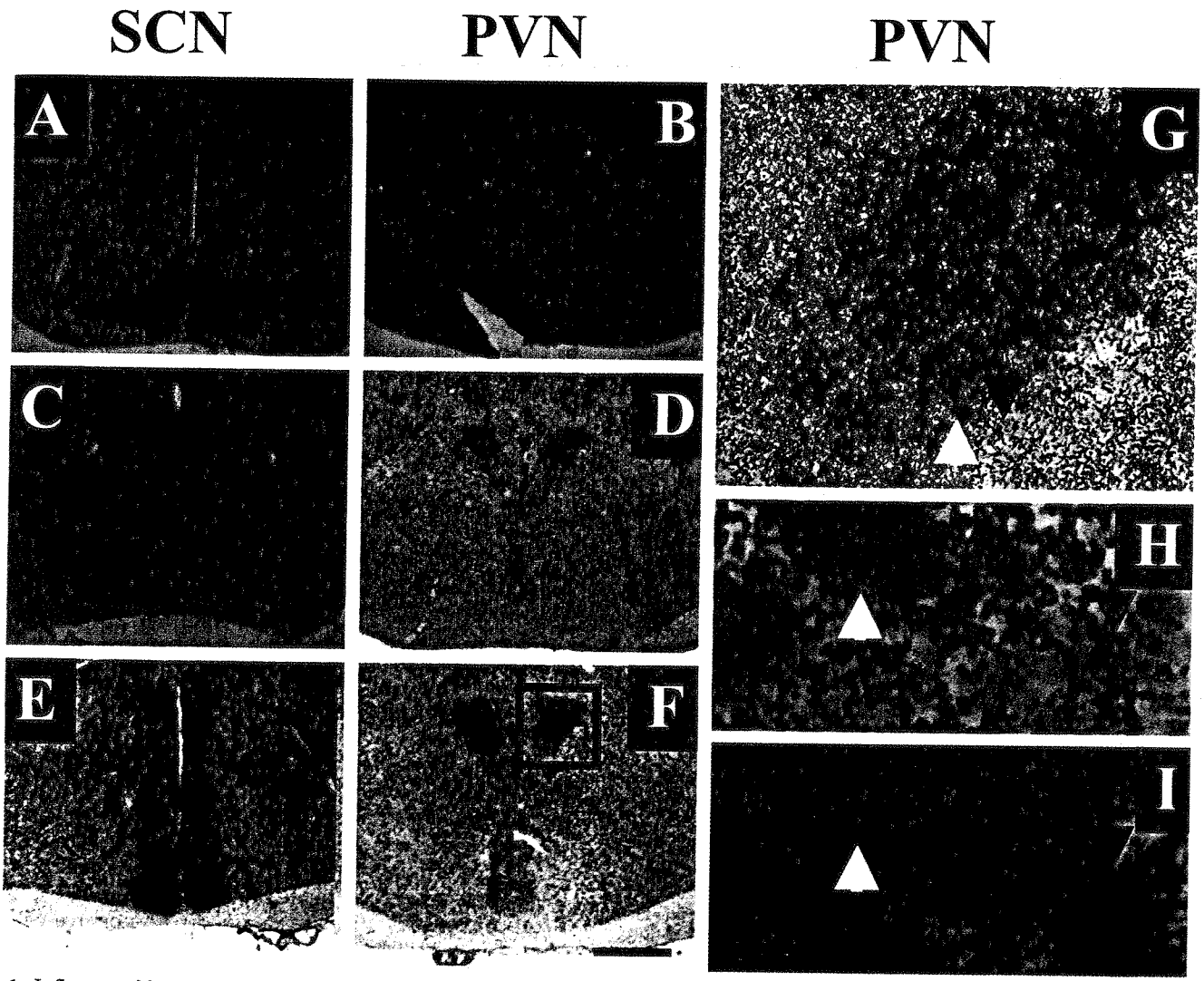

FIG. 1. Influence of forced swimming on *mPer1* expression in the SCN and PVN. Representative emulsion autoradiograms of *mPer1* and CRF immunohistochemistry using a double-staining method. A, B, Control mouse not subjected to stress. C, D, Forced swim-treated mouse. E, F, Forced swim-treated mouse pretreated with colchicine (10 mg/kg) 24 h before swim. G, Enlargement (×4) of rectangular area in F. H, I, Enlargement (×5) of *arrowhead* areas in G. Focus of microscope was adjusted to silver grains of *mPer1* mRNA in H and CRF-immunolabeling in I, respectively. Stress increased *mPer1* expression in the PVN (exhibited by a *black dot*) (D, F, G). There were many dots in some cells *(white arrowhead)*, but few dots *(background level, black arrowhead)* in the other cells showing CRF immunoreactivity (H, I). CRF immunoreactive cells were stained with a *brown color. Scale bar* indicates 0.5 mm.

mPer2 expression during the nighttime, a time during which *mPer* mRNA was low in the SCN (Fig. 3). Results indicated that the basal level of *mPer* gene expression was low in the SCN but high in the PVN during the night (Fig. 3A). The daily rhythm of *mPer1* expression was diurnal in the SCN and nocturnal in the PVN (Fig. 3A). Forced swimming failed to affect *mPer1* or *mPer2* expression in the SCN at ZT17 and ZT7. Figure 3 confirms that forced swimming elevated *mPer1* expression in the PVN during the day (ZT7), but *mPer1* or *mPer2* expression showed no response in any of the brain regions tested during the nighttime (ZT17) (Fig. 3B).

There is a clear day/night difference in the expression of D site-binding protein mRNA in the SCN; however, such a difference was not observed in the PVN (Fig. 3B). The forced swim did not cause any change in *DBP* mRNA expression in the PVN or SCN during either the daytime or nighttime.

Effect of LPS injection on mPer1 and mPer2 expression in the PVN and SCN

Because physical stress caused an increase in *mPer1* expression in the PVN, we examined whether inflammatory stress via LPS injection affected *mPer1* expression in the PVN. Injection of LPS (50 μg/kg) at ZT24 significantly increased body temperature 1, 3, and 24 h after injection (Fig. 4C). Because this body temperature increase lasted for 24 h, we examined *mPer1* and *mPer2* expression in the SCN and PVN 1, 3, and 24 h after LPS injection. One hour after LPS injection, *mPer1* expression in the PVN was significantly increased, but this increment returned to the level of the control saline-injection group (Fig. 4, A and B). Similar to physical stress, LPS injection did not affect *mPer2* expression in the PVN or *mPer1* and *mPer2* expression in the SCN.

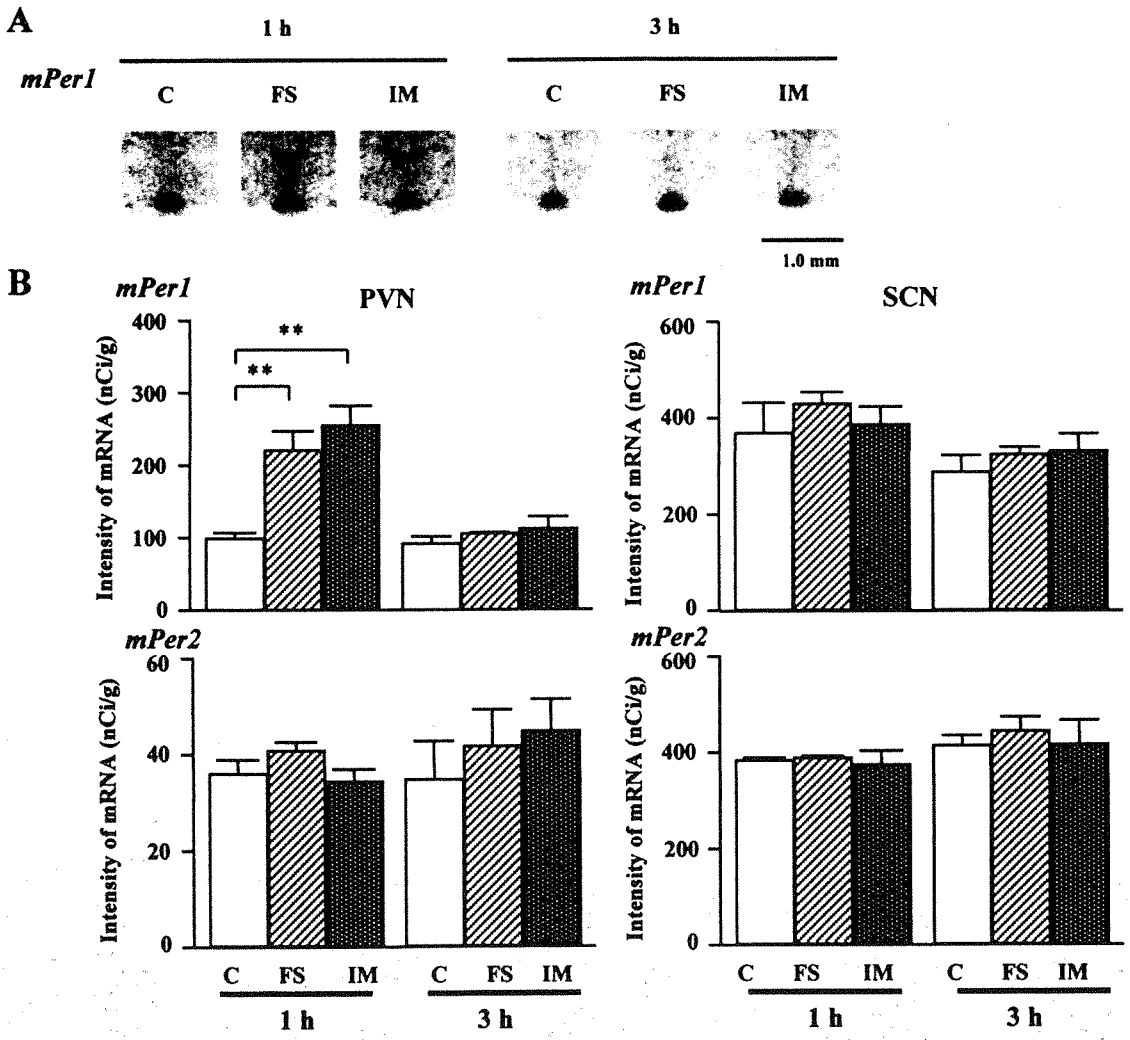

FIG. 2. Influence of the forced swimming or immobilization on *mPer1* and *mPer2* expression in the SCN and PVN of mice. A, Representative *in situ* hybridization autoradiograms of *mPer1* showing the PVN 1 and 3 h after the stressor. Note the strong expression of *mPer1* in the PVN 1 h after stress treatment. B, RNA abundance was determined by quantitative *in situ* hybridization using isotope-labeled probes. C, Control; FS, forced swimming; IM, immobilization. Each value represents the mean ± SEM of three to seven animals. **, $P < 0.01$ *vs.* control (Dunnett's test).

Effect of stressor application on mPer expression in the liver

Day/night differences in *mPer1* and *mPer2* expression in the liver were observed (Fig. 5A). The peak expression of both *mPer1* and *mPer2* mRNAs occurred at ZT11, and the profile was similar to that of the PVN but not the SCN. Administration of similar doses of LPS did not affect liver *mPer1* or *mPer2* expression (Fig. 5B). In the next experiment, we examined the effect of forced swimming on *mPer1* and *mPer2* expression in the liver and obtained negative data (Fig. 5C).

Discussion

The present results clearly demonstrate that forced swimming, immobilization, and LPS injection caused a rapid induction of *mPer1* but not *mPer2* mRNA in the PVN. This increase in *mPer1* returned to the basal level 3 h after stress application. Thus, the present results suggest that *mPer1* gene expression in the PVN is associated with stress-induced responses. The present results also demonstrate a nocturnal expression of *mPer1* and *mPer2* in the PVN and liver tissue and a diurnal expression in the SCN.

It is well known that there is a robust circadian rhythm for corticosterone release thought to be primarily controlled by the SCN because lesion of the SCN abolished this rhythm (10). In intact animals, the circadian rhythm of corticosterone release may be controlled by the circadian oscillation of *mPer1* and/or *mPer2* in the PVN under the influence of the SCN. The following lines of evidence support this conjecture: A recent report (21) demonstrated that the SCN regulates corticosterone release via the HPA and sympathetic pathway through the spinal cord. Because the light-induced rapid increase of *mPer1* in the SCN causes behavioral phase shifts (20, 22), it is important to know how *mPer1* may be involved in regulating the expression and release of CRF or other relevant factors such as vasopressin by parvocellular neurosecretory neurons. Furthermore, daily restricted feeding,

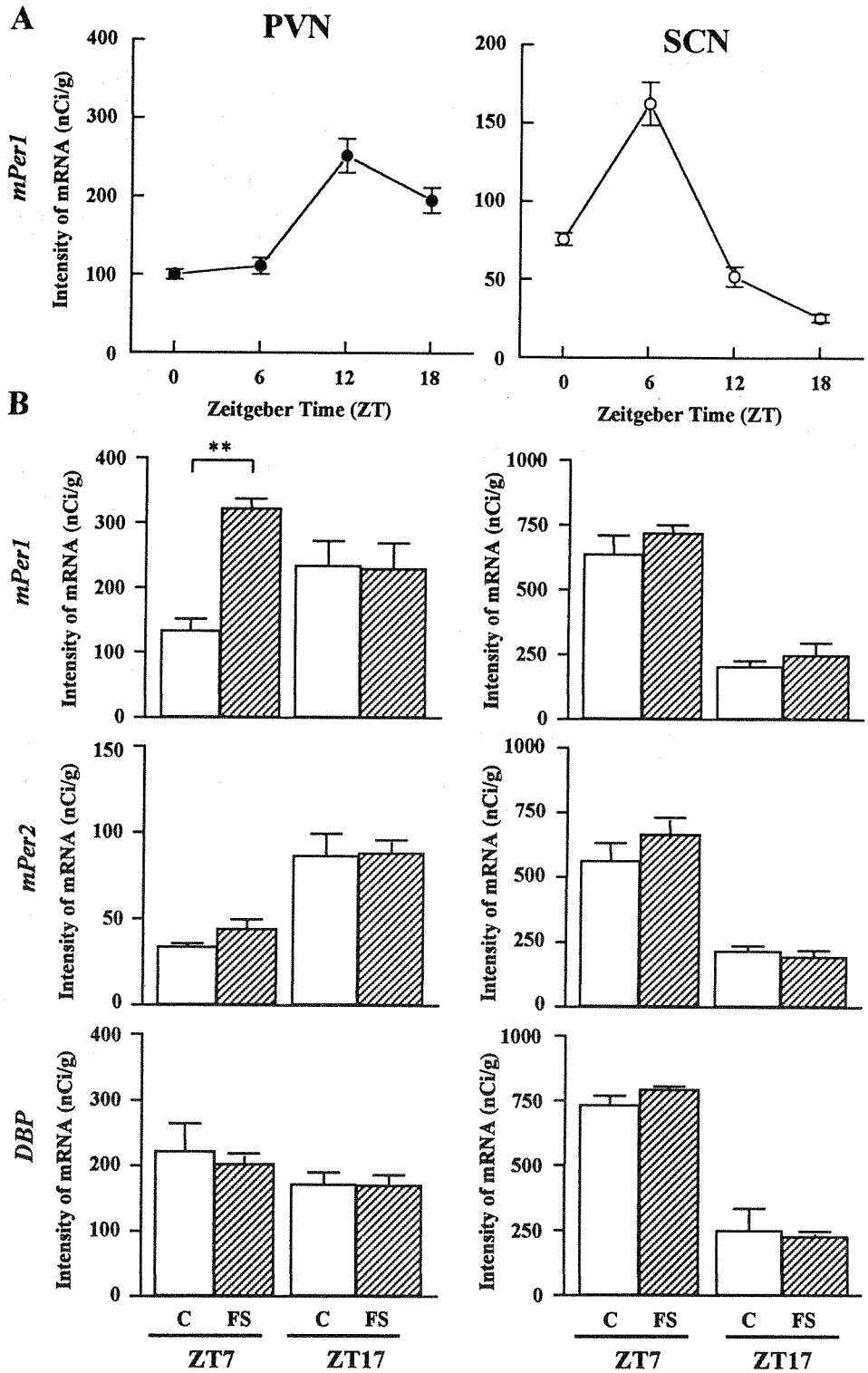

FIG. 3. Influence of forced swimming during the day or night on *mPer1*, *mPer2*, and *DBP* mRNA levels in the PVN and SCN of mice. A, Daily expression of *mPer1* mRNA levels in the PVN and SCN. B, RNA abundance was determined by quantitative *in situ* hybridization using isotope-labeled probes. C, Control; FS, forced swimming. Each value represents the mean ± SEM of three to seven animals. **, $P < 0.01$ *vs.* control (Dunnett's test).

which causes a kind of chronic mild stress, is known to reset not only circadian corticosterone release (14) but also the PVN *mPer1* expression rhythm (23).

The present results clearly reveal that not all stressors affect *mPer1* and *mPer2* expression in the SCN, suggesting an independence of the main circadian clock from stressful cir-

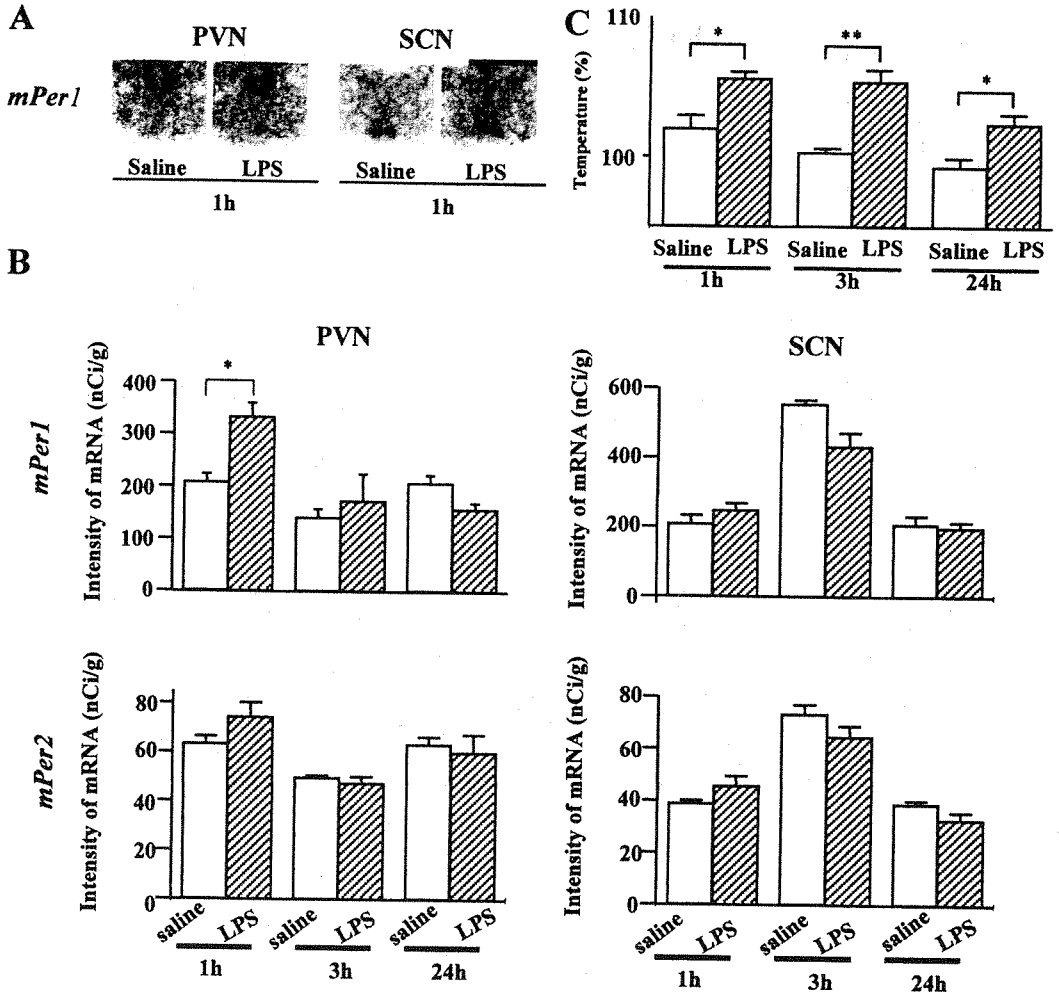

FIG. 4. Effect of LPS (50 μg/kg) injection on *mPer1* and *mPer2* mRNA levels in the PVN and SCN of mice. A, Representative *in situ* hybridization autoradiograms of *mPer1* showing the PVN and SCN 1 h after drug treatment. Note the strong expression of *mPer1* signals in the PVN 1 h after PVN injection. *Scale bar* indicates 1.0 mm. B, RNA abundance was determined by quantitative *in situ* hybridization using isotope-labeled probes. Samples were obtained 1, 3, and 24 h after LPS injection at ZT22. C, Time course of body temperature change after LPS injection at ZT22. Body temperature before injection was set at 100%. Each value represents the mean ± SEM of three to five animals. *, $P < 0.05$, **, $P < 0.01$ *vs.* control saline-injected mice (*t* test).

cumstances, which is also supported by our previous finding (23, 24) that oscillation of SCN *mPer1* and *mPer2* expression was unaffected by daily restricted feeding.

In this experiment, stress-induced *mPer1* expression was observed with only daytime treatment. Consistent with our results, Kelliher *et al.* (25) demonstrated that rats experienced less stress when placed in a test situation during the active (dark period) phase of their circadian cycle during the assessment of neurochemical and neuroendocrine indices of stress. Notably, there was no stress-induced *mPer1* expression in the PVN at night when the basal level of *mPer1* expression was elevated.

Plasma corticosterone levels were elevated 15–30 min after the onset of forced swimming (26), suggesting this hormonal response was not regulated by the expression of *mPer1* or *mPer2* mRNA. Thus, stress affects ACTH and/or corticosterone release and *mPer1* and *mPer2* expression independently. Balsalobre *et al.* (18) recently reported that the circadian clock in peripheral tissues was reset by glucocorticoid signaling. It is well known that forced swimming and LPS injection produce a corticosterone secretion (2), and we observed the effect of these two stressors on *mPer1* expression in the liver. However, *mPer1* and *mPer2* expression in the liver demonstrated no response to these stressors, possibly because they were too weak to produce *mPer1* expression in the liver but of sufficient strength to cause *mPer1* expression in the PVN. When we examined the effect of LPS on body temperature, injection of LPS exhibited a long-lasting effect of up to 24 h after injection. LPS-induced PVN *mPer1* expression, on the other hand, occurred 1 h after injection and returned to the control level 3 or 24 h later.

DBP, a member of the PAR leucine zipper transcription factor family, is reportedly a clock-controlled gene as well as a factor related to the promotion of the *mPer1* gene (27). Because acute stress did not affect *DBP* mRNA in the present study, it was ascertained that *DBP* failed to respond to environmental stimuli.

Although both forced swimming and immobilization caused strong increase in the *mPer1* mRNA in the PVN, these stressors only slightly enhanced CRF-immunolabeling cells

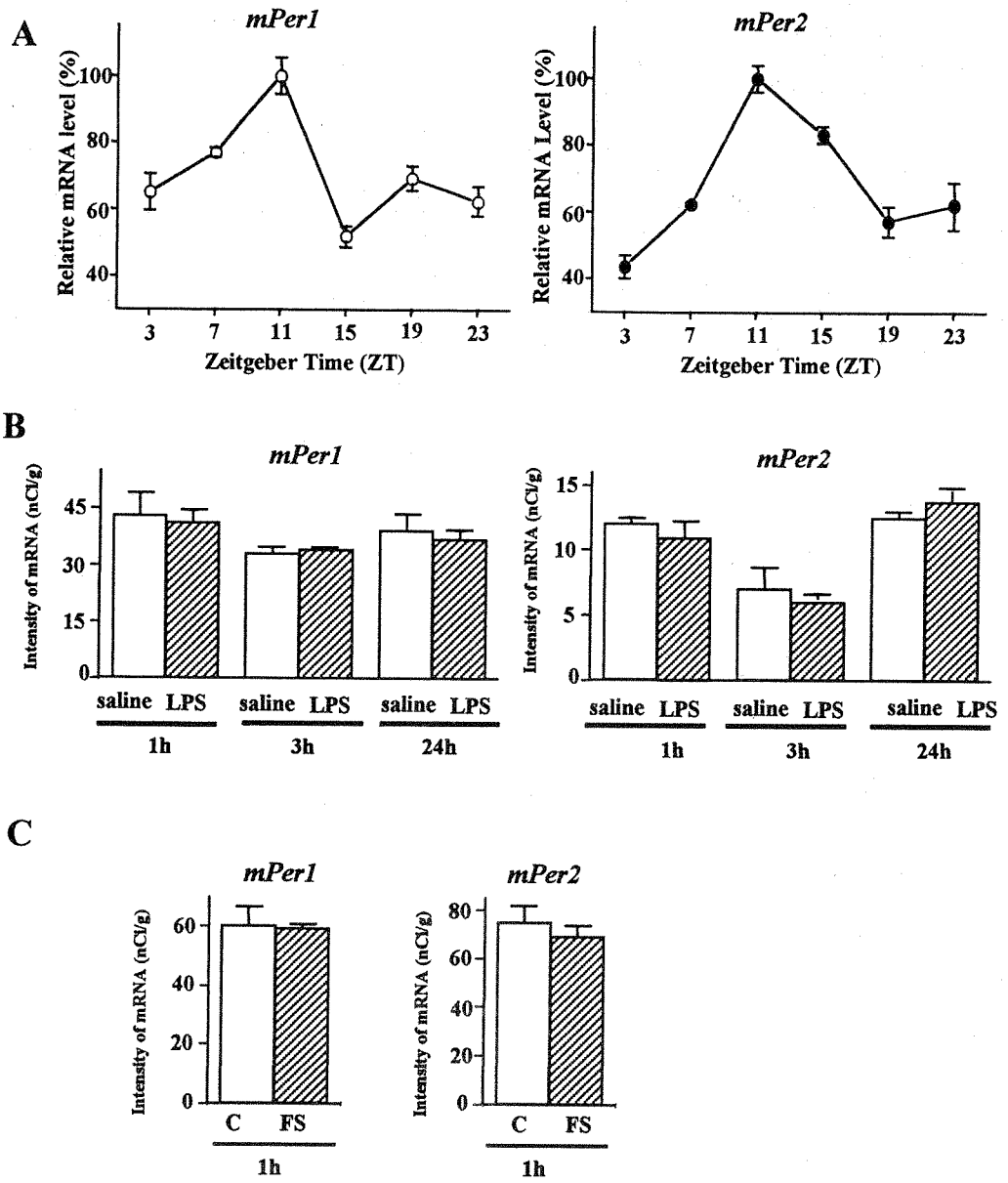

FIG. 5. Effect of LPS injection or forced swimming on *mPer1* and *mPer2* mRNA levels in the liver of mice. A, Daily expression of *mPer1* and *mPer2* mRNA levels in the liver. We used relative mRNA abundance, which means that the intensity values of the peak point (ZT11) were adjusted to 100%. B, RNA abundance was determined by quantitative *in situ* hybridization using isotope-labeled probes. Samples were obtained 1, 3, and 24 h after LPS injection at ZT22 or 1 h after forced swimming at ZT7. C, Control; FS, forced swimming. Each value represents the mean ± SEM of three to seven animals.

in the PVN (data not shown). In the following experiment, therefore, mice were treated with colchicine to enhance CRF immunolabeling before they were subjected to stress. Colchicine is itself a stressor and would have been sufficient to induce *mPer1* expression in its own right. In fact, our preliminary experiment demonstrated that colchicine application alone moderately induced *mPer1* expression in the PVN (data not shown). Thus, the present results demonstrate that *mPer1* responds in this instance to both the drug and the stressors.

Acute stress elevated both CRF mRNA in the PVN (28) and *fos* immunoreactivity in CRF-positive cells of the PVN (29). Thus, the *mPer1* response to acute stress closely resembled that of *fos*, suggesting that *mPer1* behaves as a kind of immediate early gene. Reportedly, the rapid expression of *mPer1* mRNA does not require any translational steps because serum-induced expression of these genes is not blocked by anisomycin (22, 29).

The mechanism of rapid increase in *mPer1* mRNA remains unknown at present. Several researchers have reported that *mPer1* mRNA was induced by a high concentration of serum (29), forskolin (PKA activator), and phorbolester (PKC activator) (30, 31). Activation of PKA and PKC followed by cAMP responsive element binding protein phosphorylation may be an important step in producing the *mPer1* expression. Neural inputs to the PVN from monoaminergic systems may

be important regulators for the induction of *CRF* and *mPer1* genes. The PVN is innervated by the serotonergic and noradrenergic systems, both of which are stimulated in response to stress (32–35) and have been implicated in the regulation of CRF release (36, 37). Therefore, such transmitters may facilitate *mPer1* expression, although further experiments are required for their identification. Recently, Takekida *et al.* (38) demonstrated that an adrenaline receptor agonist, isoproterenol, elevates *mPer1* and *mPer2* expression in the pineal body, suggesting such a possibility.

In summary, the present results indicate that upregulation of the *mPer1* gene in the PVN CRF neurons is suggestive of a mechanism in which stress signals affect corticosterone secretion.

Acknowledgments

Received March 27, 2001. Accepted July 18, 2001.

Address all correspondence and requests for reprints to: Shigenobu Shibata, Department of Pharmacology and Brain Science, School of Human Sciences, Waseda University, Tokorozawa, Saitama 359-1192, Japan. E-mail: shibata@human.waseda.ac.jp.

This work was partially supported by grants awarded to S.S. from the Japanese Ministry of Education, Science, Sports, and Culture (11170248, 11233207, 12877385, 13470016), The Special Coordination Funds of the Japanese Science and Technology Agency, Waseda University, and Kyowa Hakko, Inc.

References

1. **Munck A, Guyre PM, Holbrook NJ** 1984 Physiological functions of glucocorticoids in stress and their relation to pharmacological actions. Endocr Rev 5:25–44
2. **Tilders FJ, DeRijk RH, Van Dam AM, Vincent VA, Schotanus K, Persoons JH** 1994 Activation of the hypothalamus-pituitary-adrenal axis by bacterial endotoxins: routes and intermediate signals. Psychoneuroendocrinology 19: 209–232
3. **Koob GF, Heinrichs SC, Pich EM, Menzaghi F, Baldwin H, Miczek K, Britton KT** 1993 The role of corticotropin-releasing factor in behavioural responses to stress. Ciba Found Symp 172:277–89; discussion 290–295
4. **Bhatnagar S, Dallman M** 1998 Neuroanatomical basis for facilitation of hypothalamic-pituitary-adrenal responses to a novel stressor after chronic stress. Neuroscience 84:1025–1039
5. **Givalois L, Siaud P, Mekaouche M, Ixart G, Malaval F, Assenmacher I, Barbanel G** 1995 Early hypothalamic activation of combined Fos and CRH41 immunoreactivity and of CRH41 release in push-pull cannulated rats after systemic endotoxin challenge. Mol Chem Neuropathol 26:171–186
6. **Teclemariam-Mesbah R, Ter Horst GJ, Postema F, Wortel J, Buijs RM** 1999 Anatomical demonstration of the suprachiasmatic nucleus-pineal pathway. J Comp Neurol 406:171–182
7. **Hermes ML, Coderre EM, Buijs RM, Renaud LP** 1996 GABA and glutamate mediate rapid neurotransmission from suprachiasmatic nucleus to hypothalamic paraventricular nucleus in rat. J Physiol 496:749–757
8. **Kalsbeek A, Buijs RM, van Heerikhuize JJ, Arts M, van der Woude TP** 1992 Vasopressin-containing neurons of the suprachiasmatic nuclei inhibit corticosterone release. Brain Res 580:62–67
9. **Kalsbeek A, Fliers E, Franke AN, Wortel J, Buijs RM** 2000 Functional connections between the suprachiasmatic nucleus and the thyroid gland as revealed by lesioning and viral tracing techniques in the rat. Endocrinology 141:3832–3841
10. **Inouye ST, Shibata S** 1994 Neurochemical organization of circadian rhythm in the suprachiasmatic nucleus. Neurosci Res 20:109–130
11. **Ottenweller JE, Natelson BH, Pitman DL, Drastal SD** 1989 Adrenocortical and behavioral responses to repeated stressors: toward an animal model of chronic stress and stress-related mental illness. Biol Psychiatry 26:829–841
12. **Kant GJ, Leu JR, Anderson SM, Mougey EH** 1987 Effects of chronic stress on plasma corticosterone, ACTH and prolactin. Physiol Behav 40:775–779
13. **Fleshner M, Deak T, Spencer RL, Laudenslager ML, Watkins LR, Maier SF** 1995 A long-term increase in basal levels of corticosterone and a decrease in corticosteroid-binding globulin after acute stressor exposure. Endocrinology 136:5336–5342
14. **Honma K, Noe Y, Honma S, Katsuno Y, Hiroshige T** 1992 Roles of paraventricular catecholamines in feeding-associated corticosterone rhythm in rats. Am J Physiol 262:E948–E955
15. **Dunlap JC** 1999 Molecular bases for circadian clocks. Cell 96:271–290
16. **Young MW** 2000 Life's 24-hour clock: molecular control of circadian rhythms in animal cells. Trends Biochem Sci 25:601–606
17. **Reppert SM, Weaver DR** 2001 Molecular analysis of mammalian circadian rhythms. Annu Rev Physiol 63:647–676
18. **Balsalobre A, Brown SA, Marcacci L, Tronche F, Kellendonk C, Reichardt HM, Schutz G, Schibler U** 2000 Resetting of circadian time in peripheral tissues by glucocorticoid signaling. Science 289:2344–2347
19. **Porsolt RD, Bertin A, Blavet N, Deniel M, Jalfre M** 1979 Immobility induced by forced swimming in rats: effects of agents which modify central catecholamine and serotonin activity. Eur J Pharmacol.57:201–210
20. **Takumi T, Taguchi K, Miyake S, Sakakida Y, Takashima N, Matsubara C, Maebayashi Y, Okumura K, Takekida S, Yamamoto S, Yagita K, Yan L, Young MW, Okamura H** 1998 A light-independent oscillatory gene *mPer3* in mouse SCN and OVLT. EMBO J 17: 4753–4759
21. **Buijs RM, Wortel J, Van Heerikhuize JJ, Feenstra MG, Ter Horst GJ, Romijn HJ, Kalsbeek A** 1999 Anatomical and functional demonstration of a multisynaptic suprachiasmatic nucleus adrenal (cortex) pathway. Eur J Neurosci 11:1535–1544
22. **Akiyama M, Kouzu Y, Takahashi S, Wakamatsu H, Moriya T, Maetani M, Watanabe S, Tei H, Sakaki Y, Shibata S** 1999 Inhibition of light- or glutamate-induced *mPer1* expression represses the phase shifts into the mouse circadian locomotor and suprachiasmatic firing rhythms. J Neurosci 19:1115–1121
23. **Wakamatsu H, Takahashi S, Moriya T, Inouye ST, Okamura H, Akiyama M, Shibata S** 2001 Additive effect of *mPer1* and *mPer2* antisense oligonucleotides on light-induced phase shift. NeuroReport 12:127–131
24. **Hara R, Wan K, Wakamatsu H, Aida R, Moriya T, Akiyama M, Shibata S** 2001 Restricted feeding entrains liver clock without participation of the suprachiasmatic nucleus. Genes Cells 6:269–378
25. **Kelliher P, Connor TJ, Harkin A, Sanchez C, Kelly JP, Leonard BE** 2000 Varying responses to the rat forced-swim test under diurnal and nocturnal conditions. Physiol Behav 69:531–539
26. **Connor TJ, Kelly JP, Leonard BE** 1997 Forced swim test-induced neurochemical endocrine, and immune changes in the rat. Pharmacol Biochem Behav 58:961–967
27. **Yamaguchi S, Mitsui S, Yan L, Yagita K, Miyake S, Okamura H** 2000 Role of DBP in the circadian oscillatory mechanism. Mol Cell Biol 20:4773–4781
28. **Hsu DT, Chen FL, Takahashi LK, Kalin NH** 1998 Rapid stress-induced elevations in corticotropin-releasing hormone mRNA in rat central amygdala nucleus and hypothalamic paraventricular nucleus: an *in situ* hybridization analysis. Brain Res 788:305–310
29. **Balsalobre A, Damiola F, Schibler U** 1998 A serum shock induces circadian gene expression in mammalian tissue culture cells. Cell 93:929–937
30. **Yagita K, Okamura H** 2000 Forskolin induces circadian gene expression of *rPer1, rPer2* and *dbp* in mammalian rat-1 fibroblasts. FEBS Lett 465:79–82
31. **Akashi M, Nishida E** 2000 Involvement of the MAP kinase cascade in resetting of the mammalian circadian clock. Genes Dev 14:645–649
32. **Abercrombie ED, Jacobs BL** 1987 Single-unit response of noradrenergic neurons in the locus coeruleus of freely moving cats. I. Acutely presented stressful and nonstressful stimuli. J Neurosci 7:2837–2843
33. **Abercrombie ED, Jacobs BL** 1987 Single-unit response of noradrenergic neurons in the locus coeruleus of freely moving cats. II. Adaptation to chronically presented stressful stimuli. J Neurosci 7:2844–2848
34. **Vahabzadeh A, Fillenz M** 1994 Comparison of stress-induced changes in noradrenergic and serotonergic neurons in the rat hippocampus using microdialysis. Eur J Neurosci 6:1205–1212
35. **McKittrick CR, McEwen BS** 1996 Regulation of serotonergic function in the CNS by steroid hormones and stress. In: Stone TW, ed. CNS neurotransmitters and neuromodulators: neuroactive steroids. Boca Raton, FL: CRC; 37–76
36. **Plotsky PM, Cunningham ET, Widmaier EP** 1989 Catecholaminergic modulation of corticotropin-releasing factor and adrenocorticotropin secretion. Endocr Rev 10:437–458
37. **Pan L, Gilbert F** 1992 Activation of 5-HT1A receptor subtype in the paraventricular nuclei of the hypothalamus induces CRH and ACTH release in the rat. Neuroendocrinology 56:797–802
38. **Takekida S, Yan L, Maywood ES, Hastings MH, Okamura H** 2000 Differential adrenergic regulation of the circadian expression of the clock genes period1 and period2 in the rat pineal gland. Eur J Neurosci 12:4557–4561

Nonphotic Entrainment by 5-HT$_{1A/7}$ Receptor Agonists Accompanied by Reduced *Per1* and *Per2* mRNA Levels in the Suprachiasmatic Nuclei

Kazumasa Horikawa,[1] Shin-ichi Yokota,[1] Kazuyuki Fuji,[1] Masashi Akiyama,[1] Takahiro Moriya,[2] Hitoshi Okamura,[3] and Shigenobu Shibata[1,2]

[1]Department of Pharmacology and Brain Science and [2]Advanced Research Center for Human Sciences, School of Human Sciences, Waseda University, Tokorozawa, Saitama 359-1192, Japan, and [3]Department of Anatomy and Brain Science, Kobe University School of Medicine, Chuo-ku, Kobe 650-0017, Japan

In mammals, the environmental light/dark cycle strongly synchronizes the circadian clock within the suprachiasmatic nuclei (SCN) to 24 hr. It is well known that not only photic but also nonphotic stimuli can entrain the SCN clock. Actually, many studies have shown that a daytime injection of 8-hydroxy-2-(di-n-propylamino) tetralin (8-OH DPAT), a serotonin 1A/7 receptor agonist, as a nonphotic stimulus induces phase advances in hamster behavioral circadian rhythms *in vivo*, as well as the neuron activity rhythm of the SCN *in vitro*. Recent reports suggest that mammalian homologs of the *Drosophila* clock gene, *Period* (*Per*), are involved in photic entrainment. Therefore, we examined whether phase advances elicited by 8-OH DPAT were associated with a change of *Period* mRNA levels in the SCN. In this experiment, we cloned partial cDNAs encoding hamster *Per1*, *Per2*, and *Per3* and observed both circadian oscillation and the light responsiveness of *Period*. Furthermore, we found that the inhibitory effect of 8-OH DPAT on hamster *Per1* and *Per2* mRNA levels in the SCN occurred only during the hamster's mid-subjective day, but not during the early subjective day or subjective night. The present findings demonstrate that the acute and circadian time-dependent reduction of *Per1* and/or *Per2* mRNA in the hamster SCN by 8-OH DPAT is strongly correlated with the phase resetting in response to 8-OH DPAT.

Key words: suprachiasmatic nucleus; 8-OH DPAT; Per mRNA; 5-HT$_{1A/7}$ receptor; hamster; circadian rhythm; NIH Image

In mammals, the suprachiasmatic nucleus (SCN) of the hypothalamus has been shown to be a primary circadian pacemaker of locomotor activity and various physiological phenomena (Hastings, 1997). Recent studies on the molecular aspects of clock genes have produced a functional model of circadian rhythms (for review, see Dunlap, 1999).

mPer1, *mPer2*, and *mPer3*, cloned as mouse homologs of the *Drosophila* clock gene, *Period* (*Per*), exhibit circadian rhythmic expressions in the SCN (Albrecht et al., 1997; Shearman et al., 1997; Sun et al., 1997; Tei et al., 1997; Takumi et al., 1998a,b; Zylka et al., 1998). Brief exposure to light during subjective night results in a large and rapid induction of *mPer1* expression (Albrecht et al., 1997; Shigeyoshi et al., 1997). *mPer2* mRNA expression in the SCN is also induced in response to light stimuli (Shearman et al., 1997; Takumi et al., 1998a). On the other hand, *mPer3* mRNA levels do not respond to light during either the subjective night or subjective day (Takumi et al., 1998b; Zylka et al., 1998). Recently, we demonstrated that light-induced phase delays in locomotor activity at CT16 were significantly inhibited when mice were pretreated with *mPer1* antisense phosphorothioate oligodeoxynucleotide (ODN) (Akiyama et al., 1999). Therefore, we suggest that the gated expression of *mPer1* may be an important step in causing photic entrainment.

On the other hand, nonphotic manipulation such as novel wheel-running (Reebs and Mrosovsky, 1989), social interaction (Mrosovsky, 1988), and saline injection and/or handling (Mead et al., 1992) reportedly causes big phase advances in the hamster circadian clock when performed during subjective day. Additionally, many studies have shown that a daytime injection of 8-hydroxy-2-(di-n-propylamino) tetralin (8-OH DPAT), a serotonin 1A/7 receptor agonist, induces a phase advance in hamster behavioral circadian rhythms *in vivo* (Tominaga et al., 1992; Edgar et al., 1993; Cutrera et al., 1996; Mintz et al., 1997), as well as the neuron activity rhythm of the SCN *in vitro* (Shibata et al., 1992; Prosser et al., 1993). Thus, serotonin (5-HT) has been implicated in phase shifts of the circadian system during subjective day in response to nonphotic stimuli. Because light exposure induces *mPer1* and *mPer2* expression during subjective night, we questioned whether injection of 8-OH DPAT modifies the *Per* mRNA levels during subjective day. Almost all behavioral experiments investigating nonphotic-induced phase advances were performed using hamsters, so we attempted to clone partial cDNAs encoding the golden hamster *Per1*, *Per2*, and *Per3*. Therefore, we first established that oscillations and light responses of hamster *Per* gene mRNA were similar to what has previously been published in the mouse. Second, we found that injection of 8-OH DPAT at CT6, but not at CT1 or CT20, reduced the amount of *Per1* and *Per2*, but not *Per3* mRNA in the hamster SCN. Third, we demonstrated that nonphotic phase shifting with 8-OH DPAT is strongly correlated with an 8-OH DPAT-dependent, transient decrease in *Per1* and *Per2* mRNA levels.

MATERIALS AND METHODS

Cloning of partial cDNAs encoding hamster Per *genes.* For analysis of *Per* gene expression by *in situ* hybridization, we attempted to clone partial cDNAs encoding the golden hamster *Per* genes. Total RNA was extracted from the golden hamster brain using Trizol (BRL, Bethesda, MD) and was reverse-transcribed using the Superscript one-step RT-PCR system (BRL). RT-PCR was performed using a DNA Thermal Cycler 9600 (Perkin-Elmer, Norwalk, CT) with specific primers derived from mouse and human sequences of *Per* genes. The sequences of the primers were as follows: *Per2* (nucleotide position 822–1601 of *mPer2*; GenBank accession number AF035830): 5′-ACACCACCCCTTACAAGCTTCC-3′, 5′-CGCTGGATGATGTCTGGCTC-3′; *Per3* (nucleotide position 1956–2754 of *mPer3*; GenBank accession number AF050182): 5′-GAACTGTATCG-

Received Sept. 7, 1999; revised April 27, 2000; accepted May 11, 2000.

This study was partially supported by grants awarded to S.S. from the Research Project for the Future Program (RFTF96L00310), the Japanese Ministry of Education, Science, Sports, and Culture (11170248, 1123207, 11145240), and The Special Coordination Funds of the Japanese Science and Technology Agency.

Correspondence should be addressed to Shigenobu Shibata, Department of Pharmacology and Brain Science, School of Human Sciences, Waseda University, Tokorozawa, Saitama 359-1192, Japan. E-mail address: shibata@human.waseda.ac.jp.

 0270-6474/00/205867-07$15.00/0

ACAGTGTCATC-3′, 5′-GGCCATATCTTGGAGGGGAAA-3′. The PCR protocol was executed under the following conditions: cDNA synthesis and predenaturation at 50°C for 30 min followed by 94°C for 2 min, PCR amplification for 35 cycles with denaturation at 94°C for 15 sec, annealing at 55°C for 30 sec, extension at 72°C for 1 min, and final extension at 72°C for 5 min. These PCR products were subcloned into the pGEM-T Easy Vector (Promega, Madison, WI) and were sequenced using ABI PRISM Dye Terminator Cycle Sequencing Ready Reaction Kit (Perkin-Elmer). A partial cDNA encoding hamster *Per1* corresponding to the nucleotide position 726–1367 of *mPer1* (GenBank accession number AB002108) was also cloned (S. Yamamoto and H. Okamura, data not shown).

Animals. Male golden hamsters (*Mesocricetus auratus*, Tokyo Laboratory Animals Science Co. Ltd., Tokyo, Japan) purchased 6 weeks postpartum were maintained on a 12 hr light/dark cycle with lights on at 8:30 A.M. (room temperature at 23 ± 2°C). Animals were given food and water *ad libitum*. For assessment of wheel-running activity, hamsters were housed individually in transparent plastic cages (36 × 20 × 20 cm) equipped with a running wheel (13 cm in diameter) that closed a microswitch with each revolution. The number of wheel rotations was measured, and data were stored on a personal computer.

Behavioral experiment. Because 8-OH DPAT has an asymmetrical carbon, this compound has two optical isomers: *R*(+) and *S*(−) 8-OH DPAT. A few studies have investigated the relationship between binding affinity of 5-HT_{1A} and 5-HT_7 receptors and the effect of each optical isomer on circadian rhythms (Lovenberg et al., 1993; Eriksson and Evrin, 1996; Miller et al., 1996; Ying and Rusak, 1997). After free-running for 14–20 d in constant darkness, hamsters were randomly assigned to an intraperitoneal injection of 8-OH DPAT (1.0 or 5.0 mg/kg; Research Biochemicals, Natick, MA), (+) 8-OH DPAT (2.5 mg/kg, Research Biochemicals), triazolam (20 mg/kg, Upjohn), or vehicle [sterilized saline for both 8-OH DPAT and (+) 8-OH DPAT or dimethyl sulfoxide (Wako) for triazolam]. Injection was performed at circadian time (CT; CT12: onset time of wheel-running activity) 1, CT6, CT8, CT14, or CT20. Animals were then returned to their individual cages. The phase of the rhythm was assessed visually by applying a straight edge to the onset of activity on successive days before and after drug injection and determining the difference in phases on the day of drug injection (Daan and Pittendrigh, 1976).

In situ *hybridization using digoxigenin. In situ* hybridization using digoxigenin (DIG) was applied to determine the semiquantity or histochemical distribution of *Per* mRNA levels in coronal sections of the hypothalamus. Hamsters were entrained to the light/dark cycle for at least 14 d and then kept in constant dark conditions. On the third day of constant darkness at CT6 or CT20, hamsters were intraperitoneally injected with each drug and then deeply anesthetized with ether 1, 2, or 4 hr after injection and intracardially perfused with 0.1 M phosphate buffer (PB) containing 4% paraformaldehyde (PFA). In some cases, hamster brains were obtained for observation of circadian changes in *Per* gene expression in the SCN. To make this observation, light (60 lux, 15 min) was applied at CT14 or CT20, and hamsters were killed 1 or 2 hr after the initiation of light exposure. Brains were removed, post-fixed in 0.1 M PB containing 4% PFA for 24 hr at 4°C, and transferred into 20% sucrose in PBS for 24 hr at 4°C. Frontal sections (40 μm thick) were collected and placed in PBS for 30 min, followed by treatment with 6 × SSC for 30 min. Sections were incubated in hybridization buffer [50% formamide, 6 × SSC, 0.1 mg/ml denatured salmon sperm DNA, 1 × Denhardt's solution (0.02% Ficoll, 0.02% polyvinyl pyrolidone, 0.02% bovine serum albumin), and 10% dextran sulfate] containing labeled cRNA probes overnight at 60°C. DIG-UTP (Roche Molecular Biochemicals, Indianapolis, IN)-labeled antisense cRNA was made using a standard protocol for cRNA synthesis. After hybridization, these sections were rinsed in 2 × SSC/50% formamide for 45 min followed by 15 min at 60°C and treated with RNase A for 30 min at 37°C, 2 × SSC/50% formamide for 2 × 15 min at 60°C, and 0.4 × SSC for 30 min at 60°C. Sections were processed for immunocytochemistry by following the DIG nucleic acid detection kit (Roche Molecular Biochemicals) protocol. Photomicrographs were taken with a Fujix digital camera (HC-300, Fujifilm, Tokyo Japan) and captured with photograb-300 (Fujifilm). The density of *Per* gene expression was semiquantified on a Macintosh computer using the public domain NIH Image program (written by Wayne Rasband, National Institutes of Health).

In situ *hybridization using radioisotope. In situ* hybridization using radioisotope (RI)-labeled probes was applied to determine the quantity of *Per1*, *Per2*, and *Per3* mRNA levels in coronal sections of the hypothalamus. Hamsters were entrained to the light/dark cycle for at least 14 d and then kept in constant dark conditions. On the third day of constant darkness at CT1, CT6, or CT20, hamsters were intraperitoneally injected with each drug and then deeply anesthetized for 2 hr after injection and intracardially perfused with 0.1 M PB containing 4% PFA. Brains were removed, post-fixed in 0.1 M PB containing 4% PFA for 24 hr at 4°C, and transferred into 20% sucrose in PBS for 24 hr at 4°C. Frontal sections (30 μm thick) were collected and placed in 2 × SSC and then treated with proteinase K (1.0 μg/ml, 10 mM Tris buffer, pH 7.5, 10 mM EDTA) for 10 min at 37°C, 4% PFA in 0.1 M PB for 5 min, and 2 × SSC for 5 min followed by 0.25% acetic anhydride in 0.1 M triethanolamine for 10 min and 2 × SSC for 2 × 5 min. RI [α[^{33}P]UTP (New England Nuclear)]-labeled antisense cRNA was made using a standard protocol for cRNA synthesis. Hybridization and posthybridization washing steps were the same as the protocol for DIG *in situ* hybridization. RI *in situ* hybridization images were visualized by autoradiogram and BioMax film (Kodak) and analyzed using an image analyzing system (MCID, Imaging Research Inc.) after conversion into optical density by ^{14}C-autoradiographic microscales (Amersham, Arlington Heights, IL). The values were expressed as means ± SEM. For statistical analysis, one-way ANOVA followed by the Student's *t* test was applied.

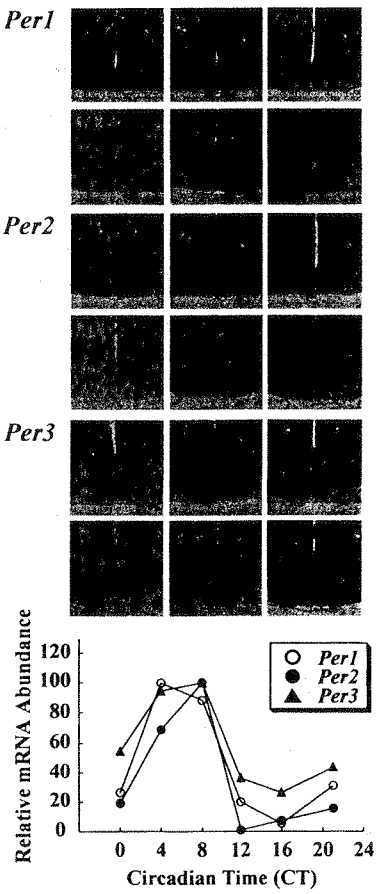

Figure 1. Circadian expressions of (*A*) *Per1*, (*B*) *Per2*, and (*C*) *Per3* in the hamster suprachiasmatic nucleus. mRNA expression was demonstrated by DIG *in situ* hybridization and semiquantified by a Macintosh computer using the public domain NIH Image program (*D*). There are clear circadian rhythms of *Per1*, *Per2*, and *Per3* expression in the hamster SCN with a peak at CT4 for *Per1* and at CT8 for both *Per2* and *Per3*.

RESULTS

Oscillation and light response of SCN *Per* mRNA expression

To evaluate the topographic differences of expression profile in hamster *Per* genes of the SCN, *in situ* hybridizations using digoxigenin-labeled probes of hamster *Per1*, *Per2*, and *Per3* were performed. DIG *in situ* hybridization showed clear signals with the antisense probes in the hamster SCN (Fig. 1). These antisense probe signals were suppressed by competition experiments using the unlabeled antisense probes. Furthermore, the sense probes demonstrated specificity of the antisense hybridization by exhibiting no signals within the SCN (data not shown). The distribution or expression patterns of hamster *Per* mRNA inside and outside the SCN were consistent with those of already published findings in the mouse (Albrecht et al., 1997; Shearman et al., 1997; Sun et al., 1997; Tei et al., 1997; Takumi et al., 1998a,b; Zylka et al., 1998). Next, we examined the circadian pattern of *Per* gene expression in the hamster SCN. There were clear circadian rhythms of *Per1*, *Per2*, and *Per3* expression in the hamster SCN with a peak at CT4 for *Per1* and at CT8 for both *Per2* and *Per3* (Fig. 1). In nocturnal rodents, it is well established that light pulses administered during the early subjective night cause phase delays of the circadian rhythm, whereas pulses delivered during the latter half of the

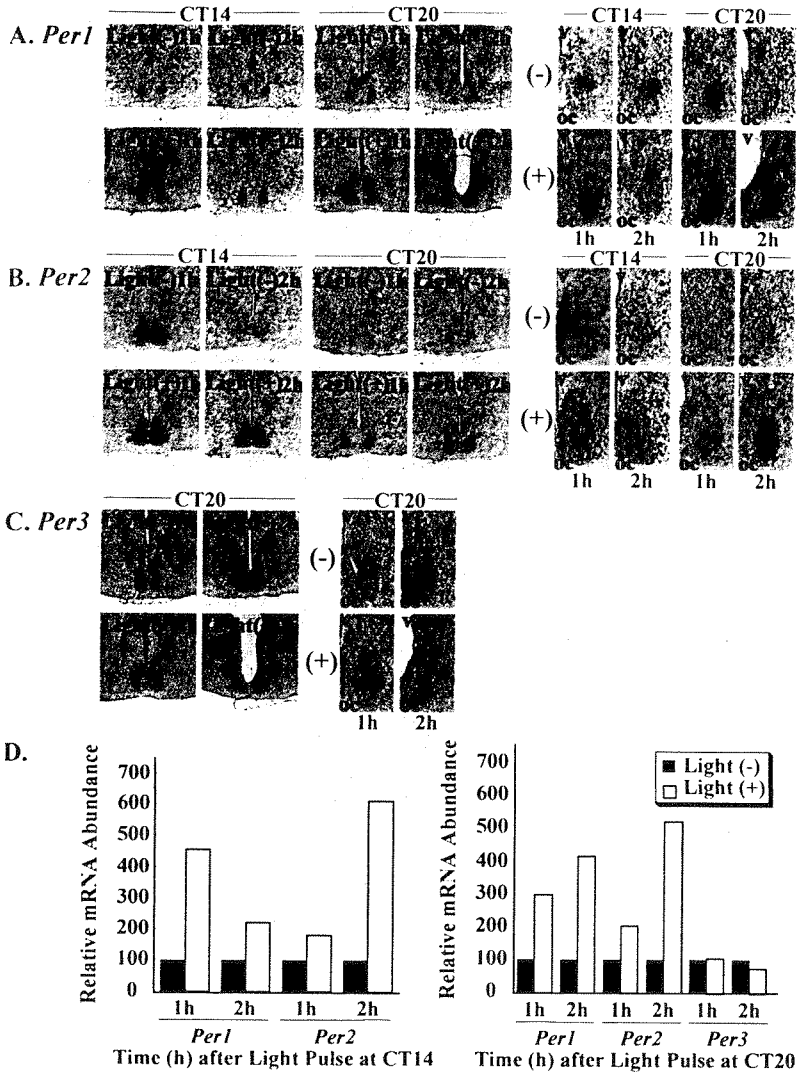

Figure 2. Effect of light exposure on the expression of (*A*) *Per1*, (*B*) *Per2*, and (*C*) *Per3* in the hamster suprachiasmatic nucleus. mRNA expression was demonstrated by DIG *in situ* hybridization, and a more magnified picture is shown. *Per* mRNA expression was semiquantified by a Macintosh computer using the public domain NIH Image program (*D*). Hamster was exposed to light (60 lux, 15 min) at CT14 or CT20 and then killed 60 or 120 min after light pulse. Light at CT14 or CT20 induced *Per1* and *Per2* expression in the SCN; however, *Per3* expression was not affected by light exposure at CT20. *oc*, Optic chiasma; *v*, third ventricle; *(+)*, light pulses were applied; *(−)*, light pulses were not applied.

subjective night cause phase advances. Recent reports indicated that *mPer1* and *mPer2* expression in the mouse SCN was increased rapidly and transiently after brief light exposure during both early and late subjective night, whereas *mPer3* expression was not (Takumi et al., 1998b; Zylka et al., 1998). We also observed that *Per1* and *Per2* expression in the hamster SCN was induced in response to brief light exposure at CT14 or CT20, and *Per3* expression was not affected by light stimulation at CT20 (Fig. 2). In both *Per1* and *Per2* cases, we found that signal intensities were more likely to be stronger in the ventrolateral part of the SCN than in the dorsomedial part. These results were consistent with previous data found in the mouse.

Wheel-running activity in response to 8-OH DPAT

Vehicle administration at CT6 did not show any change in phase (Fig. 3*A*); however, 8-OH DPAT (5.0 mg/kg) administration at CT6 produced a clear phase advance (Fig. 3*B*). Administration of this compound at CT20 did not affect the wheel-running rhythm (Fig. 3*C*). Administration of 8-OH DPAT (5.0 mg/kg) at various CTs (CT1, CT6, CT8, CT14, CT20) was compared with vehicle administration (Fig. 3*D*). Significant phase advances were observed when this compound was administered at CT6 or CT8. There were no significant differences at other CTs. Administration of triazolam (20 mg/kg) at CT6 also caused a phase advance in hamster wheel-running rhythm (data not shown).

Effect of 8-OH DPAT on SCN *Per* mRNA

Administration of 8-OH DPAT (5.0 mg/kg) reduced the levels of *Per1* in the entire SCN and *Per2* preferentially in the ventrolateral part of the SCN (Fig. 4*A*,*B*). Four hours after drug injection, however, reduced *Per1* and *Per2* levels recovered to the control level of vehicle-treated animals. Injection of 8-OH DPAT at CT20 did not change the *Per1* and *Per2* levels in the SCN. (+) 8-OH DPAT (2.5 mg/kg)-induced reduction of *Per1* and *Per2* was similar to 8-OH DPAT (5.0 mg/kg)-induced reductions (Fig. 4*A*,*B*). Injection of 8-OH DPAT did not reduce the *Per3* mRNA levels (Fig. 4*C*). For quantitative measurements of *Per* mRNA levels, *in situ* hybridizations using RI-labeled probes were performed. In Figure 5, the mean values for *Per1*, *Per2*, and *Per3* in the hamster SCN of 8-OH DPAT and vehicle-treated groups at various CTs are shown. Vehicle-treated hamsters exhibit clear circadian rhythms of *Per1* (ANOVA, $F_{(2,12)} = 9.363$, $p = 0.0032$), *Per2* (ANOVA, $F_{(2,13)} = 62.375$, $p = 0.0001$), and *Per3* (ANOVA, $F_{(2,13)} = 39.892$, $p = 0.0001$) expression in the SCN. High expression of these genes was seen at CT6. Two hours after the administration of 8-OH DPAT (5.0 mg/kg) at CT6, the amount of both *Per1* and *Per2* mRNA was significantly reduced in comparison with the group receiving vehicle treatment (Fig. 5*A*,*B*). On the other hand, injection of 8-OH DPAT at CT1 or CT20 did not affect the amount of *Per1* and *Per2* mRNA. Interestingly, this drug did not change the *Per3* mRNA of the SCN at any CTs. In the next experiment, we examined whether 8-OH DPAT reduced *Per1* and *Per2* mRNA in a dose-dependent manner (Fig. 6). Administration of 8-OH DPAT caused a phase advance in hamster wheel-running rhythm in a dose-dependent manner (Fig. 6*A*), and this compound also reduced the amount of both *Per1* and *Per2* mRNA in a dose-related fashion (Fig. 6*B*,*C*). Thus, the effective dose for behavioral phase shift induction and

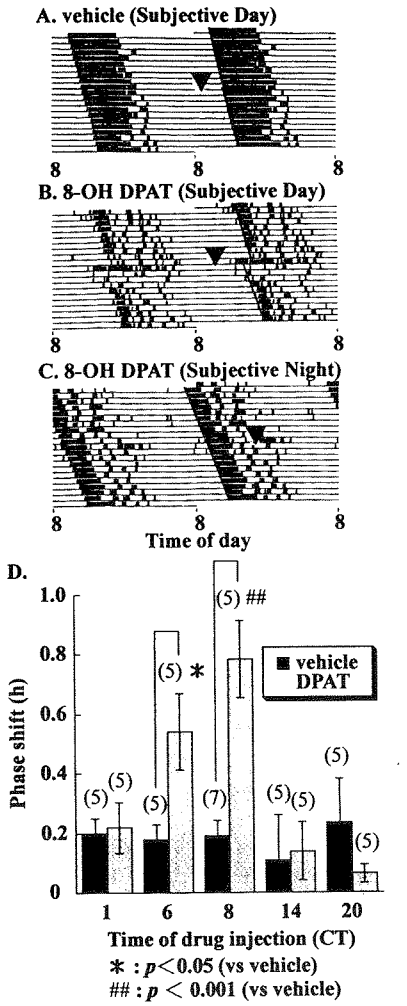

Figure 3. Effects of 8-OH DPAT administration on the hamster circadian wheel-running rhythm. Double-plotted actogram shows wheel-running activity records of (*A*) vehicle and (*B*) 8-OH DPAT (5.0 mg/kg, i.p.)-injected hamster at CT6, and (*C*) 8-OH DPAT (5.0 mg/kg, i.p.) injection at CT20. Each animal was injected at CT6 or CT20 (*arrowheads*) and returned to constant darkness. *D*, Mean phase advances induced by 8-OH DPAT (5.0 mg/kg, i.p.) administration at CT1, CT6, CT8, CT14, and CT20. *Numbers in parentheses* indicate the number of experiments. Injection of 8-OH DPAT at CT6 or CT8 induced a significant phase advance ($^{*}p < 0.05$, $^{**}p < 0.001$, Student's *t* test).

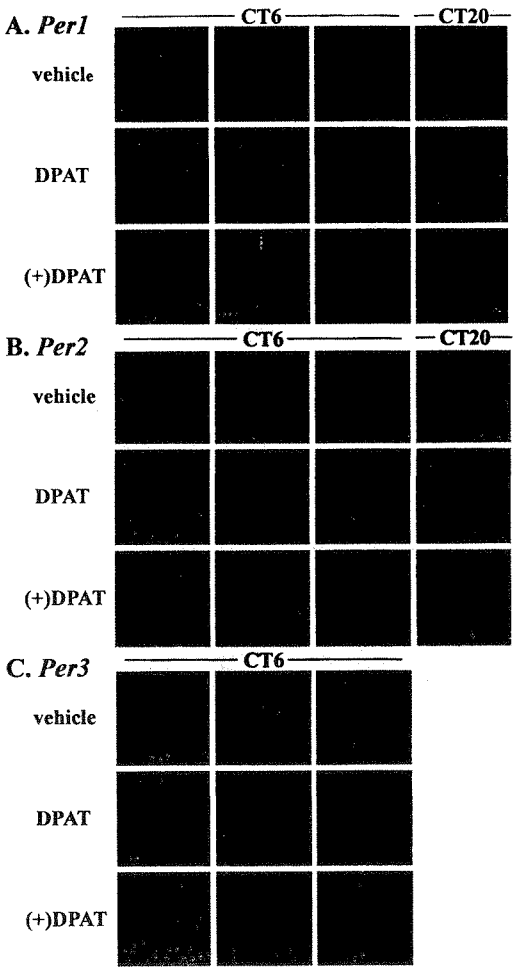

Figure 4. Effects of 8-OH DPAT (5.0 mg/kg, i.p.) or (+) 8-OH DPAT (2.5 mg/kg, i.p.) on the expression of (*A*) *Per1*, (*B*) *Per2*, and (*C*) *Per3* in the hamster suprachiasmatic nucleus. mRNA levels were demonstrated by DIG *in situ* hybridization. Drug was administered at CT6 or CT20, and *Per* mRNA levels were examined 60–240 min after drug injection. 8-OH DPAT reduced *Per1* and *Per2* mRNA levels in the SCN 120 min after injection at CT6, but mRNA levels returned to the control level 240 min after injection. Injection of 8-OH DPAT at CT20 did not affect *Per1* or *Per2* mRNA levels. The amount of *Per3* mRNA was not affected by injection of 8-OH DPAT.

reduction of *Per1* and *Per2* was very similar. Amplitude of *Per1* and *Per2* reduction by (+) 8-OH DPAT (5.0 mg/kg) was similar to that of (+) 8-OH DPAT (2.5 mg/kg) (Fig. 6). Administration of triazolam (20 mg/kg), a central-type benzodiazepine receptor ligand, at CT 6 also reduced the amount of SCN *Per1* and *Per2* but not *Per3* mRNA.

DISCUSSION

In situ hybridizations using digoxigenin-labeled probes of hamster *Per* genes revealed clear circadian expressions of *Per1*, *Per2*, and *Per3* in the hamster SCN. The pattern of expression of these genes is very similar to that observed in the mouse (Albrecht et al., 1997; Shearman et al., 1997; Sun et al., 1997; Tei et al., 1997; Takumi et al., 1998a,b; Zylka et al., 1998) and rat (Sakamoto et al., 1998; Yan et al., 1999) SCN, with peak expression of hamster *Per1*, *Per2*, and *Per3* found at CT4, CT8, and CT8, respectively. Reportedly, light exposure during subjective night causes a rapid induction of *mPer1* and *mPer2* in the SCN (Albrecht et al., 1997; Shearman et al., 1997; Takumi et al., 1998a). In the hamster, we also observed that *Per1* and *Per2* have light-responsive characters similar to mouse *period* genes.

Anatomical subdivisions such as the ventrolateral and dorsomedial parts in the rat SCN have been well established (Moore, 1982). Recently, we reported that light exposure at CT16 induced the expression of rat *Per1* and *Per2* in SCN neurons of the ventrolateral part, although the circadian rat *Per1* and *Per2* mRNA oscillations in light/dark and constant dark conditions occurred strongly in neurons in the dorsomedial part but weakly in neurons in the ventrolateral part of the SCN (Yan et al., 1999). In the hamster SCN, light-induced expression of *Per1* and *Per2* was preferential to the ventrolateral part of the SCN. Although the basic compartment profile of *Per* gene expression may be preserved in the hamster SCN, however, anatomical subdivision of the hamster SCN is vague compared with the rat SCN. Therefore, further experiments are needed to elucidate the compartmentalization of circadian profiles in *Per* genes in the hamster in detail.

In the present experiment, we demonstrated that 8-OH DPAT reduces SCN *Per1* and *Per2* mRNA in a circadian time-dependent manner. Actually, 8-OH DPAT reduced these gene mRNAs when administered at CT6 but not at CT1 or CT20. This result relates to the behavioral result showing a large phase advance at CT6 and CT8 but not at CT1 or CT20. In addition, 8-OH DPAT reduced *Per1* and *Per2* in a dose-dependent fashion. The dose and threshold closely correlated with *Per1* and *Per2* reduction in the SCN. *mPer1* and *mPer2* transcription is rapidly induced by light in a time-of-

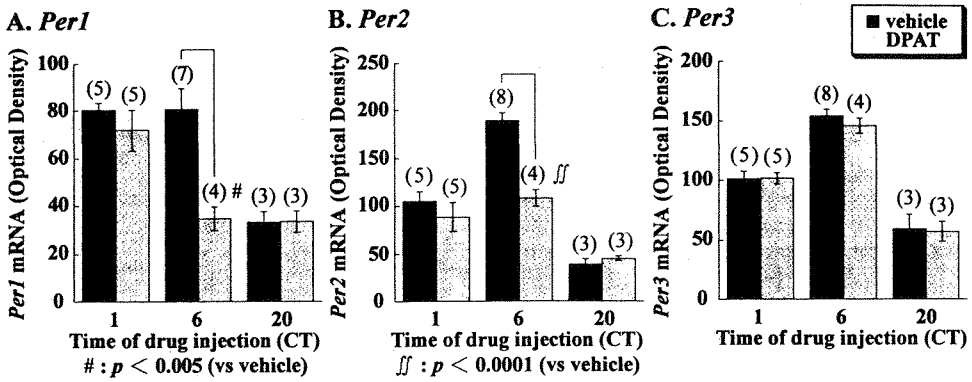

Figure 5. Effect of 8-OH DPAT at various CTs on *Per1*, *Per2*, and *Per3* expression in the hamster suprachiasmatic nucleus. RI *in situ* hybridization was performed for the quantitative analysis. Circadian expression of these genes was observed at (*A*) *Per1* (ANOVA, $F_{(2,12)} = 9.363$, $p = 0.0032$), (*B*) *Per2* (ANOVA, $F_{(2,13)} = 62.375$, $p = 0.0001$), and (*C*) *Per3* (ANOVA, $F_{(2,13)} = 39.892$, $p = 0.0001$). 8-OH DPAT (5.0 mg/kg, i.p.) significantly reduced *Per1* ($^{\#}p < 0.005$, Student's *t* test) and *Per2* ($^{\int\int}p < 0.0001$, Student's *t* test) but not *Per3* mRNA levels 2 hr after drug injection at CT6. *Numbers* in *parentheses* indicate the number of experiments.

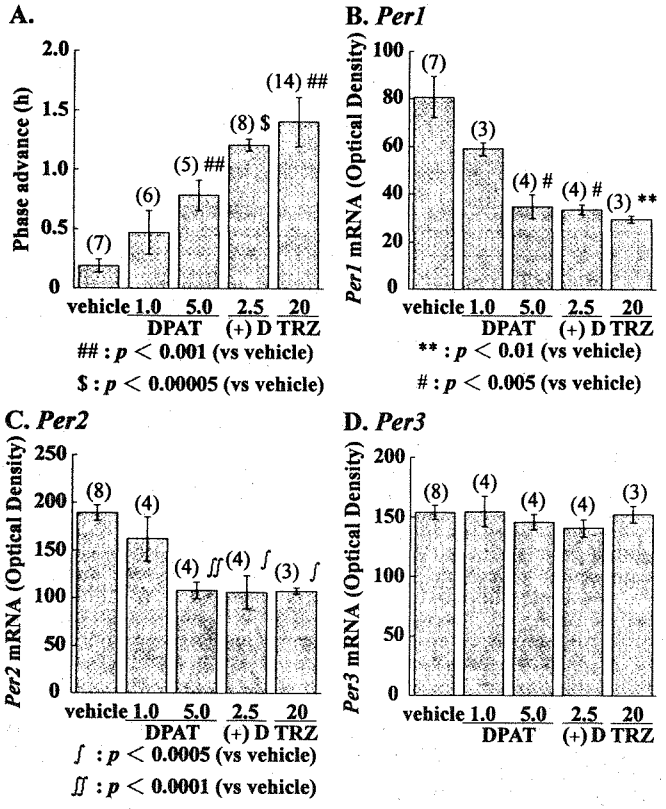

Figure 6. Dose-dependent advance of behavioral rhythms (*A*) and dose-dependent reduction of *Per1* (*B*), *Per2* (*C*), and *Per3* (*D*) mRNA levels by 8-OH DPAT (1.0 or 5.0 mg/kg, i.p.), (+) 8-OH DPAT (2.5 mg/kg, i.p.), or triazolam (20 mg/kg, i.p.). mRNA levels were quantified using RI *in situ* hybridization. $^{**}p < 0.01$, $^{\#}p < 0.005$, $^{\#\#}p < 0.001$, $^{\int}p < 0.0005$, $^{\int\int}p < 0.0001$, $^{\$}p < 0.00005$ versus vehicle alone, Student's *t* test. *Numbers* in *parentheses* indicate the number of experiments. *DPAT*, 8-OH DPAT; *(+)D*, (+) 8-OH DPAT; *TRZ*, triazolam.

day-dependent manner (Shigeyoshi et al., 1997; Takumi et al., 1998b). Gating is known to play a role in the light-induced phase shifts of behavioral rhythms. The responsiveness of *mPer1* mRNA to light is closely related to behavioral phase delays induced by light (Shigeyoshi et al., 1997). In addition, we previously demonstrated that light-induced phase delays in locomotor activity at CT16 were significantly inhibited when the mice were pretreated with *mPer1* antisense ODN before light exposure (Akiyama et al., 1999). Therefore, the gated induction of *mPer1* is a step necessary for producing behavioral phase shifts. These results along with our present results suggest that gated inhibition of *Per1* and/or *Per2* expression by nonphotic stimulation may facilitate *Per* gene reduction resulting in the onset of the next circadian induction of *Per* gene expression.

(+) 8-OH DPAT exhibited a higher affinity for 5-HT_7 receptors than for 5-HT_{1A} receptors, and amplitude of *Per1* and *Per2* reduction by 8-OH DPAT (5 mg/kg) was similar to that of (+) 8-OH DPAT (2.5 mg/kg). Thus, we estimate that the potential effect of (+) 8-OH DPAT is two times higher than that of 8-OH DPAT. The present results suggest that 5-HT_7 receptors, rather than 5-HT_{1A} receptors, have a more important role in phase shifting, as pointed out by Ying and Rusak (1997) during investigation of the inhibitory effect of 5-HT_7 receptors on light-sensitive SCN neurons. Challet et al. (1998) reported that bilateral 8-OH DPAT injections into either the SCN or the intergeniculate leaflet cause significant phase advances in hamster wheel-running activity. Additional studies proposed that perfusion of 8-OH DPAT at CT6–CT8 advances neuron activity rhythm of the SCN *in vitro* (Shibata et al., 1992; Prosser et al., 1993). These reports prefer the direct action of 8-OH DPAT on SCN *Per* gene expression. On the other hand, Schuhler et al. (1998) demonstrated that the 5-HT fibers connecting the median raphe to the SCN are essential for the phase-shifting action of peripheral 8-OH DPAT injections into the SCN using microinjections of 5-HT neurotoxin. The present results demonstrate that 8-OH DPAT reduces *Per1* mRNA levels in the entire SCN and preferentially reduces *Per2* mRNA in the ventrolateral part of the SCN. Because serotonergic fibers from the median raphe nucleus innervate the ventrolateral part of the hamster SCN (Meyer-Bernstein and Morin, 1996; Leander et al., 1998), the reduction of this SCN serotonergic input may be one of the possible outcomes of 8-OH DPAT-induced reductions of *Per* mRNA. It is interesting that triazolam (20 mg/kg) causes not only a big phase advance but also a strong inhibition of *Per1* and *Per2* mRNA. Thus, reduction of *Per1* and *Per2* mRNA correlates well with phase advances induced by 8-OH DPAT as well as triazolam.

The SCN entrains to the environmental light/dark cycle via a retinal projection called the retinohypothalamic tract (RHT). Glutamate, which acts as an RHT transmitter (de Vries et al., 1993), and glutamate and NMDA application to the rat SCN *in vitro* reportedly causes phase delays in SCN firing rhythms when applied during early subjective night (Ding et al., 1994; Shibata et al., 1994; Shirakawa and Moore, 1994; Ding et al., 1997). Excitation of glutamate receptors is reported to facilitate the phosphorylation of cAMP response element binding protein (CREB) (Ding et al., 1997; McNulty et al., 1998). Furthermore, light exposure at night is reported to produce mitogen-activated protein kinase phosphorylation and CREB phosphorylation (Obrietan et al., 1998). Thus, the signal cascade of photic entrainment is well documented, whereas the signal cascade of nonphotic entrainment is obscure at present.

Currently, we do not know the mechanism of *Per1* and *Per2* reduction in the SCN by 8-OH DPAT or triazolam.

Treatments using pituitary adenylate cyclase-activating polypeptide or cAMP during subjective day are reported to induce the phase shift of circadian rhythm, apparently via activation of adenylate cyclase and PKA activity (Prosser and Gillette, 1989; Hannibal et al., 1997; Harrington et al., 1999). 5-HT_7 receptors are positively coupled to adenylate cyclase (Lovenberg et al., 1993; Tsou AP et al., 1994), and activation of both PKA and K^+ channels is necessary for 5-HT-induced phase advances of circadian rhythm (Prosser et al., 1994). Therefore, we speculate that activation of PKA may be involved in the 8-OH DPAT-induced phase advance and transient reduction of *Per* mRNA levels.

In this experiment, we demonstrated that administration of triazolam and 8-OH DPAT during subjective day reduces *Per1* and *Per2* mRNA in the hamster SCN. Nonphotic resetting by benzodiazepine or novel wheel-running requires neuropeptide Y innervation of the SCN from the thalamus (Biello et al., 1994; Maywood et al., 1997). Recently, Maywood et al. (1999) also demonstrated the acute downregulation of SCN *Per1* and *Per2*, whereas there was no significant change in SCN PER1 immunoreactivity by novel wheel-running during the daytime under a light/dark cycle. Our present results are highly consistent with the data of Maywood et al. (1997, 1999). Although we do not know whether the signal transduction mechanism of benzodiazepine-GABA, 8-OH DPAT, and novel wheel-running are identical, it is strongly suggested that nonphotic stimuli presented during subjective day cause a phase advance through the reduction of *Per1* and *Per2* mRNA in the hamster SCN. However, further experiments are needed to investigate the response of other clock elements such as *Clock*, *Bmal1*, *Cry1*, *Cry2* (Gekakis et al., 1998; Thresher et al., 1998; Griffin et al., 1999; Jin et al., 1999; Kume et al., 1999; Miyamoto and Sancar, 1999; Okamura et al., 1999; van der Horst et al., 1999; Vitaterna et al., 1999), or other *Per* proteins in the hamster SCN after nonphotic stimuli, because these assessments will better clarify the cascading effects of nonphotic stimuli on the clock loop.

The levels of *mPer3* mRNA are not affected by light exposure (Takumi et al., 1998b; Zylka et al., 1998). In the present experiment, *Per3* mRNA levels in the hamster SCN were unresponsive to light exposure at CT20 or to administration of 8-OH DPAT at various CTs. Triazolam also did not affect *Per3* mRNA levels. We do not know why *Per3* mRNA levels in the SCN are insensitive to both photic and nonphotic stimuli. It could be that acute changing of the expression of *Per3* is not required for phase shifts in mice and hamster circadian rhythms.

In summary, we found that the acute and circadian time-dependent reduction of *Per1* or *Per2* mRNA, or both, in the hamster SCN by 8-OH DPAT strongly correlates with the phase resetting in response to 8-OH DPAT. Therefore, the present findings suggest that nonphotic shifts involve alteration in *Per1* or *Per2* mRNA levels, or both, in the SCN.

REFERENCES

Akiyama M, Kouzu Y, Takahashi S, Wakamatsu H, Moriya T, Maetani M, Watanabe S, Tei H, Sakaki Y, Shibata S (1999) Inhibition of light- or glutamate-induced *mPer1* expression represses the phase shifts into the mouse circadian locomotor and suprachiasmatic firing rhythms. J Neurosci 19:1115–1121.

Albrecht U, Sun ZS, Eichele G, Lee CC (1997) A differential response of two putative mammalian circadian regulators, *mPer1* and *mPer2*, to light. Cell 91:1055–1064.

Biello SM, Janik D, Mrosovsky N (1994) Neuropeptide Y and behaviorally induced phase shifts. Neuroscience 62:273–279.

Challet E, Scarbrough K, Penev PD, Turek FW (1998) Roles of suprachiasmatic nuclei and intergeniculate leaflets in mediating the phase-shifting effects of a serotonergic agonist and their photic modulation during subjective day. J Biol Rhythms 13:410–421.

Cutrera RA, Sabourcau M, Pevet P (1996) Phase-shifting effect of 8-OH DPAT, a 5-HT_{1A}/5-HT_7 receptor agonist, on locomotor activity in golden hamster in constant darkness. Neurosci Lett 210:1–4.

Daan S, Pittendrigh C (1976) A functional analysis of circadian pacemakers in nocturnal rodents II. The variability of phase response curves. J Comp Physiol [A] 106:253–266.

de Vries MJ, Nunes Cardozo B, van der Want J, de Wolf A, Meijer JH (1993) Glutamate immunoreactivity in terminals of the retinohypothalamic tract of the brown Norwegian rat. Brain Res 612:231–237.

Ding JM, Chen D, Weber ET, Faiman LE, Rea MA, Gillette MU (1994) Resetting the biological clock: mediation of nocturnal circadian shifts by glutamate and NO. Science 266:1713–1717.

Ding JM, Faiman LE, Hurst WJ, Kuriashkina LR, Gillette MU (1997) Resetting the biological clock: mediation of nocturnal CREB phosphorylation via light, glutamate, and nitric oxide. J Neurosci 17:667–675.

Dunlap JC (1999) Molecular bases for circadian clocks. Cell 96:271–290.

Edgar DM, Miller JD, Prosser R, Dean RR, Dement WC (1993) Serotonin and the mammalian circadian system: II. Phase-shifting rat behavioral rhythms with serotonergic agonists. J Biol Rhythms 8:17–31.

Eriksson H, Evrin K (1996) An evaluation of the 5-HT_7 receptor mediated signal transduction pathway in a transfected cell line by using the cytosensor microphysiometer. Soc Neurosci Abstr 22:1782.

Gekakis N, Staknis D, Nguyen HB, Davis FC, Wilsbacher LD, King DP, Takahashi JS, Weitz CJ (1998) Role of the CLOCK protein in the mammalian circadian mechanism. Science 280:1564–1569.

Griffin Jr EA, Staknis D, Weitz CJ (1999) Light-independent role of CRY1 and CRY2 in the mammalian circadian clock. Science 286:768–771.

Hannibal J, Ding JM, Chen D, Fahrenkrug J, Larsen PJ, Gillette MU, Mikkelsen JD (1997) Pituitary adenylate cyclase-activating peptide (PACAP) in the retinohypothalamic tract: a potential daytime regulator of the biological clock. J Neurosci 17:2637–2644.

Harrington ME, Hoque S, Hall A, Golombek D, Biello S (1999) Pituitary adenylate cyclase activating peptide phase shifts circadian rhythms in a manner similar to light. J Neurosci 19:6637–6642.

Hastings MH (1997) Central clocking. Trends Neurosci 20:459–464.

Jin X, Shearman LP, Weaver DR, Zylka MJ, de Vries GJ, Reppert SM (1999) A molecular mechanism regulating rhythmic output from the suprachiasmatic circadian clock. Cell 96:57–68.

Kume K, Zylka MJ, Sriram S, Shearman LP, Weaver DR, Jin X, Maywood ES, Hastings MH, Reppert SM (1999) mCRY1 and mCRY2 are essential components of the negative limb of the circadian clock feedback loop. Cell 98:193–205.

Leander P, Vrang N, Moller M (1998) Neuronal projections from the mesencephalic raphe nuclear complex to the suprachiasmatic nucleus and the deep pineal gland of the golden hamster (*Mesocricetus auratus*). J Comp Neurol 14:73–93.

Lovenberg TW, Baron BM, de Lecea L, Miller JD, Prosser RA, Rea MA, Foye PE, Racke M, Slone AL, Siegel BW, Danielson PE, Sutcliffe JG, Erlander MG (1993) A novel adenylyl cyclase-activating serotonin receptor (5-HT_7) implicated in the regulation of mammalian circadian rhythms. Neuron 11:449–458.

Maywood ES, Smith E, Hall SJ, Hastings MH (1997) A thalamic contribution to arousal-induced, non-photic entrainment of the circadian clock of the Syrian hamster. Eur J Neurosci 9:1739–1747.

Maywood ES, Mrosovsky N, Field MD, Hastings MH (1999) Rapid down-regulation of mammalian period genes during behavioral resetting of the circadian clock. Proc Natl Acad Sci USA 96:15211–15216.

McNulty S, Schurov IL, Sloper PJ, Hastings MH (1998) Stimuli which entrain the circadian clock of the neonatal Syrian hamster in vivo regulate the phosphorylation of the transcription factor CREB in the suprachiasmatic nucleus in vitro. Eur J Neurosci 10:1063–1072.

Mead S, Ebling FJ, Maywood ES, Humby T, Herbert J, Hastings MH (1992) A nonphotic stimulus causes instantaneous phase advances of the light-entrainable circadian oscillator of the Syrian hamster but does not induce the expression of c-fos in the suprachiasmatic nuclei. J Neurosci 12:2516–2522.

Meyer-Bernstein EL, Morin LP (1996) Differential serotonergic innervation of the suprachiasmatic nucleus and the intergeniculate leaflet and its role in circadian rhythm modulation. J Neurosci 16:2097–2111.

Miller JD, Liu ZW, Tenner T (1996) Activity of 8-OH-DPAT enantiomers at the 5-HT_7 receptor in SCN and transfected CHO cells. Soc Neurosci Abstr 22:1142.

Mintz EM, Gillespie CF, Marvel CL, Huhman KL, Albers HE (1997) Serotonergic regulation of circadian rhythms in syrian hamsters. Neuroscience 79:563–569.

Miyamoto Y, Sancar A (1999) Circadian regulation of cryptochrome genes in the mouse. Brain Res Mol Brain Res 71:238–243.

Moore RY (1982) The suprachiasmatic nucleus and the organization of a circadian system. Trends Neurosci 5:404–407.

Mrosovsky N (1988) Phase response curves for social entrainment. J Comp Physiol [A] 162:35–46.

Obrietan K, Impey S, Storm DR (1998) Light and circadian rhythmicity regulate MAP kinase activation in the suprachiasmatic nuclei. Nat Neurosci 1:693–700.

Okamura H, Miyake S, Sumi Y, Yamaguchi S, Yasui A, Muijtjens M, Hoeijmakers JH, van der Horst GT (1999) Photic induction of mPer1 and mPer2 in cry-deficient mice lacking a biological clock. Science 286:2531–2534.

Prosser RA, Gillette MU (1989) The mammalian circadian clock in the suprachiasmatic nuclei is reset in vitro by cAMP. J Neurosci 9:1073–1081.

Prosser RA, Dean RR, Edgar DM, Heller HC, Miller JD (1993) Serotonin and the mammalian circadian system: I. In vitro phase shifts by serotonergic agonists and antagonists. J Biol Rhythms 8:1–16.

Prosser RA, Heller HC, Miller JD (1994) Serotonergic phase advances of

the mammalian circadian clock involve protein kinase A and K+ channel opening. Brain Res 644:67–73.
Reebs SG, Mrosovsky N (1989) Effects of induced wheel running on the circadian activity rhythm of Syrian hamsters: entrainment and phase response curve. J Biol Rhythms 4:39–48.
Sakamoto K, Nagase T, Fukui H, Horikawa K, Okada T, Tanaka H, Sato K, Miyake Y, Ohara O, Kako K, Ishida N (1998) Multitissue circadian expression of rat period homolog (rPer2) mRNA is governed by the mammalian circadian clock, the suprachiasmatic nucleus in the brain. J Biol Chem 273:27039–27042.
Schuhler S, Saboureau M, Pitrosky B, Pevet P (1998) In Syrian hamsters, 5-HT fibres within the suprachiasmatic nuclei are necessary for the expression of 8-OH-DPAT induced phase-advance of locomotor activity rhythm. Neurosci Lett 256:33–36.
Shearman LP, Zylka MJ, Weaver DR, Kolakowski Jr LF, Reppert SM (1997) Two *period* homologs: circadian expression and photic regulation in the suprachiasmatic nuclei. Neuron 19:1261–1269.
Shibata S, Tsuneyoshi A, Hamada T, Tominaga K, Watanabe S (1992) Phase-resetting effect of 8-OH DPAT, a serotonin 1A receptor agonist, on the circadian rhythm of firing rate in the rat suprachiasmatic nuclei *in vitro*. Brain Res 582:353–356.
Shibata S, Watanabe A, Hamada T, Ono M, Watanabe S (1994) *N*-methyl-D-aspartate induces phase shifts in circadian rhythm of neuronal activity of rat SCN *in vitro*. Am J Physiol 267:R360–R364.
Shigeyoshi Y, Taguchi K, Yamamoto S, Takekida S, Yan L, Tei H, Moriya T, Shibata S, Loros JJ, Dunlap JC, Okamura H (1997) Light-induced resetting of a mammalian circadian clock is associated with rapid induction of the *mPer1* transcript. Cell 91:1043–1053.
Shirakawa T, Moore RY (1994) Glutamate shifts the phase of the circadian neuronal firing rhythm in the rat suprachiasmatic nucleus in vitro. Neurosci Lett 178:47–50.
Sun ZS, Albrecht U, Zhuchenko O, Bailey J, Eichele G, Lee CC (1997) *RIGUI*, a putative mammalian ortholog of the *Drosophila period* gene. Cell 19:1003–1011.
Takumi T, Matsubara C, Shigeyoshi Y, Taguchi K, Yagita K, Maebayashi Y, Sakakida Y, Okumura K, Takashima N, Okamura H (1998a) A new mammalian *period* gene predominantly expressed in the suprachiasmatic nucleus. Genes Cells 3:167–176.
Takumi T, Taguchi K, Miyake S, Sakakida Y, Takashima N, Matsubara C, Maebayashi Y, Okumura K, Takekida S, Yamamoto S, Yagita K, Yan L, Young MW, Okamura H (1998b) A light-independent oscillatory gene *mPer3* in mouse SCN and OVLT. EMBO J 17:4753–4759.
Tei H, Okamura H, Shigeyoshi Y, Fukuhara C, Ozawa R, Hirose M, Sakaki Y (1997) Circadian oscillation of a mammalian homologue of the *Drosophila period* gene. Nature 389:512–516.
Thresher RJ, Vitaterna MH, Miyamoto Y, Kazantsev A, Hsu DS, Petit C, Selby CP, Dawut L, Smithies O, Takahashi JS, Sancar A (1998) Role of mouse cryptochrome blue-light photoreceptor in circadian photoresponses. Science 282:1490–1494.
Tominaga K, Shibata S, Ueki S, Watanabe S (1992) Effects of 5-HT_{1A} receptor agonists on the circadian rhythm of wheel-running activity in hamsters. Eur J Pharmacol 214:79–84.
Tsou AP, Kosaka A, Bach C, Zuppan P, Yee C, Tom L, Alvarez R, Ramsey S, Bonhaus DW, Stefanich E (1994) Cloning and expression of a 5-hydroxytryptamine7 receptor positively coupled to adenylyl cyclase. J Neurochem 63:456–464.
van der Horst GT, Muijtjens M, Kobayashi K, Takano R, Kanno S, Takao M, de Wit J, Verkerk A, Eker AP, van Leenen D, Buijs R, Bootsma D, Hoeijmakers JH, Yasui A (1999) Mammalian Cry1 and Cry2 are essential for maintenance of circadian rhythms. Nature 398:627–630.
Vitaterna MH, Selby CP, Todo T, Niwa H, Thompson C, Fruechte EM, Hitomi K, Thresher RJ, Ishikawa T, Miyazaki J, Takahashi JS, Sancar A (1999) Differential regulation of mammalian period genes and circadian rhythmicity by cryptochromes 1 and 2. Proc Natl Acad Sci USA 96:12114–12119.
Yan L, Takekida S, Shigeyoshi Y, Okamura H (1999) *Per1* and *Per2* gene expression in the rat suprachiasmatic nucleus: circadian profile and the compartment-specific response to light. Neuroscience 94:141–150.
Ying SW, Rusak B (1997) 5-HT_7 receptors mediate serotonergic effects on light-sensitive suprachiasmatic nucleus neurons. Brain Res 755:246–254.
Zylka MJ, Shearman LP, Weaver DR, Reppert SM (1998) Three *period* homologs in mammals: differential light responses in the suprachiasmatic circadian clock and oscillating transcripts outside of brain. Neuron 20: 1103–1110.

0026-895X/01/5904-894–900$3.00
MOLECULAR PHARMACOLOGY

Mol Pharmacol 59:894–900, 2001

Vol. 59, No. 4
556/891083
Printed in U.S.A.

Sensitized Increase of *Period* Gene Expression in the Mouse Caudate/Putamen Caused by Repeated Injection of Methamphetamine

TAKATO NIKAIDO, MASASHI AKIYAMA, TAKAHIRO MORIYA, and SHIGENOBU SHIBATA

Department of Pharmacology and Brain Science (T.N., M.A., S.S.) and Advanced Research Center for Human Sciences (T.M., S.S.), School of Human Sciences, Waseda University, Tokorozawa, Saitama, Japan

Received September 8, 2000; accepted December 5, 2000

This paper is available online at http://molpharm.aspetjournals.org

ABSTRACT

Methamphetamine (MAP) causes the sensitization phenomena not only in MAP-induced locomotor activity, dopamine release, and Fos expression, but also in MAP-induced circadian rhythm. Cocaine-induced sensitization is reportedly impaired in *Drosophila melanogaster* mutant for the *Period* (*Per*) gene. Thus, sensitization may be related to induction of the *Per* gene. A rapid induction of *mPer1* and/or *mPer2* in the suprachiasmatic nucleus after light exposure is believed to be necessary for light-induced behavioral phase shifting. Although the caudate/putamen (CPu) expresses *mPer1* and/or *mPer2* mRNA, the function of these genes in this nucleus has not yet been elucidated. Therefore, we examined whether MAP affects the expression of *mPer1* and/or *mPer2* mRNA in the mouse CPu. Injection of MAP augmented the expression of *mPer1* but not *mPer2* or *mPer3* in the CPu, and this MAP-induced increase in *mPer1* expression lasted for 2 h. Also, the MAP-induced increase of *mPer1* mRNA was strongly antagonized by pretreatment with a dopamine D1 receptor and *N*-methyl-D-aspartate (NMDA) receptor antagonist, but not by a D2 receptor antagonist. Interestingly, application of either the D1 or the D2 agonist alone did not cause *mPer1* expression. The present results demonstrate that activation of both NMDA and D1 receptors is necessary to produce MAP-induced *mPer1* expression in the CPu. Repeated injection of MAP caused a sensitization in not only the locomotor activity but also *mPer1* expression in the CPu without affecting the level of *mPer2*, *mPer3*, or *mTim* mRNA. Thus, these results suggest that MAP-induced *mPer1* gene expression may be related to the mechanism for MAP-induced sensitization in the mouse.

A core clock mechanism in the mouse suprachiasmatic nucleus (SCN) seems to involve a transcriptional feedback loop in which CLOCK and BMAL1 function as positive regulators and the three *mPeriod* (*mPer*) genes, *Per1* (Sun et al., 1997; Tei et al., 1997), *Per2* (Albrecht et al., 1997; Shearman et al., 1997; Takumi et al., 1998), and *Per3* (Zylka et al., 1998) are involved in negative feedback (Dunlap, 1999). In addition, it was determined that two mouse cryptochrome genes, *mCry1* and *mCry2*, act in the negative limb of the clock feedback loop (Kume et al., 1999). It is already well known that the SCN contains a master pacemaker that regulates behavioral and physiological circadian rhythms such as locomotor activity, body temperature, and endocrine release (Inouye and Shibata, 1994). Interestingly, expression of the *Per* gene occurs not only in the SCN but also in other brain areas such as the cerebral cortex, caudate/putamen (CPu), and cerebellum (Albrecht et al., 1997; Shearman et al., 1997). However, the function of clock genes outside of the SCN has not been fully elucidated.

Destruction of the SCN abolishes the circadian rhythms of many physiological functions (Inouye and Shibata, 1994). On the other hand, there are at least two oscillators outside the SCN: a food-associated oscillation entrained by daily restricted feeding (Mistlberger, 1994) and methamphetamine (MAP)-induced oscillation produced by its daily injection (Shibata et al., 1994, 1995). In addition, oral administration of MAP through drinking bottle initiates a circadian rhythm with a long free-running period even after SCN ablation (Honma et al., 1987). Based on these facts, it has been suggested that other circadian oscillators such as the MAP-induced rhythm exist in areas other than the SCN. Thus, it is possible that *mPer* mRNA outside of the SCN regulates the SCN-independent circadian rhythm, and rapid induction of *mPer* outside of the SCN by MAP may entrain the SCN-independent oscillation.

This study was partially supported by grants awarded to S.S. from the Japanese Ministry of Education, Science, Sports, and Culture (11170248, 11233207, and 11145240), and by a grant-in-aid for Encouragement of Young Scientists to T.M. from the Japan Society for the Promotion of Science (11771503).

ABBREVIATIONS: SCN, suprachiasmatic nucleus; MAP, methamphetamine; CPu, caudate/putamen; NMDA, *N*-methyl-D-aspartate; *Per*, *Period*; *Tim*, *timeless*; PB, phosphate buffer; PFA, paraformaldehyde.

Recently it was reported that sensitization to repeated cocaine exposure, a phenomenon also seen in humans and animal models and associated with enhanced drug craving, is eliminated in flies mutant for *period*, *clock*, *cycle*, and *double-time*, but not in flies mutant for *timeless* (Andretic et al., 1999) We demonstrated that the MAP-induced free-running oscillation of rat locomotion with drinking application of MAP exhibits a sensitization phenomenon (Nikaido et al., 1999). Therefore, the next progressive step was to examine whether MAP induces *Per* expression in the CPu, and whether sensitization is involved in MAP-induced *Per* expression but not *timeless* expression.

Treatment with MAP is known to increase locomotor activity and Fos expression in the CPu (Graybiel et al., 1990). Pharmacological studies have further revealed that both MAP-induced hyperlocomotion and Fos expression in the CPu are attenuated by pretreatment with dopamine D1, D2, or NMDA receptor antagonists (Ujike et al., 1989; Kuribara and Uchihashi, 1993; Kuribara, 1994, 1995, 1996; Yoshida et al., 1995). Thus, it has been suggested that D1, D2, and NMDA receptors play an important role in the sensitization induced by repeated injection of MAP. This evidence suggests that MAP-induced *Per* expression may be involved in the activation of both dopamine and NMDA receptors. Therefore, in the first part of our present experiment, we examined the pharmacological characteristics of MAP-induced *Per* gene expression in the mouse CPu. Then, in the latter part, we examined the expression pattern of *Per* and *timeless* mRNA using animals sensitized to MAP.

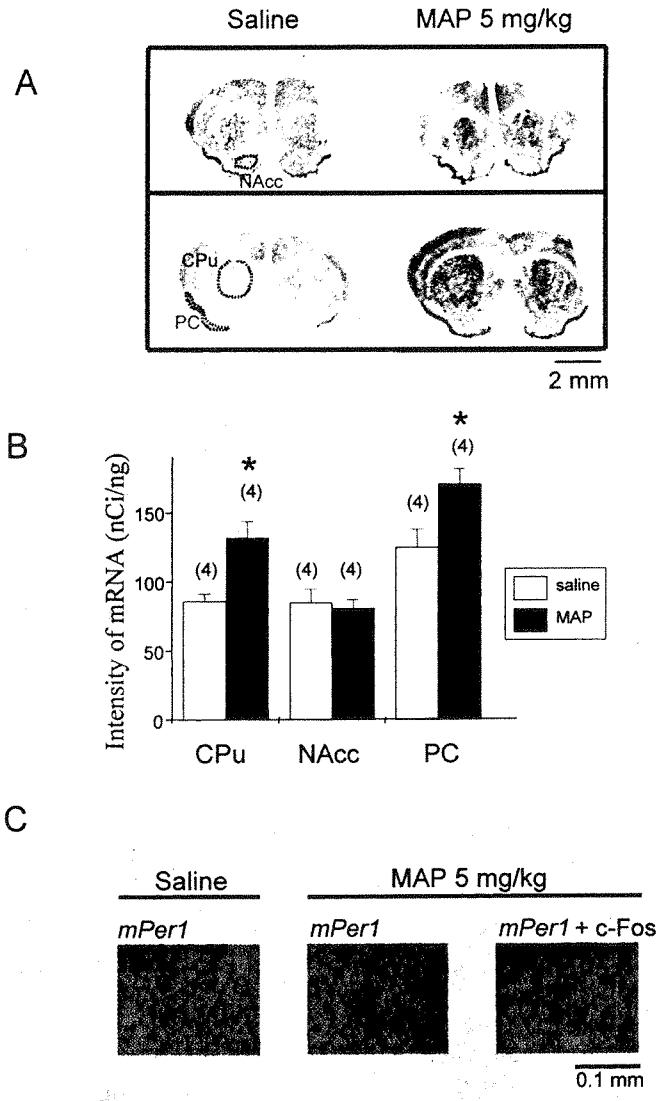

Fig. 1. Effect of 5 mg/kg of MAP on *mPer1* expression in CPu, accumbens (NAcc), and piriform cortex (PC). Mice were decapitated 60 min after MAP injection. A, representative in situ hybridization autoradiograms of *mPer1* on X-ray film. The brain areas surrounded by a broken line exhibit the NAcc, CPu, and PC areas. B, radioisotope in situ hybridization was performed for quantitative analysis purposes. Numbers in parentheses indicate the number of animals ($^*P < 0.05$ in comparison with saline by Student's *t* test). C, emulsion autoradiograms of *mPer1* in the dorsal caudate. A 5-mg/kg injection of MAP increased *mPer1* expression (black dots, middle panel), and there were many dots on cells showing the Fos immunoreactivity (right panel). Fos immunoreactive cells were stained by a brown color.

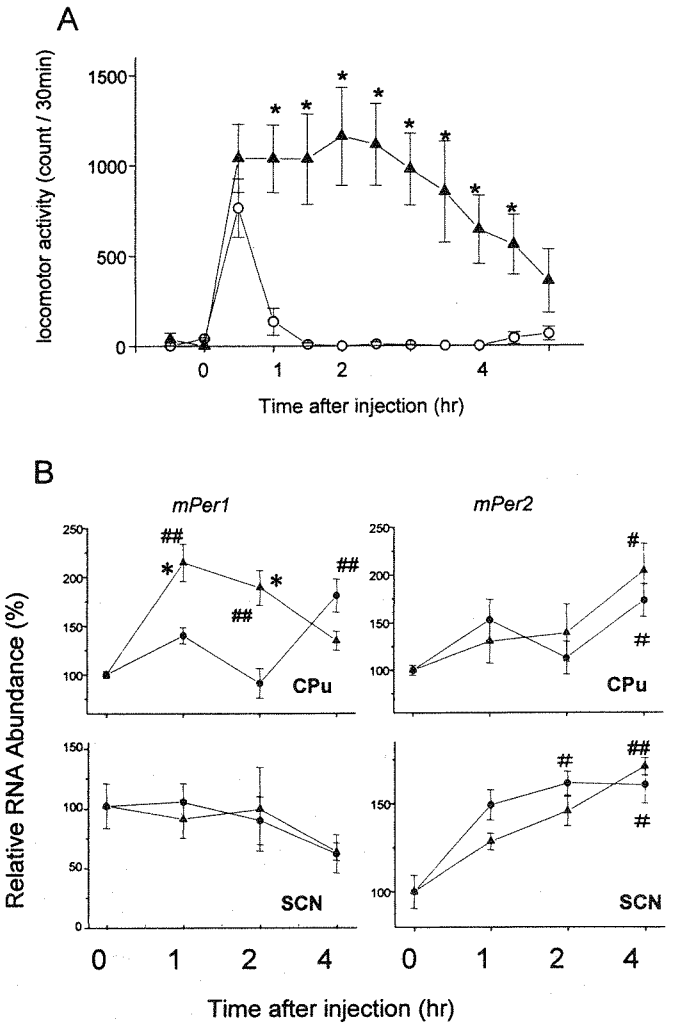

Fig. 2. Time course of MAP-induced locomotor activity (A) and *mPer* expression in the CPu or SCN (B). A, MAP increased mouse locomotion for 4 h. ○, saline injection ($n = 4$); ▲, 5 mg/kg MAP injection ($n = 4$) ($^*P < 0.05$ in comparison with saline by Student's *t* test). B, relative value of *mPer1* and *mPer2* mRNA expression in the CPu. ●, saline injection; ▲, 5 mg/kg MAP injection. *Per* expression observed in the saline group immediately after saline injection was set as 100%. Three to four animals made up each point ($^*P < 0.05$ in comparison with saline by Student's *t* test; $^\#P < 0.05$, $^{\#\#}P < 0.01$ in comparison with 0-min point by Dunnett's test).

Materials and Methods

Animals. In all experiments, we used 4- to 6-week-old male *ddY* mice (Takasugi, Saitama, Japan) maintained under a 12 h:12 h light/dark cycle. All animals were allowed free access to food and water and were treated in accordance with the Law no. 105 and Notification no. 6 of the Japanese Government.

Locomotor Activity Measurement. For assessment of the locomotor activity, mice were housed individually in transparent plastic cages (31 × 20 × 13 cm). Motor activity was measured using an infrared area sensor (F5B; Omron, Tokyo, Japan), and the activity count (number of movements) was recorded by computer and stored on disk at 5-min intervals.

Sample Preparation. Mice were deeply anesthetized with ether and intracardially perfused with 0.1 M phosphate buffer (PB), pH 7.4, containing 4% paraformaldehyde (PFA). Brains were removed, postfixed in 0.1 M PB containing 4% PFA for 24 h at 4°C, and transferred into 20% sucrose in PB for 72 h at 4°C. Brain slices (40 μm thick) including the CPu, accumbens, piriform cortex, and SCN were made using a cryostat (HM505E; Microm, Walldorf, Germany) and placed in 2× standard saline citrate until processing for hybridization.

In Situ Hybridization. The quantity of *mPer1*, *mPer2*, *mPer3*, or *mTim* mRNA expression in the various brain areas was studied by means of in situ hybridization. Slices were treated with 1 μg/ml proteinase K in 10 mM Tris-HCl buffer, pH 7.5, containing 10 mM EDTA for 10 min at 37°C followed by 0.25% acetic anhydride in 0.1 M triethanolamine and 0.9% NaCl for 10 min. The slices were then incubated in the hybridization buffer [60% formamide, 10% dextran sulfate, 10 mM Tris-HCl, pH 7.4, 1 mM EDTA, 0.6 M NaCl, 1× Denhardt's solution (0.02% Ficoll, 0.02% polyvinyl pyrrolidone, 0.02% bovine serum albumin), 0.2 mg/ml transfer RNA, 0.25% sodium dodecyl sulfate] containing ^{33}P-labeled cRNA probes for 16 h at 60°C. Radioisotope ([α-^{33}P]UTP)-labeled antisense cRNA probes (PerkinElmer Life Sciences, Boston, MA) were made from restriction enzyme-linearized cDNA templates [nucleotide positions: *mPer1* (538–1752), *mPer2* (1–638), *mPer3* (814–1955), *mTim* (236–909)] kindly provided by Dr. Okamura (Kobe University, Kobe, Japan). After a high-stringency posthybridization wash in 2× standard saline citrate/50% formamide, slices were treated with RNaseA (10 μg/ml) for 30 min at 37°C.

The radioactivity of each slice visualized on BioMax MR film (Eastman Kodak, Rochester, NY) was analyzed using a microcomputer interface to an image analysis system (MCID; Imaging Research Inc., ON, Canada) after conversion into optical density by ^{14}C-autoradiographic microscales (Amersham Pharmacia Biotech, Buckinghamshire, UK). For data analysis, we subtracted the intensities of the optical density in sections from the corpus callosum from those in the SCN, CPu, piriform cortex, and accumbens and regarded this value as the net intensity for these areas. The intensity values of sections from the rostral to the caudal part of the SCN, CPu, piriform cortex, and accumbens (three to five sections per mouse brain) were then summed; the sum was considered to be a measure of the amount of *mPer1*, *mPer2*, *mPer3*, or *mTim* mRNA in this region. To express the relative mRNA abundance (Figs. 2–5 and 7), the intensity values of vehicle treatment were adjusted to 100.

Immunohistochemistry of Fos Protein and Emulsion Autoradiography of *mPer1*. The slices were fixed with 4% PFA and processed for immunohistochemistry according to the avidin-biotin-peroxidase complex method. Primary antibody (anti-Fos, 1:5000; Cambridge Research Biochemical, Northwich, UK) was diluted in 0.1 M phosphate buffer containing 1% normal goat serum in 0.3% Triton X-100.

For emulsion autoradiography, slices already processed for immunohistochemistry were dipped into emulsion (NTB2, Eastman Kodak; diluted 1:1 with distilled water) after hybridization with the *mPer1* probe, air dried for 3 h, and stored in light-tight slide boxes at 4°C for 2 weeks. The slides were developed using a D19 developer (Eastman Kodak) and then fixed with Fujifix (Fujifilm, Tokyo, Japan). Subnuclear sliver grain distribution in the CPu was examined using an optical microscope. We did not adopt the quantitative analysis of emulsion autoradiogram because thickness of the coating could not be controlled using the present emulsion-dipping method.

Drugs and Application Schedule. The drugs used in this experiment consisted of methamphetamine HCl (Dainippon Co., Tokyo, Japan); SCH23390 (Funakoshi, Tokyo, Japan); (+)-sulpiride (Sigma, St. Louis, MO); and MK-801, SKF38393, and quinpirole (RBI/Sigma, Natick, MA). All drugs were dissolved into the physiological saline. Drugs were injected during the daytime because spontaneous locomotor activity and *mPer1* expression in the CPu were low at this time (data not shown). To examine the blocking effect of receptor antagonists on MAP-induced *mPer1* expression, these receptor antagonists were injected 15 min before MAP injection.

A single high-dose exposure to MAP or amphetamine sufficiently induces long-term behavioral and neurochemical sensitization (Ohno et al., 1994; Vanderschuren et al., 1999). Therefore, for sensitization experiments, MAP (5 mg/kg) was injected once, and then a small dose of MAP (0.5 mg/kg) was injected again after a 7-day interval.

Statistics. Results are expressed as the mean ± S.E.M. The significance of differences between groups was determined by two-way or one-way analysis of variance followed by Dunnett's test or Student's *t* test.

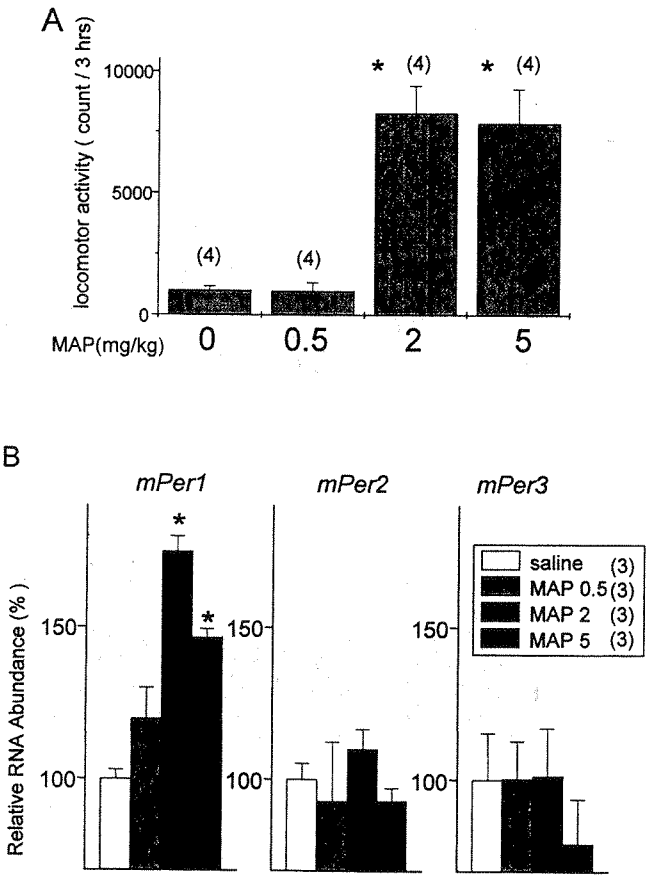

Fig. 3. Dose-response of MAP-induced locomotor activity (A) and *mPer* expression in the CPu (B). A, vertical values exhibit total locomotor counts 3 h after MAP injection. Numbers in parentheses indicate the number of animals (*$P < 0.05$ in comparison with saline by Dunnett's test). B, relative value of *mPer1*, *mPer2*, and *mPer3* mRNA expression in the CPu. *Per* expression observed in the saline group was set as 100%. Three animals made up each point (*$P < 0.05$ in comparison with saline by Dunnett's test).

Results

Methamphetamine-Induced *mPer1* Expression in the Various Brain Areas. It is well known that dopaminergic neurons innervate the CPu, accumbens, and piriform cortex. Therefore, we examined the amount of *mPer1* expression in these brain areas. Figure 1A shows the representative brain areas responding to MAP and the sampling area for each brain slice. Basal level *mPer1* expression was high in the piriform cortex but low in the CPu and accumbens (Fig. 1, A and B). Unrelated to basal expression, MAP significantly induced *mPer1* expression in the CPu ($P < 0.05$, Student's t test) and piriform cortex ($P < 0.05$, Student's t test) but not in the accumbens (Fig. 1, A and B). Previous papers demonstrated a strong induction of Fos protein in the dorsal CPu (Yoshida et al., 1995); therefore, we examined the Fos expression and *mPer1* induction using CPu slices. Interestingly, *mPer1* mRNA and Fos immunoreactivity were coexpressed in the same striatal cells (Fig. 1C).

Time Course of MAP-Induced Locomotion and *mPer1* Expression. A 5-mg/kg injection of MAP significantly increased the locomotion, which was maintained for 4 h (Fig. 2A). Two-way analysis of variance revealed an interaction between drug treatment and time course in CPu *mPer1* [$F(3,23) = 13.1$, $P < 0.01$]. Post hoc Dunnett's test demonstrated that the same dose of MAP increased *mPer1* expression in the CPu 1 h ($P < 0.05$) and 2 h ($P < 0.05$) after MAP injection, but not 4 h after injection. On the other hand, MAP did not increase *mPer2* expression in the CPu. In the SCN, MAP did not affect the expression of *mPer1* or *mPer2* at any time point after MAP injection. The increased basal level of *mPer1* and *mPer2* in the CPu and *mPer2* in the SCN may reflect a circadian change in expression of these genes (Fig. 2).

Dose-Response Curve for MAP-Induced Locomotion and *mPer* mRNA. At a dose of 0.5 mg/kg, MAP did not change the locomotion or *mPer* expression in the CPu (Fig. 3). Two milligrams per kilogram was a sufficient dose to produce significant increase in locomotion ($P < 0.05$, Dunnett's test) and also *mPer1* expression in the CPu [$F(3,8) = 29.9$, $P < 0.01$; $P < 0.05$, Dunnett's test]. In this experiment, MAP at any dose did not affect the expression of *mPer2* [$F(3,8) = 0.6$, $P > 0.05$] or *mPer3* [$F(3,8) = 0.5$, $P > 0.05$] in the CPu.

Effect of DA and NMDA Receptor Antagonists on MAP-Induced Locomotion and *mPer1* Expression in the CPu. Next, we examined the pharmacological profile of MAP-induced *mPer1* expression in the CPu. MAP (5 mg/kg)-induced hyperlocomotion was significantly blocked by SCH23390 ($P < 0.01$, Dunnett's test) and sulpiride ($P < 0.01$) but not by MK-801 ($P > 0.05$) (Fig. 4A). Treatment with MAP produced a strong increase in the expression of *mPer1* in the CPu (Fig. 4, B and C) that was completely attenuated by SCH23390 ($P < 0.01$, Dunnett's test), moderately attenuated by MK-801 ($P < 0.01$), and unaffected by sulpiride ($P > 0.05$) (Fig. 4, B and C). The basal level of *mPer1* in the CPu was also significantly reduced by SCH23390 ($P < 0.05$, Dunnett's test) and MK-801 ($P < 0.01$) but increased by sulpiride ($P < 0.05$) (Fig. 4C).

Effect of D1 and D2 Receptor Agonist on *mPer* Expression in the CPu. Because MAP-induced *mPer1* expres-

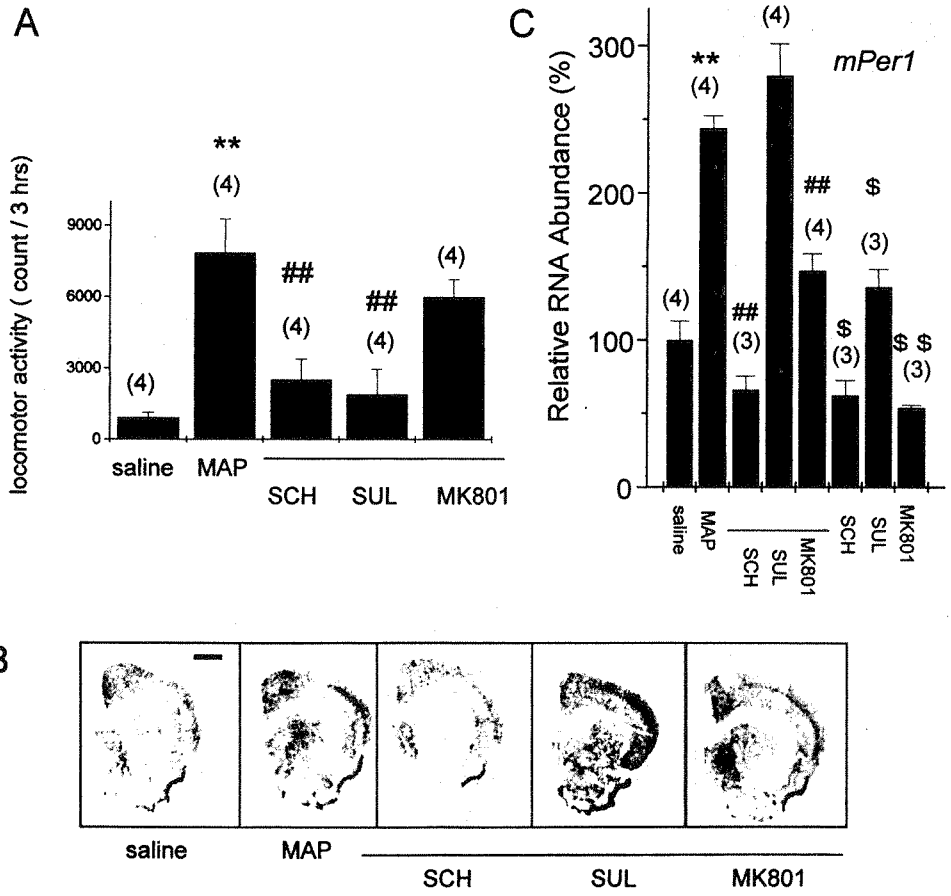

Fig. 4. Effects of D1, D2, and NMDA receptor antagonists on MAP-induced locomotor activity (A) and *mPer1* expression in the CPu (B and C). A, vertical values exhibit total locomotor counts 3 h after saline or MAP injection. Antagonists were injected 15 min before the 5-mg/kg MAP injection. Numbers in parentheses indicate the number of animals ($^{**}P < 0.01$ in comparison with saline by Student's t test; $^{\#\#}P < 0.01$ in comparison with MAP injection only by Dunnett's test). B, representative in situ hybridization autoradiograms of *mPer1* were developed on X-ray film. The D1 receptor antagonist (SCH) and NMDA receptor antagonist (MK-801), but not the D2 receptor antagonist (SUL), antagonized MAP-induced *mPer1* expression. Calibration on the saline panel is 1 mm. C, relative value of *mPer1* mRNA expression in the CPu. *Per* expression observed in the saline group was set as 100%. Antagonists were injected 15 min before the 5-mg/kg MAP injection, and then mice were decapitated 60 min after MAP injection. Numbers in parentheses indicate the number of animals ($^{**}P < 0.01$ in comparison with saline by Student's t test; $^{\#\#}P < 0.01$ in comparison with MAP injection only; $^{\$}P < 0.05$, $^{\$\$}P < 0.01$ in comparison with saline by Dunnett's test). SCH, SCH23390; SUL, sulpiride.

sion in the CPu was attenuated by the D1 receptor antagonist and facilitated by the D2 receptor antagonist, we examined the effect of D1 and D2 receptor agonists on the basal level of *mPer1* expression. Application of D1 receptor agonist SKF38393 did not affect *mPer1* and *mPer2* expression in the CPu (Fig. 5), whereas the D2 receptor agonist, quinpirole, slightly reduced *mPer1* and *mPer2* expression (Fig. 5).

Sensitized Expression of Locomotion and *mPer* mRNA in the CPu with Repeated Injection of MAP. In preparing the four experimental groups, MAP or saline was injected initially into all mice, then half of the MAP- (5 mg/kg) or saline-injected groups received another injection of MAP (0.5 mg/kg) or saline. Figure 6, A and B demonstrates the time course of locomotion (Fig. 6A) after injection of saline or MAP (0.5 mg/kg) and total locomotor counts (Fig. 6B) 60 min after injection, respectively. Small doses of MAP at 0.5 mg/kg did not increase locomotion in the saline-pretreated group but significantly increased locomotion in MAP (5 mg/kg)-pretreated mice [$F(3,12) = 6.9$, $P < 0.01$] (Fig. 6B).

A second injection of MAP (0.5 mg/kg) strongly increased *mPer1* mRNA in the CPu of mice pretreated with MAP at 5 mg/kg [$F(3,12) = 20.1$, $P < 0.01$] (Fig. 7, A and B), but 0.5 mg/kg of MAP did not affect the expression of *mPer2* [$F(3,12) = 1.8$, $P > 0.05$] or *mTim* mRNA [$F(3,12) = 1.1$, $P > 0.05$] (Fig. 7B).

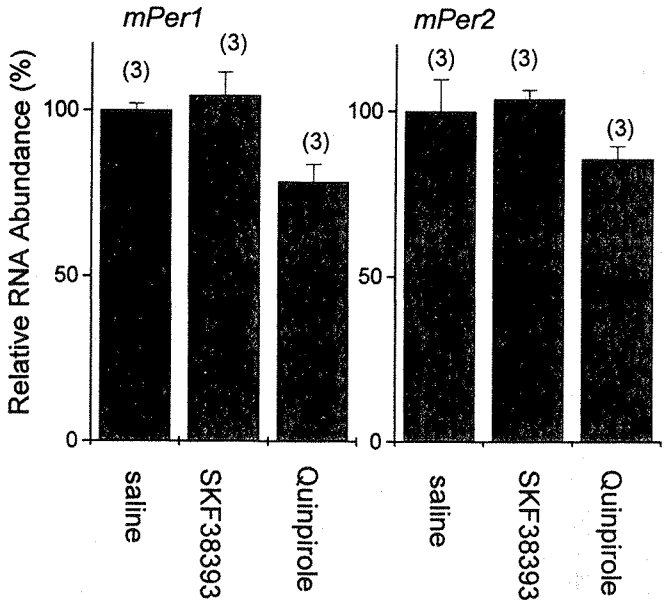

Fig. 5. Effect of the D1 (SKF38393) and D2 (quinpirole) receptor agonists on *mPer1* and *mPer2* expression in the CPu. Mice were decapitated 60 min after each agonist injection. Columns represent the relative value of m*Per1* mRNA expression in the CPu. *Per* expression observed in the saline group was set as 100%. Numbers in parentheses indicate the number of animals.

Discussion

In the present experiment, we demonstrated that MAP dose dependently induces the expression of *mPer1* in the CPu and piriform cortex but not in the accumbens or SCN, whereas MAP did not affect the levels of *mPer2* and *mPer3* in these brain areas. Coadministration of D1 receptor antagonist SCH23390 or NMDA receptor antagonist MK-801 significantly attenuated MAP-induced expression of *mPer1*, but D2 receptor antagonist sulpiride did not block this expression. Interestingly, Fos induction in the CPu by MAP injection was reportedly attenuated by either SCH23390 or MK-801 (Konradi et al., 1994, 1996; Ohno et al., 1994; Yoshida et al., 1995). Treatment with MK-801 attenuated MAP-induced *mPer1* expression in the CPu. Previous reports demonstrated that MK-801 inhibited amphetamine-induced glutamate release in the ventral tegmental area (Wolf and Xue, 1999), MAP-induced striatal dopamine release (Finnegan and Taraska, 1996), and striatal Fos expression (Ohno et al., 1994). Thus, NMDA receptor mechanisms are also involved in MAP-induced biochemical responses such as *mPer1* and Fos expression. From a pharmacological point of view, abovementioned articles have suggested that there may be common neural mechanisms between the expression of Fos and of *mPer1* induced by MAP. The present double-staining experiment demonstrated a dense expression of both Fos and *mPer1* mRNA in the dorsomedial regions of the CPu, which also support the above possibility.

In the present experiment, MAP increased the level of *mPer1* but did not affect the levels of *mPer2* and *mPer3* in the CPu. Application of forskolin induced *Per1* but not *Per2* expression in Rat-1 cells with the induction of cyclic AMP-responsive element binding protein phosphorylation; then it initiated the oscillation of *Per2* expression (Yagita and Oka-

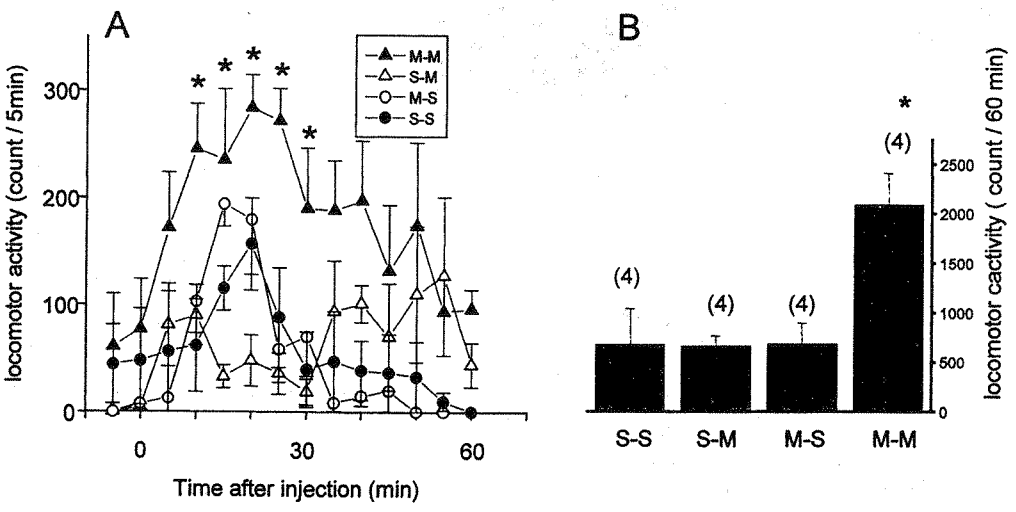

Fig. 6. Sensitization of locomotor activity induced by repeated application of MAP. A, time course of locomotor activity. M-M, MAP (5 mg/kg) injection followed by MAP (0.5 mg/kg) injection with 7-day withdrawal; S-M, saline injection followed by MAP (0.5 mg/kg) injection with 7-day interval; M-S, MAP (5 mg/kg) injection followed by saline injection with 7-day withdrawal; S-S, saline injection followed by saline injection with 7-day interval (*$P < 0.05$ in comparison with S-M group by Student's t test). B, total activity counts over a duration of 60 min (*$P < 0.05$ in comparison with S-M group by Dunnett's test). Numbers in parentheses indicate the number of animals.

mura, 2000). Interestingly, we found that the promoter region of *mPer1* contains a total of four cyclic AMP-responsive elements (Yamaguchi et al., 2000). This cyclic AMP-responsive element site may be responsible for the *mPer1* induction that occurs with MAP application. In fact, not only D1 and NMDA receptor activation (Das et al., 1997) but also MAP application (Muratake et al., 1998) reportedly cause cyclic AMP-responsive element binding protein phosphorylation.

Light exposure strongly increases *Per1* and *Per2* but not *Per3* expression in the SCN of mice, rats, and hamsters (Shigeyoshi et al., 1997; Yan et al., 1999; Horikawa et al., 2000); however, in our study, MAP failed to change *mPer* gene expression in the SCN. We found a significant circadian oscillation of *Per1* and *Per2* in the hamster SCN with a peak at subjective day (Horikawa et al., 2000). Local injection of NMDA into the SCN at subjective night causes the induction of *Per1* in the hamster (Moriya et al., 2000). On the other hand, stimulation of the D1 receptor in the SCN produces Fos induction in early developmental rodents but not in adults (Viswanathan et al., 1994; Weaver and Reppert, 1995; Grosse and Davis, 1999). Thus, the reason why MAP failed to produce *mPer1* expression in the SCN may be related to weak contribution of D1 receptors in the adult SCN. Changes in *mPer1* mRNA levels of CPu detected by in situ hybridization exhibited a circadian rhythm with a peak at early subjective night (data not shown). Therefore, it is interesting to determine whether transiently induced *mPer1* in the CPu at subjective day may cause a phase shift of circadian rhythm of *mPer1* expression in the CPu. The answer requires an examination of circadian time course of *mPer1* expression in the CPu subsequent to MAP treatment, and this important question should be the follow-up to this article.

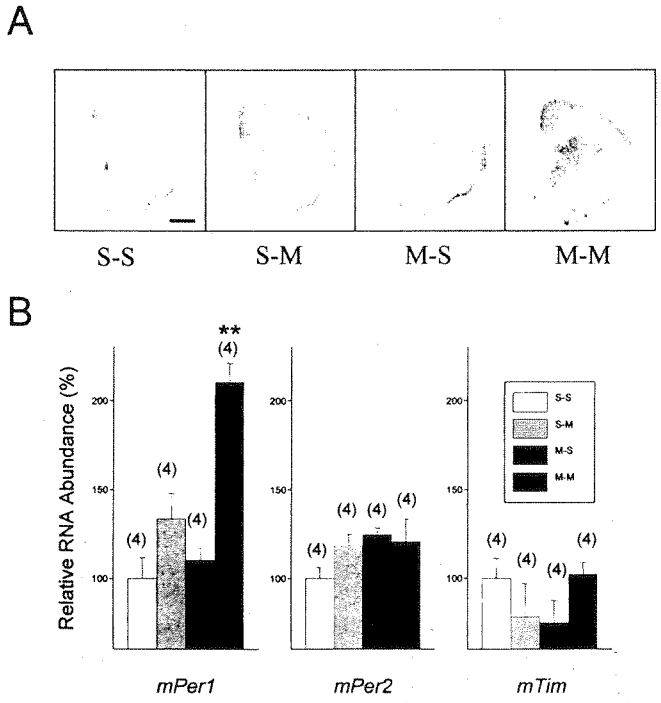

Fig. 7. Sensitization of *mPer1*, but not of *mPer2* or *mTim*, induced by repeated application of MAP. A, representative in situ hybridization autoradiograms of *mPer1* developed on X-ray film. M-M, MAP (5 mg/kg) injection followed by MAP (0.5 mg/kg) injection with 7-day withdrawal; S-M, saline injection followed by MAP (0.5 mg/kg) injection with 7-day interval; M-S, MAP (5 mg/kg) injection followed by saline injection with 7-day withdrawal; S-S, saline injection followed by saline injection with 7-day interval. As shown in panel M-M, a small doses of MAP (0.5 mg/kg) augmented *mPer1* expression in the dorsal caudate of the MAP (5 mg/kg)-pretreated mouse. Calibration on the S-S panel is 1 mm. B, relative value of *mPer1*, *mPer2*, or *mTim* mRNA expression in the CPu. *Per* expression observed in the S-S group was set as 100%. Mice were decapitated 60 min after the last MAP or saline injection. Numbers in parentheses indicate the number of animals (**$P < 0.01$ in comparison with S-S by Dunnett's test).

In this experiment, SCH23390 and MK-801 administration alone lowered the expression of *mPer1* in the CPu, suggesting a tonic activation of the *mPer1* gene through D1 and/or NMDA receptors in the CPu. Actually, MK-801 decreased the MAP-induced *mPer1* expression but slightly augmented the MAP-induced locomotion. On the contrary, sulpiride strongly attenuated the MAP-induced locomotion without affecting *mPer1* expression. These results seemingly indicate that MAP-induced locomotor stimulation is not sufficient for induction of *mPer1* by MAP. One of our previous articles supports this idea by showing that the D1 and NMDA receptor blockade abolished MAP-induced anticipatory behavior without attenuating its induction of hyperlocomotion (Shibata et al., 1995).

In the present experiments, repeated administration of MAP caused sensitization in *mPer1* expression but not in *mPer2*, *mPer3*, or *mTim* expression in the CPu. Therefore, behavioral sensitization is associated with *mPer1* expression in the CPu but not that in the SCN, suggesting the important role of *mPer1* gene expression in MAP-induced behavioral sensitization. Furthermore, we demonstrated that the MAP-induced free-running oscillation of rat locomotion with drinking application of MAP exhibited a sensitization phenomenon (Nikaido et al., 1999). Interestingly, Andretic et al. (1999) reported that flies mutant for *period*, *clock*, *cycle*, and *doubletime* lack sensitization to repeated cocaine administration, but flies mutant for *timeless* do not. On the other hand, in contrast to *Drosophila melanogaster,* mutation of the *Clock* gene that regulates circadian rhythm in mice does not affect acute or sensitized responses to cocaine (Sidiropoulou et al., 2000). Thus, in mammals, the *Clock* gene is not required for the induction of behavioral sensitization to cocaine. Therefore, we should investigate whether the sensitized increase in *mPer1* expression reflects the result or cause using *mPer1* gene mutant mice. Taken together, the results seem to indicate that MAP-induced sensitized expression of *mPer1* may be related, at least, to the sensitized phenomenon.

In conclusion, the present results demonstrate that the activation of both D1 and NMDA receptors plays an important role in causing MAP-induced expression of *mPer1* in the CPu. Furthermore, behavioral sensitization induced by repeated MAP injection is associated with sensitization of MAP-induced *mPer1* expression.

References

Albrecht U, Sun ZS, Eichele G and Lee CC (1997) A differential response of two putative mammalian circadian regulators, mper1 and mper2, to light. *Cell* **91:** 1055–1064.

Andretic R, Chaney S and Hirsh J (1999) Requirement of circadian genes for cocaine sensitization in *Drosophila*. *Science (Wash DC)* **285:**1066–1068.

Das S, Grunert M, Williams L and Vincent SR (1997) NMDA and D1 receptors regulate the phosphorylation of CREB and the induction of c-fos in striatal neurons in primary culture. *Synapse* **25:**227–233.

Dunlap JC (1999) Molecular bases for circadian clocks. *Cell* **96:**271–290.

Finnegan KT and Taraska T (1996) Effects of glutamate antagonists on methamphetamine and 3,4-methylenedioxymethamphetamine-induced striatal dopamine release in vivo. *J Neurochem* **66:**1949–1958.

Graybiel AM, Moratalla R and Robertson HA (1990) Amphetamine and cocaine induce drug-specific activation of the c-fos gene in striosome-matrix compartments and limbic subdivisions of the striatum. *Proc Natl Acad Sci USA* **87:**6912–6916.

Grosse J and Davis FC (1999) Transient entrainment of a circadian pacemaker during development by dopaminergic activation in Syrian hamsters. *Brain Res Bull* **48:**185–194.

Honma K, Honma S and Hiroshige T (1987) Activity rhythms in the circadian domain appear in suprachiasmatic nuclei lesioned rats given methamphetamine. *Physiol Behav* **40:**767–774.

Horikawa K, Yokota S, Fuji K, Akiyama M, Moriya T, Okamura H and Shibata S (2000) Nonphotic entrainment by 5-$HT_{1A/7}$ receptor agonists accompanied by reduced *Per1* and *Per2* mRNA levels in the suprachiasmatic nuclei. *J Neurosci* **20:**5867–5873.

Inouye ST and Shibata S (1994) Neurochemical organization of circadian rhythm in the suprachiasmatic nucleus. *Neurosci Res* **20:**109–130.

Konradi C, Cole RL, Heckers S and Hyman SE (1994) Amphetamine regulates gene expression in rat striatum via transcription factor CREB. *J Neurosci* **14:**5623–5634.

Konradi C, Leveque JC and Hyman SE (1996) Amphetamine and dopamine-induced immediate early gene expression in striatal neurons depends on postsynaptic NMDA receptors and calcium. *J Neurosci* **16:**4231–4239.

Kume K, Zylka MJ, Sriram S, Shearman LP, Weaver DR, Jin X, Maywood ES, Hastings MH and Reppert SM (1999) mCRY1 and mCRY2 are essential components of the negative limb of the circadian clock feedback loop. *Cell* **98:**193–205.

Kuribara H (1994) Can posttreatment with the selective dopamine D2 antagonist, YM-09151-2, inhibit induction of methamphetamine sensitization? Evaluation by ambulatory activity in mice. *Pharmacol Biochem Behav* **49:**323–326.

Kuribara H (1995) Dopamine D1 receptor antagonist SCH 23390 retards methamphetamine sensitization in both combined administration and early posttreatment schedules in mice. *Pharmacol Biochem Behav* **52:**759–763.

Kuribara H (1996) Effects of sulpiride and nemonapride, benzamide derivatives having distinct potencies of antagonistic action on dopamine D2 receptors, on sensitization to methamphetamine in mice. *J Pharm Pharmacol* **48:**292–296.

Kuribara H and Uchihashi Y (1993) Dopamine antagonists can inhibit methamphetamine sensitization, but not cocaine sensitization, when assessed by ambulatory activity in mice. *J Pharm Pharmacol* **45:**1042–1045.

Mistlberger RE (1994) Circadian food-anticipatory activity: Formal models and physiological mechanisms. *Neurosci Biobehav Rev* **18:**171–195.

Moriya T, Horikawa K, Akiyama M and Shibata S (2000) Correlative association between *N*-methyl-D-aspartate receptor-mediated expression of period genes in the suprachiasmatic nucleus and phase shifts in behavior with photic entrainment of clock in hamsters. *Mol Pharmacol* **58:**1554–1562.

Muratake T, Toyooka K, Hayashi S, Ichikawa T, Kumanishi T and Takahashi Y (1998) Immunohistochemical changes of the transcription regulatory factors in rat striatum after methamphetamine administration. *Ann NY Acad Sci* **844:**21–26.

Nikaido T, Moriya T, Takabayashi R, Akigama M and Shibata S (1999) Sensitization of methamphetamine-induced disorganization of daily locomotor activity rhythm in male rats. *Brain Res* **845:**112–116.

Ohno M, Yoshida H and Watanabe S (1994) NMDA receptor-mediated expression of Fos protein in the rat striatum following methamphetamine administration: Relation to behavioral sensitization. *Brain Res* **665:**135–140.

Shearman LP, Zylka MJ, Weaver DR, Kolakowski LF Jr and Reppert SM (1997) Two period homologs: Circadian expression and photic regulation in the suprachiasmatic nuclei. *Neuron* **19:**1261–1269.

Shibata S, Minamoto Y, Ono M and Watanabe S (1994) Aging impairs methamphetamine-induced free-running and anticipatory locomotor activity rhythms in rats. *Neurosci Lett* **172:**107–110.

Shibata S, Ono M, Fukuhara N and Watanabe S (1995) Involvement of dopamine, *N*-methyl-D-aspartate and sigma receptor mechanisms in methamphetamine-induced anticipatory activity rhythm in rats. *J Pharmacol Exp Ther* **274:**688–694.

Shigeyoshi Y, Taguchi K, Yamamoto S, Takekida S, Yan L, Tei H, Moriya T, Shibata S, Loros JJ, Dunlap JC, et al. (1997) Light-induced resetting of a mammalian circadian clock is associated with rapid induction of the *mPer1* transcript. *Cell* **91:**1043–1053.

Sidiropoulou K, Cooper DC, Baker L, Vitaterna MH, Takahashi JS and White FJ (2000) Basal hyperactivity and behavioral sensitization to cocaine in *Clock* mutant mice. *Soc Neurosci Abstr* **26:**525.

Sun ZS, Albrecht U, Zhuchenko O, Bailey J, Eichele G and Lee CC (1997) RIGUI, a putative mammalian ortholog of the *Drosophila period* gene. *Cell* **90:**1003–1011.

Takumi T, Matsubara C, Shigeyoshi Y, Taguchi K, Yagita K, Maebayashi Y, Sakakida Y, Okumura K, Takashima N and Okamura H (1998) A new mammalian *period* gene predominantly expressed in the suprachiasmatic nucleus. *Genes Cells* **3:**167–176.

Tei H, Okamura H, Shigeyoshi Y, Fukuhara C, Ozawa R, Hirose M and Sakaki Y (1997) Circadian oscillation of a mammalian homologue of the *Drosophila period* gene. *Nature (Lond)* **389:**512–516.

Ujike H, Onoue T, Akiyama K, Hamamura T and Otsuki S (1989) Effects of selective D-1 and D-2 dopamine antagonists on development of methamphetamine-induced behavioral sensitization. *Psychopharmacology (Berl)* **98:**89–92.

Vanderschuren LJ, Schmidt ED, De Vries TJ, Van Moorsel CA, Tilders FJ and Schoffelmeer AN (1999) A single exposure to amphetamine is sufficient to induce long-term behavioral, neuroendocrine, and neurochemical sensitization in rats. *J Neurosci* **19:**9579–9586.

Viswanathan N, Weaver DR, Reppert SM and Davis FC (1994) Entrainment of the fetal hamster circadian pacemaker by prenatal injections of the dopamine agonist SKF 38393. *J Neurosci* **14:**5393–5398.

Weaver DR and Reppert SM (1995) Definition of the developmental transition from dopaminergic to photic regulation of c-fos gene expression in the rat suprachiasmatic nucleus. *Brain Res Mol Brain Res* **33:**136–148.

Wolf ME and Xue CJ (1999) Amphetamine-induced glutamate efflux in the rat ventral tegmental area is prevented by MK-801, SCH 23390, and ibotenic acid lesions of the prefrontal cortex. *J Neurochem* **73:**1529–1538.

Yagita K and Okamura H (2000) Forskolin induces circadian gene expression of *rPer1*, *rPer2* and *dbp* in mammalian rat-1 fibroblasts. *FEBS Lett* **465:**79–82.

Yamaguchi S, Mitsui S, Miyake S, Yan L, Onishi H, Yagita K, Suzuki M, Shibata S, Kobayashi M and Okamura H (2000) The 5′ upstream region of *mPer1* gene contains two promoters and is responsible for circadian oscillation. *Curr Biol* **10:**873–876.

Yan L, Takekida S, Shigeyoshi Y and Okamura H (1999) *Per1* and *Per2* gene expression in the rat suprachiasmatic nucleus: Circadian profile and the compartment-specific response to light. *Neuroscience* **94:**141–150.

Yoshida H, Ohno M and Watanabe S (1995) Roles of dopamine D1 receptors in striatal fos protein induction associated with methamphetamine behavioral sensitization in rats. *Brain Res Bull* **38:**393–397.

Zylka MJ, Shearman LP, Weaver DR and Reppert SM (1998) Three *period* homologs in mammals: Differential light responses in the suprachiasmatic circadian clock and oscillating transcripts outside of brain. *Neuron* **20:**1103–1110.

Send reprint requests to: Shigenobu Shibata, Department of Pharmacology and Brain Science, School of Human Sciences, Waseda University, Tokorozawa, Saitama 359-1192, Japan. E-mail: shibata@human.waseda.ac.jp

Journal of Neurochemistry, 2001, 77, 618–627

Involvement of calcium–calmodulin protein kinase but not mitogen-activated protein kinase in light-induced phase delays and *Per* gene expression in the suprachiasmatic nucleus of the hamster

Shin-ichi Yokota,* Masakazu Yamamoto,* Takahiro Moriya,† Masashi Akiyama,* Kohji Fukunaga,‡ Eishichi Miyamoto‡ and Shigenobu Shibata*,†

**Department of Pharmacology and Brain Science Waseda University, Tokorozawa, Saitama, Japan*

†ARCHS, School of Human Sciences, Waseda University, Tokorozawa, Saitama, Japan

‡Department of Pharmacology, Kumamoto University School of Medicine, Kumamoto, Japan

Abstract

It is known that Ca^{2+}-dependent phosphorylation of cAMP response element binding protein (CREB) and the rapid induction of *mPer1* and *mPer2,* mouse *period* genes in the suprachiasmatic nucleus (SCN) are associated with light-induced phase shifting. The CREB/CRE transcriptional pathway has been shown to be activated by calcium/calmodulin dependent kinase II (CaMKII) and mitogen-activated protein kinase (MAPK); however, there is a lack of evidence concerning whether the activation of CaMKII and/or MAPK elicited by photic stimuli are associated with the change in *Per* gene expression and behavioral phase shifting. In this experiment, we found there was an inhibitory effect by KN93, CaMKII inhibitor, on hamster *Per1* and *Per2* expression in the SCN and on phase delays in wheel running rhythm induced by light pulses. PD98059 and U0126, MAPK kinase inhibitors, however, affected neither light-induced *Per1* and *Per2* expression nor behavioral phase delays, even though PD98059 attenuated the light-induced phosphorylation of MAPK in the SCN. The present findings demonstrate that the light-induced activation of CaMKII plays an important role in the induction of *Per1* and *Per2* mRNA in the hamster SCN as well as phase shifting. These results suggest that gated induction of *Per1* and/or *Per2* genes through CaMKII-CREB/CRE accompanied with photic stimuli may be a critical step in phase shifting.

Keywords: calcium/calmodulin dependent kinase, circadian rhythm, hamster, mitogen-activated protein kinase, *Per* genes, suprachiasmatic nucleus.

J. Neurochem. (2001) **77**, 618–627.

In mammals, daily physiological and behavioral rhythms are governed by a biological clock located in the suprachiasmatic nucleus (SCN) of the hypothalamus (Hastings 1997). Recent studies on the molecular aspects of clock genes have produced a functional model of circadian rhythms (for review, see Dunlap 1999), in which *mPer1*, *mPer2* and *mPer3* exhibit circadian rhythmic expression in the SCN (Albrecht *et al.* 1997; Shearman *et al.* 1997; Sun *et al.* 1997; Tei *et al.* 1997; Takumi *et al.* 1998a; Takumi *et al.* 1998b; Zylka *et al.* 1998). Light exposure induces *mPer1* and *mPer2* mRNA expression in the SCN (Shearman *et al.* 1997; Shigeyoshi *et al.* 1997; Takumi *et al.* 1998a). Thus, environmental light strongly synchronizes these endogenous circadian rhythms by conveying photic signals from the retina to the SCN via the retinohypothalamic tract. Released glutamate from the retinohypothalamic tract activates NMDA receptors (Ebling 1996; Ding *et al.* 1997), which

Received July 27, 2000; revised manuscript received December 11, 2000; accepted January 12, 2001.

Address correspondence and reprint requests to Dr Shigenobu Shibata, Department of Pharmacology and Brain Science, School of Human Sciences, Waseda University, Tokorozawa, Saitama 359–1192, Japan. E-mail: shibata@human.waseda.ac.jp

Abbreviations used: CaMKII, calcium/calmodulin dependent kinase II; CREB, cAMP response element binding protein; CT, circadian time; DMSO, dimethyl sulfoxide; ECL, enhanced chemiluminescence; i.c.v., intracerebroventricular; MAPK, mitogen-activated protein kinase; PBS, phosphate-buffered saline; PKA, protein kinase A; PVDF, polyvinylidene difluoride; SCN, suprachiasmatic nucleus; SSC, standard saline citrate; TCA, trichloroacetic acid; ZT, zeitgeber time.

in turn mediate Ca^{2+} entry and Ca^{2+}-dependent phosphorylation of cAMP response element binding protein (CREB). Cyclic AMP response element binding protein regulates the expression of many immediate-early genes such as *c-fos* and *jun-B* through downstream gene transcription (Sassone-Corsi *et al.* 1988; Nakajima *et al.* 1993; Amato *et al.* 1996). Interestingly, the promoters for these immediate-early genes contain at least one CRE. Therefore, it is reasonable to hypothesize that CRE may play a central role in mediating the ability of light to trigger *Per1* induction.

The CREB/CRE transcriptional pathway has been shown to be activated by various kinases such as protein kinase A (PKA), calcium/calmodulin dependent kinase II (CaMKII) and mitogen-activated protein kinase (MAPK)(Gonzalez and Montminy 1989; Sheng *et al.* 1991; Xing *et al.* 1996; Impey *et al.* 1998). Inhibition of PKA in the SCN *in vivo* did not affect light-induced phase shifts (Mathur *et al.* 1996). Our recent works along with other papers have demonstrated that CaM inhibitors or CaMKII inhibitor, KN-62, suppressed light pulse-induced phase shift of activity rhythm (Golombek and Ralph 1994, 1995), c-Fos expression (Fukushima *et al.* 1997), CREB phosphorylation in the SCN (Golombek and Ralph 1995). In addition, Hallbeck *et al.* (1996) showed the abundant expression of CaMKII in the rat SCN. Recently, Schurov *et al.* (1999) revealed an important role for CaMKII/IV in the glutamatergic induction of CREB phosphorylation in SCN neurons *in vitro*. These papers strongly suggest the importance of CaMKII in light-induced phase shifting.

On the other hand, Obreitan *et al.* (1998, 1999) prefer the critical role of MAPK phosphorylation in the SCN as an explanation for light-induced phase shifts. Recent papers have demonstrated the importance of MAPK in corresponding with light-induced phase shifts of the chick pineal clock oscillation (Sanada *et al.* 2000) and with TPA-induced oscillations of *Per1* and *Per2* gene expression in NIH-3T3 fibroblasts (Akashi and Nishida 2000). At present, we do not know whether CaMKII and/or MAPK activate a CREB/CRE transcriptional pathway eliciting light-induced *Per1* and/or *Per2* gene expression in the SCN. Therefore, in the present experiments we examined the effects of CaMKII or MAPKK (MAPK kinase) inhibitors on light-induced behavioral phase shifts and *Per1* and *Per2* expression in the hamster SCN.

Materials and methods

Animals

Male golden hamsters (*Mesocricetus auratus*, Tokyo Laboratory Animal Co. Ltd, Tokyo, Japan) weighing 140–240 g were used for this study. All animals were maintained under controlled environmental conditions (23 ± 2°C room temperature; 12–12 h light-dark cycle, lights on at 08 : 30 h) for at least 2 weeks before experimental use. Food and water were provided *ad libitum*. Animals were treated in accordance with the Law (No. 141) and Notification (No. 6) of Japanese Government. Under the light–dark cycle, zeitgeber time (ZT) referred to the animal colony light–dark cycle. ZT0 was designated as lights-on and ZT12 as lights-off time. In free-running conditions under constant darkness, circadian time (CT) was defined instead of ZT, and CT 12 referred to the onset of wheel-running.

Drugs and antibodies

All drugs were freshly prepared. KN-93 (Research Biochemical Inc., Natick, MA, USA), a CaMKII/IV inhibitor, KN-92 (Research Biochemical Inc.), an inactive analog, PD98059 (Research Biochemical Inc.), U0126 (Promega, Madison, WI, USA) MAPKK inhibitors, and SB203580 (Research Biochemical Inc.), a p38 kinase inhibitor, were dissolved in 10% dimethyl sulfoxide (DMSO) and administered by intracerebroventricular (i.c.v.) injection.

The Thr286/287 phospho-specific antibody, used as a phosphorylated CaMKII antibody, and the anti-CaMKII antibody, used as a nonphosphorylated CaMKII antibody (raised in rabbits by injecting the peptide) were obtained as previously reported (Fukunaga *et al.* 1988). The phospho MAPK antibody was purchased from Cell Signaling Technology (Beverly, MA, USA).

Recording of wheel-running rhythm

For recording of the locomotor activity, hamsters were housed individually in transparent plastic cages (35 × 20 × 20 cm), each equipped with a running wheel 15 cm in diameter, that closed a microswitch with each revolution. Wheel-running activity was continuously recorded in 6 min epochs by a PC-9801 computer.

Surgery

A stainless steel guide cannulae (8.0 mm, external diameter 0.7 mm and internal diameter 0.35 mm) for i.c.v. injection was implanted into the lateral ventricle by using a stereotaxic apparatus (Narishige Co., Tokyo, Japan). Hamsters were anesthetized with Nembutal and then mounted in a stereotaxic apparatus. Stereotaxic coordinates were 0.5 mm anterior, 1.8 mm lateral to the bregma, and 3.8 mm ventral to the skull face. After fixing the guide cannulae to the skull, a dummy cannulae (8.5 mm, external diameter 0.35 mm) was inserted into the guide cannulae to prevent a block of tubing until i.c.v. injection. After 2 days recovery, animals were moved to continuous darkness for at least 2 weeks before drug administration.

Intracerebroventricular injections

After free-running for 14–20 days in constant darkness, each hamster was randomly assigned to KN-93 (1.5 nmol/5 μL), KN-92 (1.5 nmol/5 μL), PD98059 (5.0 nmol/5 μL), U0126 (5.0 nmol/5 μL), SB203580 (10.0 nmol/5 μL), or vehicle (10% DMSO 5 μL/hamster). Each drug was unilaterally injected into the lateral ventricle via an injection cannulae (external diameter 0.35 mm) extending 0.5 mm below the tip of the guide cannulae at a rate of 1 μL/min using a 10-μL Hamilton syringe. Under a dim red light, animals were anesthetized with ether, and then drugs were injected into the lateral ventricle. Injection was performed at CT 13.25 (15 min prior to light application) and followed by light application (300 lux for 15 min) at CT 13.5. After light application, animals were returned to their home cages in constant darkness.

Immunohistochemistry

After 2 days of being kept in constant darkness, some hamsters received a 300-lux light pulse for 5 min or 15 min at CT 13.5,

while others were kept in darkness. Hamsters were then perfused immediately after the offset of light exposure, or 15 or 75 min after 15 min light exposure. For some studies, hamsters received an i.c.v. injection of the drug 15 min prior to light exposure. Hamsters were deeply anesthetized with an overdose of Nembutal and perfused transcardially with 50 mL of saline, followed by 50 mL of ice-cold 4% paraformaldehyde−0.1 M phosphate-buffered saline (PBS; pH 7.4). Brains were removed from the skull, fixed with 30 mL of 4% paraformaldehyde−0.1 M PBS, and transferred to 20% and 30% sucrose−0.1 M PBS solution for 24 h and 48 h at 4°C, respectively. Hypothalamic blocks were cut into 40 μm-thick sections from the rostral to caudal SCN on a freezing microtome. Alternate sections were incubated for 48 h at 4°C with one of the following: an anti-pCaMKII antibody diluted at 1 : 2000, or a CaMKII antibody diluted at 1 : 1000, or a pMAPK antibody diluted at 1 : 1000 in 0.1 M PBS containing 1% normal goat serum and 0.3% Triton X-100 (PBSGT). All sections were then washed three times with 0.1 M PBS (10 min each) and incubated for 2 h with biotinylated goat anti-rabbit antibody (diluted to 1 : 200 with PBSGT; Vectastain). The sections were washed again three times with 0.1 M PBS and this time incubated for 2 h in an avidin–biotin complex solution (Vectastain ABC kit, Burlingame, CA, USA). After a third wash with 0.1 M PBS, sections were visualized with diaminobenzidine as a chromogen and mounted on gelatin-coated glass slides. Except for the incubation with a primary antibody, all procedures were performed at room temperature. The numbers of cells expressing CaMKII and pCaMKII immunoreactivity were counted on selected sections (8–10 sections) from rostral to caudal SCN by an independent observer. The average cell numbers per hamster were calculated, and then average cell numbers/SCNs were calculated for each treatment group. Unfortunately, we could not count the number of cells expressing a pMAPK positive reaction. Therefore, in order to confirm the effect of PD98059 on the phosphorylation level of MAPK, we measured the density of the stained SCN area and lateral hypothalamus area as a control area using the public domain NIH Image program (written by Wayne Rasband at the U.S. National Institute of Health).

Western blot analysis

After 2 days of constant darkness, some hamsters received an i.c.v. injection of KN-93, KN-92 or vehicle (10% DMSO) 15 min prior to light pulse, and then some hamsters received a 300-lux light pulse for 15 min at CT 13.5, and colleagues remained in darkness. After offset of the light pulse, the hamsters were returned to constant darkness. Fifteen minutes after the onset of light, hamsters were deeply anesthetized with ether and perfused transcardially with 50 mL of ice-cold saline, containing 25 mM NaF, 15 mM $Na_4P_2O_7$ and 1 mM Na_3VO_4. The brain was rapidly removed from the skull and quickly frozen using the powder from dry ice, and then fixed with a solution containing 10% trichloroacetic acid (TCA) for 24 h at 4°C. After fixing with 10% TCA solution, hypothalamic blocks were cut into 300-μm thick sections (two slices/hamster) from the rostral to caudal SCN on a freezing microtome. Under a microscope, a couple of SCNs were then punched out by a stainless steel cannulae (internal diameter 0.6 mm), collected into 200 μL of 10% TCA solution (pooled for two hamsters), and sonicated by Handy Sonic (Tomy Seiko Co. Ltd, Japan). After centrifugation at 20 000 *g* for 5 min at 4°C, the supernatant was removed and 0.5 mL of sterile water was added in order to wash out the TCA remaining in the tissue. Next, samples were centrifuged and the water was exchanged with 50 μL of homogenizing solution: 50 mM MOPS [100 mM KCl, 0.5 mM $MgCl_2$, 0.1 mM EDTA, 1 mM EGTA, 0.32 M sucrose, 1 mM Na_3VO_4, 1 mM (DL)-dithiothreitol, 0.2 mM (*p*-amidinophenyl)-methanesulfonyl fluoride hydrochloride, 5 μg/ml pepstatin A, 50 μg/ml leupeptin, 100 nM calyculin A]. This solution was mixed with 3 × SDS buffer [50 mM Tris-HCl (pH 6.8), 2% SDS, 10% glycerol, 6% 2-mercaptoethanol and 0.02% bromophenol blue] and then boiled for 2 min. Samples were electrophoresed on a 7.5% polyacrylamide gel (Laemmli 1970) and transferred onto a polyvinylidene difluoride (PVDF) membrane (Millipore Corporation, Bedford, MA, USA). After a treatment with blocking buffer, the membrane was incubated with an anti-CaMKII or pCaMKII antibody (1 : 500 dilution, respectively) at 4°C overnight and visualized by an enhanced chemiluminescence (ECL) kit (Amersham Pharmacia Biotech Inc., Buckinghamshire, UK). The immunological activity was analyzed by use of an image analyzing system (GS-250 Molecular Imager, Bio-Rad Laboratories, Hercules, CA, USA).

***In situ* hybridization using an RI**

After 2 days of constant darkness, hamsters received an i.c.v. injection of each drug 15 min prior to light pulse at CT 13.5. Some hamsters then received a 300-lux light pulse for 15 min at CT 13.5, while others were kept in darkness. After the offset of light exposure, the hamsters were returned to constant darkness. At CT 15 (90 min after light onset), hamsters were deeply anesthetized with an overdose of Nembutal and perfused transcardially with 50 mL of ice-cold 4% paraformaldehyde−0.1 M phosphate buffer (PB; pH 7.4). Brains were removed from the skull, fixed with 30 mL of 4% paraformaldehyde−0.1 M PB, and transferred to a 20% sucrose-0.1 M PB solution for 24 h at 4°C, respectively. Coronal hypothalamic sections (30 μm thick) were made with a cryostat and an alternative series of sections were collected into 2 × standard saline citrate (SSC) for *Per1*, *Per2* and *Per3*. These sections were then treated with proteinase K [1.0 μg/mL, 10 mM Tris buffer (pH 7.5), 10 mM EDTA] for 10 min at 37°C, 4% paraformaldehyde−0.1 M PB for 5 min, 2 × SSC for 5 min, followed by 0.25% acetic anhydride in 0.1 M triethanolamine for 10 min and 2 × SSC for 5 min. Hybridization was carried out overnight at 60°C in 4 mL of hybridization solution buffer [50% formamide, 6 × SSC, 0.1 mg/mL denatured salmon sperm DNA, 1 × Denhardt's solution (0.02% Ficoll, 0.02% polyvinyl pyrolidone, 0.02% bovine serum albumin) and 10% dextran sulfate] containing ^{33}P-labeled cRNA probes. Radioisotope [RI: a[^{33}P]UTP (Perkin Elmer Inc., Boston, MA, USA)]-labeled antisense cRNA was made from restriction enzyme-linearized cDNA templates as described in our recent paper (Horikawa *et al.* 2000). All steps prior to and including hybridization were conducted under RNase-free conditions. Following hybridization, these sections were rinsed in 2 × SSC/50% formamide for 45 min followed by 15 min at 60°C, treated with RNase A for 30 min at 37°C, 2 × SSC/50% formamide for 15 min twice at 60°C, and 0.4 × SSC for 30 min at 60°C. Then each section was mounted on a glass. RI *in situ* hybridization images were visualized by autoradiograms of BioMax film (Kodak) and analyzed using an image analyzing system (MCID, Imaging Research Inc., St Catharines, Ontario, Canada) after conversion into the optical densities by ^{14}C-autoradiographic microscales (Amersham).

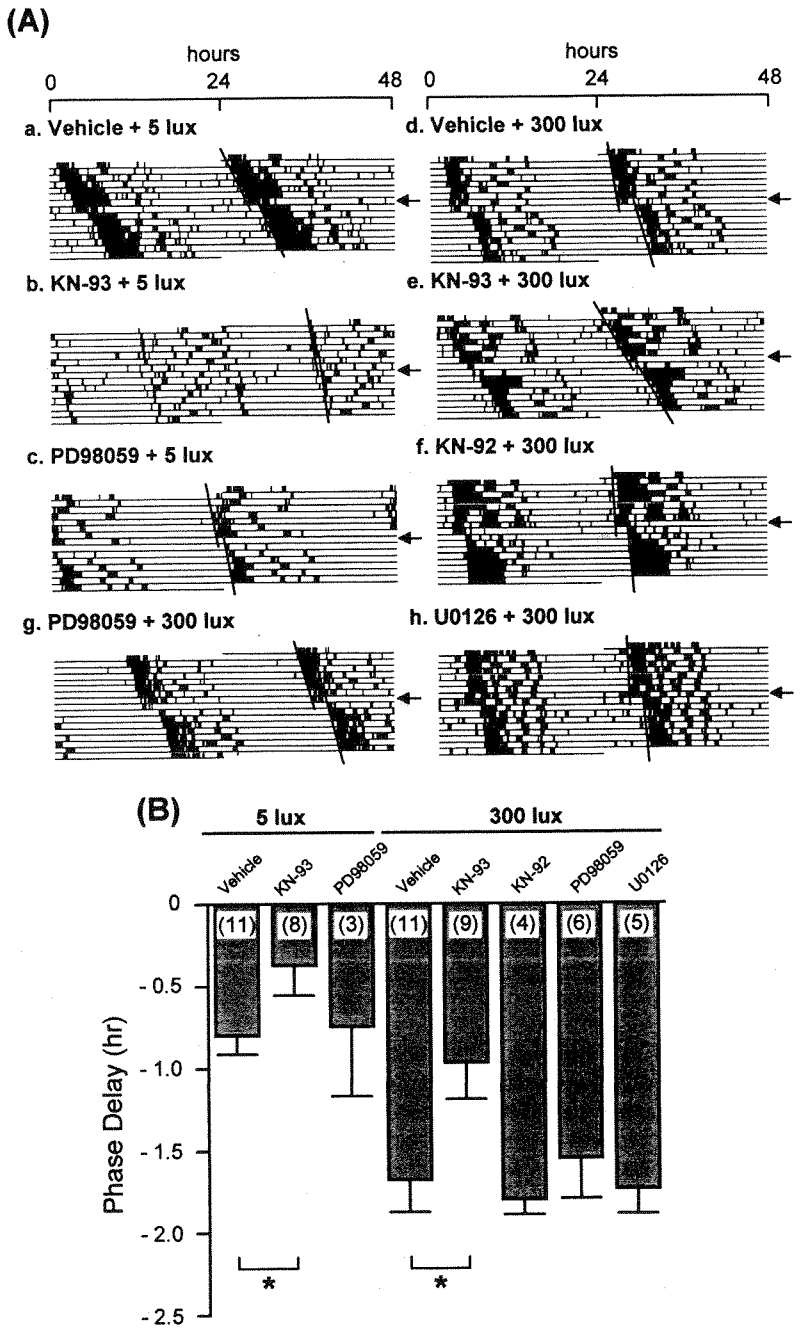

Fig. 1 Effect of KN-93, KN-92, PD98059 and U0126 on light-induced phase delays in wheel-running rhythm. (A) Double-plotted actogram shows wheel-running activity records of hamsters in constant darkness. Time of day is indicated horizontally and consecutive days vertically. Arrows indicate the day when light pulse and drug injection were administered. Eye-fitted lines to activity onset are shown in each actogram, and the difference between these two lines indicates a phase change. Each hamster received an intracerebroventricular injection of vehicle (a and d), KN-93 (1.5 nmol/5 μL; i.c.v.; b and e), KN-92 (1.5 nmol/5 μL; i.c.v.; f), PD98059 (5.0 nmol/5 μL; i.c.v.; c and g), or U0126 (5.0 nmol/5 μL; i.c.v.; h), followed by 15 min of light application of low (5 lux; a, b and c) or high (300 lux; d–h) intensity at CT 13.5. (B) Mean value of phase delay, as observed in (A). The number of animals is shown in parentheses. *$p < 0.05$ (Dunnett's test).

Statistics

The data are expressed as the mean ± SEM, and statistical analysis was performed using a one-way analysis of variance followed by Dunnett's test or the Student's *t*-test. Differences were considered significant if $p < 0.05$.

Results

Effect of KN-93 on light-induced phase delays in wheel-running rhythm

In the behavioral experiment (Fig. 1), we examined whether KN-93 attenuated the light-induced phase delays in hamster wheel-running activity rhythm under constant darkness. High (300 lux for 15 min) or low (5 lux for 15 min) intensity light pulses at CT 13.5 caused clear phase delays (an averaged value of −1.65 ± 0.23 h and −0.81 ± 0.10 h, respectively). Pre-treatment with KN-93 (1.5 nmol/5 μL; i.c.v.) significantly attenuated the high or low intensity light-induced phase delays. Whereas, KN-92 (1.5 nmol/5 μL; i.c.v.) did not reduce light-induced phase delays (Fig. 1B). Pre-injection of PD98059 (5.0 nmol/5 μL; i.c.v.), however, failed to attenuate the high or low light-induced phase delays. In addition, U0126 (5.0 nmol/5 μL;

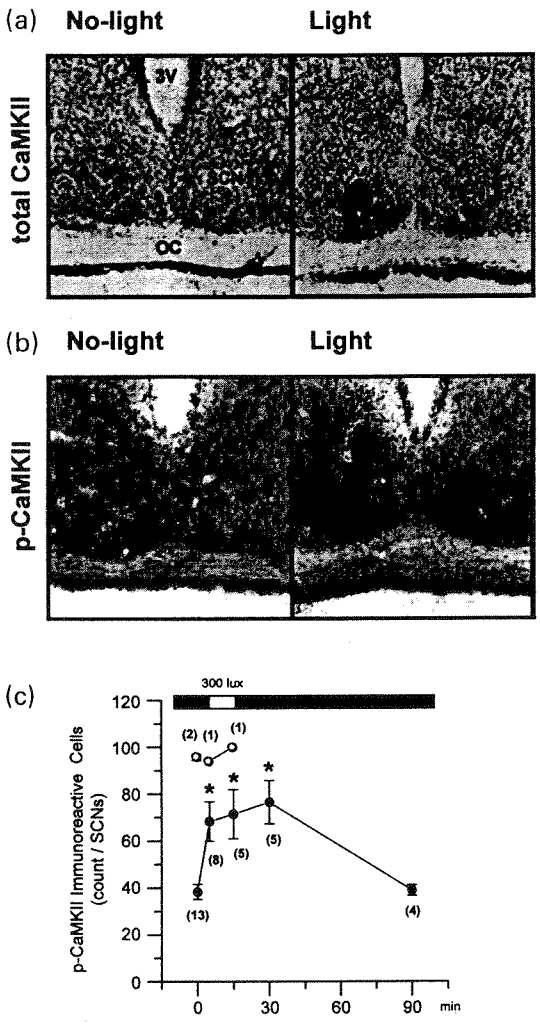

Fig. 2 Effect of light exposure on the phosphorylation of CaMKII. (a) and (b) representative photomicrographs of cells immunoreactive to anti-CaMKII (a) or anti-pCaMKII (b) antibody in the hamster SCN. Some hamsters received a light pulse (300 lux for 15 min) at CT 13.5 and were killed 15 min later (right) and colleagues did not receive a light pulse (left). Figure 2(C) shows the time course for the number of immunoreactive cells to anti-CaMKII (○) or anti-pCaMKII (●) in the hamster SCN. The number of animals is shown in parentheses. 3 V, third ventricle; OC, optic chiasm; SCN, suprachiasmatic nuclei. $^*p < 0.01$ (Dunnett's test versus no-light control).

i.c.v.), a more effective MAPKK inhibitor did not affect high light-induced phase delays. A kinase inhibitor of p38 (10 nmol/5 μL; i.c.v.), SB203580 (10 nmol/5 μL; i.c.v.), did not affect low intensity light-induced phase delays (data not shown).

Effect of light exposure on the phosphorylation of CaMKII

Figure 2 shows typical photomicrographs of cells immunoreactive to anti-CaMKII or anti-pCaMKII antibody in the hamster SCN. Large numbers of CaMKII- or pCaMKII-immunoreactive cells were seen in the SCN (Figs 2a and b). As revealed by pCaMKII immunoreactivity, light exposure (300 lux for 15 min) at CT 13.5 significantly enhanced the phosphorylation of CaMKII, especially in the ventrolateral part of the SCN where the retinohypothalamic pathways arrive (Fig. 2b). On the other hand, the amount of total CaMKII immunoreactive cells was not affected by light application (Fig. 2a). Figure 2(c) shows the time course of light-induced phosphorylation of CaMKII in the hamster SCN. Light pulse application for 5 min (68.4 ± 8.4 cells/SCN, $n = 8$) and 15 min (71.4 ± 10.5 cells/SCN, $n = 5$) immediately induced the phosphorylation of CaMKII in the SCN. The peak level of CaMKII phosphorylation occured 15 min after light application for 15 min (76.5 ± 9.2 cells/SCN, $n = 5$), in comparison to the no light controls (38.3 ± 3.2 cells/SCN, $n = 13$). Ninety minutes after the light application, phosphorylation of CaMKII returned to the base line level of nonlight controls (39.0 ± 2.3 cells/SCN, $n = 4$).

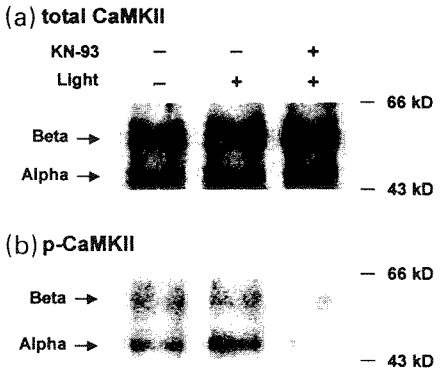

Fig. 3 Effect of KN-93 on light-induced phosphorylation of CaMKII. We examined whether or not KN-93 attenuated the light-induced phosphorylation of CaMKII using western blot analysis. Immunoreactive bands to anti-CaMKII (a) or anti-pCaMKII (b) antibodies are shown in (a) and (b). The upper band probably represents the β-subtype (≈ 60 kDa) and the lower band probably represents the α-subtype (≈ 50 kDa). Some hamsters received a 300-lux light pulse for 15 min at CT 13.5 (center and right) and were then killed 15 min later, while others did not receive any light pulses (left; control). Injection of KN-93 (1.5 nmol/5 μL; i.c.v.) was given 15 min prior to the light pulse (right).

Effect of KN-93 on light-induced phosphorylation of CaMKII

In this experiment, we examined whether KN-93 attenuated the light-induced phosphorylation of CaMKII using western blot analysis. Figure 3 shows the bands immunoreactive to anti-CaMKII (Fig. 3a) or anti-pCaMKII (Fig. 3b) antibody. It is known that among the four subtypes of CaMKII termed α, β, γ, δ, the α (≈ 50 kDa) and β (60 kDa) subtypes are dominant in the brain (Tobimatsu and Fujisawa 1989). In Figs 3(a and b), the upper bands probably represent

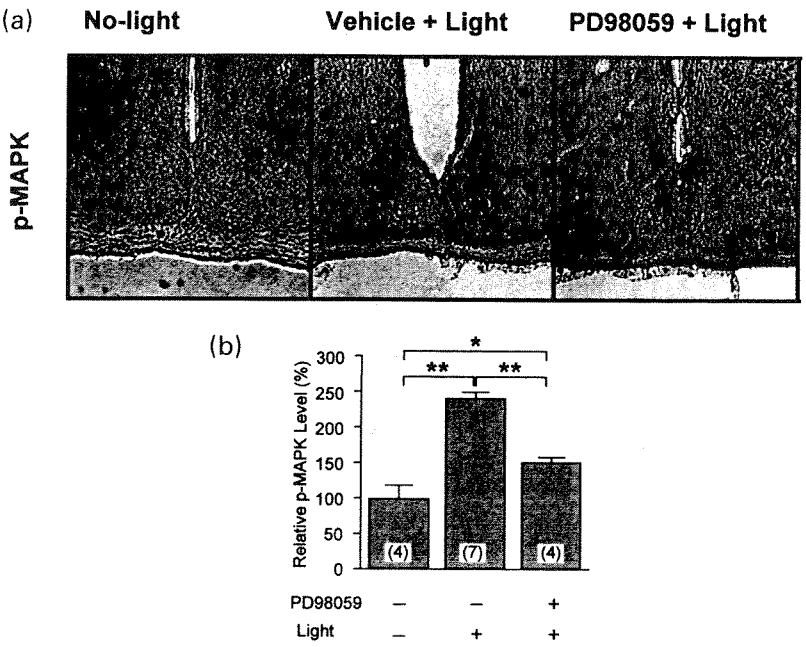

Fig. 4 Effect of PD98059 on light-induced phosphorylation of MAPK. (a) Representative photomicrographs of cells immunoreactive to the anti-pMAPK antibody in the hamster SCN. Vehicle (middle) or PD98059 (5.0 nmol/5 μL; i.c.v.)(right), a MAPKK inhibitor, was administered 30 min prior to the light pulse (300 lux for 15 min) at CT 13.5. Animals were killed 15 min after the 15-min light exposure. For control experiment, vehicle (left) was administrated without light. (b) Relative value of pMAPK immunoreactivity in the SCN. The level of pMAPK immunoreactivity was determined by examining the density of stained SCN area and the adjusted lateral hypothalamic area as a control area using the public domain NIH Image program (written by Wayne Rasband at the U.S. National Institutes of Health). Control tissue density was set at 100%. pMAPK staining density decreased with preinjection of PD98059 in comparison to the vehicle injection group. The number of animals is shown in parentheses. $^*p < 0.05$ (Student's *t*-test).

the β-subtype and the lower bands probably represent the α-subtype. As revealed by the immunoreactive bands of pCaMKII (Fig. 3b), light exposure (300 lux for 15 min) at CT 13.5 rapidly induced phosphorylation of the CaMKII α-subtype (38% of total CaMKII for non-light control and 49% of total CaMKII for light control) but not β-subtype (33% of total CaMKII for non-light control and 29% of total CaMKII for light control). Pre-injection with KN-93 strongly suppressed the light-induced phosphorylation of both CaMKII α- and β-subtypes (α: 6.4%, β: 7.4% of total CaMKII, respectively). Administration of KN-93 without light exposure moderately reduced phosphorylation of CaMKII α- (45% for vehicle injection and 38% for KN-93 injection) and β-subtype (72% for vehicle injection and 28% for KN-93 injection). On the other hand, light-induced phosphorylation of CaMKIIα- and β-subtypes was slightly attenuated by pre-injection of KN-92 (α: 80% for vehicle injection and 70% for KN-92 injection, β: 121% for vehicle injection and 95% for KN-92 injection, respectively). The intensity of total CaMKII immunoreactive bands (Fig. 3a) was not affected by light exposure (α: 112.7%, β: 103.1% of controls, respectively) or by injection of KN-93 (α: 118.6%, β: 113.6% of controls, respectively).

Effect of PD98059 on light-induced phosphorylation of MAPK

Previous reports show that light stimulation during subjective night causes the phosphorylation of MAPK in the SCN (Obrietan *et al.* 1998). In order to confirm whether light can induce the phosphorylation of MAPK, we examined light pulse (300 lux for 15 min)-induced MAPK phosphorylation at CT 13.5 (Fig. 4). Light exposure caused the phosphorylation of MAPK in the hamster SCN, as previous reports suggested (Obrietan *et al.* 1998). Intracerebroventricular injection of PD98059 (5.0 nmol/5 μL) 15 min prior to light application succeeded in suppressing the light-induced expression of MAPK immunoreactive cells (62.8% of vehicle light controls).

Effect of KN-93 on the light-induced expression of hamster *Per1*, *Per2* and *Per3* mRNAs

In the next experiment, we examined whether KN-93 attenuated the light-induced rapid induction of *Per1* and *Per2* mRNAs in the hamster SCN using an RI *in situ* hybridization method (Fig. 5). Light exposure (300 lux for 15 min) strongly induced *Per1* (250% of controls) and *Per2* (200% of controls) but not *Per3* expression 90 min after light application at CT 13.5. Pre-treatment with KN-93 (1.5 nmol/5 μL; i.c.v.) significantly attenuated light-induced *Per1* and *Per2* induction, whereas KN-92 (1.5 nmol/5 μL; i.c.v.), an inactive analog of KN-93 did not. Injection of KN-93 alone without light exposure did not reduce, but instead weakly increased *Per1* expression. Pre-injection with PD98059 (5.0 nmol/5 μL; i.c.v.) or U0126 (5.0 nmol/5 μL; i.c.v.) failed to suppress the light-induced expression of *Per1* and *Per2* mRNAs. *Per3* was unaffected by KN-92, KN-93, PD98059 and U0126.

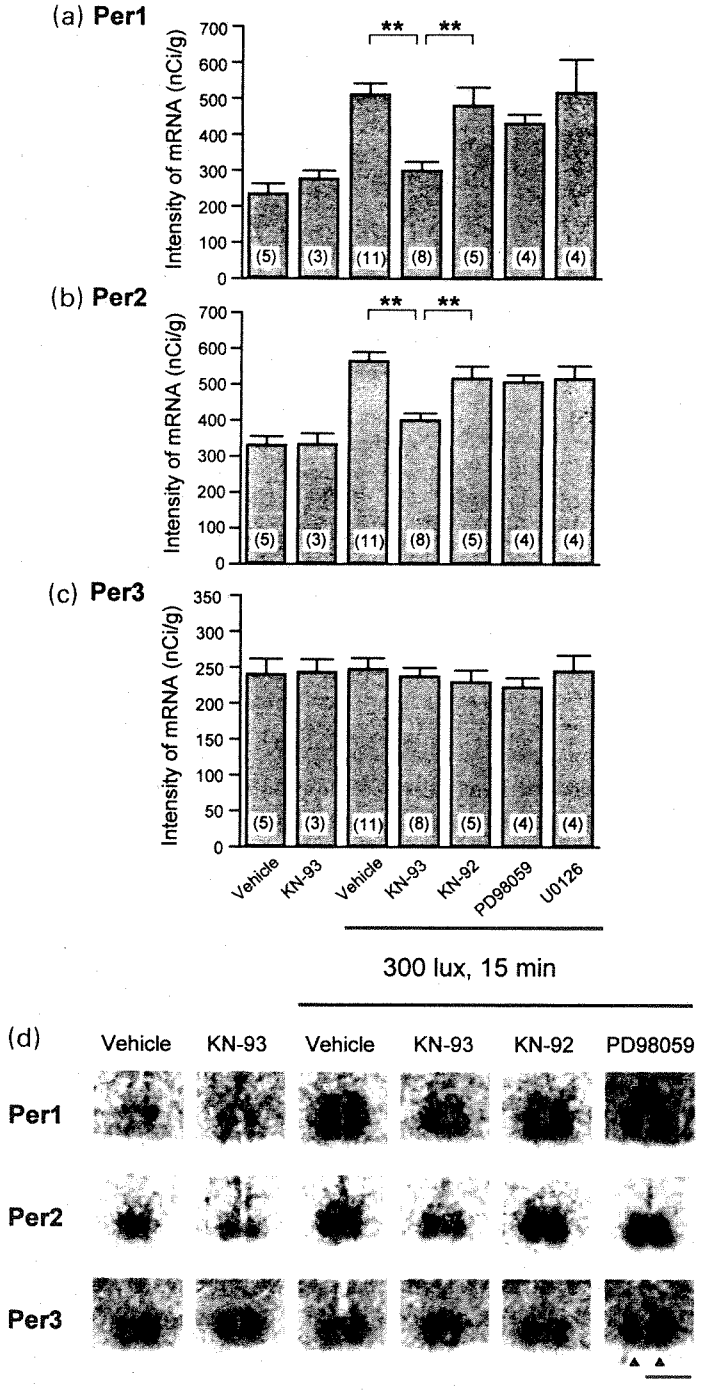

Fig. 5 Effect of KN-93, KN-92, PD98059 and U0126 on the light-induced expression of hamster *Per1* (a), *Per2* (b) and *Per3* (c) mRNAs. The mRNA expression was demonstrated by use of an RI [^{33}P] *in situ* hybridization. Each drug was administered at CT 13 and followed by a light pulse (300 lux for 15 min) at CT 13.5. *Per* gene expression was examined 90 min after light onset. Light exposure strongly induced *Per1* (250% of control) and *Per2* (200% of control). The number of animals is shown in parentheses. Representative *in situ* hybridization autoradiograms are shown in (d). Arrows in the figure indicate the SCN area, and bars are indicative of 0.5 mm $^{**}p < 0.01$ (Dunnett's test).

Discussion

In the present experiments, we demonstrated that light-pulse-induced *Per1* and *Per2* expression in the hamster SCN was attenuated by CaMKII/IV inhibitor KN-93, but not by the inactive isomer KN-92 or the MAPK inhibitors PD98059 and U0126. Similar to the molecular experiment, phase delays produced by light-exposure at CT 13.5 were blocked by KN-93, but not by PD98059 or U0126. Thus, the present results strongly suggest that the rapid increase in *Per1* and/or *Per2* in the SCN via activation of CaMKII/IV may be involved in the resetting of the circadian clock by light exposure. Golombek and Ralph (1994) suggested that circadian responses to light are mediated by CREB phosphorylation through the activation of CaMKII. In accordance with the above papers, we reported that

light-induced c-Fos expression in the SCN *in vivo* was attenuated by calmodulin inhibitors and the CaMKII inhibitor KN-62, and that glutamate-induced phase delays in SCN firing rhythm *in vitro* were inhibited by these inhibitors (Fukushima *et al.* 1997). Thus, all of these reports support the idea pointing to the importance of CaMKII/IV activation in light-induced *Per1* and *Per2* expression and in resetting of the clock. Therefore, inhibition of *Per1* and *Per2* expression in the hamster SCN by KN-93 application may explain the reduction in light-induced behavioral phase resetting.

Zylka *et al.* (1998) demonstrated both temporal and quantitative differences in *mPer2* regulation following light exposure at CT 14 (strong expression) and CT 23 (weak expression). Golombek and Ralph (1994) demonstrated that central administration of KN-62 inhibited phase delays and advances induced by light pulses. In the present experiment, we found that KN-93 preferentially attenuated *Per1* expression (60% of control) rather than *Per2* expression (70% of control) induced by light at CT 13.5. Shigeyoshi *et al.* (1997) and Akiyama *et al.* (1999) elucidated that *mPer1* induction in the SCN shows both reciprocity and a strong correlation with phase delays of the mouse overt rhythm. Therefore it is suggested that induction of *Per1* rather than *Per2* in the SCN may contribute to both phase advances and delays. However, further detailed experiments are required to distinguish the contribution of *Per1* and *Per2* to the phase shifting effects of these genes.

At present we do not know the mechanism for how CaMKII/IV inhibitor attenuates the light-induced expression of *Per1* and *Per2*. We reported that the promoter for the *mPer1* gene contains four CRE sites and the CREB/CRE transcriptional pathway has the capacity to activate *Per1* gene expression (Yamaguchi *et al.* 2000). Morgan *et al.* (1998) already suggested the possibility of the regulation of ovine *Per1* gene by a CRE. Recently, Obrietan *et al.* (1999) demonstrated that light exposure stimulated the CRE-mediated gene expression in the SCN using mice transgenic for the CRE-regulated reporter gene construct. Thus, CRE may play a central role in mediating the ability of light-induced resetting through the activation of *Per1*. Multiple kinases, including PKA, CaMKII/IV, and MAPK (Gonzalez and Montminy 1989; Sheng *et al.* 1991; Xing *et al.* 1996; Impey *et al.* 1998) activate the CREB/CRE pathway. Interestingly, Marthur *et al.* (1996) have demonstrated that inhibition of PKA in the SCN *in vivo* does not affect light-induced phase shifts. This correlates with a report that light pulses did not affect cAMP content or PKA activity in the SCN (Ferreyra and Golombek 2000). Actually, cAMP and PKA have been implicated in the control of light-independent, nonphotic regulation of circadian rhythms. Indeed, cAMP application *in vitro* (Prosser and Gillette. 1989; Ruby *et al.* 1998) as well as 5-HT receptor agonist application (Shibata *et al.* 1992; Prosser *et al.* 1994; Horikawa *et al.* 2000) produce a phase advance of the clock during the daytime by changing *Per1* and *Per2* expression in the SCN (Horikawa *et al.* 2000).

In accordance with a previous paper (Obrietan *et al.* 1999), we elucidated in the present experiment that light exposure elicits the phosphorylation of CaMKII and MAPK in the SCN. Therefore, activation of CREB via CaMKII/IV and/or MAPK may be involved in the induction of *Per1* and *Per2* in the hamster SCN. In the present experiment, injection of KN-93 inhibited both CaMKII phosphorylation and light-induced *Per1* and *Per2* expression in the SCN. Although the injection of PD98059 (5.0 nmol/hamster) into the i.c.v. inhibited the light-induced phosphorylation of MAPK in the SCN (Fig. 4), Administration of PD98059 or U0126 did not inhibit light-induced *Per1* and *Per2* expression in the SCN or the behavioral phase delays. We also found that SB203580 (p38 kinase inhibitor) failed to produce an inhibitory effect on light-induced phase delay in hamster wheel-running rhythm (data not shown). Thus, the present result strongly suggests that MAPK phosphorylation is not involved in light-induced phase delays, even though phosphorylation of MAPK is induced in the SCN by light exposure. There is an apparent discordance between our results and the conclusions of Obrietan *et al.* (1998). Their experiments are based predominantly on *in vitro* studies with transfected cells rather than *in vivo* application of inhibitors. Therefore, present discordance may reflect differences of such experimental design.

Recently, Sanada *et al.* (2000) demonstrated that activated MAPK was rapidly dephosphorylated in the chick pineal clock after light illumination during the night-time. Akashi and Nishida (2000) showed that induction of the circadian oscillation of *Per* gene expression was triggered by TPA treatment of NIH-3T3 fibroblasts and inhibited by the MAPKK inhibitor U0126. These recent papers strongly suggest the importance of the MAPK cascade in clock resetting. Treatment with serum shock or forskolin in rat-1 cells caused a transient induction of *Per1* and *Per2* and of several immediately early genes such as *c-fos* (Balsalobre *et al.* 1998; Yagita and Okamura 2000). The serum shock caused a MAPK induction in the rat-1 cells, while forskolin inhibited the level of MAPK (our unpublished observation). After taking into account the above-mentioned observations, we suggest that various stimuli which produce resetting of the circadian clock use various kinases for CREB phosphorylation, such as CaMKII/IV, MAPK and PKA depending on the cell type; the SCN and pineal clocks and fibroblasts, and circadian entrainment by light, drugs, and humoral factors may not employ the same signal transduction mechanisms.

In conclusion, the present results strongly indicate the involvement of CaMKII/IV as a signal transducer in light-induced *Per1* and *Per2* expression in the hamster SCN and the subsequent resetting of the clock.

Acknowledgements

This study was partially supported by grants awarded to SS from the Japanese Ministry of Education, Science, Sports and Culture (11170248, 11233207, 12877385) and The Special Coordination Funds of the Japanese Science and Technology Agency and Kyowa Hakko Kogyo Co. (Japan).

References

Akashi M. and Nishida E. (2000) Involvement of MAP kinase cascade in resetting of the mammalian circadian clock. *Genes Dev.* **14**, 645–649.

Akiyama M., Kouzu Y., Takahashi S., Wakamatsu H., Moriya T., Maetani M., Watanabe S., Tei H., Sakaki Y. and Shibata S. (1999) Inhibition of light- or glutamate-induced mPer1 expression represses the phase shifts into the mouse circadian locomotor and suprachiasmatic firing rhythms. *J. Neurosci.* **19**, 1115–1121.

Albrecht U., Sun Z. S., Eichele G. and Lee C. C. (1997) A differential response of two putative mammalian circadian regulators, mPer1 and mPer2, to light. *Cell* **91**, 1055–1064.

Amato S. F., Nakajima K., Hirano T. and Chiles T. C. (1996) Transcriptional regulation of the junB promoter in mature B lymphocytes. Activation through a cyclic adenosine 3′,5′-monophosphate-like binding site. *J. Immunol.* **157**, 146–155.

Balsalobre A., Damiola F. and Schibler U. (1998) A serum shock induces circadian gene expression in mammalian tissue culture cells. *Cell.* **93**, 929–937.

Ding J. M., Faiman L. E., Hurst W. J., Kuriashkina L. R. and Gillette M. U. (1997) Resetting the biological clock: mediation of nocturnal CREB phosphorylation via light, glutamate, and nitric oxide. *J. Neurosci.* **17**, 667–675.

Dunlap J. C. (1999) Molecular bases for circadian clocks. *Cell* **96**, 271–290.

Ebling F. J. (1996) The role of glutamate in the photic regulation of the suprachiasmatic nucleus. *Prog. Neurobiol.* **50**, 109–132.

Ferreyra G. A. and Golombek D. A. (2000) Cyclic AMP and protein kinase A rhythmicity in the mammalian suprachiasmatic nuclei. *Brain Res.* **858**, 33–39.

Fukunaga K., Goto S. and Miyamoto E. (1988) Immunohistochemical localization of Ca^{2+}/calmodulin-dependent protein kinase II in rat brain and various tissues. *J. Neurochem.* **51**, 1070–1078.

Fukushima T., Shimazoe T., Shibata S., Watanabe A., Ono M., Hamada T. and Watanabe S. (1997) The involvement of calmodulin and Ca^{2+}/calmodulin-dependent protein kinase II in the circadian rhythms controlled by the suprachiasmatic nucleus. *Neurosci Lett.* **227**, 45–48.

Golombek D. A. and Ralph M. R. (1994) KN-62, an inhibitor of Ca^{2+}/calmodulin kinase II, attenuates circadian responses to light. *Neuroreport* **5**, 1638–1640.

Golombek D. A. and Ralph M. R. (1995) Circadian responses to light: the calmodulin connection. *Neurosci. Lett.* **192**, 101–104.

Gonzalez G. A. and Montminy M. R. (1989) Cyclic AMP stimulates somatostatin gene transcription by phosphorylation of CREB at serine 133. *Cell* **17**, 675–680.

Hallbeck M., Blomqvist A. and Hermanson (1996) Ca^{2+}/calmodulin-dependent kinase II immunoreactivity in the rat hypothalamus. *Neuroreport* **7**, 1957–1960.

Hastings M. H. (1997) Central clocking. *Trends Neurosci.* **20**, 459–464.

Horikawa K., Yokota S., Fuji K., Akiyama M., Moriya T., Okamura H. and Shibata S. (2000) Non-photic entrainment by 5-HT1A/7 receptor agonists accompanied by reduced Per1 and Per2 expression. *J. Neurosci.* **20**, 5867–5873.

Impey S., Obrietan K., Wong S. T., Poser S., Yano S., Wayman G., Deloulme J. C., Chan G. and Storm D. R. (1998) Cross talk between ERK and PKA is required for Ca2+ stimulation of CREB-dependent transcription and ERK nuclear translocation. *Neuron* **21**, 869–883.

Laemmli U. K. (1970) Cleavage of structural proteins during the assembly of the head of bacteriophage T4. *Nature.* **227**, 680–685.

Mathur A., Golombek D. A. and Ralph M. R. (1996) cGMP-dependent protein kinase inhibitors block light-induced phase advances of circadian rhythms in vivo. *Am. J. Physiol.* **270**, R1031–R1036.

Morgan P. J., Ross A. W., Graham E. S., Adam C., Messager S. and Barrett P. (1998) oPer1 is an early response gene under photoperiodic regulation in the ovine pars tuberalis. *J. Neuroendocrinol.* **10**, 319–323.

Nakajima K., Kusafuka T., Takeda T., Fujitani Y., Nakae K. and Hirano T. (1993) Identification of a novel interleukin-6 response element containing an Ets-binding site and a CRE-like site in the junB promoter. *Mol. Cell Biol.* **13**, 3027–3041.

Obreitan K., Impey S. and Storm D. R. (1998) Light and circadian rhythmicity regulate MAP kinase activation in the suprachiasmatic nuclei. *Nat. Neurosci.* **1**, 693–700.

Obrietan K., Impey S., Smith D., Athos J. and Storm D. R. (1999) Circadian regulation of cAMP response element-mediated gene expression in the suprachiasmatic nuclei. *J. Biol. Chem.* **274**, 17748–17756.

Prosser R. A. and Gillette M. U. (1989) The mammalian circadian clock in the suprachiasmatic nuclei is reset *in vitro* by cAMP. *J. Neurosci.* **9**, 1073–1081.

Prosser R. A., Macdonald E. S. and Heller H. C. (1994) c-fos mRNA in the suprachiasmatic nuclei *in vitro* shows a circadian rhythm and responds to a serotonergic agonist. *Brain Res. Mol. Brain Res.* **25**, 151–156.

Ruby N. F., Edgar D. M., Heller H. C. and Miller J. D. (1998) The aged suprachiasmatic nucleus is phase-shifted by cAMP *in vitro*. *Brain Res.* **779**, 338–341.

Sanada K., Hayashi Y., Harada Y., Okano T. and Fukada Y. (2000) Role of circadian activation of mitogen-activated protein kinase in chick pineal clock oscillation. *J. Neurosci.* **20**, 986–991.

Sassone-Corsi P., Visvader J., Ferland L., Mellon P. L. and Verm I. M. (1988) Induction of proto-oncogene fos transcription through the adenylate cyclase pathway: characterization of a cAMP-responsive element. *Genes Dev.* **2**, 1529–1538.

Schurov I. L., McNulty S., Best J. D., Sloper P. J. and Hastings M. H. (1999) Glutamatergic induction of CREB phosphorylation and Fos expression in primary cultures of the suprachiasmatic hypothalamus *in vitro* is mediated by co-ordinate activity of NMDA and non-NMDA receptors. *J. Neuroendocrinol.* **11**, 43–51.

Shearman L. P., Zylka M. J., Weaver D. R., Kolakowski L. F. Jr and Reppert S. M. (1997) Two period homologs: circadian expression and photic regulation in the suprachiasmatic nuclei. *Neuron* **19**, 1261–1269.

Sheng M., Thompson M. A. and Greenberg M. E. (1991) CREB: a Ca (2+)-regulated transcription factor phosphorylated by calmodulin-dependent kinases. *Science* **252**, 1427–1430.

Shibata S., Tsuneyoshi A., Hamada T., Tominaga K. and Watanabe S. (1992) Phase-resetting effect of 8-OH-DPAT, a serotonin1A receptor agonist, on the circadian rhythm of firing rate in the rat suprachiasmatic nuclei *in vitro*. *Brain Res.* **582**, 353–356.

Shigeyoshi Y., Taguchi K., Yamamoto S., Takekida S., Yan L., Tei H., Moriya T., Shibata S., Loros J. J., Dunlap J. C. and Okamura H. (1997) Light-induced resetting of a mammalian circadian clock is associated with rapid induction of the mPer1 transcript. *Cell* **91**, 1043–1053.

Sun Z. S., Albrecht U., Zhuchenko O., Bailey J., Eichele G. and Lee C. C. (1997) RIGUI, a putative mammalian ortholog of the *Drosophila* period gene. *Cell.* **19**, 1003–1011.

Takumi T., Taguchi K., Miyake S., Sakakida Y., Takashima N., Matsubara C., Maebayashi Y., Okumura K., Takekida S., Yamamoto S., Yagita K., Yan L., Young M. W. and Okamura H. (1998a) A light-independent oscillatory gene mPer3 in mouse SCN and OVLT. *EMBO J.* **17**, 4753–4759.

Takumi T., Matsubara C., Shigeyoshi Y., Taguchi K., Yagita K., Maebayashi Y., Sakakida Y., Okumura K., Takashima N. and Okamura H. (1998b) A new mammalian period gene predominantly expressed in the suprachiasmatic nucleus. *Genes Cells* **3**, 167–176.

Tei H., Okamura H., Shigeyoshi Y., Fukuhara C., Ozawa R., Hirose M. and Sakaki Y. (1997) Circadian oscillation of a mammalian homologue of the Drosophila period gene. *Nature* **389**, 512–516.

Tobimatsu T. and Fujisawa H. (1989) Tissue-specific expression of four types of rat calmodulin-dependent protein kinase II mRNAs. *J. Biol. Chem.* **264**, 17907–17912.

Xing J., Ginty D. D. and Greenberg M. E. (1996) Coupling of the RAS-MAPK pathway to gene activation by RSK2, a growth factor-regulated CREB kinase. *Science* **16**, 959–963.

Yagita K. and Okamura H. (2000) Forskolin induces circadian gene expression of rPer1, rPer2 and dbp in mammalian rat-1 fibroblasts. *FEBS Lett.* **465**, 79–82.

Yamaguchi S., Mitsui S., Miyake S., Yan L., Onishi H., Yagita K., Suzuki M., Shibata S., Kobayashi M. and Okamura H. (2000) The 5′ upstream region of mPer1 gene contains two promoters and is responsible for circadian oscillation. *Curr. Biol.* **10**, 873–876.

Zylka M. J., Shearman L. P., Weaver D. R. and Reppert S. M. (1998) Three period homologs in mammals: differential light responses in the suprachiasmatic circadian clock and oscillating transcripts outside of brain. *Neuron* **20**, 1103–1110.

5）ヒトの概日リズム障害に伴う疾患における生体時計関連遺伝子の解析及び治療法の開発（研究代表者：海老澤尚（埼玉医科大学））

研究代表者：　海老澤尚　（埼玉医科大学医学部　講師）
研究分担者：　池田正明　（埼玉医科大学医学部　講師）

Ⅰ．はしがき

24 時間活動し続ける現代社会のなかで、健康的な生活を送るために、また、産業事故を防ぐためにもヒトの概日リズムに関する知識の集積は欠かせない。他のほ乳動物などと同様、ヒトの場合もその概日リズムは時計遺伝子が形成する転写・翻訳を介するフィードバックループによって構成されている。我々は、概日リズムの異常に基づく睡眠障害の原因を探り、ヒトの概日リズムの個体差を遺伝子レベルで解析するため、睡眠相後退症候群(Delayed sleep phase syndrome; DSPS)、非２４時間睡眠覚醒症候群（non-24-hour sleep-wake syndrome; N-24）を対象に時計遺伝子の多型解析を続けている。この成果により、概日リズム障害発症の分子メカニズムの解明や新規治療法の開発の他、概日リズムの個体差を遺伝子レベルで掌握することが可能になると思われる。

Ⅱ．研究成果

(1) 概日リズム障害における生体時計遺伝子の多型解析

a) メラトニン受容体遺伝子の解析；ヒトメラトニン 1a, 1b 受容体遺伝子の多型解析により、それぞれから 2 種類ずつ計 4 種類のミスセンス多型を検出した。うち 1a 受容体の R54W 多型は非 24 時間睡眠覚醒症候群（N-24）に多く、受容体の発現量・メラトニンとの親和性が変化することを見出した（発表済み）。また、G 蛋白キメラ cDNA（慶應大学西本教授より提供）を使い、R54W 多型を持つ受容体は Gq 蛋白との結合性が弱まり、Gi 蛋白との結合がやや強化ることも見出した。

b) Per3 遺伝子の解析；ヒト *Per3* 遺伝子から 6 個のミスセンス多型を含む 20 個の多型を見出した。[G647, P864, 4-repeat, T1037, R1158]の組み合わせ（ハプロタイプ）が睡眠相後退症候群発症（DSPS）の危険因子になっていることを見出した。V647G 多型により PER3 蛋白のリン酸化が変化する可能性を指摘した。(報告済み)。また、少数例（21 例）での研究ながら、概日リズム障害との関連が想定されている季節性感情障害（SAD）でも V647G 多型が有意に高頻度でみられることを見出し(P=0.019)、その発症との関わりを指摘した。

c) CLOCK 遺伝子；CLOCK 遺伝子の多型解析により、ミスセンス多型を２個見出したほか、既に朝型・夜型生活パターンとの相関が報告されていた T3111C 多型が DSPS 発症に関与する可能性を見出した。(報告済み)

d) Casein kinase I epsilon（CK I ε）遺伝子；CK I ε遺伝子の全翻訳領域での多型解

析により、ミスセンス多型1個を含む4個の多型を見いだした。ミスセンス多型は概日リズム障害群で有意に低頻度だった（P=0.013)。また、この多型を導入したCK Ⅰε cDNAを発現ベクターに挿入し、大腸菌で蛋白を発現させてin vitroで酵素蛋白を発現させて活性を測定すると、野生型の酵素蛋白に比べ、酵素活性が約1.8倍に増加すること（大阪大学蛋白質研究所高野氏・礒島氏との共同研究）を見出した。従ってこのミスセンス多型は酵素活性の増加を介して、概日リズム障害の発症を抑制する働きを持つと考えられた（投稿準備中)。

概日リズム形成の中枢に関わる遺伝子の数は限定されており、我々が行っているヒト生体時計遺伝子の多型のリスト作製及びその機能解析により、ヒトの概日リズム障害・概日リズムの個体差と遺伝子多型との関連を包括的に理解することが可能となると思われる。

(2) マウス *Bmal1* のゲノム構造の解析

a) マウス *Bmal1* BAC クローンの翻訳領域塩基配列を解析し、その構造を明らかにした。マウス *Bmal1* の翻訳領域は17個のエクソンからなり、メジャートランスクリプトである *Bmal1b* はエクソン 2 を除いた 16 個のエクソンから構成されていた。*Bmal1b* 以外にスプライスバリアントとして *Bmal1g'*, *Bmal1b'* があり、*Bmal1g'* はエクソン 7 が短くなったためにフレームシフトを起こし、PAS ドメインの途中でストップコドンが挿入された短い蛋白をコードすること、*Bmal1b'* は21bpのエクソン2が含まれており、7アミノ酸長い蛋白をコードすることを明らかにした。

b) *Bmal1* の発現調節機構とそのリズム性発現の解析；視交叉上核での *Per1, Per2* などのいわゆる抑制系因子の mRNA は明期にピークを示すリズムがあり，*Bmal1* に対して正反対の位相を有している．また視交叉上核以外の器官においても，それぞれの因子発現のピーク位相は異なるものの，逆位相性の発現は保存されている．私達はこの逆位相発現の分子機構を明らかにするためマウス *Bmal1* BAC クローン非翻訳領域の塩基配列解析，5' RACE 法による転写開始点の決定およびマウス *Bmal1* プロモーター領域の同定を行なった.マウス *Bmal1* プロモーター領域にはSP1サイトのほか、ROR-RE 4 箇所などが存在した。プロモーター領域の解析から抑制系因子の転写抑制因子であるCRY1, PER2がマウス *Bmal1* プロモーターに対しては転写促進因子として働いていることを明らかにした.

c) *Bmal2* のクローニングと機能解析;BMAL1と相同性の高い因子を検索する目的で *Bmal1* cDNA 配列情報を用いてヒト cDNA データベースを検索し、BMAL1 と相同性の高い cDNA 断片配列を見いだしその全長をクローニングした。この cDNA がコードするタンパクはBMAL1と49%の相同性があり、BMAL1と同様にbHLH-PAS型転写因子であり、BMAL1 に最も相同性が高いことから BMAL2 と命名した。この cDNA は視交叉上核に発現するが、*Bmal1* とは異なり、明らかなリズム性発現は示さなかった。

d) *Bmal1* の発現と ROR レスポンスエレメントの役割；*mBmal1* プロモーターにある ROR レスポンスエレメントの *Bmal1* 発現における役割を解析した。ROR レスポンスエレ

メント2個を含むBP/527-LUCレポーターはRORα、RORβ、RORγによって転写活性化が起こり、REV-ERBでは変化が認められなかった。

(3) 今後の計画

今後は、見出された時計遺伝子多型について機能解析を行い、概日リズム表現型に及ぼす影響を詳細に調べる予定である。

参考文献

1. Namihira M, Honma S, Abe H, Tanahashi Y Ikeda M, Honma K. Circadian rhythms and light responsiveness of mammalian clock gene, Clock and BMAL1, transcripts in the rat retina. *Neurosci Lett.*271:1-4,1999.

2. Namihhira M, Honma S, Abe H, Tanahashi Y, Ikeda M, Honma K. Daily variation and light responsiveness of mammalian clock gene, Clock and BMAL1, transcripts in the pineal body and different areas of brain in rats. *Neurosci Lett.*267:69-72,1999.

3. Abe H, Honma S, Namihira M, Tanahashi Y, Ikeda M, Yu W, Honma K. Phase-dependent induction by light of rat Clock gene expression in the suprachiasmatic nucleus. *Mol Brain Res.*66:104-110,1999.

4. Yu W, Ikeda M, Abe H, Honma S, Ebisawa T, et al. Characterization of three splice variants and genomic organization of the mouse BMALL1 gene. *Biochem. Biophys. Res. Commun.*260:760-767.1999.

5. Ebisawa T, et al. Alleic variants of human melatonin 1a receptor: function and prevalence in subjects with circadian rhythm sleep disorders. *Biochem. Biophys. Res. Commun.*260:832-837,1999.

6. Masubuchi S, Honma S, Abe H, Ishizaki K, Namihira M, Ikeda M, Honma K. Clock genes outside the suprachiasmatic nucleus involved in manifestation of locomotor activity rhythm in rats. *Eur J Neurosci.*12:4206-4214,2000.

7. Ebisawa T, et al. Genetic polymorphisms of human melatonin 1b receptor gene in circadian rhythm sleep disorders and controls. *Neurosci Lett.*280:29-32,2000.

8. Ikeda M, Ikeda M, Yu W, Hirai M, Ebisawa T, et al. cDNA cloning of a novel bHLH-PAS transcription factor superfamily gene, BMAL2: Its mRNA expression, subcellular distribution, and chromosomal localization. *Biochem. Biophys. Res. Commun.*275:493-502,2000.

9. Namihira M, Honma S, Abe H, Masubuchi S, Ikeda M, Honma K. Circadian pattern, light responsiveness and localization of rPer1 and rPer2 gene expression in the rat retina. *NeuroReport.*12:471-475,2001.

10. Abe H, Honma S, Namihira M, Masubuchi S, Ikeda M, Ebisawa T, Honma K. Clock gen expression in the suprachiasmatic mucleus and other areas of the brain during rhythm splittinf in CS mice. *Mol.Blain Res.*87:92-99,2001.

11. Ebisawa T, et al. Association of structural polymorphisms in the human *period3* gene with delayed sleep phase syndorome. *EMBO Reports.*2:342-346,2001.

12. Yu W, Nomura M, Ikeda M. Interactivating feedback loops within the mammalian clock : BMAL1 is negatively autoregulated and upregulated by CRY1, CRY2, and PER2. *Biochem. Biophys. Res. Commun.*290:933-341,2002.

13. Yamashita H, Kazamwa T, Minatogawa Y, Ebisawa T, and Yamauchi T. Time course of hepatic crtochrome P450 subfamily induction by chronic carbamazapine administration in rats. *Int J Neurophychopharmacol.*5:47-52,2002.

14. Uchiyama M, Shibui K, Hayakawa T, Kamei Y, Ebisawa T, et al. Larger phase angle between sleep propensity and melatonin rhythm in sighted humans with non-24-hour sleep-wake syndrome. *Sleep.*25:83-88,2002.

15. Iwase T, Kajimura N, Uchiyama M, Ebisawa T, et al. Mutation screening of the human Clock gene in circadian rhythm sleep disorders. *Psychiatry Reseach.*109:121-128,2002.

16. Satoh K, Mishima K, Inoue Y, Ebisawa T, Shimizu T. Two pedigrees of familial advanced sleep phase syndrome in Japan. *Sleep.*in press.2003.

総説

1. 海老沢尚、概日リズム障害と遺伝子変異、日本時間生物学会会誌 5(1): 49-51,1999.

2. 海老沢尚、サーカディアンリズム異常の分子生物学、医学のあゆみ 190(4): 281,1999.

3. 海老沢尚、メラトニンと生体リズムの遺伝機構、Molecular Medicine 36(10): 1150-1159,1999.

4. 山内俊雄、海老澤尚、生物学的精神医学研究の限界と将来、精神医学 42(3): 263-271,2000.

5. 池田正明、BMAL1と生体リズム、日本神経精神薬理学雑誌 20: 189-198,2000.

6. 池田正明、－生物時計関連遺伝子－、PASドメインとPAS因子 －PAS因子は環境適応素子として生まれた－、日本時間生物学会会誌 6:12-25,2000.

7. 池田正明、体内時計は転写因子で刻まれる？、バイオサイエンスとインダストリー 58: 16-2,2000.

8. 海老澤尚、概日リズム障害と遺伝子変異、脳と精神の医学 11(1): 1-7,2000.

9. 海老澤尚、睡眠覚醒リズム障害と遺伝子変異、自律神経 37(2): 158-162,2000.

10. 海老沢尚、生体リズム障害の分子生物学、臨床脳波 42(10): 629-633,2000.

11. 海老沢尚、家族性致死症不眠症、Clinical Neuroscience 18(10): 94-95,2000.

12. 海老沢尚、生体時計の分子機構－ストレスへの時間生物学的アプローチに向けて－、日本神経精神薬理学雑誌 20: 107-111,2000.

13. 海老澤尚、睡眠覚醒リズム障害と時計遺伝子、神経研究の進歩 44(6): 891-897,2000.

14. 池田正明、PAS因子の構造と機能、神経研究の進歩 45: 744-754,2001.

15. 池田正明、海老澤尚、概日リズム障害と時計遺伝子、分子精神医学 1(5): 31-38,2001.

16. 海老澤尚、睡眠覚醒リズム障害の遺伝子解析、神経研究の進歩 45(5): 840-846,2001.

17. 海老沢尚、生体リズム障害と睡眠異常の分子医学、現代医療　33(11): 126-131,2001.

18. 海老澤尚、概日リズム障害、最新精神医学　6(6): 559-566,2001.

19. 海老澤尚、メラトニン受容体および時計遺伝子多型と概日リズム障害、現代医療　34: 63-67,2002.

20. 海老澤尚、生体リズム障害の分子生物学的背景、Prog.Med.　22: 1385-1389,2002.

21. 海老澤尚、概日リズム障害の遺伝子解析、内分泌・糖尿病科　14(4): 408-413,2002.

22. 海老澤尚、時計遺伝子と睡眠覚醒障害、脳と精神の医学　13(3): 289-295,2002.

23. 海老沢尚、時計遺伝子の発見と時間生物学、精神科　1(5): 382-387,2002.

24. 海老澤尚、体内時計機構の分子医学、Molecular Medicine　40(3): 318-325,2003.

25. 海老澤尚、概日リズムと睡眠障害－時計遺伝子からみた睡眠障害、医学のあゆみ　204(11): 799-802,2003.

ELSEVIER

Psychiatry Research 109 (2002) 121–128

PSYCHIATRY RESEARCH

www.elsevier.com/locate/psychres

Mutation screening of the human *Clock* gene in circadian rhythm sleep disorders

Toshio Iwase[a], Naofumi Kajimura[c], Makoto Uchiyama[d], Takashi Ebisawa[a,*], Kimio Yoshimura[e], Yuichi Kamei[f], Kayo Shibui[d], Keiko Kim[g], Yoshinao Kudo[f], Masaaki Katoh[c], Tsuyoshi Watanabe[c], Toru Nakajima[c], Yuji Ozeki[h], Mariko Sugishita[a], Toru Hori[c], Masaaki Ikeda[b], Ryoichi Toyoshima[a], Yuichi Inoue[i], Naoto Yamada[h], Kazuo Mishima[j], Masahiko Nomura[b], Norio Ozaki[k], Masako Okawa[h], Kiyohisa Takahashi[c,f], Toshio Yamauchi[a]

[a]*Department of Neuropsychiatry, Saitama Medical School, 38 Morohongo, Moroyama-cho, Iruma-gun, Saitama 350-0495, Japan*
[b]*Department of Physiology, Saitama Medical School, 38 Morohongo, Moroyama-cho, Iruma-gun, Saitama 350-0495, Japan*
[c]*Musashi Hospital, National Center of Neurology and Psychiatry (NCNP), Tokyo 187-0031, Japan*
[d]*Department of Psychophysiology, NCNP, Chiba 272-0827, Japan*
[e]*Cancer Information and Epidemiology Division, National Cancer Center Research Institute, Tokyo 104-0045, Japan*
[f]*Kohnodai Hospital, NCNP, Chiba 272-0827, Japan*
[g]*Department of Psychiatry, Tokyo Women's Medical College, Tokyo 162-8666, Japan*
[h]*Department of Psychiatry, Shiga University of Medical Science, Shiga 520-2192, Japan*
[i]*Department of Psychiatry, Juntendo University, School of Medicine, Tokyo 113-8431, Japan*
[j]*Department of Psychiatry, Akita University School of Medicine, Akita 010-8543, Japan*
[k]*Department of Psychiatry, Fujita Health University School of Medicine, Aichi 470-1192, Japan*

Received 4 June 2001; received in revised form 2 January 2002; accepted 15 January 2002

Abstract

We tested whether the human *Clock* (*hClock*) gene, one of the essential components of the circadian oscillator, is implicated in the vulnerability to delayed sleep phase syndrome (DSPS) and non-24-hour sleep–wake syndrome (N-24). Screening in the entire coding region of the *hClock* gene with PCR amplification revealed three polymorphisms, of which two predicted the amino acid substitutions R533Q and H542R. The frequencies of the R533Q and H542R alleles in patients with DSPS or N-24 were very low and not significantly different from those in control subjects. A T3111C polymorphism in the 3′-untranslated region of *hClock*, which had been reportedly associated with morning or evening preference for activity, was also investigated; the results showed that the 3111C allele frequency decreased in DSPS. Polymorphisms in the coding region of the *hClock* gene are unlikely to play an important role in the development of DSPS or N-24. The possible contribution of the T3111C polymorphism to DSPS susceptibility should be studied further.

Keywords: Delayed sleep phase syndrome; Non-24-hour sleep–wake syndrome; Single-strand conformation polymorphism; Transcription factors; Missense mutation; Genetic screening

*Corresponding author. Tel.: +81-492-76-1213; fax: +81-492-76-1622.
E-mail address: tebisawa@saitama-med.ac.jp (T. Ebisawa).

0165-1781/02/$ - see front matter
PII: S0165-1781(02)00006-9

1. Introduction

Circadian (~24 h) rhythmicity of biological processes is a conserved feature of most organisms, and is controlled by endogenous self-sustaining oscillators (Hastings, 1997). Recent genetic studies revealed that the circadian clock system consists of transcriptional/translational feedback loops, of which the molecular components have been isolated from bacteria, plants, insects, and mammals, with circadian rhythm mutants (Dunlap, 1999). The mammalian circadian clock is located principally in the suprachiasmatic nuclei in the hypothalamus. Mutations in clock-relevant genes, such as *Clock*, *BMALI* (*Mop3*), *Period2* (*Per2*), *Per3*, *Cryl/2*, and *Casein Kinaselepsilon* (*CKIε*), alter or abolish the circadian rhythmicity in mice and hamsters (Bunger et al., 2000; King and Takahashi, 2000; Lowrey et al., 2000; Shearman et al., 2000).

In humans, sleep and wakefulness, cognitive function, body temperature, and hormonal secretion cycles are regulated by an endogenous circadian clock, which is synchronized to the 24-h day by environmental stimuli, notably light (Hastings, 1997). However, patients with circadian rhythm sleep disorders, such as delayed sleep phase syndrome (DSPS) and non-24-hour sleep–wake syndrome (N-24), fail to adapt their sleep–wake cycle to the environmental time cues (Regestein and Monk, 1995). Patients with DSPS show sleep-onset insomnia and difficulties in awaking at the desired time in the morning. Patients with N-24 exhibit daily delay of the sleep–wake phase, which apparently is not entrained to the environmental light–dark cycles. Although melatonin administration and chronological treatment, such as morning bright light exposure or a daily 3-h delay of bedtimes for several nights, sometimes improve symptoms, patients often suffer from difficulties in social and family life and a high incidence of depression (Czeisler et al., 1981; Dahlitz et al., 1991; Regestein and Monk, 1995). Because some of the circadian rhythm sleep disorders occur in families (Fink and Ancoli-Israel, 1997; Jones et al., 1999), polymorphisms in the human clock genes may lead to the development of DSPS and N-24. A recent study reported that a polymorphism in the human *Per2* gene, one of the three human homologs of the *Drosophila* Clock gene *Per*, causes another type of circadian rhythm sleep disorder, advanced sleep phase syndrome, in which both sleep onset and offset occur much earlier than the desired time (Toh et al., 2001). We have already reported that one of the haplotypes of the *hPer3* gene, another human homolog of the *Drosophila Per*, is significantly associated with the susceptibility to DSPS (Ebisawa et al., 2001).

The *Clock* gene is the first essential component of the mammalian clock. A point mutation in the mouse *Clock* gene, which causes skipping of exon 19, reduces the transcriptional activity of the CLOCK protein and lengthens the period of the locomotor activity rhythm in a dominant-negative fashion (King et al., 1997; Gekakis et al., 1998). These results suggest that the human Clock *hClock* gene is another potential candidate for susceptibility to circadian rhythm sleep disorders.

In this study, mutation screening was performed in the complete coding region of the *hClock* gene in circadian rhythm sleep disorders and controls. The distribution of the T3111C polymorphism in the 3′-untranslated region (3′-UTR) of the gene, which is reportedly associated with morning or evening preference for activity, was also investigated (Katzenberg et al., 1998).

2. Methods

2.1. Subjects

We screened 96 patients with circadian rhythm sleep disorders (59 with DSPS, 37 with N-24) diagnosed according to the International Classification of Sleep Disorders (ICSD, 1990, 1997) criteria and 109 healthy controls.

Brief descriptions of the diagnostic criteria are as follows.

DSPS: (1) inability to fall asleep and wake up spontaneously at the desired time; (2) persistent phase delay of the major sleep episode in relation to the desired time for sleep; (3) symptoms present for at least 1 month; and (4) sleep of normal quality and duration when not required to maintain a conventional sleep–wake schedule.

N-24: (1) difficulty either in falling asleep or in awaking; (2) progressive delay of sleep–wake

phase with inability to be entrained to a 24-h day; and (3) sleep pattern present for at least 6 weeks. Patients with symptoms that met the criteria for any other sleep disorder were excluded.

All participants were Japanese and recruited at the participating institutions in mainland Japan. None of them were blind. Patients with DSPS were 39 men and 20 women (mean age 28.0±9.7 years), and patients with N-24 were 27 men and 10 women (mean age 27.0±8.3 years). The control subjects were 56 men and 53 women (mean age 33.1±8.1 years), without sleep disorders or difficulty in waking up at the desired time. The study subjects were unrelated except for two sibling pairs, of which each consisted of a patient with DSPS and a patient with N-24. Another patient with DSPS had a sibling with probable DSPS, who was not involved in this study, and the other patient with N-24 had a first-degree relative with severe insomnia. Three patients with DSPS had first-degree relatives with depression. Previous research involving part of this study population has been reported (Ebisawa et al., 2001). Genomic DNA was extracted from blood with a commercial kit (QIAamp DNA Blood Maxi Kit, QIAGEN, Hilden, Germany) and subjected to the mutation analysis. The protocol was approved by the Institutional Ethical Board of the Saitama Medical School and the corresponding committees at the participating institutions. Written informed consent was obtained from subjects or the parents of minor subjects.

2.2. DNA analysis

The genomic structure of the *hClock* gene was determined by alignment of the cDNA sequence with the genomic DNA obtained from the database (AF011568 for the cDNA sequence and AC069200.3 for the genomic sequence), revealing the same exon–intron structure as was reported previously (Steeves et al., 1999). On the basis of the genomic sequence, we generated 23 sets of fluorescein-labelled oligonucleotide primers to amplify all of the 20 coding exons and the adjacent exon–intron boundaries for single-strand conformation polymorphism (SSCP) analysis. We also generated a set of primers identical in sequence to the reported primers for detecting the T3111C polymorphism in the 3′-UTR (Katzenberg et al., 1998) (Table 1). Because the subsequent direct sequence analysis revealed that the 3′ end of the forward primer for exon 18b corresponded to the polymorphic locus 2121(C→T), either of the two sequence-specific primers was used as shown in Table 1.

SSCP analysis was performed as described previously (Ebisawa et al., 2001). Briefly, polymerase chain reaction (PCR) amplification was carried out with approximately 100 ng of genomic DNA, 0.5 μM of each primer, 0.2 mM of dNTPs, 0.5 unit of AmpliTaq Gold® (Applied Biosystems, Foster City, CA), 1.5 mM Mg^{2+}, and 1×PCR II buffer in a total volume of 20 μl. After activation of AmpliTaq Gold® at 95 °C for 9 min and initial denaturation at 98 °C for 1 min, 45 cycles were performed at 98 °C for 10 s, 53 °C for 45 s, and 72 °C for 60 s, followed by the last extension at 72 °C for 10 min. Then 2.0-μl aliquots of the PCR products were mixed with 18.0 μl of loading solution containing 90% deionized formamide, 5 mM EDTA, and 1% blue dextran. After denaturation at 80 °C for 7 min, 1.5 μl was loaded on an SSCP gel containing 1×TBE, 6% Long Ranger® Gel Solution (BioWhittaker Molecular Applications, Rockland, ME) with or without 5% glycerol. To study the distributions of 1955(G→A) [R533Q] and 1982(A←G) [H542R] polymorphisms in exon 17, another set of primers (5′-TTA GGA GCC ATG CAA CAT CTG AAA GAC C-3′ and 5′-CCT GAC CAT GGA CCA TCT GAA GTT GTT C-3′) was used for SSCP analysis to get better resolution of electrophoretic mobility shifts. Electrophoresis was performed at 20 °C for 5 h at 500 V/21 cm gel length with 0.6×TBE and the gel was analyzed on a DNA sequencer (model DSQ-1000S, Shimadzu, Kyoto, Japan) with PCR–SSCP analysis software (Shimadzu). Variants detected by SSCP were subjected to direct sequence analysis of PCR products re-amplified from genomic DNA samples with primers encompassing the SSCP fragment. Nucleotide sequences were determined with internal primers by a commercial kit (BigDye Terminator Cycle Sequencing Ready Reaction Kit, Applied Biosystems) on an

Table 1
Primers for SSCP analysis of the *hClock* gene

Exon	Forward primer (5′-3′)	Reverse primer (5′-3′)	PCR product size
2	CTG TGA TAA CAT ATA GTA TTT CTC	ATA GAC CAT TAT TCT AAT AGT GC	251
3	TCA CTT TAG TAT TGC TGT TGC TTA G	CAC ATA GCT TTT GGA AAT CAT TTA TTC AC	219
4	AAC ATT GTA TTA AAC TAC TTG TG	ACT AAT GCT TTG AGA GTC TGT TC	265
5	GTT GGA GTA TGC CAC TAA TAT GTC	GAT ATT AAG TCA CCC TGT GAT TTC	198
6	TTC TGT CCT GCA AAA TAC TTT TTT C	AGC TCT GAT TCC TAC CCC TTT AAC G	272
7	GTC TCT TGA ATC ATT GAA GTT ATT TTA C	GCA AAA GGA TAG TGC TAC TGA ATA C	231
8	ACT TTT ATG ATC TTA CTT TAT GTG G	TCA CTG ATA TTC AAA CAT CTA TGT C	283
9	CTG TGC TCT TAA AGA CAT AGA TGT TTG	TAA TGA CTC ATA GCC ATT CCA CCT C	311
10	GGC CAT GAC TTA TTT TTA TAT GTA GC	AAA TGG GAA CAG GTT TCA AAG TC	283
11	CCC CCC CAA AGT TTA TTT CTA GTT G	CTT ACT ACC TAT CAT TTC AGG ACA G	266
12	GAT AGC TTT TGG TTA AAA AAC AAT C	ATC ATA GGA TGT TAC AGT AAT TCA G	270
13	TTG TGT AGC ACA TAG CAA ATA GTC	TTG AGT TTC ATC TTT TAT TGG GGA G	267
14	TCT CTG AAC TGA ACC ACA AGA AAA C	TTG ATG AGA AAT GCT GAT ATA AGT AAC	273
15	CTA ATG CTC TTC TGA TTT TGT TG	AGA TTT AGA TCA TTT TTC CCC TC	197
16	ATG TAT GGG AAT GAG AAT CAC TTC AG	GCA ATT TAT CAT ATT CAA ATA CGC AAC	188
17	GTT AT CTG CTT ACT TTT CAT GTT G	AAA TGT GAA TGG GAT GCT TTG TTT G	286
18a	TTA ATG CTC ATT CTT CTT TTC AAT C	ACT CTG TAA AGT CTG TTG TTG TAT C	260
18b	ACT TTC TTC TGG AAA TTC ATC TAA T(C)	ACT CTC AAT ACT ATA CTT TCT AAA TAC	300
19a	TGC CAC TTC TTT CTC TGT CAT ATT G	ATA CTA GAT GGA ATC TGG ACC ATG C	256
19b	ATC TCT ACC CAG TCA GAC ACA G	CAA ATT ATT GTT TTC TAA TCA ATC GGT TTA C	231
20a	TTA GGT AAG TAT TTA CTC CAC TGC G	GTC TGT GAC TGT TGC TGT TGT GTA G	228
20b	GTC AAC AAC TTG TGA CCA AAT TAG	ATG AAA GTA AAT GAG TTT GAA GCA GC	291
21	GGG AGT AAA GCA ATG CTG CAT AAT C	TCT GAG TAA CTC TTA ATG GGC CAT C	282
3′-UTR	TCC AGC AGT TTC ATG AGA TGC	GAG GTC ATT TCA TAG CTG AGC	221

Exons are numbered according to a previous report (Steeves et al., 1999). For exon 18b, either of the two forward primers was used as described in Section 2.

Table 2
Genotype and allele distribution of the 1982 (A→G) [H542R] polymorphism in the *hClock* gene in circadian rhythm sleep disorder patients and contols

Subjects	*N*	Genotypes (%)			Alleles (%)	
		A/A	A/G	G/G	A	G
Controls	109	107 (98.2)	2 (1.8)	0 (0)	216 (99.1)	2 (0.9)
DSPS	59	57 (96.6)	2 (3.4)	0 (0)	116 (98.3)	2 (1.7)
N-24	37	37 (100)	0 (0)	0 (0)	74 (100)	0 (0)

The amino acid position is given relative to the first methionine. To be consistent with the previous reports, the nucleotide number is based on AF011568. Values in parentheses represent percentage frequencies.

automatic sequencer (model AB1310, Applied Biosystems).

2.3. Data analysis

Fisher's exact test with two-tailed probability was used to compare genotype distributions and allele frequencies between controls and patients with DSPS, and between controls and patients with N-24. The Hardy–Weinberg equilibrium was calculated with the Arlequin software package (obtained from http://lgb.unige.ch/arlequin/software/).

3. Results

With SSCP analysis and subsequent direct sequencing, 32 patients (22 with DSPS and 10 with N-24) were screened for nucleotide sequence variations in the entire coding region of the *hClock* gene and the adjacent exon–intron boundaries. Two polymorphisms were identified in the coding regions of the gene. The first sequence variation is an A to G change occurring at nucleotide position 1982 in exon 17, which alters the coding sequence from a histidine to an arginine at amino acid 542. The second variation, a C to T change at nucleotide 2121 in exon 18, is a silent polymorphism. The genotype and allele distribution of the 1982(A→G) polymorphism, which induces an amino acid substitution, were investigated in the total study population; during the course of the distribution analysis, a third polymorphism, 1955(G→A) [R533Q], was identified. The 1955(G→A) [R533Q] polymorphism was observed in one allele of a control, while the 1982(A→G) [H542R] polymorphism was observed in two patients with DSPS and two controls (Table 2). Neither of the missense polymorphisms showed significant differences in genotype or allele distribution between patients with DSPS or N-24 and controls.

The 3111(T→C) polymorphism in the 3′-UTR of the *hClock* gene has been reportedly associated with morning–evening activity preferences (Katzenberg et al., 1998). Therefore, we studied the distribution of the polymorphism in our study population. The SSCP analysis in the 32 patients suggested the presence of two different alleles in this locus, and subsequent sequencing revealed that each allele corresponds to either 3111C or 3111T. All of the study samples were subjected to SSCP analysis; direct sequencing was performed for variants which showed a SSCP band shift that suggested the presence of at least one 3111C allele. Direct sequencing analysis was also performed on seven randomly selected samples which had a SSCP migration pattern consistent with the homozygous 3111T allele, resulting in the confirmation of the SSCP genotyping results. Genotype frequencies for the T3111C polymorphism were not significantly different from that expected by Hardy–Weinberg equilibrium, both in the control population and the total study population. The 3111C allele frequency, which is reported to be significantly increased in evening types, was lower in patients with DSPS than in controls ($P=0.0152$), whereas Bonferroni's correction for multiple comparisons abolished the significance of the difference ($P=0.061$) (Table 3). In patients with N-24, the 3111C allele exhibited reduced frequen-

Table 3
Genotype and allele distribution of the 3111 (T→C) polymorphism in the 3′-UTR of the *hClock* gene in circadian rhythm sleep disorder patients and controls

Subjects	*N*	Genotypes (%)			Alleles (%)	
		T/T	T/C	C/C	T	C
Controls	109	63 (57.8)	40 (36.7)	6 (5.5)	166 (76.1)	52 (23.9)
	M 56	M 35 (62.5)	M 16 (28.6)	M 5 (8.9)	M 86 (76.8)	M 26 (23.2)
	F 53	F 28 (52.8)	F 24 (45.3)	F 1 (1.9)	F 80 (75.5)	F 26 (24.5)
DSPS	59	45 (76.3)	13 (22.0)	1 (1.7)	103 (87.3)	15 (12.7)*
	M 39	M 31 (79.5)	M 7 (17.9)	M 1 (2.6)	M 69 (88.5)	M 9 (11.5)
	F 20	F 14 (70.0)	F 6 (30.0)	F 0 (0.0)	F 34 (85.0)	F 6 (15.0)
N-24	37	26 (70.3)	9 (24.3)	2 (5.4)	61 (82.4)	13 (17.6)**
	M 27	M 20 (74.1)	M 5 (18.5)	M 2 (7.4)	M 45 (83.3)	M 9 (16.7)
	F 10	F 6 (60.0)	F 4 (40.0)	F 0 (0.0)	F 16 (80.0)	F 4 (20.0)

Values in parentheses represent percentage frequencies compared to controls. M, males; F, females.
* $P=0.0152$ vs. controls. Bonferroni's correction $P=0.061$. Becuase the R533Q polymorphism was found in only one control, it was not included in calculation of the multiplier for Bonferroni's correction.
** $P=0.332$ vs. controls.

cy compared to the controls; however, the difference was not statistically significant.

4. Discussion

We have identified three polymorphisms, of which two predict the amino acid substitutions [R533Q] and [H542R]. Both of the missense polymorphisms are located in exon 17, which is equal to exon 19 in the mouse *Clock* (*mClock*) gene (Steeves et al., 1999). Exon 19 in *mClock* encodes the only region of amino acid sequence similarity between CLOCK and another bHLH-PAS protein, MOP4 (NPAS2), in the glutamine-rich C-terminal half of the protein (King et al., 1997). The mutant mCLOCK protein derived from the exon-19-deleted *Clock* allele formed heterodimers with BMAL1 that bound DNA but failed to activate transcription, which indicates that exon 19 is located within the transcriptional regulatory domain (Gekakis et al., 1998). A point mutation in the *mClock* gene, which causes skipping of exon 19, induces elongation of the locomotor activity rhythm in heterozygotes and abolition of the rhythmicity in homozygotes, as well as alteration of the homeostaic regulation of sleep (King et al., 1997; Naylor et al., 2000). The amino acid R533 is conserved in fish, amphibians, birds, rodents and humans, while H542 is conserved in birds, rodents and humans. Therefore, the R533Q and/or H542R polymorphism in exon 17 of the *hClock* gene might result in some alteration in the transcriptional activity of the hCLOCK protein. Although the frequencies of the R533Q and H542R polymorphisms were very low compared to that of the 3111C polymorphism and not significantly different between sleep disorder patients and controls in our study population (Table 2), the polymorphisms could be associated with other disorders related to circadian rhythm or sleep regulation.

Previous study showed that the 3111C allele frequency was slightly higher in evening types (i.e. people who prefer evening activity) (Katzenberg et al., 1998); the higher frequency was not associated with major depression (Desan et al., 2000). DSPS is thought to be an extreme form of evening preference, because patients with DSPS score very low values on the morningness–eveningness scale derived from Horne and Osteberg's Morningness–Eveningness Questionnaire (Horne and Osteberg, 1976; Weitzman et al., 1981). Therefore, we expected that the 3111C allele frequencies in patients with DSPS and N-24 would be higher than in controls. In contrast to this hypothesis, we observed reduced frequency of the 3111C allele in patients with DSPS (0.127) compared to that in

control subjects (0.239). Our results could have occurred by chance, because the difference did not remain significant after Bonferroni's correction for multiple comparisons. The discrepancy may have arisen from a difference of the study population; we used circadian rhythm sleep disorder patients who suffered from social difficulty and sought medical help, while the previous study used a population-based random sample whose sleep–wake patterns seemed to be within normal limits. Alternatively, the lower frequency finding may reflect the presence of underlying common etiologies between DSPS and morning preference. Recent studies suggest that people with DSPS or N-24 and people with morning preference exhibit similar physiological features in the phase relationship between endogenous circadian rhythm and sleep–wake cycle, a prolonged interval between the core body temperature trough and the natural wake time (Ozaki et al., 1996; Duffy et al., 1999; Uchiyama et al., 2000). Further studies are required to confirm the possible contribution of the T3111C polymorphism to the susceptibility to sleep disorders and the aberrant coupling between circadian rhythm and sleep–wake cycle.

The possibility remains that we have missed another polymorphisms because the sensitivity of SSCP is not 100%, although the possibility has been reduced by performing SSCP under two different conditions. The T3111C polymorphism may be associated with other functional polymorphisms, located in untranslated regions, which act as regulatory domains of the gene.

In conclusion, in performing the first systematic screening for sequence polymorphisms in the entire coding region of *hClock* gene, we found two missense polymorphisms, R533Q and H542R, which do not appear to play important roles in the development of DSPS or N-24. A silent polymorphism, C2121T, was detected and will be useful for other studies. The possible functional relevance of the T3111C polymorphism to sleep disorders should be studied further. Identification of genetic components of circadian rhythm sleep disorders will lead not only to the elucidation of the pathophysiology of the disorders but also to the general understanding of interindividual variations in circadian rhythms.

Acknowledgments

The nucleotide sequences containing the missense polymorphisms reported in this manuscript have been submitted to the DDBJ/EMBL/GenBank databases under the accession numbers AB059556 and AB061682. The authors are grateful to Mr Eiichi Yamada, Ms Kyoko Ohnishi, and Mr Masakazu Kinoshita for their expert technical assistance. This work was supported by research grants from the Ministry of Health and Welfare, and the Ministry of Education, Science, Sports, and Culture (10557089, 11233206, 11770558, 12470198), and by Saitama Medical School.

References

Bunger, M.K., Wilsbacher, L.D., Moran, S.M., Clendenin, C., Radcliffe, L.A., Hogenesch, J.B., Simon, M.C., Takahashi, J.S., Bradfield, C.A., 2000. *Mop3* is an essential component of the master circadian pacemaker in mammals. Cell 103, 1009–1017.

Czeisler, C.A., Richardson, G.S., Coleman, R.M., Zimmerman, J.C., Moore-Ede, M.C., Dement, W.C., Weitzman, E.D., 1981. Chronotherapy: resetting the circadian clocks of patients with delayed sleep phase insomnia. Sleep 4, 1–21.

Dahlitz, M., Alvarez, B., Vignau, J., English, J., Arendt, J., Parkes, J.D., 1991. Delayed sleep phase syndrome response to melatonin. Lancet 337, 1121–1125.

Desan, P.H., Oren, D.A., Malison, R., Price, L.H., Rosenbaum, J., Smoller, J., Charney, D.S., Gelernter, J., 2000. Genetic polymorphism at the *CLOCK* gene locus and major depression. American Journal of Medical Genetics 96, 418–421.

Duffy, J.F., Dijk, D.-J., Hall, E.F., Czeisler, C.A., 1999. Relationship of endogenous circadian melatonin and temperature rhythms to self-reported preference for morning or evening activity in young and older people. Journal of Investigative Medicine 47, 141–150.

Dunlap, J.C., 1999. Molecular basis for circadian clocks. Cell 96, 271–290.

Ebisawa, T., Uchiyama, M, Kajimura, N., Mishima, K., Kamei, Y., Katoh, M., Watanabe, T., Sekimoto, M., Shibui, K., Kim, K., Kudo, Y., Ozeki, Y., Sugishita, M., Toyoshima, R., Inoue, Y., Yamada, N., Nagase, T., Ozaki, N., Ohara, O., Ishida, N., Okawa, M., Takahashi, K., Yamauchi, T., 2001. Association of structural polymorphisms in the human *period3* gene with delayed sleep phase syndrome. EMBO Reports 2, 342–346.

Fink, R., Ancoli-Israel, S., 1997. Pedigree of one family with delayed sleep phase syndrome. Sleep Research 26, 713.

Gekakis, N., Staknis, D., Nguyen, H.B., Davis, F.C., Wilsbacher, L.D., King, D.P., Takahashi, J.S., Weitz, C.J., 1998. Role of the CLOCK protein in the mammalian circadian mechanism. Science 280, 1564–1569.

Hastings, M.H., 1997. Central clocking. Trends in Neuroscience 20, 459–464.

Horne, J.A., Osteberg, O., 1976. A self-assessment questionnaire to determine morningness-eveningness in human circadian rhythms. International Journal of Chronobiology 4, 97–110.

Jones, C.R., Campbell, S.S., Zone, S.E., Cooper, F., DeSano, A., Murphy, P.J., Jones, B., Czajkowski, L., Ptacek, L.J., 1999. Familial advanced sleep-phase syndrome: a short-period circadian rhythm variant in humans. Nature Medicine 5, 1062–1065.

Katzenberg, D., Young, T., Finn, L., Lin, L., King, D.P., Takahashi, J.S., Mignot, E., 1998. A *CLOCK* polymorphism associated with human diurnal preference. Sleep 21, 569–576.

King, D.P., Takahashi, J.S., 2000. Molecular genetics of circadian rhythms in mammals. Annual Review of Neuroscience 23, 713–742.

King, D.P., Zhao, Y., Sangoram, A.M., Wilsbacher, L.D., Tanaka, M., Antoch, M.P., Steeves, T.D.L., Vitaterna, M.H., Kornhauser, J.M., Lowrey, P.L., Turek, F.W., Takahashi, J.S., 1997. Positional cloning of the mouse circadian *Clock* gene. Cell 89, 641–653.

Lowrey, P.L., Shimomura, K., Antoch, M.P., Yamazaki, S., Zemenides, P.D., Ralph, M.R., Menaker, M., Takahashi, J.S., 2000. Positional syntenic cloning and functional characterization of the mammalian circadian mutation *tau*. Science 288, 483–492.

Naylor, E., Bergmann, B.M., Krauski, K., Zee, P.C., Takahashi, J.S, Vitaterna, M.H., Turek, F.W., 2000. The circadian clock mutation alters sleep homeostasis in the mouse. Journal of Neuroscience 20, 8138–8143.

Ozaki, S., Uchiyama, M., Shirakawa, S., Okawa, M., 1996. Prolonged interval from body temperature nadir to sleep offset in patients with delayed sleep phase syndrome. Sleep 19, 36–40.

Regestein, Q.R., Monk, T.H., 1995. Delayed sleep phase syndrome: a review of its clinical aspects. American Journal of Psychiatry 152, 602–608.

Shearman, L.P., Jin, X., Lee, C., Reppert, S.M., Weaver, D.R., 2000. Targeted disruption of the *mPer3* gene: subtle effects on circadian clock function. Molecular and Cellular Biology 20, 6269–6275.

Steeves, T.D.L., King, D.P., Zhao, Y., Sanogram, A.M., Du, F., Bowcock, A.M., Morre, R.Y., Takahashi, J.S., 1999. Molecular cloning and characterization of the human CLOCK gene: expression in the suprachiasmatic nuclei. Genomics 57, 189–200.

Toh, K.L., Jones, C.R., He, Y., Eide, E.J., Hinz, W.A., Virshup, D.M., Ptacek, L.J., Fu, Y.-H., 2001. An *hPer2* phosphorylation site mutation in familial advanced sleep phase syndrome. Science 291, 1040–1043.

Uchiyama, M., Okawa, M., Shibui, K., Kim, K., Tagaya, H., Kudo, Y., Kamei, Y., Hayakawa, T., Urata, J., Takahashi, K., 2000. Altered phase relation between sleep timing and core body temperature rhythm in delayed sleep phase syndrome in humans. Neuroscience Letters 294, 101–104.

Weitzman, E.D., Czeisler, C.A., Coleman, R.M., Spielman, A.J., Zimmerman, J.C., Dement, W., 1981. Delayed sleep phase syndrome. Archives of General Psychiatry 38, 737–746.

EMBO reports

scientific report

Association of structural polymorphisms in the human *period3* gene with delayed sleep phase syndrome

Takashi Ebisawa[1,+], Makoto Uchiyama[2], Naofumi Kajimura[3], Kazuo Mishima[4], Yuichi Kamei[5], Masaaki Katoh[3], Tsuyoshi Watanabe[3], Masanori Sekimoto[3], Kayo Shibui[2], Keiko Kim[6], Yoshinao Kudo[5], Yuji Ozeki[7], Mariko Sugishita[1], Ryoichi Toyoshima[1], Yuichi Inoue[8], Naoto Yamada[7], Takahiro Nagase[9], Norio Ozaki[10], Osamu Ohara[9], Norio Ishida[11], Masako Okawa[7], Kiyohisa Takahashi[3,5] & Toshio Yamauchi[1]

[1]Department of Psychiatry, Saitama Medical School, 38 Morohongo, Saitama 350-0495, [2]Department of Psychophysiology, National Center of Neurology and Psychiatry (NCNP), 1-7-3 Kohnodai, Chiba 272-0827, [3]Musashi Hospital, NCNP, 4-1-1 Ogawa-cho, Tokyo 187-0031, [4]Department of Psychiatry, Akita University School of Medicine, 1-1-1 Hondo, Akita 010-8543, [5]Kohnodai Hospital, NCNP, 1-7-1 Kohnodai, Chiba 272-0827, [6]Department of Psychiatry, Tokyo Women's Medical College, 8-1 Kawata-cho, Tokyo 162-8666, [7]Department of Psychiatry, Shiga University of Medical Science, Seta Tsukinowa-cho, Shiga 520-2192, [8]Department of Psychiatry, Juntendo University, School of Medicine, 2-1-1 Hongo, Tokyo 113-8431, [9]Kazusa DNA Research Institute, 1532-3 Yana, Chiba 292-0812, [10]Department of Psychiatry, Fujita Health University School of Medicine, Machida Rakugabuchi, Aichi 470-1192 and [11]National Institute of Bioscience and Human Technology, Agency of Industrial Science and Technology, 1-1 Higashi, Ibaraki 305-8566, Japan

Received November 23, 2000; revised and accepted February 12, 2001

Recent progress in biological clock research has facilitated genetic analysis of circadian rhythm sleep disorders, such as delayed sleep phase syndrome (DSPS) and non-24-h sleep–wake syndrome (N-24). We analyzed the human *period3* (*hPer3*) gene, one of the human homologs of the *Drosophila* clock-gene *period* (*Per*), as a possible candidate for rhythm disorder susceptibility. All of the coding exons in the *hPer3* gene were screened for polymorphisms by a PCR-based strategy using genomic DNA samples from sleep disorder patients and control subjects. We identified six sequence variations with amino acid changes, of which five were common and predicted four haplotypes of the *hPer3* gene. One of the haplotypes was significantly associated with DSPS (Bonferroni's corrected $P = 0.037$; odds ratio = 7.79; 95% CI 1.59–38.3) in our study population. Our results suggest that structural polymorphisms in the *hPer3* gene may be implicated in the pathogenesis of DSPS.

INTRODUCTION

Most living organisms exhibit a circadian (~24 h) rhythm in their physiology and behavior, which is generated by an endogenous biological oscillator (Hastings, 1997). Genetic mutational studies using *Drosophila* led to the identification of the *period* (*Per*) gene, the first essential component of the circadian oscillator, which was followed by the isolation of various clock-relevant genes not only from *Drosophila*, but also from various species including mammals (Dunlap, 1999).

In mammals, clock-relevant genes such as *Per1/2/3*, *CLOCK*, *Cry1/2*, *BMAL1* and *Casein Kinase I epsilon* (*CK I* ε) are expressed in the hypothalamic suprachiasmatic nuclei (SCN), the site of the principal circadian oscillator, and are thought to play a role in the clock mechanism (Dunlap, 1999; Lowrey *et al.*, 2000). Mutations in *Per2*, *CLOCK*, *Cry1/2* and *CK I* ε genes are known to modulate circadian rhythms in hamsters and mice (King and Takahashi, 2000; Lowrey *et al.*, 2000); therefore, it is likely that human clock-relevant genes with mutations could also cause abnormal circadian rhythms.

In humans, sleep, plasma melatonin and the body core temperature show circadian rhythmicity, which is adjusted to 24 h by the environmental light–dark cycle and other stimuli such as social time cues (Hastings, 1997), whereas patients with circadian rhythm sleep disorders can not synchronize their sleep–wake cycle to the desired time schedule and have difficulties in their social lives (Campbell *et al.*, 1999). Delayed sleep phase syndrome (DSPS) patients exhibit sleep-onset insomnia with an inability to wake up at a conventional time for school or work.

+Corresponding author. Tel: +81 492 76 1213; Fax: +81 492 76 1622; E-mail: tebisawa@saitama-med.ac.jp

Cases with non-24-h sleep–wake syndrome (N-24) show a daily delay of the sleep phase, resulting in cyclic episodes of insomnia. Recently, genetic contributions to the pathogenesis of DSPS and advanced sleep phase syndrome (ASPS), in which patients wake up and fall asleep too early relative to the desired time schedule, have been suggested by clinical genetic studies (Fink and Ancoli-Israel, 1997; Jones *et al.*, 1999).

These results indicate that mutations in the clock-relevant genes may be involved in the susceptibility to circadian rhythm sleep disorders. To test this hypothesis, in this study we screened polymorphisms in the human *Per3* (*hPer3*) gene, one of the three human homologs of the *Drosophila* clock-gene *Per* (Takumi *et al.*, 1998; Zylka *et al.*, 1998), and identified 20 sequence variations, of which six predicted amino acid changes. We characterized the polymorphisms and investigated their distribution in circadian rhythm sleep disorder patients and controls.

RESULTS

hPer3 cDNA was isolated from a size-fractionated cDNA library of the human brain (DDBJ/EMBL/GenBank accession No. AB047686). Sequence analysis of the cDNA revealed that the human chromosome 1 contig with accession No. Z98884 contained all of the coding sequences of *hPer3* gene, as was suggested previously (Zylka *et al.*, 1998). Table I summarizes the exon structure of the *hPer3* gene, which consisted of 21 exons spanning >50 kbp. Based on the exon organization of the gene, polymerase chain reaction–single-strand conformation polymorphism (PCR-SSCP) analysis was performed, and genomic DNA from 36 patients (23 cases with DSPS and 13 with N-24) was screened for sequence variations in the *hPer3* gene. Polymorphisms in DNA samples displaying aberrant SSCP migration patterns were identified by direct sequence analysis. A total of 20 sequence variations were detected: 13 single-nucleotide polymorphisms (SNPs) and a polymorphic repeat region with four or five copies of a 54 bp repetitive sequence in the exons, and four SNPs and two insertion/deletions in the portion of the introns examined (Table II). Five of the SNPs in the exons predicted amino acid substitutions: V420M, V647G, P864A, M1037T and H1158R. Exon 18 contained a polymorphic repeat domain, which harbored four or five copies of a tandemly repeated 54 bp sequence encoding 18 amino acids, in addition to the M1037T polymorphism (Figure 1A, 2). The prevalence of the six variations with putative amino acid changes was investigated in a total of 78 patients (48 with DSPS and 30 with N-24) and 100 controls by PCR-SSCP and subsequent direct sequence analysis. For exon 18, PCR–restriction fragment length polymorphism (RFLP) analysis was also used to

Table I. Exon structure of the *hPer3* gene

Exon	Amino acids	Nucleotides (in Z98884)
1	1–43	(–224)–128 (61873–62224)
2	43–92	129–274 (62660–62805)
3	92–130	275–390 (63940–64055)
4	131–198	391–592 (65264–65465)
5	198–215	593–644 (71176–71227)
6	215–265	645–793 (75744–75892)
7	265–291	794–872 (78332–78410)
8	291–327	873–979 (80266–80372)
9	327–379	980–1136 (80911–81067)
10	379–414	1137–1242 (86112–86217)
11	415–457	1243–1371 (87112–87240)
12	458–508	1372–1522 (87657–87807)
13	508–553	1523–1658 (96504–96639)
14	553–595	1659–1783 (97334–97458)
15	595–653	1784–1957 (97686–97859)
16	653–730	1958–2188 (103699–103929)
17	730–962	2189–2886 (104337–105034)
18	963–1072	2887–3214 (107053–107380)
19	1072–1133	3215–3398 (112981–113164)
20	1133–1183	3399–3549 (114218–114368)
21	1184–1210	3550–3630 (119891–119971)

In parentheses are the nucleotide positions in the sequence of accession No. Z98884.

Table II. Sequence variations detected in the *hPer3* gene

Region	Nucleotide change	Amino acid change
Intron 1	128 + 22(G→A)	none
Exon 2	195(C→T)	none
Intron 6	794–20insT	none
Intron 6	794–15(T→G)	none
Intron 7	872 + 53(T→C)	none
Intron 8	980–16delTTA	none
Exon 11	1258(G→A)	V420M
Exon 11	1338(T→C)	none
Exon 15	1881(G→A)	none
Exon 15	1940(T→G)	V647G
Exon 17	2259(G→A)	none
Exon 17	2415(C→T)	none
Exon 17	2484(A→G)	none
Exon 17	2590(C→G)	P864A
Exon 17	2616(G→A)	none
Exon 18	2934(C→T)	none
Exon 18	del(3031–3084 nt)	del(1011–1028 aa)
Exon 18	3110(T→C)	M1037T
Exon 20	3473(A→G)	H1158R
Intron 20	3549 + 19(G→A)	none

To avoid complications, nucleotide and amino acid positions are numbered according to the full-length *hPer3* cDNA sequence containing five copies of a 54 bp repeat (AB047686). The 3110(T→C) [M1037T] and the 3473(A→G)[H1158R] polymorphisms are estimated to be exclusively on a 4-repeat allele; therefore, actual nucleotide (nt) and amino acid (aa) positions relative to the putative initiation site are 3056 nt (1019 aa) and 3419 nt (1141 aa), respectively.

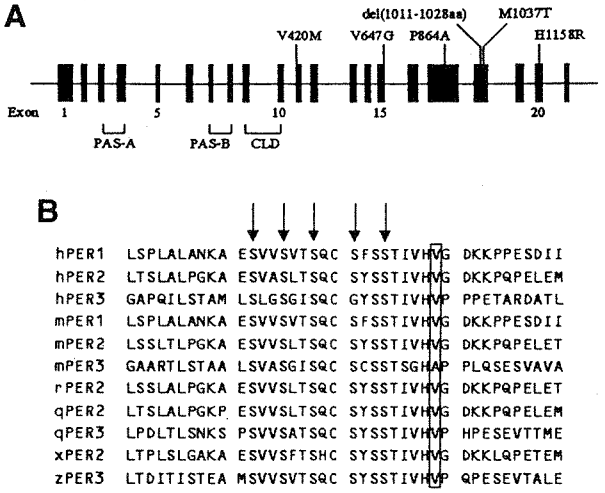

Fig. 1. (**A**) Schematic diagram of the *hPer3* gene illustrating the locations of six polymorphisms with putative amino acid changes. Exons 1–21 are depicted as closed boxes and are numbered intermittently for clarity. Sizes of the introns and exons are not to scale. Polymorphisms with putative amino acid changes are shown above the gene. At the bottom are summarized the locations of the coding sequences for domains of hPER3. CLD, cytoplasmic localization domain. (**B**) Alignment of the amino acid sequences of vertebrate PER homologs. Only the region adjacent to the V647G polymorphism is shown. Amino acid residues that correspond to V647 in hPER3 are boxed. Arrows indicate the putative target residues of CK I ε (Toh *et al.*, 2001). hPER1/2/3, human PER1/2/3; mPER1/2/3, mouse PER1/2/3; rPER2, rat PER2; qPER2/3, Japanese quail PER2/3; xPER2, *Xenopus* PER2; zPER3, zebrafish PER3.

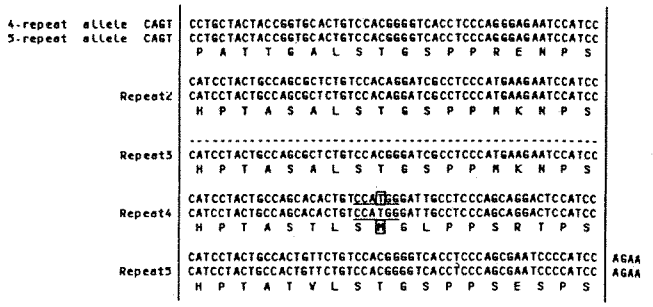

Fig. 2. Nucleotide and amino acid sequences of each allele in the polymorphic repeat region of the *hPer3* gene. The 4-repeat and 5-repeat alleles are aligned for optimal homology. The dotted line indicates a gap in the sequence created for optimal alignment. The nucleotide and amino acid that are subject to 3110(T→C) [M1037T] polymorphism, which was exclusively observed on a 4-repeat allele, are boxed. The *Nco*I restriction site used in RFLP analysis is underlined.

confirm the number of repetitive sequences and the presence of M1037T polymorphism (data not shown). M1037T polymorphism was observed exclusively on a 4-repeat allele (Figure 2). Because V420M polymorphism was found only in one allele in one DSPS case out of the total study population, it was not included in further analyses. Genotype frequencies for the other five polymorphisms (V647G, P864A, 4-repeat/5-repeat, M1037T and H1158R) were not significantly different from those expected by Hardy–Weinberg equilibrium, both in the control population and the total study population. There was a marked linkage disequilibrium among the five polymorphisms. The V647G polymorphism was in complete concordance with H1158R. M1037T was always accompanied either by P864A or [V647G, H1158R]. On the basis of an expectation-maximization algorithm, we predicted four haplotypes, [V647, P864, 4-repeat, M1037, H1158] (designated as the H1 haplotype), [V647, P864, 5-repeat, M1037, H1158] (H2), [V647, A864, 4-repeat, T1037, H1158] (H3) and [G647, P864, 4-repeat, T1037, R1158] (H4), with a cumulative frequency of 100%. We could not identify a single recombinant event within these haplotypes in any of the patients or control individuals, who were unrelated except for one of the DSPS patients and one of the N-24 patients, who were siblings.

Carrier and estimated haplotype frequencies are reported in Table III. The frequency of the H4 haplotype was substantially higher in DSPS patients [7 (7.3%) of 96] than in controls [2 (1.0%) of 200], giving an odds ratio of 7.79 (95% CI 1.59–38.3; $P = 0.0062$). This difference remained significant after Bonferroni's correction for two disorders and four haplotypes ($P = 0.037$). These results indicate that the H4 haplotype in the *hPer3* gene is associated with increased susceptibility to DSPS. None of the other haplotypes showed any significant association with the disorders. Neither member of the sibling pair carried the H4 haplotype.

DISCUSSION

There are two possibilities that might explain the association between the H4 haplotype of the *hPer3* gene and DSPS. First, the H4 haplotype may be in linkage disequilibrium with functional mutations elsewhere within the *hPer3* gene or a susceptibility locus nearby. Secondly, the polymorphisms on the H4 haplotype may directly contribute towards the increased susceptibility to DSPS. Out of the five polymorphisms on the H4 haplotype, G647 and R1158 are exclusively observed on the H4 haplotype, and G647 is a substitute of V647, which is conserved among most of the vertebrate PER homologs in the database (Table III; Figure 1B). Therefore, it is likely that G647 may be the causative variant. Of note, G647 is located within the region of amino acid similarity to the CK I ε binding domain of hPER1 and hPER2 (Vielhaber *et al.*, 2000; Toh *et al.*, 2001). Moreover, G647 is situated only five residues C-terminal relative to the region that corresponds to the putative phosphorylation site for CK I ε in hPER2 (Toh *et al.*, 2001) (Figure 1B). Although CK I ε-dependent phosphorylation of PER3 protein has not been reported yet, structural conservation of the putative CK I ε phosphorylation site among PER1/2/3 indicates that PER3 is another substrate of CK I ε. In addition, substrate recognition of kinases can be affected by amino acid residues surrounding the consensus sequence (Pinna and Ruzzene, 1996). Taken together, we speculate that G647 polymorphism in the H4 haplotype may alter the CK I ε-dependent phosphorylation of hPER3. In our study population, two of the H4 haplotype carriers were controls (Table III); therefore, we can not exclude the possibility that an additional unknown polymorphism, such as one in CK I ε, might be

Table III. Carrier and estimated haplotype frequencies of *hPer3* polymorphisms in patients and controls

Haplotype	Carrier frequency (%)			Haplotype frequency (%)		
	DSPS	N-24	Controls	DSPS	N-24	Controls
H1[V647,P864,4-repeat,M1037,H1158]	40/48 (83.3)	28/30 (93.3)	89/100 (89.0)	62/96 (64.6)	42/60 (70.0)	137/200 (68.5)
H2[V647,P864,5-repeat,M1037,H1158]	16/48 (33.3)	7/30 (23.3)	34/100 (34.0)	19/96 (19.8)	7/60 (11.7)	39/200 (19.5)
H3[V647,A864,4-repeat,T1037,H1158]	7/48 (14.6)	10/30 (33.3)	19/100 (19.0)	8/96 (8.3)	10/60 (16.7)	22/200 (11.0)
H4[G647,P864,4-repeat,T1037,R1158]	7/48 (14.6)[a]	1/30 (3.3)	2/100 (2.0)	7/96 (7.3)[b]	1/60 (1.7)	2/200 (1.0)

Underlined are minor alleles in each polymorphic locus.
Statistical comparisons were performed using a two-tailed Fisher's exact test.
[a]$P = 0.0055$ versus controls, Bonferroni's corrected $P = 0.033$.
[b]$P = 0.0062$ versus controls, odds ratio = 7.79, 95% CI 1.59–38.3, Bonferroni's corrected $P = 0.037$.

necessary to exhibit an apparent alteration in phosphorylation of hPER3 and cause DSPS.

Phosphorylation of PER1 and PER2 by CK I ε seems to play an essential role in the circadian system (Keesler *et al.*, 2000; Vielhaber *et al.*, 2000; Toh *et al.*, 2001). However, at the present time, it is difficult to elucidate how the G647-induced alteration of hPER3 phosphorylation, if any, could lead to the susceptibility to DSPS. While it is reported that a targeted disruption of the *Per3* gene induced a subtle but significant alteration in the circadian cycle length in mice, the specific functional role of the *Per3* gene in the clock system is not yet clearly understood (Shearman *et al.*, 2000). The PER3 protein forms heterodimers with PER1/2 and CRY1/2, respectively, and enters into the nucleus, resulting in inhibition of CLOCK/BMAL1-mediated transcription. (Kume *et al.*, 1999; Yagita *et al.*, 2000). A possible contribution of PER3 in an output pathway of circadian oscillation is also proposed (Shearman *et al.*, 2000). Altered phosphorylation of hPER3 might affect these functions. Alternatively, PER3 might act as a competitor for CK I ε binding against PER1/2 proteins. It is assumed that DSPS may be caused by subsensitivity to light, a prolonged endogenous circadian period, or abnormal coupling of the sleep–wake cycle to the circadian rhythm (Ozaki *et al.*, 1996; Campbell *et al.*, 1999). Functional analysis of the predicted form of the mutated hPER3 protein, in addition to the search for another polymorphism in *CK I ε*, may reveal the specific function of PER3 and the underlying physiological mechanism of developing DSPS.

No significant association was observed between the H4 haplotype and N-24, which often shows symptoms of DSPS during the course of the illness and is supposed to be caused by common underlying mechanisms (Weitzman *et al.*, 1981; Campbell *et al.*, 1999). In our study, 41 (85%) of the 48 DSPS patients did not carry the H4 haplotype (Table III); therefore, it is likely that DSPS is genetically heterogeneous with residual unknown genetic factors, of which some confer susceptibility to both DSPS and N-24.

A human *CLOCK* (*hCLOCK*) gene polymorphism in the 3′-untranslated region was reported to be associated with morningness–eveningness tendencies (individual differences in preferred timing of behavior) (Katzenberg *et al.*, 1998). A recent study has revealed that a missense mutation in hPER2 causes familial ASPS (Toh *et al.*, 2001). It is possible that the polymorphisms identified in this study, in combination with additional ones in other clock-relevant genes such as *CLOCK* and *hPER2*, may lead to physiological or pathological variations in circadian rhythmicity among individuals.

To our knowledge, this is the first study analyzing the *hPer3* gene for polymorphisms in circadian rhythm sleep disorders. Our findings suggest that the H4 haplotype of the *hPer3* gene may confer susceptibility to DSPS in ~15% of affected people. Verification using other populations or familial based internal controls allowing for a linkage disequilibrium study is needed. Identification of a genetic factor will provide valuable insights into the pathogenesis of DSPS and in developing therapeutic strategies to treat patients with the disorder.

METHODS

Subjects. Cases and healthy control subjects, all of whom were sighted, were recruited at the participating institutes on mainland Japan. Cases comprised 48 patients with DSPS and 30 with N-24, and satisfied the International Classification of Sleep Disorders (ICSD1990) criteria. Cases with DSPS consisted of 29 males and 19 females (mean age 28.4 ± 10.0 years), and those with N-24 consisted of 22 males and eight females (mean age 26.4 ± 8.2 years). A total of 100 control subjects were recruited, 47 of whom were males and 53 were females (mean age 33.2 ± 7.9 years). All control subjects with a history of sleep disorders or psychoses were excluded. A part of the study population was reported previously (Ebisawa *et al.*, 1999). Blood was aspirated and genomic DNA was prepared from white blood cells with a QIAamp DNA Blood Maxi Kit (Qiagen, Hilden) for use in the genetic analysis. The design of the study was approved by the ethics committees of the Saitama Medical School and the respective institutes from which blood samples were obtained. Each individual signed an informed consent form.

Isolation and sequencing of *hPer3* cDNA. The *hPer2* nucleotide sequence (DDBJ/EMBL/GenBank accession No. AB002345) was used to perform a BLAST search against expressed sequence tags (ESTs) of ~10 000 cDNA clones isolated from size-fractionated human brain cDNA libraries (Ohara *et al.*, 1997). Several clones showed high sequence similarity to the open reading frame (ORF) of *hPer2*. Sequence analysis of the full-length cDNAs suggested that they comprised two groups, of which one was made up of *hPer1* cDNAs. cDNA clones in the second group showed 66% identity with mouse *Per3* cDNA at the amino acid level, and >99% identity at the nucleotide level, to the corresponding sequences in a human chromosome 1 genomic contig,

Z98884, which contains the sequence of the *hPer3* gene (Zylka *et al.*, 1998). Thus, we identified the second group clones as *hPer3* cDNAs. The nucleotide sequence of a *hPer3* cDNA with the longest 5′ region contained the first in-frame ATG preceded by a stop codon and encoded an ORF of 1210 amino acids, suggesting that the cDNA clone (AB047686) comprises a whole coding region of the *hPer3* gene. The deduced amino acid sequence of the ORF showed 66, 39 and 42% identity with that of mouse PER3, human PER1 and human PER2 protein, respectively. From the comparison with the nucleotide sequence of Z98884, four discrepancies [1338(T→C), 2504(T→C)[L835P], 2852(A→G)[Q951R] and 3057(A→G)] were identified. After we had finished analyzing the sequence of the isolated clone, an *hPer3* cDNA sequence assembled from public domain ESTs was independently released into the DDBJ/EMBL/GenBank database with the accession No. AL157954. The nucleotide sequence of AL157954 was >99% identical to that of AB047686.

SSCP and sequencing. Fluorescein-labeled oligonucleotide primers for SSCP analysis were synthesized based on the genomic sequence of the *hPer3* gene to amplify all of the coding exons and the flanking exon–intron boundaries, generating PCR products of 209–414 bp (primer sequences are given in the Supplementary data, available at *EMBO reports* Online). SSCP analysis was performed as described previously (Ebisawa *et al.*, 1999). Nucleotide sequences for the polymorphic repeat region and the insertion/deletions were confirmed by direct sequencing of the DNA samples homozygous for each variation.

RFLP analysis of the repeat domain. Exon 18 and adjacent introns were amplified using forward (5′-CAAAATTTTATGAC-ACTACCAGAATGGCTGAC-3′) and reverse (5′-AACCTTGTAC-TTCCACATCAGTGCCTGG-3′) primers, the resultant PCR products separated on 1.5% agarose gels after digestion with *Nco*I, and visualized using SYBR Green I Stain (FMC BioProducts, Rockland, ME).

Statistical analysis. The calculations of Hardy–Weinberg equilibrium, pairwise linkage disequilibrium and haplotype frequencies were computed using the Arlequin software package (obtained from http://lgb.unige.ch/arlequin/software/). Fisher's exact test was performed using Prism software (Graphpad Software Inc., San Diego, CA).

DDBJ/EMBL/GenBank accession Nos. The novel sequence data reported in this manuscript have been submitted to the DDBJ/EMBL/GenBank databases under accession Nos AB047520–AB047539 and AB047686.

Supplementary data. Primers used for SSCP analysis of the *hPer3* gene are available as Supplementary data at *EMBO reports* Online.

ACKNOWLEDGEMENTS

Technical contributions by Eiichi Yamada, Kyoko Ohnishi and Masakazu Kinoshita are gratefully acknowledged. This work was supported by research grants from the Ministry of Health and Welfare, and the Ministry of Education, Science, Sports, and Culture (10557089, 11233206, 12470198) and Saitama Medical School.

REFERENCES

Campbell, S.S., Murphy, P.J., van den Heuvel, C.J., Roberts, M.L. and Stauble, T.N. (1999) Etiology and treatment of intrinsic circadian rhythm sleep disorders. *Sleep Med. Rev.*, **3**, 179–200.

Dunlap, J.C. (1999) Molecular basis for circadian clocks. *Cell*, **96**, 271–290.

Ebisawa, T. *et al.* (1999) Allelic variants of human melatonin 1a receptor: function and prevalence in subjects with circadian rhythm sleep disorders. *Biochem. Biophys. Res. Commun.*, **262**, 832–837.

Fink, R. and Ancoli-Israel, S. (1997) Pedigree of one family with delayed sleep phase syndrome. *Sleep Res.*, **26**, 713.

Hastings, M.H. (1997) Central clocking. *Trends Neurosci.*, **20**, 459–464.

Jones, C.R., Campbell, S.S., Zone, S.E., Cooper, F., DeSano, A., Murphy, P.J., Jones, B., Czajkowski, L. and Ptacek, L.J. (1999) Familial advanced sleep-phase syndrome: a short-period circadian rhythm variant in humans. *Nature Med.*, **5**, 1062–1065.

Katzenberg, D., Young, T., Finn, L., Lin, L., King, D.P., Takahashi, J.S. and Mignot, E. (1998) A *CLOCK* polymorphism associated with human diurnal preference. *Sleep*, **21**, 569–576.

Keesler, G.A., Camacho, F., Guo, Y., Virshup, D., Mondadori, C. and Yao, Z. (2000) Phosphorylation and destabilization of human period1 clock protein by human casein kinase I ε. *Neuroreport*, **11**, 951–955.

King, D.P. and Takahashi, J.S. (2000) Molecular genetics of circadian rhythms in mammals. *Annu. Rev. Neurosci.*, **23**, 713–742.

Kume, K., Zylka, M.J., Sriram, S., Shearman, L.P., Weaver, D.R., Jin, X., Maywood, E.S., Hastings, M.H. and Reppert, S.M. (1999) *mCry1* and *mCry2* are essential components of the negative limb of the circadian clock feedback loop. *Cell*, **98**, 193–205.

Lowrey, P.L., Shimomura, K., Antoch, M.P., Yamazaki, S., Zemenides, P.D., Ralph, M.R., Menaker, M. and Takahashi, J.S. (2000) Positional syntenic cloning and functional characterization of the mammalian circadian mutation *tau*. *Science*, **288**, 483–492.

Ohara, O., Nagase, T., Ishikawa, K.-I., Nakajima, D., Ohira, M., Seki, N. and Nomura, N. (1997) Construction and characterization of human brain cDNA libraries suitable for analysis of cDNA clones encoding relatively large proteins. *DNA Res.*, **4**, 53–59.

Ozaki, S., Uchiyama, M., Shirakawa, S. and Okawa, M. (1996) Prolonged interval from body temperature nadir to sleep offset in patients with delayed sleep phase syndrome. *Sleep*, **19**, 36–40.

Pinna, L.A. and Ruzzene, M. (1996) How do protein kinases recognize their substrates? *Biochim. Biophys. Acta*, **1314**, 191–225.

Shearman, L.P., Jin, X., Lee, C., Reppert, S.M. and Weaver, D.R. (2000) Targeted disruption of the *mPer3* gene: subtle effects on circadian clock function. *Mol. Cell. Biol.*, **20**, 6269–6275.

Takumi, T. *et al.* (1998) A light-independent oscillatory gene *mPer3* in mouse SCN and OVLT. *EMBO J.*, **17**, 4753–4759.

Toh, K.L., Jones, C.R., He, Y., Eide, E.J., Hinz, W.A., Virshup, D.M., Ptacek, L.J. and Fu, Y.-H. (2001) An h*Per2* phosphorylation site mutation in familial advanced sleep-phase syndrome. *Science* online, 10.1126/science.1057499.

Vielhaber, E., Eide, E., Rivers, A., Gao, Z.-H. and Virshup, D.M. (2000) Nuclear entry of the circadian regulator mPER1 is controlled by mammalian casein kinase I ε. *Mol. Cell. Biol.*, **20**, 4888–4899.

Weitzman, E.D., Czeisler, C.A., Coleman, R.M., Spielman, A.J., Zimmerman, J.C. and Dement, W. (1981) Delayed sleep phase syndrome. *Arch. Gen. Psychiatr.*, **38**, 737–746.

Yagita, K., Yamaguchi, S., Tamanini, F., van der Horst, G.T.J., Hoeijmakers, J.H.J., Yasui, A., Loros, J.J., Dunlap, J.C. and Okamura, H. (2000) Dimerization and nuclear entry of mPER proteins in mammalian cells. *Genes Dev.*, **14**, 1353–1363.

Zylka, M.J., Shearman, L.P., Weaver, D.R. and Reppert, S.M. (1998) Three *period* homologs in mammals: differential light responses in the suprachiasmatic circadian clock and oscillating transcripts outside of brain. *Neuron*, **20**, 1103–1110.

DOI: 10.1093/embo-reports/kve070

Biochemical and Biophysical Research Communications **262**, 832–837 (1999)
Article ID bbrc.1999.1308, available online at http://www.idealibrary.com on IDEAL®

Alleic Variants of Human Melatonin 1a Receptor: Function and Prevalence in Subjects with Circadian Rhythm Sleep Disorders

Takashi Ebisawa,*[,1] Naofumi Kajimura,† Makoto Uchiyama,‡ Masaaki Katoh,† Masanori Sekimoto,† Tsuyoshi Watanabe,† Yuji Ozeki,§ Masaaki Ikeda,[¶] Takako Jodoi,‖ Mariko Sugishita,* Toshio Iwase,* Yuichi Kamei,** Keiko Kim,†† Kayo Shibui,‡ Yoshinao Kudo,‡‡ Naoto Yamada,§ Ryoichi Toyoshima,* Masako Okawa,‡ Kiyohisa Takahashi,† and Toshio Yamauchi*

**Department of Psychiatry and [¶]Department of Physiology, Saitama Medical School, Saitama, Japan; †Musashi Hospital, National Center of Neurology and Psychiatry (NCNP), Tokyo, Japan; ‡Department of Psychophysiology, National Institute of Mental Health, NCNP, Chiba, Japan; **Kohnodai Hospital, NCNP, Chiba, Japan; ‖Department of Child Development, Kumamoto University School of Medicine, Kumamoto, Japan; ‡‡Department of Psychiatry, Nippon Medical School, Tokyo, Japan; ††Department of Psychiatry, Tokyo Women's Medical College, Tokyo, Japan; and §Department of Psychiatry, Shiga University of Medical Science, Shiga, Japan*

Received July 28, 1999

The human melatonin 1a (hMella) receptor gene was screened for mutations using genomic DNA samples from patients with circadian rhythm sleep disorders and control subjects by single strand conformational polymorphism analysis (SSCP). We found seven mutations, two of which predict amino acid changes R54W and A157V, respectively. The prevalence of the R54W variant and that of the A157V variant were several times more common in non-24-h sleep-wake syndrome subjects than among control subjects, although the incidence was not significant in our study group. When expressed in COS-7 cells, the R54W mutant receptor exhibited significantly reduced B_{max} and slightly enhanced affinity (reduced K_d) compared to the wild type receptor, while the A157V variant receptor showed similar binding characteristics to the wild type. The identification of variants in the hMella receptor will provide a useful tool for analyzing genetic predisposition toward various diseases related to melatonin function and to clarify the physiological role of melatonin receptors in humans. © 1999 Academic Press

Melatonin, a hormone principally produced in the pineal gland, is controlled by endogenous circadian clock and light-dark cycle, showing striking rhythm with high levels at night (1). Exogenous melatonin phase shifts the circadian rhythm of mammals, including humans, through its high-affinity cell-surface receptors expressed in the hypothalamic suprachiasmatic nuclei (SCN), where the mammalian circadian oscillator exists (2, 3, 4, 5, 6). Although the physiological role of endogenous melatonin in mammals is not as clear as that in birds and reptiles, several reports suggest that it may modify the entrainment of the circadian pacemaker by the light-dark cycle (7, 8, 9).

People with circadian rhythm sleep disorders, such as delayed sleep phase syndrome (DSPS; major symptoms of which are chronic difficulty in falling asleep at the appropriate clock time in the evening and inability to wake up at the desired time in the morning) and non-24-hour sleep-wake syndrome (N-24; which is characterized by a chronic pattern of daily delays in sleep onsets and wake times resulting in cyclic shifting of the sleep-wake phase) are known to express an altered melatonin secretion pattern and administration of melatonin at a certain time is effective for such patients, presumably through entrainment of the endogenous circadian rhythm (10, 11, 12, 13). In addition, it is reported that some of the circadian rhythm sleep disorders have a genetic component (14), therefore, we

[1] To whom correspondence should be addressed at Department of Psychiatry, Saitama Medical School, 38 Morohongo, Moroyama-cho, Iruma-gun, Saitama 350-0495, Japan. Fax: 81-492-76-1622. E-mail: tebisawa@saitama-med.ac.jp.

0006-291X/99 $30.00

analyzed the genetic variations of melatonin receptor genes in these disorders.

In mammals, two subtypes of melatonin receptors have been isolated, melatonin 1a (Mella) and melatonin 1b (Mellb) receptors, both of which are coupled to Gi protein. Mella subtype is expressed in the SCN, whereas Mellb subtype is detected in the retina (15, 16, 17). Polymorphisms of the Mella receptor in sheep have been already reported, but those in humans have not (18). In this study, we examined whether there was a mutation in the gene coding for human Mella (hMella) receptor in patients with circadian rhythm sleep disorders.

Using a PCR-based strategy, we identified seven polymorphisms, two of which resulted in amino acid substitutions. To test for the potential involvement of these mutations in the pathogenesis of the diseases, we studied the prevalence of the mutations in 66 patients with sleep disorders and 67 control subjects. To our knowledge, this is the first report of naturally-occurring missense mutations in the hMella receptor gene. Binding characteristics of each mutant receptor were also determined by expression studies.

MATERIAL AND METHODS

Study subjects. All protocols were approved by the Institutional Ethical Board of the Saitama Medical School and the corresponding committees at the respective institutions from which blood samples were obtained. Informed written consent was obtained from all subjects. Seventeen patients with circadian rhythm sleep disorders (5 of N-24, 11 of DSPS, and 1 of irregular sleep-wake pattern [ISWP]) diagnosed according to the International Classification of Sleep Disorders (ICSD 1990) criteria and 21 healthy control subjects were recruited at the participating institutions in Japan. Blood was aspirated and genomic DNA was extracted from EDTA anticoagulated blood using Qiagen Blood & Cell Culture DNA Midi Kit. The whole length of the coding region of hMella receptor gene was screened by SSCP analysis and the nucleotide substitutions were determined by direct sequencing of the PCR product. To investigate the prevalance of mutations in a larger sample size, additional recruitment was performed and genomic DNAs were extracted from the blood of 49 patients and 46 control subjects, resulting in 66 patients (22 of N-24, 43 of DSPS, 1 of ISWP) and 67 controls in total. The patients were consisted of 42 men and 24 women, aged 13–56 (mean age 28.6 ± 9.6). The control subjects comprised of 33 men and 34 women, aged 22–53 (mean age 34.0 ± 8.3), without sleep disorders nor difficulty in waking up at the desired wake time. For additionally recruited genomic DNAs, only regions that showed missense mutations in the first screening were analyzed by SSCP analysis and mutations were identified by nucleotide sequence analysis.

Preparation of vectorette library. The hMella receptor gene consists of two exons (15). We have defined the genomic sequences adjacent to each of the exons to provide primers for mutation scanning in the entire coding region of hMella receptor. Vectorette libraries of human genomic DNA were constructed according to the procedure described by Morrison *et al.* (19), and were used for the analysis of genomic sequence. Genomic DNA from a human male (Clontech) was digested with one of the four restriction enzymes (Dra I, Bcl I, Bgl II, Hinc II). The appropriate annealed vectorette unit was ligated to each digested DNA, thereby generating four libraries. PCR was then carried out on each library in 20 μl reactions with 2 μl of vectorette library, 1 × TaKaRa LA PCR buffer containing 2.5 mM $MgCl_2$, 0.4 mM of dNTPs, 1 unit of TaKaRa LA Taq, 0.2 μM of universal vectorette primer (5′-CGA ATC GTA ACC GTT CGT ACG AGA ATC GCT-3′), and 0.2 μM of one of the gene-specific primers (5′-CAG GAT GAC CAG GAG GTT GCC CAG GAT GTC-3′ for amplifying the 5′-untranslated region [5′-UTR], 5′-CCC TAG CCT GCG TCCTCA TCT TCA CCA TCG TG-3′ for the 3′-intronic region adjacent to the first exon [3′-IR/1], 5′-GTA GGC GGAGCT GAC GGA CTG GGC GAA GGT GC-3′ for the 5′-intronic region adjacent to the second exon [5′-IR/2], and 5′-GGC TCC TCT GAA CTT CAT TGG CCT GGC CGT GG-3′ for the 3′-untranslated region [3′-UTR], respectively) derived from the published sequence of hMella receptor cDNA (15). After an initial denaturation at 98°C for 2 min, samples were amplified for 30 cycles of denaturation at 98°C for 10 sec and annealing and extension at 68°C for 5 min, followed by a final 10 min extension at 72°C. For the second round of PCR, 0.5 μl of the PCR product above was used as a template and was amplified with 0.2 μM nested vectorette primer (5′-ACC GTT CGT ACG AGA ATC GCT GTCCTCTCC-3′) and 0.2 μM one of the nested gene-specific primers (5′-GAT GGTGAA GAT GAGGAC GCA GGCTAG GG-3′ for 5′-UTR, 5′-GCA ACC TCC TGGTCA TCC TGT CGGTGT ATC GG-3′ for 3′-IR/1, 5′-CGA TGA CGC TCA GGC CCA TCA GGA ACC CAC TG-3′ for 5′-IR/2, and 5′-CCC GCC AGC ATG GTG CCT AGG ATC CCA GAG TG-3′ for 3′-UTR), using the same cycling condition as in the first-round PCR. The product of the second-round PCR was electrophoresed on a 1.2% agarose gel. DNAs eluted from the gel were ligated in to the pCR II vector (Invitogen) and the sequence was determined in both strands. After we have completed analyzing the genomic sequence of hMella receptor gene, Petit *et al.* independently released the sequence of 3′-UTR for the gene into the DDBJ/EMBL/GenBank database with the accession No. AF085498, the sequence of which was 99.5% identical to that we determined.

SSCP and DNA sequence analysis. Nine sets of fluorescein-labelled oligonucleotide primers were used to cover the whole length of the gene by overlapping segments (Table 1). PCR was carried out with approximately 100 ng of genomic DNA, 0.2 μM each primer, 0.2 mM dNTPs, 0.5 unit AmpliTaq Gold (Perkin-Elmer), and 1.5 mM Mg^{2+} in a total volume of 20 μl. After an activation of AmliTaq Gold at 95°C for 7 min and initial denaturation at 98°C for 2 min, 45 cycles were performed at 98°C for 10 sec, 60°C for 45 sec, and 72°C for 1 min, followed by the last extention at 72°C for 10 min. Then 0.4 μl aliquots of the PCR products were diluted in 19.6 μl of loading solution containing 90% deionized formamide, 5 mM EDTA, and 1% blue dextran. After denaturation at 80°C for 7 min, 1.5 μl was applied to an SSCP gel containing 1 × TBE, 6% Long Ranger Gel Solution with or without 5% glycerol. Electrophoresis was performed at 20°C for 6 h at 500V/21 cm gel length with 0.6 × TBE buffer and was analyzed on a DNA sequencer DSQ-1000S with PCR-SSCP Analysis Software (Shimadzu).

The samples that exhibited altered SSCP migration patterns were PCR-amplified using primers that encompass the SSCP fragment and both strands were sequenced using internal primers.

Cloning of hMella receptor cDNA. Marathon-Ready cDNA from human hypothalamus (Clontech) was PCR-amplified using two primers corresponding to 5′-UTR (5′-CGG AAT TCC GGC GGA GCCTTA ACA AGT GGT CGGGC-3′) and 3′-UTR (5′-CGG AAT TCC GCTTTC CCA GAC ATC TGTCAA GAGCGAGG-3′) of the hMella receptor cDNA. EcoR I site was incorporated to the 5′-portion of each primer. The reaction was performed with cloned Pfu DNA Polymerase (Stratagene) in order to minimize the misincorporation frequency. The amplified cDNA was separated on an agarose gel, recovered using QIAquick Gel Purification Kit (Qiagen), restricted by EcoR I, and ligated into pcDNA1.1/Amp (hMella-pcDNA1.1/Amp, Invitrogen). The sequence was confirmed on both strands.

Mutagenesis. Missense mutations were introduced by PCR-based site-directed mutagenesis method using hMella-pcDNA1.1/Amp as a

TABLE 1

Primer Sets for PCR SSCP Analysis of the hMella Receptor Gene

Primer set	Exon	Forward primer (5′-3′)	Reverse primer (5′-3′)	PCR product size (bp)
1	I	CCG GCG GAG CCT TAA CAA GTG GTC	CAA GTG CTT GGG GAA GGC TGG CTG	344
2	II	ATT GTA ACA GAA AAC CCA CTG TGA ACT G	CAG ATG TAG CAG TAG CGG TTG ATG	268
3	II	GTG GAA CCT GGG CTA TCT GCA CTG	ATC CTC GGG TCG TAC TGG AGA GTC	246
4	II	ACT GCT ACA TCT GCC ACA GTC TCA AG	TCC ATA TTC TCA GGT AAC AGA AGA TGA C	258
5	II	CGT GCA GGG ACT CTC CAG TAC GAC	AGT TCA GAG GAG CCC AGC AAA TGG	277
6	II	TCT GTT ACC TGA GAA TAT GGA TCC TGG	GCT GTT GAA ATA CGC CAT GTA GTA ACT G	251
7	II	CTC CTC TGA ACT TCA TTG GCC TGG	ATT GTT GGT CAT CAG TGG AGA CGG	272
8	II	CTA CAT GGC GTA TTT CAA CAG CTG CCT C	ATC TGT CAA GAG CGA GGC CTT GCG	270
9	II	CCG TCT CCA CTG ATG ACC AAC AAT AAT G	TAG AAT TGG AGG GGT TTA TAA CGC TGA C	214

template. To introduce 160(C→T) mutation, an oligonucleotide corresponding to T7 promoter region of pcDNA1.1/Amp (5′-GCT TAT CGA AAT TAA TAC GAC TCA CTA TAG GG-3′) was used in combination with a mutagenic primer1 (5′-CCA CCA CCA GGT CTG CCA CCG CTA AGC TCA CCA CAA AGA TGT TTC CTG CGT TCC TGA GCT TCT TGT TCC AAT ACA CCG AC-3′) corresponding to a unique Bpu1 102I site to allow for polymerase extention of a Hind III/Bpu 1102I fragment, Hind III site of which is in the vector sequence. This fragment was digested with Hind III and Bpu1 102I, and ligated into digested hMella-pcDNA1.1/Amp. 470(C→T) mutation was introduced using the PCR mutagenesis method reported by Nelson *et al.* (20). First round PCR was performed using a hybrid primer, with the 3′ segment derived from the template sequence upstream of the Bpu1102I site and the 5′ segment non-complementary to the template (5′-ATG CTA TTC ACT CAC TAT AGG GCT CGA GCG GCT TCCTGG TCA TCC TGT CGG TGT ATC G-3′), and a mutagenic primer2 (5′-GCA GGA CGG CCA CCA GCG TCA GGA G-3′). Purified DNA fragment was denatured and used as a primer to synthesize a template for the 2nd round PCR. Briefly, 4 ng of hMella-pcDNA1.1/Amp was mixed with 10 pmol dNTPs, 20 ng purified product from the 1st round PCR, and 5 μl of 10 × cloned Pfu DNA polymerase reaction buffer to make 46.5 μl of reaction mixture. After preheating to 98°C for 2 min, 5 units of cloned Pfu DNA polymerase was added and 5 cycles of 98°C for 10 sec, 68°C for 45 sec, and 72°C for 5 min were performed. Then, 25 pmols of primer (5′-ACT CAC TAT AGG GCT CGA GCG GC-3′), which is identical to the non-complementary 5′ segment of the hybrid primer, and 25 pmols of the primer corresponding to the vector sequence (5′-AGG TAG TTT GTC CAA TTA TGT CAC-3′) were used to amplify the hMella receptor cDNA containing 470(C→T) mutation. After digestion with Bpu1102I, Bsm B I, and Eag I, the fragment was ligated with digested hMella-pcDNA1.1/Amp and sequenced both directions.

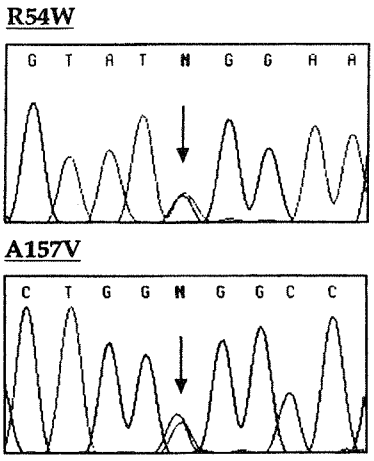

FIG. 1. DNA sequences showing the missense mutations. Examples of DNA sequences are shown from individuals who were heterozygotes for the variant allele. The arrows indicate the position of nucleotide substitution, with the adjacent sequences shown.

Expression study. COS-7 cells were grown in monolayers in Ham's F-12 media supplemented with 10% fetal bovine serum, 100 units/ml penicillin, 100 μg/ml streptomycin at 37°C in a 5% CO_2 atmosphere. For ligand-binding studies, 15 μg of each plasmid DNA per 15 cm dish was introduced into COS-7 cells using LIPOFECTAMINE Reagent (Gibco-BRL) according to the manufacturer's protocol. Medium was removed 3 days after transfection, the dishes were washed with phosphate-buffered saline, and the cells were harvested. The cells were then pelleted (2500 rpm, 10 min at 4°C) and stored at −80°C. Whole cell binding studies were performed by thawing the cells and resuspending them in binding buffer (50 mM Tris-HCl pH 7.4 with 5 mM $MgCl_2$) at a concentration of 5-24 μg of protein per milliliter. The cell suspension was incubated with 2-[^{125}I] iodomelatonin (^{125}I-Mel, New England Nuclear) with or without melatonin in a total reaction volume of 0.2 ml of binding buffer. The suspension was incubated in a shaker bath for 1.5 hr at 25°C. Reaction was terminated by dilution with several volumes of ice-cold binding buffer, followed by rapid vacuum filtration through Whatman GF/B glass fiber filters. All determinations were done in either duplicate or triplicate. Protein measurements were performed using BCA Protein Assay Kit (Pierce). Binding data were analyzed by computer using the LIGAND Program by Munson and Rodbard (21).

RESULTS AND DISCUSSION

By direct sequencing of PCR-amplified DNA from fifteen of the control subjects, we defined the sequence of the most common allele for hMella receptor gene in our ethnic group. The result was identical with that of the previous report by Reppert *et al.* (15) except for the nucleotide substitutions 90(A→G), 738(C→T) in the coding region and −25(T→C), −10(A→C) in the 5′-UTR (The nucleotide sequence data reported in this paper will appear in the DDBJ/EMBL/GenBank nucleotide sequence databases with the accession numbers AB029932 and AB029933), none of which led to amino acid substitution. These base changes are not likely to

TABLE 2

Variants of hMella Receptor and Their Prevalence in Patients with Circadian Rhythm Sleep Disorders and Control Subjects

Nucleotide change	Amino acid change	Number of carrier/total (allele frequency)			
		N-24	DSPS	ISWP	Control
160(C→T)	R54W	3/22 (0.068) *P = 0.162	2/43 (0.023)	0/1 (0)	3/67 (0.022)
470(C→T)	A157V	2/22 (0.045) *P = 0.598	2/43 (0.023)	0/1 (0)	3/67 (0.022)

Note. The nucleotide position is given relative to the start of the coding sequence.
* Fisher's exact test with two-tailed probability in comparison with allele frequency in control subjects.

have been PCR artifacts because they were detected by direct sequencing. These differences may indicate alleic heterogeneity among ethnic groups.

The whole coding region of the two exons that encode the hMella receptor was screened for the presence of genetic polymorphism by SSCP analysis, using DNA samples from 17 subjects with circadian rhythm sleep disorders and 21 control subjects, which revealed aberrant SSCP migration patterns in primer sets #1, 3, 4, 7, and 8 (Table 1). DNA samples which showed aberrant patterns were subjected to PCR using primers that spanned the region. Nucleotide variations were determined by direct sequencing of the PCR products on both strands. We detected seven polymorphisms [160(C→T), 417(C→T), 470(C→T), 534(C→T), 867(C→T), 924(A→G), 945(A→G)], two of which [160(C→T) and 470(C→T)] predicted amino acid change (missense mutations, Fig. 1, Table 2) while the others did not (silent mutations).

To determine the prevalence of the two variants with missense mutations, additional samples were recruited and SSCP analysis was performed using primer sets #1 and 4 on a total of 66 subjects with sleep disorders and 67 control subjects. Nucleotide substitutions of the samples which exhibited aberrant migration patterns were confirmed by direct sequencing of the PCR product. As for 160(C→T) substitution, an additional migration band caused by the mutation was only weakly visible on SSCP non-denatured gel, therefore, all of the study samples were amplified by PCR and dedicated to direct sequencing of the site of nucleotide substitution to avoid missing the mutation, the result of which was consistent with that expected from the SSCP analysis.

The 160(C→T) substitution results in a nonconservative amino acid change from Arg54 to Trp (R54W) in the first cytoplasmic loop of the receptor, while the 470(C→T) substitution induces a conservative amino acid change A157V in the fourth transmembrane domain. R54W variant was found in 3 of 22 N-24, 2 of 43 DSPS, 0 of 1 ISWP, and 3 of 67 control subjects. The A157V substitution was present in 2 of 22 N-24, 2 of 43 DSPS, 0 of 1 ISWP, and 3 of 67 control subjects (Table 2). We could not find homozygotes for either of the missense mutations in our study group and none of the subjects carried both mutations. The frequency of the R54W allele and that of the A157V allele were approximately 3-fold and 2-fold higher in N-24 subjects, respectively, compared to those in controls, although the incidence was not significant in our study group (P = 0.162 and 0.598, respectively, Fisher's exact test, Table 2). Genetic analysis of a larger sample size will clarify whether these variants represent predisposing alleles in a subgroup of N-24 subjects.

To assess whether these amino acid substitutions induce an alteration in binding characteristics of the receptor, hMella receptor cDNA bearing R54W or A157V mutation was constructed, respectively. We performed radioligand-binding assays with COS-7 cells transiently transfected with either of the variants, or the wild type receptor, using ^{125}I-Mel as a ligand. On Scatchard analysis, the R54W variant receptor showed an approximate 70% reduction in the Bmax and slightly reduced Kd (enhanced binding affinity) compared to the wild type receptor (Fig. 2a, Table 3), which is consistent with several studies demonstrating that mutagenesis in the first cytoplasmic loop of G protein-coupled receptor affects ligand binding (22, 23). Correspondance of Arg54 to a highly conserved amino acid residue among melatonin receptors in various species also support the idea that this region may play an important role in the function of melatonin receptors (24, 25). The A157V variant showed similar Bmax and Kd to the wild type receptor. Competitive binding analysis was also performed to investigate the binding characteristics of the variant receptors to the endogenous ligand, melatonin, which revealed slightly reduced Kd of the R54W mutant compared to that of the wild type receptor (Fig. 2b, Table 3).

It is reported that targeted disruption of the Mella receptor in mice abolishes the inhibitory effect of melatonin on SCN neuronal firing, but only slightly

changes the melatonin-induced phase-shift (26). Administration of melatonin can entrain the circadian rhythm in Siberian hamsters with nonfunctional Mellb receptor (25). These results indicate that both receptor subtypes contribute to mediating the phase-shift effect of melatonin in mammals. It is therefore possible that mutations of the hMella receptor gene are involved in developing sleep disorders in combination with those of the hMellb receptor gene. Mutation analysis of hMellb receptor gene is now in progress.

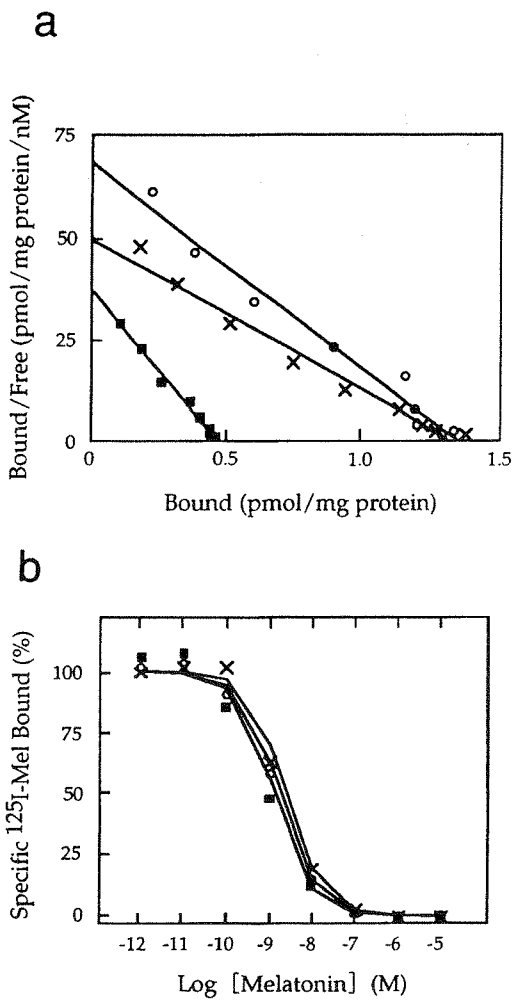

FIG. 2. (a) Scatchard analysis of ^{125}I-Mel binding to membranes from COS-7 cells expressing the hMella receptor variants. The specific binding of increasing concentrations of ^{125}I-Mel to COS-7 cells expressing either of the mutant hMella receptors or the wild-type receptor was determined in triplicate as described under Material and Methods. Nonspecific binding was defined using 10 μM melatonin. Scatchard plots of representative binding data from four separate experiments are presented. Wild type (○), R54W mutant (■), A157V mutant (×). Similar results were obtained with another clone for each variant. (b) Displacement of ^{125}I-Mel binding at wild type and mutated hMella receptors by melatonin. Cell suspensions were incubated at 25°C for 1.5 h in the presence of 100 pM ^{125}I-Mel and increasing concentration of melatonin. The results are representative of three independent experiments carried out in duplicate whose mean values are reported in Table 3. Wild type (○), R54W mutant (■), A157V mutant (×).

TABLE 3

Ligand Binding Parameters Observed in COS-7 Cells Expressing the Wild Type and Mutated hMella Receptors

Mutant	^{125}I-Mel binding		Melatonin competition
	B_{max} (pmol/mg)	K_d (pM)	K_i (pM)
Wild type	1.42 ± 0.10	24.7 ± 2.1	348 ± 22
R54W	0.44 ± 0.04	15.7 ± 1.3	173 ± 4
A157V	1.37 ± 0.06	27.9 ± 2.4	498 ± 16

Note. The results from ^{125}I-Mel saturation and melatonin competition binding assays performed using COS-7 cells transfected with either of the mutants or wild type hMell, a receptor as described under Material and Methods are shown. Results are the means ± S.E. of three or four independent experiments. K_d, equilibrium dissociation constant for ^{125}I-Mel; K_i, equilibrium dissociation constant for melatonin.

To our knowledge, this is the first report of naturally-occurring missense mutations in the hMella receptor gene. The identification of variants in hMella receptor could provide a useful tool for testing the gene in the predisposition to various melatonin-related diseases, especially to circadian rhythm sleep disorders, and for clarifying the physiological role of melatonin receptors in humans.

ACKNOWLEDGMENTS

The authors thank Dr. Hiroshi Aikawa for statistical analysis, Dr. Shin-ichiro Sawada for critical reading of the manuscript, Mr. Eiichi, Yamada, Ms. Kyoko Ohnishi, and Mr. Masakazu Kinoshita for expert technical assistance. This work was supported by research grants from the Ministry of Health and Welfare, and the Ministry of Education, Science, Sports and Culture (09770758, 10557089), Saitama Medical School, and Pharmacopsychiatry Research Foundation.

REFERENCES

1. Tamarkin, L., Baird, C. J., and Almeida, O. F. X. (1985) *Science* **227,** 714–720.
2. Cassone, V. M. (1990) *Trends Neurosci.* **13,** 457–464.
3. McArthur, A. J., Hunt, A. E., and Gillette, M. U. (1997) *Endocrinology* **138,** 627–634.
4. Reppert, S. M., Weaver, D. R., Rivkees, S. A., and Stopa, E. G. (1988) *Science* **242,** 78–81.
5. Lewy, A. J., Ahmed, S., Jackson, J. M. L., and Sack, R. L. (1992) *Chronobiol. Int.* **9,** 380–392.
6. Zaidan, R., Geoffriau, M., Brun, J., Taillard, J., Bureau, C., Chazot, G., and Claustrat, B. (1994) *Neuroendocrinol.* **60,** 105–112.
7. Quay, W. B. (1970) *Physiol. Behav.* **5,** 353–360.
8. Finkelstein, J. S., Baum, F. R., and Campbell, C. S. (1978) *Physiol. Behav.* **21,** 105–111.

9. Kopp, C., Vogel, E., Rettori, M-C., Delagrange, P., Guardiola-Lemaître, B., and Misslin, R. (1998) *Physiol. Behav.* **63,** 577–585.
10. Rodenbeck, A., Huether, G., Rüther, E., and Hajak, G. (1998) *J. Pineal Res.* **25,** 201–210.
11. Shibui, K., Uchiyama, M., and Okawa, M. (1999) *J. Biol. Rhythms* **14,** 72–76.
12. Dahlitz, M., Alvarez, B., Vignau, J., English, J., Arendt, J., and Parkes, J. D. (1991) *Lancet* **337,** 1121–1124.
13. McArthur, A. J., Lewy, A. J., and Sack, R. L. (1996) *Sleep* **19,** 544–553.
14. Fink, R., and Ancoli-Israel, S. (1997) *Sleep Res.* **26,** 713.
15. Reppert, S. M., Weaver, D. R., and Ebisawa, T. (1994) *Neuron* **13,** 1177–1185.
16. Reppert, S. M., Godson, C., Mahle, C. D., Weaver, D. R., Slaugenhaupt, S. A., and Gusella, J. F. (1995) *Proc. Natl. Acad. Sci. USA* **92,** 8734–8738.
17. Weaver, D. R., and Reppert, S. M. (1996) *Neuroreport* **8,** 109–112.
18. Barret, P., Conway, S., Jockers, R., Strosberg, A. D., Guardiola-Lemaitre, B., Delagrange, P., and Morgan, P. J. (1997) *Biochim. Biophys. Acta.* **1356,** 299–307.
19. Morrison, J. F. J., and Markham, A. F. (1995) *in* PCR2, A Practical Approach (McPherson, M. J., Hames, B. D., and Taylor, G. R., Eds.), pp. 171–181, Oxford University Press, Oxford, UK.
20. Nelson, R. M., and Long, G. L. (1989) *Anal. Biochem.* **180,** 147–151.
21. Munson, P. J., and Rodbard, D. (1980) *Anal. Biochem.* **107,** 220–239.
22. O'Dowd, B. F., Hnatowich, M., Regan, J. W., Leader, W. M., Caron, M. G., and Lefkowitz, R. J. (1988) *J. Biol. Chem.* **263,** 15985–15992.
23. Dixon, R. A. F., Sigal, I. S., Candelore, M. R., Register, R. B., Scattergood, W., Rands, E., and Strader, C. D. (1987) *EMBO J.* **6,** 3269–3275.
24. Ebisawa, T., Karne, S., Lerner, M. R., and Reppert, S. M. (1994) *Proc. Natl. Acad. Sci. USA* **91,** 6133–6137.
25. Weaver, D. R., Liu, C., and Reppert, S. M. (1996) *Mol. Endocrinol.* **10,** 1478–1487.
26. Liu, C., Weaver, D. R., Jin, X., Shearman, L. P., Pieschl, R. L., Gribkoff, V. K., and Reppert, S. M. (1997) *Neuron* **19,** 91–102.

METHODS

Isolation and sequencing of genomic clones. Using an 858-bp fragment of the *hBMAL1a* sequence (nucleotides −380 to 478 relative to the translation initiation codon, 8) as the hybridization probe, Genome Systems Inc. (St. Louis, USA) screened a mouse ES-129/SVJI BAC library at our request. Two clones, BAC-mb53 and BAC-mb54, were isolated (28, Fig. 1A). We determined the sequences using a primer-walking method. The dideoxy chain termination method (BigDye Terminator Kit, PE Applied Biosystems) and an automated sequencer (377 DNA Sequencer, PE Applied Biosystems) were used to carry out DNA sequencing.

RT-PCR. The total RNA of NIH3T3 cells was extracted using Trizol Reagent (Gibco-BRL). First strand cDNAs were synthesized using random hexamers. First strand cDNAs were subjected to PCR directly. PCR was performed using two different primer pairs (primer pair A: 5′-GCAATCGCAAGAGGAAAGGCA-3′ and 5′-CTTTGGCAATATCTTTTGGA-3′; primer pair B: 5′-ACCCATACACAGAAGCAAAC-3′ and 5′-CTTTGGCAATATCTTTTGGA-3′) derived from the sequence of *mBmal1b* (28). The PCR products were electrophoresed in an agarose gel.

5′ RACE. A 5′ RACE system (Version 2.0, Gibco-BRL) was used. The total RNA of BALB/c mouse testis was extracted using Trizol reagent (Gibco-BRL). First-strand cDNA synthesis was performed using ThermoScript RT (Gibco-BRL) and the primer 5′-GTTTGCTTCTGTGTATGGGT-3′, followed by tailing using a terminal deoxynucleotidyl transferase and dATP. Second-strand cDNA synthesis was carried out using SuperScript II RT (Gibco-BRL) and the linker primer 3RACE-AP (5′-GGCCACGCGTCGACTAGTAC(T)17-3′). The first PCR reaction employed the primers: AUAP (5′-GGCCACGCGTCGACTAGTAC-3′) and 5′-TGTCCCGACGCCTCTTTTC-3′. The nested PCR reaction was performed using primers AUAP and 5′-CCGCCATTGGAAGGAAGGTGCTTGC-3′. The products of the nested PCR were cloned into a TA-vector (pCR2.1, Invitrogen) and sequenced.

Bmal1 promoter reporter. An 8096 bp 5′-upstream fragment containing 99 bp of the first exon (accession number AB064982) was excised from the BAC clone mB-53 (Fig. 1A) using *Aat*I and *Sac*II (Fig. 4) and cloned into pBluescript II KS+. This fragment was then subcloned into the pGL3-Basic vector (Promega) and named Bp/8096-LUC (Fig. 4). Bp/4103-LUC was derived from Bp/8096-LUC by *Pst*I digestion at two sites; one site originated 3993 bp downstream from the 5′ end of the 8096 bp fragment (Fig. 4), and the other in the 5′ upstream region of the 8096 bp fragment derived from pBluescript II KS+. Other deletions in the *mBmal1* promoter constructs were generated from Bp/4103-LUC using exonuclease III (Takara, Japan) and mung bean nuclease (Takara).

Per1 promoter reporter. A 2.0-kb upstream fragment of *mPer1* was isolated by PCR amplification from a BALB/c mouse genomic DNA library, as described previously (12), and subcloned into the pGL3-promoter luciferase vector (Promega).

Expression constructs. The expression constructs consisted of the full-ORF cDNAs encoding mBMAL1 (*mBmal1b,* 28), hCLOCK, mPER1, mCRY1, or hCRY2, which had been subcloned into the pcDNA3 expression vector (Invitrogen). All expression constructs were checked by restriction digestion and the sequences around the cloning sites were verified by automated DNA sequencing. The full-ORF cDNA of rPER2, cloned in the expression vector pCAGGS, was kindly provided by Dr. N. Ishida. The full-ORF cDNAs encoding mPER1, hCLOCK (KIAA0334), and mCRY1 were kindly provided by Dr. H. Tei, Dr. T. Nagase, and Dr. A. Yasui, respectively. An *hCry2* cDNA clone (KIAA0658), a gift from Dr. T. Nagase, lacked 7 N-terminal amino acid residues. Using PCR, the 5′ end sequence of the 7 amino acid residues of mCRY2 (AF156987) was combined with the *hCry2* clone. Briefly, a 610 bp fragment was amplified by PCR using the *hCry2*/R-U (5′-ATTCTAGAAAGCTTAATGGCGGCGGCTGCTGTGGTGGCAGCTGTGGCCCCGGCG-3′) and *hCry2*-590L (5′-CGGCCCTGCAGCTCTCCATCT-3′) primers and the original *hCry2* clone as template. The resulting PCR products were cloned and sequenced. Using *Eco*RI sites, the 450 bp fragment at the 5′ end of this construct was ligated to the original *hCry2* clone. The resulting chimeric ORF was designated *hCry2.*

Cell transfection and luciferase assay. Transfected NIH-3T3 cells were used in the luciferase assays. One day before transfection, the cells were seeded (5×10^4 per well) in 24-well plates containing Dulbecco's Modified Eagle medium (DMEM, Gibco-BRL), supplemented with 10% fetal bovine serum (Gibco-BRL) and 0.1 mM MEM nonessential amino acids. Cells were transfected using Lipofectamine-Plus (Gibco-BRL). Transfected DNA (200 ng) was added to each well; the amount of added DNA per well was kept constant by adding pBluescript II KS+ DNA. In order to measure the transcriptional activities of the various *mBmal1* promoter reporters without interference from other clock gene products, the cells in each well were transfected with 5 ng of pRL-TK (*Renilla* luciferase internal control plasmid, Promega), and a constant molar concentration of pGL3 firefly luciferase reporter constructs. A total of 195 ng of the longest reporter construct (Bp/8096-LUC) was added. The plasmid pGL3-Basic (without inserted DNA) was used as a control. In order to assess the effects of various clock gene products on *mBmal1* or *mPer1* transcription, each transfection mixture contained 3 ng of pRL-TK and 57 ng of the indicated reporter and gene expression constructs. At 24–28 h post-transfection, the cells were disrupted with 100 μl of passive lysis buffer (Promega). The luciferase activity was determined using a Dual-Luciferase Reporter Assay System (Promega) and an Ascent FS II luminometer (Labsystems). For each sample, the measured luciferase activity was corrected for transfection efficiency by dividing the firefly luciferase activity (expressed from the reporter construct) by the *Renilla* luciferase activity (expressed from pRL-TK). The transcription activity value in individual experiments was normalized to the corresponding control (set at 1-fold or 100%).

RESULTS

Genomic Structure and Promoter Activity of mBmal1

Sequence analysis of two BAC clones (BAC-mb53 and BAC-mb54) showed that *mBmal1* consists of 23 exons and spans more than 110 kb (Fig. 1A). The exon–intron splice junctions, including the alternative splice acceptors, have the GT/AG consensus sequence, except for intron 19, which begins with GC at the 5′ end (donor) and ends in AG at the 3′ end (acceptor). The 23 exons result in several splice variants. The major transcript suggested by RT-PCR analysis consists of 20 exons—designated as *mBmal1b* (28, Fig. 1B). The length of this predicted major transcript was consistent with the reported results of Northern blot analysis in which the main band of the human *Bmal1* transcript was located at about 3 kb (8).

We performed 5′ RACE and mapped the transcriptional start site to a site 486 bp upstream from ATG (*mBmal1b)* and 154 bp upstream of the 3′ end of the first exon (Fig. 2). The first residue, a guanosine, was designated as nucleotide (nt) +1. An extremely CG-rich region, possibly representing CpG islands, was identified in proximity to the transcriptional start site. To define the *mBmal1* gene promoter, an 8096 bp 5′ flanking fragment containing 99 bp of the first exon

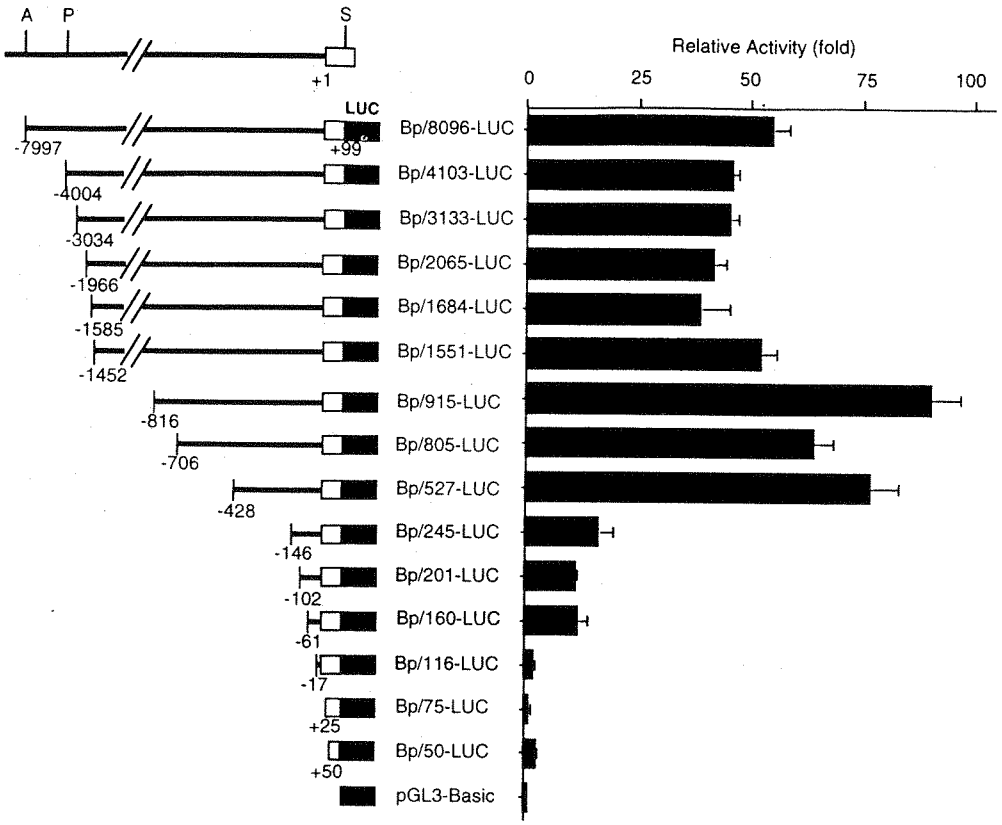

FIG. 4. *mBmal1* promoter activity in NIH3T3 cells. NIH3T3 cells were transfected with a constant molar concentration of *mBmal1* promoter luciferase reporters. The relative activities are shown as fold increases (mean ± SEM, $n = 4$) compared with the control vector pGL3-Basic. A schematic diagram of the *mBmal1* promoter reporters is shown on the left, with the names of the reporters listed in the middle and their corresponding relative activities shown on the right. Nucleotide positions demarcate the boundaries of the *mBmal1* promoter constructs whose 3′ termini are identical. +1, transcriptional start site; A, *Aat*I site; P, *Pst*I site; S, *Sac*II site; LUC, sequence of firefly luciferase gene.

and PER2 are indispensable for the upregulation of *Bmal1*.

BMAL1-CLOCK Inhibits Bmal1 Transcription

In *Drosophila,* mutants lacking functional dCLOCK or CYCLE had high levels of *dclock* mRNA. Consequently, CYCLE-dCLOCK was proposed to represses *dclock* expression through a mediator (26). We hypothesized that BMAL1-CLOCK dimers negatively regulate *Bmal1*. To test this hypothesis, we co-transfected BMAL1 or CLOCK expression plasmids with a Bp/915-LUC reporter. The introduction of BMAL1 or CLOCK alone had no effect on the *Bmal1* promoter, but a combination of BMAL1 and CLOCK decreased transcriptional activity by 38% compared to the control (Fig. 7). This suggests that BMAL1-CLOCK dimers act as transcriptional repressors of *Bmal1*.

Our results are corroborated by the recent finding that dimers of BMAL1 and NPAS2 (an analog of CLOCK; also called MOP4) inhibit the activity of a *Bmal1* promoter-driven luciferase reporter (32). The lack of NPAS2 expression (33) in the SCN indicates that BMAL1-NPAS2-mediated autoregulation of *Bmal1* does not function in the core clock, as it appears to do in peripheral tissues (32). These findings, along with our present results, indicate that BMAL1 autoregulation in the core clock is mediated by BMAL1-CLOCK.

We assessed whether BMAL1-CLOCK was capable of quenching the activation of *Bmal1* induced by CRY1, CRY2. and PER2 (Fig. 7). The results showed that when BMAL1 and CLOCK were co-transfected with CRY1 or CRY2, there were no changes in the activity of the *Bmal1* promoter. BMAL1-CLOCK caused a small decrease (to 77% of the control level) in PER2-induced activation (Fig. 7). These data lead us to conclude that: (i) PER2 is associated with BMAL1-CLOCK in the transcriptional machinery, either directly or through mediators, (ii) activation of *Bmal1* by CRY is independent of BMAL1-CLOCK, and (iii) CRY/PER2-dependent activation of *Bmal1* overcomes transcription suppression by BMAL1-CLOCK.

DISCUSSION

The negative component CRY/PER2 and the positive component BMAL1/CLOCK appear to be crucial com-

```
GGGACGACGGCGAGCTCGCAGAGTCCGCAACGCAGTGGCCTCAGCGAGCT        -379

TTAGACCTGAGGGGGAAAACCGAGGGCTGGGGCAAGAAATCCACAGAGCG        -329

TGCCAATTGGTCCACTCCTCGGGGCGTGTGCTTCTGTGCGCCAAATGATT        -279
  E-box/NF-Y                                  E-box/NF-Y

GGTGAAGGGAAAGTAGCAGGTAAACCAGCCCTGCCGTCTTGCCATTGGTC        -229
                                                NF-Y/AP1

AGAGGCTTTCCTATCGGTCACTCGATTGGCTAGCCTAACGCAGAGCAGAA        -179
                          NF-Y

CGCGAATTGGTTTGGGTTGTCCGCCAAGACAACTCCGTTCGCTCTCTCTG        -129
     NF-Y

ATTGGCTAACGGGAAGAGGCAGGTATCCGGGCTGCGCGGCTCCTCCATTG         -79
NF-Y                                                  NF-Y

GTGGGCGGGGAAGGGGGGTTGGGCACAGCGATTGGTGGGCGGGGGGCCGG         -29
    SP1                          NF-Y    SP1   SP1

GCCTGGGCCGGCGGGGAGCGGATTGGTCGGAAAGTAGGTTAGTGGTGCGA         +22
=                        NF-Y  +1

CATTTAGGGAAGGCAGAAAGTAGGTCAGGGACGGAGGTGCCTGTTTACCC         +72
                         AP1
```

FIG. 2. Nucleotide sequence of the 5′-flanking region of the *mBmal1* gene. A 428-bp fragment from the 5′-flanking region containing the putative core promoter is shown. The transcription start site is shown in bold and is designated as nt +1. SP1 binding sites are double-underlined. Other putative *cis*-elements are single-underlined.

Although PER1 (at a dosage of 140 ng) induced a 2.0-fold increase in the transcriptional activity of the *Bmal1* promoter *in vitro* (Fig. 5A), it probably does not function as an effective transcription regulator *in vivo*. In *mPer1*-deficient mice, *Per2*, *Cry1*, and *Bmal1* expression levels were reported to be unchanged (14). Indeed, of the three PER, only PER2 appears to play a role in the regulation of clock gene expression. In the SCN of *mPer3*-deficient mice, the circadian oscillations in *Per1*, *Per2*, and *Bmal1* mRNA levels were not altered (27). Furthermore, behavior rhythms were sustained in mice deficient in either *mPer1* (14) or *mPer3* (18).

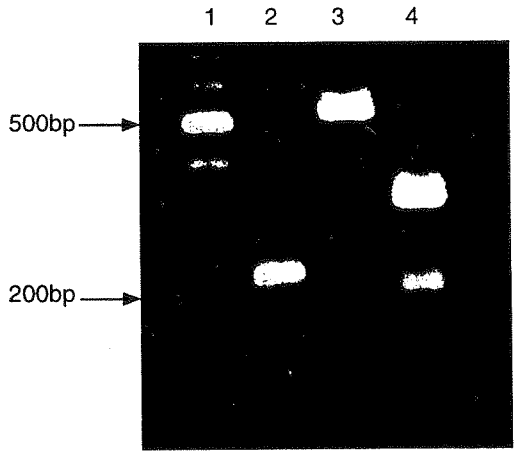

FIG. 3. RT-PCR assay of *mBmal1* gene expression in NIH3T3 cells. Lane 1, DNA ladder; lane 2, RT-PCR product of primer pair A; lane 3, RT-PCR product of primer pair B; lane 4, *Kpn*I digestion of the PCR product from lane 3 (refer to Methods).

Interactions between different negative components that contribute to the nuclear translocation of PER have been reported (17, 29–31). We tested the effects of each pair-wise combination of CRY1, CRY2, PER1, and PER2 on *Bmal1* transcription (Fig. 6). No synergism was observed, although PER2 appeared to augment CRY2 activity partially, and PER1 partially augments PER2 activity. These results imply that CRY and PER2 modulate *Bmal1* transcription independently, with a certain degree of redundancy. However, reduced *Bmal1* mRNA levels reported in *Cry1-Cry2* double-deficient and *Per2*-deficient mice (27) suggest that CRY

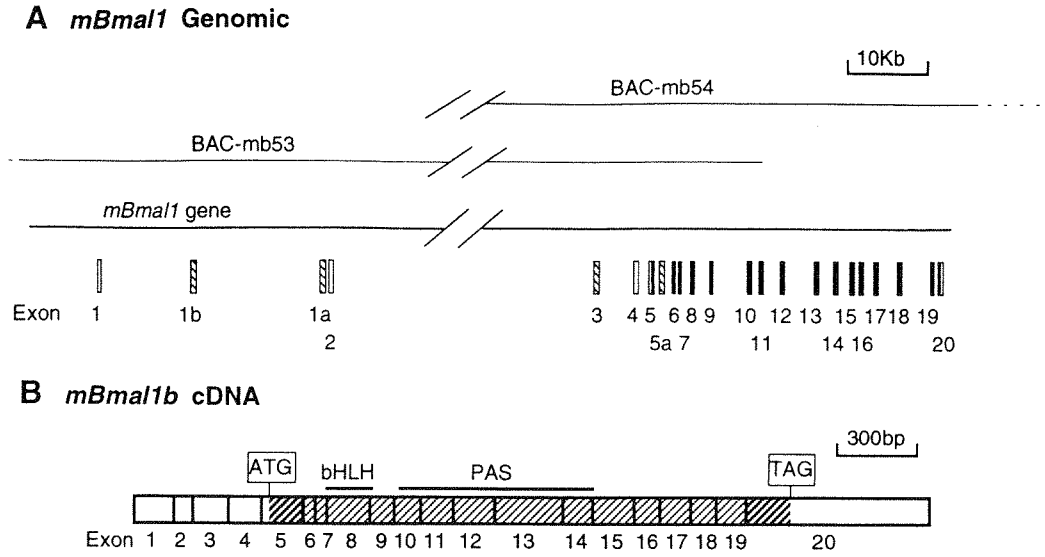

FIG. 1. The genomic structure and the major transcript of the *mBmal1* gene. (A) Schematic representation of sequence and relative positions of exons. // represents the unidentified sequence. Filled boxes indicate coding exons, open boxes indicate untranslational exons, and hatched boxes indicate alternative splice exons. (B) Organization of the predicted major transcript to the conserved domain structure. Hatched boxes indicate the coding region; open boxes indicate the untranslated region.

from the BAC clone mB-53 (Fig. 1A) was isolated. The 8069-bp fragment was ligated upstream of the firefly luciferase gene in the promoterless pGL3-Basic vector. A series of luciferase reporter constructs with an identical 3′ sequence were generated by 5′ deletion (Fig. 4).

Induction of the circadian oscillation of *Per1, Per2* expression was triggered by TPA treatment of NIH3T3 cells (6). Our RT-PCR assay showed that NIH3T3 cells express the *Bmal1* gene (Fig. 3). Consequently, NIH3T3 cells were used in a transient transfection assay to examine *mBmal1* transcriptional activity. The various reporter plasmids with a constant molar concentration were transiently transfected into NIH3T3 cells and the promoter activities were determined by luciferase assay. Bp/915-LUC (from nt −816 to +99) showed the highest promoter activity (Fig. 4). A deletion in the 5′ region extending upstream from nt −146 (Bp/245-LUC) resulted in a drastic reduction in promoter activity. However, Bp/245-LUC, Bp/201-LUC, and Bp/160-LUC retained approximately 10-fold greater activity over the control. A deletion extending to nt −17, present in Bp/116-LUC, showed only control levels of promoter activity (Fig. 4). These results suggest that the core promoter is located between nt +146 and −17, and that important cis-acting regulatory elements are present in the region from nt −428 to −146. Computer analysis revealed three SP1, one AP1, and eight NF-Y binding sites within the nt −428 to −17 (411 bp) region. Two E-boxes were also found in the 411 bp region, although they did not perfectly match the CACGTG consensus sequence (Fig. 2). The nucleotide sequence of this 411 bp region shares 79% identity with the corresponding region of the human *Bmal1* gene, as revealed by alignment using GeneWorks 2.2.1 (data not shown).

Bmal1 is Activated by CRY1, CRY2, and PER2

Using the luciferase assay, the effects of CRY1, CRY2, PER1, and PER2 on *Bmal1* expression were tested by co-transfecting expression plasmids with Bp/915-LUC into NIH3T3 cells. CRY1, CRY2, and PER2 produced a substantial increase in *mBmal1* transcriptional activity (6.6-, 3.3-, and 3.4-fold increases, respectively, at doses of 140 ng; Fig. 5A). These transcriptional enhancements were dose-dependent (Fig. 5A). These data, taken together with the finding that *Cry1-Cry2* double-deficient mice and *Per2*-deficient mouse mutants had reduced *Bmal1* mRNA levels (15, 27), suggest that CRY1, CRY2, and PER2 act as transcriptional activators of *Bmal1*. In contrast to the enhancing effects on *Bmal1* transcription described above, CRY1 and PER2 had inhibitory effects on *Per1* transcription, when CRY1 and PER2 expression plasmids were co-transfected with an *mPer1* promoter driven reporter. PER2 partially inhibited BMAL1-CLOCK-mediated *mPer1* transcription, as reported previously (17, Fig. 5B). CRY1 repressed BMAL1-CLOCK-mediated *mPer1* transcriptional activity to a level below that observed in controls, which were cells carrying the reporter construct alone (17, Fig. 5B). This suggests that inhibition by CRY1 overcomes *Per1* transcription activation by BMAL1-CLOCK. The strong bi-directional effects of CRY on *Bmal1* and *Per1* transcription indicate a central role for CRY in the transcriptional control of clock genes.

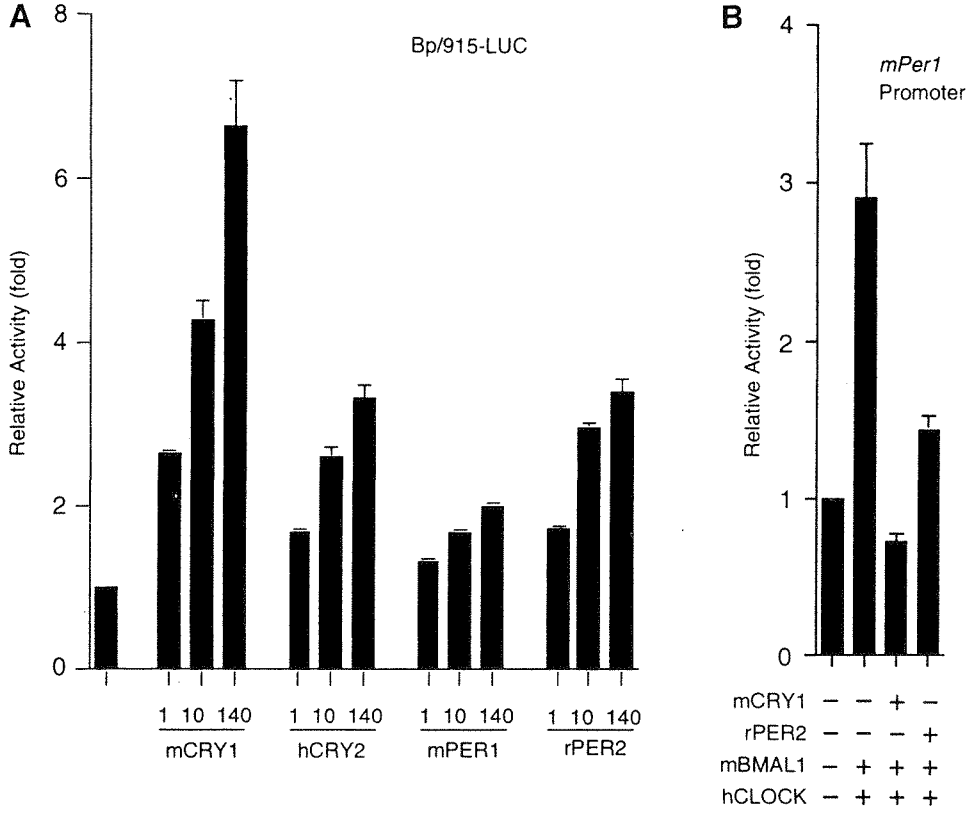

FIG. 5. Contrasting effects of CRY/PER2 on *mBmal1* and *mPer1* transcription. (a) CRY1, CRY2, and PER2 potently induced *mBmal1* transcription. Bp/915-LUC (57 ng) was co-transfected with the indicated amount (in nanograms) of expression plasmids. The values are shown as fold increases (mean ± SEM, $n = 6$) compared to the control (without expression plasmid). (b) CRY1 and PER2 inhibited BMAL1-CLOCK-mediated *mPer1* transcription. *mPer1* promoter-driven reporters (57 ng) were co-transfected with (+; 46 ng) or without (−) the indicated expression plasmids. All values are shown as fold increases (mean ± SEM, $n = 6$) compared to the control (without expression plasmid).

ponents in the core clock transcriptional control apparatus (10–18, present data). All of the negative regulatory components are cyclically expressed (2, 4). Among the positive components, *Bmal1* mRNA and protein are cyclic (20, 21) and in opposite phase to the negative components, whereas CLOCK is constant. The oscillations in clock gene expression are believed to control output rhythms. Transcriptional regulation appears to be fundamental to circadian oscillations. Negative components are activated by BMAL1-CLOCK heterodimers through the E-box (12) and are strongly repressed by CRY (17). Our results showed that the cyclic positive component BMAL1 is transcriptionally activated by CRY/PER2, but is repressed by BMAL1-CLOCK. Together with the time course of BMAL1 (mRNA and protein) nocturnal rhythm (20, 21) and CRY/PER2 (mRNAs and proteins) diurnal rhythms (1, 2, 4), our results imply that CRY/PER2 activate *Bmal1* and simultaneously represses gene expression of themselves by late day (at high levels), and that BMAL1-CLOCK heterodimers activate the expression of negative components and simultaneously repress *Bmal1* by midnight, when BMAL1 is at a high level. The bi-directional transcriptional roles of both CRY/PER2 and BMAL1-CLOCK at opposite circadian time points underlie the opposite phase of BMAL1 compared to CRY and PER. This feature of an opposite phase between negative and positive components in *Neurospora* has been proposed to contribute to the robustness of overt rhythm (34).

Both negative and positive components consist of three loops. The first of these is the negative autoregulatory CRY/PER2 feedback loop. The second is the negative autoregulatory BMAL1 feedback loop. These two anti-phased loops combine to form the third positive forward loop through inter-activation—CRY/PER2 activate *Bmal1* by late day when at high levels, and subsequently BMAL1 accumulates, and when a high level is reached by midnight, BMAL1, together with CLOCK, activates CRY and PER gene expression. Our results, along with studies demonstrating the different circadian time courses for oscillations of negative components and BMAL1 (2, 4, 20, 21), suggest a model for the transcriptional control of the mammalian clock that incorporates transcriptional switching at late day and midnight (Fig. 8). Multi-loops are apparently well

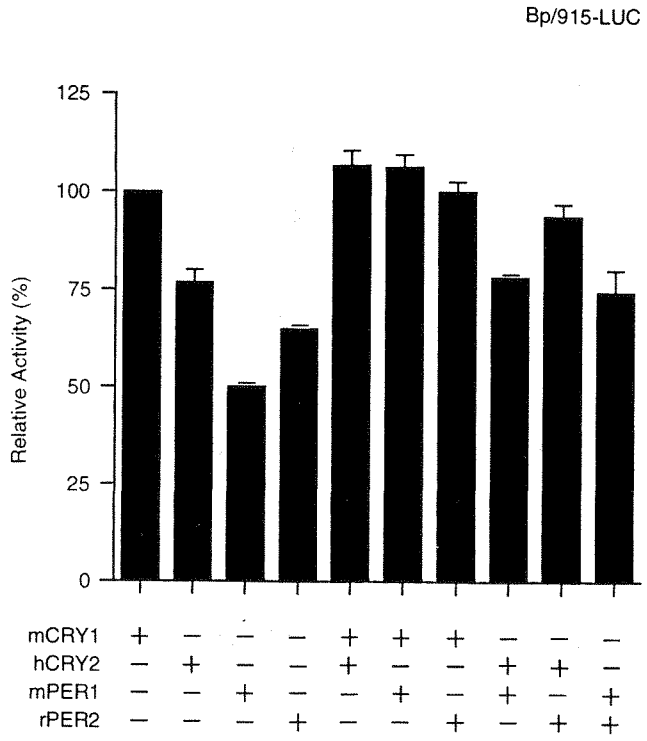

FIG. 6. Lack of synergistic effects on *Bmal1* transcription of pair-wise combinations of CRY1, CRY2, PER1, and PER2. The Bp/915-LUC (57 ng) reporters were co-transfected with (+; 10 ng) or without (−) the indicated expression plasmids. Luciferase activity values in each experiment are normalized to the activity produced with 10 ng of CRY1 alone (set at 100%). Values shown are plotted as the mean % ± SEM (n = 6).

conserved among fungi, insects, and mammals. In *Neurospora,* WC-1 is cyclically expressed, although its mRNA is constant. Surprisingly, WC-1 is upregulated by FRQ at the translational level (34, 35).

Circadian rhythms are remarkably stable, persistent and display precision of period in the absence of environmental cues, such as light. It is conceivable that multi-loops are more stable than a single loop in feedback regulatory systems. The CRY/PER2 loop appears to be critical to the regulatory process. The BMAL1 loop is interlocked with the main CRY/PER2 loop, and lends stability to the clock. Inter-activation between two loops may maintain the amplitude of mRNA oscillation of the clock and clock-controlled genes, thus providing a potential basis for the persistence of circadian clocks. The period precision may involve much more complicated mechanisms. Both CRY/PER2 and anti-phased BMAL1, at high levels and at opposite circadian time points, provide feedback to repress their own gene transcription in nuclei. This event simultaneously sows the seed for the next circadian cycle through a positive forward loop, thereby setting up the timed suppression and promotion of self-oscillations, and forming a timing device.

Our data shows that in both *Per1* and *Bmal1* transcription, inhibition or activation by CRY significantly dominates BMAL1-CLOCK-mediated regulation (Fig. 5B, Fig. 7). This implies that the transcriptional potency of CRY is predominant within the mammalian clock. It is conceivable that, in the presence of CRY, the BMAL1-CLOCK dimers cannot function. This requires a mechanism whereby CRY and PER2 are removed from the nuclei at some time before midnight, just when BMAL1-CLOCK turns on the negative components and simultaneously turns off *Bmal1* transcription. Such clearance mechanisms, working in concert with CKI epsilon-PER2-related cytoplasmic delay of negative components (36, 37), might contribute to period precision. PER1 does not appear to have a direct role in clock gene transcription. Conversely, the ability of PER1 to suppress PER2 at the post-transcriptional level (14) may contribute to the period precision of the clock. Additional interactions between negative regulatory factors and nucleus translocation mechanisms may be involved in controlling the periodicity of the clock.

Much of our understanding of the mammalian clock is derived from studies of the *Drosophila* clock. Among the positive components in *Drosophila,* dCLOCK is

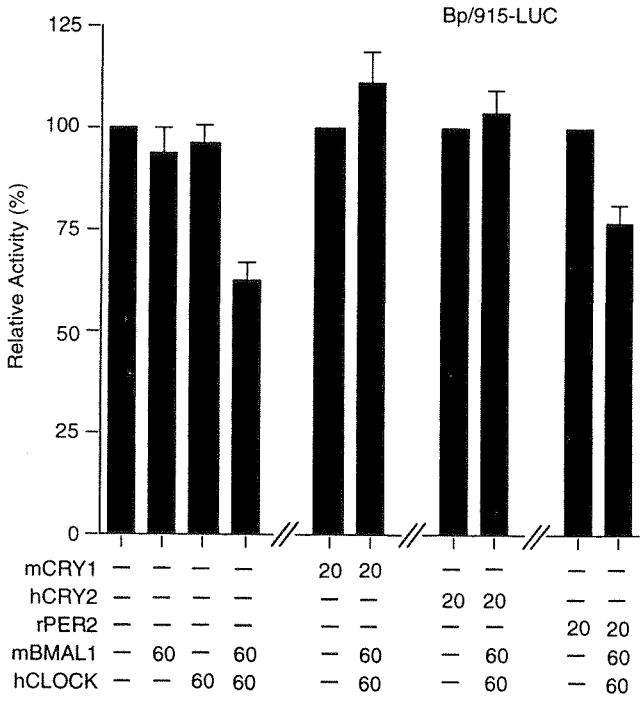

FIG. 7. BMAL1 and CLOCK in combination repress *mBmal1* transcription independent of CRY1 and CRY2. The Bp/915-LUC (57 ng) reporters were co-transfected without (−) or with the indicated amount (in nanograms) of expression plasmids. The luciferase activity values in each experiment are normalized to the activities of appropriate controls (without expression plasmids, CRY1 alone, CRY2 alone, PER2 alone, respectively; set at 100%). The values are plotted as the mean % ± SEM (n = 6).

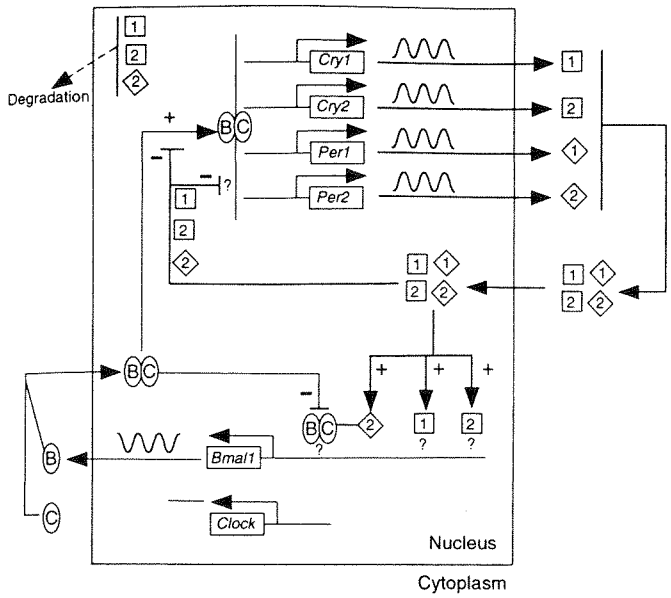

FIG. 8. A model for transcriptional control within the mammalian clock. During late day (right), dimers or multi-complexes of CRY and PER enter the nucleus, thereby activating *Bmal1* transcription either via direct activation or intermediate factors, and repressing *Cry/Per* transcription, probably through sequestration of BMAL1-CLOCK dimers. By midnight (left), when CRY and PER have been removed from the nucleus, high levels of BMAL1-CLOCK dimers activate *Cry/Per* transcription and repress *Bmal1* transcription. Subsequently, CRY and PER accumulate and are retained in the cytoplasm by CKI epsilon (and other unknown mechanisms) until late day. At this point, CRY and PER enter the nucleus and start the cycle anew. Square with 1, CRY1; square with 2, CRY2; diamond with 1, PER1; diamond with 2, PER2; oval with B, BMAL1; oval with C, CLOCK; +, activation; −, repression; wavy lines, cyclic mRNA; straight lines, constant mRNA.

cyclic (19) and CYCLE is constant. The *dclock* mRNA levels are low in *per* mutant flies, and high in *dclock* or *cycle* mutants and in *per-dclock* or *per-cycle* double mutants. An interlocked loops model was proposed, in which CYCLE-dCLOCK represses *dclock,* probably through a mediator, and PER-TIM de-represses the CYCLE-dCLOCK mediated repression, and an unknown activator of *dclock,* independent of PER, dCLOCK and CYCLE was predicted (26). In mammals, *Period2*^{Brdm1} mutants or *Cry1-Cry2* double deficient mice had low *Bmal1* mRNA levels in SCN (27), which is also found in flies. Unlike flies, *Bmal1* mRNA levels are low in the SCN of *Clock* homozygous mutants (27). Our data implicates CRY as the major activator of *Bmal1.* We propose that the low level of *Bmal1* mRNA in *Clock* homozygous mutants results from the low level of CRY (17), whose activation on *Bmal1* transcription overcomes the repression of BMAL1-CLOCK. The high levels of *dclock* mRNA in *dclock* or *cycle* mutant flies and in *per-dclock* or *per-cycle* double mutant flies implies that the unknown activator of *dclock* is independent of dCLOCK and CYCLE, whereas CRY, the major activator of *Bmal1* in mammals, is under the control of BMAL1-CLOCK.

In conclusion, our data reveal that BMAL1 is activated by CRY1, CRY2, and PER2, but is repressed by BMAL1-CLOCK. Both negative components (CRY/PER2) and positive components (BMAL1-CLOCK) play bi-directional transcription roles when at high levels during late day and at midnight. The bi-directional transcription roles at these opposite circadian time points underlies the opposite phase of BMAL1 compared to PER and CRY. A BMAL1 negative feedback loop interlocks with the CRY/PER2 negative feedback loop by inter-activation, forming a third positive forward loop in the mammalian clock. This transcriptional model suggests a molecular basis for maintenance of the stability, persistence, and period of circadian rhythms. The transcriptional potency of CRY is predominant within the mammalian clock, suggesting a clearance mechanism for CRY/PER2 is involved in period maintenance.

ACKNOWLEDGMENTS

We thank M. Muramatsu and P. E. Hardin for a critical review of the manuscript, N. Takehara for technical assistance, and members of the Division of Analytic Science at the Biomedical Research Center of Saitama Medical School for the use of their 377 sequencer, PCR thermal cycler, and luminometer. W.Y. was supported by the Uehara Memorial Foundation. This work was supported by research grants from the Ministry of Education, Science, Sports, and Culture of Japan (10670914 and 11233206), the Pharmacopsychiatry Research Foundation, and the Saitama Medical School.

REFERENCES

1. Dunlap, J. C. (1999). Molecular bases for circadian clocks. *Cell* **96,** 271–290.
2. Lowrey, P. L., and Takahashi, J. S. (2000). Genetics of the mammalian circadian system: Photic entrainment, circadian pacemaker mechanisms, and posttranslational regulation. *Annu. Rev. Genet.* **34,** 533–562.
3. Williams, J. A., and Sehgal, A. (2001). Molecular components of the circadian system in *Drosophila. Annu. Rev. Physiol.* **63,** 729–755.
4. Reppert, S. M., and Weaver, D. R. (2001). Molecular analysis of mammalian circadian rhythms. *Annu. Rev. Physiol.* **63,** 647–676.
5. Balsalobre, A., Damiola, F., and Schibler, U. (1998). A serum shock induces circadian gene expression in mammalian tissue culture cells. *Cell* **93,** 929–937.
6. Akashi, M., and Nishida, E. (2000). Involvement of the MAP kinase cascade in resetting of the mammalian circadian clock. *Genes Dev.* **14,** 645–649.
7. McNamara, P., Seo, S. P., Rudic, R. D., Sehgal, A., Chakravarti, D., and FitzGerald, G. A. (2001). Regulation of CLOCK and MOP4 by nuclear hormone receptors in the vasculature: A humoral mechanism to reset a peripheral clock. *Cell* **105,** 877–889.
8. Ikeda, M., and Nomura, M. (1997). cDNA cloning and tissue-specific expression of a novel basic helix–loop–helix/PAS protein (BMAL1) and identification of alternatively spliced variants with alternative translation initiation site usage. *Biochem. Biophys. Res. Commun.* **233,** 258–264.

9. Hogenesch, J. B., Chan, W. K., Jackiw, V. H., Brown, R. C., Gu, Y. Z., Pray-Grant, M., Perdew, G. H., and Bradfield, C. A. (1997). Characterization of a subset of the basic-helix–loop–helix–PAS superfamily that interacts with components of the dioxin signaling pathway. *J. Biol. Chem.* **272,** 8581–8593.
10. King, D. P., Zhao, Y., Sangoram, A. M., Wilsbacher, L. D., Tanaka, M., Antoch, M. P., Steeves, T. D., Vitaterna, M. H., Kornhauser, J. M., Lowrey, P. L., Turek, F. W., and Takahashi, J. S. (1997). Positional cloning of the mouse circadian clock gene. *Cell* **89,** 641–653.
11. Antoch, M. P., Song, E. J., Chang, A. M., Vitaterna, M. H., Zhao, Y., Wilsbacher, L. D., Sangoram, A. M., King, D. P., Pinto, L. H., and Takahashi, J. S. (1997). Functional identification of the mouse circadian Clock gene by transgenic BAC rescue. *Cell* **89,** 655–667.
12. Gekakis, N., Staknis, D., Nguyen, H. B., Davis, F. C., Wilsbacher, L. D., King, D. P., Takahashi, J. S., and Weitz, C. J. (1998). Role of the CLOCK protein in the mammalian circadian mechanism. *Science* **280,** 1564–1569.
13. Bunger, M. K., Wilsbacher, L. D., Moran, S. M., Clendenin, C., Radcliffe, L. A., Hogenesch, J. B., Simon, M. C., Takahashi, J. S., and Bradfield, C. A. (2000). Mop3 is an essential component of the master circadian pacemaker in mammals. *Cell* **103,** 1009–1017.
14. Zheng, B., Albrecht, U., Kaasik, K., Sage, M., Lu, W., Vaishnav, S., Li, Q., Sun, Z. S., Eichele, G., Bradley, A., and Lee, C. C. (2001). Nonredundant roles of the mPer1 and mPer2 genes in the mammalian circadian clock. *Cell* **105,** 683–694.
15. Zheng, B., Larkin, D. W., Albrecht, U., Sun, Z. S., Sage, M., Eichele, G., Lee, C. C., and Bradley, A. (1999). The mPer2 gene encodes a functional component of the mammalian circadian clock. *Nature* **400,** 169–173.
16. van der Horst, G. T., Muijtjens, M., Kobayashi, K., Takano, R., Kanno, S., Takao, M., de Wit, J., Verkerk, A., Eker, A. P., van Leenen, D., Buijs, R., Bootsma, D., Hoeijmakers, J. H., and Yasui, A. (1999). Mammalian Cry1 and Cry2 are essential for maintenance of circadian rhythms. *Nature* **398,** 627–630.
17. Kume, K., Zylka, M. J., Sriram, S., Shearman, L. P., Weaver, D. R., Jin, X., Maywood, E. S., Hastings, M. H., and Reppert, S. M. (1999). mCRY1 and mCRY2 are essential components of the negative limb of the circadian clock feedback loop. *Cell* **98,** 193–205.
18. Shearman, L. P., Jin, X., Lee, C., Reppert, S. M., and Weaver, D. R. (2000). Targeted disruption of the mPer3 gene: Subtle effects on circadian clock function. *Mol. Cell Biol.* **20,** 6269–6275.
19. Bae, K., Lee, C., Hardin, P. E., and Edery, I. (2000). dCLOCK is present in limiting amounts and likely mediates daily interactions between the dCLOCK-CYC transcription factor and the PER-TIM complex. *J. Neurosci.* **20,** 1746–1753.
20. Honma, S., Ikeda, M., Abe, H., Tanahashi, Y., Namihira, M., Honma, K., and Nomura, M. (1998). Circadian oscillation of BMAL1, a partner of a mammalian clock gene Clock, in rat suprachiasmatic nucleus. *Biochem. Biophys. Res. Commun.* **250,** 83–87.
21. Tamaru, T., Isojima, Y., Yamada, T., Okada, M., Nagai, K., and Takamatsu, K. (2000). Light and glutamate-induced degradation of the circadian oscillating protein BMAL1 during the mammalian clock resetting. *J. Neurosci.* **20,** 7525–7530.
22. Tei, H., Okamura, H., Shigeyoshi, Y., Fukuhara, C., Ozawa, R., Hirose, M., and Sakaki, Y. (1997). Circadian oscillation of a mammalian homologue of the Drosophila period gene. *Nature* **389,** 512–516.
23. Sakamoto, K., Nagase, T., Fukui, H., Horikawa, K., Okada, T., Tanaka, H., Sato, K., Miyake, Y., Ohara, O., Kako, K., and Ishida, N. (1998). Multitissue circadian expression of rat period homolog (rPer2) mRNA is governed by the mammalian circadian clock, the suprachiasmatic nucleus in the brain. *J. Biol. Chem.* **273,** 27039–27042.
24. Okamura, H., Miyake, S., Sumi, Y., Yamaguchi, S., Yasui, A., Muijtjens, M., Hoeijmakers, J. H., and van der Horst, G. T. (1999). Photic induction of mPer1 and mPer2 in cry-deficient mice lacking a biological clock. *Science* **286,** 2531–2534.
25. Abe, H., Honma, S., Namihira, M., Tanahashi, Y., Ikeda, M., Yu, W., and Honma, K. (1999). Phase-dependent induction by light of rat Clock gene expression in the suprachiasmatic nucleus. *Brain Res. Mol. Brain Res.* **66,** 104–110.
26. Glossop, N. R., Lyons, L. C., and Hardin, P. E. (1999). Interlocked feedback loops within the Drosophila circadian oscillator. *Science* **286,** 766–768.
27. Shearman, L. P., Sriram, S., Weaver, D. R., Maywood, E. S., Chaves, I., Zheng, B., Kume, K., Lee, C. C., van der Horst, G. T., Hastings, M. H., and Reppert, S. M. (2000). Interacting molecular loops in the mammalian circadian clock. *Science* **288,** 1013–1019.
28. Yu, W., Ikeda, M., Abe, H., Honma, S., Ebisawa, T., Yamauchi, T., Honma, K., and Nomura, M. (1999). Characterization of three splice variants and genomic organization of the mouse BMAL1 gene. *Biochem. Biophys. Res. Commun.* **260,** 760–767.
29. Field, M. D., Maywood, E. S., O'Brien, J. A., Weaver, D. R., Reppert, S. M., and Hastings, M. H. (2000). Analysis of clock proteins in mouse SCN demonstrates phylogenetic divergence of the circadian clockwork and resetting mechanisms. *Neuron* **25,** 437–447.
30. Griffin, E. A., Jr., Staknis, D., and Weitz, C. J. (1999). Light-independent role of CRY1 and CRY2 in the mammalian circadian clock. *Science* **286,** 768–771.
31. Yagita, K., Yamaguchi, S., Tamanini, F., van Der Horst, G. T., Hoeijmakers, J. H., Yasui, A., Loros, J. J., Dunlap, J. C., and Okamura, H. (2000). Dimerization and nuclear entry of mPER proteins in mammalian cells. *Genes Dev.* **14,** 1353–1363.
32. Reick, M., Garcia, J. A., Dudley, C., and McKnight, S. L. (2001). NPAS2: An analog of clock operative in the mammalian forebrain. *Science* **293,** 506–509.
33. Shearman, L. P., Zylka, M. J., Reppert, S. M., and Weaver, D. R. (1999). Expression of basic helix–loop–helix/PAS genes in the mouse suprachiasmatic nucleus. *Neuroscience* **89,** 387–397.
34. Cheng, P., Yang, Y., and Liu, Y. (2001). Interlocked feedback loops contribute to the robustness of the Neurospora circadian clock. *Proc. Natl. Acad. Sci. USA* **98,** 7408–7413.
35. Lee, K., Loros, J. J., and Dunlap J. C. (2000). Interconnected feedback loops in the Neurospora circadian system. *Science* **289,** 107–110.
36. Lowrey, P. L., Shimomura, K., Antoch, M. P., Yamazaki, S., Zemenides, P. D., Ralph, M. R., Menaker, M., and Takahashi, J. S. (2000). Positional syntenic cloning and functional characterization of the mammalian circadian mutation *tau*. *Science* **288,** 483–492.
37. Toh, K. L., Jones, C. R., He, Y., Eide, E. J., Hinz, W. A., Virshup, D. M., Ptacek, L. J., and Fu, Y. H. (2001). An hPer2 phosphorylation site mutation in familial advanced sleep phase syndrome. *Science* **291,** 1040–1043.

6）kai 時計遺伝子の分子遺伝学的解析による概日振動発生機構の解明（研究代表者：近藤孝男（名古屋大学））

研究代表者：　近藤孝男（名古屋大学大学院理学研究科　教授）
研究分担者：　岩崎秀雄
　　小山時隆

Ⅰ．研究成果

我々はシアノバクテリアで生物発光を利用した実験系を開発し（PNAS 1993)、多くの概日時計突然変異体を分離し(Science 1994)、分子遺伝的方法によってその時計遺伝子群 *kaiABC* をクローニングし、その発現のフィードバック制御が概日振動を発生しうることを示すことが出来た(Science 1998)。しかし概日振動のプロセスを「矢印」で結んだだけでは、進化適応の所産である概日時計を理解したとは言えない。このフィードバックが概日振動の発生原因であったとしても、その振動が安定した 24 時間周期となる生化学的根拠はまったく説明されていない。この概日時計の特性こそがその環境適応機能の前提であってみれば、その生化学的基礎を解明することが重要であろう。そして、この安定した周期決定機構こそが進化を通して開発された概日時計の本質であろう。我々はシアノバクテリアの概日周期が Kai 蛋白質のアミノ酸の変更で大幅に変化するが、他の関連遺伝子の変異や生理学的条件の変更は、振幅の低下はもたらしても、周期をあまり変化させないことを経験しており、Kai 蛋白質とそのパートナーの生化学的性質に振動の特性を規定する謎が潜んでいるのではないかと考え、*kai* 遺伝子の発現制御機構、Kai 蛋白質の生化学的性質、あるいは振動を補佐する他の要素について分子レベルの解析を試みた。

1．Kai 蛋白質の相互作用と高次複合体

Kai 蛋白質は新規の蛋白質であり、その配列から機能を推測することは困難であるが、我々は３つの Kai 蛋白質が酵母の細胞内もしくは *in vitro* で、様々な組み合わせの相互作用することを確認し、この相互作用が概日振動の発生やその周期の決定に大きな意味を持つものではないかと考えている。事実、KaiA と KaiB の結合活性が突然変異により変化する。また KaiC は KaiA と KaiB の結合活性を大幅に増大させることも確認されており、夫々のホモダイマーも確認されている。従って、Kai 蛋白質は細胞内ではさまざまな結合の可能性をもっており、その結合が概日振動の発生に深く係っていると考えられた(1)。

さらに、抗 KaiC 抗体で免疫沈降反応を行い，細胞中での各 Kai 蛋白質と SasA の相互作用の時間変動を確認した。KaiA，KaiB，SasA 共に KaiC と夜間に強く相互作用していることが明らかになった。次に，ゲルろ過法により分画し，Kai 蛋白質，SasA を含む蛋白質複合体のサイズを明らかにした。全ての Kai 蛋白質，SasA が形成する複合体のサイズは顕著な日周変動を示した。各複合体は夜間に約 500kDa と巨大になり，それらのサ

イズからはKai/SasAの高次複合体が夜間に形成され,昼間に分離することを思わせた。続いて各Kai蛋白質，SasAの欠失株を用いて同様の解析をすることにより，KaiCがこの複合体の中心的な分子になっていることや,KaiAとKaiBが共役的にKaiCを含む複合体と相互作用することなど，400-600 kDa複合体の構造が明らかにされた。実際に，免疫沈降法によって複合体中で各Kai蛋白質とSasAが夜間に相互作用していることが明らかになった。以上の結果から *kaiBC* オペロンの転写活性における400-600kDa複合体の役割を推定しモデルを提出した（8)。

2．Kai蛋白質の動態

Western解析により3つのKai蛋白質がいずれもmRNAのリズムに比べ8時間ほど遅れた位相で振動することが確認された。また、この時、KaiC蛋白質は2つのバンドになるが、フォスファターゼの処理により高分子量のバンドが消失するのでKaiC蛋白質は細胞内でリン酸化されていることが示された。このリン酸化のレベルも概日振動を示し、さらに、いくつかの突然変異体ではこのリン酸化レベルの異常が確認され、概日振動の過程でKaiC蛋白質のリン酸化が重要なステップであることが示された。

上記の相互作用解析からKaiC上にはKaiAと結合する2つの領域が特定されており、この領域には多くの時計突然変異がマップされ、結合の強さが突然変異により変化することが確認されている。また、*kaiA* 遺伝子上の時計変異のサプレッサーが *kaiC* 遺伝子のこの領域にみいだされている。これらのデータはKaiA, KaiC蛋白質間の相互作用が概日振動の性質に大きな影響を持つことを示している。事実、KaiAの共存によりKaiCのリン酸化が著しく促進されることがシアノバクテリアの細胞内でも、*in vitro* でも確認され、KaiCとKaiAの共役による振動活性化が示唆されている。この事実はKai蛋白質による周期の決定機構の解析の糸口になるであろう(5)。今後、シアノバクテリアの細胞内での相互作用の変動、翻訳速度、分解速度の時間変動や細胞内分布およびリン酸化の時間変動を調査する。またKai蛋白質のリン酸化などのタンパク質修飾を、SDS-PAGEや二次元電気泳動によるバンドシフト，フォスファターゼなどをもちいた修飾検定，被修飾アミノ酸残基の決定などで調査する必要があり、さらにこれらを様々な変異体で比較することで、24時間周期を成立させる要因を探りたいと考えている。

3．Kai蛋白質の機能とリン酸化

KaiCの配列には2つのATP/GTP結合モチーフ(Walker's p-loop)が見出されている。またKaiCの配列は重複構造をとっており、N端側(CI)とC端側(CII)とはよく類似しており、p-loopも夫々対応する位置にあることが確認された。さらにCIとCIIは相互作用すること、単独でも *kaiBC* の発現を抑制することが確認された(4)。また、KaiCのP-loopによって、KaiC蛋白質はATPと結合することも確認されている。またこのモチーフへ変異を導入するとこのATP結合能も概日リズムも消失してしまい、KaiC蛋白質のATPとの結合が概日周期の決定に重要であることが示された(2)。さらに *in vitro* でKaiCがそのセリ

ン/スレオニン残基を自己リン酸化することも見出されている。KaiC には既知のキナーゼ・モチーフは存在せず、新規の自己リン酸化蛋白質（autokinase）と考えられる。シアノバクテリアでは今までに Ser/Thr autokinase の報告例はなく、その意味でも貴重な知見を提供するものである。

我々は KaiC 蛋白質のリン酸化についてさらに以下の２つの事実を明らかにした。

・KaiA 蛋白質による KaiC 蛋白質のリン酸化

細胞内においても、試験管内でも KaiC 蛋白質のリン酸化が KaiA 蛋白質により大きく促進されることを明らかにした。またこの KaiA による促進に KaiC が必要であることも示され、この２つの蛋白質が協同して *kaiBC* の発現を促進しており、振動持続のための正のフィードバックを起していることが示唆された。これらの生化学的な事実は *kaiA* の点突然変異と *kaiC* に見いだされたその抑制変異の解析からも裏付けられた。これらの事実をもとに KaiA と KaiC の共同によるフィードバック機構を提案した。(7)

・KaiB 蛋白質による KaiC 蛋白質のリン酸化抑制。

細胞内の Kai 蛋白質の解析を行い、各蛋白質の存在量とその細胞内分布を解析した。その結果細胞質内の KaiB は他のものに遅れて極大となり、さらに免疫沈降法による解析では、まず KaiA がの作用について KaiC 蛋白質のリン酸化を促進し、KaiA-C 複合体を形成し、次に KaiB がこれに結合することで、KaiC 蛋白質のリン酸化を低下させることが示された (9)。

４．KaiC による包括的遺伝子発現制御

シアノバクテリアの概日振動は時計蛋白質 KaiC による *kaiBC* プロモーターのフィードバック制御を骨格として発生していると考えられている(Ishiura et al. 1998)。この様式は真核生物の時計モデルと共通であるが、これまでのところ、真核生物の様に時計遺伝子の上流領域に対する KaiC の特異的な制御は確認されていない。一方、プロモータートラップ法による調査ではシアノバクテリアの概日時計はすべての遺伝子発現を制御していることが示されている (Liu et. al 1995)。そこで、シアノバクテリアの概日システムの特徴を裏付けている機構を探るべく、解析を行ない、以下の結果を得た。１）KaiC の過剰発現は *kaiBC* プロモーターのみならずべてのプロモーターのリズム成分だけを選択的に抑制する。２）*kaiBC* 欠損株において、大腸菌由来のプロモーターにより *kaiCB* を発現させた場合でも、発現レベルを調整すると、ほぼ完全な概日振動を回復することが出来た。従って、シアノバクテリアでは KaiC は遺伝子発現の包括的制御を行っており、細胞の遺伝子発現を包括的に制御するとともに、概日振動の発生を実現していると考えられる（投稿中)。

５．概日振動を構成する要素の探索

シアノバクテリアの概日振動を理解するためには、さらに多くの概日振動発生系に関与

する分子の同定も不可欠である。先にも述べたように我々はEMS処理により、100個以上の時計突然変異体を分離したが、これまで *kai* 遺伝子群以外に変異のあるものは見いだされていない。*kai* 遺伝子群以外の時計関連遺伝子は、突然変異により機能を失うと致死になるのかもしれない。従ってこれらの遺伝子を同定するためには、酵母のtwo-hybrid系あるいは他の生化学的方法などの異なった戦略が必要であろう。我々はすでに酵母のtwo-hybrid法を用いて、KaiC結合蛋白質の探索を行い、二成分情報伝達系(two-component regulatory system) のセンサー（ヒスチジン）キナーゼSasAを同定した。*sasA* 遺伝子破壊株では、*kaiBC* の発現量が著しく低下し、概日振動の振幅（振動の強さ)も大きく低下した。一過的な *sasA* の過剰発現は概日時計の位相変化をもたらし、さらに、*sasA* の構成的な過剰発現により、時計機能は完全に停止した。これらの知見は、KaiCがSasAの活性を制御するいっぽう、SasAが *kaiBC* の発現を調節することで安定な概日振動を実現していることを強く示唆している。SasAがない状態でも *kai* に基づく振動は持続しているが、その振幅は生理的な意味を持たないと思われ無いほど弱く、SasAは *kai* に基づく振動の重要な増幅装置として機能しているようである (3)

6．環境情報による時計同調メカニズムおよび概日振動による遺伝子発現制御

光による同調は概日時計の基本的要件である。この光信号伝達経路を探るためまず、光による位相合わせを調査した。概日時計の位相の変化は光信号の与えられる時刻によって異なっており、生物種を越えた共通の性質を持っている。この性質は位相応答曲線として表されるが、シアノバクテリアではこれまで位相応答曲線は調査されていないので、まずこれを調査した。連続明下で持続しているシアノバクテリアのリズムは強光、暗期（弱光)、低温、高温といった外部刺激に対して、真核生物で知られている位相応答と同様な反応を示すことが確認されたさらに位相変位を引き起こす暗パルスの替りに単色光を照射することで、この光刺激を受容する光受容体の分光学的性質を調査した。この作用スペクトルは、基礎生物学研究所の大型スペクトログラフを利用し測定されたが、450nmと660nmに極大をもつ光合成型のものであった。したがって暗パルスによる位相変位は、代謝の変動を介した振動の速度変更に基づくもの（いわゆるparametric effect)と、明暗の切り替えによる位相変位（いわゆるnon-parametric effect)いずれもが係わっている現象であると考えられる。したがってこの二つの効果を分別するため、暗期中の光パルスによる位相変位を解析するプロトコルを開発し、光パルスによる位相変位の突然変異体を多数分離し、解析を進めている。

またこの光リセット過程に対する分子遺伝学的アプローチ、すなわち位相変位の異常体の分離も進行中である。なお、米国の共同研究者 S. Golden 博士らを中心として、暗パルスによる位相変位に係るフィトクロム類似の蛋白質をコードする遺伝子 *cikA* を見出した(4)。

参考文献

1. Iwasaki, H.,Taniguchi, Y., Ishiura, M. and T. Kondo: Physical interactions among circadian clock proteins, KaiA, KaiB and KaiC, in cyanobacteria. EMBO J (1999) 18: 1137-1145

2. Nishiwaki T, Iwasaki, H., Ishiura, M. and T. Kondo: Nucleotide binding and autophosphorylation of the clock protein KaiC as a circadian timing process of cyanobacteria. Proc. Natl. Acad. Sci. (2000) 97: 495-499.

3. Iwasaki, H.,Williams SB, Kitayama Y, Ishiura, M., Golden SS and T. Kondo: A KaiC-interacting sensory histidine kinase, SasA, necessary to sustain robust circadian oscillation in cyanobacteria. Cell 101: 223-233 (2000)

4. Schmitz,O, M Katayama, S. B. Williams, T. Kondo, S. S. Golden. CikA, a bacteriophytochrome that resets the cyanobacterial circadian clock. Science 289: 765-768 (2000)

5. Taniguchi Y, Yamaguchi A, Hijikata A, Iwasaki H, Kamagata K, Ishiura M, Go M and Kondo T: Two KaiA-binding domains of cyanobacterial circadian clock protein KaiC , FEBS lett. 496: 86-90, (2001)

6. Nishimura H, Nakahira Y, Imai K, Tsuruhara A, Kondo H, H ayashi H, Hirai M, Saito H, and Kondo T. Mutations in KaiA, a clock protein, extend the period of circadian rhythm of cyanobacterium Synechococcus elogatus PCC7942. Microbiology (2002), 148, 2903 ≒ 2909

7. Iwasaki, H., T. Nishiwaki, Y. Kitayama, M Nakajima and T. Kondo. KaiA-Stimulated KaiC Phosphorylation in Circadian Timing Loops in Cyanobacteria. Proc. Natl. Acad. Sci. 99: 15788-15793 (2002)

8. Kageyama H, T. Kondo and H. Iwasaki Circadian Formation of Clock Protein Complexes by KaiA, KaiB, KaiC and SasA in Cyanobacteria J. Biol. Chem. 278:2388-2395 (2003)

9. Kitayama Y., H. Iwasaki, T. Nishiwaki and T. Kondo. KaiB functions as an attenuator of KaiC phosphorylation in the cyanobacterial circadian clock system. EMBO J in press (2003)

総説

1. Kondo T. and Ishiura M. (1999) The circadian clocks of plants and cyanobacteria. Trends Plant Sci. 4: 171-176

2. Kondo T. and Ishiura M. Circadian clock of cyanobacteria. BioEssays (2000) 22:10-15

3. Iwasaki H, Kondo T. (2000) The current state and problems of circadian clock studies in cyanobacteria. Plant Cell Physiol.41: 1013-1020

和文総説

1. 近藤孝男・石浦正寛 (1999) 光合成生物の概日時計遺伝子 Molecular Medicine 36 巻 10 号 1120-1127

2. 岩崎秀雄・近藤孝男 (2001) 多重フィードバック制御による概日時計の振動安定化機構 細胞工学 20: No. 6, 801-807

3. 近藤孝男 (2002) 概日時計による生命活動の統合 数理科学 468：19-24

出版物

1. Iwasaki H, Kondo T. (2002) "Histidine kinases in the cyanobacterial circadian system" Histidine Kinases (Eds. M. Inouye and R. Dutta), Academic Press

2. Kondo T. (2002) Molecular Basis for Circadian Oscillation in Cyanobacteria. In Circadian organization Eds K. Honma and S. Honma, Hokkaido Univ. Press

3. 近藤孝男 (2002) 植物にとっての昼と夜ー生物時計について 「植物が未来を拓く」 67-90 ページ 共立出版

Cell, Vol. 101, 223–233, April 14, 2000, Copyright ©2000 by Cell Press

A KaiC-Interacting Sensory Histidine Kinase, SasA, Necessary to Sustain Robust Circadian Oscillation in Cyanobacteria

Hideo Iwasaki,* Stanly B. Williams,†
Yohko Kitayama,* Masahiro Ishiura,*‡
Susan S. Golden,† and Takao Kondo*§
*Division of Biological Science
Graduate School of Science
Nagoya University
Nagoya 464-8602
Japan
†Department of Biology
Texas A&M University
College Station, Texas 77843

Summary

Both regulated expression of the clock genes *kaiA*, *kaiB*, and *kaiC* and interactions among the Kai proteins are proposed to be important for circadian function in the cyanobacterium *Synechococcus* sp. strain PCC 7942. We have identified the histidine kinase SasA as a KaiC-interacting protein. SasA contains a KaiB-like sensory domain, which appears sufficient for interaction with KaiC. Disruption of the *sasA* gene lowered *kaiBC* expression and dramatically reduced amplitude of the *kai* expression rhythms while shortening the period. Accordingly, *sasA* disruption attenuated circadian expression patterns of all tested genes, some of which became arrhythmic. Continuous *sasA* overexpression eliminated circadian rhythms, whereas temporal overexpression changed the phase of *kaiBC* expression rhythm. Thus, SasA is a close associate of the cyanobacterial clock that is necessary to sustain robust circadian rhythms.

Introduction

Circadian clocks are endogenous biological timing processes that have been observed ubiquitously in organisms from cyanobacteria to green plants and humans. Temporal regulation of various metabolic and behavioral activities by the clock (circadian rhythmicity) is thought to be adaptive for organisms to survive under daily alteration in environmental conditions, such as light, temperature, and humidity (Pittendrigh, 1993; Ouyang et al., 1998). To elucidate the molecular mechanism of the circadian oscillator, several clock genes and clock-related genes have been cloned and analyzed in various organisms (reviewed by Dunlap, 1999).

Cyanobacteria are the simplest organisms that exhibit circadian rhythms (reviewed by Golden et al., 1997). Using a bioluminescence reporter gene, we monitored circadian gene expression in the cyanobacterium *Synechococcus* sp. strain PCC 7942 (hereafter referred to as *Synechococcus*) (Kondo et al., 1993) and isolated various rhythm mutants (Kondo et al., 1994). A locus composed of three genes, *kaiA*, *kaiB*, and *kaiC*, was cloned previously by genetic complementation (Ishiura et al., 1998). All three genes are essential for circadian rhythms of gene expression. Detailed genetic analyses suggested that negative feedback control of KaiC on *kaiBC* expression helps to generate circadian oscillation, and that KaiA sustains the oscillation by increasing the *kaiC* expression (Ishiura et al., 1998).

The Kai proteins interact in various combinations in yeast cells, in vitro, and in *Synechococcus* (Iwasaki et al., 1999). More recently, we found that KaiC has ATP-binding and autophosphorylating activities that are likely important for the circadian feedback processes (Nishiwaki et al., 2000). These observations provided some biochemical characteristics of the Kai-based oscillator. However, to elucidate a molecular mechanism by which Kai proteins contribute to generation of circadian rhythms, it is necessary to identify and characterize other clock-associated genes.

We used a yeast two-hybrid screen to search for genes that encode KaiC-associating proteins, and identified a histidine protein kinase gene, *sasA*. The functional relevance of SasA to the cyanobacterial circadian clock was analyzed by examining cyanobacterial transformants in which *sasA* was disrupted or overexpressed. The results indicated that SasA activates *kaiBC* expression and is important for maintaining robust rhythmicity in *Synechococcus*. Moreover, *sasA* contributes to adaptation of the cells to grow in light/dark cycles.

Results

Identification of SasA as a KaiC-Interacting Protein

To identify *Synechococcus* genomic DNA encoding potential KaiC-binding proteins, we used a LexA-KaiC hybrid protein as bait in a yeast two-hybrid screen (Fields and Song, 1989; Iwasaki et al., 1999). The *Synechococcus* genomic library, which was constructed in the two-hybrid vector pVP16 (Vojtek et al., 1993), was prepared from a *kaiABC*-deficient *Synechococcus* strain (Ishiura et al., 1998) to exclude the Kai proteins from the screening. Yeast transformants (5×10^6 independent clones) were screened, and 5 library clones were obtained for KaiC-dependent dual reporter gene activation (see Experimental Procedures). Four of these plasmids carried identical 0.3 kb DNA segments that encode the N-terminal portion of the two-component system histidine protein kinase, SasA (*Synechococcus* adaptive sensor) (Nagaya et al., 1993) (Figure 1A). The fifth plasmid was probably not significant as it contained *Synechococcus* DNA encoding only 6 amino acid residues.

Interestingly, the KaiC-interacting portion of SasA (amino acyl residues 1–97) is similar to the full-length KaiB protein (Figure 1A). Identity and similarity between the two polypeptides are approximately 26% and 60%, respectively. Indeed, we independently found SasA by its similarity to KaiB in a database (BLAST) (Altschul et al., 1990) search during the course of the two-hybrid screening.

§To whom correspondence should be addressed (e-mail: kondo@bio.nagoya-u.ac.jp).
‡Present address: Center for Gene Research, Nagoya University, Furo-cho, Chikusa-ku, Nagoya 464-8602, Japan.

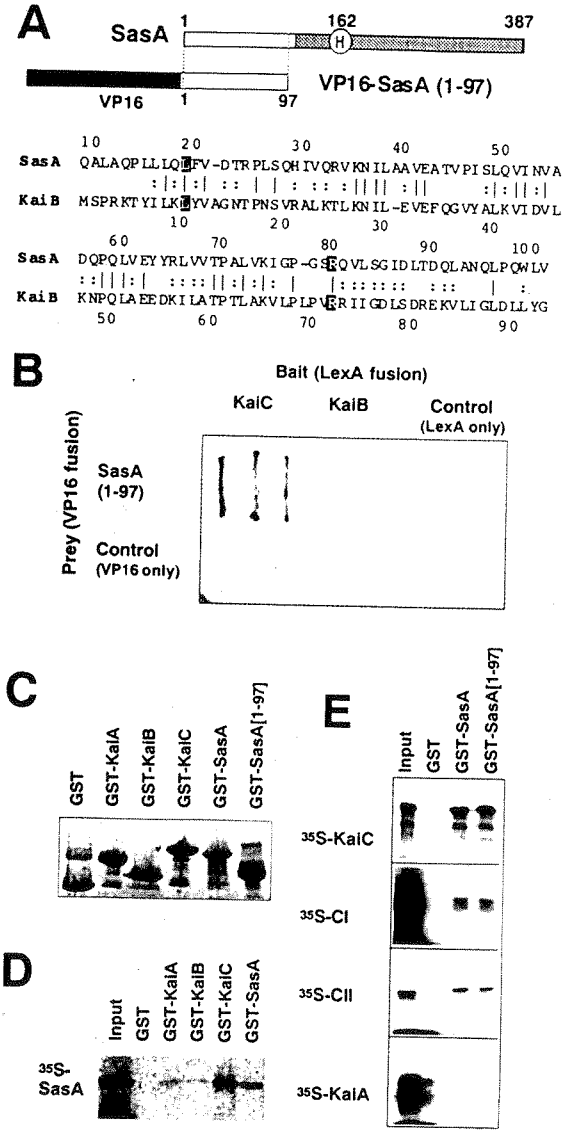

Figure 1. Identification of SasA as a KaiC-Interacting Factor

(A) Schematic representation of SasA (top) and the VP16:SasA-C-terminal domain fusion (middle). Putative histidyl residue for autophosphorylation (His 162) and conserved C-terminal kinase domain are indicated by shadowing on the SasA molecule. The amino acid sequence of the N-terminal SasA sequence was aligned with that of KaiB (bottom).

(B) Specific interaction of SasA(1–97) and KaiC in the two-hybrid system. Shown is the result of the filter assay for β-galactosidase reporter of yeast colonies cotransformed with the combination of bait and prey constructs indicated.

(C) Production of fusion proteins in *E. coli*. GST, GST fused to KaiA, KaiB, KaiC, SasA, or the N-terminal SasA fragment (residues 1–97) were produced in *E. coli* and purified by affinity chromatography with glutathione Sepharose 4B resin. The fusion proteins (about 5 μg each) were eluted from the resin and fractionated by SDS-PAGE on 10%–15% gradient gels, then stained with Coomassie brilliant blue (CBB).

(D) In vitro binding assay. GST, GST-KaiA, -KaiB, -KaiC, and -SasA (2 μg each) were immobilized on glutathione Sepharose 4B and then incubated with 2 μl of the reticulocyte reaction mixture containing ^{35}S-labeled SasA. Proteins associated with the resin were detected by SDS-PAGE on 12% gels followed by autoradiography.

(E) In vitro binding assay. GST, GST-SasA, and -SasA(1–97) (5 μg each) were immobilized on glutathione Sepharose 4B and then incubated with 3 μl of the reticulocyte reaction mixture containing ^{35}S-labeled intact KaiC, CI domain, CII domain, or KaiA. Proteins associated with the resin were detected by SDS-PAGE on 10% gels followed by autoradiography. Residues L11 and R76 in KaiB, whose mutations alter circadian periods, and the corresponding L19 and R80 in SasA, respectively, are reversed.

Although homotypic interaction of KaiB has been demonstrated using both yeast two-hybrid and in vitro binding assays (Iwasaki et al., 1999), and by bioluminescence resonance energy transfer (Xu et al., 1999), the hybrid protein VP16-SasA(1–97) (VP-16 fused to just the first 97 amino acyl residues of SasA) failed to interact with a hybrid LexA-KaiB protein in our yeast two-hybrid assay (Figure 1B).

We further established interaction between SasA and KaiC using an in vitro binding assay. Each protein, truncated SasA(1–97), full-length SasA(1–387), KaiA, KaiB, and KaiC, was individually expressed and purified with GST (glutathione-S-transferase) fused at the amino terminus (Figure 1C). The fusion proteins were immobilized on a glutathione sepharose affinity resin and incubated with in vitro–translated, ^{35}S-labeled SasA ([^{35}S]SasA). Resin-bound protein was eluted and analyzed by SDS-polyacrylamide gel electrophoresis followed by autoradiography. As shown in Figure 1D, significant amounts of [^{35}S]SasA were retained by both immobilized GST-KaiC and GST-SasA fusions, but not by the GST, GST-KaiA, or GST-KaiB. In reciprocal assays, [^{35}S]KaiC interacted with both GST-SasA and GST-SasA(1–97), but not with the GST control (Figure 1E). [^{35}S]KaiA failed to interact with GST-SasA derivatives (Figure 1E).

The primary structure of KaiC contains a tandem repeat. The sequence of the first half, KaiC(1–260) called the CI domain, is easily aligned with and very similar to the sequence of the second half, KaiC(261–519), called the CII domain. Each half interacts separately with KaiA, KaiB, and KaiC in vitro (Iwasaki et al., 1999). Using the same procedure, we examined interaction between SasA and each half of KaiC, CI, and CII. Both [^{35}S]CI and [^{35}S]CII bound to both GST-SasA and GST-SasA(1–97) (Figure 1E). In summary, SasA interacted only with itself and KaiC. Either CI or CII was sufficient for the latter interaction. Interestingly, the first 97 amino acyl residues of SasA seem sufficient for all demonstrated interactions with KaiC and its derivative proteins.

Effects of *sasA* Disruption on Circadian Gene Expression

To test its function, we inactivated the *sasA* gene in a variety of reporter strains and monitored circadian gene expression patterns in continuous light (LL). The *sasA*-disrupted strains grew as well as their parental strains in LL (Nagaya et al., 1993) (for example, see Figure 6). Using promoter fusions to the *luxAB* genes encoding bacterial luciferase proteins, we determined patterns of gene expression from the *kaiA*, *kaiBC*, and *psbAI* promoters at two different light intensities after a single 12 hr dark period to synchronize the clock (Kondo et al., 1993; Ishiura et al., 1998).

At the higher light intensity (50 μE m^{-2} s^{-1}), amplitudes

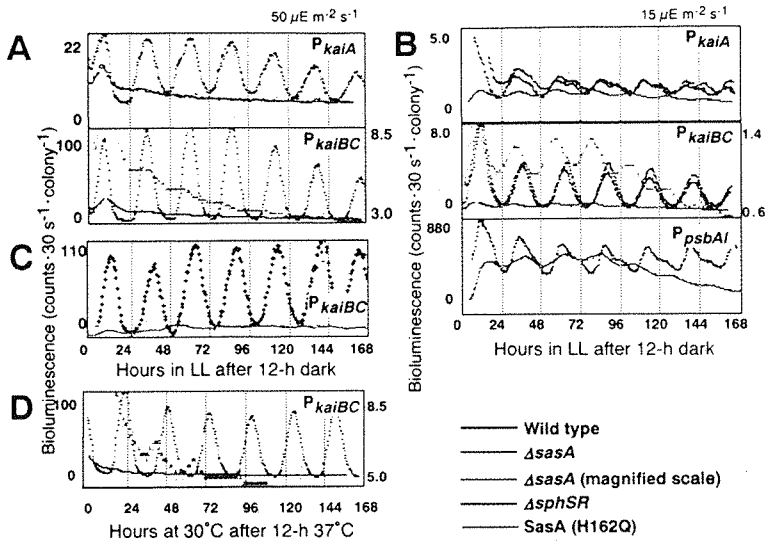

Figure 2. Disruption of *sasA* Attenuates Circadian *kai* Gene Expression

(A and B) Very low amplitude, short period bioluminescence rhythms in the absence of *sasA*. Wild type (black trace), *sasA*-disrupted (Δ*sasA*, red trace), and *sphSR*-disrupted (Δ*sphSR*, blue trace) cells that carry P_{kaiA}-, P_{kaiBC}-, or P_{psbAI}-reporter cassette were grown for 3–4 days on solid medium in LL at 50 μE m^{-2} s^{-1} (A) or 30 μE m^{-2} s^{-1} (B) to give 30 to 60 colonies (0.2 mm diameter). After a 12 hr dark treatment, cells were transferred to LL at 50 μE m^{-2} s^{-1} (A) or 15 μE m^{-2} s^{-1} (B), and the bioluminescence was measured by a photomultiplier tube. For clarity, bioluminescence profiles of the P_{kaiBC}-reporter strain lacking *sasA* are also shown in magnified scales (purple trace, maginified scale shown on the right).

(C) *kaiBC* expression profile in the H162Q mutant, in which a putative autophosphorylation residue was substituted with Gln. Bioluminescence from wild type (black) and the mutant (green) was monitored in LL at 50 μE m^{-2} s^{-1} as in (A).

(D) Nonphotic zeitgeber (temperature step-up) did not restore normal circadian phenotype in the *sasA*-disrupted strain. Cells were grown under LL (50 μE m^{-2} s^{-1}) at 30°C, treated with a temperature shift (37°C) for 12 hr, and then returned to 30°C. Other details are the same as described above.

of expression rhythms driven from both *kaiA* and *kaiBC* promoters (P_{kaiA} and P_{kaiBC}, respectively) were dramatically reduced and damped out to be arrhythmic within a few days (Figure 2A). Moreover, the magnitude of P_{kaiA} and P_{kaiBC} activity were lowered in the *sasA* disruptant cells to 40%–60% and 5%–10% of the peak levels, respectively.

At the lower light intensity (15 μE m^{-2} s^{-1}), the residual rhythmicity was more robust than at 50 μE m^{-2} s^{-1} (Figure 2B). Disruption of *sasA* shortened the period length of the P_{kaiBC} expression rhythm by 3 hr (23.0 ± 0.3 hr versus 25.8 ± 0.1 hr, n = 3). Both the magnitude of expression and the amplitude of the P_{kaiBC} rhythm were still diminished by inactivation of *sasA* (Figure 2B), but the magnitude of expression from both P_{kaiA} and P_{psbAI} was less affected.

In *Synechococcus*, expression of most or all genes is controlled by the circadian clock (Liu et al., 1995). Monitoring a larger set of reporter strains under low intensity LL revealed at least two classes of altered gene expression patterns in a *sasA* null background (Figure 3). In one class, which includes bioluminescence from *luxAB* gene reporter fusions to the *psbAII* (Golden et al., 1986), *cikA* (O. Schmitz, M. Katayama, and S. S. G., unpublished data) and *opcA* (Scanlan et al. 1992; H. Min and S. S. G., unpublished data) genes, inactivation of the *sasA* gene did not dramatically reduce bioluminescence levels but did result in arrhythmic, essentially constitutive, expression patterns (Figure 3A). In the other class, which includes *luxAB* fusions to the *rpoD2* and *ndhD* genes (Tsinoremas et al., 1996), *sasA* inactivation altered period, amplitude, or phase angle of the circadian expression rhythms (Figure 3B). Both phase angle and amplitude of the *rpoD2* expression rhythm were affected by inactivation of *sasA*, whereas the expression pattern from the *ndhD::luxAB* fusion retained little rhythmicity after *sasA* inactivation (Figure 3B).

Reduced amplitude of bioluminescence rhythms could be caused by availability of reduced flavin mononucleotide, a bacterial luciferase substrate. Thus, we also monitored expression patterns from a P_{kaiBC} gene fusion to the firefly luciferase gene, *luc*, which has different substrate requirements from the bacterial luciferase. Choice of reporter enzyme made no difference in the circadian phenotype of our wild-type or *sasA*-inactivated strains (data not shown).

Attenuation of *kaiBC* Expression Rhythm by Mutation in the Putative Autophosphorylation Site of SasA

To examine whether histidine kinase function of SasA is involved in circadian *kaiBC* expression, we substituted the conserved histidine at residue 162 (H162) (Figure 1A), a putative autophosphorylation site expected to be essential for phosphoryl transfer activity, with glutamine (H162Q). As shown in Figure 2C, H162Q mutation dramatically reduced *kaiBC* promoter activity and lowered amplitude of the rhythm, as did disruption of *sasA*. Thus, this residue of SasA is indeed necessary for normal robust rhythmicity in *Synechococcus*, consistent with a requirement for autophosphorylation.

Both *sasA* and another *Synechococcus* histidine protein kinase gene, *sphS*, were originally cloned by heterologous complementation of sensor kinase function in *Escherichia coli* (Aiba et al., 1993; Nagaya et al., 1993). Because both SasA and SphS belong to the EnvZ-type histidine kinase subfamily, we measured bioluminescence from a P_{kaiBC} reporter strain that lacked both *sphS* and its cognate response regulator, *sphR* (Aiba et al.,1993). The *sphS/sphR* disruptant exhibited wild-type bioluminescence expression rhythms (Figure 2B, blue line). Therefore, although SasA and SphS behave similarly in a heterologous complementation assay that is fairly nonspecific for sensor kinase function, only SasA has a role in circadian control in *Synechococcus*.

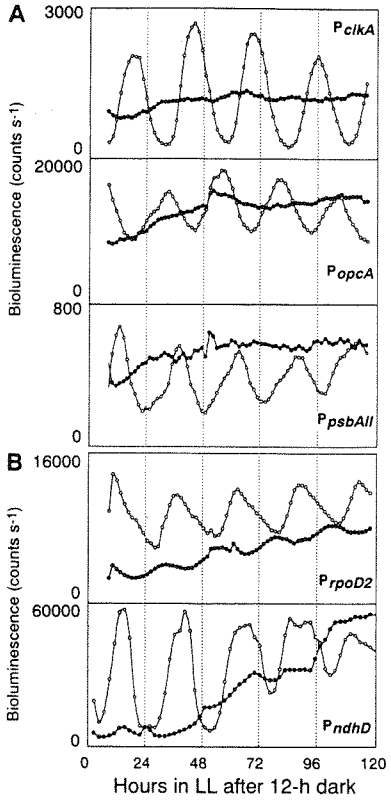

Figure 3. Two Phenotypic Classes Emerge after *sasA* Disruption

Bioluminescence rhythms comparing wild-type (open circles) to *sasA*-disrupted (filled circles) reporter strains. The promoter driving *luxAB* is indicated for each panel. Traces are from individual microtiter wells, but are representative of multiple independent experiments (see Experimental Procedures).

(A) Three reporter strains with arhythmic circadian phenotypes after *sasA* disruption are shown. Note that the P_{opcA} rhythm has a class 2 (180° offset) phase angle. (B) Two additional reporter strains that maintain detectable rhythmic expression patterns are shown.

Clock Resetting in the *sasA* Disruptant

Although unstable, the circadian clock in the *sasA*-disrupted strain is still entrainable by a 12 hr dark treatment (Figures 2A, 2B, and 3). To test whether a nonphotic zeitgeber (entrainment signal) is able to synchronize the circadian oscillator in the *sasA*-inactivated strain, we assayed P_{kaiBC} in wild-type and *sasA* backgrounds after a 12 hr exposure to high temperature. As shown in Figure 2D (red and purple lines), a 12 hr high temperature treatment (37°C) synchronized the *Synechococcus* clock to circadian time 12 (CT 12), which is subjective dusk, in both strains. Thus, *sasA* is not essential to reset the circadian clock by light or temperature. However, note that a 12 hr temperature step-up, concurrent with a 12 hr dark treatment still failed to recover robust rhythmicity in the *sasA*-disrupted strain (Figure 2D). Thus, attenuated circadian rhythmicity in this strain cannot be attributed to a defect in a light-specific signal transduction pathway to the clock.

Accumulation of *kai* Gene Products in the Absence of SasA

Inactivation of the *sasA* gene had dramatic effects on the expression of the *kai* genes without complete loss of the circadian timing mechanism (Figures 2 and 3). We examined the accumulation levels of *kai* mRNAs in an *sasA* strain by Northern (RNA) blot analysis. In wild-type cells, robust circadian rhythms of *kaiA* and *kaiBC* mRNA levels were observed under standard LL conditions (Ishiura et al., 1998) (Figure 4A). By contrast, no circadian fluctuations in these mRNA levels were evident in the *sasA* disruptant (Figure 4A). The levels of *kaiBC* and *kaiA* mRNAs were lowered in the mutant to 5%–15% and 40%–70%, respectively of those in wild-type cells at peak, correlating well with the bioluminescence profiles shown in Figure 2A.

Accumulation of the Kai proteins was also compared between wild-type and the *sasA* null strains. In wild-type cells, Y. Xu, T. Mori, and C. H. Johnson found KaiB and KaiC abundances exhibit circadian rhythms peaking at circadian time (CT) 15–16 (15–16 hr after lights-on) and troughing at CT 3–4, while the amplitude of KaiA accumulation rhythm is low (Figure 4B) (C. H. Johnson, personal communication; T. Nishiwaka, J. Tomita, and H. I., unpublished data). Accumulation of both KaiB and KaiC was dramatically reduced in the absence of SasA. KaiA accumulation was somewhat lower in the *sasA*-disruptant (~70% of wild-type level), although to a lesser degree than that of KaiB and KaiC. These data are again consistent with our bioluminescence and Northern blot analyses.

Expression of *sasA* and Formation of SasA:KaiC Complex in *Synechococcus*

We monitored *sasA* expression patterns by inserting a promoterless *luxAB* gene set immediately downstream of the gene. As expected from evidence for global circadian control of gene expression (Liu et al., 1995), *sasA* promoter activity showed a circadian rhythm with period and phase angle similar to those of *kaiA* and *kaiBC*, while its amplitude was relatively low (Figure 4C). In correlation with the low amplitude expression rhythm, SasA protein appeared to accumulate constitutively throughout the day (Figure 4B and data not shown). As is the case for other clock-controlled genes in *Synechococcus*, the *kai* genes were required for rhythmic *sasA* gene expression (data not shown). However, disruption of the *kai* genes did not affect the magnitude of the *sasA* promoter activity (data not shown) nor SasA abundance (Figure 4B).

Because the KaiC-interacting portion of SasA is similar to KaiB, the two proteins may compete for binding to KaiC, and their relative ratios or affinities at different times of day could be important for their clock-related functions. To test whether KaiC and SasA/KaiB can be found in the same protein complex in vivo, we performed coimmunoprecipitation assays. *Synechococcus* lysates prepared from wild-type and *kaiABC*-deficient strains were separately immunoprecipitated with anti-KaiC antiserum, and the immunoprecipitated materials were blotted and probed with either anti-SasA or anti-KaiB antiserum. The results indicated that SasA and KaiC constitutively form a complex regardless of circadian time (Figure 4B and data not shown). In contrast, KaiC:KaiB complex is apparently more abundant at CT 16 than at CT 4 (Figure 4B).

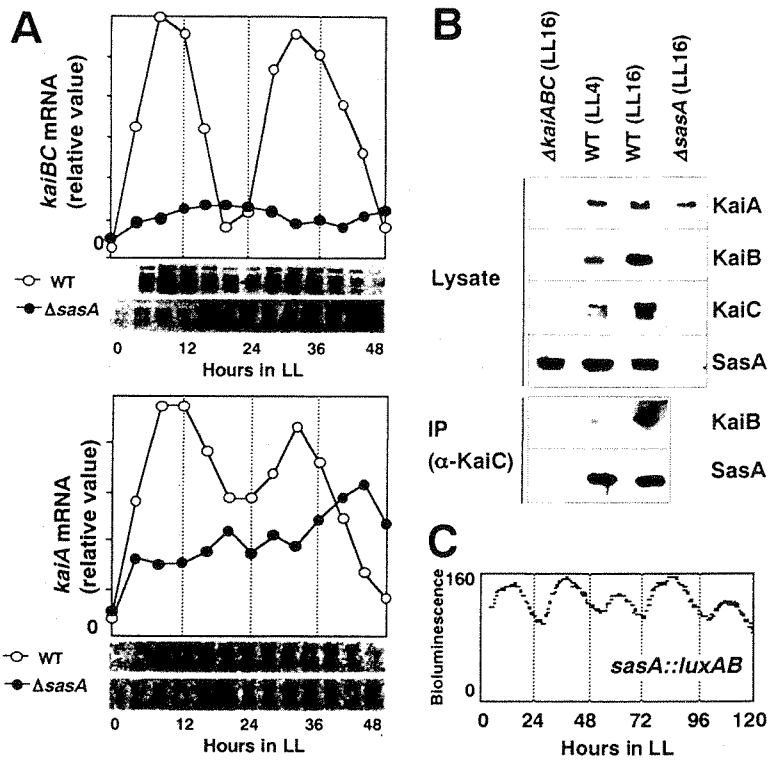

Figure 4. Expression of *kaiABC* and *sasA* Gene Products and SasA:KaiC Complex Formation

(A) Northern blot analysis. *kaiA* and *kaiBC* mRNA levels were examined in wild-type and *sasA*-disrupted strains at 4 hr intervals during hours 0–48 in LL (80 μE m^{-2} s^{-1}). Densitometric data of the blot are also shown. Multiple bands are due to both mRNA degradation and separation caused by the presence of rRNA. Abundance of *kai* mRNA was normalized for total RNA loading by using the signal of rRNA detected with ethidium bromide.

(B) Western blot analysis and coimmunoprecipitation assay. Accumulation levels of KaiA, KaiB, KaiC, and SasA were examined. Cells were collected at hours 4 and 16 in LL. Proteins (10 μg) were prepared from cells of wild-type, *kaiABC*-deficient, and *sasA*-disrupted strains, subjected to SDS-PAGE on 10% gels, and then analyzed by immunoblotting using each anti-Kai antiserum (upper four panels). The protein extracts were also used for immunoprecipitation (IP) with anti-KaiC IgG as a primary antiserum. Immune complexes were resolved and analyzed by Western blotting with anti-KaiB or anti-SasA antiserum.

(C) Low amplitude rhythm of *sasA* gene expression in LL, monitored by a bioluminescence reporter inserted just downstream of the *sasA* gene in the chromosome. Bioluminescence was monitored as described in Figure 2.

Effects of *sasA* Overexpression on *kai* Gene Expression

We also determined the effects of both constitutive and temporal overexpression of the *sasA* gene by placing its transcription under control of the IPTG (isopropyl β-thiogalactoside)–inducible *trc* promoter. The effects of overexpression were assayed in a P_{kaiBC} reporter strain (Figure 5A). Sustained overexpression of *sasA* was induced at hour 24 in LL (see Experimental Procedures). After one cycle, *kaiBC* expression became arrythmic with low bioluminescence levels (Figure 5A). Note that the subsequent circadian cycle after IPTG treatment was somewhat phase advanced relative to the uninduced control cycle. Loss of P_{kaiBC} activity after the subsequent cycle suggests that SasA has some role in negative regulation of *kai* gene expression as well as positive control of it (see Discussion).

In addition, we examined the effect of temporal overexpression of *sasA* on the phase angle of the expression rhythm from P_{kaiBC} by 6 hr administration of IPTG (Figures 5B and 5C). Transient elevation of *sasA* expression delayed oscillation when native *kaiBC* mRNA levels were increasing (from midsubjective day to midsubjective night, hours 24 to 30 and 30 to 36 in LL) and advanced the oscillation when these levels were decreasing (from midsubjective night to midsubjective day, hours 36 to 42). Based on Western blot analysis, our 6 hr administration of IPTG during hours 30 to 46 increased SasA protein levels 4- to 5-fold over endogenous levels (data not shown). This significant phase shifting by increased levels of SasA further suggests a close association of this protein with normal circadian clock function (see Discussion).

Growth of *sasA*-Disrupted Cells under Light/Dark Cycles

Inactivation of *sasA* did not affect the growth rate of *Synechococcus* under various LL conditions (light fluences of 6, 30, and 60 μE m^{-2} s^{-1} on agar plates) (Nagaya et al., 1993) (Figure 6A). However, we found that a *sasA*-disrupted strain grows much slower than the wild-type or a *kaiABC*-deficient strain under LD cycles (periodic alteration of 12 hr light and 12 hr darkness, 12L12D) of various light fluences (6, 30, or 60 μE m^{-2} s^{-1}). In addition, the *sasA*-disrupted strain in 12L12D (60 μE m^{-2} s^{-1}) appears to form colonies slower than it does in dim LL (6 μE m^{-2} s^{-1}), whereas wild-type cells grew faster in 12L12D (60 μE m^{-2} s^{-1}) than in dim LL. Thus, slower growth under LD cycles in the absence of SasA reflects a defect in adapting to light/dark transitions rather than by a simple difference in the quantity of light irradiation each day. Cells lacking both the *sphS* and *sphR* genes grew at similar rates to the wild-type strain in both LL and LD (Figure 6B). In addition, the *sasA*-deficient cells grew normally in LL at 6 or 60 μE m^{-2} s^{-1} under a temperature cycling regime (12 hr at 37°C and 12 hr at 30°C or 12 hr at 30°C and 12 hr at 25°C) (Figure 6B and data not shown). These results suggest a role for SasA in adapting the cell's metabolism specifically to natural light and dark transitions rather than in setting the circadian clock.

It should be noted that the abnormal circadian phenotypes observed in *sasA*-inactivated strains (Figures 2–4) cannot be attributed simply to a growth abnormality. This follows from two observations. First, the slow growth phenotype was not observed in the *sasA* null strains under LL conditions after the single 12 hr dark

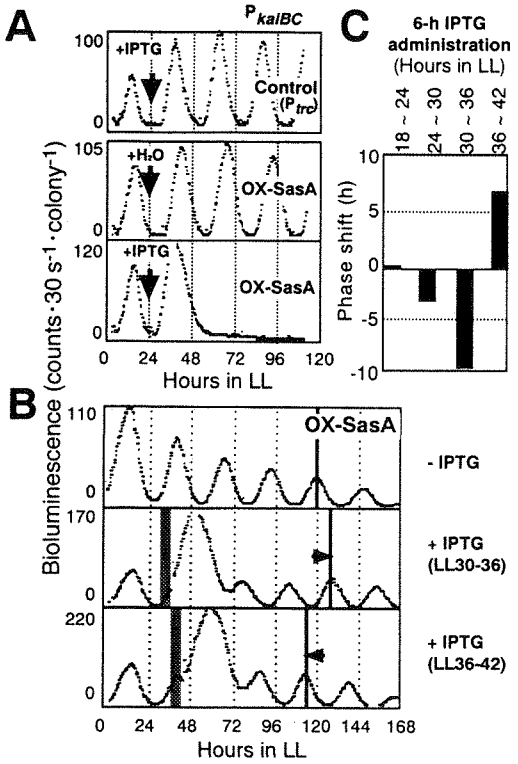

Figure 5. Overexpression of *sasA* Affects Circadian Rhythms

(A) Continuous overexpression of *sasA* disrupts circadian rhythms. Bioluminescence from a P_{kaiBC} reporter strain carrying a P_{trc} vector only or a P_{trc}::*sasA* construct (for overexpression of SasA) was monitored. Cells were grown on agar plates in LL, exposed to darkness for 12 hr to synchronize their clocks, returned to LL (50 μE m^{-2} s^{-1}) and treated with 2 mM IPTG or water at hour 24 in LL after the dark exposure (the arrows indicate the timing of addition of IPTG or water). Monitoring of bioluminescence and representation of data were the same as described in Figure 2.

(B and C) Transient (6 hr) SasA induction changes the phase of the circadian clock in a phase-dependent manner. Bioluminescence from P_{kaiBC}-reporter strains carrying the P_{trc}::*sasA* construct was monitored. Cells were grown and treated with IPTG within indicated duration (gray zone). Phase responses to *sasA* overexpression administrated at four distinct circadian times are indicated.

period used to entrain the clock (data not shown). In addition, expression levels from P_{kaiBC} were greatly reduced in the *sasA* inactivated strains even in the absence of any light to dark cues (Figure 6B).

Discussion

We have identified and characterized the *sasA* gene as encoding a salient function within the *Synechococcus* circadian timing mechanism. Although *sasA* was originally isolated from *Synechococcus* via heterologous complementation of two-component-type histidine protein kinase function in *E. coli* (using *envZ* or *phoR/creC* backgrounds, see Nagaya et al., 1993), its physiological functions were unknown. We have revealed functions of SasA which include: (1) physical interaction with the circadian clock protein KaiC through a KaiB-like region, (2) maintenance of robust circadian oscillation of gene expression under continuous light conditions, (3) enhancement of *kaiBC* expression, and (4) adaptation of growth to LD cycles. This is the first report of a two-component system signaling molecule that is intimately involved in circadian timing.

SasA as a Circadian Amplifier for Robust Rhythmicity

We conclude that SasA is necessary to maintain robust circadian oscillations in *Synechococcus*. This may arise through enhancement of transcription of the *kaiBC* genes, suggested to be a "state variable" of the cyanobacterial oscillator (Ishiura et al., 1998). The following data from our *sasA* null strains support this initial conclusion: (1) both promoter activities and *kai* mRNA levels, especially those from the *kaiBC* operon, were greatly reduced; (2) the average levels of expression of genes other than *kaiBC* were much less affected; (3) accumulation levels of the KaiB and KaiC proteins were reduced, whereas that of KaiA was less affected; (4) the amplitude and period of the circadian expression of all clock-controlled genes tested were evidently altered—in some cases, expression patterns were completely arhythmic.

It is important to note that the *sasA*-disrupted strain did not completely lose rhythmicity, whereas rhythmicity is completely abolished by disruption of any *kai* gene (Ishiura et al., 1998). However, the rhythms in the *sasA* null strain appear too weak to function as a global, temporal coordinator of cellular metabolism. Also, in spite of severe reduction of *kaiBC* expression (less than 10% of wild-type levels) by *sasA* disruption, the period of the residual rhythm was shortened but surprisingly still in a circadian range. Therefore, SasA is not an essential component of the basic timing loop, but evidently a close associate of the oscillator to amplify it to be sufficient as a robust temporal coordinator.

Continuous overexpression of *sasA* completely suppressed the *kaiBC* promoter (Figure 5A), and temporary elevation of SasA advanced or delayed the phase of the *kaiBC* expression rhythm in a phase-dependent manner (Figure 5B). Interestingly, the overexpression of *sasA* allowed one additional, robust *kaiBC* expression cycle before strong suppression of P_{kaiBC} activity. In contrast, *kaiC* overexpression immediately represses *kaiBC* expression (Ishiura et al., 1998). Phase shifting patterns after pulsed *sasA* overexpression were also different from those created by *kaiC* temporal overexpression. These results not only support a close association between SasA function and the central oscillatory mechanism, but also provide both functional differences between SasA and KaiC (Figure 7A and see below).

KaiC Interacts with the Sensor Domain of SasA

The sensory histidine kinase and the response regulator are two families of phosphorylation-based signal transduction proteins that constitute the two-component regulatory system (Stock et al., 1989; Parkinson, 1993). In sensory kinases, the amino-terminal portion of the protein is thought to be a signal input domain. As demonstrated above (Figure 1), only the amino-terminal, 97 amino acyl residues of SasA are necessary for its interactions with KaiC. Moreover, we confirmed that disruption of His 162 of SasA, presumably an essential residue for histidine kinase function, abolished SasA's function in circadian gene regulation (Figure 2C). Thus, it is plausible that binding to KaiC changes enzymatic activity of

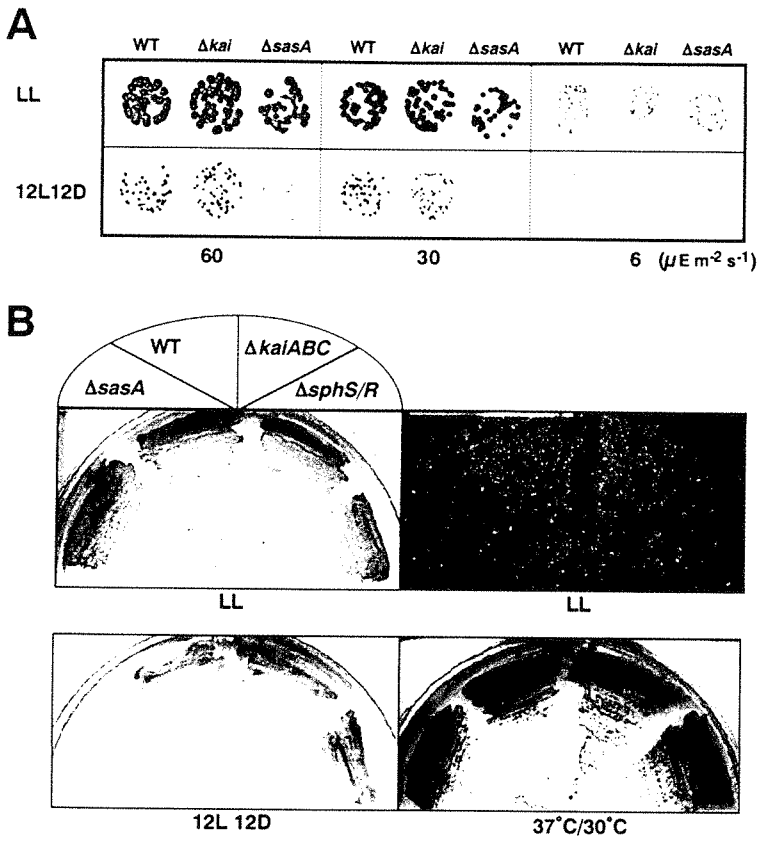

Figure 6. Slow Growth Phenotype in the Absence of *sasA* in LD but Not in LL or Temperature Cycle Conditions

(A) Colonies of wild-type, *kaiABC*-deficient or *sasA*-disrupted strains were allowed to form on solid media for 10 days under continuous illumination (LL) or 12 hr light/12 hr dark (12L 12D) conditions at the indicated light intensity.

(B) Growth phenotypes of wild type and strains lacking *sasA*, *kaiABC*, or *sphSR* on agar plates grown under LL (50 μE m^{-2} s^{-1}) and 12L (50 μE m^{-2} s^{-1}) 12D at 30°C, or LL (50 μE m^{-2} s^{-1}) with 12 hr 30°C/12 hr 37°C cycles. These strains carried a P_{kaiBC}::*luxAB* reporter. Bioluminescence image of the cells grown in LL was captured by a cooled CCD camera (upper right panel).

SasA and thereby mediates a clock-controlled, phosphoryl relay system (see below).

Regardless of the evolutionary relationships among the circadian timing mechanisms in prokaryotes and eukaryotes, it seems evident that "clocks" have recruited similar regulatory mechanisms to exhibit their control of cellular activities (Dunlap, 1999). Note that an open reading frame (ORF sll0750) that encodes a protein similar to SasA and structural homologs of *kaiABC* genes are present in the genome of *Synechocystis* sp. strain PCC 6803 (Mizuno et al., 1996), in which we have found circadian rhythms (Aoki et al., 1995). These cyanobacterial circadian-timing systems will provide an instructive evolutionary contrast to the fungal, insect, and mammalian systems (reviewed by Dunlap, 1999). It is also possible that identification of SasA will uncover phylogenic "missing-links" of circadian systems between prokaryotes and eukaryotes. Recent studies have revealed many proteins belonging to the two-component regulatory families in diverse eukaryotic species including yeast, *Neurospora*, *Dictyostelium*, and higher plants (reviewed by Wurgler-Murphy and Saito, 1997).

Implications of Similarity between SasA and KaiB

It is intriguing that the presumed input domain of SasA and KaiB share similar amino acid sequence. Moreover, SasA and KaiB exhibit similar protein-binding profiles in yeast or in vitro: (1) binding to KaiC, (2) lesser interaction with KaiA, and (3) homotypic interaction (Figure 1) (Iwasaki et al., 1999). Surprisingly, KaiB and SasA do not bind to each other in our assays.

Previous studies identified two mutations in the *kaiB* gene that cause a period shortening of approximately 3 hr in the expression rhythm from a *kaiBC* promoter (Ishiura et al., 1998). Recall that inactivation of *sasA* also reduces the period of this rhythm to a similar extent (Figure 2). Interestingly, both *kaiB* mutations result in amino acid changes (L11F, a leucine to phenylalanine change at residue 11, and R76W, an arginine to tryptophan substitution at residue 76) at positions that are identical in our sequence alignment of these proteins (L19 and R80, respectively, in SasA) (Figure 1A). These similarities suggest commensurate or overlapping function for SasA and KaiB in the circadian clock mechanism. It is likely that their mutual interactions with KaiC results in this functional overlap. KaiC and SasA form a complex constitutively in vivo, whereas KaiC-KaiB complex is more prevalent at CT 16 than at CT 4. KaiB and SasA may have similar affinities for KaiC, hence, the ratio of KaiB-KaiC complex and SasA-KaiC complex may simply reflect the relative abundance of KaiB and SasA (Figure 4B). It is possible that KaiB additionally binds to a KaiC molecule in the KaiC-SasA complex to form a larger multimer when KaiB levels are high at CT 16 (Figure 7A, right).

Function of SasA:KaiC Complex

How does SasA modulate *kaiBC* gene expression? In general, sensory kinases function by autophosphorylation and phospho-transfer activities at the beginning of a phosphoryl-relay system that terminates by modifying

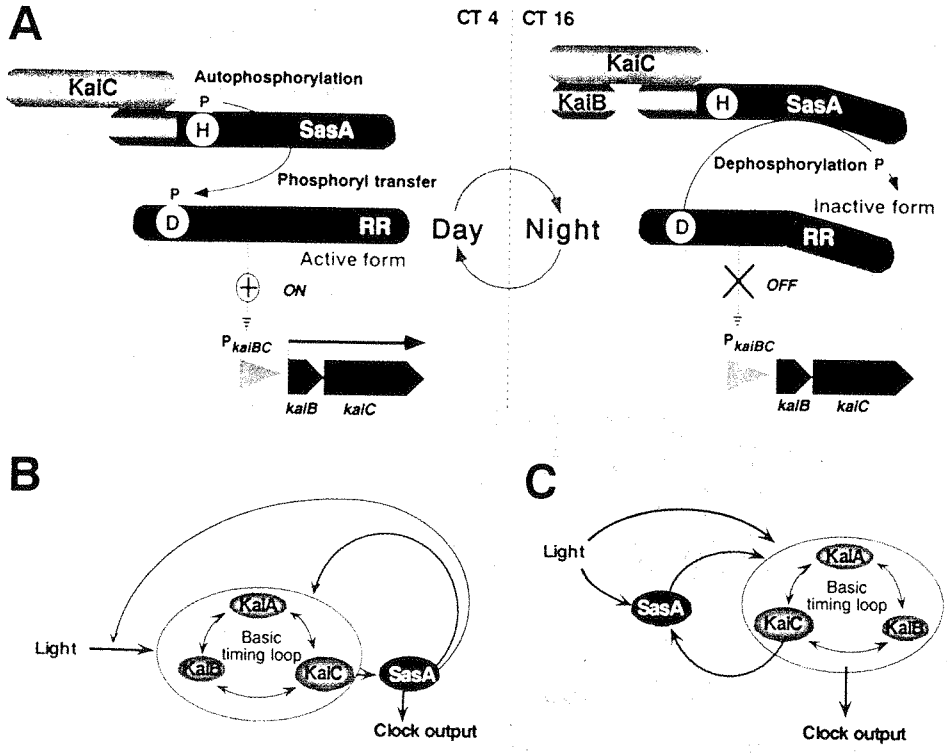

Figure 7. Possible Models for SasA Function in the Circadian System

(A) A model for function of the SasA:KaiC complex in *kaiBC* expression. In the early morning, when total KaiC abundance is low, SasA may bind with KaiC, stimulating autophosphorylation to activate its cognate response regulator (RR) through phosphoryl transfer from His (H) to Asp (D). Activated RR directly or indirectly activates expression of *kaiBC* genes from P_{kaiBC} (left). As the KaiBC concentration gets higher in the evening, KaiC:SasA complex is additionally bound with KaiC or KaiB to form a larger complex(es), which reduces SasA autophosphorylation. Hence, SasA may then act as a phosphoryl protein phosphatase, inhibiting RR-mediated stimulation of P_{kaiBC} activity (right).

(B and C) SasA may function as the first output of the clock to regulate downstream clock-controlled processes (B) or as an element of redundant input pathways (C). In both models, SasA and clock protein KaiC form an outer feedback loop (red arrows) to amplify the KaiABC-based basic timing process (gray circle) by modulating the *kai* gene expression as depicted in (A). In model (B), KaiC:SasA complex controls its cognate response regulator and thereby directly controls downstream gene expression. In model (C), SasA controls robustness of the circadian oscillation in a light-dependent manner, although SasA is not essential to entrain the clock. SasA may sense light signals directly or indirectly, and binding of SasA to KaiC would alter SasA's enzymatic activity. See Discussion for more detail.

function of a DNA-binding, transcription-regulating, response regulator. Thus, SasA-mediated phosphoryl relay would, by necessity, include at least one additional component—the SasA cognate response regulator. Considering the negative effects of *sasA* gene inactivation on expression levels from the *kaiBC* promoter (Figures 2 and 4), this response regulator may function to activate *kaiBC* gene transcription. The role for this postulated response regulator in the *Synechococcus* circadian oscillator would thus be comparable to those described for PAS-containing transcription factors, the dClock/Cycle (dBmal1) and CLOCK /BMAL1 proteins in *Drosophila* and mammals, and the WC-1 and WC-2 proteins in *Neurospora* (reviewed in Dunlap, 1999). Most histidine protein kinases like SasA have both kinase and phosphoryl-protein phosphatase activities with respect to their cognate regulatory proteins (Pratt and Silhavy, 1995). In the absence of the phosphatase activity, such as in a *sasA* null strain, low levels of phosphorylated (activated) response regulator can accumulate via nonspecific kinase activities (Kim et al., 1996). This nonspecific response regulator activation could account for the residual rhythmicity seen in *sasA* null strains (Figures 2 and 3).

Based on these considerations and data described in this paper, we propose a model for SasA-mediated modulation of the *kaiBC* expression (Figure 7A). In this model, both SasA and KaiC can be positive and negative elements in feedback control of *kai* gene expression. During subjective day, total KaiC level is relatively low, but considerable amounts of KaiC:SasA complex exist in the cell (Figure 4B). This complex functions as a positive element, possibly through stimulating SasA autophosphorylation, and thereby activating a SasA-coupled response regulator that directly or indirectly enhances *kaiBC* expression (Figure 7A, left). A positive function of KaiC for *kaiBC* expression has been suggested by our previous observation that P_{kaiBC} activity is somewhat downregulated in an arhythmic mutant mapped on *kaiC* (Ishiura et al., 1998).

By contrast, SasA may inactivate its cognate response regulator with its phosphoryl-protein phosphatase activity when SasA does not bind to KaiC or when KaiB (or/and KaiC itself) additionally binds the SasA:KaiC complex. During subjective night such KaiB:KaiC:SasA (Figure 7A, right) or/and multimerized KaiC:SasA complexes can be formed to negatively regulate *kaiBC* expression. It is still possible that KaiB could compete with SasA

for binding KaiC to release free SasA molecules functioning as negative elements, although we failed to detect reduction in the SasA:KaiC complex level at CT 4 in our experimental condition (Figure 4B).

Our model accounts for the additional expression cycle followed by loss of *kaiBC* expression when *sasA* is continuously overexpressed. Within several hours after IPTG administration at CT 0, when the KaiC level is not very high, the SasA level gradually increases and forms a complex with KaiC to enhance *kaiBC* expression. About 10 hr after induction, in turn, abnormally highly accumulating KaiC-uncoupled SasA gradually inactivates *kaiBC* expression to close one cycle and further abolishes recovery of its activation.

SasA Function in Cyanobacterial Circadian Organization

In theory, circadian organization can be divided into three major constituents: input pathways, the central oscillator, and output pathways. The oscillator generates fundamental circadian timing. Input pathways mediate environmental stimuli to synchronize the oscillator with environmental cycles. The oscillator is coupled to clock-controlled processes through output pathways. Based on our observations presented here, two alternative possibilities for the function of SasA in the cyanobacterial circadian organization can be assigned (Figures 7B and 7C).

The first possibility is that SasA functions as the first output from the circadian timing mechanism, and thus transmits timing signals to all clock-controlled processes (Figure 7B). This regulation includes feedback upon *kai* gene expression, upon light sensitivity of the oscillator, and also, necessarily, upon gene expression responsible for metabolic adaptation to natural growth conditions, which include light to dark transitions (see below).

An alternative possibility is that SasA modulates a photic input pathway(s) into the oscillator to act as a circadian amplifier (Figure 7C). Because the attenuated clock in the *sasA*-inactivated strain is still entrainable to both 12 hr darkness and 12 hr temperature shifts (Figure 2), SasA is not essential to entrain the clock. Nonetheless, SasA may function in one of several potential photic-input pathways because the amplitude of the circadian oscillation in a *sasA* mutant is more sensitive to light fluence than a wild-type strain (Figures 2A and 2B). This model postulates that SasA senses light signals either directly or indirectly, and that binding of SasA to KaiC would alter its sensitivity to further regulate SasA's enzymatic activity. Both models reflect both light-regulated *kaiBC* expression and a feedback control of the *kai*-based oscillator to its input. More importantly, as depicted in Figures 7B and 7C, SasA-KaiC interaction amplifies a KaiABC-based fundamental timing process (gray circle) by forming an outer feedback loop that modulates *kai* gene expression (red arrows and Figure 7A).

SasA as an Adaptive Sensory Kinase for Light/Dark Cycles

Growth is severely suppressed in a *sasA*-disrupted strain only under LD cycles (Figure 6). Microscopic observation did not reveal any morphological difference in cell shape and cell size between the *sasA* null and wild-type strains grown in LD conditions (data not shown). These results suggest that *sasA* is important for normal growth under natural diurnal conditions. The cause of slower LD growth in the absence of SasA could be perturbation of general metabolism in the dark. Alternatively, *sasA* mutant cells may be very sensitive to stress caused by abrupt light/dark transitions. Because *kaiABC*-deficient cells grow as well as wild-type cells in 12L12D, the effect of *sasA* disruption on circadian function alone is not likely to explain the maladaption to diurnal growth. However, it is still possible that the function of SasA in adaptation to LD transitions is regulated by the circadian clock through the SasA–KaiC interaction. In either case, SasA may allow *Synechococcus* to adapt to day–night alternation by maintenance of robust circadian rhythms and by directly adjusting metabolism to LD transitions.

Experimental Procedures

Bacterial and Yeast Strains

Saccharomyces cerevisiae strain L40 was used for the two-hybrid analysis (Vojtek et al., 1993). As hosts for transgenic analyses of *sasA*, we used wild-type *Synechococcus* reporter strains CR1 (P_{psbAI}::*luxAB* strain) (Kutsuna et al., 1998), NUC35, and NUC39 (P_{kaiA}::*luxAB* and P_{kaiBC}::*luxAB* strains carrying a chloramphenicol-resistance gene as a selective marker gene at a specific targeting site called NSI). NUC38 (Iwasaki et al., 1999) was used as a *kaiABC*-deficient P_{kaiBC} reporter strain. The *sphS/sphR*-deficient reporter strain was generated by transformation of NUC39 with pHAI140 (Aiba et al., 1993). *Synechococcus* was cultured in modified BG-11 medium (BG-11M) (Bustos and Golden, 1991).

Library Construction

Synechococcus genomic DNA was prepared from NUC39, partially digested with DNaseI (50 mM $MnCl_2$), and the resulting DNA fragments were repaired with T4 DNA polymerase and Klenow polymerase, and size-fractionated. Five-tenths to three kb fragments were ligated with NotI linkers and cloned into the NotI site of pVP16 (Vojtek et al., 1993). The resulting ligation products were transformed by electroporation into *E. coli* DH10B. Plasmid DNA was prepared from 1×10^6 transformant colonies. Approximately 70% of the clones were estimated to be recombinant, and inserts ranged from 0.3 to 2 kb.

Two-Hybrid Screening

The yeast strain L40 expressing LexA-KaiC (Iwasaki et al., 1999) was transformed with the *Synechococcus* genomic DNA library as described (Gietz et al., 1992). Approximately 5×10^6 transformants were screened for activation of the *HIS3* reporter gene (30°C for 3 days). Five of twenty-two of His^+ clones exhibited strong β-galactosidase activity. Library plasmids were then recovered from these clones and reintroduced into appropriate yeast reporter strains to verify a plasmid-linked, KaiC-dependent, His^+ $LacZ^+$ phenotype.

In Vitro Binding Assay

GST fused to either full-length SasA or N-terminal SasA fragments at the N terminus was produced by induction of derivatives of the pGEX-3X vector (Pharmacia) with 1 mM IPTG in an *E. coli* DH5α background. The resulting inclusion bodies were purified as described (Aiba et al., 1989), lysed with 1× PBS containing 6 M urea, and collected by centrifugation. The supernatant was dialyzed with 1× PBS containing 2 M urea and then with 1× PBS for 20 hr each. Then, fusion proteins were purified with and immobilized on glutathione Sepharose 4B (Pharmacia) as described (Iwasaki et al., 1999). ^{35}S-labeled KaiA, KaiC, CI, or CII was synthesized in vitro and interaction assays were performed as described previously (Iwasaki et al., 1999).

Disruption of the *sasA* Gene

One plasmid for disruption of *sasA*, pDsasA, carries three DNA segments in succession: a 2.1 kb DNA fragment carrying the upstream region of *sasA* (nucleotides [nt] 2 to 2099 relative to the left BamHI site of the 4.8 kb BamHI-KpnI segment from plasmid pCS33 [Nagaya et al., 1993] [A gift from Dr. H. Aiba]), a 1.5 kb HpaI fragment from plasmid pCKm carrying a kanamycin resistance gene (M. I., unpublished data); and the 1.8 kb SmaI-KpnI segment from pCS33. This 5.4 kb fragment was cloned into pBluescript KSII (Stratagene) to complete pDsasA. An additional disruption plasmid, pAM2076, was constructed by cloning the 4.8 kb BamHI-KpnI fragment from plasmid pCS33 into plasmid pUC19 (Promega) and then inserting a 1.4 kb XmnI-SmaI fragment from pDAH346 (provided by Dr. D. Hodgson) into the SmaI site within *sasA*. The pDAH346 fragment encodes a gentamycin resistance gene derived from pXS1 (Hirsch et al., 1986). *Synechococcus* strains NUC35 and NUC39 were transformed with pDsasA. Strains AMC520 (*psbAII::luxAB*), AMC538 (*rpoD2::luxAB*), AMC551 (*ndhD::luxAB*), AMC589 (*cikA::luxAB*), and AMC617 (*opcA::luxAB*) were transformed with pAM2076. The clones resistant to kanamycin sulfate (33 μg/ml) or gentamycin (2 μg/ml) were checked by Southern blot and PCR to confirm disruption of the *sasA* gene.

H162Q Mutant Strain

A 3.6 kb SacII-KpnI fragment of pCS33 (nt 1284 to 4850) was inserted into pBluescript KSII to construct pBSSA2. Next, the Ω fragment carrying a spectinomycin resistance gene (Prentki and Krisch, 1984) was inserted into the BstBI site of pBSSA2 (corresponding to nt 3491 of pCS33) to create pCsasΩ. Site-directed mutagenesis of pCsasΩ was performed as described (Horton, 1993) and designated pCsasΩHQ. NUC39 was transformed with pCsasΩHQ and selected with spectinomycin (40 μg/ml). Transformant colonies on agar plates were subjected to bioluminescence assay (Kondo and Ishiura, 1994) to screen for reduced bioluminescence clones. Seven low bioluminescent clones were identified from ~2000 transformants, and their *sasA* loci were confirmed for the H162Q mutation.

Northern Hybridization

Cells were grown with aeration in LL of 80 μE s^{-1} m^{-2} at 30°C to maintain an optical density of 0.3 at 730 nm (OD_{730}) using a continuous culturing system. The culture was exposed to 12 hr of darkness to synchronize the circadian clock, and then returned to LL. At 4 hr intervals in LL, cells were harvested, immediately frozen, and stored at −80°C. RNA extraction and Northern hybridization were performed using digoxigenin-labeled *kaiA* and *kaiC* probes as described (Ishiura et al., 1998).

Monitoring *sasA* Gene Expression as Bioluminescence from a Luciferase Reporter

The coding region of *luxAB* gene set from *Vibrio harveyi* (Baldwin et al., 1984) was inserted into the XbaI site of pCsasΩ (corresponding to nt 3398 of pCS33, ~50 bp downstream of the stop codon of *sasA*) to construct pCsas-lux. Then, *Synechococcus* was transformed with pCsas-lux to target *luxAB* just downstream of the *sasA* ORF of the chromosome. Transformant clones were selected with spectinomycin, grown under LL on BG-11M agar plates until colonies were 0.2 mm in diameter, and then assayed for bioluminescence rhythms.

Preparation of Anti-SasA Antiserum

Purified GST-SasA(1–97) was used to immunize rabbits. Antigen specificity of antisera was confirmed by Western blotting using cell extract prepared from NUC39 and pDsasA-transformed NUC39 as described previously (Iwasaki et al., 1999) except anti-SasA antiserum at 1000-fold dilution as a primary probe. The antiserum specifically detects SasA protein with molecular mass of ~45 kDa (Figure 4B).

Immunoprecipitation

Cells were grown with aeration in LL of 30 μE s^{-1} m^{-2} at 30°C to maintain the optical density at 730 nm of 0.2 as described above. After treatment with 12 hr of darkness, cells were returned to LL and harvested. Cyanobacterial cell extracts were prepared as described (Iwasaki et al., 1999). Protein content of each extract was adjusted to 200 μg in 400 μl of extraction buffer and incubated with 25 μl bed volume of AffiGel-Hz beads (BioRad) coupled to purified rabbit anti-KaiC IgG at 4°C for 12 hr. After six washes with 1 ml of extraction buffer, the beads were resuspended in 80 μl of SDS-sample buffer without reducing agent. Proteins were eluted by vortexing gently for 10 min at room temperature. After centrifugation, the supernatant was collected, supplemented with 0.1% 2-mercaptoethanol and 0.1% bromophenol blue, and subjected to SDS-PAGE and immunoblotting. KaiB, KaiC, and SasA were reacted with specific antisera at 1:1000, 1:2000, and 1:1000 dilution, respectively, and detected with the enhanced chemiluminescence (ECL) method (Pharmacia), according to the manufacturer's protocol.

Overexpression of the *sasA* Gene

Nco-BamHI segments carrying a sequence encoding SasA were ligated with NcoI- and BamHI-digested p322P*trc* (Kutsuna et al., 1998) to obtain p322P_{trc}::*sasA*. The smaller BglII fragment from p322P_{trc}::*sasA* was inserted into the BamHI site of the pTS2KC (Kutsuna et al., 1998) to obtain pTS2C-P_{trc}::*sasA*. NUC35 and NUC39 were transformed with each plasmid as described previously (Kutsuna et al., 1998) to harbor the expression construct at a specific genomic targeting site of the chromosome (NSII) (Andersson et al., 2000). Conditions for overexpression were the same as described previously (Ishiura et al., 1998), except that 2 mM IPTG was used for induction.

Bioluminescence Assays

Most bioluminescence rhythms were monitored and processed as described previously (Ishiura et al., 1998), except that we used a higher sensitivity photomultiplier tube (Hamamatsu R329P). For Figure 6B, bioluminescence from streaks of *Synechococcus* on agar plates was analyzed by a cooled CCD camera system as described previously (Kondo and Ishiura, 1994). For the data shown in Figure 3, cultures were grown for 3 to 4 days under standard LL conditions in liquid BG-11M containing the appropriate antibiotic before being transferred to 96-well microtiter plates containing BG-11M agar medium. Eighty wells, 40 for wild type and 40 for *sasA*-disrupted reporter strains, were used on each plate. The cultures were incubated in situ in the microtiter wells for 24 hr in LL before being subjected to a 12 hr dark interval to synchronize the circadian clock. Bioluminescence rhythms were subsequently measured and recorded in LL using a Packard TopCount luminometer as described elsewhere (Katayama et al., 1999; Andersson et al., 2000).

Acknowledgments

We thank C. H. Johnson (Vanderbilt University) for sharing unpublished results, H. Aiba and T. Mizuno (Nagoya University) for the kind gift of pCS33 and pHAI140, H. Min and O. Schmitz for use of the *opcA* and *cikA* reporter strains, respectively, and D. Hodgson (University of Warwick) for pDAH346. We are grateful to members of the Kondo lab for fruitful discussion and advice, especially T. Nishiwaki and J. Tomita for Western blotting, C. Inouye for the continuous culturing system, S. Kutsuna for RNA techniques, and Y. Taniguchi for the two-hybrid screen.

This research was supported by grants from the Japanese Ministry of Education, Science and Culture (11233203, 11440234, 11151213, 11558089, and 11694199), Research for the Future Program of the Japan Society for the Promotion of Science (JSPS, JSPS-RFTF96L00601) and the Mitsubishi Foundation to T. K., by NSF grant MCB9513367 to S. S. G., and by Human Frontier Science Program grants (to both T. K. and S. S. G.). H. I. was supported by JSPS Fellowship 09001527, and S. B. W. by NRSA Fellowship F32 GM19644 from the National Institutes of Health.

Received November 11, 1999; revised March 15, 2000.

References

Aiba, H., Mizuno, T., and Mizushima, S. (1989). Transfer of phosphoryl group between two regulatory proteins involved in osmoregulatory expression of the *ompF* and *ompC* genes in *Escherichia coli*. J. Biol. Chem. *264* 8563–8567.

Aiba, H., Nagaya, M. and Mizuno, T. (1993). Sensor and regulator proteins from the cyanobacterim *Synechococcus* species PCC7942 that belong to the bacterial signal-transduction protein families: implication in the adaptive response to phosphate limitation. Mol. Microbiol. *8*, 81–91.

Altschul, S.F., Gish, W., Miller, W., Myers, E.W., and Lipman, D.J. (1990). Basic local alignment search tool. J. Mol. Biol. *215*, 403–410.

Andersson, C.R., Tsinoremas, N.F., Shelton, J., Lebedeva, N.V., Yarrow, J., Min, H. and Golden, S.S. (2000). Application of bioluminescence to the study of circadian rhythms in cyanobacteria. Methods Enzymol., in press.

Aoki, S., Kondo, T., and Ishiura, M. (1995). Circadian expression of the *dnaK* gene in the cyanobacterium *Synechocystis* sp. strain PCC 6803. J. Bacteriol. *177*, 5606–5611.

Baldwin, T.O., Berends, T., Bunch, T.A., Holzman, T.F., Rausch, S.K. Shamansky, L., Treat, M.L., and Ziegler, M.M. (1984). Cloning of the luciferase structural genes from *Vibrio harveyi* and expression of bioluminescence in Escherichia coli. Biochemistry *23*, 3663–3667.

Bustos, S.A., and Golden, S.S. (1991). Expression of the *psbDII* gene in *Synechococcus* sp. strain PCC 7942 requires sequences downstream of the transcription start site. J. Bacteriol. *173*, 7525–7533.

Dunlap, J.C. (1999). Molecular bases for circadian clocks. Cell *96*, 271–290.

Fields, S., and Song, O. (1989). A novel genetic system to detect protein-protein interactions. Nature *340*, 245–246.

Gietz, D., St. Jean, A., Woods, R.A., and Schiestl, R.H. (1992). Improved methods for high efficiency transformation of intact yeast cells. Nucleic Acid Res. *20*, 1425.

Golden, S.S., Brusslan, J., and Haselkorn, R. (1986). Expression of a family of *psbA* genes encoding a photosystem II polypeptide in the cyanobacterium *Anacystis nidulans* R2. EMBO J. *5*, 2789–2798.

Golden, S.S., Ishiura, M., Johnson, C.H., and Kondo, T. (1997). Cyanobacterial circadian rhythms. Annu. Rev. Plant Physiol. Mol. Biol. *48*, 327–354.

Hirsch, P.R., Wang, C.L. and Woodward, M.J. (1986). Construction of a Tn5 derivative determining resistance to gentamicin and spectinomycin using a fragment cloned from R1033. Gene *48*, 203–209.

Ishiura, M., Kutsuna, K., Aoki, S., Iwasaki, H., Andersson, C.R., Tanabe, A., Golden, S.S., Johnson, C.H., and Kondo, T. (1998). Expression of a gene cluster *kaiABC* as a circadian feedback process in cyanobacteria. Science *281*, 1519–1523.

Iwasaki, H., Taniguchi, Y., Ishiura, M., and Kondo, T. (1999). Physical interactions among circadian clock proteins, KaiA, KaiB and KaiC, in cyanobacteria. EMBO J. *18*, 1137–1145.

Katayama, M., Tsinoremas, N.F., Kondo, T., and Golden, S.S. (1999). *cpmA*, a gene involved in an output pathway of the cyanobacterial circadian system. J. Bacteriol. *181*, 3616–3624.

Kim, S., Wilmes-Riesenberg, M.R., and Wanner, B.L. (1996). Involvement of the sensor kinase EnvZ in the in vivo activation of the responsse-regulator PhoB by acetyl phosphate. Mol. Microbiol. *22*, 135–147.

Kondo, T., and Ishiura, M. (1994). Circadian rhythms of cyanobacteria: monitoring the biological clocks of individual colonies by bioluminescence. J. Bacteriol. *176*, 1881–1885.

Kondo, T., Strayer, C.A., Kulkarni, R.D., Taylor, W., Ishiura, M., Golden, S.S., and Johnson, C.H. (1993). Circadian rhythms in prokaryotes: luciferase as a reporter of circadian gene expression in cyanobacteria. Proc. Natl. Acad. Sci. USA *90*, 5672–5676.

Kondo,T., Tsinoremas, N.F., Golden, S.S., Johnson, C.H., Kutsuna, S., and Ishiura, M. (1994). Circadian clock mutants of cyanobacteria. Science *266*, 1233–1236.

Kutsuna, S., Kondo, T., Aoki, S., and Ishiura, M. (1998). A period-extender gene, *pex*, that extends the period of the circadian clock in the cyanobacterium *Synechococcus* sp. PCC 7942. J. Bacteriol. *180*, 2167–2174.

Liu, Y., Tsinoremas, N.F., Johnson, C.H., Lebedeva, N.V., Golden, S.S., Ishiura, M., and Kondo, T. (1995). Circadian orchestration of gene expression in cyanobacteria. Genes Dev. *9*, 1469–1478.

Mizuno, T., Kaneko, T., and Tabata, S. (1996). Compilation of all genes encoding bacterial two-component signal transducers in the genome of the cyanobacterium, *Synechocystis* sp. strain PCC6803. DNA Res. *3*, 407–414.

Nagaya, M., Aiba, H., and Mizuno, T. (1993). Cloning of a sensory-kinase-encoding gene that belongs to the two-component regulatory family from the cyanobacterium *Synechococcus* sp. strain PCC7942. Gene *131*, 119–124.

Nishiwaki, T., Iwasaki, H., Ishiura, M. and Kondo, T. (2000). Nucleotide binding and autophosphorylation of clock protein KaiC as a circadian timing process of cyanobacteria. Proc. Natl. Acad. Sci. USA *97*, 495–499.

Ouyang, Y., Andersson, C.R., Kondo, T., Golden, S.S., and Johnson, C.H. (1998). Resonating circadian clocks enhance fitness in cyanobacteria. Proc. Natl. Acad. Sci. USA *95*, 8660–8664.

Parkinson, J.S. (1993). Signal transduction schemes of bacteria. Cell *73*, 857–871.

Pratt, L.A. and Silhavy, T.J. (1995). Porin regulon of *Escherichia coli*. In Two-Component Signal Reduction, J. Hoch and T.J. Silhavy, eds. (Washington, DC: ASM Press), pp. 105–127.

Prentki, P., and Krisch, H.M. (1984). In vitro insertional mutagenesis with a selectable DNA fragment. Gene *29*, 303–313.

Scanlan, D.J., Newman, J., Sebaihia, M., Mann, N.H., and Carr, N.G. (1992). Cloning and sequence analysis of the glucose-6-phosphate dehydrogenase gene from the cyanobacterium *Synechococcus* PCC 7942. Plant Mol. Biol. *19*, 877–880.

Stock, J.B., Ninfa, A.D., and Stock, A.M. (1989). Protein phosphorylation and regulation of adaptive response in bacteria. Microbiol. Rev. *53*, 450–490.

Tsinoremas, N.F., Ishiura, M., Kondo, T., Tanaka, K., Takahashi, H., Johnson, C.H., and Golden, S.S. (1996). A sigma factor that modifies the circadian expression of a subset of genes in cyanobacteria. EMBO J. *15*, 2488–2495.

Vojtek, A.B., Hollenberg, S.M., and Cooper, J. (1993). Mammalian Ras interacts directly with the serine/threonine kinase Raf. Cell *74*, 205–214.

Wurgler-Murphy, S.M. and Saito, H. (1997). Two-component signal transducers and MAPK cascades. Trends Biol. Sci. *22*, 172–176.

Xu, Y., Piston, D.W., and Johnson, C.H. (1999). A bioluminescence resonance energy transfer (BRET) system: application to interacting circadian clock proteins. Proc. Natl. Acad. Sci. USA *96*, 151–156.

Nucleotide binding and autophosphorylation of the clock protein KaiC as a circadian timing process of cyanobacteria

Taeko Nishiwaki*†, Hideo Iwasaki*, Masahiro Ishiura*§, and Takao Kondo*§

Divisions of *Biological Science and †Material Science, Graduate School of Science, Nagoya University, Furo-cho, Chikusa-ku, Nagoya 464-8602, Japan

Edited by Robert Haselkorn, University of Chicago, Chicago, IL, and approved November 10, 1999 (received for review August 3, 1999)

A negative feedback control of *kaiC* expression by KaiC protein has been proposed to generate a basic oscillation of the circadian clock in the cyanobacterium *Synechococcus* sp. PCC 7942. KaiC has two P loops or Walker's motif As, that are potential ATP-/GTP-binding motifs and DXXG motifs conserved in various GTP-binding proteins. Herein, we demonstrate that *in vitro* KaiC binds ATP and, with lower affinity, GTP. Point mutation by site-directed mutagenesis of P loop 1 completely nullified the circadian rhythm of *kaiBC* expression and markedly reduced ATP-binding activity. Moreover, KaiC can be autophosphorylated *in vitro*. These results suggest that the nucleotide-binding activity of KaiC plays important roles in the generation of circadian oscillation in cyanobacteria.

Circadian rhythms, biological oscillations with 24-h periodicity, are observed ubiquitously among eukaryotes and cyanobacteria. An endogenous oscillator named the circadian clock temporally regulates various biological activities to match them with daily environmental alterations (1). To elucidate the molecular mechanism of the circadian clock, several clock genes and clock-related genes have been cloned and analyzed in cyanobacteria, *Neurospora*, *Drosophila*, *Arabidopsis*, and mammals (2).

Cyanobacteria are the simplest organisms known to have the circadian clock. An essential clock gene cluster *kaiABC* was cloned from the cyanobacterium *Synechococcus* sp. strain PCC 7942 (3). Various circadian phenotypes can arise from mutations in any of the *kai* genes. In particular, 14 distinct clock mutations including those for period length and arrhythmia were mapped to *kaiC*. Experiments on the promoters of *kai* genes suggest that KaiC suppresses its own (*kaiBC*) expression in a basic negative feedback loop, and KaiA enhances *kaiBC* expression to make the system oscillate (3). Moreover, the KaiA, KaiB, and KaiC proteins directly associate in all possible combinations in the yeast two-hybrid system, *in vitro*, and in cyanobacterial cells, and a long-period allele, *kaiA1*, markedly enhances KaiA–KaiB interaction (4). These observations suggest that physical interactions among the Kai proteins are crucial to the circadian timing mechanism.

Although the biochemical functions of the Kai proteins remain unknown, the amino acid sequence of KaiC contains two ATP-/GTP-binding motifs (P loops or Walker's motif As) whose consensus is GXXXXGKT/S (X represents any amino acid) in the tandem duplicated domains of KaiC (CI and CII domains) (Fig. 1*A*; refs. 3–6). In addition, two DXXG motifs that are highly conserved in the GTPase superfamily (7, 8) are found in the CI domain. These motifs could provide clues to the biochemical function of KaiC in circadian rhythm generation. In this report, we show that KaiC binds ATP and, to a lesser extent, GTP *in vitro*, and disruption of the P loop in the CI domain causes arrhythmia and a marked reduction in ATP-binding activity. Moreover, we have identified autophosphorylation activity of KaiC *in vitro*. These observations strongly suggest that the ATP-binding activity of KaiC is important for the generation of circadian oscillation in *Synechococcus*.

Materials and Methods

Bacterial Strains, Media, Cultures, and Manipulation of DNA. Because the expression of the *kaiBC* operon was assumed to be the key process of the cyanobacteria oscillator (3), we used a reporter strain of *Synechococcus*, NUC39 (4), that carried a bacterial luciferase gene set *luxAB* fused to a promoter of *kaiBC* operon (P_{kaiBC}) at a specific site of the chromosome (neutral site I) as the control strain of this study. The *Synechococcus* cells were grown at 30°C in BG-11 liquid medium or solid medium that contained 1.5% (wt/vol) Bacto Agar (Difco) under continuous light (LL) conditions of 46 μmol $m^{-2}\cdot s^{-1}$ from white fluorescent lamps. Plasmids were introduced into *Escherichia coli* DH10B by electroporation. *Synechococcus* cells were transformed with plasmid DNA by natural transformation and selected with 40 μg/ml of spectinomycin sulfate (9).

Site-Directed Mutagenesis of the *kai* Locus. pCkaiABC targeting vector (3) containing the *kaiABC* cluster and a spectinomycin-resistant gene was mutagenized with the overlap extension method by PCR (10). All of the resulting mutations were confirmed by sequencing with a *Taq* DyeDeoxy terminator cycle sequencing kit (Applied Biosystems). The mutant plasmids were introduced into *kaiABC*-deficient P_{kaiBC} reporter cells (NUC38) as described (4).

***In Vitro* Translation of KaiC and Its Derivatives.** Expression vectors for *in vitro* transcription/translation were generated by inserting a wild-type or mutagenized PCR fragment into the *SalI–BamHI* site of pSP64-poly(A) vector (Promega). The TNT rabbit reticulocyte system (Promega) was used for *in vitro* production and labeling of each KaiC-derived protein as described (4). Briefly, 25 μl of reaction mixture containing 1 μg each of the pSP64-poly(A) derivatives, SP6 RNA polymerase, and 12.5 μl of rabbit reticulocyte was incubated for 2 h at 30°C in the presence of 10 μCi of [^{35}S]methionine (>1,000 Ci/mmol; 1 Ci = 37 GBq). Labeled proteins were confirmed by SDS/10% PAGE and analyzed by autoradiography with a BAS2000 Image Analyzer (Fuji).

Binding of *in Vitro* Translated Proteins to ATP- or GTP-Agarose. An *in vitro* ATP-/GTP-binding assay was performed as described by Iismaa *et al.* (11) with minor modifications. A fraction of the radioactivity (3.0×10^5 cpm) of the *in vitro* translation reaction

This paper was submitted directly (Track II) to the PNAS office.

Abbreviations: CI, tandem duplicated domain of KaiC (N-terminal half); CII, tandem duplicated domain of KaiC (C-terminal half); LL, continuous light; GST, glutathione *S*-transferase.

‡Present address: Center for Gene Research, Nagoya University, Furo-cho, Chikusa-ku, Nagoya 464-8602, Japan.

§To whom reprint requests should be addressed. E-mail: kondo@bio.nagoya-u.ac.jp or ishiura@bio.nagoya-u.ac.jp.

The publication costs of this article were defrayed in part by page charge payment. This article must therefore be hereby marked "*advertisement*" in accordance with 18 U.S.C. §1734 solely to indicate this fact.

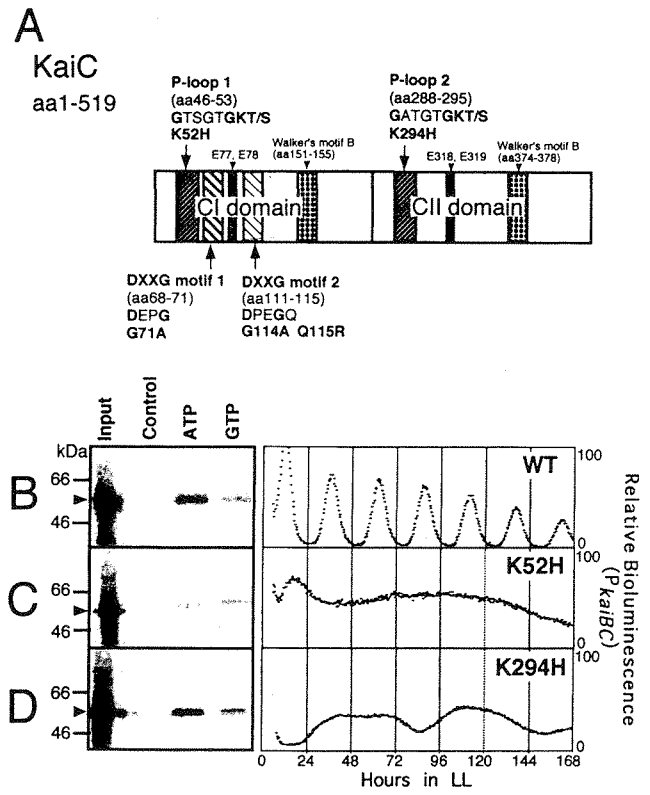

Fig. 1. Effects of point mutations on nucleotide-binding motifs of KaiC and bioluminescence rhythm of P_{kaiBC}. (*A*) Point mutations introduced to nucleotide-binding motifs (P loops and DXXG motifs) of KaiC are illustrated. The amino acid (aa) sequences of these motifs and point mutations are designated by their one-letter codes. Tandem duplicated domains of KaiC, N-terminal and C-terminal halves, are indicated as CI (amino acids 1–250) and CII (amino acids 251–519), respectively. Locations of P loops, DXXG motifs, Walker's motif Bs, and putative catalytic carboxylates are illustrated. Conserved amino acids of each motif are shown in boldface, and X represents any residue. (*B–D*) *In vitro* nucleotide binding assay (*Left*) and bioluminescence profiles for P_{kaiBC} promoter activity (*Right*). ^{35}S-labeled KaiC was incubated with ATP agarose (lane 3), GTP agarose (lane 4), or control agarose (lane 2) resin. Input controls are shown in lane 1. Autoradiograms for ^{35}S-labeled KaiC are shown. Arrowheads indicate the position of the KaiC band (≈57 kDa). For monitoring bioluminescence rhythm, cells were grown to give 30–70 colonies 0.2 mm in diameter under LL conditions. After a 12-h dark treatment, the bioluminescence from each dish was measured with a photomultiplier tube. Bioluminescence intensity per colony was normalized to 100 by the peak value of the first day for wild-type cells (*y* axes). (*B*) Binding to wild-type (WT) KaiC and bioluminescence from wild-type cells. (*C*) Lysine-to-histidine substitution in P loop 1 (K52H). (*D*) Lysine-to-histidine substitution in P loop 2 (K294H).

mixture was diluted to 450 μl with binding buffer [20 mM Tris·HCl, pH 7.0/150 mM NaCl/5 mM $MgCl_2$/0.1% (vol/vol) Triton X-100] and incubated with 50 μl of ATP-agarose or GTP-agarose beads (2.2 μmol/ml; Sigma) at room temperature for 30 min. The beads were pelleted by centrifugation, and the supernatant containing unbound protein was retained. The beads were washed five times with 1 ml of binding buffer to reduce nonspecific protein binding before the subsequent 3-h incubation with the supernatant. Bound protein was eluted by boiling in SDS/PAGE loading buffer and analyzed by SDS/10% PAGE followed by autoradiography.

UV Crosslink Assay. Glutathione *S*-transferase (GST) fused to KaiC, CI, and CII was prepared as described (4). To assess ATP crosslink to KaiC derivative proteins, 1.5 μg each of the fusion proteins was incubated with 0.1 mM [α-^{32}P]ATP (10,000 Ci/mmol) or 0.2 mM [^{35}S]ATPγS (1,000 Ci/mmol) in 20 μl of reaction buffer (100 mM Tris·HCl, pH 7.6/50 mM KCl/5 mM $MgCl_2$/0.4 mM DTT) at 25°C for 30 min. Reactions were terminated by placing the mixture on ice. The mixture was exposed to UV light (Stratalinker 1800, Stratagene) for 40 min at 4°C, and 4 μl of 6× SDS/PAGE loading buffer was added to the mixture. After boiling for 5 min, samples were subjected to SDS/PAGE with 10% gels and autoradiography and then analyzed with the BAS2000 Image Analyzer.

Assay of Bioluminescence Rhythm. *Synechococcus* cells were inoculated onto BG-11 agar plates in a plastic dish (30 mm in diameter) and incubated under LL conditions (46 μmol m^{-2}·s^{-1}) to form 50–100 colonies. Then, cells were subjected to 12 h of darkness to synchronize the circadian clocks, and bioluminescence from the agar plates was automatically monitored under LL in the presence of decanal solution with a photomultiplier-tube-based bioluminescence-monitor system (3).

Protein Phosphorylation Assay. GST and GST fused to KaiA, KaiB, or KaiC were prepared as described (4). An autophosphorylation assay was performed as described by Aiba *et al.* (12) and McCleary and Zusman (13) with some modifications. The protein sample (1.0 μg) was added to 15 μl of a reaction mixture {50 mM Tris·HCl, pH 7.5/100 mM KCl/5 mM $MgCl_2$/0.5 mM EDTA/2 mM DTT/0.1 mM [γ-^{32}P]ATP (10,000 cpm/mmol) or [α-^{32}P]ATP (30,000 cpm/mmol)} at 25°C for 30 min. Reactions were terminated by the addition of 3 μl of 6× SDS/PAGE loading buffer. After heating at 65°C for 5 min, samples were subjected to SDS/PAGE with 10% gels and then blotted onto Immobilon-P membranes (Millipore). The radioactivities of phosphorylated proteins were analyzed with the BAS2000 Image Analyzer.

Chemical Stability Assay of Phospho-Linkage. A chemical stability assay was performed as described by McCleary and Zusman (13) with minor modifications. Equal amounts of GST-KaiC were phosphorylated and blotted onto an Immobilon-P membrane as described above. Individual blots were excised from the membrane and separately incubated in 50 mM Tris·HCl, pH 7.5/3 M NaOH/1 M HCl or 0.8 M hydroxylamine (pH 6.8) at 42°C. After incubation for 1 h, the membranes were washed with distilled water and dried in air, and then the radioactivities were analyzed with the BAS2000 Image Analyzer.

Results

KaiC Binds to ATP and GTP. ^{35}S-labeled KaiC was translated *in vitro* and incubated with ATP-agarose or GTP-agarose. As shown in Fig. 1*B*, radioactive KaiC was detected after incubation with ATP-agarose or GTP-agarose followed by SDS/PAGE (Fig. 1*B*, lanes 3 and 4). The binding of KaiC to ATP was much stronger than that to GTP. No activity was detected after incubation with control agarose resin (Fig. 1*B*, lane 2). In addition, [^{35}S]KaiA associated with neither ATP- nor GTP-agarose (data not shown). These results indicate specific binding of KaiC to ATP and to GTP with lower affinity.

Point Mutations of the P Loops Affect Both ATP-/GTP-Binding of KaiC and Circadian Rhythm. As illustrated in Fig. 1*A*, the first and second P loops (P loop 1 and P loop 2, respectively) were disrupted separately by substitution of the conserved lysine residues with histidine (K52H and K294H, respectively) to examine the effects of these mutations on the ATP-/GTP binding activity of KaiC. Fig. 1*C* shows that the K52H substitution in P loop 1 markedly reduced the ATP-binding activity; however, the P loop 2 mutation (K294H) failed to alter the ATP-binding profile (Fig. 1*D*), and neither mutation altered the GTP-binding activities.

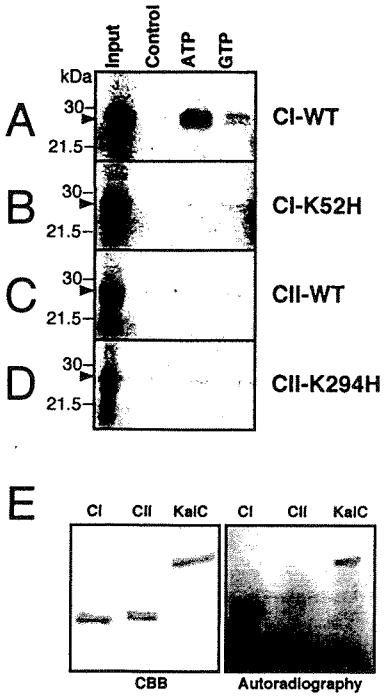

Fig. 2. Nucleotide binding to the CI or CII domain of KaiC. (*A–D*) *In vitro* nucleotide binding to the ^{35}S-labeled CI or CII domain of KaiC was examined. Experimental conditions and the presentation of data were the same as described for Fig. 1 *B–D Left*, except that the ^{35}S-labeled CI or CII domain of KaiC was used instead of full-length KaiC. (*A*) Wild-type (WT) CI domain. (*B*) CI domain containing K52H mutation. (*C*) Wild-type CII domain. (*D*) CII domain containing the K294H mutation. (*E*) UV crosslink assays. Purified GST-KaiC, GST-CI, and GST-CII proteins were visualized by staining with Coomassie brilliant blue (CBB) after SDS/PAGE (*Left*). Each fusion protein was incubated with [α-^{32}P]ATP, crosslinked by UV irradiation, and then analyzed by SDS/PAGE followed by autoradiography (*Right*).

Next, we analyzed the effect of these mutations on the circadian oscillation of *kaiBC* expression. Initially, we constructed a DNA fragment that contained the entire *kai* gene cluster in which the *kaiC* ORF was modified to carry mutations in the nucleotide-binding motifs. Each mutant *kai* cluster was introduced into a *kai*-deficient strain at the original locus. Although the control strain that had regained the normal *kai* cluster had a robust circadian rhythm (Fig. 1*B*), the P loop 1-disrupted transformant (K52H) completely lost the rhythmicity (Fig. 1*C*), suggesting that the lysine residue in P loop 1 was indispensable to the generation of the circadian oscillation. The amino acid substitution at P loop 2 (K294H) resulted in an extremely long-period phenotype ($\approx$70 h; Fig. 1*D*) with lowered amplitude. Neither of these mutations altered the average level of bioluminescence (compare the values of the vertical axes in Fig. 1 *B–D*). Moreover, substitutions of threonine residues with alanine in both P loop 1 and P loop 2 instead of lysine-to-histidine mutations disrupted the rhythm completely (data not shown). These results imply that both P loops are crucial for the circadian clock of cyanobacteria.

ATP Binds Mainly to the CI Domain. Although mutation in either P loop significantly altered the rhythm, binding to ATP was lowered only by the mutation in P loop 1. The contribution of P loop 2 to ATP-binding seemed to be minor. To examine this point, we produced CI and CII domains of KaiC with or without the point mutations by *in vitro* translation. ATP and, to a lesser extent, GTP bound to CI domains (Fig. 2*A*), and the P loop 1 mutation lowered the ATP binding as was the case of full-length

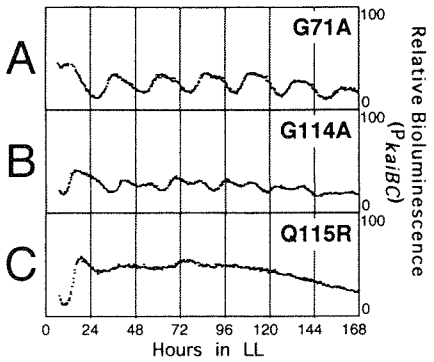

Fig. 3. Effects of point mutations in DXXG motifs on circadian rhythm. Bioluminescence profiles of P_{kaiBC}:*luxAB* reporter strains carrying mutations in each DXXG motif under LL conditions are shown. Measurement of the bioluminescence and representation of data were the same as described for Fig. 1 *B–D Right*. (*A*) Glycine-to-alanine substitution in DXXG motif 1 (G71A). (*B*) Glycine-to-alanine substitution in DXXG motif 2 (G114A). (*C*) Glutamine-to-arginine substitution at position 115.

KaiC (Fig. 2*B*). On the other hand, only a faint signal of ATP-binding was detected for either normal or mutated CII domains (Fig. 2 *C* and *D*). To exclude a possibility that CII is merely inaccessible to agarose-linked ATP, we also performed a UV crosslinking assay to assess the ATP-binding profile of KaiC, CI, and CII fusion proteins. GST fused to KaiC, CI, or CII was incubated with [α-^{32}P]ATP or [^{35}S]ATPγS, and UV crosslinked ATP was analyzed by SDS/PAGE and autoradiography. The results confirmed that ATP bound to KaiC and CI but failed to associate with CII (Fig. 2*E* and data not shown). These results suggest that ATP-binding activity mainly resides on the CI domain and that the P loop 1 is responsible for this activity.

Mutation in DXXG Motifs Affects the Clock. Two DXXG motifs (DXXG1 and DXXG2) in the CI domain were disrupted individually by substitution of the conserved glycine residues with alanine (G71A and G114A). DXXG2 is followed by a glutamine residue (Q115) that is a cognate to the glutamine residue at position 61 in Ras protein. The glutamine of Ras is one of the main sites of oncogenic transformation (14) and is required for GTP hydrolysis (15, 16). Therefore, we also changed the residue Q115 to arginine (Q115R). The G71A mutation in DXXG1 lowered the amplitude and distorted the waveform (Fig. 3*A*). The G114A mutation in DXXG motif 2 extended the period to 27 h and caused a bimodal waveform (Fig. 3*B*). Thus, the circadian oscillation in *kaiBC* expression was modified considerably by these mutations, although periodicity remained in the circadian range. On the other hand, Q115R mutation abolished the circadian rhythm (Fig. 3*C*). None of these mutations affected the average level of *kaiBC* expression. We could not detect any effect of these mutations on nucleotide-binding activities by the method with GTP agarose (data not shown).

Autophosphorylation of KaiC. It is known that some bacterial proteins that contain the P loop and Walker's motif B have autokinase activity (17, 18). To examine the autophosphorylation of KaiC, GST-KaiC (4) was produced in *E. coli*, purified with an affinity resin, and then incubated with [γ-^{32}P]ATP or [α-^{32}P]ATP in the presence of Mg^{2+}. As shown in Fig. 4*A*, GST-KaiC was labeled with ^{32}P after incubation with [γ-^{32}P]ATP but not with [α-^{32}P]ATP. No phosphorylation activity was detected in unfused GST and GST fused to KaiA or KaiB. Therefore, GST-KaiC was specifically autophosphorylated by γ-phosphate.

Based on the stability of the phosphate bond in various ionic

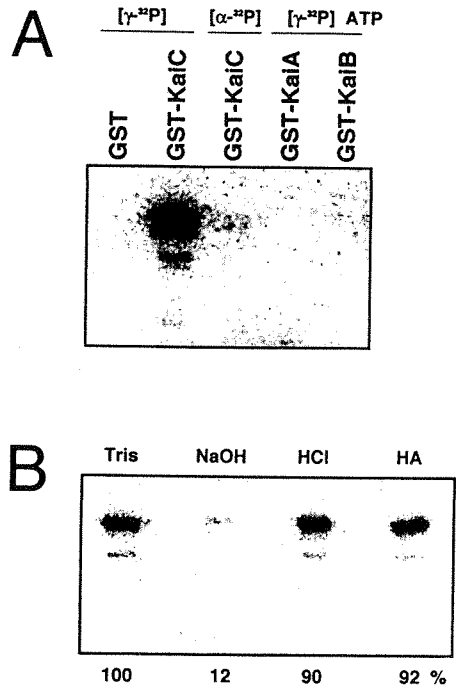

Fig. 4. Autophosphorylation of Kai by ATP and its chemical stability profiles. (*A*) GST fusions of KaiA, KaiB, and KaiC as well as a GST control were incubated with [γ-^{32}P]ATP or [α-^{32}P]ATP in the presence of Mg^{2+}. Proteins were subjected to SDS/PAGE and detected by autoradiography. (*B*) Phosphorylated KaiC separated by electrophoresis was blotted to Immobilon-P membrane. Fractions of the membrane were treated under various ionic conditions and then assayed for binding. Numbers at the bottom are the relative intensity of signal that was normalized with that treated by neutral buffer.

conditions, phosphorylated GST-KaiC was assayed to determine the class of phosphorylated amino acid residue (19). As shown in Fig. 4*B*, 90% or more radioactivity was retained after treatments with HCl and hydroxylamine, whereas base (NaOH) treatment markedly reduced the level to 12% of the control. These results suggest that the phosphate link in phosphorylated GST-KaiC is an *O*-phosphate linkage. Among *O*-phosphate bonds, phosphotyrosine is base stable, whereas phosphoserine and phosphothreonine are base labile (19). Therefore, KaiC was likely to be autophosphorylated at serine or/and threonine residue or residues.

Discussion

Ishiura *et al.* (3) proposed a model of circadian oscillation of cyanobacteria in which negative feedback of the *kaiBC* expression by KaiC and positive regulation by KaiA play key roles. Thus, Kai proteins, especially KaiC, are evidently key components of the circadian oscillator of cyanobacteria (3). In this report, we have presented evidence of the biochemical activity of KaiC. The ATP-binding of KaiC could be essential to generate the circadian oscillation, because a marked decrease in ATP-binding activity caused by the disruption of P loop 1 was strikingly correlated with the complete nullification of circadian rhythms (Fig. 1*B*). Moreover, note that a point mutation of P loop 1 did not alter the average level of bioluminescence from P_{kaiBC} reporter strains. Therefore, a point mutation in P loop 1 likely caused arrhythmicity, not by lowering the average level of *kaiBC* transcription, but by affecting an as-yet unknown biochemical function or functions of KaiC that are driven by bound ATP.

KaiC is composed of two tandem duplicated domains, CI and CII (4). Our results strongly suggest that ATP bound mainly to the CI domain (Fig. 2) and that P loop 1 was a main active site for ATP-binding of KaiC. This observation also suggests distinct functions of CI and CII domains. This possibility is pertinent to our previous findings that the KaiA–KaiB association was enhanced by the CI but not the CII domain (4). However, note also that substitution of the lysine residue of P loop 2 with histidine extremely extended the period of the rhythms ($\approx$70 h) and of conserved threonine with alanine induced arrhythmicity. Thus, it is evident that this region of P loop 2 is also important for normal rhythmicity. Mutation of P loop 2 might affect some unknown function (e.g., maintaining a functional configuration of KaiC) and have a large effect on the circadian oscillator; however, it is still possible that P loop 2 is also a functional ATP-binding motif but that its ATP/GTP-binding affinity is below the detection limit of the current assay.

The GTP-binding activity detected in this study was much weaker than the ATP-binding activity and was not altered by point mutations in the P loops and DXXG motifs (Fig. 1 *B–D Left*; Fig. 2; data not shown). Mutations of invariant glycine to alanine in GXXG motifs 1 and 2 altered the circadian rhythm phenotype; however, rhythmicity still remained obvious, and the period length was in the circadian range (Fig. 3). Moreover, KaiC contained P loops and DXXG motifs but not NXKD and (C/S)AX motifs that are conserved in many GTP-binding proteins (7, 8). Thus, the GTP binding to KaiC seems not to be essential to the timing mechanism of the circadian oscillator. However, because a substitution of Q115, which is cognate to Q61 of Ras (7, 8), with arginine resulted in complete arrhythmia (Fig. 3*C*), it is still possible that GTP hydrolysis by this residue is responsible for the generation of circadian rhythm, as is the case for signal transduction by Ras (15, 16).

Yoshida and Amano (20) revealed a consistency in topologies of ATPases whose crystal structures had already been solved, such as F1-ATPase and RecA. These investigators identified catalytic carboxylate 24 $\pm$ 2 residues from the lysine residue of P loop and Walker's motif B 50–130 residues from the C-terminal side of the P loop (20). In the case of KaiC, the distances between P loops and Walker's motif Bs in CI and CII domains are 87 and 78 residues, respectively, and two continuous glutamate residues are located 25 and 24 residues from the lysine residues of P loops in CI and CII domains, respectively (Fig. 1*A*; ref. 3). Therefore, it is likely that the topology of the CI and CII domains of KaiC are similar to that of the ATPases.

In this study, we have identified *O*-autokinase activity of KaiC at the serine and/or threonine residue or residues in KaiC (Fig. 3). *O*-phosphorylation has been widely found in eukaryotes and prokaryotes including cyanobacteria (21–26). However, to the best of our knowledge, ours is the first report of *O*-autophosphorylation in cyanobacteria. Conserved sequences were found among various *O*-kinases, but such sequences are not found in KaiC (3). It was reported recently that several proteins that contain a P loop have autokinase activities. Point mutations in P loop and Walker's motif B of Ptk protein of *Acinetobacter johnsonii* decreased ATP binding and autophosphorylation activity (17). EpsE protein of *Vibrio cholerae* decreased the autokinase activity by a point mutation in the P loop (18). Therefore, it is possible that KaiC also uses P loops in autophosphorylation.

In various clock models, phosphorylation of clock proteins is considered to be an important part of the circadian timing loop (2). In *Drosophila*, phosphorylation of Period (PER) controls the initial rate of PER accumulation and seems necessary for PER cycling. Double-time (Dbt), a *Drosophila* homolog of casein kinase Iε, was revealed to phosphorylate PER (27, 28). As is the case for PER, autophosphorylation of KaiC, revealed in this study, could alter the stability of KaiC that regulates negative feedback of *kaiBC* transcription. Alternatively, after autophosphorylation, KaiC might change its conformation to regulate as-yet unknown biochemical activities. Our previous analysis

revealed that KaiC interacted with both KaiA and KaiB (4). Autophosphorylated KaiC may alter affinities between the Kai proteins. Conversely, it is possible that the binding of KaiA and/or KaiB regulates the autophosphorylation activity of KaiC.

We thank Dr. C. H. Johnson (Vanderbilt University) and his colleagues for discussions on our study, Dr. Osamu Yamauchi (Nagoya University) for supporting T.N., and members of the Kondo–Ishiura labs for fruitful discussions and advice. This research was supported by Japanese Ministry of Education, Science, and Culture Grants 11440234, 11694199, 11558089, 11151213, 11233203, and 11304055, by Research for the Future Program of the Japanese Society for the Promotion of Science Grant JSPS-RFTF96L00601, by the Human Frontier Science Program, and by the Mitsubishi Foundation (to T.K. and M.I.). T.N. and H.I. were supported by the Hayashi memorial foundation for female natural scientists and Research Fellowship for Young Scientists 09001527 from the Japanese Society for the Promotion of Science, respectively.

1. Bünning, E. (1973) *The Physiological Clock* (Springer, Heidelberg), 3rd Ed.
2. Dunlap, J. C. (1999) *Cell* **96,** 271–290.
3. Ishiura, M., Kutsuna, S., Aoki, S., Iwasaki, H., Andersson, C. R., Tanabe, A., Golden, S. S., Johnson, C. H. & Kondo, T. (1998) *Science* **281,** 1519–1523.
4. Iwasaki, H., Taniguchi, Y., Ishiura, M. & Kondo, T. (1999) *EMBO J.* **18,** 1137–1145.
5. Walker, J. E., Saraste, M., Runswick, M. J. & Gay, N. J. (1982) *EMBO J.* **1,** 945–951.
6. Saraste, M., Sibbald, P. R. & Wittinghofer, A. (1990) *Trends Biochem. Sci.* **15,** 430–434.
7. Bourne, H. R., Sanders, D. A. & McCormick, F. (1991) *Nature (London)* **349,** 117–127.
8. Kjeldgaard, M., Nyborg, J. & Clark, B. F. C. (1996) *FASEB J.* **10,** 1347–1368.
9. Kutsuna, S., Kondo, T., Aoki, S. & Ishiura, M. (1998) *J. Bacteriol.* **180,** 2167–2174.
10. Noumi, T., Beltran, C., Nelson, H. & Nelson, N. (1991) *Proc. Natl. Acad. Sci. USA* **88,** 1938–1942.
11. Iismaa, S. E., Chung, L., Wu, M.-J., Teller, D. C., Yee, V. C. & Graham, R. M. (1997) *Biochemistry* **36,** 11655–11664.
12. Aiba, H., Nagaya, M. & Mizuno, T. (1993) *Mol. Microbiol.* **8,** 81–91.
13. McCleary, W. R. & Zusman, D. R. (1990) *J. Bacteriol.* **172,** 6661–6668.
14. Namba, H., Rubin, S. A. & Fagin, J. A. (1990) *Mol. Endocrinol.* **4,** 1474–1479.
15. Pai, E., Krengel, U., Petsko, G. A., Goody, R. S., Kabsch, W. & Wittinghofer, A. (1990) *EMBO J.* **9,** 2351–2359.
16. Privé, G. G., Milburn, M. V., Tong, L., deVos, A. M., Yamaizumi, Z., Nishimura, S. & Kim, S. H. (1992) *Proc. Natl. Acad. Sci. USA* **89,** 3649–3653.
17. Doublet, P., Vincent, C., Grangeasse, C., Cozzone, A. J. & Duclos, B. (1999) *FEBS Lett.* **445,** 137–143.
18. Sandkvist, M., Bagdasarian, M., Howard, S. P. & DiRita, V. J. (1995) *EMBO J.* **14,** 1664–1673.
19. Duclos, B., Marcandier, S. & Cozzone, A. J. (1991) *Methods Enzymol.* **201,** 10–21.
20. Yoshida, M. & Amano, T. (1995) *FEBS Lett.* **359,** 1–5.
21. Kennelly, P. J. & Potts, M. (1999) *Front. Biosci.* **4,** 372–385.
22. Zhang, C. C. (1996) *Mol. Microbiol.* **20,** 9–15.
23. Forchhammer, K. & de Marsac, N. T. (1994) *J. Bacteriol.* **176,** 84–91.
24. Warner, K. M. & Bullerjahn, G. S. (1994) *Plant Physiol.* **105,** 629–633.
25. McCartney, B., Howell, L. D., Kennely, P. J. & Potts, M. (1997) *J. Bacteriol.* **179,** 2314–2318.
26. Taylor, S. S., Knighton, D. R., Zheng, J., TenEyck, L. F. & Sowadski, J. M. (1992) *Annu. Rev. Cell Biol.* **8,** 429–462.
27. Price, J. L., Blau, J., Rothenfluh, A., Abodeely, M., Kloss, B. & Young, M. W. (1998) *Cell* **94,** 83–95.
28. Kloss, B., Price, J. L., Saez, L., Blau, J., Rothenfluh, A., Wesley, C. S. & Young, M. W. (1998) *Cell* **94,** 97–107.

FEBS Letters 496 (2001) 86–90

FEBS 24836

Two KaiA-binding domains of cyanobacterial circadian clock protein KaiC

Yasuhito Taniguchi[a], Akihiro Yamaguchi[a], Atsushi Hijikata[a], Hideo Iwasaki[a,b], Kyoko Kamagata[a], Masahiro Ishiura[a,1], Mitiko Go[a], Takao Kondo[a,b,*]

[a] *Division of Biological Science, Graduate School of Science, Nagoya University, Furo-cho, Chikusa-Chikusa-ku, Nagoya 464-8602, Japan*
[b] *CREST, Japan Science and Technology Corporation (JST), Japan*

Received 26 March 2001; revised 26 March 2001; accepted 30 March 2001

First published online 24 April 2001

Edited by Gianni Cesareni

Abstract ***kaiABC*, a gene cluster, encodes KaiA, KaiB and KaiC proteins that are essential to circadian rhythms in the unicellular cyanobacterium *Synechococcus* sp. strain PCC 7942. Kai proteins can interact with each other in all possible combinations. This study identified two KaiA-binding domains (C_{KABD1} and C_{KABD2}) in KaiC at corresponding regions of its duplicated structure. Clock mutations on the two domains and *kaiA* altered the strength of C_{KABD}–KaiA interactions assayed by the yeast two-hybrid system. Thus, interaction between KaiA and KaiC through C_{KABD1} and C_{KABD2} is likely important for circadian timing in the cyanobacterium.**

Key words: Circadian rhythm; *kai* gene; Protein–protein interaction; Cyanobacterium; *Synechococcus*

1. Introduction

Circadian rhythms, biological oscillations with a period of about 24 h, have been found in organisms ranging from cyanobacteria to green plants and mammals. These rhythms regulate various metabolic and behavioral activities and have evolved as an adaptation to daily changes in environmental conditions: such as light, temperature and humidity [1,2]. The circadian clock, an endogenous mechanism that generates the ca. 24 h oscillation, has been postulated as a basis for those rhythms.

Cyanobacteria are the simplest organisms that exhibit circadian rhythms [4,5]. We introduced a bioluminescence reporter gene into the unicellular cyanobacterium *Synechococcus* sp. strain PCC 7942 to monitor circadian gene expression [6], isolated various clock mutants [7] and identified the clock gene cluster *kaiABC* composed of three genes, *kaiA*, *kaiB* and *kaiC*, that was cloned [8]. While no similarity was found between Kai proteins and clock proteins from other organisms, disruption of any one of the *kai* genes completely abolished circadian rhythm. Disruption and overexpression experiments on the *kai* genes suggested that KaiC represses its own (*kaiBC*) expression, while KaiA enhances it. Thus, KaiC and KaiA have been proposed as negative and positive elements, respectively, of the molecular feedback loop of *kaiBC* expression [8]. 19 distinct mutants exhibiting a wide range of period length and arhythmia mapped onto the *kaiC* gene. It is therefore likely that the biochemistry of KaiC protein is a key to understanding circadian characteristics. ATP-binding and autophosphorylation activities of KaiC [9] have been demonstrated as important functional processes in the circadian timing mechanism. More recently, SasA, a regulatory system consisting of a two-component sensory kinase, has been found to amplify the *kai*-based oscillation by interacting with KaiC [10].

Feedback loops for molecular circadian cycling have also been proposed for *Neurospora*, *Drosophila* and mammals [3]. These models involve interactions among clock proteins as crucial step for the feedback loop within the circadian period [3]. A previous study [11] has revealed that KaiA (a positive regulator) and KaiC (a negative regulator) interact with each other in the yeast two-hybrid system, both in vitro and in *Synechococcus*. Each of homologous two half units of KaiC (the first (CI) and second (CII) half domains) interacts with KaiA. In the present study, we identify two KaiA-binding domains (C_{KABD1} and C_{KABD2}) in KaiC by using the yeast two-hybrid system and an in vitro interaction assay. C_{KABD1} and C_{KABD2} were found on corresponding C-terminal regions of CI and CII, respectively. We demonstrated that many of the known clock mutations on C_{KABD1} and C_{KABD2} and on *kaiA* [8] altered C_{KABD}–KaiA interactions, suggesting that a direct interaction between KaiA and KaiC through C_{KABD1} and C_{KABD2} is crucial for circadian timing in the cyanobacterium. Moreover, molecular modeling of KaiC based on similarity of KaiC with many ATP-binding proteins suggested that two domains are configured in the native form of KaiC so as to be accessed by other proteins.

2. Materials and methods

2.1. Bacterial and yeast strains

Escherichia coli strains DH5α and DH10B were used as hosts for both plasmid construction and bacterial expression of GST fusion proteins. *Saccharomyces cerevisiae* strain L40 was used for two-hybrid analysis [12]. The *Synechococcus* arhythmic mutant ALAb, which carries the *kaiA4* mutation (T. Kondo and M. Ishiura, unpublished data), was isolated from the chemically mutagenized P_{psbAI} reporter strain AMC149 [7]. Wild-type and mutant *Synechococcus* strains listed

*Corresponding author. Fax: (81)-52-789 2963.
E-mail: kondo@bio.nagoya-u.ac.jp

[1] Present address: Center for Gene Research, Nagoya University, Furo-cho, Chikusa-Chikusa-ku, Nagoya 464-8602, Japan.

0014-5793/01/$20.00
PII: S0014-5793(01)02408-5

Table 1
Cyanobacterial strains used in this study

Strains	Clock phenotypes	*kai* mutations[a]	References
AMC149[b]	wild-type (period: 24 h)	none	[6]
ALAb	arhythmia	*kaiA4* (Y166→C)	this study
A30a	long period (30 h)	*kaiA2* (R249→H)	[8]
C16a	short period (16 h)	*kaiC3* (R215→C)	[8]
CLAd	low amplitude	*kaiC6* (P248→L)	[8]
C44a	long period (44 h)	*kaiC11* (G421→R)	[8]
C60a	long period (60 h)	*kaiC12* (Y442→H)	[8]
CLAc	arhythmia	*kaiC14* (T495→A)	[8]

[a]Name of mutations and amino acid substitutions are listed.
[b]AMC149 is a derivative of wild-type *Synechococcus* that carries a *psbAI* reporter construct, P*psbAI*::*luxAB*. All mutant strains listed below were originally isolated from chemically mutagenized AMC149.

in Table 1 were each used for their respective genomic DNA preparations.

2.2. Plasmid construction

To construct expression vectors for KaiC deletion fragments (fragments 1–6) fused to LexA (pLexA-f1, -f2, -C_{KABD1}, -f4, -f5 and -C_{KABD2}), PCR was performed (primers listed in Table 2) on a wild-type *Synechococcus* genomic DNA template. For construction of point-mutated C_{KABD1} and C_{KABD2} fusions, PCR was performed similarly using a mutant *Synechococcus* genomic DNA (listed in Table 1) template. PCR products were cloned into the *Bam*HI site of pBTM116. Expression vectors for full-length KaiA, KaiB and KaiC protein fused to VP16 were designated as pLexA-KaiA, -KaiB and -KaiC [12]. For construction of point-mutated LexA-KaiA fusions, PCR was performed using *kaiA*-specific primers (listed in Table 2; [11]) and a mutant *Synechococcus* genomic DNA template (listed in Table 1). Each PCR product was cloned into the *Bam*HI site of pVP16 [12]. Plasmids expressing GST fused to the N-terminus of C_{KABD1} or C_{KABD2} (pGST-C_{KABD1} or -C_{KABD2}) were constructed by insertion of the smaller *Bam*HI fragment of pLexA-C_{KABD1} or -C_{KABD2} into the unique *Bam*HI site of pGEX-3X.

2.3. Yeast two-hybrid assay

The β-galactosidase filter assay was performed as described previously [11,13]. A quantitative liquid culture assay using *o*-nitrophenyl β-D-galactopyranoside (ONPG) as a substrate for β-galactosidase was performed as described [13].

2.4. Production of GST fusion proteins

GST, GST-C_{KABD1}, and GST-C_{KABD2} proteins were prepared and immobilized to glutathione Sepharose 4B (Pharmacia) as described previously [11], except that cells were induced with isopropyl-β-D-thiogalactopyranoside (IPTG) for 6 h prior to cell harvesting.

2.5. Production of ^{35}S-labeled KaiA

[^{35}S]Methionine-labeled KaiA was produced using the rabbit reticulocyte system as described previously [11].

2.6. In vitro assay for protein–protein interaction

An in vitro binding assay was performed as described previously [11].

2.7. Assay for bioluminescence rhythms

Bioluminescence rhythms were monitored as described previously [7].

2.8. Molecular modeling of KaiC

A three-dimensional (3D) structure for KaiC was modeled as follows. The amino acid sequence of KaiC was analyzed by a custom program developed to align its Walker motifs A and B, and its catalytic Glu to be configured in a fashion similar to other ATP-binding proteins such as RAS, F1-ATPase, elongation factor Tu and RecA. RecA had the best sequence match with half domains C1 and C2 of KaiC. Then, we applied a homology modeling technique to each half domain of KaiC, using the 3D structure of RecA as a template. The atomic coordinates of regions having no counterpart in RecA were estimated from corresponding regions of F1-ATPase. The homology module from insightII (SGI) was used in modeling of the half domains of KaiC. Molecular dynamics on the C1 and C2 domains of KaiC were carried out for 100 ps at 300 K, after which energy minimization was conducted with insightII.

3. Results and discussion

3.1. Identification of two KaiA-binding domains on KaiC

To identify KaiA-binding regions in KaiC by the yeast two-hybrid system, we first generated six deletion fragments (60–110 amino acid residues) of KaiC by exploiting an appropriate combination of restriction sites (Fig. 1A), then fused them to LexA, a DNA-binding protein. Each of the six deletion fusions was co-expressed in yeast cells with KaiA fused to a transcriptional activation domain of VP16 [11]. A filter assay

Table 2
Oligonucleotide primers used for amplification of full-length *kaiA* and deleted *kaiC* open reading frames

Fragment 1	5′-CCCTCTT**GGATCC**TGACTTCCGCT-3′ (−12 to +12)
	5′-AGCATCAA**GGATCC**ATAGTTTGCC-3′ (+324 to +301)
Fragment 2	5′-GTCAAG**GGATCC**TTGGCGGCTTCGATCTC-3′ (+341 to +369)
	5′-CGTAGCT**GGATCC**TTTAGAGGGTGCGGCG-3′ (+671 to +649)
Fragment 3	5′-AACGTCG**GGATCC**TCCGCAACGTT-3′ (+610 to +630)
[C_{KABD1}]	5′-TCGGAC**GGATCC**AGATTAAACACGCAC-3′ (+807 to +781)
Fragment 4	5′-GTGGGG**GGATCC**TTAAGGACTCAATCATT-3′ (+824 to +852)
	5′-TTGGCG**GGATCC**TTAGTTGCTAACGCCCCG-3′ (+1182 to +1153)
Fragment 5	5′-CTCTCTG**GGATCC**CGCGGGGCGTTAGCA-3′ (+1138 to +1165)
	5′-CATTTC**GGATCC**AATCTAGACGTATTGGAG-3′ (+1347 to +1318)
Fragment 6	5′-AATACCA**GGATCC**AATTTATGGGA-3′ (+1240 to +1263)
[C_{KABD2}]	5′-AAGCG**GGATCC**CTGGCTAGCTCTC-3′ (+1575 to +1552)
Full-length KaiA	5′-AGGAGCG**AGATCT**TGCTCTCGCAA-3′ (−12 to +12)
	5′-AGCCGAGC**AGATCT**CCTCCTTTAC-3′ (+884 to +860)

As shown in Fig. 1, fragments 1–6 are partial sequences of KaiC. Bold letters indicate *Bam*HI and *Bgl*II sites. Stop codons are underlined. Numbers in parentheses indicate nucleotide position within the *kaiC* or *kaiA* gene; the first nucleotide, A (*kaiC*) or G (*kaiA*), of the translation initiation codon of each gene is numbered +1.

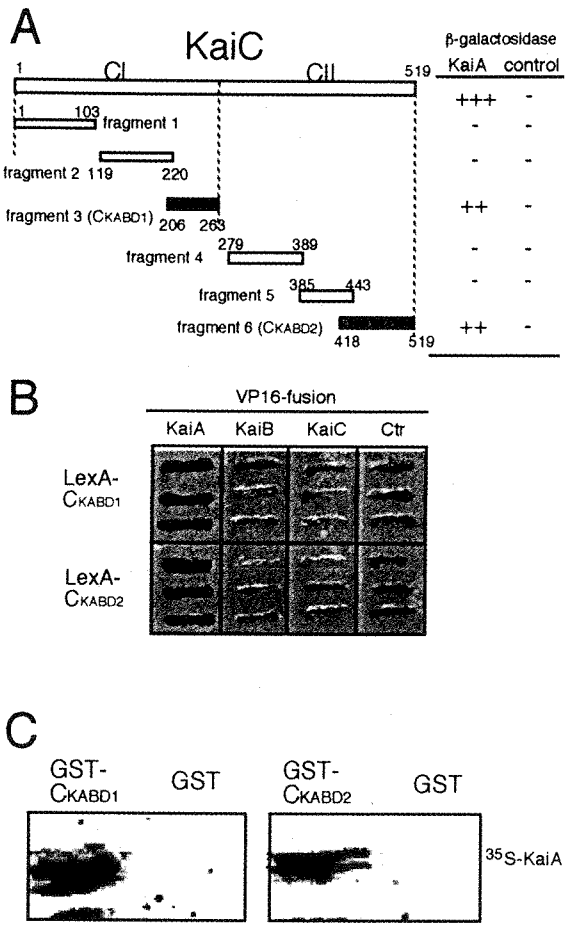

Fig. 1. Identification of two KaiA-binding domains in KaiC. A: Deletion analysis of KaiC for KaiA binding in the yeast two-hybrid system. Left: Open bars represent regions represented by expressed fusion proteins. Numeric labels refer to the first and last amino acid residues included. LexA domains, which were fused to the N-terminal end of each protein (the left of each bar), are not shown. Right: Results of two-hybrid tests. Two-hybrid interactions were estimated by the filter assay for β-galactosidase at 30°C for 3 h. +++, strongly positive interaction (cells were dark blue); ++, positive interaction (cells were blue); −, no interaction (cells remained white). Quantitative data for KaiA–fragment 3 (C_{KABD1}) and KaiA–fragment 6 (C_{KABD2}) interactions are shown in Table 2. B: C_{KABD1} and C_{KABD2} specifically interact with KaiA in yeast cells. β-Galactosidase was monitored by the filter assay as described in A. C: In vitro KaiA–C_{KABD} binding assay. GST, GST-C_{KABD1} or GST-C_{KABD2} were separately immobilized on glutathione Sepharose 4B and incubated with an equivalent volume of a reticulocyte reaction mixture containing ^{35}S-labeled KaiA. Proteins binding to the resin were eluted and then detected by SDS–PAGE on 10% acrylamide gels followed by autoradiography.

for β-galactosidase demonstrated that KaiA interacts with both a 58 amino acid fragment (fragment 3) and a 102 amino acid fragment (fragment 6) (Fig. 1B). In contrast, the other four fragments did not associate with KaiA (Fig. 1A). As shown in Fig. 1B, neither fragment 3 nor 6 interacted with KaiB or KaiC, suggesting that KaiC binds to KaiA through these two fragments exclusively. Therefore, fragments 3 and 6 were designated C_{KABD1} and C_{KABD2}, respectively. As expected from the repeat structure of KaiC, both C_{KABD1} and C_{KABD2} are located at equivalent C-terminal regions of the CI and CII domains, respectively. These observations support the general correlation of primary structure repeats and functional duplication in KaiC, but additional data also have uncovered some specific functional differences between CI and CII as well [8,13].

We confirmed the association between C_{KABD} and KaiA with an in vitro binding assay. Glutathione *S*-transferase (GST) fused to C_{KABD1} or C_{KABD2} and unfused control GST were separately expressed in *E. coli* and immobilized to an affinity resin. KaiA was labeled with ^{35}S using a rabbit reticulocyte system and incubated with each protein-bound resin. The amount of ^{35}S-labeled protein bound to, and subsequently eluted from, each resin was then analyzed by sodium dodecyl sulfate–polyacrylamide gel electrophoresis (SDS–PAGE) followed by autoradiography. The autoradiogram demonstrated that both C_{KABD1} and C_{KABD2} bind KaiA in vitro (Fig. 1C). The doublet bands of in vitro translated KaiA may be due to alternative translation or degradation of KaiA in the rabbit reticulocyte system [11].

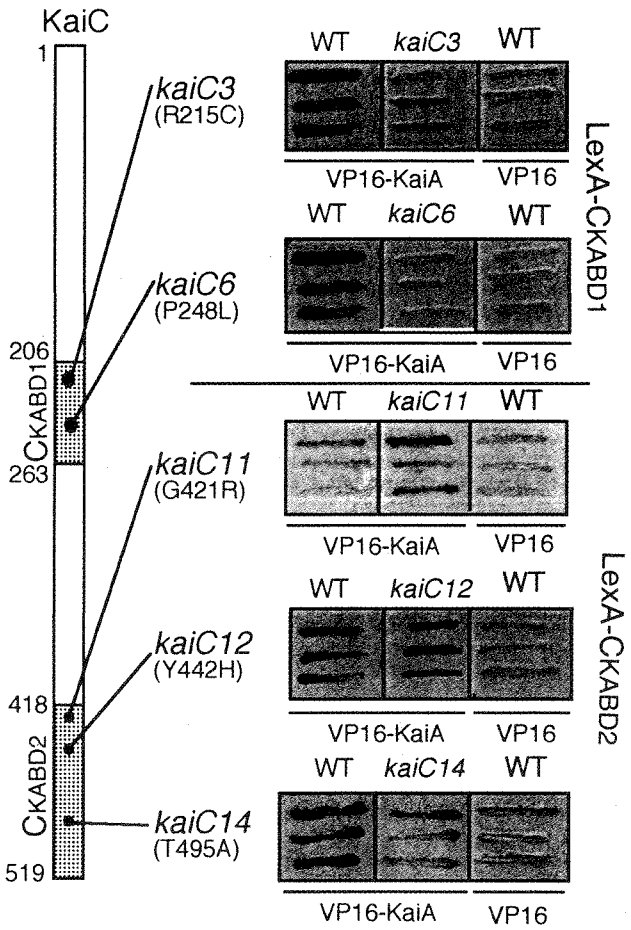

Fig. 2. *kaiC* clock mutations alter KaiA–C_{KABD} interactions. Left: Schematic representation of five clock mutations on either C_{KABD1} or C_{KABD2}. Filled bars indicate C_{KABD1} and C_{KABD2} segments. Numeric labels refer to the amino acid residue number. Black dots indicate locations of various mutations causing the indicated rhythm variations. Right: Effects of KaiC mutations on KaiA–C_{KABD} binding. LexA-C_{KABD1} or LexA-C_{KABD2} was used as bait in the two-hybrid system, while either VP16-KaiA or unfused VP16 was used as prey. β-Galactosidase filter assays were performed as described for Fig. 1A. Photographs show interaction profiles at different reaction times for clarity: incubation for 80 min (*kaiC12*), 120 min (*kaiC11*), 150 min (*kaiC14*), or 180 min (*kaiC3* and *kaiC6*). Note that introduction of each mutation did not alter the background signal of cells expressing C_{KABD} hybrid and unfused VP16 control (data not shown).

3.2. Clock mutations of KaiA-binding domains of kaiC alter C_{KABD}–KaiA interactions

More than half (64%) of the missense mutations in *kaiC* localize to 31% (160 amino acids of C_{KABD1} and C_{KABD2} per 519 amino acids of KaiC) of the *kaiC* gene [8]. Therefore, we examined the effects of these mutations on the association between C_{KABD} and KaiA by the yeast two-hybrid assay. As shown in Fig. 2 and Table 3, we found that five *kaiC* mutations altered the C_{KABD}–KaiA interaction in yeast cells. C_{KABD1}–KaiA interaction was greatly reduced by *kaiC3* (substitution at residue R215 to C) and *kaiC6* (P248 to L) mutations (Fig. 2). *kaiC3* shortens the period to 16 h with a reduced amplitude and *kaiC6* exhibits arhythmia [7,8]. In contrast, C_{KABD2}–KaiA interaction was enhanced by *kaiC11* (G421 to R) and *kaiC12* (Y442 to H) mutations, while it was reduced by *kaiC14* (T495 to A). *kaiC11* and *kaiC12* lengthen the period to 44 and 60 h, respectively, and *kaiC14* abolishes rhythmicity [7,8]. These observations suggest that both KaiA–C_{KABD1} and KaiA–C_{KABD2} interactions may play a role in the generation of circadian rhythms in *Synechococcus*. Binding of KaiC to KaiA is thought to enhance KaiA activity, promoting *kaiBC* expression. Arhythmicity or damping of the oscillation caused by *kaiC3*, *kaiC6* and *kaiC14* mutations could be ascribed to a change in KaiA activity by losing KaiC binding. In contrast, enhanced KaiA–C_{KABD2} binding by the two long-period mutations (*kaiC11* and *kaiC12*) suggests that the more strongly KaiA and C_{KABD} interact, the more slowly the clock proceeds. Elevation of KaiA–C_{KABD} binding would induce a higher level of KaiA activation, which would extend the period. Further studies of *kaiBC* expression profiles and Kai protein complex formation in *Synechococcus* are necessary to address these possibilities.

Four other C_{KABD} mutations did not alter KaiA–C_{KABD} binding profiles (data not shown). Our assay might not be able to detect slight alterations in KaiA–C_{KABD} binding that could be generated by these mutations. Alternatively, these mutations could affect properties of KaiC other than KaiA binding, which are currently unknown but should be assessed. We have not yet found a *kaiC* mutation that affects the interaction between full-length KaiC and KaiA in yeast cells. The duplication of C_{KABD} in KaiC may explain these results, because loss of affinity of either C_{KABD1} or C_{KABD2} could be compensated by the other binding domain. However, even using CI- or CII-VP16 protein, we have not yet found clock mutations that alter the interaction of CI or CII with KaiA (H. Iwasaki, unpublished data), suggesting that the effects of these mutations on binding are too small to alter the configuration of entire domains.

Table 3
Quantitative liquid assay for yeast two-hybrid interactions between KaiA and C_{KABD}

Bait	Prey	β-Galactosidase activity, mean value ± S.D. (arbitrary units)
LexA-C_{KABD1} (wild-type)	VP16	< 0.07
LexA-C_{KABD1} (wild-type)	VP16-KaiA	5.4 ± 0.74
LexA-C_{KABD1} (*kaiC3*)	VP16-KaiA	0.22 ± 0.06
LexA-C_{KABD1} (*kaiC6*)	VP16-KaiA	ND
LexA-C_{KABD2} (wild-type)	VP16	0.12 ± 0.03
LexA-C_{KABD2} (wild-type)	VP16-KaiA	5.5 ± 1.3
LexA-C_{KABD2} (*kaiC11*)	VP16-KaiA	8.0 ± 1.8
LexA-C_{KABD2} (*kaiC12*)	VP16-KaiA	15.0 ± 2.6
LexA-C_{KABD2} (*kaiC14*)	VP16-KaiA	ND

ND, not determined.

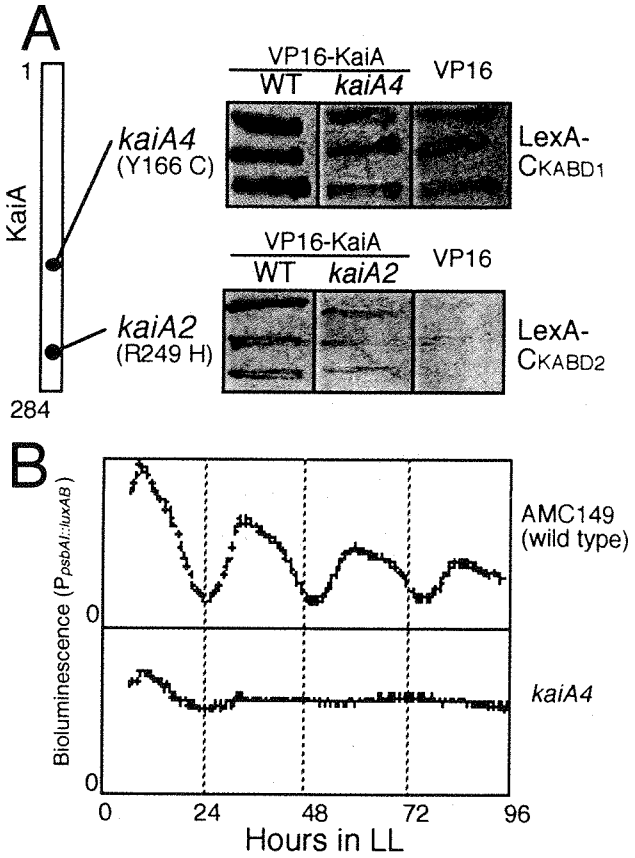

Fig. 3. *kaiA* clock mutations alter KaiA–C_{KABD} interactions. A: Left: Schematic representation of five *kaiA* clock mutations. Reaction conditions were as described in Fig. 2 (left). Black dots mark locations of the indicated mutations. Right: Effects of mutations on KaiA–C_{KABD} binding. Each KaiA mutation was introduced into the VP16-KaiA prey construct. Then, the yeast reporter strain was transformed with the resulting prey plasmid and either LexA-C_{KABD1} or LexA-C_{KABD2} as bait. β-Galactosidase filter assays were performed as described for Fig. 1A. B: Temporal pattern of expression of a clock-controlled gene (*psbAI*) monitored by a bioluminescence reporter in wild-type and ALAb (*kaiA4*) mutant strains.

3.3. Clock mutations of kaiA alter C_{KABD}–KaiA interactions

Reciprocally, we also examined whether clock mutations at KaiA altered binding between KaiA and C_{KABD} in yeast cells (Fig. 3A). *kaiA4*, that causes arhythmicity (Fig. 3B), exhibited reduced KaiA–C_{KABD1} binding. *KaiA4* mapped to the middle of *kaiA* (A to G transition at nucleotide +497, where the first G of the initiator GTG codon is numbered +1) causing an expanded 30 h period [7,8] demonstrated reduced KaiA–C_{KABD2} binding. While reduction of KaiA–C_{KABD2} association by the long period *kaiA2* mutation deviates from the possibilities mentioned in Section 3.2, it is still likely that KaiA–C_{KABD} interaction is an important process to determine parameters of the circadian oscillator of *Synechococcus*, such as period or amplitude.

These observations also support the notion that the C_{KABD}–KaiA interaction plays a role in circadian rhythms in cyanobacteria, and in that period would be extended by alteration of C_{KABD}–KaiA interaction both to tighter or weaker.

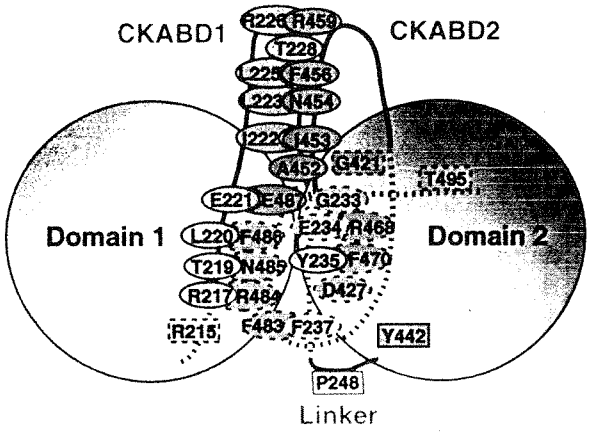

Fig. 4. Putative molecular structure of KaiA-binding domains of KaiC. A putative structure of the two KaiA-binding domains of KaiC is illustrated. Blue and red lines represent C_{KABD1} and C_{KABD2}, respectively. Solid lines depict peptide chains exposed to solvent, and dashed lines indicate buried regions. Each oval indicates a non-polar amino acid residue. Predicted interactions between amino acid side chains are illustrated. Boxes indicate KaiC mutations that modify C_{KABD}–KaiA binding. Amino acid residues near P248 form an interface between the CI and CII domains, and are colored with green and pink circles, respectively.

3.4. Structural modeling of the two KaiA-binding domains

To discuss the functions of the two KaiA-binding domains identified in this study, a 3D structure of KaiC would be extremely helpful. While no 3D structural information is available for KaiC, the similarity of KaiC sequence to those of several nucleotide-binding proteins, such as RAS, F1-ATPase, adenylate cyclase and RecA [14], might help to model the 3D structure. Based on the assumption that common functional motifs of these proteins (Walker's motif A, Walker's motif B, and catalytic Glu) would exhibit structural conservation, the 3D structure of KaiC was computed, based on homology of each half domain of KaiC (CI and CII) to RecA (Yamaguchi et al., in preparation). The predicted structure, as shown in Fig. 4, suggests that both C_{KABD1} and C_{KABD2} are located at the interface between the CI and CII domains, and are stabilized by forming hydrophobic contacts. Two domains seem to be exposed to the surface, which can be accessed by KaiA. This computational model is consistent with our observations that mutations in KaiC profoundly affect KaiA–KaiC association, resulting in abnormality in circadian timing processes.

Acknowledgements: This research was supported by grants from the Japanese Ministry of Education, Science and Culture (11233203, 11440234, 11558089, 11694199 to T.K. and M.I. and 12207002, 12208006, 1559007, 11480189 to M.G.).

References

[1] Bünning, E. (1973) The Physiological Clock, 3rd Edn., Springer, Heidelberg.
[2] Ouyang, Y., Andersson, C.R., Kondo, T., Golden, S.S. and Johnson, C.H. (1998) Proc. Natl. Acad. Sci. USA 95, 8660–8664.
[3] Dunlap, J.C. Molecular bases for circadian clocks, (1999) Cell 96, 271–290.
[4] Golden, S.S., Ishiura, M., Johnson, C.H. and Kondo, T. (1997) Annu. Rev. Plant Physiol. Mol. Biol. 48, 327–354.
[5] Iwasaki, H. and Kondo, T. (2000) Plant Cell Physiol. 41, 1013–1020.
[6] Kondo, T., Strayer, C.A., Kulkarni, R.D., Taylor, W., Ishiura, M., Golden, S.S. and Johnson, C.H. (1993) Proc. Natl. Acad. Sci. USA 90, 5672–5676.
[7] Kondo, T., Tsinoremas, N.F., Golden, S.S., Johnson, C.H., Kutsuna, S. and Ishiura, M. (1994) Science 266, 1233–1236.
[8] Ishiura, M., Kutsuna, K., Aoki, S., Iwasaki, H., Andersson, C.R., Tanabe, A., Golden, S.S., Johnson, C.H. and Kondo, T. (1998) Science 281, 1519–1523.
[9] Nishiwaki, T., Iwasaki, H. and Ishiura, M. (2000) Proc. Natl. Acad. Sci. USA 97, 495–499.
[10] Iwasaki, H., Williams, S.B., Kitayama, Y., Ishiura, M., Golden, S.S. and Kondo, T. (2000) Cell 101, 223–233.
[11] Iwasaki, H., Taniguchi, Y., Ishiura, M. and Kondo, T. (1999) EMBO J. 18, 1137–1145.
[12] Vojtek, A.B., Hollenberg, S.M. and Cooper, J. (1993) Cell 74, 205–214.
[13] Ausubel, F.M., Brent, R., Kingston, R.E., Moore, D.D., Seidman, J.G., Smith, J.A. and Struhl, K., Eds. (1996) Current Protocols in Molecular Biology, Vol. 3, Wiley, New York.
[14] Leipe, D.D., Aravind, L., Grishin, N.V. and Koonin, E.V. (2000) Genome Res. 10, 5–16.

KaiA-stimulated KaiC phosphorylation in circadian timing loops in cyanobacteria

Hideo Iwasaki*†, Taeko Nishiwaki*, Yohko Kitayama, Masato Nakajima, and Takao Kondo†

Division of Biological Science, Graduate School of Science, Nagoya University, and Core Research for Evolutional Science and Technology (CREST), Japan Science and Technology Corporation (JST), Furo-cho, Chikusa, Nagoya 464-8602, Japan

Edited by Robert Haselkorn, University of Chicago, Chicago, IL, and approved September 12, 2002 (received for review August 5, 2002)

Cyanobacterial clock proteins KaiA and KaiC are proposed as positive and negative regulators in the autoregulatory circadian *kaiBC* expression, respectively. Here, we show that activation of *kaiBC* expression by *kaiA* requires KaiC, suggesting a positive feedback control in the cyanobacterial clockwork. We found that robust circadian phosphorylation of KaiC. KaiA was essential for *in vivo* KaiC phosphorylation and activated *in vitro* KaiC autophosphorylation. These effects of KaiA were attenuated by the *kaiA2* long period mutation. Both the long period phenotype and the abnormal KaiC phosphorylation in this mutant were suppressed by a previously undocumented *kaiC* mutation. We propose that KaiA-stimulated circadian KaiC phosphorylation is important for circadian timing.

Cyanobacteria are the simplest organisms known to generate circadian rhythms (1, 2). In the cyanobacterium, *Synechococcus elongatus* PCC 7942, three *kai* genes (*kaiA*, *kaiB*, and *kaiC*) are essential for circadian function and form a gene cluster (3). A transcription/translation-based autoregulatory loop by these Kai proteins is proposed as an important process in circadian *kaiBC* gene expression (3). This type of feedback regulation of clock genes has also been suggested as a key process to generate circadian oscillation also in eukaryotic clock systems in *Drosophila*, *Neurospora*, *Arabidopsis*, and mammals (4). Nevertheless, no similarity was found between the Kai proteins and eukaryotic clock proteins. We know some biochemical properties of the Kai proteins. First, all three Kai proteins interact with each other to form protein complexes (5), and KaiC also interacts with the SasA histidine kinase (6). Second, KaiC has ATP-binding and autokinase activities (7). Third, the KaiB and KaiC proteins accumulate in a circadian fashion in free-running conditions (8). However, it is unknown how these properties are related to each other and function for circadian *kaiBC* expression.

We report here genetic and biochemical data that provide a previously undocumented regulatory link among these properties. Combinatorial studies of genetic inactivation and overexpression of *kai* genes revealed coordinated functions of KaiA and KaiC for both positive and negative limbs of the circadian feedback process for *kaiBC* expression. We also provide genetic evidence for cooperative KaiA-KaiC functions in determining the period length by identification of a previously undocumented *kaiC* allele (*kaiC15*) that suppresses a *kaiA2* long period phenotype. At the molecular level, KaiA was found to enhance *in vitro* KaiC autokinase activity. Moreover, we found that KaiC is phosphorylated *in vivo* in a robust circadian manner. KaiA was essential for this *in vivo* KaiC phosphorylation. Finally, we found that the level of KaiC phosphorylation is lowered in the *kaiA2* mutant, whereas *kaiC15* restores it. Thus, we propose that KaiA and KaiC cooperatively function in both positive and negative feedback processes in the cyanobacterial clock by controlling the state of KaiC phosphorylation in a circadian fashion.

Materials and Methods

Bacterial Strains, Media, and Culture. We used wild-type, *kaiA*-inactivated and *kaiC*-depleted *Synechococcus* strains that harbor the P_{kaiBC}::*luxAB* reporter gene set. The mutant reporter strains were newly generated by mutagenesis of a wild-type P_{kaiBC}::*lux* luciferase reporter strain, NUC42 (9), as described (3). For overexpression of *kaiA* and *kaiC* genes, these reporter strains were transformed with pTS2KP$_{trc}$::*kaiA* or pTS2KP$_{trc}$::*kaiC* (3). For the suppressor mutant screen, we also used a *kaiA2* mutant reporter strain, A30a, which harbors a P_{psbAI}::*luxAB* reporter unit (3).

Suppressor Mutant Screen. *kaiA2* mutant strain A30a was mutagenized with ethylmethane-sulfonate, and the bioluminescence profiles of mutagenized cells were monitored by a chilled charge-coupled device (CCD) camera-based multiplate bioluminescence monitoring system as described (10). Among ≈50,000 independent clones screened, we isolated one mutant that restored a period length of ≈24 h. Potential causal mutation *kaiC15* was mapped to the *kaiC* gene by sequencing the entire *kai* locus. To confirm that this mutation is responsible for the *kaiA2*-suppressor phenotype, we generated *kaiBC* reporter strains that contain the *kaiC15* mutation and/or the *kaiA2* mutation by introduction of a mutagenized pCkaiABC vector (3) in the *kaiABC*-depleted reporter strain NUC42 (9) to regain a different mutant *kai* cluster at the original *kai* locus. Data in Fig. 1*D* illustrate bioluminescence profiles from these strains.

Bacterial Expression and Purification of Kai Proteins. The *kaiB* and *kaiC* ORFs were cloned into the pGEX-6P-1 vector (Amersham Pharmacia) and then transformed into *Escherichia coli* DH 10B. GST-fusion proteins were produced and affinity-purified in *E. coli* as described (5), and the GST-tag was then cleaved and removed with PreScission Protease (Amersham Pharmacia) according to the manufacturer's protocol. The *kaiA* ORF was cloned into pQE32 (Qiagen, Valencia, CA) and transformed with *E. coli* M15(pRep4) (Qiagen). The KaiA protein was produced and purified according to the manufacturer's protocol.

Protein Phosphorylation Assay. Autokinase assay was performed at 30°C as described (7), with some modifications. Briefly, 8.6 pmol (1 μg) of KaiC was incubated with 10 μl of TD buffer (100 mM Tris·Cl/100 mM KCl/5 mM $MgCl_2$,pH 7.6) in the presence or absence of KaiA (8.6 pmol), KaiB (38 pmol), or BSA (8.6 pmol) at 4°C for 40 min. ATP was supplemented to a final concentration of 0.05 mM (10,000 cpm/pmol) and incubated at 30°C. Time 0 was taken from when ATP was added (for data in Fig. 3*A* and *E*). Reaction mixtures were subjected to SDS/PAGE on 10–12% gels followed by autoradiography as described (7). For data on Fig. 3*D*, KaiC was produced in *E. coli* and purified in the presence of 5 mM ATP. KaiC protein (1.4 μg) was incubated with 1.9 μg of KaiA in a reaction buffer (150 mM NaCl/20 mM

This paper was submitted directly (Track II) to the PNAS office.

Abbreviations: λPPase, λ phosphatase; LL, continuous illumination; CBB, Coomassie brilliant blue.

*H.I. and T.N. contributed equally to this work.

†To whom correspondence should be addressed. E-mail: iwasaki@bio.nagoya-u.ac.jp or kondo@bio.nagoya-u.ac.jp.

www.pnas.org/cgi/doi/10.1073/pnas.222467299

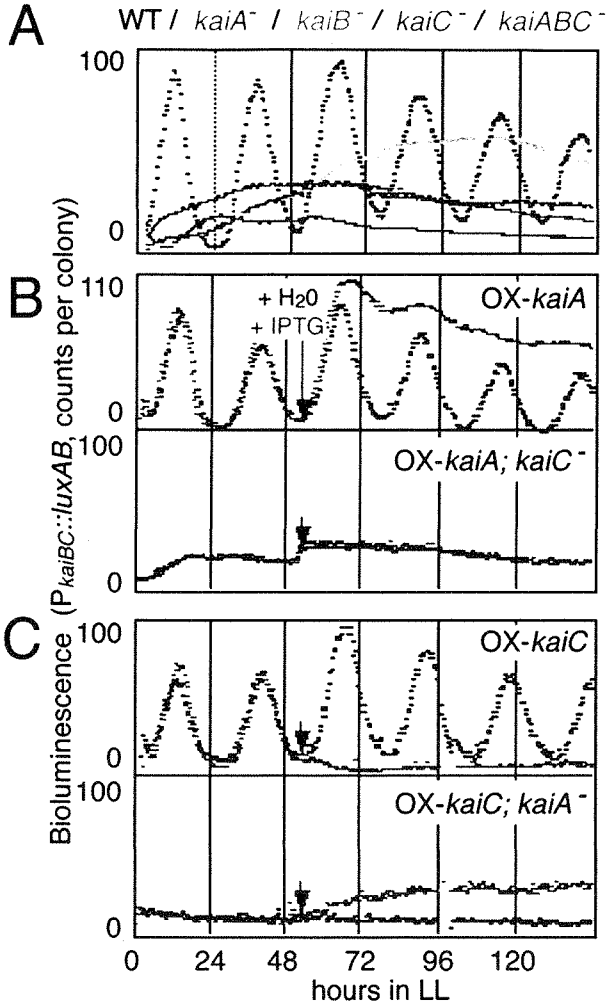

Fig. 1. (*A*) *kaiBC* promoter (P_{kaiBC}) activity was monitored with a luciferase reporter gene set fused to P_{kaiBC} in the wild-type (WT; black), *kaiA*$^-$ (blue), *kaiB*-inactivated (*kaiB*$^-$; yellow), *kaiC*$^-$ (red), and *kaiABC*-cluster-depleted (*kaiABC*$^-$; green) strains. The bioluminescence profiles of four independent clones for each mutant were measured in LL after two cycles of 12 h light:12 h dark (LD) alternations with a photomultiplier tube as described (3). Representative bioluminescence profiles normalized to that of the wild type are shown. (*B*) The effect of overexpression of the *kaiA* gene on P_{kaiBC} activity in the wild-type and *kaiC*-disrupted strains. Bioluminescence from P_{kaiBC} reporter strains carrying a P_{trc}::*kaiA* construct (for *kaiA* overexpression) was monitored. Cells were grown on agar plates as described above and treated with 500 μM isopropyl β-D-thiogalactopyranoside or water after 50 h in LL (arrows). (*C*) The effect of overexpression of the *kaiC* gene on P_{kaiBC} activity in wild-type and *kaiA*-disrupted strains.

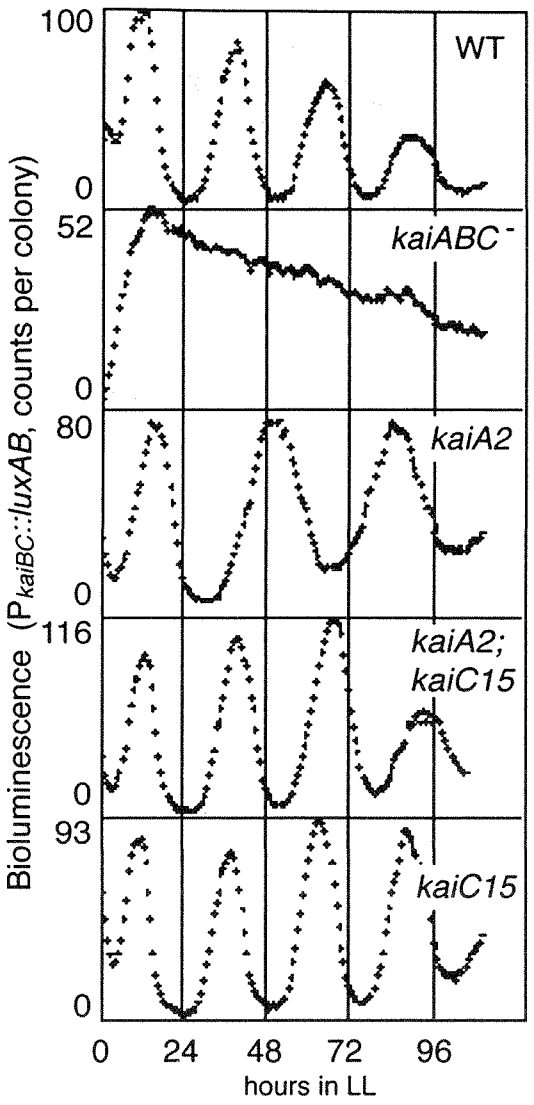

Fig. 2. Suppression of *kaiA2* long period phenotype by the *kaiC15* mutation. *kaiBC* expression profiles in the wild-type, *kaiABC*$^-$, *kaiA2*, *kaiC2;kaiC15*, and *kaiC15* strains are shown. Measurement of the bioluminescence and representation of data are the same as described for Fig. 1.

Tris·Cl/0.4 mM EDTA/5 mM ATP/5 mM $MgCl_2$, pH 8.0) at 30°C and then subjected to SDS/PAGE on 7.5% gels and Coomassie brilliant blue (CBB) staining.

2D-TLC Analysis. 2D-TLC analysis was performed as described (11) with some modifications. KaiC (1 μg) was subjected to an autokinase assay, as described in the text, in the presence or absence of 1 μg of KaiA. After SDS/PAGE analysis, proteins were blotted onto poly(vinylidene difluoride) membranes. The phosphorylated bands were dissected from the membranes and digested with 6 M HCl at 110°C for 1 h. After centrifugation, the supernatants were lyophilized and spotted onto cellulose plates. Thin-layer electrophoresis was performed initially in 2% formic acid, 8.3% acetate (pH 1.9; 1D electrophoresis) and then in 0.5% pyridine, 10% acetate (pH 3.5; 2D electrophoresis) with the Multiphore II electrophoresis apparatus (Amersham Pharmacia). Phosphoserine, phosphothreonine, and phosphotyrosine (Sigma) were used as standard control samples.

λ Phosphatase (λPPase) Assay. *Synechococcus* protein extracts were prepared with a French pressure cell press in buffer A (20 mM Hepes, pH 7.5/150 mM NaCl/1 mM EDTA/1 μg/ml PMSF/1 μg/ml pepstatin A/1 μg/ml leupeptin), and then supplemented with Triton X-100 (final 1%), sodium deoxycholate (0.5%), and SDS (0.1%). Five-hundred-microliter aliquots of the resulting protein extracts (1.4 mg/ml) were immunoprecipitated by incubation with 25 μl (bed volume) of AffiGel-Hz resin (Bio-Rad), immobilizing anti-KaiC IgG (6) at 4°C for 12 h. After washing five times with buffer A supplemented with 1% Triton X-100, 0.5% sodium deoxycholate, and 0.1% SDS, the resin was equilibrated with λPPase buffer (50 mM Tris·Cl/0.1 mM EDTA/2 mM $MnCl_2$/5 mM DTT/0.01% (wt/vol) Brij 35, pH 7.5). The resin was then incubated with 25 μl of λPPase buffer containing 100 or 1,000 units of λPPase (NEB) with or without inhibitors (50 mM NaF/20 mM Na_3VO_4) at 30°C for 1 h. The digested

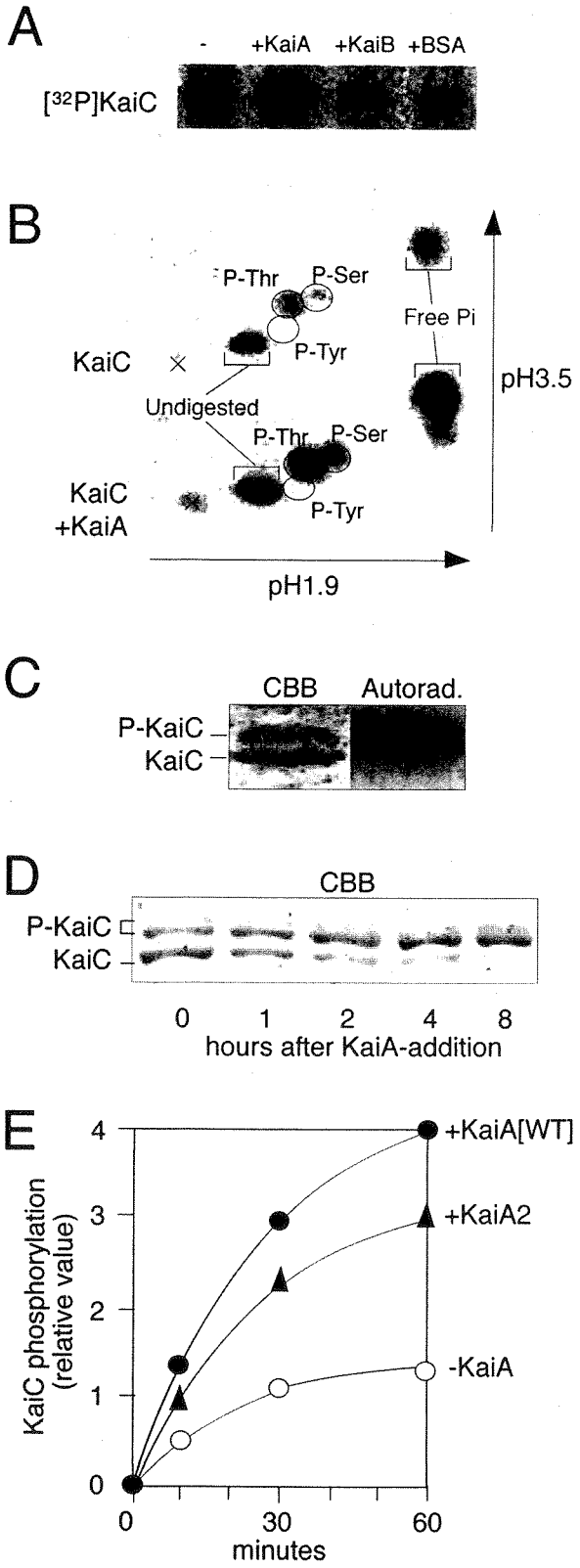

Fig. 3. KaiA-stimulated KaiC autokinase activity. (*A*) Autophosphorylation of the KaiC protein with [γ-^{32}P]ATP in the presence or absence of KaiA, KaiB, and BSA. Autokinase assays were performed at 30°C for 60 min and then analyzed by SDS/PAGE and autoradiography. (*B*) Determination of phosphorylated aminoacyl species for KaiC autophosphorylation by the 2D thin-layer electrophoresis assay. Crosses indicate the sample origin positions. (*C*) Separation of phosphorylated and nonphosphorylated forms of KaiC by SDS/PAGE on 10% gels (acrylamide:*N,N'*-methylenebisacrylamide = 29.8:0.2). KaiC incubated with [γ-^{32}P]ATP was subjected to SDS/PAGE followed by CBB staining (*Left*) and autoradiography (*Right*). (*D*) The effect of KaiA on the mobility of the KaiC protein on 7.5% SDS-polyacrylamide gels. (*E*) Effects of KaiA2 mutant proteins on KaiC autokinase activity. The graph shows the time course profile of KaiC autophosphorylation with or without the wild-type or *kaiA2*-mutation-introduced KaiA proteins (KaiA and KaiA2, respectively).

immune-complexes were resolved in an SDS sample buffer and then subjected to SDS/PAGE and Western blotting with anti-KaiC antisera (5).

Results

Cooperative Functions of KaiA and KaiC in *kaiBC* Expression Feedback Loops. In the previous transcriptional feedback model, KaiA was suggested as a positive regulator for *kaiBC* expression (3). As described previously (3), a *kaiA*-inactivated (*kaiA*$^-$) strain consistently reduces *kaiBC* promoter (P_{kaiBC}) activity, as monitored by a luciferase reporter (Fig. 1*A*), and continuous *kaiA* overexpression enhances it and abolishes rhythmicity (Fig. 1*B*). On the other hand, KaiC has been proposed as a negative element for *kaiBC* expression (3). As shown in Fig. 1*C Upper*, *kaiC* overexpression consistently suppresses *kaiBC* expression (3). However, *kaiC*-disrupted (*kaiC*$^-$) strains did not enhance but reduced *kaiBC* expression to ≈20% of the wild-type strain (Fig. 1*A*), which cannot be explained by the simple negative feedback model (1, 3). This result is in contrast to enhanced expression of the *frequency* (*frq*) gene, a negative element in the *Neurospora* clock, in *frq*-null mutants (12). Our observation in *Synechococcus* raises the possibility that KaiC may also function in the positive limb of the *kaiBC* oscillatory loop.

To examine whether the positive function of KaiA requires KaiC, we overexpressed *kaiA* in the wild-type and *kaiC*$^-$ strains under the control of an isopropyl-β-D-thiogalactopyranoside-inducible *trc* promoter. Although overexpression of *kaiA* enhanced *kaiBC* expression and abolished its rhythmicity in the wild-type strain (Fig. 1*B*; ref. 3), that of *kaiA* in the *kaiC*$^-$ strain failed to up-regulate *kaiBC* transcription (Fig. 1*B*). Thus, KaiC seems required for a positive effect of KaiA in the expression of *kaiBC*. Moreover, KaiC additionally participates in activation of *kaiBC* expression independently of KaiA function. As shown in Fig. 1*C*, KaiC overexpression reduces its own transcription (3), whereas in the *kaiA*$^-$ mutant it failed to exhibit the inhibitory effect and instead gradually enhanced *kaiBC* expression.

Identification of a *kaiC* Allele That Suppresses *kaiA2* Long Period Phenotype. The KaiA–KaiC cooperation was further supported by identification of a previously undocumented *kaiC* allele named *kaiC15*, which suppresses a *kaiA2* rhythm mutant, by a suppressor mutagenesis screen (Fig. 2). The *kaiA2* mutation (Arg-249 to His in KaiA) lengthens the period by 6–7 h (3). We screened ethylmethane-sulfonate-mutagenized *kaiA2* mutant strain A30a for suppressor mutants, which restore a wild-type period phenotype. The A30a strain contains a bioluminescence reporter to monitor the *psbAI* clock-controlled gene expression (3). Among ≈50,000 independent clones screened, we isolated a mutant that restored a period length of ≈24 h. Because most chemically mutagenized strains that impair period length have mutations in the *kaiABC* genes (3), we sequenced the *kai* locus of the genomic DNA prepared from the potential *kaiA2* suppressor mutant. A mutation, designated *kaiC15*, was found in the *kaiC* ORF, which caused an amino acid substitution at the amino terminus of the KaiC (Ala-422 to Thr). To confirm that the *kaiC15* mutation is responsible for the *kaiA2*-suppressor phenotype, we generated *kaiBC* reporter strains that contain the *kaiC15* mutation and/or the *kaiA2* mutation by site-directed mutagenesis (see *Materials and Methods*). As shown in Fig. 2, the *kaiC15* mutation shortened the period of *kaiA2* by ≈6 h. The

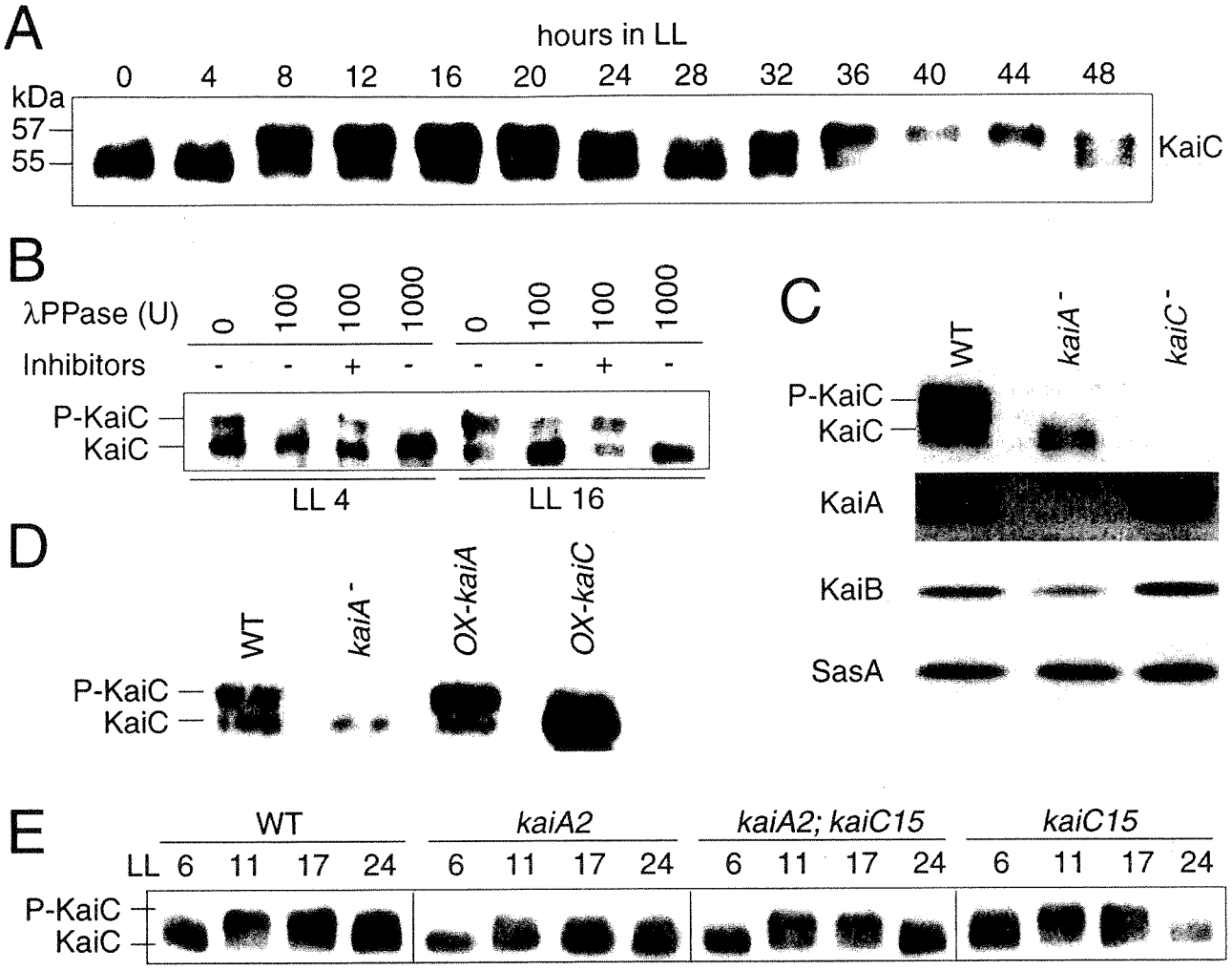

Fig. 4. (*A*) KaiC protein expression profile examined by Western blotting. Cells were cultured in a continuous culture system in BG-11 liquid medium to maintain an OD_{730} of 0.18 under LL (50 $\mu E \cdot m^{-2} \cdot s^{-1}$, in which E indicates an einstein, 1 mol of photons). After two LD cycles, cells were returned to LL conditions and then collected every 4 h. Total proteins were extracted by sonication of cell pellets in SDS-sample buffer and then subjected to SDS/PAGE with 10% gels (acrylamide:*N,N'*-methylenebisacrylamide = 29.8:0.2), followed by Western blotting assay (4.0 μg protein per lane). (*B*) λPPase assay. Soluble protein extracts were prepared from *Synechococcus* culture collected at hours 4 and 16 under LL (LL 4 and LL 16), immunoprecipitated with anti-KaiC IgG, digested with 100 or 1,000 units of λPPase in the presence or absence of λPPase inhibitors (NaF and Na_3VO_4), and then subjected to Western blotting with anti-KaiC antisera. (*C*) Expression of clock proteins in wild-type, *kaiA*-null, and *kaiC*-null mutant strains by Western blotting. Note that no circadian fluctuation was observed in both *kai*-gene mutants in terms of the state of KaiC phosphorylation throughout the circadian cycle (data not shown). We show here Western blots using cells collected at LL 16, when the level of KaiC phosphorylation is maximal in the wild-type strain. (*D*) KaiC phosphorylation profile in *kaiA*$^-$, *kaiA*-overexpressing (ox-*kaiA*), and *kaiC*-overexpressing (ox-*kaiC*) cells (Western blotting). Cells were cultured in BG-11 liquid medium (100 μM isopropyl-β-D-thiogalactopyranoside) and collected at LL 16. Total proteins (8 μg) were extracted from the collected cells and subjected to 10% gels followed by Western blotting assay. (*E*) Circadian KaiC phosphorylation profiles in the wild-type, *kaiA2*, *kaiC15*, and *kaiA2;kaiC15* strains. Total proteins (8 μg) were analyzed by Western blotting as described above.

average period length was 25.2 h in the wild-type strain, 33.0 h in the *kaiA2* mutant, and 27.3 h in the *kaiA2;kaiC15* strain. Note that *kaiC15* mutation alone affected the period length to a lesser extent (24.7 h; Fig. 2). This finding presents genetic evidence for interactive KaiA–KaiC functions in determining the circadian period length (see *Discussion*).

KaiA Enhances KaiC Autophosphorylation Activity. Then, how are KaiA and KaiC functions coordinated in the circadian system at the molecular level? We previously showed that all three Kai proteins interact in all possible combinations (5) and that the KaiC protein undergoes autophosphorylation *in vitro* (7). Thus, we examined whether the association of KaiC with KaiA (or KaiB) directly affects *in vitro* KaiC autokinase activity by incubation of KaiC with [γ-^{32}P]ATP in the presence or absence of KaiA or KaiB protein. We found KaiC autokinase activity to be dramatically enhanced by KaiA (Fig. 3*A*). Addition of KaiB affected KaiC phosphorylation less (Fig. 3*A*). To examine phosphorylated aminoacyl species in KaiC, we performed 2D-TLC analysis for phosphorylated KaiC in the presence or absence of KaiA. KaiC was found to be autophosphorylated at both threonine and serine residues at a 2:1 ratio, and KaiA enhanced KaiC phosphorylation without affecting the ratio (Fig. 3*B*).

Circadian Rhythm in KaiC Phosphorylation *in Vivo*. We found that KaiC is also phosphorylated *in vivo*. Under continuous illumination (LL) conditions, KaiB and KaiC accumulate in a circadian fashion, peaking at circadian time (CT) 16 (Fig. 4*A*), whereas KaiA accumulation shows much lower amplitude rhythm or even arrhythmia (8). We noted that KaiC shows circadian fluctuation in mobility shift on SDS–polyacrylamide gels (Fig. 4*A*). KaiC signal appeared as doublet bands, and the upper band is dom-

inant at subjective early night (CT 12–16), whereas in subjective early day (CT 0–4), it is dramatically reduced. λPPase treatment abolished the upper band for KaiC, and this effect was inhibited by the λPPase inhibitors vanadate and fluoride (Fig. 4*B*). Thus, KaiC undergoes robust circadian phosphorylation, peaking at CT 16. The λPPase removes a phosphoryl group from phosphorylated Ser, Thr, Tyr, and His residues (13, 14), and our preliminary chemical stability assay suggested that KaiC is phosphorylated *in vivo* at Ser and/or Thr residues (T.N., unpublished results), as it is *in vitro* (Fig. 3*B*).

KaiA Is Essential for *in Vivo* KaiC Phosphorylation. To address whether KaiA protein also affects KaiC phosphorylation *in vivo*, we analyzed expression of KaiC and other clock proteins in the *kaiA*- and *kaiC*-null mutant strains (Fig. 4*C*). These mutants are arrhythmic (3) but did not affect the level of SasA protein. On the other hand, the *Upper* band in Fig. 4*C* (a phosphorylated form) of KaiC was evidently diminished in the *kaiA*$^-$ strain. Abnormality in the phosphorylation state of KaiC in the *kaiA*-null mutant was observed throughout the circadian cycle (data not shown). Thus, KaiA is essential for accumulation of phosphorylated KaiC protein *in vivo*. Decrease in the levels of KaiB and KaiC in the *kaiA*$^-$ cells (Fig. 4*C*) is most likely due to inactivation of *kaiBC* expression (3). The *kaiA*-overexpressor consistently enhanced the magnitudes of both KaiC phosphorylation and accumulation, whereas the *kaiC*-overexpressor accumulated a nonphosphorylated form of KaiC (Fig. 4*D*). Hyperphosphorylation of KaiC in the arrhythmic *kaiA*-overexpressor strain further supports that abolishment of KaiC phosphorylation in the *kaiA*-null mutant is not due to lack of circadian oscillation but to lack of the KaiA protein.

Because KaiA enhances both *in vivo* and *in vitro* KaiC phosphorylation, we tested whether activation of KaiC autophosphorylation by KaiA *in vitro* is accompanied by any mobility shift of the KaiC protein on SDS-polyacrylamide gels as observed *in vivo*. KaiC was autophosphorylated by incubation with [γ-^{32}P]ATP, subjected to SDS/PAGE, and stained by CBB. As shown in Fig. 3*C*, KaiC appeared as doublet bands on 10% gels. Autoradiography of the gel revealed that the *Upper* band is the phosphorylated form as observed *in vivo*. To test the effect of KaiA on the mobility of the KaiC protein on gels, we purified KaiC protein in the presence of ATP, incubated it with KaiA, and then analyzed by SDS/PAGE. As shown in Fig. 3*D*, KaiC purified in the presence of ATP appeared as three bands on 7.5% gels. Incubation with KaiA attenuated the *Bottom* band signal, whereas it enhanced accumulation of the *Top* and *Middle* band signals. Incubation of KaiC without KaiA protein did not enhance accumulation of the *Top* and *Middle* bands (data not shown). Thus, KaiA enhances both *in vitro* and *in vivo* KaiC phosphorylation with a similar mobility shift profile of KaiC on SDS/PAGE gels.

Reduction in KaiA-Mediated KaiC Phosphorylation by *kaiA2* Mutation. To test whether KaiA-modulated KaiC phosphorylation is important for the timing mechanism in *Synechococcus*, we examined the effects of *kaiA* period mutations on the phosphorylation state of KaiC. We found that, in the *kaiA2* mutant, the nonphosphorylated form of KaiC was highly accumulated throughout the circadian cycle (Fig. 4*E*). In contrast, the *kaiA2;kaiC15* suppressor strain regained the wild-type circadian phosphorylation pattern, as did the *kaiC15* single mutant strain (Fig. 4*E*). The *kaiA2* mutation consistently reduced the enhancing effect of KaiA on *in vitro* KaiC autokinase activity to ≈70% of that of the wild-type protein (Fig. 3*E*). The abnormality in the *in vivo* KaiC phosphorylation state by the long period mutant thus strongly suggests a physiological relevance for the activation of KaiC phosphorylation by KaiA in determining the circadian period length in *Synechococcus*.

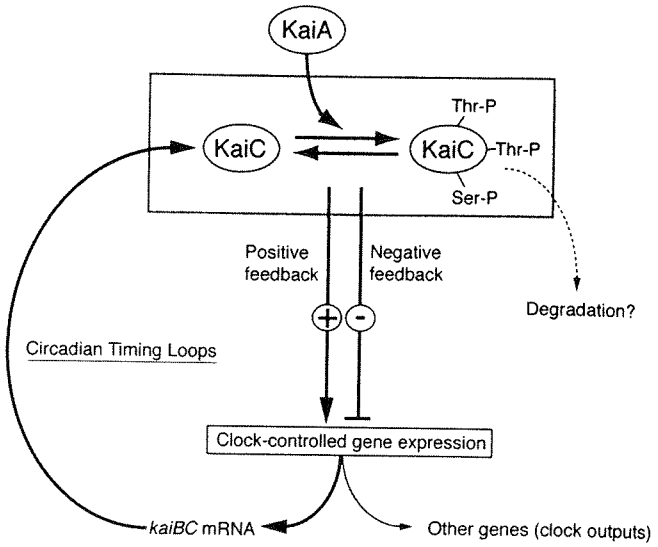

Fig. 5. A model for KaiA–KaiC functions in the *Synechococcus* clock. KaiA protein activates KaiC autokinase activity. The state of KaiC phosphorylation would regulate *kaiBC* expression. KaiC protein (complex) might affect its own promoter indirectly through controlling a clock output mechanism, such as regulation of the state of chromosome condensation (2), or by regulating SasA kinase activity (6). Phosphorylation also possibly affects the stoichiometry of clock protein complex(es) and/or the turnover of the KaiC protein (complex), which will affect the equilibrium state between nonphosphorylated and phosphorylated forms of KaiC. Because KaiC autophosphorylates at multiple residues, multiple phosphorylated forms of KaiC may be able to play different biochemical roles.

Discussion

The previously proposed simple negative feedback model for the *Synechococcus* clock (3) focused on KaiC function as a negative factor. In addition to this role, our genetic study (Fig. 1*B*) supported the idea that KaiA-mediated activation of *kaiBC* is KaiC dependent, and thus KaiC could be involved in the positive limb to form a positive feedback process. A certain state of KaiA–KaiC complex would activate the *kaiBC* promoter activity. Alternatively, KaiA may derepress *kaiBC* expression by affecting an inhibitory KaiC-containing complex. Moreover, it is also possible that KaiA is partly involved in KaiC-dependent repression of *kaiBC* expression because, in the absence of KaiA, overexpression of KaiC failed to repress *kaiBC* expression (Fig. 1*C*). In either case, the state of interaction between KaiA and KaiC determines both positive and negative feedback effects on *kaiBC* expression. The moderate reduction in the magnitude of *kaiBC* expression in the *kaiC*-null mutant is thus most likely due to the lack of the KaiC-dependent positive function. Note that many biological oscillations such as cell cycle control, glycolytic oscillations, and Ca^{2+} oscillations contain positive feedback (self-amplifying) processes (15), in addition to negative feedback regulations that are well described in circadian clock models (4). Coupling of the previously proposed negative feedback loop in the *Synechococcus* oscillator (3) with the positive feedback process revealed here would be important to make oscillation robust.

Our biochemical and genetic studies strongly suggest that KaiA-stimulated phosphorylation of KaiC is an important process in the coordination of the KaiA–KaiC functions. Phosphorylation may affect the stability of the KaiC protein (and/or KaiC-containing complexes) as proposed for some eukaryotic clock proteins (4), or it might affect the formation of different stoichiometric complexes of the Kai and/or SasA proteins (5, 6). Alternatively, circadian KaiC phosphorylation may modulate the

state of chromosome condensation for global circadian gene expression (2). In any case, changes in the rate of KaiC phosphorylation by the KaiA protein could affect the rate of *kaiBC* repression, which is important for circadian rhythm generation (Fig. 5).

Moreover, our study revealed a similarity between *in vivo* and *in vitro* KaiC phosphorylation. Both types of phosphorylation (*i*) are stimulated by KaiA, (*ii*) occur at Ser and/or Thr residues, (*iii*) are accompanied by similar mobility shift profiles on SDS/PAGE gels, and (*iv*) are affected equivalently by the *kaiA2* long period mutation. Thus, we suggest that *in vivo* KaiC phosphorylation is most likely due to KaiA-activated KaiC's autokinase activity, although we do not rule out the possibility that KaiC is additionally phosphorylated by other kinases, which are activated by KaiA.

Consistent changes by *kaiA2* mutation, both in the KaiC phosphorylation profile and the period length, further support the physiological importance of KaiC phosphorylation for circadian timing. The *kaiA2* mutation most likely reduces the rate of KaiC phosphorylation, and so it would retard the timing of KaiC degradation and/or that of activation (or derepression) of the *kaiBC* genes to lengthen the period. The *kaiC15* mutation may compensate such effects to regain the wild-type period length. Consistently, *kaiC15* has been mapped to one of two KaiA-binding domains (C_{KABD2}) of KaiC (16) and *kaiA2* to a KaiC-interacting, C-terminal domain of KaiA (amino acyl residues 180–286) that is sufficient for enhancing KaiC phosphorylation (17).

We thank Stanly B. Williams, Ioannis Vakonakis, Andy LiWang, and Susan S. Golden (Texas A&M University, College Station, TX) for sharing unpublished results and comments on the manuscript. We thank Jun Tomita, Hakuto Kageyama, and Yoriko Murayama (Nagoya University) for technical help, and our lab members for discussion. This research was partly supported by grants-in-aid from the Japanese Society for Promotion of Science (13680778 to H.I.), from the Japanese Ministry of Education, Culture, Sports, Science, and Technology (11233203 to H.I. and T.K., and COE 13CE2005 to T.K.), and from the Kurata Memorial Hitachi Science and Technology Foundation (to H.I.), and by Inoue Research Award for Young Scientists from the Inoue Foundation (to H.I.). T.N. was supported by the Hayashi Memorial Foundation for female natural scientists, and Y.K. by the Japanese Society for Promotion of Science fellowship for young scientists (13001761).

1. Iwasaki, H. & Kondo, T. (2000) *Plant Cell Physiol.* **41,** 1013–1020.
2. Mori, T. & Johnson, C. H. (2001) *Semin. Cell Dev. Biol.* **12,** 271–278.
3. Ishiura, M., Kutsuna, S., Aoki, S., Iwasaki, H., Andersson, C. R., Johnson, C. H., Golden, S. S. & Kondo, T. (1998) *Science* **281,** 1519–1523.
4. Young, M. W. & Kay, S. A. (2001) *Nat. Rev. Genet.* **2,** 702–715.
5. Iwasaki, H., Taniguchi, Y., Ishiura, M. & Kondo, T. (1999) *EMBO J.* **18,** 1137–1145.
6. Iwasaki, H., Williams, S. B., Kitayama, Y., Ishiura, M., Golden, S. S. & Kondo, T. (2000) *Cell* **101,** 223–233.
7. Nishiwaki, T., Iwasaki, H., Ishiura, M. & Kondo, T. (2000) *Proc. Natl. Acad. Sci. USA* **97,** 495–499.
8. Xu, Y., Mori, T. & Johnson, C. H. (2000) *EMBO J.* **19,** 3349–3357.
9. Nishimura, H., Nakahira, Y., Imai, K., Tsuruhara, A., Kondo, H., Hayashi, H., Hirai, M., Saito, H. & Kondo, T. (2002) *Microbiology* **148,** 2903–2909.
10. Kondo, T., Tsinoremas, N. F., Golden, S. S., Johnson, C. H., Kutsuna, S. & Ishiura, M. (1994) *Science* **266,** 1233–1236.
11. Hardie, D. G. (1993) *Protein Phosphorylation: A Practical Approach* (Oxford Univ. Press, Oxford).
12. Aronson, B. A., Johnson, K. A., Loros, J. J. & Dunlap, J. C. (1994) *Science* **263,** 1578–1584.
13. Cohen, P. T. & Cohen, P. (1989) *Biochem. J.* **260,** 931–934.
14. Zhuo, S., Clemens, J. C., Hakes, D. J., Barford, D. & Dixon, J. E. (1993) *J. Biol. Chem.* **268,** 17754–17761.
15. Goldbeter, A. (1996) *Biochemical Oscillations and Cellular Rhythms* (Cambridge Univ. Press, Cambridge, U.K.).
16. Taniguchi, Y., Yamahuchi, A., Hijikata, A., Iwasaki, H., Kamagata, K., Ishiura, M. & Kondo, T. (2001) *FEBS Lett.* **496,** 86–90.
17. Williams, S. B., Vakonakis, I., Golden, S. S. & LiWang, A. (2002) *Proc. Natl. Acad. Sci. USA* **99,** 15357–15362.

THE JOURNAL OF BIOLOGICAL CHEMISTRY

Vol. 278, No. 4, Issue of January 24, pp. 2388–2395, 2003
Printed in U.S.A.

Circadian Formation of Clock Protein Complexes by KaiA, KaiB, KaiC, and SasA in Cyanobacteria*

Received for publication, August 30, 2002, and in revised form, October 9, 2002
Published, JBC Papers in Press, November 18, 2002, DOI 10.1074/jbc.M208899200

Hakuto Kageyama, Takao Kondo, and Hideo Iwasaki‡

From the Division of Biological Science, Graduate School of Science, Nagoya University and Core Research for Evolutional Science and Technology (CREST), Japan Science and Technology Corporation (JST), Furo-cho, Chikusa, Nagoya 464-8602, Japan

Physical interactions among clock-related proteins KaiA, KaiB, KaiC, and SasA are proposed to be important for circadian function in the cyanobacterium *Synechococcus elongatus* PCC 7942. Here we show that the Kai proteins and SasA form heteromultimeric protein complexes dynamically in a circadian fashion. KaiC forms protein complexes of ~350 and 400–600 kDa during the subjective day and night, respectively, and serves as a core of the circadian protein complexes. This change in the size of the KaiC-containing complex is accompanied by nighttime-specific interaction of KaiA and KaiB with KaiC. In various arrhythmic mutants that lack each functional Kai protein or SasA, circadian rhythms in formation of the clock protein complex are abolished, and the size of the protein complexes is dramatically affected. Thus, circadian-regulated formation of the clock protein complexes is probably a critical process in the generation of circadian rhythm in cyanobacteria.

Circadian rhythms, biological oscillations with a period of ~24 h, are observed in many physiological events of a wide variety of organisms. At the molecular level, several clock-related genes have been identified and intensively analyzed in cyanobacteria, *Neurospora*, *Arabidopsis*, *Drosophila*, and mammals (1, 2).

Cyanobacteria are the simplest organisms known to have the circadian clock and provide both genetic and physiological model systems (3, 4). Previously we have monitored circadian gene expression in the cyanobacterium *Synechococcus elongatus* PCC 7942 using a bioluminescence (luciferase) reporter gene set (5), isolated various mutants that impaired normal circadian phenotypes (6), and identified the clock gene cluster *kaiABC* (7). Molecular genetic studies suggested functions of KaiA and KaiC as positive and negative elements for *kaiBC* expression, respectively, to form a negative feedback loop (7). This regulatory loop has been proposed as an important step to drive circadian oscillation in *kaiBC* expression (7).

To elucidate the molecular mechanism of the cyanobacterial circadian clock, it is essential to discover the biochemical properties of the Kai proteins. KaiB and KaiC accumulate in a circadian fashion in cyanobacterial cells, peaking at circadian time (CT)[1] 15–16 in continuous light conditions. (CT indicates the subjective time of a day (h) in constant environmental conditions; CT 0 corresponds to the subjective dawn. In contrast, Zeitgeber time (ZT) is used to indicate time in a light-day cycle; ZT 0 indicates dawn time in a light-day cycle.) This accumulation follows *kaiBC* mRNA rhythms by ~8 h (8). KaiC binds to ATP *in vitro* through nucleotide-binding domains (P-loops), and mutations of these motifs severely alter the circadian function (4, 9). Moreover, KaiC undergoes autophosphorylation *in vitro* (9). Another important characteristic of the Kai proteins is their physical association in various combinations in yeast cells, *in vitro*, and in *Synechococcus* cells (10). A long period mutation of KaiA affects the strength of the KaiA-KaiC interaction, suggesting an important role of such protein interactions in circadian time-keeping (10). We have also identified another KaiC-interacting partner, SasA, which is a sensory histidine kinase (11). Although SasA is not an essential oscillator component, SasA is important in enhancing *kaiBC* expression and likely forms a secondary loop with KaiC to stabilize the Kai-based primary molecular circuit. SasA is also involved in metabolic growth control under day/night cycle conditions (11). However, biochemical functions and molecular behaviors of the Kai proteins and SasA remain largely unknown in *Synechococcus* cells.

In this study, we biochemically examined temporal profiles of the clock protein interactions in *Synechococcus*. Gel filtration chromatographic analysis demonstrated that the Kai proteins and SasA form large protein complexes and suggested that the complexes change their stoichiometry during the circadian cycle. Immunoprecipitation studies confirmed that the Kai proteins and SasA circadianly associate in large KaiC-containing protein complexes. Dramatic changes in the size of Kai/SasA-containing complexes in *kaiA*-, *kaiB*-, *kaiC*-, and *sasA*-inactivated strains further support that circadian formation of the clock protein complexes has a function in the circadian regulatory mechanism.

EXPERIMENTAL PROCEDURES

Bacterial Strains and Cultures—NUC39 and NUC38 (10) were used as the wild-type and *kaiABC*-depleted *Synechococcus* strains, respectively. We also used *kaiA*-, *kaiB*-, and *kaiC*-inactivated strains (7), a *sasA*-disrupted strain (11), and the KaiC(K52H) mutant strain (9). *Synechococcus* cells were grown at 30 °C in BG-11 liquid medium under continuous light (LL) conditions of 46 μmol^{-2} s^{-1} from white fluorescent lamps.

* This research was supported in part by grants-in-aid from the Japanese Society for Promotion of Science (13680778 to H. I.), the Japanese Ministry of Education, Culture, Sports, Science, and Technology (11233203 to H. I. and T. K. and COE 13CE2005 to T. K.), and the Kurata Memorial Hitachi Science and Technology Foundation (to H. I.) and by the Inoue Research Award for Young Scientists from the Inoue Foundation (to H. I.). The costs of publication of this article were defrayed in part by the payment of page charges. This article must therefore be hereby marked "*advertisement*" in accordance with 18 U.S.C. Section 1734 solely to indicate this fact.

‡ To whom correspondence should be addressed: Division of Biological Science, Graduate School of Science, Nagoya University, Furo-cho, Chikusa, Nagoya 464-8602, Japan. Tel.: 81-52-789-2507; Fax: 81-52-789-2963; E-mail: iwasaki@bio.nagoya-u.ac.jp.

[1] The abbreviations used are: CT, circadian time; ZT, Zeitgeber time; LL, continuous light; LD, 12-h light/12-h dark.

Immunoblotting Analysis—*Synechococcus* cells were grown in BG-11 liquid medium to an optical density of 0.2 at 730 nm (OD_{730}). The cells were exposed to two cycles of 12-h light/12-h dark (LD) alternation and then placed in LL conditions and harvested in LD and LL. The cell pellets were collected from the culture and then immediately resuspended in 200 μl of binding buffer, BB5 (50 mM Tris-HCl, 100 mM KCl, 5 mM $MgCl_2$, 0.2% glycerol, 0.1 mM EDTA, 1 mM phenylmethylsulfonyl fluoride, 3 μg/ml leupeptin, 3 μg/ml pepstatin, 0.1 mM NaF, 0.1 mM Na_3VO_4, 0.1 mg/ml DNase I, pH 8.0), and disrupted by sonication using the Ultrasonic Liquid Processor (Misonix) or the BioRupter (Cosmo) at 4 °C. After centrifugation, the resulting supernatant was used for immunoblotting, immunoprecipitation, or gel filtration chromatographic analyses. Immunoblot analyses, shown in Figs. 1 and 4*B*, were performed with 5 μg of total cell extracts that were subjected to SDS-PAGE on 10 or 15% gels and blotted onto nitrocellulose membranes. The KaiA, KaiB, KaiC, and SasA proteins were analyzed with specific antisera (10, 11) at a 1:500, 1:2000, 1:2000, and 1:2000 dilution, respectively, and detected with the enhanced chemiluminescence (ECL) method (Amersham Biosciences) according to the manufacturer's protocol. The specificities of these antibodies have been confirmed and described previously (10, 11).

Immunoprecipitation—Immunoprecipitation was performed as described previously (11) with some modifications. Briefly, protein extracts in 360 μl of BB5 (total, 500 μg of protein) were prepared as described above. Then the extracts were supplemented with 40 μl of 5% bovine serum albumin in 0.1 M KCl and then incubated with a 10-μl bed volume of prewashed AffiGel-Hz beads (Bio-Rad) coupled to purified rabbit anti-KaiC IgG at 4 °C for 2 h. After six washes with 1 ml of BB5 without DNase I, the beads were resuspended in 80 μl of SDS sample buffer without reducing agents. Proteins were eluted by vortexing gently for 10 min at room temperature. After centrifugation, the supernatant was collected, supplemented with 0.1% 2-mercaptoethanol and 0.1% bromphenol blue, and subjected to SDS-PAGE and immunoblotting.

Gel Filtration Chromatography—All protein chromatographic steps were performed with an Amersham Biosciences FPLC system. Aliquots (100 μl) of cell extracts in BB5 as prepared above were size-fractionated by gel filtration chromatography with Superdex 200 (Amersham Biosciences) at 4 °C. Protein standards used for calibration of the gel filtration column included thyroglobulin (669 kDa), ferritin (440 kDa), catalase (232 kDa), lactose dehydrogenase (140 kDa), bovine serum albumin (67 kDa), carbonic anhydrase (30 kDa), and α-lactalbumin (14.4 kDa). The protein samples fractionated by gel filtration chromatography were precipitated with trichloroacetate, and each was resolved in 50 μl of the SDS sample buffer. Five microliters of each sample were subjected to SDS-PAGE and immunoblotting. Two or three independent experiments obtained similar results at each time point.

RESULTS

KaiA, KaiB, and SasA Interact with KaiC in a Circadian Manner—To analyze temporal dynamics of clock protein interactions, we first evaluated the temporal accumulation profiles of the Kai proteins and SasA in *Synechococcus* cells. Soluble protein extracts were prepared from cells that had been collected at 4-h intervals either during one LD cycle or during LL conditions. Immunoblotting analysis confirmed that the amounts of the KaiB and KaiC proteins oscillate, peaking at subjective dusk, and the amount of KaiA protein oscillates with a low amplitude rhythm under an LD cycle or LL conditions (Fig. 1*A*) as reported previously (8).

KaiC is a master circadian regulator, proposed to be a negative factor for *kaiBC* expression (7). Recent analysis suggested that KaiC is also responsible for activation of the *kaiBC* promoter (11). To examine whether KaiC interacts with other clock-related proteins, such as positive factors KaiA and SasA, in a phase-dependent manner, we performed co-immunoprecipitation analysis using anti-KaiC antiserum. The resulting immunoprecipitated materials were blotted and probed with anti-KaiA, anti-KaiB, anti-KaiC, or anti-SasA antiserum. The results demonstrated that KaiC interacts rhythmically with KaiA, KaiB, and SasA (Fig. 1*B*). KaiA, KaiB, and SasA bound to KaiC more abundantly during subjective night in LL. The

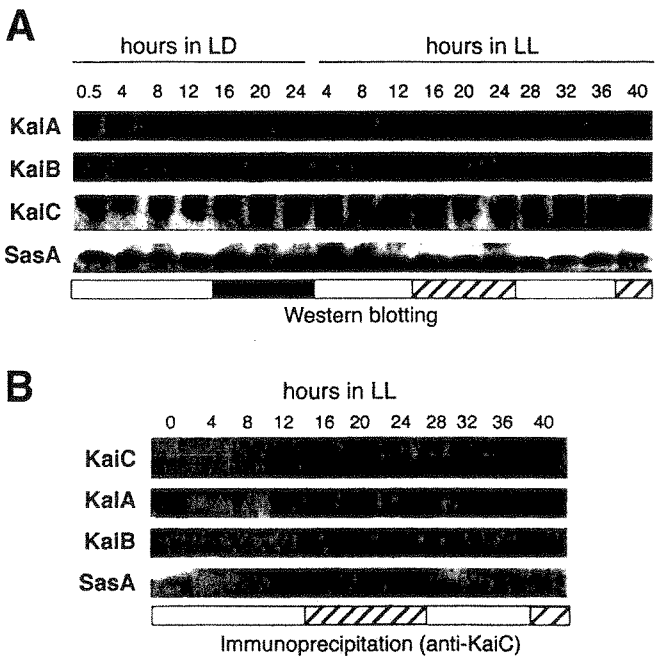

FIG. 1. **Circadian rhythms of the KaiC protein in its accumulation and association with other clock proteins.** *A*, Western blot analysis. Accumulation levels of KaiA, KaiB, KaiC, and SasA were examined. *Synechococcus* cells were collected at the indicated timing in LD and LL conditions. Total proteins (5 μg) were fractionated by SDS-PAGE on 15% gels and then analyzed by immunoblotting using antibodies of each of the anti-Kai or anti-SasA antisera. The *white*, *hatched*, and *black bars* indicate subjective day, subjective night, and darkness, respectively. *B*, co-immunoprecipitation assay. The protein extracts were used for immunoprecipitation with anti-KaiC IgG as a primary antiserum. Immune complexes were resolved and analyzed by Western blotting with specific antisera.

level of SasA interacting with KaiC was abundant at 12–16 in LL; KaiC also accumulated abundantly at this time. On the other hand, the levels of KaiA and KaiB interacting with KaiC followed the KaiC accumulation rhythms with a 4-h delay, peaking at hours 20–24 in LL (see "Discussion").

KaiA, KaiB, KaiC, and SasA Form Large Protein Complexes in a Circadian Fashion—The Kai proteins and SasA interact in a circadian manner, but the *in vivo* dynamics of their complex formation is still largely unknown. To estimate the size of clock protein-containing complexes in cells, soluble protein extracts were prepared from *Synechococcus* cells at hours 4, 10, 16, and 22 in LD cycles, size-fractionated by filtration chromatography, and then subjected to immunoblotting analyses.

As shown in Fig. 2*A*, KaiA showed a dramatic change in its size throughout an LD cycle. KaiA occurred as a complex of ~60 kDa, which is close to the size of a KaiA dimer at ZT 10, whereas it occurred as both a ~500-kDa complex and as the ~60-kDa complex at ZT 16. At ZT 22 and ZT 4, KaiA was fractionated more broadly, and the ~60-kDa complex and a fraction tail of smaller size were more abundant at ZT 4. These results indicate that KaiA forms larger protein complexes in the night and is present in smaller forms in the day.

KaiB was fractionated mainly as two portions: a broad tail of the larger fractions (200–600 kDa) and a smaller ~20-kDa fraction, which is close to the size of a KaiB dimer. At ZT 10, KaiB was mainly found in the ~20-kDa fraction. By contrast, at ZT 22 most of KaiB molecules were present in larger complex fractions, and only faint signals were detected from the ~20-kDa portion.

KaiC forms protein complexes of ~350 kDa at ZT 4 and 10, whereas it was present in larger complexes of 500–670 kDa at ZT 16 and 22. Less KaiC was detected at ZT 10 and 16 in a

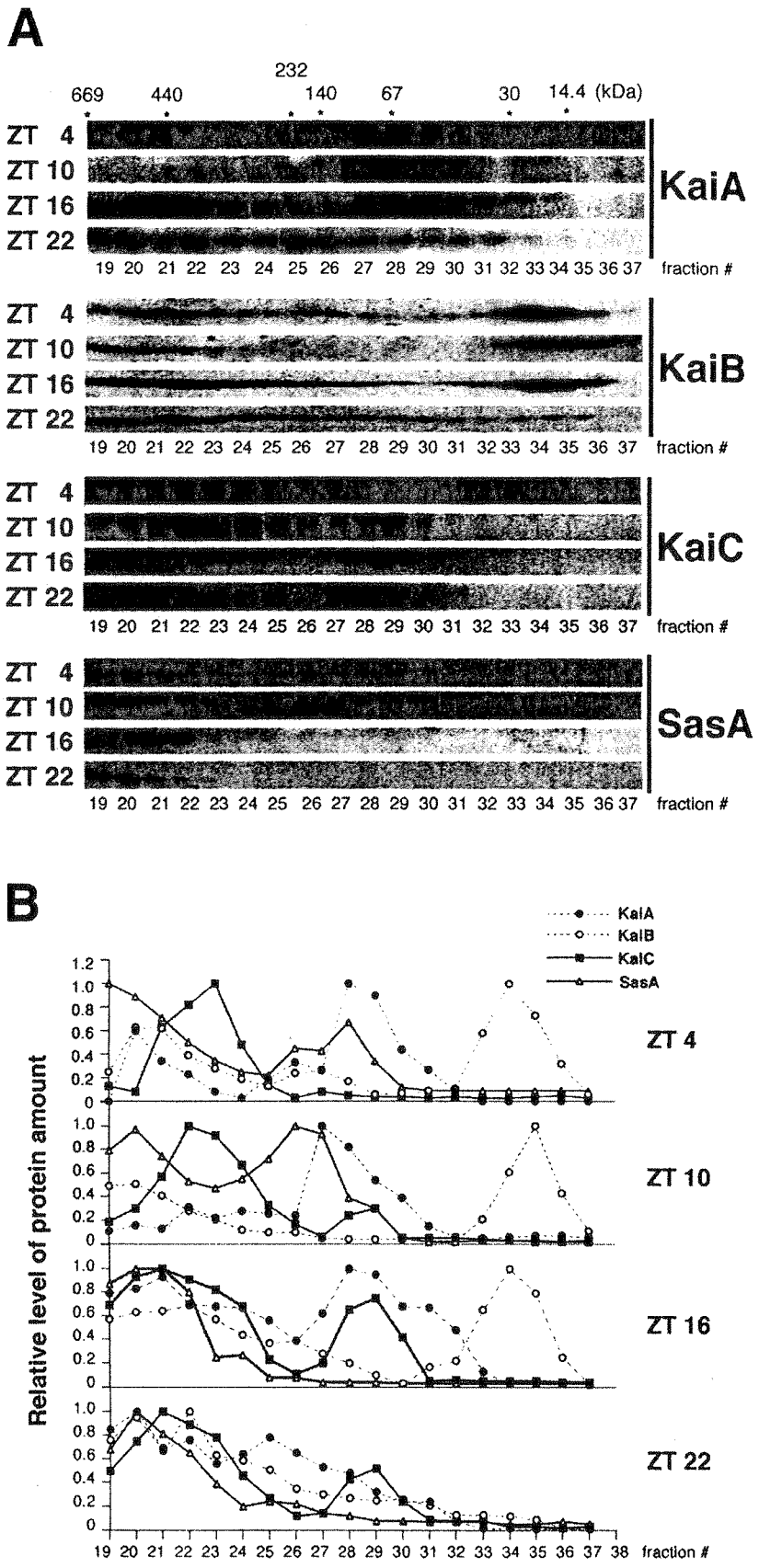

FIG. 2. **Nighttime-specific formation of clock protein complexes under LD cycle conditions.** *A*, *Synechococcus* cells were collected at hours 4, 10, 16, and 22 in an LD cycle (noted as ZT 4, 10, 16 and 22; ZT 0 indicates dawn time in an LD cycle), and cell extracts were size-fractionated by gel filtration chromatography. Each fraction was analyzed by immunoblotting with specific antisera. *Asterisks* indicate the peaks of standard proteins and their native molecular size. Two or three independent experiments obtained essentially the same patterns: representative data are shown here. *B*, densitometric data of *panel A* are shown to emphasize that clock-related proteins were detected in different fractions from each other in a daytime, whereas they were co-fractionated in a nighttime. The maximal level for each protein was set as 1.

fraction of the ~60-kDa portion, which might corresponded to its monomeric form.

SasA was found during the daytime (ZT 4 and 10) in mainly two portions, peaking at 400–600 and 200 kDa, respectively. In the nighttime (ZT 16 and 22), the 200-kDa signal disappeared, and SasA was present as large protein complexes of 400–600 kDa. As summarized in Fig. 2*B*, these data show that during the night all four clock-related proteins were mainly co-frac-

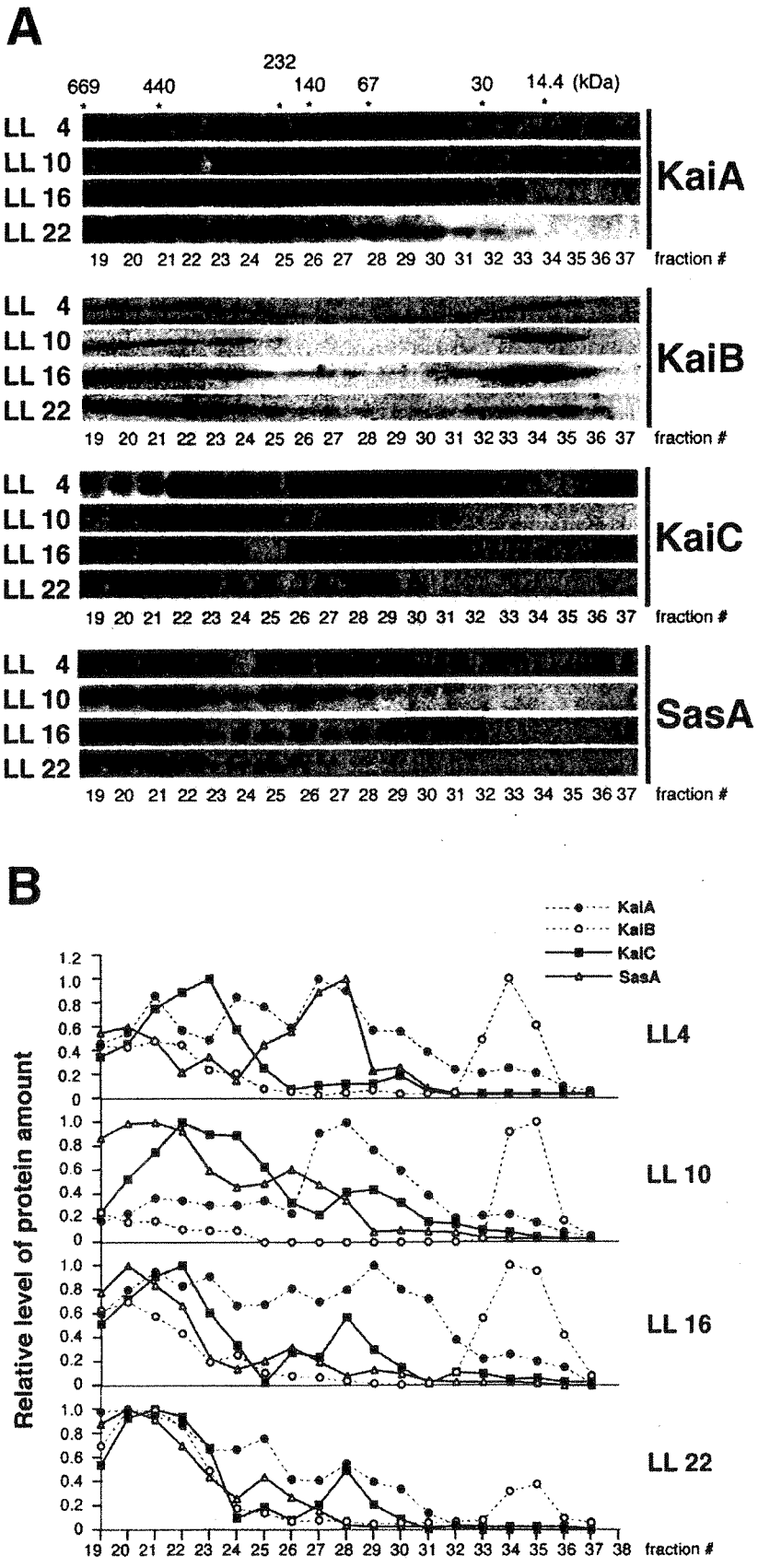

FIG. 3. **Circadian rhythm in clock protein complex formation under LL conditions.** *A*, *Synechococcus* cells were collected at hours 4, 10, 16, and 22 in LL, and cell extracts were size-fractionated by gel filtration chromatography followed by immunoblotting as described in Fig. 2*A*. Similar data were obtained from two or three independent experiments for each time point: representative data are shown here. *B*, densitometric data of *panel A* are shown. Note that in LL conditions, the clock-related proteins were detected in different fractions from each other during subjective daytime, whereas they were co-fractionated during subjective nighttime. The maximal level for each protein was set as 1.

tionated in ~400–600-kDa portions, whereas they separated into different fractions during the daytime, especially at ZT 10.

Next we examined the size of the clock-related proteins in cells cultured under LL conditions after two LD cycles (Fig. 3*A*). The results were essentially similar to those under LD cycles. Clock-related protein molecules were more abundant during subjective night, occurring as 400–600-kDa protein complexes, and they separated into different fractions during

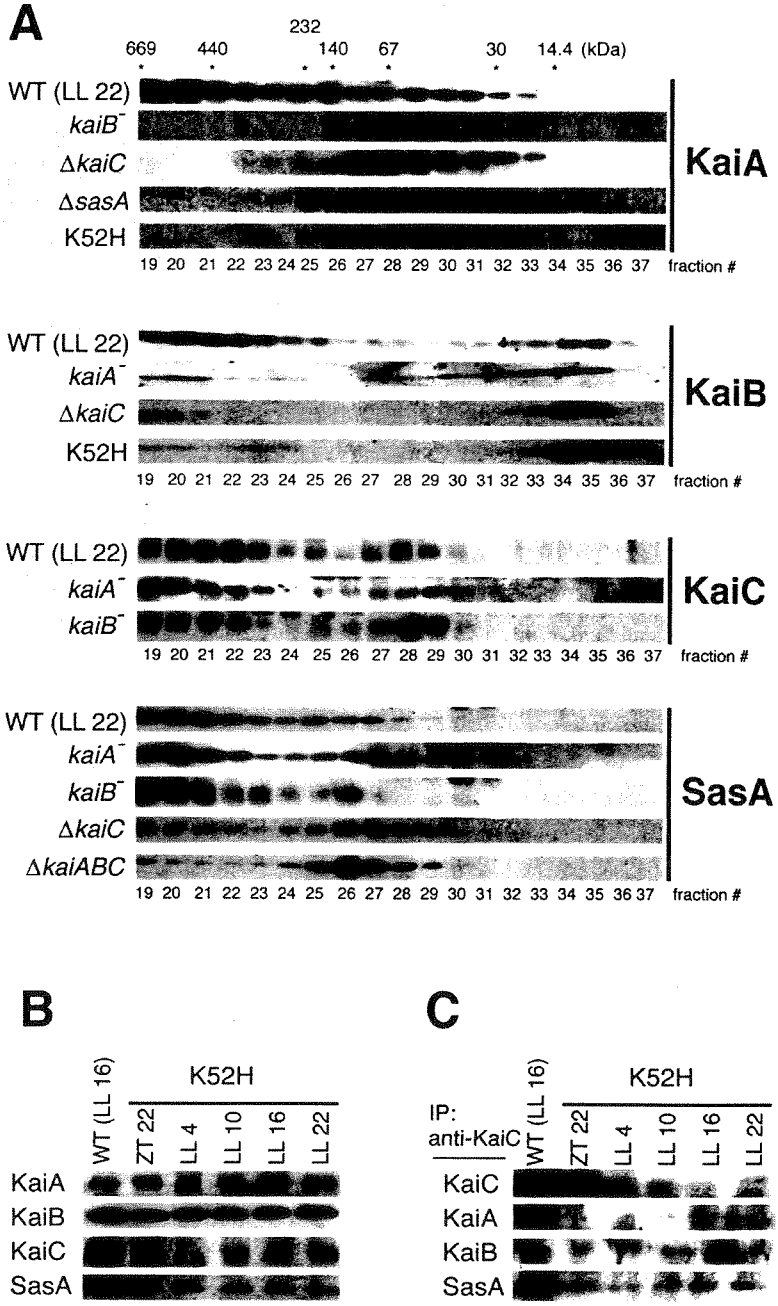

FIG. 4. **Effects of inactivation of *kai* genes and *sasA* on formation of clock protein complexes.** *A*, gel filtration assay followed by immunoblotting analysis. Cell extracts were collected from *kaiA*-inactivated (*kaiA*$^-$), *kaiB*-inactivated (*kaiB*$^-$), *kaiC*-disrupted (Δ*kaiC*), *kaiABC* cluster-depleted (Δ*kaiABC*), and *sasA*-disrupted (Δ*sasA*) strains and an arrhythmic KaiC P-loop mutant (K52H) strain. Gel filtration and immunoblotting assays were performed as described in Fig. 2*A*. Profiles of subjective night-specific large clock protein complex formations in wild-type strains are also shown as a control (*WT*). The Kai proteins and SasA did not form large protein complexes in the *kaiC*-disrupted and K52H strains. *kaiA*- and *kaiB*-null mutants also showed abnormalities in clock protein complex formation (see text). Note that in these arrhythmic mutants, each clock protein showed no circadian change in its size by the gel filtration assay (data not shown). *B*, expression of KaiABC and SasA proteins in the KaiC(K52H) mutant strain examined by immunoblotting. Note that accumulation of KaiC was dramatically lowered in the mutant throughout a day. *C*, immunoprecipitation analysis using anti-KaiC antibody for the KaiC(K52H) strain. The cell extracts were analyzed as described in Fig. 1*B*. The *asterisks* indicate cross-reacting signals due to anti-IgG. *IP*, immunoprecipitation.

subjective day (Fig. 3*B*). All these results support the hypothesis that the clock-related proteins interact with each other and form large protein complexes during (subjective) night and tend to dissociate from each other during (subjective) day.

Effects of Disruption of Clock Genes on the Size of the Clock Protein Complexes—To characterize the nighttime-specific large complexes, we performed gel filtration chromatography on the Kai and SasA proteins from various clock gene-inactivated strains (Fig. 4*A*). Inactivation of the *kaiA*, *kaiB*, or *kaiC* gene each abolishes circadian rhythms (7), and disruption of the *sasA* gene reduces *kaiBC* expression with lowered amplitude and a shortened period length in a light intensity-dependent manner (11).

In both *kaiB*- and *kaiC*-null mutants, KaiA failed to form the 400–500-kDa complex and was present predominantly as the ~60-kDa form throughout the day (Fig. 4*A*; data not shown). These results indicate that both KaiB and KaiC are required for the 400–600-kDa KaiA-containing complex during the (subjective) night. KaiB also failed to form the large complex in both *kaiA*- and *kaiC*-null mutants and was exclusively present as a 20-kDa form. Thus, both KaiA and KaiC are necessary for the large KaiB-containing protein complex.

In both *kaiA*- and *kaiB*-null strains, KaiC and SasA were co-present as 440–670-kDa forms, which are significantly larger than the major form of the night-specific KaiC complex. The size of these complexes is, however, very close to that of the larger SasA complex or larger tail of the KaiC complex in the wild-type strain in LL 22 (Fig. 4*A*). The 440–670-kDa SasA-containing complex in the mutant strains probably contains KaiC because this form is dramatically reduced in the *kaiC*-null mutant (Fig. 4*A*). These results support the hypothesis that SasA serves as a main partner for KaiC in the absence of KaiA or KaiB (see "Discussion").

We also characterized the size of Kai protein complexes in the *sasA*-deficient strain under LL conditions (50 μmol m^{-2} s^{-1}). Under these conditions, the mutant strain is arrhythmic with severely reduced levels of KaiB and KaiC (11). KaiA was fractionated as ~60-kDa proteins in the *sasA*-null mutant and

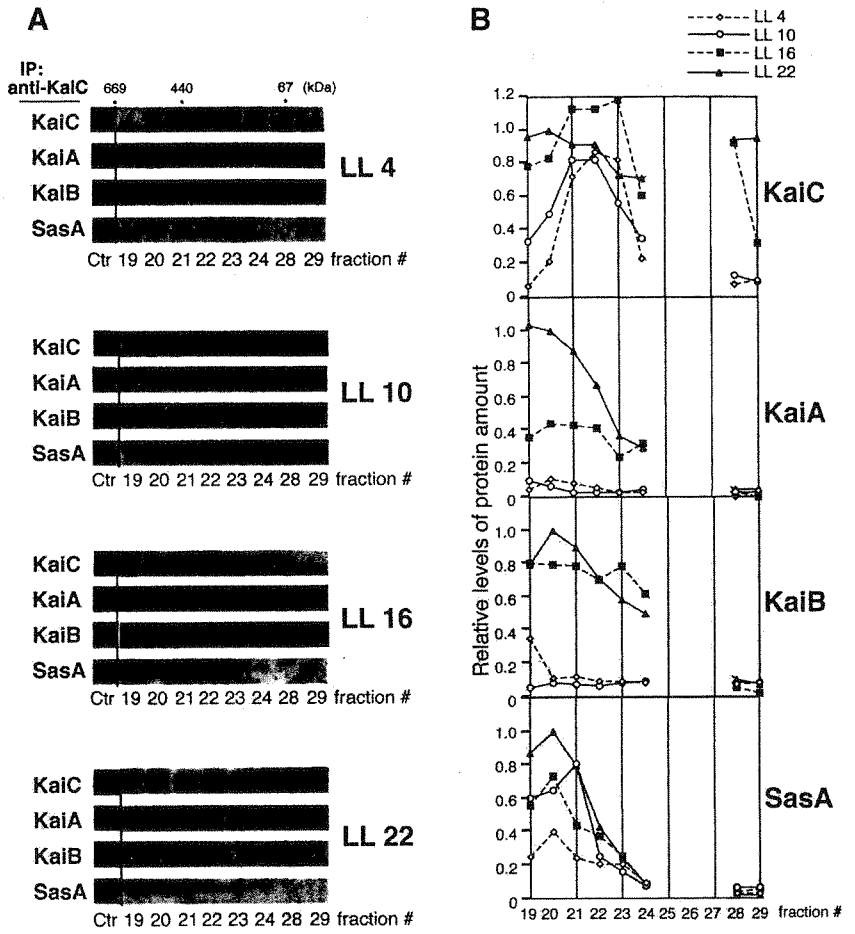

FIG. 5. **KaiA, KaiB, and SasA co-exist in the large KaiC-containing protein complexes.** *A*, co-immunoprecipitation assay following the gel filtration chromatography analysis. Cell extracts from the wild-type *Synechococcus* strain were prepared at the indicated times in LL and were size-fractionated by gel filtration chromatography as described in Fig. 3*A*. The KaiC-containing fractions (19–24, 28, and 29 in Fig. 3*A*) were then subjected to immunoprecipitation assay with anti-KaiC IgG followed by immunoblotting as described in Fig. 1*B*. Five micrograms each of total cell extracts were used as control input samples (*Ctr*). *B*, densitometric data of *panel A* were used to compare the strength of interactions between KaiC and KaiA, KaiB, or SasA in each fraction, dependent on circadian time. The maximal level of each protein in a circadian cycle was set to 1. *IP*, immunoprecipitation.

was not present in the 400–600-kDa fractions as was the case in the *kaiC*-deficient strain (Fig. 4*A*). We were unable to obtain reliable data on the size of these proteins by gel filtration because of their low concentrations.

To better understand the relationship between a biochemical property of KaiC and the protein complex formation, we analyzed *in vivo* clock protein behaviors in a KaiC(K52H) strain in which an ATP-binding domain of KaiC (P-loop1) was mutated (9). This mutation dramatically reduces the ATP binding activity of KaiC *in vitro*, and the mutant cyanobacterial strain nullifies the circadian clock (9). We first examined the level of the Kai proteins and SasA in the mutant. Accumulation of all four proteins did not exhibit any detectable circadian fluctuations (Fig. 4*B*). Compared with wild-type strains, KaiA and KaiB were present constitutively at relatively high levels. In contrast, the accumulation level of KaiC was reduced dramatically in this strain (Fig. 4*B*). Because the *kaiBC* promoter activity is not evidently down-regulated in the KaiC(K52H) strain (9), it is plausible that the ATP binding property is important for stability of the KaiC protein. The level of SasA in the mutant strain was similar to that in the wild-type cells. Immunoprecipitation analysis using anti-KaiC antiserum failed to detect KaiC-interacting KaiA or KaiB protein, but faint signals were observed for SasA bound to KaiC (Fig. 4*C*). Gel filtration analysis followed by immunoblotting confirmed that, in the KaiC(K52H) mutant, KaiA and KaiB did not form the protein complexes of >400 kDa and instead were found only in distinct fractions of ~60 and ~14 kDa, respectively (Fig 4*A*). SasA was dominantly found as a complex of ~140 kDa, while lesser amounts of SasA were also detected broadly in fractions of ~400–600 kDa (data not shown). These profiles were essentially the same as in the *kaiC*-deficient mutant (Fig. 4*A*) and were the same as the day phase patterns in the wild-type strain (Fig. 3).

KaiC Forms Large Protein Complexes with KaiA, KaiB, and SasA—All the results mentioned above support KaiC as a scaffold protein for the heteromultimeric clock protein complexes. Thus, an immunoprecipitation assay with anti-KaiC antiserum was performed using KaiC-containing fractions after the gel filtration assay (fractions 19–24, 28, and 29), and results were examined to determine whether KaiA, KaiB, and SasA were co-precipitated with KaiC. As shown in Fig. 5, *A* and *B*, KaiA and KaiB interacted with KaiC solidly in the 400–600-kDa fractions, peaking at ~500 kDa during the subjective night. The SasA protein interacted with KaiC in the 400–670-kDa complexes, especially in the 500–670-kDa region. The level of SasA bound to KaiC also exhibited a circadian rhythm, while the amplitude was lower compared with the rhythms of KaiA and KaiB interacting with KaiC. These results further confirmed that the Kai proteins and SasA interact to form 400–670-kDa protein complexes in a circadian fashion.

DISCUSSION

We have previously demonstrated that KaiC enhances KaiA-KaiB interaction *in vitro* and in the yeast two-hybrid system and predicted formation of a heteromultimeric complex that contains the three Kai proteins (10). We also reported limited information on KaiC-SasA and KaiB-SasA interactions in cyanobacteria by immunoprecipitation analysis at two points of the day (11). In contrast, this report provides more comprehensive details on *in vivo* dynamics of the clock protein complex formation, which must be a basis for understanding molecular actions of these circadian clock elements in the cell.

Our results showed that the Kai proteins and SasA are present in various complexes during the circadian cycle. In the subjective day, KaiC forms complexes ranging from 350 to 440 kDa. The small KaiC-containing complex (350 kDa; *fraction 23* in Figs. 2 and 3) corresponds to the size of a KaiC hexamer (calculated mass of 354 kDa). This could be possible because the amino acid sequence of KaiC is similar to those of RecA/DnaB superfamily proteins, which generally form hexamers (12). In the subjective night, KaiC additionally forms larger protein complexes, most commonly around 500 kDa (Figs. 2 and 3). Importantly, in *kaiC*-null mutant strains, KaiA, KaiB, and SasA did not form the large complexes, and all four clock proteins were dissociated from each other (Fig. 4*A*). Therefore, we propose a role for KaiC (or the KaiC hexamer) as a scaffold protein to form the large heteromultimeric clock protein complexes.

In addition to the complexes of >300 kDa, we observed that KaiA and KaiC from wild-type cells were also co-fractionated in ~60-kDa fractions (Fig. 3). Two observations suggest that KaiA and KaiC are not associating with each other in a 60-kDa complex. First, these small KaiA and KaiC signals were not affected in *kaiC*- and *kaiA*-inactivated mutants, respectively (Fig. 4*A*). Second, these ~60-kDa forms of KaiA and KaiC did not co-immunoprecipitate (Fig. 5). Thus, these signals might simply represent a KaiA dimer (calculated mass of 65.2 kDa) and a KaiC monomer (58.0 kDa).

Our results also revealed the importance of SasA for formation of heteromultimeric clock protein complexes. Because the KaiC-interacting sensory domain of SasA is similar to the full-length KaiB protein, KaiB and SasA have been proposed to compete with each other for binding to KaiC (11). Consistently in the *kaiB*-inactivated strain we found abnormal dominance of 500–670-kDa forms of KaiC, which co-fractionated with SasA. Dominance of these forms of KaiC was also observed in *kaiA*-null mutants, in which the levels of KaiB and KaiC were reduced, although the level of SasA was not affected (Fig. 4*A*). Thus, molecular excess of SasA compared with KaiB and the absence of KaiA-KaiC interaction both could enhance KaiC-SasA interaction and reduce KaiB-KaiC association in the *kaiA*-inactivated strain.

SasA is dominantly present as a 140–200-kDa form at CT 4 in the wild-type strain and throughout the circadian cycle in the *kaiC*-null and *kaiABC*-null mutants. Thus, SasA is capable of forming a multimeric protein complex even without the Kai proteins. Because histidine kinases often dimerize, a SasA dimer may be interacting solidly with a still unknown cognate response regulator to form the 140–200-kDa complex. Note that homotypic interaction of SasA has been demonstrated *in vitro* previously (11). The night-specific 500–670-kDa KaiC-containing complex might be formed by the binding of a 140–200-kDa SasA complex to a KaiC hexamer, which conjugates with KaiA and/or KaiB according to subjective time. So far, however, we do not have any evidence that SasA binds indirectly to KaiA or KaiB through association with a KaiA/KaiB-interacting KaiC complex. This lack of evidence is because our anti-KaiA, anti-KaiB, and anti-SasA antisera are not sufficient for immunoprecipitation studies. Nevertheless, it is plausible that there are several co-existing populations of multimeric complexes even during the late subjective night. It is necessary to find detailed stoichiometry of the complexes to gain a better understanding of the characteristics of the clock proteins.

How do the clock protein complexes function for circadian timing in the cell? Considering a temporal profile of the clock protein complexes and a circadian *kaiBC* expression pattern, we speculate a certain day/night-specific Kai/SasA complex could be either a positive or negative regulator at certain times

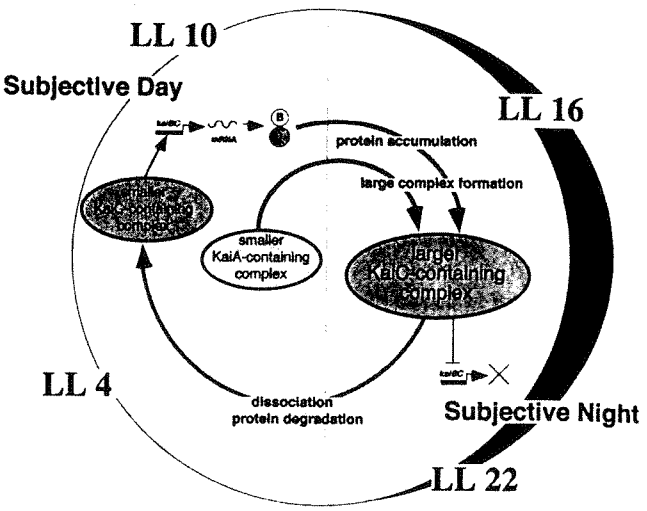

FIG. 6. **A possible model for circadian formation and functions of clock protein complexes.** The details of this model are described in the text (see "Discussion"). *B* and *C* in *white* and *gray circles* indicate KaiB and KaiC proteins respectively. × represents transcriptional inactivation of KaiBC mRNA.

of the day for *kaiBC* gene expression. When the *kaiBC* expression level is low at CT 0 the Kai/SasA proteins form large complexes. By contrast, when the *kaiBC* mRNA level is high at CT 8–10 (7, 11), the Kai proteins and SasA dissociate from each other. Fig. 6 illustrates one possibility for a *kaiBC* regulatory loop by these protein complexes. In the early subjective day, a smaller (~60-kDa) KaiA-containing protein complex, possibly a KaiA dimer or a KaiB monomer or dimer, and a ~350-kDa KaiC-containing protein complex (a hexamer?) accumulate in the *Synechococcus* cells. Thus, the small KaiA complex and/or the 350-kDa (smaller) KaiC complex may function as positive elements. There has been a speculation that the KaiC protein has some positive function (11, 13). As a result, KaiB and KaiC accumulate, peaking at CT 16 at which time KaiA, KaiB, and SasA interact with the KaiC hexamer and *kaiBC* expression becomes reduced. At around CT 22, most KaiA, KaiB, and SasA molecules are complexed with KaiC, and the *kaiBC* mRNA reaches its trough level. We suggest the large KaiC complexes containing KaiA, KaiB, and SasA as negative regulators. When these complexes start dissociating and the KaiB and KaiC protein levels decrease in the next subjective early morning, the *kaiBC* transcription begins increasing by derepression. Interestingly, the peak of the Kai protein association is delayed several hours compared with that of KaiB and KaiC accumulation (Figs. 1 and 2). This may be an important step for producing a delay in the negative action to achieve proper 24-h molecular periodicity.

We do not yet know how these protein complexes activate or inhibit the *kaiBC* promoter. It is possible that these protein complexes contain as yet unknown transcriptional activators or inhibitors. Alternatively, the circadianly changing KaiC-containing complexes might affect the topology or superhelicity of the chromosomal DNA, thereby affecting gene expression, as proposed (4) with respect to a similarity of the primary structure of KaiC to those of RecA (recombinase) and DnaB (DNA helicase). Moreover, KaiC was recently found to be phosphorylated in a circadian fashion (13), and protein-protein interaction would affect this KaiC phosphorylation to modulate activities of the complexes.

Finally, we found the accumulation level of KaiC was severely reduced in the KaiC(K52H) strain (Fig. 4*B*). As the *kaiBC* promoter activity is not evidently down-regulated in this mutant (9), an ATP binding activity is probably important for

the stability of the KaiC protein. Dissociation between the KaiA and KaiB proteins and their failure to form large protein complexes in the P-loop mutant seem primarily due to a dramatic loss of KaiC accumulation (Fig. 4*B*). The KaiC level was too low in this mutant to obtain reliable information on the size of the mutant KaiC complex by the gel filtration assay under our experimental conditions. Another discovery related to the stability of the Kai proteins is the relatively enhanced accumulation levels of KaiB and KaiC in ZT 12–24 compared with those in CT (LL) 12–24 in the wild-type strains (Fig. 1). Although we do not know whether this is due to a dark/light-dependent control on transcription, translation, or degradation, this phenomenon might be related to entrainment of the clock by photic stimuli.

Acknowledgments—We thank Takahiro Nakamura (Nagoya University), Takashi Kageyama (Kyoto University), and Toshio Iwasaki (Nippon Medical School) for technical suggestions, Jun Tomita (Nagoya University) for helpful discussion on the Kai protein accumulation profiles, Taeko Nishiwaki (Nagoya University) for the *Synechococcus* KaiC(K52H) strain, and our laboratory members for valuable comments.

REFERENCES

1. Dunlap, J. C. (1999) *Cell* **96,** 271–290
2. Young, M. W., and Kay, S. A. (2001) *Nat. Rev. Genet.* **2,** 702–715
3. Iwasaki, H., and Kondo, T. (2000) *Plant Cell Physiol.* **41,** 1013–1020
4. Mori, T., and Johnson, C. H. (2001) *Semin. Cell Dev. Biol.* **12,** 271–278
5. Kondo, T., Strayer, C. A., Kulkarni, R. D., Taylor, W., Ishiura, M., Golden, S. S., and Johnson, C. H. (1993) *Proc. Natl. Acad. Sci. U. S. A.* **90,** 5672–5676
6. Kondo, T., Tsinoremas, N. F., Golden, S. S., Johnson, C. H., Kutsuna, S., and Ishiura, M. (1994) *Science* **266,** 1233–1236
7. Ishiura, M., Kutsuna, S., Aoki, S., Iwasaki, H., Andersson, C. R., Tanabe, A., Golden, S. S., Johnson, C. H., and Kondo, T. (1998) *Science* **281,** 1519–1523
8. Xu, Y., Mori, T., and Johnson, C. H. (2000) *EMBO J.* **19,** 3349–3357
9. Nishiwaki, T., Iwasaki, H., Ishiura, M., and Kondo, T. (2000) *Proc. Natl. Acad. Sci. U. S. A.* **97,** 495–499
10. Iwasaki, H., Taniguchi, Y., Ishiura, M., and Kondo, T. (1999) *EMBO J.* **18,** 1137–1145
11. Iwasaki, H., Williams, S. B., Kitayama, Y., Ishiura, M., Golden, S. S., and Kondo, T. (2000) *Cell* **101,** 223–233
12. Leipe, D. D., Aravind, L., Grishin, N. V., and Koonin, E. V. (2000) *Genome Res.* **10,** 5–16
13. Iwasaki, H., Nishiwaki, T., Kitayama, Y., Nakajima, M., and Kondo, T. (2002) *Proc. Natl. Acad. Sci. U. S. A.* **99,** 15788–15793

7）体内時計の光位相同調とメラトニン出力系の調節メカニズム（研究代表者：深田吉孝（東京大学））

研究代表者：　深田吉孝　（東京大学大学院理学系研究科　教授）
研究分担者：　岡野俊行　（東京大学大学院理学系研究科　講師）

Ⅰ．研究目的と概要

多くの生物が持つ概日時計は、自らの位相を外界の周期的な環境変化に応じて調節できるという特徴をもつ。概日時計の同調因子としては、温度変化や摂餌など様々な要因が知られているが、全ての生物に共通、かつ最も重要な同調因子が光、すなわち外界の明暗周期である。本研究では、約24時間周期で自己発振する概日時計が、外界の環境因子の周期的変動に同調する分子メカニズムを細胞レベルで明らかにすることを目標とした。このような解析には、培養条件においても自律的な時計発振機構を保持し、メラトニンの分泌プロファイルや時計遺伝子の発現パターンなどが顕著な概日リズムを示す細胞が適している。これらの特徴を備えた材料として、ニワトリ松果体・ゼブラフィッシュ松果体・マウス視交叉上核・哺乳類培養細胞株を選び、研究対象とした。なかでもニワトリやゼブラフィッシュの松果体は、個体や培養条件下において敏感に光に感じて内在性の時計が同調するという特徴を示すので、その利点を生かし、発振系に入力する光情報伝達経路に重点を置いた研究を行った。

Ⅱ．研究成果

(1) ニワトリ松果体に特異的に発現する光受容体ピノプシンの大量発現系を構築し、その光反応特性を網膜の光受容分子と比較解析した。その結果、ピノプシンは錐体型光受容体と桿体型光受容体の両方の機能を併せ持つユニークな光受容体であることを見出した[原著論文(3, 13)]。一方、ピノプシン遺伝子の転写が光刺激と共に誘導されることを見出し、これまで動物遺伝子では未知であった光誘導に関わるシスエレメントの同定を試みた。その結果、ピノプシン遺伝子上流のEボックス配列CACGTGを含む18塩基のDNA配列が光転写誘導に必須であることを突きとめた［原著論文(21)]。

(2) ニワトリ松果体におけるピノプシン下流の光情報伝達経路を調べ、ピノプシンと共役する分子として3量体G蛋白質である網膜桿体型トランスデューシン(Gt1)とG11を同定した。Gt1は百日咳毒素感受性のG蛋白質であり、従来の薬理学的知見と考え併せると、松果体のGt1経路はおそらく光によるメラトニン分泌の急性抑制効果を担うと考えられた。一方、ニワトリ松果体G11αのcDNAクローニングや蛋白質の局在・性状解析などから、G11を介する情報伝達経路が概日時計の位相シフトを引き起こすことを示した［原著論文(8, 9, 23)]。

(3) 1990 年代後半から、ショウジョウバエ時計遺伝子のホモログが哺乳類において相次いでクローニングされ、ショウジョウバエで提唱された時計発振の自律制御フィードバックループモデルが哺乳類の時計発振系にもあてはまると考えられた。私共は、ニワトリ松果体に発現する時計遺伝子（候補）*cPer2*, *cPer3*, *cBmal1*, *cClock*, *cCry1*, *cCry2* の全長 cDNA を単離・同定し、その過程で BMAL1 と相同性を示す新規 bHLH-PAS 型転写因子 BMAL2 を発見した。これら一群のニワトリ松果体時計遺伝子産物の性状を詳細に解析した結果、bHLH-PAS 型転写因子である cCLOCK と cBMAL1/2 が正の制御因子として E ボックスを介して *cPer2* の転写を活性化し、その産物である cPER2 が負の制御因子として自分自身の転写を抑制するというフィードバックモデルが推定された [原著論文(14, 18, 19)]。

(4) ディファレンシャルディスプレイ法を用いて新規の時計構成分子・光入力関連分子を探索し[原著論文(22)]、bZIP 型の転写因子 cE4BP4 を同定した。ショウジョウバエにおいて、*cE4bp4* 遺伝子に最も高い相同性を示す遺伝子 *vri* は、遺伝学的解析によって概日時計との関連が示唆されていたものの、時計システムにおける機能は全く未知であった。そこで、ニワトリ松果体における *cE4bp4* 遺伝子の機能を解析した結果、光刺激によってニワトリ松果体の時計位相が後退する時に *cE4bp4* 遺伝子が光誘導を受け、増加した cE4BP4 蛋白質が *cPer2* の転写抑制を行うことを明らかにした。つまり cE4BP4 は、ニワトリ松果体の光位相シフト、特に光位相後退を調節する重要な時計因子と考えられた [原著論文(17)]。

(5) 光入力系と発振系との接点に注目して研究を進める過程で、ニワトリ松果体細胞の MAP キナーゼが暗期に活性化するという、明暗サイクルに同調した日周変動を示すことを見出した。この MAP キナーゼは、恒暗条件においても主観的夜に活性化する概日リズムを示すことから、時計発振系に制御されていることが判明した [原著論文(5)]。MAP キナーゼ上流の Ras、Raf1 および MEK の活性も同じ位相で変動しており、時刻情報が Ras を介して MAP キナーゼカスケードに入力していると考えられた [原著論文(15)]。また、視交叉上核においてリズミックに発現している SCOP は、ラフトにおいて K-Ras の働きを抑制することから、MAP キナーゼカスケードのリズム生成において重要な役割を果たす可能性が示唆された[原著論文(27)]。一方、MAP キナーゼの上流キナーゼ MEK に対する阻害剤を投与したところ、培養松果体の時計位相が約 8 時間も後退した。つまり MAP キナーゼは、時計の出力支配を受けつつ発振系に入力するというフィードバック効果をもち、発振系コアループに対してサブループを形成すると考えられた。MAP キナーゼの活性リズムは、ウシガエル網膜やマウス視交叉上核などでも観察され、脊椎動物の時計発振系において普遍的な役割を果たす可能性が示唆された [原著論文(10); Nakaya *et al. (submitted)*]。

(6) 概日時計発振系における MAP キナーゼカスケードの作用点を探るため、時計遺伝子産物と MAP キナーゼの相互作用を調べた。その結果、MAP キナーゼは BMAL1 と会合し、特定の

アミノ酸残基（Thr534）をリン酸化することによって BMAL1 の転写活性を抑制していることを明らかにした。また、MAP キナーゼは CRY1 や CRY2 とも結合し、リン酸化を介して CRY の転写抑制活性を阻害することを見出した［原著論文(20); Sanada *et al. (submitted)*］。

(7) 松果体や視交叉上核などの中枢組織だけでなく、肝臓や心臓などの末梢組織も時計機能をもち、これらは末梢時計と呼ばれる。末梢時計の位相同調においては、光ではなく食餌のタイミングが重要な役割を果たすが、同調因子の分子実体は未だ謎に包まれている。私共は、末梢時計のモデル系である rat-1 細胞を用いた研究から、食餌の主要成分であるグルコースが同調因子として働くことを見出した。従来から、時計同調時においては *Per* 遺伝子の急激な発現上昇が見られることが知られていたが、これとは対照的に、グルコースによる時計同調の際には *Per* 遺伝子発現のゆるやかな低下が見られた。このことから、グルコースによる時計同調には、新規の細胞内分子メカニズムが関わっていると考えられた。そこで、DNA マイクロアレイ解析によってグルコース応答遺伝子を網羅的に解析した結果、時計同調に関与する候補因子として、転写制御因子 TIEG1 と VDUP1 を同定した［原著論文(24)］。

(8) 多くの脊椎動物においては、網膜や松果体だけでなく脳深部にもオプシンタイプの光受容体が発現している。これらの脳深部光受容体は、時計の位相調節の他に、光周性や体色変化の制御など多様な生理現象に関与すると考えられてきたが、その分子実体は全く不明であった。これらの光受容分子の実体を明らかにし、その生理機能を調べるため、ゼブラフィッシュ・カエル・ハト・トカゲなどの脳内オプシンを遺伝子クローニングおよび免疫染色法により検索した［原著論文(6, 7, 11, 16)］。その結果、ゼブラフィッシュにおいては脳深部と網膜水平細胞に新規オプシンである VAL オプシンが発現していることを見出した［原著論文(6)］。また、ハトの光周性（日長変化を基にした季節性の生殖応答など）に関わる光受容分子候補として、ロドプシンが外側中隔の脳脊髄液接触ニューロンに発現していることを見出した。このロドプシン陽性細胞には、トランスデューシンをはじめ網膜視細胞と類似の光情報伝達蛋白質が共存しており、日長識別という生理機能に対する分子的な手掛かりが初めて得られた［原著論文(11)］。

(9) 個体の生理・行動リズムを支配している生物時計のメカニズムを知るためには、これまで記したような分子レベル・細胞レベルでの解析と併せて個体レベルの研究が必須である。そこで、ゼブラフィッシュを用いた実験系を構築し、サーカディアンリズム発現に重要な脳内器官である松果体を対象にして研究を行った。まず発現オプシンの同定を試みた結果、ゼブラフィッシュ松果体にはピノプシンではなく、ロドプシンに類似した新規オプシンが発現していることを見出し、これをエクソロドプシンと命名した［原著論文(4)］。エクソロドプシンは大部分の松果体細胞で発現しているのに対し、網膜の視細胞には全く発現していなかった。そこで次に、このような組織特異的な遺伝子発現を誘導するシスエ

レメントの同定を目指して、GFP をレポーターに用いて数十系統のトランスジェニック個体を作製した。松果体特異的な遺伝子発現に必要十分なエクソロドプシンプロモーター領域を絞り込んだ結果、12 塩基のエレメントを同定することができ、これを PIPE (pineal expression promoting element)と命名した [原著論文(25)]。この PIPE を活用することにより、任意の遺伝子を松果体特異的に発現するトランスジェニックゼブラフィッシュ系統を樹立する実験が可能となり、個体レベルでの解析に向けて大きな道が拓けた。

参考文献リスト

原著論文 - Refereed Papers -

1. Mikaru Yamao, Masasuke Araki, Toshiyuki Okano, Yoshitaka Fukada and Tadashi Oishi.Differentiation of pinopsin-immunoreactive cells in the developing quail pineal organ:in vivo and in vitro immunohistochemical study.Cell Tissue Res., 296, 667-671 (1999).

2. Osamu Shouno, Kamon Sanada, Tomiko Asano and Yoshitaka Fukada.Characterization of N-acylation of Goα purified from bovine retinas.NeuroReport, 10, 2999-3002 (1999).

3. Atsushi Nakamura, Daisuke Kojima, Hiroo Imai, Akihisa Terakita, Toshiyuki Okano, Yoshinori Shichida and Yoshitaka Fukada.Chimeric nature of pinopsin between rod and cone visual pigments.Biochemistry, 38, 14738-14745 (1999).

4. Hiroaki Mano, Daisuke Kojima and Yoshitaka Fukada.Exo-rhodopsin: A novel rhodopsin expressed in the zebrafish pineal gland.Mol. Brain Res., 73, 110-118 (1999).

5. Kamon Sanada, Yuichiro Hayashi, Yuko Harada, Toshiyuki Okano and Yoshitaka Fukada.Role of circadian activation of mitogen-activated protein kinase in chick pineal clock oscillation.J. Neurosci., 20, 986-991 (2000).

6. Daisuke Kojima, Hiroaki Mano and Yoshitaka Fukada.Vertebrate ancient-long opsin: A green-sensitive photoreceptive molecule present in zebrafish deep brain and retinal horizontal cells.J. Neurosci., 20, 2845-2851 (2000).

7. Keiko Okano, Toshiyuki Okano, Tomoko Yoshikawa, Atsuko Masuda, Yoshitaka Fukada and Tadashi Oishi.Diversity of opsin immunoreactivities in the extraretinal tissues of four anuran amphibians.J. Exp. Zool., 286, 136-142 (2000).

8. Atsuko Matsushita, Tomoko Yoshikawa, Toshiyuki Okano, Takaoki Kasahara and Yoshitaka Fukada.Colocalization of pinopsin with two types of G-protein α-subunits in the chicken pineal gland. *Cell Tissue Res., 299,* 245-251 (2000).

9. Takaoki Kasahara, Toshiyuki Okano, Tomoko Yoshikawa, Kazumitsu Yamazaki and Yoshitaka Fukada.Rod-type transducin α-subunit mediates a phototransduction pathway in the chicken pineal gland.*J. Neurochem., 75,* 217-224 (2000).

10. Yuko Harada, Kamon Sanada and Yoshitaka Fukada.Circadian activation of bullfrog retinal mitogen-activated protein kinase associates with oscillator function.*J. Biol.*

Chem., 275, 37078-37085 (2000).

11. Yasutaka Wada, Toshiyuki Okano and Yoshitaka Fukada.Phototransduction molecules in the pigeon deep brain.*J. Comp. Neurol., 428,* 138-144 (2000).

12. Tsuyoshi Hirota, Satoshi Kagiwada, Takaoki Kasahara, Toshiyuki Okano, Masayuki Murata and Yoshitaka Fukada.Effect of brefeldin A on melatonin secretion of chick pineal cells.*J. Biochem., 129,* 51-59 (2001).

13. Atsushi Nakamura, Daisuke Kojima, Toshiyuki Okano, Hiroo Imai, Akihisa Terakita, Yoshinori Shichida and Yoshitaka Fukada.Regulatory mechanism for the stability of the meta II intermediate of pinopsin.*J.* Biochem., *129,* 329-334 (2001).

14. Toshiyuki Okano, Momoko Sasaki and Yoshitaka Fukada.Cloning of mouse BMAL2 and its daily expression profile in the suprachiasmatic nucleus: A remarkable acceleration of *Bmal2* sequence divergence after *Bmal* gene duplication.*Neurosci. Lett., 300,* 111-114 (2001).

15. Yuichiro Hayashi, Kamon Sanada and Yoshitaka Fukada.Circadian and photic regulation of MAP kinase by Ras- and protein phosphatase-dependent pathways in the chick pineal gland.*FEBS Lett., 491,* 71-75 (2001).

16. Tomoko Yoshikawa, Toshiyuki Okano, Koichi Kokame, Osamu Hisatomi, Fumio Tokunaga, Tadashi Oishi and Yoshitaka Fukada.Immunohistochemical localization of opsins and alpha-subunit of transducin in the pineal complex and deep brain of the Japanese grass lizard, *Takydromus tachydromoides.Zool. Sci., 18,* 325-330 (2001).

17. Masao Doi, Yoshito Nakajima, Toshiyuki Okano and Yoshitaka Fukada.Light-induced phase-delay of the chicken pineal circadian clock is associated with theinduction of *cE4bp4,* a potential transcriptional repressor of *cPer2* gene.*Proc. Natl. Acad. Sci. USA, 98,* 8089-8094 (2001).

18. Toshiyuki Okano, Kazuyuki Yamamoto, Keiko Okano, Tsuyoshi Hirota, Takaoki Kasahara, Momoko Sasaki, Yoko Takanaka and Yoshitaka Fukada.Chicken pineal clock genes: Implication of BMAL2 as a bidirectional regulator incircadian clock oscillation.*Genes Cells, 6,* 825-836 (2001).

19. Kazuyuki Yamamoto, Toshiyuki Okano and Yoshitaka Fukada.Chicken pineal *Cry* genes: Light-dependent up-regulation of *cCry1* and *cCry2* transcripts.*Neurosci. Lett., 313,* 13-16 (2001).

20. Kamon Sanada, Toshiyuki Okano and Yoshitaka Fukada.Mitogen-activated protein kinase phosphorylates and negatively regulates basic helix-loop-helix-PAS transcription factor BMAL1.*J. Biol. Chem., 277,* 267-271 (2002).

21. Yoko Takanaka, Toshiyuki Okano, Kazuyuki Yamamoto and Yoshitaka Fukada.A negative regulatory element required for light-dependent pinopsin gene expression.*J. Neurosci., 22,* 4357-4363 (2002).

22. Masao Doi, Yoshito Nakajima, Toshiyuki Okano and Yoshitaka Fukada.Light-dependent changes in the chick pineal temperature and the expression of *cHsp90α* gene: A potential contribution of *in vivo* temperature change to the

photic-entrainment of the chick pineal circadian clock.*Zool. Sci., 19,* 633-641 (2002).

23. Takaoki Kasahara, Toshiyuki Okano, Tatsuya Haga and Yoshitaka Fukada.Opsin-G11-mediated signaling pathway for photic entrainment of the chicken pineal circadian clock.*J. Neurosci., 22,* 7321-7325 (2002).

24. Tsuyoshi Hirota, Toshiyuki Okano, Koichi Kokame, Hiroko Ikejima-Shirotani, Toshiyuki Miyata, and Yoshitaka Fukada.Glucose down-regulates *Per1* and *Per2* mRNA levels and induces circadian gene expression in cultured rat-1 fibroblasts.*J. Biol. Chem., 277,* 44244-44251 (2002).

25. Yoichi Asaoka, Hiroaki Mano, Daisuke Kojima and Yoshitaka Fukada.Pineal expression-promoting element (PIPE), a *cis*-acting element, direcs pineal-specific gene expression in zebrafish.*Proc. Natl. Acad. Sci. USA., 99,* 15456-15461 (2002).

26. Fumiko Shimizu, Kamon Sanada and Yoshitaka Fukada.Purification and immunohistochemical analysis of calcium-binding proteins expressed in the chick pineal gland.*J. Pineal Res., 34,* 208-216 (2003).

27. Kimiko Shimizu, Masato Okada, Katsuya Nagai and Yoshitaka Fukada.Suprachiasmatic nucleus circadian oscillatory protein, a novel binding partner of K-Ras in the membrane rafts, negatively regulates MAPK pathway.*J. Biol. Chem.* (in press).

英文総説など - Invited Papers and Reviews -

1. Daisuke Kojima and Yoshitaka Fukada.Non-visual photoreception by a variety of vertebrate opsins.in: *"Rhodopsins and Photo-transduction"* (J.A.Goode, ed.), pp. 265-279,John Wiley & Sons, Chichester, UK (1999).

2. Toshiyuki Okano and Yoshitaka Fukada.Photoreceptors in pineal gland and brain: Cloning, localization and over-expression.in: *"Methods in Enzymology" Vol.316, "Vertebrate Phototransduction and the Visual Cycle"* Part B (K. Palczewski, ed.), pp.278-291, Academic Press (2000).

3. Takahiko Matsuda and Yoshitaka Fukada.Functional analysis of farnesylation and methylation of transducin.in: *"Methods in Enzymology" Vol.316, "Vertebrate Phototransduction and the Visual Cycle"* Part B (K. Palczewski, ed.), pp. 465-481, Academic Press (2000).

4. Toshiyuki Okano and Yoshitaka Fukada.Photoreception and circadian clock system of the chicken pineal gland.*Microscopy Research and Technique , 53,* 72-80 (2001).

5. Yoshitaka Fukada and Toshiyuki Okano.Circadian clock system in the pineal gland.*Mol. Neurobiol., 25,* 19-30 (2002).

日本語総説・著書など

1. 深田吉孝、岡野俊行 (1999) 松果体：光受容．『生物時計の分子生物学』(海老原史樹文、深田吉孝 編) pp. 139-150, シュプリンガーフェアラーク東京．

2. 深田吉孝、笠原和起 (1999) 脳内光受容タンパク質ピノプシン．『光シグナルトランスダク

ション』（蓮沼仰嗣、木村成道、徳永史生 編）pp. 146-151, シュプリンガーフェアラーク東京.

3. 深田吉孝、橋本祐一（1999）視細胞の光シグナル伝達を担うGタンパク質. 『光シグナルトランスダクション』（蓮沼仰嗣、木村成道、徳永史生 編）pp. 165-171,シュプリンガーフェアラーク東京.

4. 深田吉孝(1999)脂質共有結合による蛋白質機能調節.概説. 蛋白質 核酸 酵素 増刊号『脂質の分子生物学と病態生化学』（井上圭三・西島正弘 編集）Vol.44, No.8, pp.1319-1320.

5. 萩原健一、深田吉孝(1999)脂肪酸アシル化およびイソプレニル化による蛋白質機能の調節. 蛋白質 核酸 酵素 増刊号『脂質の分子生物学と病態生化学』（井上圭三・西島正弘 編集）Vol.44, No.8, pp.1337-1345.

6. 深田吉孝、真野弘明（1999）概日リズムと松果体の光受容分子. 生体の科学、Vol.50, No.3, 特集『時間生物学の新たな展開』、 pp.221-227.

7. 深田吉孝、林勇一郎（1999）７回膜貫通型 / G蛋白質共役レセプター / RGS. 『細胞内シグナル伝達』改訂第２版（山本雅 編）、pp.62-63, 羊土社.

8. 小島大輔、深田吉孝（1999）新規オプシンの同定：ロドプシンファミリーの多様性. 細胞工学、Vol.18, No.8, pp.1196-1204.

9. 岡野俊行、深田吉孝（1999）脳内光レセプター. 生物物理、Vol.39, No.4, pp.246-249.

10. 深田吉孝（1999）脳内光レセプターの多様性. 『遺伝子で生物の進化を考える 』（第13回「大学と科学」公開シンポジウム組織委員会編）、pp.79-90, クバプロ.

11. 岡野俊行、深田吉孝（1999）色覚の進化. 生物の科学 遺伝、特集：色覚のしくみと色覚異常、Vol.53, No.9, pp.39-44.

12. 深田吉孝、吉川朋子（1999）脳内光受容タンパク質とその役割. シリ.ズ・光が拓く生命科学、第１巻：生物の光環境センサ.（津田基之 編）、pp.40-52, 共立出版.

13. 吉川朋子、深田吉孝（2000）脳内光受容分子. 脳の科学、Vol.22, No.5, 特集『生物時計』、pp.527-532, 星和書店.

14. 深田吉孝、広田毅（2000）松果体とサーカディアンリズム. Clinical Neuroscience, Vol.18, No.10, 特集「サーカディアンリズムのしくみと働き」pp. 1147-1149, 中外医学社.

15. 岡野俊行、深田吉孝（2001）鳥類松果体細胞の概日時計システム. 細胞工学、Vol. 20, No. 6, 特集『生物時計：細胞はいかにして時を刻むか』、pp.837-842

16. 松田孝彦、深田吉孝(2001)タンパク質の脂質修飾. シリーズ・バイオサイエンスの新世紀、第４巻「糖と脂質の生物学」（川嵜敏祐・井上圭三 編）、pp. 201-213、共立出版.

17. 深田吉孝、小島大輔（2001）光を感じる脳 .生物時計の目.. 『生き物はどのように世界を見ているか』（和田 勝 編）, pp.101-126, 学会出版センター.

18. 深田吉孝、土居雅夫(2002)脳内光受容と体内時計の時刻調節.現代化学、No.370, pp.24-29, 東京化学同人.

19. 岡野俊行、深田吉孝（2002）体内時計の時刻を調節する遺伝子の発見. 生物の科学 遺伝、Vol. 56, No. 2, pp.26-28.

20. 深田吉孝、原田裕子 (2002) 体内時計とメラトニン合成. 現代医療、特集『体内時計と疾患.基礎と臨床』、Vol. 34, No. 6, pp. 35-40, 現代医療社.

21. 深田吉孝、浅岡洋一 (2003) 松果体の光受容と概日時計システム. 脳と神経、特集『睡眠障害と体内時計』、Vol. 55, No. 1, pp. 13-24, 医学書院.

日経産業新聞　2002年（平成14年）9月24日（火曜日）

体内時計

調節DNA特定

東大、睡眠障害など解明へ

東京大学の深田吉孝教授らのグループは生物が体内時計を調節するのに欠かせないDNA（デオキシリボ核酸）配列を発見した。光を感じ取るセンサー遺伝子の働きを抑える働きがあるという。体内時計がうまく調節できず昼夜が逆転する睡眠障害などの解明などにつながると期待される。

深田教授らは、脳で体内時計の調節にかかわる松果体の細胞をニワトリから採取。この培養細胞で、光を感じ取るセンサーの役割を果たすピノプシンと呼ぶ遺伝子の働きを詳しく調べた。

通常は松果体細胞に光を当てるとピノプシンは増加、逆に暗いところではピノプシンの働きが抑制される。ところがDNA配列上で、この遺伝子の上流にある特定の十八塩基に変異を加えると周囲が暗い場合にもピノプシンが増加した。別の実験でニワトリやマウス細胞などにこの十八塩基を導入すると、自分の下流にある遺伝子の働きを抑制した。

こうした結果から、この十八塩基は遺伝子の働きを抑える作用があることが確認できた。この塩基配列は通常、特定のたんぱく質が結びついた状態で下流の遺伝子を抑えるが、光を当てるとたんぱく質が離れ抑制作用が弱まると深田教授らはみている。

光センサー遺伝子はショウジョウバエなどで研究が進んでいるが、ヒトなどせきつい動物での解明は遅れている。今回の成果は、せきつい動物の光センサー研究の促進につながりそうだ。

日経産業新聞　2002年（平成14年）12月12日（木曜日）

光センサー質
センサーたんぱく質

働き調節する配列

東大、体内時計研究に

東京大学の深田吉孝教授らは、体内時計にかかわる脳内組織、松果体で遺伝子が働くのに欠かせない塩基配列を突き止めた。この配列を利用すれば、望みの遺伝子を松果体で働かせられる。生物の体内時計機能の詳細な研究に役立ち、睡眠障害などの解明につながるとみている。

深田教授らは実験動物ゼブラフィッシュの松果体で働くエクソロドプシンという遺伝子に着目した。この遺伝子は網膜で光を感じ取るセンサーたんぱく質の遺伝子の仲間で、働く場所だけが異なることが知られている。

この遺伝子周辺の配列を調べた結果、特定の十二個の塩基が遺伝子を松果体で機能させるのに必要なことが分かった。この配列を変えると遺伝子が松果体で働かなくなった。逆に、網膜にみられる遺伝子の上流にこの配列を導入すると、松果体でも働くようになったという。

従来、体内の時計機能を担う脳組織で遺伝子を働かせる仕組みは不明だった。この配列をうまく使えば、松果体などの組織で様々な遺伝子の作用を調べて体内時計を解明する実験ができるようになると期待している。

朝日新聞（夕刊） 2001年(平成13年)7月11日 水曜日

科学

進みすぎの生物時計 調整にかぎ

東大グループ

生物の体は睡眠など1日のサイクルを生み出す体内時計をもつ。この時計が進みすぎた場合に時刻を合わせる「竜頭」のような働きをする遺伝子を、東京大の研究グループが見つけ、米科学アカデミー紀要に発表した。時差ぼけの解明や治療法の開発などにつながる可能性がある。

発表したのは深田吉孝教授、大学院生の土井雅夫さんらだ。

生物は進化の長い歩みのなかで、明暗などに対応する約24時間周期のリズムを獲得した。時を刻む振り子の役割を果たす遺伝子は「ピリオド」と呼ばれる。

ところが、ピリオドがつくるリズムは正確には24時間ではない。このため、生物は環境に応じて時刻を合わせる仕組みをもつ。

たとえば、体内時計の夜明け前に光を感じると、「朝がきた」と認識し、それに合わせて時計を進める。反対に、体内時計は夜になったのに光が当たると、「まだ夕方」と時計を遅らせる。

こうした時計合わせで働く遺伝子は何か。ニワトリの細胞で探した。ニワトリは頭の薄い骨のすぐ下に光を感じるセンサーがあり、体内時計と直結している。

その結果、体内時計で夜に入ったときに光を当てると、E4BP4と呼ばれる遺伝子が働き出すことがわかった。この遺伝子はピリオドの働きを抑えることで、時計を遅らせていた。

「次は、時計を早める遺伝子を突き止めたい」と深田さんたちは話している。

夕刊讀賣新聞 2001年(平成13年)8月20日(月曜日)

生命館

体内時計

朝夕 別機構で調節

東大チームが仕組み解明

生物は、朝と夕方の光をそれぞれ別の機構で感じ分けることで体内時計を調節していることが、東京大学理学部の深田吉孝教授と大学院生の土居雅夫さんの研究で分かった。生物は早朝に光を受けると、「朝」を感知して体内時計を進め、夕暮れ時の光には、「まだ夕方」と感じて時計を遅らせるが、二つの機構を使い分けることで微妙な調節を可能にしているらしい。

体内時計をコントロールする時計遺伝子は、光で活性化され、時計を進めることが知られていたが、夕暮れ時の光で時計が遅れることについては不明な点が多かった。

深田教授らは、ニワトリの体内時計がある脳上部の松果体で「E4BP4」という遺伝子の働きが朝夕で異なり、夜前半に強く働くことに着目。この遺伝子が作るたんぱく質が時計遺伝子の働きを抑制することを明らかにした。

実際に生きたニワトリを使い、明るくする時間を延長して、昼の時間を長くする実験を行うと、光によってE4BP4の働きが活性化し、時計が遅れることが確認できた。

朝の光の場合は、E4BP4の活性が低いため、こうした抑制が働かず、時計遺伝子自身が光によって活性化されることで、時計が先に進むらしい。深田教授は「時差ボケの解消や睡眠障害の治療のヒントになるだろう」と話している。

Light-induced phase-delay of the chicken pineal circadian clock is associated with the induction of *cE4bp4*, a potential transcriptional repressor of *cPer2* gene

Masao Doi, Yoshito Nakajima, Toshiyuki Okano, and Yoshitaka Fukada*

Department of Biophysics and Biochemistry, Graduate School of Science, University of Tokyo, and Japan Science and Technology (JST), Core Research for Evolutional Science and Technology (CREST), Tokyo 113-0033, Japan

Edited by Steven L. McKnight, University of Texas Southwestern Medical Center, Dallas, TX, and approved May 3, 2001 (received for review February 22, 2001)

The chicken pineal gland contains the autonomous circadian oscillator together with the photic-input pathway. We searched for chicken pineal genes that are induced by light in a time-of-day-dependent manner, and isolated chicken homolog of bZIP transcription factor *E4bp4* (*cE4bp4*) showing high similarity to *vrille*, one of the *Drosophila* clock genes. *cE4bp4* was expressed rhythmically in the pineal gland with a peak at very early (subjective) night under both 12-h light/12-h dark cycle and constant dark conditions, and the phase was nearly opposite to the expression rhythm of *cPer2*, a chicken pineal clock gene. Luciferase reporter gene assays showed that cE4BP4 represses *cPer2* promoter through a E4BP4-recognition sequence present in the 5′-flanking region, indicating that cE4BP4 can down-regulate the chick pineal *cPer2* expression. *In vivo* light-perturbation studies showed that the prolongation of the light period to early subjective night maintained the high level expression of the pineal *cE4bp4*, and presumably as a consequence delayed the onset of the induction of the pineal *cPer2* expression in the next morning. These light-dependent changes in the mRNA levels of the pineal *cE4bp4* and *cPer2* were followed by a phase-delay of the subsequent cycles of *cE4bp4*/*cPer2* expression, suggesting that cE4BP4 plays an important role in the phase-delaying process as a light-dependent suppressor of *cPer2* gene.

Daily rhythms of biological activities observed in a variety of organisms from bacteria to humans are driven by endogenous oscillators called circadian clocks (1). The circadian clock autonomously oscillates even in the absence of external time cues, although the period length differs slightly from 24 h. Under natural conditions, the circadian clock is entrained (synchronized) to the 24-h day by environmental time cues, most commonly by light (2), but the molecular nature of the light-entrainment of the clock is not fully understood. In vertebrates, the central circadian clocks are located in several neuronal tissues such as the suprachiasmatic nucleus (SCN), the retina, and the pineal gland (3–7), and the oscillation seems to be generated by cell-autonomous mechanisms (8, 9). Among clock-containing cells, the chick pinealocyte is unique in that it retains not only the circadian oscillator but also intrinsic phototransduction pathway for the light-entrainment within a single cell (3, 4, 9, 10–14), providing a prominent model for the study of the light-entrainment mechanism, especially at the cellular and molecular levels (15).

Recent molecular and genetic analyses of clock genes have demonstrated that the transcription/translation-based autoregulatory feedback loop plays a central and common role in generating the circadian rhythmicity among various organisms (16, 17). In the case of *Drosophila*, clock genes such as *period*, *timeless*, *cycle* (*bmal*), *clock*, *cryptochrome*, *double-time*, and *vrille* were identified as necessary for normal circadian function (18). Although the role of *vrille* remains to be elucidated, the products of many clock genes seem to form interlocked negative feedback loops for stable oscillation of the *Drosophila* clock (19). Mammalian homologs of all of the *Drosophila* clock genes except *vrille* have been studied in relation to their roles in the circadian clock system. In mice, mCLOCK:mBMAL1 heteromer is suggested to drive transcription of three *period* genes (designated *mPer1*, *mPer2*, and *mPer3* in the mouse), two cryptochrome genes (*mCry1* and *mCry2*), and output (clock-controlled) genes such as vasopressin gene (20–22). mPER and mCRY proteins thus induced in turn inhibit the mCLOCK:mBMAL1-mediated transcription, and hence this feedback cycle generates rhythmic expression of several clock genes and output genes. The molecular framework of the circadian oscillator established in the mouse SCN appears to be applicable to that in the chicken pineal gland, in which the mRNA levels of chicken homologs, *cPer2*, *cClock*, *cBmal1*, and *cBmal2* exhibit diurnal fluctuations (ref. 23; T.O., K. Yamamoto, K. Okano, T. Hirota, T. Kasahara, M. Sasaki, Y. Takanaka, and Y.F., unpublished results). Functionally, both cCLOCK:cBMAL1 and cCLOCK:cBMAL2 complexes up-regulate *cPer2* transcription, which is subject to down-regulation by cPER2 protein (T.O., K. Yamamoto, K. Okano, T. Hirota, T. Kasahara, M. Sasaki, Y. Takanaka, and Y.F., unpublished results), suggesting that these chicken clock genes form the autoregulatory feedback loop as well. Now, the chicken pineal clock system provides a new avenue to understanding of a molecular link between the oscillator and the intrinsic photic-input pathway.

As a general feature of the light-entrainment of the clock, a light stimulus given at early and late subjective night induces the phase-delay and advance of the clock, respectively, whereas that at (early) subjective day gives little effect on the clock phase (2, 12). Because the product levels of many clock genes likely define, rather than simply reflect, the phase of the clock, the light-induced phase-shift is closely associated with light-dependent changes in the mRNA or protein levels of a subset of clock genes (16). In the case of *Drosophila*, the clock phase is reset by light-induced degradation of dTIM protein (24–27). On the other hand, in the mammalian SCN, the mRNA levels of *Per1*

NEUROBIOLOGY

This paper was submitted directly (Track II) to the PNAS office.

Abbreviations: LD, light/dark; DD, constant darkness; SCN, suprachiasmatic nucleus; CT, circadian time; RACE, rapid amplification of cDNA ends; RT, reverse transcription; DBP, D-site binding protein.

Data deposition: The sequences reported in this paper have been deposited in the GenBank database (accession nos. AF335427 and AF335428).

*To whom reprint requests should be addressed at: Department of Biophysics and Biochemistry, Graduate School of Science, University of Tokyo, Hongo 7-3-1, Bunkyo-Ku, Tokyo 113-0033, Japan. E-mail: sfukada@mail.ecc.u-tokyo.ac.jp.

The publication costs of this article were defrayed in part by page charge payment. This article must therefore be hereby marked "*advertisement*" in accordance with 18 U.S.C. §1734 solely to indicate this fact.

and *Per2* genes rapidly increase in response to a brief light stimulus that induces a phase-shift of the clock (28–32). In contrast to the short-light-pulse-induced phase-shift, the phase-shift induced by a nonphotic stimulus such as a wheel-running action is accompanied by a rapid decrease in the mRNA levels of the SCN *Per1* and *Per2* genes (33, 34). Thus, the changes (rise and fall) of the mRNA levels of *Per* genes seem to be important for the phase-shift of the SCN clock (30, 31). However, little is known about a molecular system that induces the changes of the expression levels of *Per* genes in response to the external time cues.

In the present study, we searched for chick pineal genes that are induced by light in a time-of-day-dependent manner, and isolated chicken homolog of bZIP transcription factor *E4bp4* (*cE4bp4*), which shows high similarity to *vrille*, one of the *Drosophila* clock genes (35). Here, we show several lines of evidence for an important role of cE4BP4 serving as a transcriptional repressor of *cPer2* gene in the chick pineal clock system. Noticeably, the prolonged light period, which induced a phase-delay of the chick pineal clock, up-regulates *cE4bp4* expression and delayed the onset of the *cPer2* induction in the next morning, suggesting that cE4BP4 contributes to the phase-delaying process as a light-responsive repressor of *cPer2* gene.

Materials and Methods

Animals. Animals were treated in accordance with the guidelines of the University of Tokyo. Newly hatched chicks were purchased from local suppliers, and housed under various light/dark conditions with a constant light intensity of ≈300 lux at the level of chicks. Pineal glands were isolated from killed chicks, frozen in liquid nitrogen, and kept at −80°C until subsequent analyses. All of the procedures during the dark-period were performed under dim red light (>640 nm).

Differential Display Analysis. One-day-old chicks were maintained in light/dark (LD) cycles for 7 days and transferred to constant darkness (DD) on day 8, when animals were exposed to light for 1 h from circadian time (CT) 0, CT14, or CT20, and their pineal glands were isolated at CT1, CT15, or CT21, respectively (40 chicks each). On the other hand, control animals were kept in the dark on day 8, and their pineal glands were isolated at CT1.5, CT15.5, or CT21.5 (40 chicks each). Total RNA extracted from each pool of the isolated pineal glands was reverse transcribed by using ThermoScript (Life Technologies, Grand Island, NY) with an anchored oligo(dT) primer at 55°C for 60 min. Briefly, a fixed amount (1.5 μg) of the total RNA preparation was incubated in a reaction mixture (30 μl) composed of 50 mM Tris acetate (pH 8.4), 75 mM potassium acetate, 8 mM magnesium acetate, 5 mM DTT, 1 mM each of the dNTPs, 2.5 μM anchored oligo(dT) primer (RNAimage kit, GenHunter, Nashville, TN), 60 units RNase Inhibitor (Life Technologies), and 22.5 units ThermoScript (Life Technologies). One-hundredth of this reaction mixture was subjected to PCR in a reaction mixture (10 μl) composed of 10 mM Tris·HCl (pH 8.3), 50 mM KCl, 1.5 mM $MgCl_2$, 200 μM each of the dNTPs, 1 μM anchored oligo(dT) primer, 1 μM H-AP primer (RNAimage kit, GenHunter), and 1 unit AmpliTaq (Applied Biosystems) under the following cycle conditions: 27 cycles of 94°C (30 s), 34°C (2 min), 72°C (30 s) for amplification, followed by 72°C (7 min) for final extension. The PCR products were subjected to 7.5% native PAGE, stained with SYBR Green I (Molecular Probes), and quantified by FLA-2000 bioimage analyzer (Fuji Film, Tokyo, Japan).

Cloning of *cE4bp4* cDNA. The PCR products selected in the differential display analysis were cut out from the gel and eluted by boiling in 50 μl distilled water at 95°C for 5 min. An aliquot (2 μl) of the eluted DNA solution was subjected to the secondary PCR under the same PCR conditions as those in the initial analysis. The reamplified DNA fragment was subcloned into pCR2.1TOPO vector (Invitrogen) and sequenced.

A cDNA clone including the entire coding region of *cE4bp4* gene was obtained by RACE (rapid amplification of cDNA ends), and the coding sequence of *cE4bp4* (GenBank accession no. AF335427) was amplified by PCR with a pair of primers, 5′-TGTGTGTGGATTTAAAACTACTG-3′ and 5′-ACTTTACTGTAGTACTCAGGTC-3′, which correspond to the 5′- and 3′-untranslated regions of *cE4bp4* gene, respectively. Possible PCR errors were identified and eliminated by sequencing a total of seven clones obtained from three independent PCRs.

Quantitative Reverse Transcription (RT)-PCR Analysis. Quantitative RT-PCR analyses were performed as previously described (36). PCR primers used were as follows: for *cE4bp4*, 5′-CCTTTCTCAGTTCAGGTGAC-3′ (forward) and 5′-TGAAATGACATCATGAGTCCAG-3′ (reverse); for *cPer2*, 5′-GGAAGTCCTTGCAGTGCATAC-3′ (forward) and 5′-ACAGGAAGCGGATATGCAG-3′ (reverse); for chicken TATA-box binding protein (*cTbp*; GenBank accession no. D83135), 5′-GTCGAATATAATCCCAAGCG-3′ (forward) and 5′-TCTGCTCGAACTTTAGCACC-3′ (reverse). The optimal cycle numbers for quantitative analyses were 19 for *cE4bp4*, 19 for *cPer2*, and 21 for *cTbp* under our experimental conditions.

Transcriptional Assay. LMH chicken hepatoma cells were grown in Waymouth's MB752/1 medium (Life Technologies) supplemented with 10% FBS, and plated at 5×10^6 cells per well in six-well plates. On the next day, cells in each well were transfected by using Lipofectamine plus (Life Technologies) with (*i*) indicated amount of expression plasmid containing the coding sequence of *cE4bp4* in pcDNA3.1/V5/His (Invitrogen) without introduction of any tags, (*ii*) 300 ng of firefly luciferase reporter (derivative of pGL3-Basic or pGL3-Promoter), and (*iii*) 1 ng of *Renilla* luciferase reporter, pRL-CMV (Promega), as an internal control. The total amount of expression plasmid DNA added to each well was adjusted to 2.0 μg by mixing pcDNA3.1/V5/His empty vector. Two days after transfection, the extract prepared from harvested cells was subjected to luminometry-based dual-luciferase assay (Promega), and the firefly luciferase activity was normalized by *Renilla* luciferase activity for each extract.

Reporter plasmids used were as follows: (*i*) *cPer2* promoter-*luc*: A 674-bp genomic DNA fragment of the 5′-flanking region of *cPer2* gene (GenBank accession no. AF335428; −607 to +67; +1 indicates a putative transcription initiation site estimated by 5′-RACE) was obtained by using LA PCR *in vitro* Cloning Kit (Takara Shuzo, Kyoto, Japan) according to the manufacturer's protocol. This fragment was subcloned into pGL3-Basic vector (Promega). (*ii*) mut. distal site-*luc*: The "distal site"-containing DNA fragment (−340 to −309; *Bsu*36I-*Not*I-digested fragment) of *cPer2* promoter-*luc* construct was substituted by a synthesized fragment in which the distal site (5′-GTGATGTAAC-3′; −334 to −325) was mutated to 5′-GGAGACGCTC-3′. (*iii*) mut. proximal site-*luc*: The "proximal site"-containing DNA fragment (−102 to −52; *Pml*I-*Asc*I-digested fragment) of *cPer2* promoter-*luc* was substituted by a synthesized fragment in which the proximal site (5′-CTTATGTAAA-3′; −96 to −87) was mutated to 5′-CGAGACGCTA-3′. (*iv*) Distal site × 3-*luc*: Three copies of a 20-bp piece, the distal binding site with its flanking sequences (5′-GAGGCGTGATGTAACCTCTG-3′; −339 to −320) were linked in tandem, and the 60-bp fragment was inserted into an SV40-driven luciferase reporter (pGL3-Promoter, Promega). (*v*) mut. distal site × 3-*luc*: The same as *iv*, except that every E4BP4-binding site was mutated to 5′-GGAGACGCTC-3′.

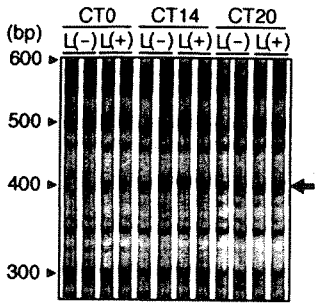

Fig. 1. A time-of-day-specific light-induced gene identified by differential display analyses. The pineal glands were isolated from chicks exposed to a 1-h light pulse [L(+)] or kept in the dark [L(−)] at indicated CT points of a day. Duplicate amplification reactions were performed with a pair of H-T11C primer (5′-AAGCTTTTTTTTTTC-3′) and H-AP21 primer (5′-AAGCTTTCTCTGG-3′, both primers from RNAimage kit, GenHunter), and the amplified products were loaded on the gel side by side. The arrow indicates the position of the amplified DNA fragment derived from *cE4bp4* transcript.

Results

Identification of a Novel Light-Controlled Gene. To approach the molecular basis of the phase-dependent phase-shifting mechanism in the chicken pineal clock system, we used a differential display-based cloning of pineal genes that are induced by light in a CT-dependent manner. We compared the effects of 1-h light stimulus given at CT0, CT14, and CT20 on the band intensities of PCR products (Fig. 1). Screening of ≈6,000 bands of the PCR products revealed that most of the light-induced products responded to light at every circadian time point tested. A phase-dependent light-induction was observed only in a few products, among which one (indicated by an arrow in Fig. 1) showed a remarkable light-induction at CT14, a time when a light stimulus induces a phase-delay of the chick pineal clock (12), whereas far less light-induction of the product was observed at both CT0 and CT20 (Fig. 1). The cloning and sequencing of the product (393-bp cDNA fragment) revealed that it encoded a peptide (60 aa) showing high similarity (70% identity) to the N-terminal region (Met-1–Cys-60) of human E4BP4 (hE4BP4), which was previously isolated as a transcriptional repressor recognizing the adenovirus E4 promoter region (37). The full-length coding sequence obtained by 3′-RACE encoded a protein of 458 aa residues 83% identical to hE4BP4 (Fig. 2*A*). This chicken homolog of *E4bp4* (*cE4bp4*) shows the highest similarity to *vrille* (*Vri*, Fig. 2*B*) among all of the coding sequences of *Drosophila* genome, and the DNA-binding domain (basic region) of E4BP4 shows high similarity not only with VRI but also with the PAR subfamily of bZIP transcription factors, including albumin gene D-site binding protein (DBP, Fig. 2*B*).

Light-Dependent and Time-of-Day-Dependent Expression of *cE4bp4*. A time course of light-dependent *cE4bp4* induction was investigated by quantitative RT-PCR analyses, in which the mRNA levels of the chick pineal *cE4bp4* were pursued during and after the 1-h light exposure from CT14 (Fig. 3*A*). The *cE4bp4* mRNA level began to increase within 30 min after the light onset, and at 60 min it reached a peak level ≈2-fold higher than the basal level. After the light was turned off, the *cE4bp4* mRNA level began to decrease and reached a level close to that of the control (dark-kept) animals within 3 h after the light offset. The light-dependent induction of *cE4bp4* was observed at any circadian time within a day (Fig. 3*B*), but this is not contradictory to the observation in Fig. 1 because both the basal levels in the dark and the light-induced levels heavily depended on circadian time (Fig. 3*B*; see also Fig. 1). A light-dependent induction of *cE4bp4* was also observed in an *in vitro* experiment with cultured chick pinealocytes (see Fig. 8, which is published as supplemental data on the PNAS web site, www.pnas.org), indicating that the pineal photoreceptive molecule(s) is responsible for the induction of *cE4bp4*.

The circadian fluctuation of the chick pineal *cE4bp4* expression under DD conditions had a peak around the day-night transition phase (between CT11 and CT15; Figs. 3*B* and 4*B*), and a similar or more pronounced fluctuation with a higher peak/trough ratio was observed in animals maintained in 12-h light/12-h dark (LD) cycles (Fig. 4A). These results indicate that the expression of *cE4bp4* is controlled not only by the external light but also by the circadian clock. In both LD and DD, the phase of the rhythmic expression of *cE4bp4* was constantly delayed by ≈8 h relative to that of *cPer2* (Fig. 4).

NEUROBIOLOGY

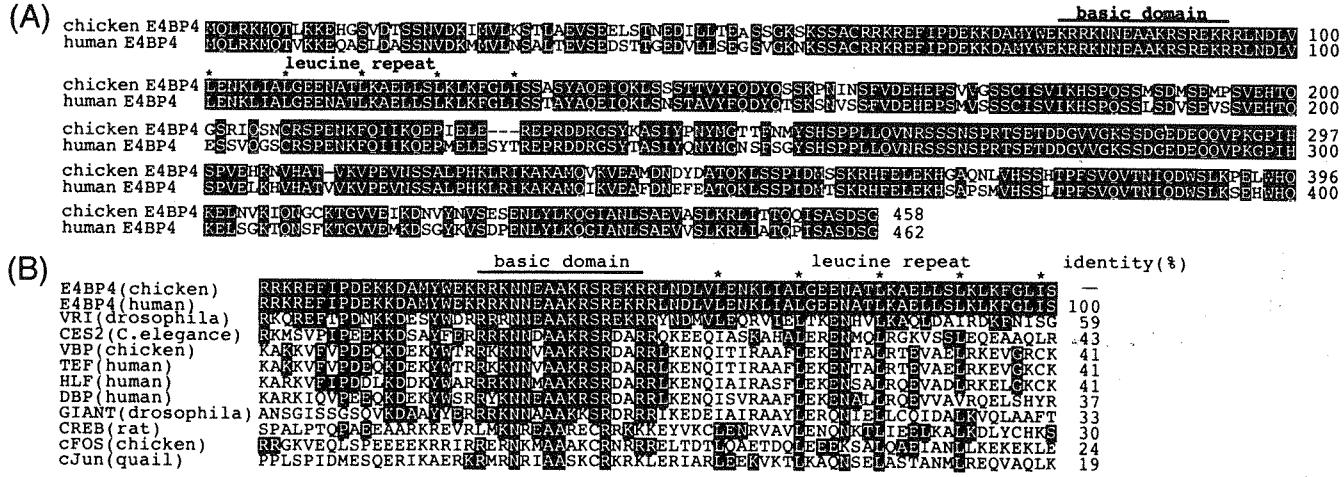

Fig. 2. Amino acid sequence of chicken E4BP4. (*A*) The deduced amino acid sequence of chicken E4BP4 is aligned with that of human E4BP4 (37), and the conserved residues are shown with white characters on black backgrounds. Asterisks and a horizontal line above the sequence represent a heptad leucine repeat and a basic domain, respectively. (*B*) Comparison of bZIP domain of chicken E4BP4 with other typical bZIP proteins; human E4BP4 (GenBank accession no. U26173), VRI (Y11837), CES-2 (U60979), VBP (U09222), TEF (U44059), HLF (M95585), DBP (U06936), GIANT (X05426), CREB (X14788), cFos (M18043), and cJun (X15547). VBP, TEF, HLF, and DBP are members of PAR bZIP protein family (38, 39). Residues identical to those of chicken E4BP4 are shown with white characters on black backgrounds. The amino acid identity (%) of each bZIP protein to chicken E4BP4 is shown on the right of the sequence.

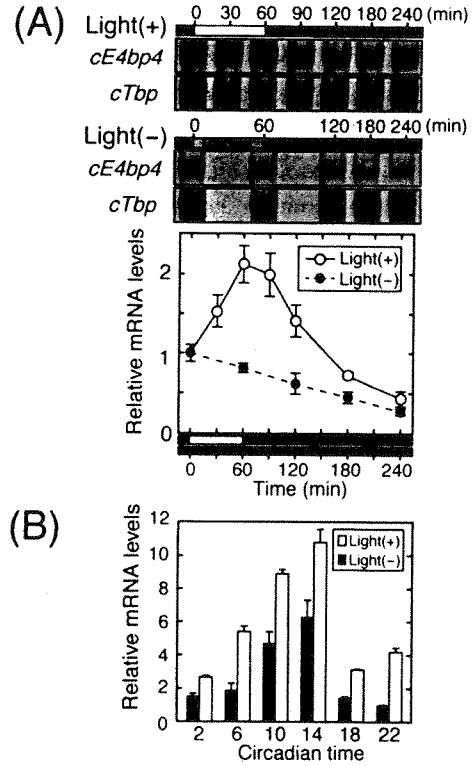

Fig. 3. Light-dependent change in *cE4bp4* mRNA levels. One-day-old chicks were maintained in LD cycles for 8 days and then transferred to DD on day 9, when animals were exposed to light for 1 h from each indicated time points [Light (+)] or kept in the dark for control [Light (−)]. (*A*) Time course of *cE4bp4* induction by light given at CT14–15. The pineal glands were isolated at indicated time points, and the relative mRNA levels of *cE4bp4* and *cTbp* in the isolated pineal glands were evaluated by RT-PCR (*Upper*). The band intensities of the amplified products of *cE4bp4* were normalized to those of *cTbp*, and the value of CT14 (0 min) was set to 1 (*Lower*). (*B*) Light-induction of *cE4bp4* at various circadian time points. The pineal glands were isolated from light-exposed animals (open bars) or dark-kept animals (filled bars) 1 h after each indicated time point. Relative mRNA levels of *cE4bp4* and *cTbp* were evaluated as described in *A*, and the value of dark-kept animals at CT22 was set to 1. All of the values are the mean ± SEM from three independent experiments.

cE4BP4 Represses Transcription from *cPer2* Promoter. The rhythmic expression of *cE4bp4* with the phase nearly opposite to that of *cPer2* (Fig. 4) suggests that cE4BP4 down-regulates *cPer2* transcription because of a possible function of cE4BP4 as a transcriptional repressor (37). To test this idea, we isolated a 5′-flanking region of *cPer2* gene (607 bp) and found two potential cE4BP4-binding sites (Fig. 5*A*). One, termed "distal site," at −334 to −325 (+1 indicates a putative transcription initiation site) matched 9 of 10 bp with the consensus hE4BP4-binding sequence (37), and the other, termed "proximal site," at −96 to −87 matched 8 of 10 bp (Fig. 5*A*). To examine whether cE4BP4 regulates *cPer2* transcription through the potential cE4BP4-binding sites, we performed transcriptional assays in chicken hepatoma LMH cells using a luciferase reporter construct that contains the 5′-flanking region of *cPer2* gene (−607 to +67, Fig. 5*A*). The transcriptional activity of the *cPer2*-promoter-containing construct was repressed by transfection of cE4BP4 expression construct in a dose-dependent manner (Fig. 5*B*, *Left*). This cE4BP4-dependent repression was completely abolished by mutation of the distal site, but not by mutation of the proximal site (Fig. 5*B*, *Center* and *Right*), indicating that the distal site is responsible for the repressing activity of cE4BP4 on *cPer2* promoter. To investigate whether the distal site is sufficient for the repressing activity of cE4BP4, we examined the

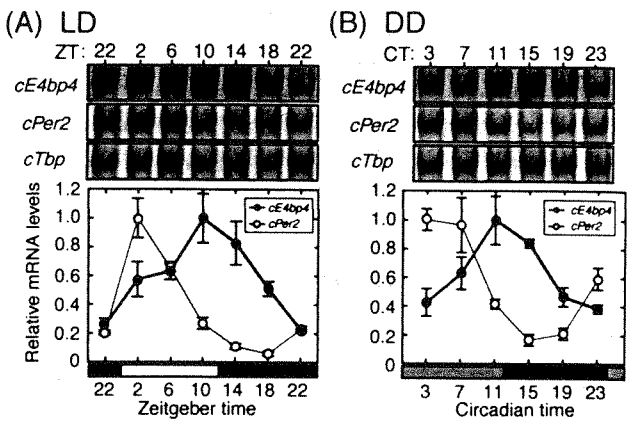

Fig. 4. Temporal changes in mRNA levels of *cE4bp4* and *cPer2* in the chicken pineal gland. One-day-old chicks were maintained in LD cycles for 8 days and then transferred to DD. The pineal glands were isolated at indicated time points of day 7–8 (*A*, in LD) and day 9 (*B*, in DD). Relative mRNA levels of *cE4bp4*, *cPer2*, and *cTbp* in the isolated pineal glands were evaluated by RT-PCR (*Upper*). The band intensities of the amplified products of *cE4bp4* and *cPer2* were normalized to those of *cTbp*, and the peak value for each gene was set to 1 (*Lower*). All of the values are the mean ± SEM from three independent experiments.

transcriptional activity of an SV40-driven reporter construct containing three copies of the distal site with its short flanking sequences (see *Materials and Methods*). As shown in Fig. 5*C*, cE4BP4 repressed strikingly the transcriptional activity of the tandem-repeat construct, and this repression was entirely abolished when the distal site sequences were all mutated. These results indicate that cE4BP4 represses transcription from the *cPer2* promoter through the distal E4BP4 recognition sequence.

Effect of the Prolongation of the Light Period on the Expression of *cE4bp4*/*cPer2*. Given that cE4BP4 would repress *cPer2* transcription *in vivo*, *cPer2* expression should be down-regulated when chicks were exposed to light that induces a sufficient amount of *cE4bp4* expression. Then, we investigated effects on the chick pineal *cE4bp4*/*cPer2* expression of a prolonged light period (18 h) extended to early subjective night, a period when *cE4bp4* mRNA levels are elevated strikingly by light (Fig. 3*B*). As shown in Fig. 6, the prolonged light period maintained the high-level expression of *cE4bp4*, and the subsequent decrease of the *cE4bp4* mRNA level was delayed relative to that in control animals exposed to the 12-h light period. In marked contrast, the pineal *cPer2* expression was maintained at low levels until the next morning, and the onset of the subsequent *cPer2* increase was delayed by ≈2 h. Then, the effect of the light prolongation on the chick pineal clock phase was evaluated by *cPer2*/*cE4bp4* expression cycles in chicks that were maintained in the dark after the prolonged light period. The phases of the rhythmic expression of both *cPer2* and *cE4bp4* were clearly delayed by ≈2 h relative to those in controls exposed to the 12-h light period (Fig. 6). These results indicate that the phase-delay induced by the light prolongation is closely associated with the light-dependent up-regulation of *cE4bp4* and with the subsequent delay of the morning induction of *cPer2*.

Discussion

In the present study, we have identified a bZIP transcription factor, *cE4bp4*, as a potential transcriptional repressor of the chick pineal *cPer2* gene. Rhythmic expression of *cE4bp4* with a phase almost opposite to that of *cPer2* was observed in LD (Figs. 4*A* and 6), in DD (Figs. 4*B* and 6), and also under the prolonged light period condition (Fig. 6). Taken together with the repress-

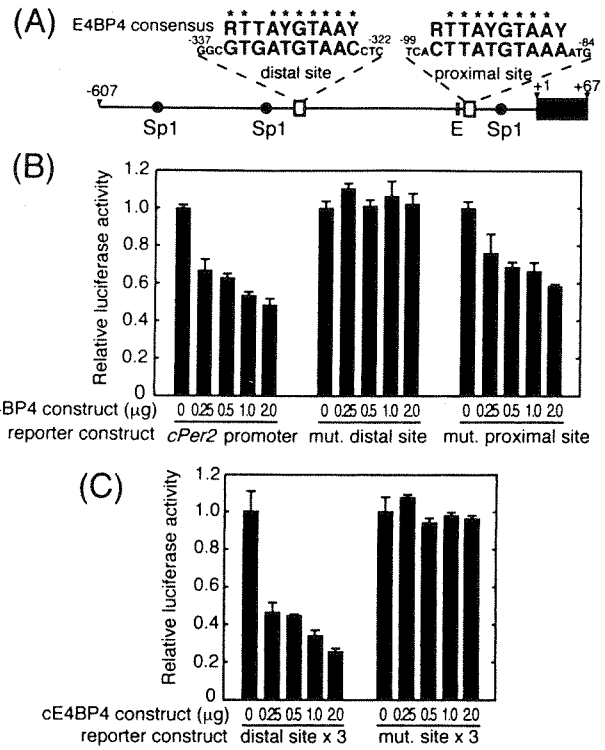

Fig. 5. cE4BP4 represses transcription from *cPer2* promoter. (*A*) *cPer2* promoter. The solid box and the horizontal line show the 5′-untranslated region and the 5′-flanking region of *cPer2* gene, respectively, with numbers representing the position relative to the transcription initiation site. The nucleotide sequences of the two potential cE4BP4 binding sites (open boxes; "distal site" and "proximal site") are compared with the hE4BP4 recognition sequence (R, purine; Y, pyrimidine) (37), and the bases conserved in the *cPer2* gene were marked with asterisks. Filled circles and a vertical bar indicate Sp1-binding sites and a CACGTG E-box, respectively. (*B*) Transcriptional assay was performed with a luciferase reporter construct containing the 5′-flanking region (−607 to +67) of *cPer2* gene (*cPer2* promoter-*luc*). The construct, "mut. distal site-*luc*" or "mut. proximal site-*luc*", is the same with "*cPer2* promoter-*luc*," except that the distal site (−334 to −325) or the proximal site (−96 to −87) was mutated, respectively (see *Materials and Methods*). (*C*) Transcriptional assay was performed with an SV40-driven luciferase reporter construct that contains three copies of the distal site sequence or the mutated sequence ("distal site × 3-*luc*" or "mut. distal site × 3-*luc*," respectively). Each value of luciferase activity was expressed relative to that of controls transfected with pcDNA3.1/V5/His empty vector alone without the cE4BP4 expression construct. All of the values are the mean ± SEM of three independent experiments.

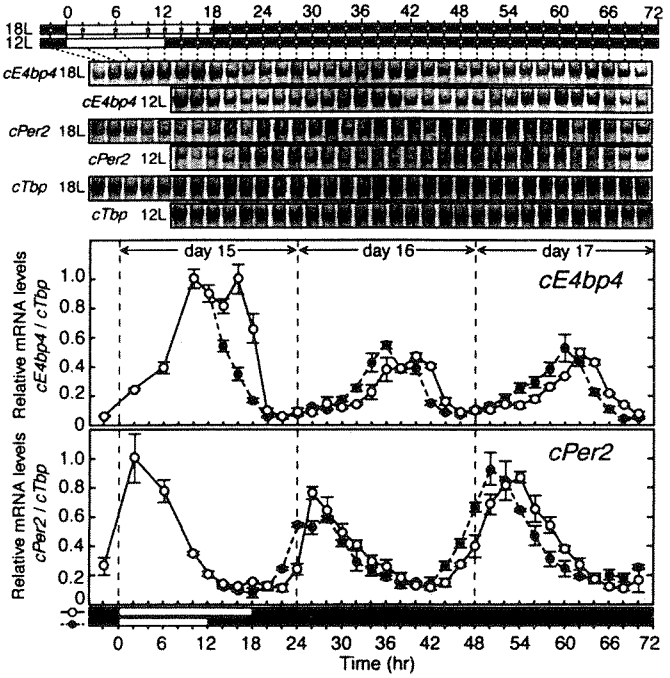

Fig. 6. Effect of the prolongation of the light period on the expression of *cE4bp4* and *cPer2*. One-day-old chicks were maintained in 12-h light/12-h dark cycles for 14 days. On day 15, a group of animals (18L) were maintained under the 18-h light/6-h dark condition, whereas control animals (12L) were maintained under the 12-h light/12-h dark condition. All of the animals were transferred and maintained in DD from day 16. The pineal glands were isolated at indicated time points of days 15–17. Relative mRNA levels of *cE4bp4*, *cPer2*, and *cTbp* were evaluated by RT-PCR (*Upper*), and each value is expressed as described in Fig. 4 (*Lower*). All of the values are the mean ± SEM from three independent experiments.

ing activity of cE4BP4 on *cPer2* promoter (Fig. 5), it is strongly suggested that cE4BP4 down-regulates the chick pineal *cPer2* transcription in light-dependent and time-of-day-dependent manners (see a model in Fig. 7).

Here, we would stress the physiological importance of cE4BP4 in the light-entrainment, especially as a key player in the phase-delaying mechanism. As shown in Fig. 6, the prolonged light period, which induced a phase-delay of the clock, maintained *cE4bp4* expression at high levels and delayed the rising phase of *cPer2* in the next morning. This observation suggests that the delay of *cPer2* induction was due to a delay of timing when its transcription became free from the suppression by cE4BP4 in the morning. Thus, cE4BP4 may play a very important role in the phase-delaying process, serving as a light-dependent transcriptional suppressor of *cPer2* gene (Fig. 7). Here, it is noteworthy that the observed suppressing effect of the light prolongation on the pineal *cPer2* expression (Fig. 6) contrasts strikingly with the effect of a 1-h light stimulus in DD that induces an acute increase of the pineal *cPer2* mRNA level (T.O., K. Yamamoto, K. Okano, T. Hirota, T. Kasahara, M. Sasaki, Y. Takanaka, and Y.F., unpublished results). These opposite effects on *cPer2* expression let us hypothesize that the phase-shift induced by the "prolonged light period" and the "short light pulse" is elicited through molecular processes totally distinct from each other.

The diurnal fluctuation of *cE4bp4* expression in LD (Figs. 4*A* and 6) and DD (Figs. 4*B* and 6) suggests that cE4BP4 protein down-regulates *cPer2* transcription in a time-of-day-dependent manner. On the assumption that E4BP4 protein levels rapidly reflect *E4bp4* mRNA levels in the chicken pineal cells as seen in

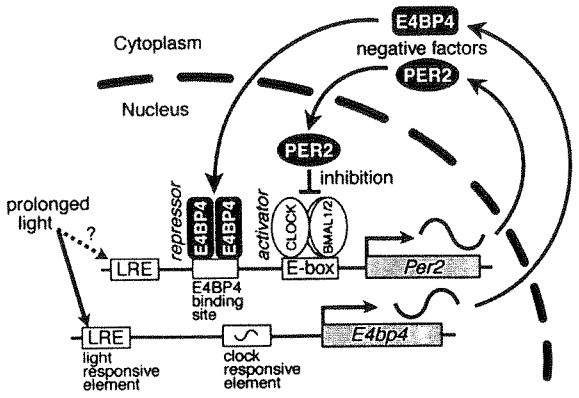

Fig. 7. A model for the role of cE4BP4 in the chicken pineal clock system.

other cells (40, 41), we can speculate that cE4BP4 proteins accumulate during the (subjective) day and go into the nucleus to repress the transcription of *cPer2* gene. This repression would lead to the gradual decrease in the mRNA level of *cPer2* in the evening. Before the dawn, in contrast, the cE4BP4 protein level may decline along with the decrease in the *cE4bp4* mRNA level, allowing the morning induction of *cPer2*. Thus, the time-of-day-specific rise and fall of cE4BP4 may contribute to the rhythmic expression of *cPer2* gene (Fig. 7). Such a circadian function of cE4BP4 could be evaluated by the temporal change in the pineal cE4BP4 protein level. Unfortunately, however, our efforts to detect the pineal cE4BP4 proteins were unsuccessful probably because of the low-level expression to be detected by antibodies that were raised against its amino-terminal or carboxyl-terminal part fused to glutathione *S*-transferase (GST; data not shown).

We found that the 5′-flanking region of *cPer2* gene contains not only the E4BP4 recognition sequence but also CACGTG E-box (Fig. 5*A*), which was demonstrated to be a functional binding site of cCLOCK:cBMAL1/2 heteromers that positively regulate *cPer2* transcription (T.O., K. Yamamoto, K. Okano, T. Hirota, T. Kasahara, M. Sasaki, Y. Takanaka, and Y.F., unpublished results). Taken together with the negative regulation by cE4BP4, the time-of-day-dependent transcription of *cPer2* gene is likely regulated by multiple factors in a well-concerted manner (Fig. 7). Interestingly, the promoter region of *mPer1* gene contains the E4BP4 recognition sequence as well, and this site is likely a target site of transcriptional activator DBP (42), which shares very similar recognition sequences with E4BP4 (37, 39). Considering that E4BP4 and DBP could compete with each other for a single binding site, a time-of-day-specific regulation exerted by two factors with apparently opposite functions may serve as a molecular switch for the robust rhythmic expression of *Per* gene.

The rhythmic expression of *cE4bp4* may contribute to the rhythmic expression of clock controlled (output) genes as well. Mouse vasopressin gene, one of the output genes, is subject to rhythmic transactivation by CLOCK:BMAL1 heteromers through CACGTG E-box found in the promoter region (21). It is also possible that cE4BP4 regulates a subset of output genes in a manner different from E-box-mediated one, and thereby cE4BP4 may diversify the output pathways from the circadian oscillator.

E4bp4 shows the highest similarity to *Vri* among all of the coding sequences of *Drosophila* genome. On the other hand, a BLAST database search (in December 2000) demonstrated that VRI protein showed higher similarity to E4BP4 than to any other members of bZIP proteins when the 70-aa stretches including the bZIP domain were compared (Fig. 2*B*). The structural similarity between E4BP4 and VRI strongly suggests that *E4bp4* is a counterpart of *Vri*, which has been identified as a *Drosophila* clock gene by genetic studies (35). Although it is unclear at present whether VRI functions as a transcriptional repressor of *dPer* gene, the observed suppression of dPER protein level because of continuous expression of *Vri* (35) implies that the time-keeping mechanism mediated by a bZIP transcriptional repressor is conserved among animal clock systems.

We thank Dr. K. Kokame at National Cardiovascular Center Research Institute (Osaka, Suita, Japan) for technical advice in the differential display analysis, and K. Yamamoto in our laboratory for assistance with the luciferase reporter gene assay. This work was supported by Grants-in-Aid for Scientific Research from the Japanese Ministry of Education, Culture, Sports, Science and Technology.

1. Pittendrigh, C. S. (1993) *Annu. Rev. Physiol.* **55,** 16–54.
2. Pittendrigh, C. S. (1981) In *Handbook of Behavioral Neurobiology, Biological Rhythms,* ed. Aschoff, J. (Plenum, New York), pp. 95–124.
3. Deguchi, T. (1979) *Nature (London)* **282,** 94–96.
4. Kasal, C. A., Menaker, M. & Perez-Polo, J. R. (1979) *Science* **203,** 656–658.
5. Green, D. J. & Gillette, R. (1982) *Brain Res.* **245,** 198–200.
6. Cahill, G. M. & Besharse, J. C. (1993) *Neuron* **10,** 573–577.
7. Tosini, G. & Menaker, M. (1996) *Science* **272,** 419–421.
8. Welsh, D. K., Logothetis, D. E., Meister, M. & Reppert, S. M. (1995) *Neuron* **14,** 697–706.
9. Nakahara, K., Murakami, N., Nasu, T., Kuroda, H. & Murakami, T. (1997) *Brain Res.* **774,** 242–245.
10. Takahashi, J. S., Hamm, H. & Menaker, M. (1980) *Proc. Natl. Acad. Sci. USA* **77,** 2319–2322.
11. Zatz, M., Mullen, D. A. & Moskal, J. R. (1988) *Brain Res.* **438,** 199–215.
12. Robertson, L. M. & Takahashi, J. S. (1988) *J. Neurosci.* **8,** 22–30.
13. Okano, T., Yoshizawa, T. & Fukada, Y. (1994) *Nature (London)* **372,** 94–97.
14. Bernard, M., Klein, D. C. & Zatz, M. (1997) *Proc. Natl. Acad. Sci. USA* **94,** 304–309.
15. Takahashi, J. S., Murakami, N., Nikaido, S. S., Pratt, B. L. & Robertson, L. M. (1989) *Recent Prog. Horm. Res.* **45,** 279–352.
16. Dunlap, J. C. (1999) *Cell* **96,** 271–290.
17. King, D. P. & Takahashi, J. S. (2000) *Annu. Rev. Neurosci.* **23,** 713–742.
18. Young, M. W. (2000) *Trends Biochem. Sci.* **25,** 601–606.
19. Glossop, N. R., Lyons, L. C. & Hardin, P. E. (1999) *Science* **286,** 766–768.
20. Gekakis, N., Staknis, D., Nguyen, H. B., Davis, F. C., Wilsbacher, L. D., King, D. P., Takahashi, J. S. & Weitz, C. J. (1998) *Science* **280,** 1564–1569.
21. Jin, X., Shearman, L. P., Weaver, D. R., Zylka, M. J., de Vries, G. J. & Reppert, S. M. (1999) *Cell* **96,** 57–68.
22. Kume, K., Zylka, M. J., Sriram, S., Shearman, L. P., Weaver, D. R., Jin, X., Maywood, E. S., Hastings, M. H. & Reppert, S. M. (1999) *Cell* **98,** 193–205.
23. Chong, N. W., Bernard, M. & Klein, D. C. (2000) *J. Biol. Chem.* **42,** 32991–32998.
24. Hunter-Ensor, M., Ousley, A. & Sehgal, A. (1996) *Cell* **84,** 677–685.
25. Lee, C., Parikh, V., Itsukaichi, T., Bae, K. & Edery, I. (1996) *Science* **271,** 1740–1744.
26. Myers, M. P., Wager-Smith, K., Rothenfluh-Hilfiker, A. & Young, M. W. (1996) *Science* **271,** 1736–1740.
27. Zeng, H., Qian, Z., Myers, M. P. & Rosbash, M. (1996) *Nature (London)* **380,** 129–135.
28. Albrecht, U., Sun, Z. S., Eichele, G. & Lee, C. C. (1997) *Cell* **91,** 1055–1064.
29. Shearman, L. P., Zylka, M. J., Weaver, D. R., Kolakowski, L. F., Jr., & Reppert, S. M. (1997) *Neuron* **19,** 1261–1269.
30. Shigeyoshi, Y., Taguchi, K., Yamamoto, S., Takekida, S., Yan, L., Tei, H., Moriya, T., Shibata, S., Loros, J. J., Dunlap, J. C. & Okamura, H. (1997) *Cell* **91,** 1043–1053.
31. Akiyama, M., Kouzu, Y., Takahashi, S., Wakamatsu, H., Moriya, T., Maetani, M., Watanabe, S., Tei, H., Sakaki, Y. & Shibata, S. (1999) *J. Neurosci.* **19,** 1115–1121.
32. Zylka, M. J., Shearman, L. P., Weaver, D. R. & Reppert, S. M. (1998) *Neuron* **20,** 1103–1110.
33. Maywood, E. S., Mrosovsky, M. D. & Hastings, M. H. (1999) *Proc. Natl. Acad. Sci. USA* **96,** 15211–15216.
34. Hirokawa, K., Yokota, S., Fuji, K., Akiyama, M., Moriya, T., Okamura, H. & Shibata, S. (2000) *J. Neurosci.* **20,** 5867–5873.
35. Blau, J. & Young, M. W. (1999) *Cell* **99,** 661–671.
36. Hirota, T., Kagiwada, S., Kasahara, T., Okano, T., Murata, M. & Fukada, Y. (2001) *J. Biochem.* **129,** 51–59.
37. Cowell, I. G., Skinner, A. & Hurst, H. C. (1992) *Mol. Cell. Biol.* **12,** 3070–3077.
38. Drolet, D. W., Scully, K. M., Simmons, D. M., Wegner, M., Chu, K. T., Swanson, L. W. & Rosenfeld, M. G. (1991) *Genes Dev.* **5,** 1739–1753.
39. Haas, N. B., Cantwell, C. A., Johnson, P. F. & Burch, J. B. (1995) *Mol. Cell. Biol.* **15,** 1923–1932.
40. Ikushima, S., Inukai, T., Inaba, T., Nimer, S. D., Cleveland, J. L. & Look, A. T. (1997) *Proc. Natl. Acad. Sci. USA* **94,** 2609–2614.
41. Kuribara, R., Kinoshita, T., Miyajima, A., Shinjo, T., Yoshihara, T., Inukai, T., Ozawa, K., Look, A. T. & Inaba, T. (1999) *Mol. Cell. Biol.* **19,** 2754–2762.
42. Yamaguchi, S., Mitsui, S., Yan, L., Yagita, K., Miyake, S. & Okamura, H. (2000) *Mol. Cell. Biol.* **20,** 4773–4781.

THE JOURNAL OF BIOLOGICAL CHEMISTRY

Vol. 277, No. 1, Issue of January 4, pp. 267–271, 2002
Printed in U.S.A.

Mitogen-activated Protein Kinase Phosphorylates and Negatively Regulates Basic Helix-Loop-Helix-PAS Transcription Factor BMAL1*

Received for publication, August 15, 2001, and in revised form, October 16, 2001
Published, JBC Papers in Press, October 30, 2001, DOI 10.1074/jbc.M107850200

Kamon Sanada‡, Toshiyuki Okano, and Yoshitaka Fukada§

From the Department of Biophysics and Biochemistry, Graduate School of Science, The University of Tokyo and Core Research for Engineering, Science, and Technology, Japan Science and Technology, Tokyo 113-0033, Japan

In vertebrates, mitogen-activated protein kinase (MAPK) exhibits circadian activation in several clock structures and likely participates in the timekeeping mechanism of the circadian clock. Here we show that MAPK associates with a basic helix-loop-helix-PAS transcription factor BMAL1, a positive regulator for the autoregulatory feedback loop of the circadian oscillator. MAPK phosphorylates BMAL1 at multiple sites, including Ser-527, Thr-534, and Ser-599, *in vitro*, and BMAL1:CLOCK-induced transactivation from the E-box element is inhibited by expression of a constitutive active form of MAPK kinase in 293 cells. The inhibitory effect is reversed by coexpression of the kinase-dead mutant of MAPK or by mutation of BMAL1 at Thr-534. These results indicate that BMAL1:CLOCK-induced transcription is negatively regulated by MAPK-mediated phosphorylation of BMAL1 at Thr-534 and suggest a molecular link between circadian-activated MAPK and the clock oscillator.

A variety of organisms show circadian rhythms in physiology and behavior under the regulation of the endogenous circadian clock. In mice, a heterodimer of two basic helix-loop-helix-PAS transcription factors, CLOCK and BMAL1, binds to CACGTG E-box elements for transcriptional activation of *Period* (*Per*) and *Cryptochrome* (*Cry*) genes (1–3). Products of *Per* and *Cry* genes feed back to inhibit BMAL1:CLOCK-induced transcription, resulting in a decrease in levels of these gene products. This then allows the molecular cycle to start again with the activation of the BMAL1:CLOCK heterodimer, forming a transcription/translation-based negative feedback loop. Behavioral and molecular analyses of mutant mice for *Clock*, *Per2*, *Cry*s, *and Bmal1* genes have clarified their circadian function (3), and in particular, *Bmal1* knock-out mice exhibit a complete loss of the circadian rhythmicity immediately upon placement in constant darkness, indicating a central role of BMAL1 in the circadian oscillator (4).

In addition to the transcriptional regulation, posttranslational modifications such as phosphorylation of clock gene products seem to regulate the stability and period length of the circadian cycle by generating an appropriate time lag (5, 6). We demonstrated previously that a transient inhibition of circadian activation of mitogen-activated protein kinase (MAPK)[1] induced a phase shift of the oscillator in the chick pineal gland (7, 8) and bullfrog retina (9), both of which are the sites of the circadian clock system (10, 11). In the chick pineal gland, MAPK appears to be regulated via the Ras-Raf-1-MEK pathway, and this classical MAPK cascade seems to form a secondary loop interconnected to the core feedback loop (7). Noticeably, the photic signal down-regulates pineal MAPK via light-activated MAPK phosphatase without affecting the Ras-MEK pathway (8). These observations indicate that MAPK activity is regulated by the clock and photic signals via independent pathways and suggest a pivotal role of MAPK in maintenance of the circadian rhythm and its photic entrainment. Despite growing evidence supporting an important contribution of MAPK to the clock system, less is known about its downstream pathway. One such candidate is the cAMP response element-binding protein/cAMP-response element transcriptional pathway (12–14), but an *in vivo* involvement of MAPK in the transcriptional activation of cAMP response element-binding protein for the clock regulation is still controversial (13–15). In this study, we examined another stream of MAPK signaling and found a direct interaction of MAPK with the clock component BMAL1 for negative regulation of BMAL1:CLOCK-induced transcription via BMAL1 phosphorylation.

EXPERIMENTAL PROCEDURES

Plasmids—The open reading frame (ORF) of chicken MAPK (GenBank™ accession no. AY033635) was amplified from chicken pineal cDNA by PCR using LA *Taq* polymerase (Takara) and a pair of primers (5′-GGGAGGAGTCGACTCATGGCGGCGGTGGCGG-3′ and 5′-CCGTCGACGAAGACTAAGATCGATATCCTGGCTGG-3′). The PCR product was digested with *Sal*I and ligated into *Sal*I-digested pCMV-Tag3C (Stratagene). For bacterial expression of myc epitope-tagged MAPK, the 1.2 kbp-*Nco*I/*Xho*I fragment of MAPK-pCMV-Tag3C was ligated into *Nco*I/*Sal*I-digested pET21d (Novagen). In reporter gene assay, we used ERK2(K54R)-pEF-BOS plasmid (a kind gift of Masato Ogata at Osaka Medical School, Osaka, Japan) for expression of human K54R-ERK2 (KR-MAPK, kinase-dead mutant). For the yeast two-hybrid assay, the ORF of human K54R-ERK2 was amplified by PCR using primers (5′-GGTCGACTTCATATGGCGGCGGCGGCGGCG-3′ and 5′-GGTGTCGACTTAAGATCTGTATCCTGGCTGGAATC-3′). The PCR product was digested with *Nde*I and *Sal*I and then ligated into *Nde*I/*Sal*I-digested pGBKT7 (CLONTECH).

The ORF of chicken CLOCK and BMAL1 (16) was ligated into *Xho*I-digested pGADT7 (CLONTECH) for the yeast two-hybrid assay. The ORF of chicken BMAL1 was ligated into *Sal*I-digested pGEX-5X-1 (Amersham Biosciences, Inc.) for its bacterial expression as a glutathi-

* This work was supported in part by grants-in-aid for Scientific Research from the Japanese Ministry of Education, Culture, Sports, Science and Technology. The costs of publication of this article were defrayed in part by the payment of page charges. This article must therefore be hereby marked "*advertisement*" in accordance with 18 U.S.C. Section 1734 solely to indicate this fact.

‡ Present address: Howard Hughes Medical Institute, Dept. of Pathology, Harvard Medical School, 200 Longwood Ave., Boston, MA 02115.

§ To whom correspondence should be addressed: Dept. of Biophysics and Biochemistry, Graduate School of Science, The University of Tokyo, Hongo 7-3-1, Bunkyo-Ku, Tokyo 113-0033, Japan; Tel. and Fax: 81-3-5802-8871; E-mail: sfukada@mail.ecc.u-tokyo.ac.jp.

[1] The abbreviations used are: MAPK, mitogen-activated protein kinase; MEK, MAPK kinase; DE-MEK, constitutive active MEK; ERK, extracellular signal-regulated protein kinase; GST, glutathione *S*-transferase; HPLC, high performance liquid chromatography; MS, mass spectrometry; MALDI-TOF/MS, matrix-assisted laser desorption/ionization time-of-flight MS; ORF, open reading frame.

one *S*-transferase (GST) fusion protein. For reporter gene assay, the ORF of chicken BMAL1 was ligated into *Sal*I-digested pCMV-Tag3C. Mutations (Ser/Thr to Ala) were introduced into BMAL1 by using a site-directed mutagenesis kit (Stratagene). Construction of a plasmid for expression of chicken CLOCK in mammalian cells was described previously (16).

The ORF of chicken MEK (GenBank™ accession no. L28703) was amplified from chicken pineal cDNA by PCR with a pair of primers (5'-GCGGGATCCCGGCCATGCCGGCCAAG-3' and 5'-GGATCCGAAGACTCACGGCAGCACGGGTGGGTG-3'). The PCR product was then digested with *Bam*HI and ligated into *Bam*HI-digested pGEX-5X-1 or pCMV-Tag3C. A constitutive active form of chicken MEK (DE-MEK) was produced by mutations of Ser-220 to Asp and Ser-224 to Glu (17) with the aid of the site-directed mutagenesis kit.

Preparation of Recombinant Proteins—GST-BMAL1 and its mutants were expressed in *Escherichia coli* strain BL21(DE3) cultured with 30 μM isopropyl-β-D-thiogalactopyranoside at 25 °C for 15–20 h. The bacteria in a 1-liter culture were then suspended with 50 ml of a lysis buffer (50 mM Tris-HCl, 250 mM NaCl, 2 mM EDTA, 2 mM EGTA, 1 mM dithiothreitol, 1 mM benzamidine, 4 μg/ml aprotinin, 4 μg/ml leupeptin, and 1% (w/v) Triton X-100, pH 7.8, at 4 °C) containing 2 mg/ml lysozyme, and the suspension was incubated for 30 min on ice for lysis followed by centrifugation (45,000 × *g* for 30 min). GST-fusion proteins in the supernatant were purified by a glutathione-Sepharose column (Amersham Biosciences, Inc.), and the glutathione used for the elution was removed by passing through a PD-10 column (Amersham Biosciences, Inc.) pre-equilibrated with buffer A (50 mM Tris-HCl, 1 mM dithiothreitol, 1 mM benzamidine, 4 μg/ml aprotinin, 4 μg/ml leupeptin, and 0.03% (w/v) Brij 35, pH 7.8, at 4 °C). After concentration by a Centricon YM-100 concentrator (Amicon), the protein content was estimated by the densitometry of SDS-PAGE gel bands in comparison with those of serial dilutions of bovine serum albumin standards in the same gel.

GST-DE-MEK was bacterially expressed in *E. coli* strain BL21(DE3) pLysS, and the bacteria were sonicated in the lysis buffer followed by centrifugation (45,000 × *g* for 30 min). GST-DE-MEK extracted in the supernatant was then purified as described above. For preparing the phosphorylated form of myc epitope-tagged MAPK (termed P-myc-MAPK), bacterially expressed myc-MAPK (1 mg) was purified to near homogeneity by a phenyl-Sepharose column (Amersham Biosciences, Inc.), dialyzed against buffer B (20 mM Tris-HCl, 2 mM $MgCl_2$, and 1 mM Na_3VO_4, pH 7.8), and then phosphorylated by incubation at 30 °C for 2 h with GST-DE-MEK (100 μg) in 10 ml of a kinase buffer (50 mM Tris-HCl, 20 mM $MgCl_2$, and 50 μM Na_3VO_4, pH 7.8) containing 1 mM ATP. This mixture was passed through a glutathione-Sepharose column to adsorb GST-DE-MEK, and the flow-through fraction containing P-myc-MAPK was dialyzed against buffer B. Based on gel shift analysis, we estimated more than 90% of MAPK to be phosphorylated.

In Vitro Binding Assay—GST-BMAL1, its mutant, or GST alone (each 3 μg) was incubated with myc-MAPK or P-myc-MAPK (0.3 μg) in 80 μl of a binding buffer (20 mM Tris-HCl, 10% (w/v) glycerol, 135 mM NaCl, 50 μM NaF, 0.5 mM benzamidine, 1 mM EDTA, and 1 mM Na_3VO_4, pH 7.8) containing 0.5 mg/ml bovine serum albumin at 4 °C for 1 h. To this mixture was added 10 μl of glutathione-Sepharose beads for sedimentation of GST-fusion protein, which was washed five times with the binding buffer containing 0.5% (w/v) Triton X-100. The bound proteins were resolved by SDS-PAGE followed by immunoblotting with anti-myc antibody (1:1000 dilution, Santa Cruz Biotechnology) or anti-GST antibody (1:10,000 dilution, Amersham Biosciences, Inc.) as described (7).

Protein Kinase Assay—Recombinant myc-MAPK or P-myc-MAPK (0.3 μg) was incubated with 1.8 μg of GST-BMAL1, its mutant, or GST alone in 80 μl of the kinase buffer at 30 °C in the presence of 400 μM [γ-^{32}P]ATP (200 Bq/pmol). The reaction mixture was then subjected to SDS-PAGE, and the phosphorylation level of GST-BMAL1 was estimated by autoradiography of the gel. For phosphopeptide analysis, recombinant GST-BMAL1 (18 μg) was incubated at 30 °C for 2 h with 1.8 μg of P-myc-MAPK in 80 μl of the kinase buffer containing 1 mM ATP. GST-BMAL1 thus phosphorylated was then separated by SDS-PAGE and transferred to a polyvinylidene difluoride membrane. The blot containing the GST-BMAL1 protein band was excised, washed five times with water, and incubated for blocking with 100 mM acetic acid containing 0.5% (w/v) polyvinylpyrrolidone-40 at 37 °C for 1 h. After washing five times with water, the blot was incubated with 0.03 μg of lysylendopeptidase *Achromobacter* protease I at 37 °C for 18 h in 200 μl of 50 mM Tris buffer (pH 8.8) containing 10% (w/v) acetonitrile. The mixture was then supplemented with 2 μg of *Staphylococcus aureus* V8 protease for further digestion at 37 °C for 18 h, and the digest was subjected to reversed-phase HPLC (18). All the fragments eluted from the column were analyzed by matrix-assisted laser desorption/ionization time-of-flight mass spectrometry (Voyager MALDI-TOF/MS spectrometer equipped with a delayed extraction ion source, operated in the linear mode, PerSeptive Biosystems). For sequence analysis of phosphopeptides (19), the HPLC-purified peptide was lyophilized, dissolved in 10 μl of 10% (w/v) HCl for incubation at 50 °C for 6 h, and subjected to MALDI-TOF/MS analysis.

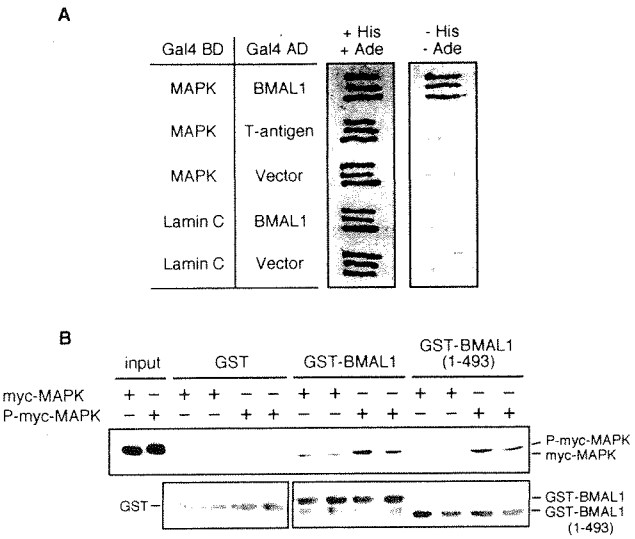

FIG. 1. **Association of MAPK with BMAL1.** *A*, Saccharomyces *cerevisiae* strain AH109 (*MATa ura3–52 his3–200 trp1–901 leu2–3,112 gal4Δ gal80Δ LYS2::GAL1-HIS3 GAL2-ADE2 URA3::MEL1-lacZ*) was cotransformed with plasmids encoding the indicated proteins fused to either GAL4 BD or GAL4 AD by the standard lithium acetate method with 0.3 μg of each plasmid. Transformants containing two independent fusion proteins were selected by culture at 30 °C on plates of synthetic dextrose medium (lacking Trp and Leu) containing His and Ade. Three independent yeast transformants were assayed for transactivation of the *HIS3* and *ADE* reporter genes, as indicated by growth on minimal medium lacking His and Ade. *B*, bacterially expressed GST-BMAL1, GST-BMAL1(residues 1–493), or GST alone was incubated with myc-MAPK or P-myc-MAPK and then sedimented with glutathione-Sepharose. The precipitated proteins were subjected to SDS-PAGE followed by immunoblotting with anti-myc (*upper panel*) or anti-GST antibody (*lower panels*). As markers, both myc-MAPK and P-myc-MAPK (10% of those used in the binding reaction) were loaded on the same gel (input).

RESULTS AND DISCUSSION

Association of MAPK with BMAL1—MAPK is known to translocate to the nucleus where activated MAPK phosphorylates and regulates nuclear proteins including transcription factors, and in some cases, MAPK forms a complex with its substrate (20). Therefore we performed a yeast two-hybrid assay to examine the possible interaction of MAPK (with kinase-dead MAPK as bait) with a couple of basic helix-loop-helix-PAS transcription factors, chicken BMAL1 and CLOCK, that are important elements in the clock function (16). In the yeast two-hybrid assay, MAPK interacted with BMAL1 (Fig. 1*A*) but not with CLOCK (data not shown). We further explored this interaction by GST pull-down assay and examined the effect of MAPK phosphorylation on the complex formation with BMAL1. GST-BMAL1 preferentially associated with phosphorylated MAPK (P-myc-MAPK) rather than with myc-MAPK, whereas GST alone interacted with neither of the proteins (Fig. 1*B*). Deletion of C-terminal 140 amino acids of BMAL1 (GST-BMAL1(1–493)) did not abrogate the interaction, implying that the C-terminal activation domain (21) is not required for the interaction with MAPK. These two analyses suggest that BMAL1 could be one of the *in vivo* targets of phosphorylated and hence activated MAPK.

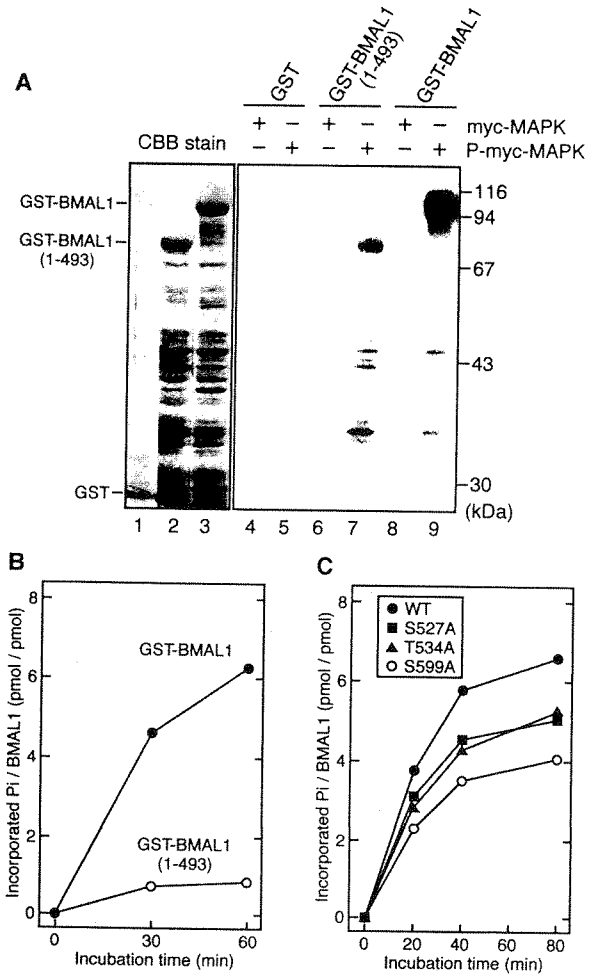

FIG. 2. **Phosphorylation of BMAL1 by MAPK.** *A*, GST (*lane 1*), GST-BMAL1(residues 1–493) (*lane 2*), or GST-BMAL1 (*lane 3*) was incubated for 30 min with myc-MAPK or P-myc-MAPK in the presence of 400 μM [γ-^{32}P]ATP followed by electrophoresis and autoradiography (*right panel*). *B*, BMAL1 and BMAL1(1–493) was phosphorylated by P-myc-MAPK as in *panel A*, and the incorporation of $^{32}P_i$ into BMAL1 protein quantified by an image analyzer (FLA2000, Fujifilm, Tokyo, Japan) was plotted against incubation time. *C*, wild-type (*WT*) BMAL1 or indicated BMAL1 mutant was incubated with P-myc-MAPK as in *panel A*, and the incorporation of $^{32}P_i$ into BMAL1 protein was quantified and plotted as in *panel B*. The data are representative results of replicate experiments with similar results. CBB, Coomassie Brilliant Blue.

MAPK Phosphorylates BMAL1 at Multiple Pro-Ser/Thr Sites—We then tested whether BMAL1 is phosphorylated by activated MAPK. In the presence of radiolabeled ATP, GST-BMAL1 was efficiently phosphorylated by P-myc-MAPK (Fig. 2*A*, *lane 9*) but not by myc-MAPK (*lane 8*). Quantitative analysis of the time-dependent change of the phosphorylated band revealed that BMAL1 incorporated 6–7 pmol of $^{32}P_i$/pmol of protein, indicating that MAPK phosphorylates BMAL1 at multiple sites (Fig. 2*B*). Noticeably, deletion of the C-terminal 140 amino acids of BMAL1 resulted in substantial loss of phosphorylation by P-myc-MAPK (Fig. 2*A*, *lane 7*) despite the MAPK binding of the truncated form being comparable with that of full-length BMAL1 (Fig. 1*B*). We speculate that the C-terminal region of BMAL1 contains the primary site(s) for MAPK phosphorylation.

Within the C-terminal 140 amino acids of BMAL1 from human, rat, mouse, chicken, and zebrafish, we find six conserved sites for putative MAPK phosphorylation (ψ*X*(S/T)P, in which ψ is aliphatic or proline; see Refs. 22 and 23). To determine the phosphorylation site(s), GST-BMAL1 was incubated with either phosphorylated or nonphosphorylated MAPK in the presence of unlabeled ATP, digested by lysylendopeptidase and V8 protease, and subjected to reversed-phase HPLC for isolating the proteolytic fragments. From nonphosphorylated BMAL1, we obtained two relevant fragments (termed A and B) showing MALDI-TOF/MS signals at *m/z* 3509.4 and 2333.2, which correspond to the BMAL1 sequences Ile-513–Lys-546 (fragment A: calculated mass 3508.9, assuming that Cys-523 is acrylamided) and Asn-583–Asp-604 (fragment B: calculated mass 2333.4), respectively (Table I). The assignment of the fragment was confirmed by MS-based sequence analysis (see below). We paid special attention to these fragments due to the accumulation of the putative phosphorylation sites within their sequences (Table I, see footnote *a* and *b*). As expected, phosphorylated BMAL1 yielded two peak fractions containing fragment A (Ile-513–Lys-546), and they displayed a MALDI-TOF/MS signal at *m/z* 3589.7 or 3669.4, which corresponds to the peptide modified by one or two phosphate groups (3508.9 plus 79.9 or 159.8 mass units, respectively; Table I). Fragment B (Asn-583–Asp-604) derived from phosphorylated BMAL1 showed MALDI-TOF/MS signal at *m/z* 2412.1, corresponding to the peptide with one phosphate group (2333.4 plus 79.9 mass units). This fragment, Asn-583–Asp-604, contains only one putative MAPK phosphorylation site, Ser-599. By contrast, fragment A contains four putative phosphorylation sites, and we performed an MS-based sequence analysis of the doubly phosphorylated fraction of fragment A to determine the phosphorylated residues. This analysis utilizes a sequential C-terminal degradation of a peptide dissolved in 10% (w/v) HCl (Ref. 19; see also "Experimental Procedures"). MALDI-TOF/MS analysis of the mixture of partially degraded fragments yielded an array of signals that were assigned to ions of fragments with 0–2 phosphate groups. As summarized in Table II, the loss of phosphate groups was observed at two distinct degradation steps, one from peptide 513–538 to 513–533 and the other from peptide 513–532 to 513–525, supporting the phosphorylation sites at Thr-534 and Ser-527 (Table II). The three sites for *in vitro* MAPK phosphorylation, Ser-527, Thr-534 (both in fragment A), and Ser-599 (in fragment B), in BMAL1 were mutated to Ala, and each mutant was subjected to an *in vitro* kinase assay (Fig. 2*C*). These BMAL1 mutants, S527A, T534A, and S599A, were phosphorylated by activated MAPK to reduced degrees (by ~24, 24, and 40%, respectively) as compared with wild-type BMAL1, which is consistent with the phosphopeptide analysis predicting *in vitro* phosphorylation at these sites. The observed multiple phosphorylation of BMAL1 (6–7 pmol phosphate/pmol of protein in average, Fig. 2, *B* and *C*) suggests the presence of the other sites to be phosphorylated quantitatively that were not identified in our analyses. Alternatively, the overall phospho-

TABLE I
Mass analysis of proteolytic fragments containing putative MAPK phosphorylation sites

Proteolytic fragments of either GST-BMAL1 or phosphorylated GST-BMAL1 were subjected to MALDI-TOF/MS. Observed masses (MH^+) of two fragments (A and B) containing putative MAPK phosphorylation sites (underlined) were shown.

Source	Observed mass	Predicted peptide structure	Calculated mass
GST-BMAL1	3509.4	fragment A[a]	3508.9
	2333.2	fragment B[b]	2333.4
Phosphorylated GST-BMAL1	3669.4	fragment A + $2PO_4$	3668.7
	3589.7	fragment A + $1PO_4$	3588.8
	2412.1	fragment B + $1PO_4$	2413.3

[a] Fragment A: IHRIRGSSPSSCGSSPLNITSTPPPDTSSPGSKK (513–546).
[b] Fragment B: NSHIGIDMIDNDQGSSSPSNDE (583–604).

TABLE II

Mass analysis of phosphopeptide Ile-513–Lys-546 based on partial degradation by dilute HCl

Doubly phosphorylated fragment A Ile-513–Lys-546 was partially degraded by incubation in 10% HCl, and the resultant products were subjected to MALDI-TOF/MS analysis. Putative MAPK phosphorylation sites were highlighted.

Mass		No. of phosphate	Predicted amino acid sequence	
Observed	Calculated			
3669.4	3668.7	2	IHRIRGSSPSSCGSSPLNITSTPPPDTSSPGSKK	(513–546)
3541.0	3540.7	2	IHRIRGSSPSSCGSSPLNITSTPPPDTSSPGSK	(513–545)
3326.0	3325.5	2	IHRIRGSSPSSCGSSPLNITSTPPPDTSSPG	(513–543)
3171.6	3171.4	2	IHRIRGSSPSSCGSSPLNITSTPPPDTSS	(513–541)
3084.6	3084.3	2	IHRIRGSSPSSCGSSPLNITSTPPPDTS	(513–540)
2997.2	2997.2	2	IHRIRGSSPSSCGSSPLNITSTPPPDT	(513–539)
2896.9	2896.1	2	IHRIRGSSPSSCGSSPLNITSTPPPD	(513–538)
2308.0	2308.5	1	IHRIRGSSPSSCGSSPLNITS	(513–533)
2221.2	2221.4	1	IHRIRGSSPSSCGSSPLNIT	(513–532)
1428.8	1428.6	0	IHRIRGSSPSSCG	(513–525)

rylation reaction may involve, in addition to physiologically important phosphorylation on certain sites, slow reaction of less importance at multiple sites that are phosphorylated to various degrees *in vitro*. The latter might account for the unsuccessful identification of the other sites in our MS-based peptide analyses.

Effect of MAPK-mediated Phosphorylation of BMAL1 on Its Transactivation Activity—A functional role of MAPK-catalyzed phosphorylation of BMAL1 was examined by a transcriptional assay in 293 cells in which coexpression of BMAL1 and CLOCK stimulated the E-box element-dependent transcription of a luciferase reporter gene (Fig. 3*A*). Under these conditions, coexpression of DE-MEK (a constitutive active form of MEK) suppressed BMAL1:CLOCK-induced transcription, and the maximal inhibition reached 23–30%. This inhibitory effect of DE-MEK was completely reversed by additional coexpression of KR-MAPK (a kinase-dead mutant of MAPK), suggesting that activated MAPK mediates the inhibition of BMAL1:CLOCK-induced transcription. To evaluate the contribution of BMAL1 phosphorylation to the inhibition, we examined the effects of BMAL1 mutations at the phosphorylation sites (S527A, T534A, and S599A) in the transcription assay. Similar to wild-type BMAL1, every mutant induced a large increase in E-box element-dependent transcription together with CLOCK in 293 cells (Fig. 3*B*). In addition, as is observed for wild-type BMAL1:CLOCK, DE-MEK-dependent suppression of the transactivation was observed for BMAL1(S527A):CLOCK and BMAL1 (S599A):CLOCK (inhibition by 21 and 25%, respectively). On the other hand, the transactivation induced by BMAL1 (T534A):CLOCK was not affected by DE-MEK (Fig. 3*B*). These results, together with the *in vitro* data (Fig. 1 and Table II), indicate that MAPK negatively regulates E-box-dependent transactivation induced by BMAL1:CLOCK heteromers via phosphorylation of BMAL1 at Thr-534. We speculate that MAPK-catalyzed phosphorylation of BMAL1 at Thr-534 may induce a conformational change of the C-terminal activation domain (21) for inhibiting its activity. At present, it is not clear whether the MAPK-catalyzed phosphorylation of BMAL1 completely inhibits its activity or attenuates it partially. Under our experimental conditions, activation of MAPK gave a modest inhibitory effect (~30% inhibition) on transactivation of BMAL1 (Fig. 3*A*). It is likely, however, that endogenous MAPK activated by DE-MEK was only able to phosphorylate a part of overexpressed BMAL1. This would lead to the weak inhibition of the transactivation even if phosphorylated BMAL1 retains no substantial activity. Protein characterization of BMAL1 is required to understand the mechanism underlying the phosphorylation-dependent inhibition of BMAL1 function.

Role of MAPK in Clockworks—MAPK activity exhibits a circadian rhythm with a peak at mid to late subjective night in various clock structures (7, 9, 24). During the nighttime, protein levels of negative regulatory elements in the circadian feedback loop (mPERs and mCRYs) are in declining phase, but

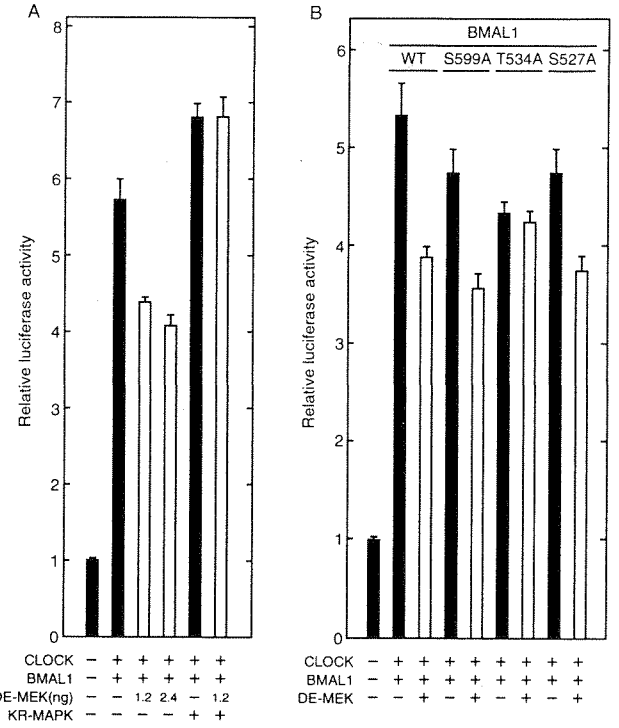

FIG. 3. **Effect of MAPK activation on BMAL1:CLOCK-induced transcription mediated by E-box element.** *A*, 293EBNA cells cultured in wells of 6-well plates were transiently transfected by LipofectAMINE PLUS reagent (Invitrogen) with various combinations of plasmids expressing BMAL1 (300 ng of plasmid), CLOCK (250 ng), DE-MEK (1.2 or 2.4 ng), and kinase-dead MAPK (KR-MAPK, 100 ng) as indicated, with 25 ng of firefly luciferase reporter plasmid (see below) and 0.25 ng of pRL-CMV (*Renilla*) luciferase plasmid (Promega) as an internal control. For construction of a firefly luciferase reporter plasmid (*mAVP* E-box3-SV40-*luc* plasmid; see Ref. 16), the CACGTG E-box element with its flanking sequences from the promoter/enhancer region of mouse *vasopressin* gene was linked in tandem (three copies), and it was inserted into pGL3-Promoter plasmid (Promega). The total amount of DNA applied per well was adjusted to 1 μg by adding pCMV-Tag3C empty plasmid. The cell extracts were prepared 36 h after the transfection and subjected to a dual-luciferase assay by luminometry (Promega) according to the manufacturer's protocol. The values were normalized to transfection efficiency with the help of the internal control in each cell culture. Presence (+) or absence (−) of plasmids expressing BMAL1, CLOCK, and KR-MAPK is denoted, and data are presented as the mean ± S.E. of six independent experiments. *B*, 293EBNA cells were transfected with plasmids expressing CLOCK (250 ng plasmid), wild-type (*WT*) BMAL1 (300 ng), BMAL1 mutant (S527A, T534A, or S599A; 300 ng), and/or DE-MEK (+, 1.2 ng). Luciferase activity was measured and normalized as described in *panel A*.

their mRNA levels do not start to increase until these protein levels reach to their circadian trough at late subjective night (2, 25). BMAL1:CLOCK-mediated transcription of *mPer/mCry* is kept suppressed during mid to late subjective night despite very low protein levels of negative elements. Therefore the negative element-independent inhibition of the BMAL1: CLOCK heteromer seems to delay the restart of the *mPer/mCRY* cycle, generating an appropriate time lag required for the circadian rhythmicity of the oscillator (5). The MAPK-mediated inhibition of BMAL1 activity observed in this study (Fig. 3) is an event capable of explaining well such a time lag for activation of E-box element-dependent transcription during the nighttime, and thereby MAPK is likely involved in the time-keeping mechanism of the circadian oscillation.

Recently a BMAL1 homolog, BMAL2 (also called MOP9 or CLIF), has been identified in various clock structures (16, 26–28), and it couples with CLOCK to activate E-box element-dependent transcription (16, 26). Interestingly, phospho-acceptor sites on chicken BMAL1 (Ser-527/Thr-534/Ser-599) are highly conserved among all of the known BMAL1s in vertebrates but are not found in any BMAL2s. Considering that BMAL1 is an essential component that cannot be compensated by any other components in the oscillator (4), it is likely that the BMAL1-specific regulation mediated by MAPK makes a fundamental contribution to the circadian regulation of E-box element-dependent transcription in the oscillator.

Acknowledgments—We thank Masato Ogata for providing human ERK2 expression plasmids, Takaoki Kasahara and Chie Higashi for cloning of chicken MAPK, and Yuko Harada for technical assistance in yeast two-hybrid assays.

REFERENCES

1. Gekakis, N., Staknis, D., Nguyen, H. B., Davis, F. C., Wilsbacher, L. D., King, D. P., Takahashi, J. S., and Weitz, C. J. (1998) *Science* **280,** 1564–1569
2. Kume, K., Zylka, M. J., Sriram, S., Shearman, L. P., Weaver, D. R., Jin, X., Maywood, E. S., Hastings, M. H., and Reppert, S. M. (1999) *Cell* **98,** 193–205
3. Chang, D. C., and Reppert, S. M. (2001) *Neuron* **29,** 555–558
4. Bunger, M. K., Wilsbacher, L. D., Moran, S. M., Clendenin, C., Radcliffe, L. A., Hogenesch, J. B., Simon, M. C., Takahashi, J. S., and Bradfield, C. A. (2000) *Cell* **22,** 1009–1017
5. Dunlap, J. C. (1998) *Science* **280,** 1548–1549
6. Price, J. L., Blau, J., Rothenfluh, A., Adodeely, M., Kloss, B., and Young, M. W. (1998) *Cell* **94,** 83–95
7. Sanada, K., Hayashi, Y., Harada, Y., Okano, T., and Fukada, Y. (2000) *J. Neurosci.* **20,** 986–991
8. Hayashi, Y., Sanada, K., and Fukada, Y. (2001) *FEBS Lett.* **491,** 71–75
9. Harada, Y. Sanada, K., and Fukada, Y. (2000) *J. Biol. Chem.* **275,** 37078–37085
10. Deguchi, T. (1979) *Science* **203,** 1245–1247
11. Cahill, G. M., and Besharse, J. C. (1995) *Prog. Retinal Eye Res.* **14,** 267–291
12. Yamaguchi, S., Mitsui, S., Miyake, S., Yan, L., Onishi, H., Yagita, K., Suzuki, M., Shibata, S., Kobayashi, M., and Okamura, H. (2001) *Curr. Biol.* **10,** 873–876
13. Obrietan, K., Impey, S., Smith, D., Athos, J., and Storm, D. R. (1999) *J. Biol. Chem.* **274,** 17748–17756
14. Obrietan, K., Impey, S., and Storm, D. R. (1998) *Nat. Neurosci.* **1,** 693–700
15. Yokota, S., Yamamoto, M., Moriya, T., Akiyama, M., Fukunaga, K, Miyamoto, E., and Shibata, S. (2001) *J. Neurochem.* **77,** 618–627
16. Okano, T., Yamamoto, K., Okano, K., Hirota, T., Kasahara, T., Sasaki, M., Takanaka, Y., and Fukada, Y. (2001) *Genes Cells* **6,** 825–836
17. Huang, W., and Erikson, R. L. (1994) *Proc. Natl. Acad. Sci. U. S. A.* **91,** 8960–8963
18. Sanada, K., Kokame, K., Takao, T., Shimonishi, Y., Yoshizawa, T., and Fukada, Y. (1994) *J. Biol. Chem.* **270,** 15459–15462
19. Takayama, M., Matsui, T., Sakai, T., and Tsugita, A. (1999) *J. Biomol. Tech.* **10,** 194–198
20. Yang, S.-H., Yates, P. R., Whitmarsh, A. J., Davis, R. J., and Sharrocks, A. D. (1998) *Mol. Cell. Biol.* **18,** 710–720
21. Takahata, S., Ozaki, T., Mimura, J., Kikuchi, Y., Sogawa, K., and Fujii-Kuriyama, Y. (2000) *Genes Cells* **5,** 739–747
22. Alvarez, E., Northwood, I. C., Gonzalez, E. A., Latour, D. A., Seth, A., Abate, C., and Curran, T. (1991) *J. Biol. Chem.* **266,** 15277–15285
23. Clark-Lewis, I., Sanghera, J. S., and Pelech, S. L. (1991) *J. Biol. Chem.* **266,** 15180–15184
24. Ko, G. Y.-P., Ko, M. H., and Dryer, S. E. (2001) *Neuron* **29,** 255–266
25. Field, M. D., Maywood, E. S., O'Brien, J. A., Weaver, D. R., Reppert, S. M., and Hastings, M. H. (2000) *Neuron* **25,** 437–447
26. Hogenesch, J. B., Gu, Y.-Z., Moran, S. M., Shinomura, K., Radcliffe, L. A., Takahashi, J. S., and Bradfield, C. A. (2000) *J. Neurosci.* **20,** RC83 (1–5)
27. Cermakian, N., Whitmore, D., Foulkes, N. S., and Sassone-Corsi, P. (2000) *Proc. Natl. Acad. Sci. U. S. A.* **97,** 4339–4344
28. Okano, T., Sasaki, M., and Fukada, Y. (2001) *Neurosci. Lett.* **300,** 111–114

THE JOURNAL OF BIOLOGICAL CHEMISTRY

Vol. 277, No. 46, Issue of November 15, pp. 44244–44251, 2002
Printed in U.S.A.

Glucose Down-regulates *Per1* and *Per2* mRNA Levels and Induces Circadian Gene Expression in Cultured Rat-1 Fibroblasts*[S]

Received for publication, June 22, 2002, and in revised form, August 20, 2002
Published, JBC Papers in Press, September 3, 2002, DOI 10.1074/jbc.M206233200

Tsuyoshi Hirota‡§, Toshiyuki Okano‡, Koichi Kokame¶, Hiroko Shirotani-Ikejima¶, Toshiyuki Miyata¶, and Yoshitaka Fukada‡‖

From the ‡Department of Biophysics and Biochemistry, Graduate School of Science, The University of Tokyo, Hongo 7-3-1, Bunkyo-ku, Tokyo 113-0033 and ¶National Cardiovascular Center Research Institute, Fujishirodai 5-7-1, Suita, Osaka 565-8565, Japan

In mammals, peripheral circadian clocks are present in most tissues, but little is known about how these clocks are synchronized with the ambient 24-h cycles. By using rat-1 fibroblasts, a model cell system of the peripheral clock, we found that an exchange of the culture medium triggered circadian gene expression that was preceded by slow down-regulation of *Per1* and *Per2* mRNA levels. This profile contrasts to the immediate up-regulation of these genes often observed for clock resetting. The screening of factor(s) responsible for the down-regulation revealed glucose as a key component triggering the circadian rhythm. The requirement of both glucose metabolism and RNA/protein synthesis for the down-regulation suggests the involvement of gene(s) immediately up-regulated by glucose metabolism. An analysis with high density oligonucleotide microarrays identified >100 glucose-regulated genes. We found among others immediately up-regulated genes encoding transcriptional regulators TIEG1, VDUP1, and HES1, in addition to cooperatively regulated genes that are associated with cholesterol biosynthesis and cell cycle. The immediate up-regulation of *Tieg1* and *Vdup1* expression was dependent on glucose metabolism but not on protein synthesis, suggesting that the transcriptional regulators mediate the glucose-induced down-regulation of *Per1* and *Per2* expression. These results illustrate a novel mode of peripheral clock resetting by external glucose, a major food metabolite.

Almost all organisms on earth exhibit daily changes in a variety of physiological processes, such as gene expression, metabolism, and behavior (1–3). Many of the daily changes persist under constant conditions with intrinsic period lengths (~24 h) under the control of autonomous biological pacemakers called circadian clocks. The circadian clock can be reset by environmental time cues (such as light) to synchronize with the ambient 24-h cycles.

In mammals, genetic and molecular analyses revealed transcription/translation-based negative feedback loop(s) that constitutes the core oscillator of the circadian clock. This loop involves a well concerted regulation of *Per*, *Cry*, *Clock*, *Bmal* genes and their products, resulting in robust oscillations of *Per* and *Bmal* mRNA levels in antiphase and of several output genes such as *Dbp* (4, 5). The core oscillatory mechanism seems to be common to both the central clock localized in the hypothalamic suprachiasmatic nucleus (SCN)[1] and peripheral clocks distributed in most tissues and cells (6–8). However, peripheral clocks are distinct from the central clock in that the circadian expression of the clock genes persists only for several days in culture (9). The cyclic gene expression in peripheral clocks is probably sustained by synchronization with some neural and/or humoral signals generated by the SCN in a circadian manner (9–11).

Recent studies showed that restricted feeding cycle synchronizes peripheral clocks independently of the central clock (12–14), suggesting that feeding may be a dominant time cue for peripheral clocks. These observations led to an interesting idea that the central clock indirectly synchronizes peripheral clocks by regulating feeding behaviors (12–14). This model predicts peripheral clocks to be reset by feeding-associated events such as food processing, metabolite absorption, and/or change in hormone levels, but little is known regarding the molecular identity of the feeding signal to be sent to peripheral clocks. Cultured cells such as rat-1 fibroblasts have been used as a model for the study on the peripheral clock system, especially on the resetting mechanism (7, 8, 15–19). This is because circadian gene expression in these cells is induced not only by serum shock that was originally found to be effective (7) but also by treatment with many chemicals that activate a variety of signal transduction pathways (8, 15–19). Such induction of circadian rhythm is always preceded by a stimulus-induced immediate up-regulation of *Per1* and/or *Per2* mRNA levels (7, 8, 15–19), an event that plays an important role in the photic-resetting of the central clock (20–22). Here we demonstrate that in rat-1 fibroblasts, an exchange of the culture medium induced circadian expression of the clock genes, which was preceded by slow down-regulation, not by rapid up-regulation, of *Per1* and *Per2* mRNA levels. An addition of glucose to the culture medium was a key step in this novel type of rhythm

* This work was supported in part by grants-in-aid from the Ministry of Education, Culture, Sports, Science and Technology of Japan. The costs of publication of this article were defrayed in part by the payment of page charges. This article must therefore be hereby marked "*advertisement*" in accordance with 18 U.S.C. Section 1734 solely to indicate this fact.

[S] The on-line version of this article (available at *http://www.jbc.org*) contains supplemental "Experimental Procedures," Figs. 1 and 2, and Table I.

§ Supported by Research Fellowships of the Japan Society for the Promotion of Science for Young Scientists.

‖ To whom correspondence should be addressed: Dept. of Biophysics and Biochemistry, Graduate School of Science, The University of Tokyo, Hongo 7-3-1, Bunkyo-ku, Tokyo 113-0033, Japan. Tel./Fax: 81-3-5802-8871; E-mail: sfukada@mail.ecc.u-tokyo.ac.jp.

[1] The abbreviations used are: SCN, suprachiasmatic nucleus; DMEM, Dulbecco's modified Eagle's medium; RT, reverse transcriptase; 3-OMG, 3-*O*-methylglucose; TIEG1, transforming growth factor β-inducible early gene 1; VDUP1, vitamin D_3 up-regulated protein 1; HES1, hairy and enhancer of split 1; CREB, cAMP-response element-binding protein; SREBP, sterol regulatory element-binding protein.

induction, and the down-regulation of *Per1* and *Per2* expression required ongoing RNA and protein synthesis. Microarray analysis revealed glucose-induced up- or down-regulation of many genes, some of which encode transcriptional regulators and may play an important role in the induction of circadian rhythm.

EXPERIMENTAL PROCEDURES

Materials—All compounds including each component of DMEM were dissolved in water before their addition to the culture medium. Compositions of solutions were as follows (final concentrations in the culture medium): salts (0.9 mM $CaCl_2$, 0.12 μM $Fe(NO_3)_3 \cdot 9H_2O$, 2.7 mM KCl, 0.41 mM $MgSO_4$, 55 mM NaCl, 22 mM $NaHCO_3$, and 0.45 mM NaH_2PO_4), glucose (2.8 mM), pyruvate (0.5 mM), amino acids (2 mM L-glutamine, 0.2 mM glycine, 0.2 mM L-serine, and 1× minimum essential medium amino acids solution (Invitrogen)), and vitamins (2× minimum essential medium vitamin solution (Invitrogen)).

Cell Culture—Rat-1 fibroblasts were cultured at 37 °C under 5% CO_2, 95% air in DMEM containing 5.6 mM glucose (Invitrogen) supplemented with 100 units/ml penicillin, 100 μg/ml streptomycin, and 5% fetal bovine serum (Invitrogen). Because light/dark cycle did not affect circadian expression of clock genes in rat-1 fibroblasts,[2] the cells were kept in darkness in the incubator and all of the manipulations were performed under the light condition. For the experiments, cells were plated at a density of ~2.5×10^5 cells/35-mm dish for reverse transcriptase (RT)-PCR analysis or ~1.2×10^6 cells/10-cm dish for microarray analysis. The cells reached confluence 2 days after the plating, and they were maintained for another day prior to the start of experiments (at time 0). In the experiments (Figs. 3–10), 10 × concentrated solution of compound(s) in one-ninth volume was added to the culture medium.

Preparation of RNA Samples and RT-PCR Analysis—The cultured cells were washed with ice-cold phosphate-buffered saline, homogenized with 1 ml (for 35-mm dish) or 3 ml (for 10-cm dish) of TRIzol reagent (Invitrogen), and stored at −80 °C until use. The extraction of total RNA and quantitative RT-PCR analysis were performed as described previously (23) with some modifications (see "Supplemental Experimental Procedures").

Microarray Analysis—Poly(A)$^+$ RNA was isolated from total RNA by Oligotex-dT30 (Roche Molecular Biochemicals) and used to prepare cRNA sample as described in the GeneChip Expression Analysis Technical Manual (Affymetrix). Double-stranded cDNA was synthesized from 1 μg of poly(A)$^+$ RNA by SuperScipt Choice System (Invitrogen) with T7-$(dT)_{24}$ primer (Amersham Biosciences). The product was used as a template to synthesize biotin-labeled cRNA by *in vitro* transcription with ENZO BioArray High Yield RNA Transcript-Labeling Kit (Affymetrix), and cRNA amplified was fragmented by heat treatment in the presence of KOAc and $Mg(OAc)_2$. 15 μg of cRNA sample then was applied to GeneChip Rat Genome U34A Array (Affymetrix). Hybridization, washing, staining, and scanning were performed according to the GeneChip Manual.

The raw data for each probe set were calculated from the scanned array image by using GeneChip Analysis Suite software (Affymetrix) and subsequently analyzed by using GeneSpring software (Silicon Genetics). To compare the data from different arrays, the signal intensity value for each probe set on each array was normalized as follows: negative control value (median intensity value of negative control genes included in the array) was subtracted from the raw values, and the calculated values were divided by their median value. The values below 0 were set to 0. The normalized values from four independent arrays were then averaged for each probe set at each time point, and they were compared between two time points (time 0 with 1 or 4 h) to select probe sets for up- or down-regulated genes with the following criteria: (i) the intensity exhibits 3-fold or greater change, (ii) the change is significant (mean ± S.E. at each time point do not overlap with each other), and (iii) the signal is marked as "present" by the GeneChip software in at least 2 of 4 arrays at the time point for the higher average intensity. Expressed sequence tags in the selected probe sets were characterized by searching GenBank™ data base using BLAST program. Nomenclature of the selected genes was updated by using OMIM and GenBank™ databases. Overlapping probe sets for the same gene were unified by leaving one that exhibited the strongest signal when their expression profiles were similar to each other. Hierarchical clustering of the selected probe sets was then carried out using Cluster program (24) in uncentered correlation/average linkage clustering mode, and the result was visualized with the aid of TreeView program (24). Functional assignment of the selected genes was performed by searching OMIM and PubMed databases.

[2] T. Hirota, T. Okano, and Y. Fukada, unpublished data.

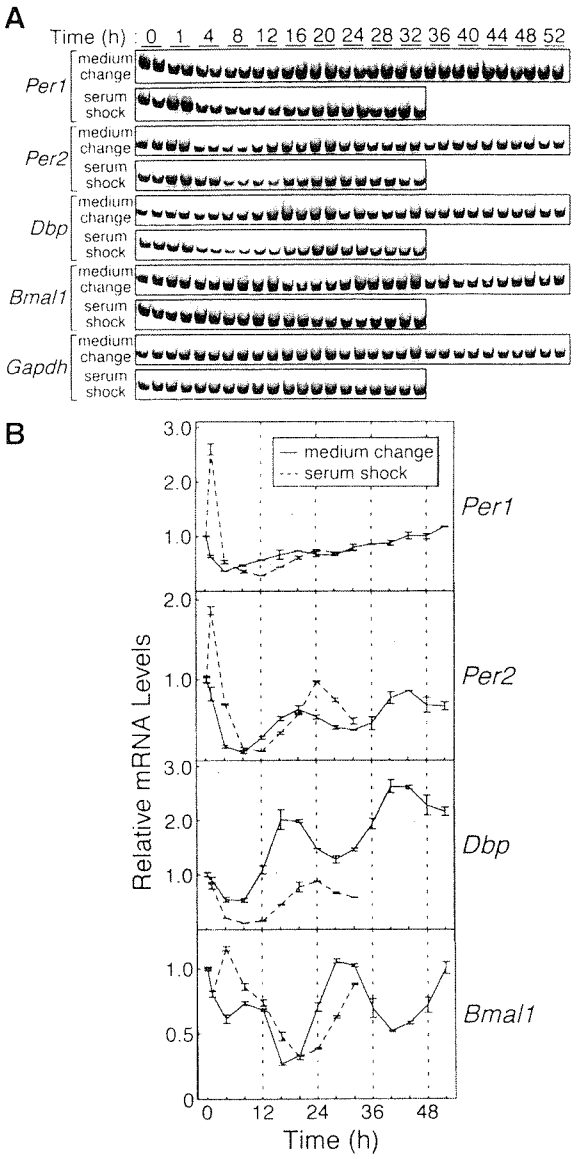

FIG. 1. **Temporal expression patterns of clock genes in rat-1 fibroblasts after medium exchange or serum shock.** *A*, at time 0, the culture medium was exchanged with serum-free medium (*medium change*) or with medium containing 50% horse serum (*serum shock*). The serum-treated cells were shifted to serum-free medium at 2 h. The cells were collected at indicated time points, and the relative mRNA levels of *Per1*, *Per2*, *Dbp*, *Bmal1*, and *Gapdh* were determined by RT-PCR analysis. *B*, the signals obtained in *panel A* for each mRNA were quantitated and normalized to those for *Gapdh* mRNA, the level of which was nearly constant throughout the experiment. The mean value at time 0 was set to 1. Data are the mean ± S.D. of two independent samples. Results for serum-treated cells were similar to those previously reported for serum- or endothelin-1-treated rat-1 fibroblasts (7, 8).

RESULTS

Exchange of Culture Medium Down-regulates Per1 and Per2 mRNA Levels and Induces Circadian Gene Expression in Rat-1 Fibroblasts—In a search for a stimulus that induces rhythmic expression of some clock genes in rat-1 fibroblasts, we unexpectedly found that an exchange of the culture medium to serum-free medium triggered circadian changes in mRNA levels of *Per2*, *Dbp*, *Bmal1*, and *Cry1* genes (Fig. 1 and Supple-

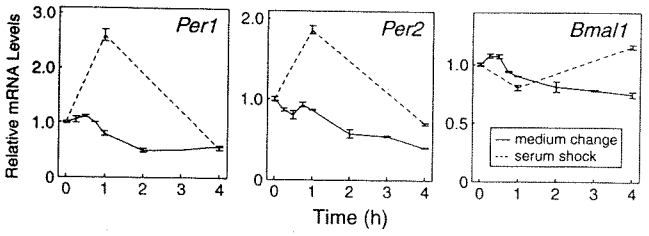

FIG. 2. **Immediate changes of *Per1*, *Per2*, and *Bmal1* mRNA levels after medium exchange.** At time 0, the culture medium was exchanged with serum-free medium. The cells were collected at indicated time points, and the relative mRNA levels of *Per1*, *Per2*, *Bmal1*, and *Gapdh* were determined by RT-PCR analysis. The signals obtained for each mRNA were normalized to those for *Gapdh* mRNA and the mean value at time 0 was set to 1 (*solid lines*). Data are the mean ± S.D. of two independent samples. The serum shock experiment data from Fig. 1*B* are replotted for comparison (*dashed lines*).

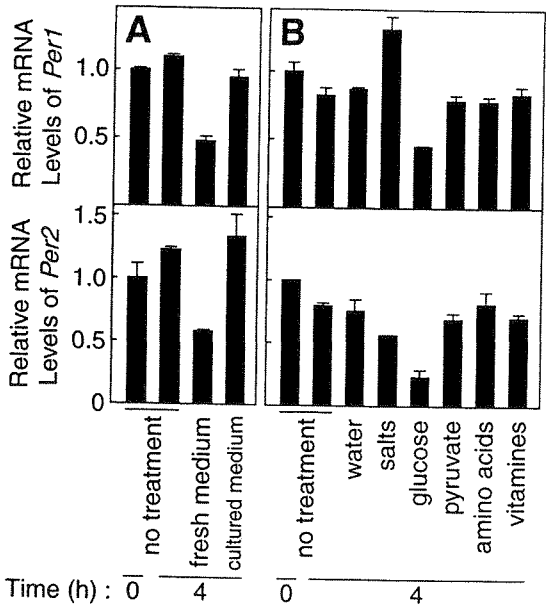

FIG. 3. **Screening of factor that down-regulates *Per1* and *Per2* expression.** *A*, effects of physical stimuli. At time 0, the culture medium was exchanged with fresh serum-free medium (*fresh medium*) or with medium recovered from another culture dish (*cultured medium*). *B*, effects of medium components. At time 0, the solution containing indicated component(s) of DMEM was added to the culture medium. Increases in the final concentrations of all of the components attributed to the addition were half of their concentrations in DMEM. In each experiment (*A* and *B*), the cells were collected at time 0 or after 4-h treatment, and the relative mRNA levels of *Per1*, *Per2*, and *Gapdh* were determined by RT-PCR analysis. The signals obtained for each mRNA were normalized to those for *Gapdh* mRNA, and the mean value at time 0 was set to 1. Data are the mean ± S.D. of two independent samples.

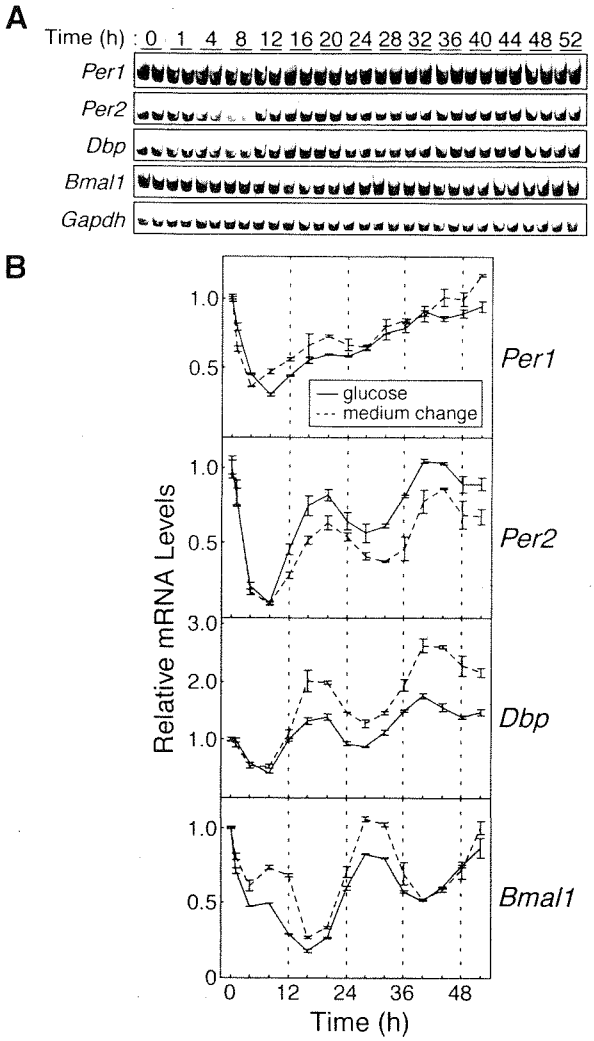

FIG. 4. **Temporal expression patterns of clock genes after addition of glucose to the culture medium.** *A*, at time 0, glucose solution (5.6 mM final concentration) was added to the culture medium. The cells were collected at indicated time points, and the relative mRNA levels of *Per1*, *Per2*, *Dbp*, *Bmal1*, and *Gapdh* were determined by RT-PCR analysis. *B*, the signals obtained in *panel A* for each mRNA were normalized to those for *Gapdh* mRNA and the mean value at time 0 was set to 1 (*solid lines*). Data are the mean ± S.D. of two independent samples. The medium exchange experiment data from Fig. 1*B* are replotted for comparison (*dashed lines*).

mental Fig. 1, *medium change*). The phase of the expression rhythm of each gene induced by the medium exchange was advanced by ~4 h relative to that observed after a pulse treatment with 50% serum (Fig. 1*B* and Supplemental Fig. 1*B*, compare *solid lines* with *dashed lines*). Notably, no immediate increase was observed in mRNA levels of *Per1* and *Per2* gene after the medium exchange, and this contrasted markedly with the rapid up-regulation of *Per1* and *Per2* expression after serum shock (Fig. 1*B*). We further analyzed immediate changes of *Per1*, *Per2*, and *Bmal1* mRNA levels after the medium exchange and found that these mRNA levels began to decrease 45–60 min after the treatment (Fig. 2). These results indicate that the circadian rhythm is induced by the medium exchange in a manner quite different from that triggered by the serum shock and predict a novel mechanism of rhythm induction that is preceded by slow down-regulation of *Per1* and *Per2* expression.

Glucose Down-regulates Per1 and Per2 mRNA Levels and Induces Circadian Gene Expression—The exchange of the culture medium might have multiple effects on the cultured cells, and hence, we searched for factor(s) that causes the down-regulation of *Per1* and *Per2* mRNA levels (Fig. 3). An exchange of the culture medium with medium recovered from another culture dish had a minimal effect on *Per1* and *Per2* expression (Fig. 3*A*), eliminating the possibility that the down-regulation was caused by any physical stimuli such as a transient change in temperature and/or pH of the medium or exposure of the cells to the air. We next screened the components of DMEM (salts, glucose, pyruvate, amino acids, and vitamins) by adding them separately to the culture medium and found that glucose remarkably reduced not only *Per1* but also *Per2* expression (Fig. 3*B*) in a manner similar to that observed after the medium exchange (Fig. 3*A*). These observations suggest glucose as a key molecule that induces the cellular circadian rhythm. We then examined whether the fresh supply of glucose can trigger

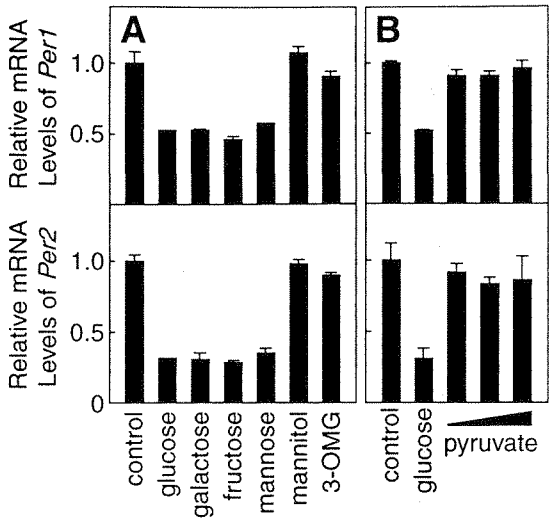

FIG. 5. **Effects of glucose-related compounds and pyruvate on *Per1* and *Per2* mRNA levels.** *A*, effects of glucose-related compounds. At time 0, the solution containing indicated compound (each 2.8 mM final concentration) or water (as a control) was added to the culture medium. Cells do not metabolize mannitol and 3-OMG. *B*, effect of pyruvate. At time 0, glucose solution (final 2.8 mM), pyruvate solution (final 0.5, 5.6, 11.2 mM), or water (as a control) was added to the culture medium. In each experiment (*A* and *B*), the cells were collected after 4-h treatment, and the relative mRNA levels of *Per1*, *Per2*, and *Gapdh* were determined by RT-PCR analysis. The signals obtained for each mRNA were normalized to those for *Gapdh* mRNA, and the mean value of the control was set to 1. Data are the mean ± S.D. of two independent samples.

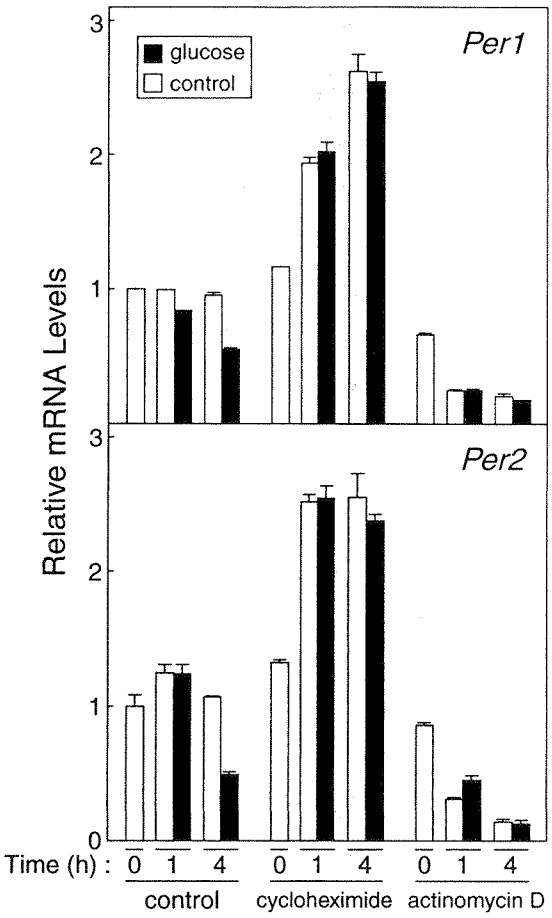

FIG. 6. **Effects of cycloheximide and actinomycin D on glucose-induced down-regulation of *Per1* and *Per2* expression.** Cycloheximide solution (36 μM final concentration, *middle group*), actinomycin D solution (final 0.8 μM, *right group*), or water (as a control, *left group*) was added to the culture medium 30 min before the addition of glucose solution (final 5.6 mM, *filled bar*) or water (as a control, *blank bar*) at time 0. The cells were collected at indicated time points, and the relative mRNA levels of *Per1*, *Per2*, and *Gapdh* were determined by RT-PCR analysis. The signals obtained for each mRNA were normalized to those for *Gapdh* mRNA, and the mean value of the control at time 0 was set to 1. Data are the mean ± S.D. of two independent samples.

the circadian gene expression as did the medium exchange (Fig. 4). After the addition of glucose solution (5.6 mM final concentration) to the culture medium, *Per2*, *Dbp*, and *Bmal1* genes exhibited robust circadian expression with profiles nearly identical to those observed after the medium exchange (Fig. 4*B*, compare *solid lines* with *dashed lines*), and the profiles were obviously different from those after the serum shock (Fig. 1*B*, *dashed lines*). These results demonstrate that glucose can trigger circadian rhythm and suggest that the induction of circadian rhythm by the medium exchange is mainly attributed to the supply of glucose.

Down-regulation of Per1 and Per2 mRNA Levels Is Dependent on Glucose Metabolism and RNA/Protein Synthesis—We were interested in the molecular mechanism underlying the induction of circadian rhythm that is preceded by the down-regulation of *Per1* and *Per2* expression, and we first investigated whether glucose itself or its metabolism is important for the down-regulation (Fig. 5*A*). Among several glucose-related compounds examined, metabolizable carbohydrates such as galactose, fructose, and mannose reduced *Per1* and *Per2* expression to the level that was achieved by the glucose addition (Fig. 5*A*). On the other hand, no significant change of the gene expression was observed with non-metabolizable mannitol and 3-*O*-methylglucose (3-OMG) (Fig. 5*A*), suggesting that metabolism of glucose is required for the down-regulation. Because NAD(P)H/NAD(P)$^+$ ratio seems to determine binding efficiencies of CLOCK-BMAL1 transcriptional activators to E-box sequences (25), glucose may directly attenuate the transcription of *Per1* and *Per2* genes by changing NAD(P)H/NAD(P)$^+$ ratio. We then examined the effect of pyruvate addition, which would change the intracellular NADH/NAD$^+$ ratio (Fig. 5*B*). Even 4-fold molar excess of pyruvate relative to glucose had minimal effect on *Per1* and *Per2* mRNA levels (Fig. 5*B*), suggesting that neither change in NADH/NAD$^+$ ratio nor metabolism of pyruvate causes the down-regulation. These observations prompted us to explore the dependence of the down-regulation on ongoing protein synthesis (Fig. 6). Although both *Per1* and *Per2* mRNA levels gradually increased after the addition of cycloheximide to the culture medium (Fig. 6, *blank bars* in *middle group*), the inhibition of protein synthesis abrogated the effect of glucose addition (Fig. 6, compare *blank bars* with *filled bars* in *middle group*). Similarly, the inhibition of RNA synthesis by actinomycin D blunted the down-regulating effect of glucose (Fig. 6, compare *blank bars* with *filled bars* in *right group*), although both *Per1* and *Per2* mRNA levels gradually decreased after the addition of the inhibitor (Fig. 6, *blank bars* in *right group*). These results indicate that the down-regulation of *Per1* and *Per2* expression by glucose requires newly synthesized RNA and protein.

Genes Associated with Transcriptional Regulation, Cholesterol Biosynthesis, and DNA Replication are Up-regulated by Glucose—We searched for genes that responded immediately or slowly to the glucose addition by using high density oligonucleotide array technology. The cells were harvested just before, 1 h after, or 4 h after the glucose addition, and the cRNA sample from each preparation was hybridized to microarray containing 8,800 probe sets, some of which recognize same genes. The array contained probe sets for *Per2*, *Dbp*, and

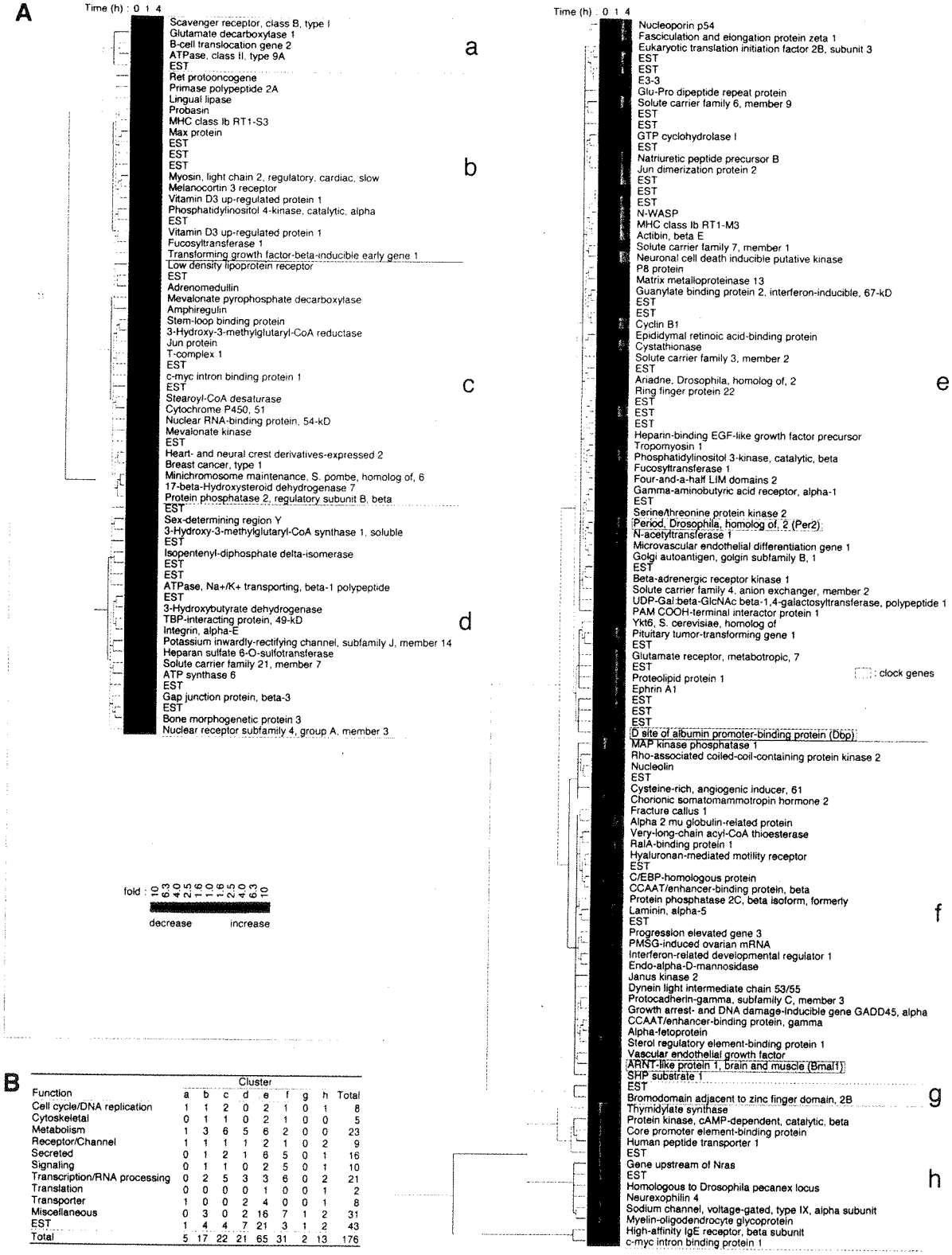

B

Function	Cluster a	b	c	d	e	f	g	h	Total
Cell cycle/DNA replication	1	1	2	0	2	1	0	1	8
Cytoskeletal	0	1	1	0	2	1	0	0	5
Metabolism	1	3	6	5	6	2	0	0	23
Receptor/Channel	1	1	1	1	2	1	0	2	9
Secreted	0	1	2	1	6	5	0	1	16
Signaling	0	1	1	0	2	5	0	1	10
Transcription/RNA processing	0	2	5	3	3	6	0	2	21
Translation	0	0	0	0	1	0	0	1	2
Transporter	1	0	0	2	4	0	0	1	8
Miscellaneous	0	3	0	2	16	7	1	2	31
EST	1	4	4	7	21	3	1	2	43
Total	5	17	22	21	65	31	2	13	176

FIG. 7. **Classification of the genes regulated by glucose addition.** *A*, at time 0, glucose solution (5.6 mM final concentration) was added to the culture medium. The cells were collected at time 0 or at 1 or 4 h after the glucose addition. They were analyzed by microarray technology, and the relative signal intensity for each probe set was calculated. The 176 probe sets for genes exhibiting 3-fold or greater changes in their signals after the glucose addition were classified by hierarchical clustering according to the temporal expression patterns (clusters *a–h*). For genes encoding c-*myc* intron-binding protein 1, fucosyltransferase 1, and vitamin D_3 up-regulated protein 1, data for two independent probe sets for each gene are shown because they exhibited expression profiles distinct from each other. Signal intensities obtained from four independent samples were averaged for each probe set at each time point, and a ratio of the value at each time point to that at time 0 is indicated by *colored boxes*. The color scale ranges from saturated *green* (10-fold decrease) to saturated *red* (10-fold increase). *Columns* represent time points, and *rows* represent genes (indicated by their names) among which clock genes are *boxed*. The dendrogram shows similarities among the selected probe sets in their temporal expression patterns. An immediate up-regulation of *Max* gene was not reproducible in RT-PCR analysis (data not shown). *B*, the 176 probe sets were classified according to the function of their corresponding gene products. The number of the genes belonging to each class is indicated.

Bmal1 genes, and their signal intensities exhibited temporal profiles similar to those measured by RT-PCR analysis (Supplemental Fig. 2), ensuring the reliability of the microarray data. We found 176 probe sets exhibiting 3-fold or greater changes in their signal intensities after the glucose addition (Supplemental Table I, representing 130 known genes with three overlapping probe sets and 43 expressed sequence tags without sequence homology to any known gene). Based on the temporal expression pattern, the 176 probe sets were grouped into eight clusters by hierarchical clustering method (Fig. 7*A*, clusters *a–h*). *Per2* and *Dbp* genes belonged to cluster *e* containing delayed down-regulated genes, and *Bmal1* gene belonged to cluster *f* containing steadily down-regulated genes (Fig. 7*A*, *boxed*). Among 24 probe sets exhibiting immediate up-regulation after the glucose addition (Fig. 7*A*, clusters *a*, *b*, and *g*), we found two genes encoding transcriptional regulators (Fig. 8*A*, *upper panel*); a transcriptional repressor TIEG1 (26) and a putative transcriptional regulator VDUP1 (27). In addition, a transcriptional repressor HES1 (28) gene was found to exhibit 2.5-fold up-regulation within 1 h after the glucose addition (Fig. 8*A*, *middle panel*). On the other hand, the glucose addition had almost no effect on the expression levels of transcription factors such as c-*fos*, *jun-B*, NGFI-A, NGFI-B, and *egr-3* (Fig. 8*A*, *lower panel*), which in the rodent SCN are immediately up-regulated by light (29). This result further supports the novelty of the mechanism underlying the glucose-dependent induction of circadian rhythm in rat-1 cells. The classification of the 176 probe sets according to the function of their corresponding gene products (Fig. 7*B*) revealed that many genes associated with cholesterol biosynthesis (Fig. 8*B*) or with the cell cycle and DNA replication (Fig. 8*C*) exhibit characteristic expression patterns after the glucose addition (see "Discussion").

Tieg1 and Vdup1 Are Glucose-responsive Immediate-early Genes—To characterize properties of the glucose-induced up-regulation of *Tieg1*, *Vdup1*, and *Hes1* expression, we investigated detailed temporal changes of their mRNA levels (Fig. 9). The addition of glucose transiently up-regulated *Tieg1* and *Hes1* expression with a peak at ~1 h after the treatment, whereas it persistently up-regulated *Vdup1* expression (Fig. 9, *solid lines*). On the other hand, the addition of non-metabolizable 3-OMG had little or no effect on *Tieg1* and *Vdup1* mRNA levels but increased *Hes1* mRNA levels in a manner similar to that after the glucose addition (Fig. 9, compare *solid lines* with *dashed lines*). It is most probable that *Tieg1* and *Vdup1* mRNA levels are immediately up-regulated by glucose metabolism, and this property is similar to that of the down-regulation of *Per1* and *Per2* expression (Fig. 5*A*). Thus, *Tieg1* and *Vdup1* genes are the candidates mediating the effect of glucose on *Per1* and *Per2* expression.

We then tested the effects of protein and RNA synthesis inhibitors on the up-regulation of *Tieg1* and *Vdup1* mRNA levels induced by glucose (Fig. 10). Even in the presence of cycloheximide, *Tieg1* and *Vdup1* mRNA levels were up-regulated by the glucose addition (Fig. 10, compare *blank bars* with *filled bars* in *middle group*), indicating that the up-regulation is independent of new protein synthesis. On the other hand, the effect of glucose addition was blunted by the actinomycin D treatment, suggesting that the glucose action centers at the level of transcription. These results indicate that *Tieg1* and *Vdup1* are glucose-responsive immediate-early genes, which may act as a direct mediator of the glucose effect.

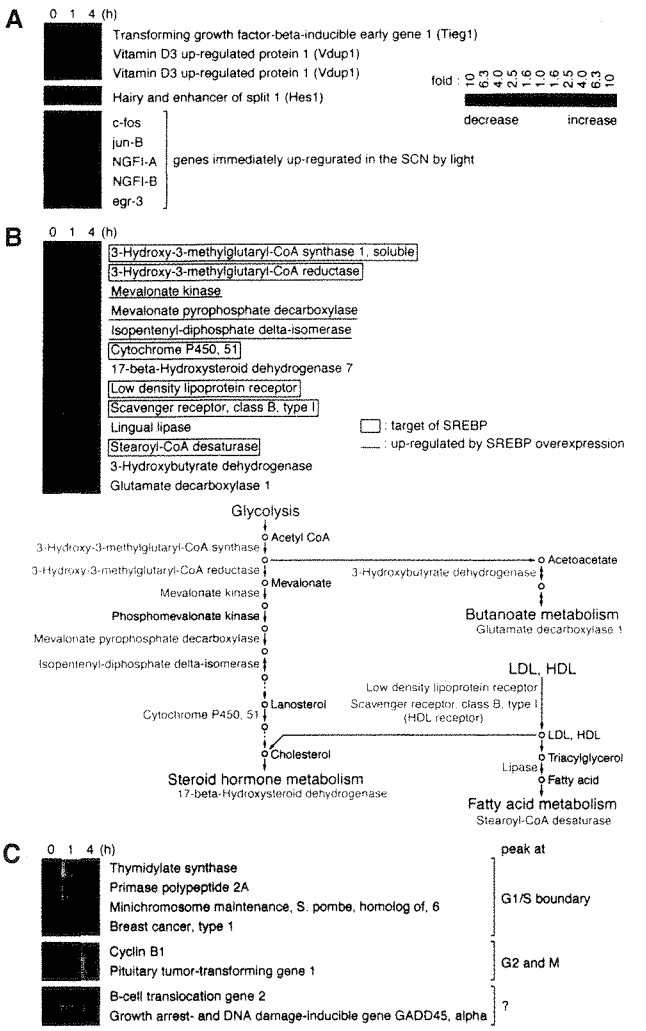

FIG. 8. **Gene groups showing characteristic expression patterns after glucose addition.** The microarray analysis was performed as described in the legend to Fig. 7. Signal intensities obtained from four independent samples were averaged for each probe set at each time point, and a ratio of the value at each time point to that at time 0 is indicated by *colored boxes*. The color scale ranges from saturated *green* (10-fold decrease) to saturated *red* (10-fold increase). *Columns* represent time points, and *rows* represent genes as indicated by their names. The probe sets exhibiting 3-fold or greater changes in their signals after the glucose addition were classified according to the function of their corresponding gene products. *A*, the immediately up-regulated genes associated with transcriptional regulation. *Upper panel*, transcriptional regulators up-regulated within 1 h after the glucose addition. For *Vdup1* gene, data for two independent probe sets are shown, because they exhibited expression profiles distinct from one another. *Middle panel*, transcriptional regulator HES1 gene exhibiting 2.5-fold up-regulation within 1 h after the glucose addition. *Lower panel*, transcription factors known to be immediately up-regulated in the rodent SCN by light. *B*, the genes associated with cholesterol biosynthesis. *Upper panel*, *boxed genes* are targets of SREBP transcription factor, and *underlined genes* are known to be up-regulated by SREBP overexpression. *Lower panel*, *scheme* of cholesterol biosynthetic pathway was constructed with the aid of KEGG data base (www.kegg.com). Genes for the enzymes shown in *red* were up-regulated by the glucose addition. The array contains no probe set for phosphomevalonate kinase gene. *C*, the genes associated with the cell cycle and DNA replication. These genes were divided into three subclasses according to their known mRNA expression patterns during the cell cycle (*upper* to *lower panels*).

DISCUSSION

Glucose as a Direct Resetting Signal for Peripheral Clocks—This study stemmed from our fortuitous observation that an exchange of the culture medium induced circadian gene expression in rat-1 fibroblasts (Fig. 1 and Supplemental Fig. 1). The screening of factors associated with the medium exchange led to the identification of glucose as the key molecule (Fig. 3), and glucose addition was shown to induce the circadian rhythm in culture (Fig. 4). Glucose is one of the major food metabolites,

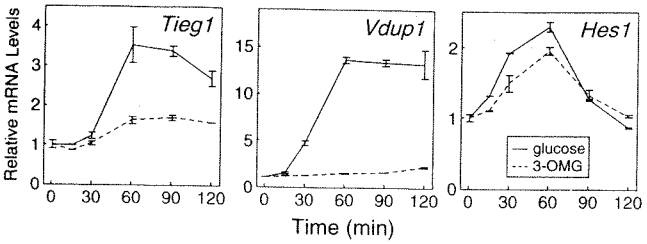

FIG. 9. **Immediate changes of *Tieg1*, *Vdup1*, and *Hes1* mRNA levels after glucose or 3-OMG addition.** At time 0, glucose (5.6 mM final concentration, *solid lines*) or 3-OMG (final 5.6 mM, *dashed lines*) solution was added to the culture medium. The cells were collected at indicated time points, and the relative mRNA levels of *Tieg1*, *Vdup1*, *Hes1*, and *Gapdh* were determined by RT-PCR analysis. The signals obtained for each mRNA were normalized to those for *Gapdh* mRNA, and the mean value at time 0 was set to 1. Data are the mean ± S.D. of two independent samples.

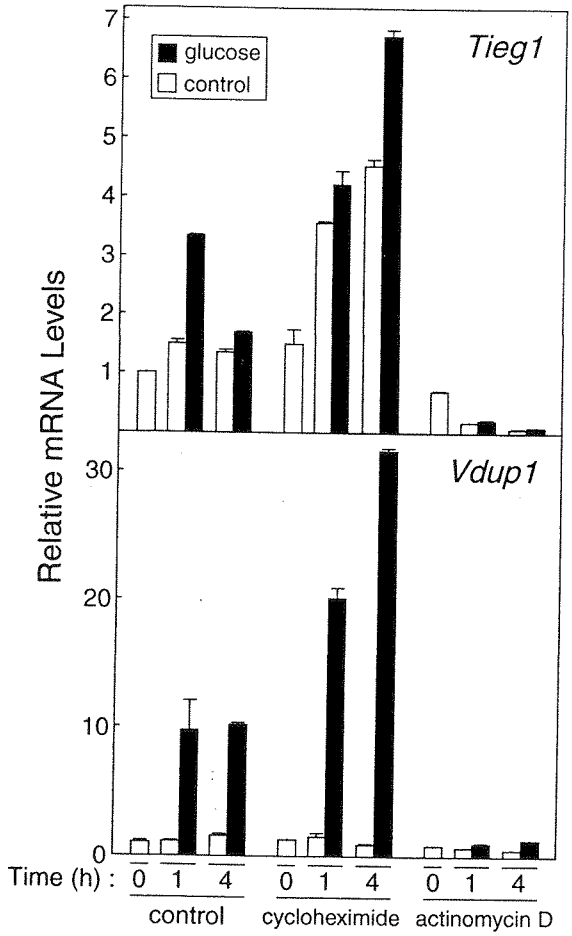

FIG. 10. **Effects of cycloheximide and actinomycin D on glucose-induced up-regulation of *Tieg1* and *Vdup1* expression.** Cycloheximide solution (36 μM final concentration, *middle group*), actinomycin D solution (final 0.8 μM, *right group*), or water (as a control, *left group*) was added to the culture medium 30 min before the addition of glucose solution (final 5.6 mM, *filled bar*) or water (as a control, *blank bar*) at time 0. The cells were collected at indicated time points, and the relative mRNA levels of *Tieg1*, *Vdup1*, and *Gapdh* were determined by RT-PCR analysis. The signals obtained for each mRNA were normalized to those for *Gapdh* mRNA, and the mean value of the control at time 0 was set to 1. Data are the mean ± S.D. of two independent samples.

and in rodents, plasma glucose level exhibits diurnal rhythm (30). In accordance with this rhythm, 3 of the 4 genes known to contain the glucose-response element (31) exhibit diurnal expression patterns in the liver (32, 33). In addition, glucose, but not fat or non-nutritive bulk, causes a phase-shift of food-anticipatory activity rhythm, which occurs after a restriction of feeding time (34, 35). Thus, our present results predict an important role of glucose as a direct resetting signal for peripheral clocks *in vivo*, and this idea would explain how the peripheral clock in the liver responds to a change in feeding time faster than the clocks in other tissues (12, 13).

Besides glucose, the levels of glucose-regulated hormones such as insulin and glucagon exhibit diurnal rhythms in plasma (30), and insulin immediately up-regulates *Per1* and *Per2* expression in rat-1 fibroblasts (18). In addition, recent studies revealed an important role of glucocorticoid hormones and vitamins in the resetting of peripheral clocks (17, 36). Taken together, peripheral clocks in various tissues may be coordinately regulated by multiple circulating factors, the levels of which are affected by the food intake. Paradoxically, because of such a network, it is not feasible to evaluate the effect of glucose as a direct resetting signal *in vivo*. It is the model cell system such as rat-1 fibroblasts that enables this study.

Down-regulation of Per1 and Per2 mRNA Levels by Glucose—The induction of circadian rhythm by glucose seems quite different in mechanism from either the rhythm induction by serum shock in cultured fibroblasts or photic resetting of the central clock (Figs. 1, 2, 4, 8*A*, and Supplemental Fig. 1). It should be stressed that the circadian gene expression induced by glucose did not accompany an immediate up-regulation of any clock gene (Figs. 1, 2, 4, and Supplemental Fig. 1). The down-regulation of *Per1* and *Per2* mRNA levels by glucose (Figs. 1, 2, and 4) is reminiscent of *in vivo* down-regulation of these genes observed in the rodent SCN during non-photic-resetting (37, 38), suggesting a common mechanism among the SCN and peripheral clocks for the resetting that is preceded by the down-regulation of *Per1* and *Per2* expression.

Characterization of the molecular mechanism by which glucose down-regulates *Per1* and *Per2* mRNA levels would be of great importance. The important role of glucose metabolism and the minimal effect of pyruvate (Fig. 5) imply that earlier metabolic process of glucose contributes to the down-regulation of *Per1* and *Per2* expression, and it is less likely that a change in NADH/NAD^+ ratio plays an essential role in it. The glucose metabolism would initiate new RNA and protein synthesis that is required for the down-regulation (Fig. 6). As the candidates for such glucose-responsive genes, we found two genes for transcriptional regulators TIEG1 and VDUP1 (Figs. 7 and 8*A*) whose mRNA levels were immediately up-regulated in a glucose metabolism-dependent manner (Fig. 9). The identification of *Tieg1* and *Vdup1* as glucose-responsive immediate-early genes (Fig. 10) may implicate these gene products in the glucose effect. TIEG1 was originally identified as a transforming growth factor β-inducible early gene, and this protein binds to Sp1 sequence to repress the transcription (26). Because several Sp1 sequences are present near transcription initiation sites of *Per1* and *Bmal1* genes (39, 40), it is possible that TIEG1 acts as glucose-dependent negative regulator of these genes. On the other hand, VDUP1 (identified as vitamin D_3 up-regulated protein) is known to negatively regulate thioredoxin, a multifunctional protein that promotes DNA binding of various transcription factors such as NFκB, AP-1, and p53 (27). Interestingly, thioredoxin enhances transactivation activities of basic helix-loop-helix-PAS transcription factors HIF1α and HLF (HIF1α-like factor) by facilitating their interaction with co-activator CREB-binding protein/p300 (41), which also mediates transactivation by CLOCK-BMAL1 heterodimer (42). Thus, VDUP1 might inactivate CLOCK-BMAL1 by inhibiting thioredoxin function and hence reduce the transcription of *Per1* and

Per2 genes. Taken together, TIEG1 and VDUP1 are candidates for clock-associated molecule(s) mediating the glucose signal.

Other Cellular Responses to Glucose—The microarray analysis revealed glucose-induced up-regulation or down-regulation of genes associated with a variety of metabolic pathways (Fig. 7). Among them, 13 genes were related to cholesterol biosynthesis (Fig. 8*B*), and they were all up-regulated within 4 h after the glucose addition. Such an up-regulation may lead to an increase of cellular activity to synthesize cholesterol from glucose newly supplied. Most of these genes are known to be under the control of common transcription factor, SREBP (43, 44), implying the activation of SREBP by the glucose addition.

The glucose addition also up-regulated four genes related to DNA replication (Fig. 8*C*, *upper panel*) and down-regulated two genes related to the cell cycle (Fig. 8*C*, *middle panel*). The former four genes are known to exhibit peak mRNA levels at the G_1/S boundary of the cell cycle (45, 46), and the latter two genes exhibit peak mRNA levels at G_2 and M phases (47, 48). Taken together, it appeared as if the cells started to progress from G_0 or G_1 phase after the glucose addition. However, the number of the cells in culture was almost constant from 24 h before to 48 h after the glucose addition (data not shown), indicating that the cells did not proliferate under the confluent condition. Considering that several genes related to the cell cycle exhibit circadian expression patterns in confluent rat 3Y1 fibroblasts (49), we assume that cell cycle-related genes play some roles other than the progression of the cell cycle when the cells are confluent. Notably, all of the four up-regulated genes are targets of a transcription factor E2F (45, 50), and this predicts glucose-dependent activation of E2F as well.

In conclusion, this study identified glucose as a key molecule that can directly reset the peripheral clock and illustrated a novel mode of the clock resetting. The finding of the genes regulated by the glucose addition suggested the activation of several transcriptional regulators and cellular pathways that have not been known to respond to glucose. Further analyses of these glucose-responsive genes including their regulatory *cis*-elements and *trans*-factors would lead to elucidation of not only a novel intracellular pathway mediating the glucose response but also an unidentified mechanism by which peripheral clocks are synchronized with feeding cycle.

Acknowledgments—We thank Dr. T. Kasahara for technical assistance and Dr. H. Itoh (Graduate School of Agricultural and Life Sciences, The University of Tokyo, Tokyo, Japan) for providing rat-1 fibroblasts.

REFERENCES

1. Pittendrigh, C. S. (1993) *Annu. Rev. Physiol.* **55,** 17–54
2. Dunlap, J. C. (1999) *Cell* **96,** 271–290
3. Cermakian, N., and Sassone-Corsi, P. (2000) *Nat. Rev. Mol. Cell Biol.* **1,** 59–67
4. King, D. P., and Takahashi, J. S. (2000) *Annu. Rev. Neurosci.* **23,** 713–742
5. Reppert, S. M., and Weaver, D. R. (2001) *Annu. Rev. Physiol.* **63,** 647–676
6. Zylka, M. J., Shearman, L. P., Weaver, D. R., and Reppert, S. M. (1998) *Neuron* **20,** 1103–1110
7. Balsalobre, A., Damiola, F., and Schibler, U. (1998) *Cell* **93,** 929–937
8. Yagita, K., Tamanini, F., van Der Horst, G. T. J., and Okamura, H. (2001) *Science* **292,** 278–281
9. Yamazaki, S., Numano, R., Abe, M., Hida, A., Takahashi, R., Ueda, M., Block, G. D., Sakaki, Y., Menaker, M., and Tei, H. (2000) *Science* **288,** 682–685
10. Brown, S. A., and Schibler, U. (1999) *Curr. Opin. Genet. Dev.* **9,** 588–594
11. Ishida, N., Kaneko, M., and Allada, R. (1999) *Proc. Natl. Acad. Sci. U. S. A.* **96,** 8819–8820
12. Damiola, F., Le Minh, N., Preitner, N., Kornmann, B., Fleury-Olela, F., and Schibler, U. (2000) *Genes Dev.* **14,** 2950–2961
13. Stokkan, K. A., Yamazaki, S., Tei, H., Sakaki, Y., and Menaker, M. (2001) *Science* **291,** 490–493
14. Hara, R., Wan, K., Wakamatsu, H., Aida, R., Moriya, T., Akiyama, M., and Shibata, S. (2001) *Genes Cells* **6,** 269–278
15. Yagita, K., and Okamura, H. (2000) *FEBS Lett.* **465,** 79–82
16. Akashi, M., and Nishida, E. (2000) *Genes Dev.* **14,** 645–649
17. Balsalobre, A., Brown, S. A., Marcacci, L., Tronche, F., Kellendonk, C., Reichardt, H. M., Schütz, G., and Schibler, U. (2000) *Science* **289,** 2344–2347
18. Balsalobre, A., Marcacci, L., and Schibler, U. (2000) *Curr. Biol.* **10,** 1291–1294
19. Nonaka, H., Emoto, N., Ikeda, K., Fukuya, H., Rohman, M. S., Raharjo, S. B., Yagita, K., Okamura, H., and Yokoyama, M. (2001) *Circulation* **104,** 1746–1748
20. Shigeyoshi, Y., Taguchi, K., Yamamoto, S., Takekida, S., Yan, L., Tei, H., Moriya, T., Shibata, S., Loros, J. J., Dunlap, J. C., and Okamura, H. (1997) *Cell* **91,** 1043–1053
21. Akiyama, M., Kouzu, Y., Takahashi, S., Wakamatsu, H., Moriya, T., Maetani, M., Watanabe, S., Tei, H., Sakaki, Y., and Shibata, S. (1999) *J. Neurosci.* **19,** 1115–1121
22. Wakamatsu, H., Takahashi, S., Moriya, T., Inouye, S. T., Okamura, H., Akiyama, M., and Shibata, S. (2001) *Neuroreport* **12,** 127–131
23. Hirota, T., Kagiwada, S., Kasahara, T., Okano, T., Murata, M., and Fukada, Y. (2001) *J. Biochem.* **129,** 51–59
24. Eisen, M. B., Spellman, P. T., Brown, P. O., and Botstein, D. (1998) *Proc. Natl. Acad. Sci. U. S. A.* **95,** 14863–14868
25. Rutter, J., Reick, M., Wu, L. C., and McKnight, S. L. (2001) *Science* **293,** 510–514
26. Cook, T., and Urrutia, R. (2000) *Am. J. Physiol.* **278,** G513–G521
27. Nishiyama, A., Masutani, H., Nakamura, H., Nishinaka, Y., and Yodoi, J. (2001) *IUBMB Life* **52,** 29–33
28. Kageyama, R., Ohtsuka, T., and Tomita, K. (2000) *Mol. Cell* **10,** 1–7
29. Morris, M. E., Viswanathan, N., Kuhlman, S., Davis, F. C., and Weitz, C. J. (1998) *Science* **279,** 1544–1547
30. Yamamoto, H., Nagai, K., and Nakagawa, H. (1987) *Chronobiol. Int.* **4,** 483–491
31. Towle, H. C. (2001) *Proc. Natl. Acad. Sci. U. S. A.* **98,** 13476–13478
32. Kinlaw, W. B., Fish, L. H., Schwartz, H. L., and Oppenheimer, J. H. (1987) *Endocrinology* **120,** 1563–1567
33. Fukuda, H., and Iritani, N. (1991) *Biochim. Biophys. Acta* **1086,** 261–264
34. Stephan, F. K. (1997) *Physiol. Behav.* **62,** 995–1002
35. Stephan, F. K., and Davidson, A. J. (1998) *Physiol. Behav.* **65,** 277–288
36. McNamara, P., Seo, S. B., Rudic, R. D., Sehgal, A., Chakravarti, D., and FitzGerald, G. A. (2001) *Cell* **105,** 877–889
37. Maywood, E. S., Mrosovsky, N., Field, M. D., and Hastings, M. H. (1999) *Proc. Natl. Acad. Sci. U. S. A.* **96,** 15211–15216
38. Horikawa, K., Yokota, S., Fuji, K., Akiyama, M., Moriya, T., Okamura, H., and Shibata, S. (2000) *J. Neurosci.* **20,** 5867–5873
39. Hida, A., Koike, N., Hirose, M., Hattori, M., Sakaki, Y., and Tei, H. (2000) *Genomics* **65,** 224–233
40. Yu, W., Nomura, M., and Ikeda, M. (2002) *Biochem. Biophys. Res. Commun.* **290,** 933–941
41. Ema, M., Hirota, K., Mimura, J., Abe, H., Yodoi, J., Sogawa, K., Poellinger, L., and Fujii-Kuriyama, Y. (1999) *EMBO J.* **18,** 1905–1914
42. Takahata, S., Ozaki, T., Mimura, J., Kikuchi, Y., Sogawa, K., and Fujii-Kuriyama, Y. (2000) *Genes Cells* **5,** 739–747
43. Shimano, H. (2001) *Prog. Lipid Res.* **40,** 439–452
44. Sakakura, Y., Shimano, H., Sone, H., Takahashi, A., Inoue, N., Toyoshima, H., Suzuki, S., Yamada, N., and Inoue, K. (2001) *Biochem. Biophys. Res. Commun.* **286,** 176–183
45. Ohtani, K. (1999) *Front. Biosci.* **4,** D793–804
46. Vaughn, J. P., Davis, P. L., Jarboe, M. D., Huper, G., Evans, A. C., Wiseman, R. W., Berchuck, A., Iglehart, J. D., Futreal, P. A., and Marks, J. R. (1996) *Cell Growth Differ.* **7,** 711–715
47. Pines, J., and Hunter, T. (1989) *Cell* **58,** 833–846
48. Yu, R., Ren, S. G., Horwitz, G. A., Wang, Z., and Melmed, S. (2000) *Mol. Endocrinol.* **14,** 1137–1146
49. Grundschober, C., Delaunay, F., Pühlhofer, A., Triqueneaux, G., Laudet, V., Bartfai, T., and Nef, P. (2001) *J. Biol. Chem.* **276,** 46751–46758
50. Wang, A., Schneider-Broussard, R., Kumar, A. P., MacLeod, M. C., and Johnson, D. G. (2000) *J. Biol. Chem.* **275,** 4532–4536

Pineal expression-promoting element (PIPE), a *cis*-acting element, directs pineal-specific gene expression in zebrafish

Yoichi Asaoka*, Hiroaki Mano*, Daisuke Kojima†, and Yoshitaka Fukada‡

Department of Biophysics and Biochemistry, Graduate School of Science, University of Tokyo, Hongo 7-3-1, Bunkyo-ku, Tokyo 113-0033, Japan

Edited by Jeremy Nathans, Johns Hopkins University School of Medicine, Baltimore, MD, and approved September 26, 2002 (received for review July 25, 2002)

The pineal gland, sharing morphological and biochemical similarities with the retina, plays a unique and central role in the photoneuroendocrine system. The unique development of the pineal gland is directed by a specific combination of the expressed genes, but little is known about the regulatory mechanism underlying the pineal-specific gene expression. We isolated a 1.1-kbp fragment upstream of the zebrafish exo-rhodopsin (*exorh*) gene, which is expressed specifically in the pineal gland. Transgenic analysis using an enhanced green fluorescent protein reporter gene demonstrated that the proximal 147-bp region of the *exorh* promoter is sufficient to direct pineal-specific expression. This region contains three copies of a putative cone rod homeobox (Crx)/Otx-binding site, which is known to be required for expression of both retina- and pineal-specific genes. Deletion and mutational analyses of the *exorh* promoter revealed that a previously uncharacterized sequence TGACCCCAATCT termed pineal expression-promoting element (PIPE) is required for pineal-specific promoter activity in addition to the Crx/Otx-binding sites. By using the zebrafish rhodopsin (*rh*) promoter that drives retina-specific expression, we created a reporter construct having ectopic PIPE in the *rh* promoter at a position equivalent to that in the *exorh* promoter by introducing five nucleotide changes. Such a slight modification in the *rh* promoter induced ectopic enhanced green fluorescent protein expression in the pineal gland without affecting its retinal expression. These results identify PIPE as a critical *cis*-element contributing to the pineal-specific gene expression, in combination with the Crx/Otx-binding site(s).

Living organisms use environmental light signals for multiple physiological functions such as vision, photoentrainment of circadian rhythms, regulation of body color, and detection of seasonal changes in photoperiod. These diverse functions are mediated not only by the retina but also by extra-ocular photoreceptive organs, such as the pineal gland. The retina and pineal gland probably arose via divergence from a common ancestral photoreceptive organ, and consistently, the pineal gland acts as a photosensory organ in the lowest vertebrate (1–3). In the course of vertebrate evolution, the physiological role of the pineal gland has been changed from a photosensory organ to a photoendocrinal organ in the lower vertebrates and eventually to a neuroendocrinal organ in mammals (4, 5). Generally, the retina receives visual images and transmits them to the brain, whereas the primary role of the pineal gland is the rhythmic production of circulating melatonin, which regulates numerous physiological activities (6). Despite such a dynamic change in the physiological function, the pineal gland displays many similarities to the retina in tissue/cellular morphology and biochemical properties (7, 8). In fish, amphibians, and lacertilian reptiles, their pineal photoreceptor cells possess well developed and lamellar outer segments, which are homologous to the outer segments of retinal photoreceptor cells. These photoreceptor cells form an ordered layer structure in both tissues. Biochemically, the retinal phototransduction proteins such as opsin, α-subunit of transducin, arrestin, and recoverin also have been localized in the pineal photoreceptor cells (9–13). These observations illustrate remarkable parallels in the pineal and retinal phototransduction pathways, but very little is known about the molecular basis that accounts for the characteristic development of the pineal gland. The regulatory mechanism responsible for tissue-specific gene expression and its evolutionary background are, therefore, important issues providing clues to the developmental control specifying the pineal or retinal identity.

In recent years, a number of studies have been reported about transcriptional regulation of the retinal genes (reviewed in ref. 14), among which the rhodopsin (*rh*) promoter has been studied extensively. Biochemical approaches and *in vitro* transcription assays have identified several *cis*-acting DNA elements, such as Ret-1 (15), BAT-1 (16), and Ret-4 (17). These studies suggest a cooperative interplay of multiple *cis*-acting elements and transcription factors for the retinal photoreceptor cell-specific gene expression. Consistent with this idea, several transcription factors have been identified and shown to regulate the *rh* gene expression. Subtraction cDNA cloning resulted in identification of neural retina leucine zipper (Nrl), a basic leucine zipper (bZIP) transcription factor that is expressed in all cell layers of adult mammalian retina (18, 19). Nrl binds to a well conserved *cis*-acting element Nrl response element (NRE) and transactivates the *rh* promoter (20, 21). On the other hand, cone rod homeobox (Crx) is an Otx-related homeodomain protein expressed exclusively in the retinal photoreceptor cells and pinealocytes (22–24). Crx transactivates the *rh* promoter by binding to BAT-1 and Ret-4 (22) and is implicated in the regulation of photoreceptor cell-specific gene expression (25). In addition to these transcription factors, Rx and Erx seem to participate in the regulation of the *rh* gene expression (26–28).

In contrast to these advances in the studies on the retina-specific gene expression, transcriptional regulation of the pineal gene remains poorly understood. The only *cis*-acting element identified so far is a pineal regulatory element (PIRE), which is recognized by Crx (29, 30). PIRE with a consensus sequence of TAATC/T is present in 5′-flanking regions of several pineal genes such as rat arylalkylamine-*N*-acetyltransferase and human hydroxyindole-*O*-methyltransferase genes (29). Recently, it has been reported that circadian gene expression in the zebrafish pineal complex requires Otx5, which is closely related to Crx (31). These studies suggest that a member of the Crx/Otx family and its binding site(s) play a common role in the transcription of

This paper was submitted directly (Track II) to the PNAS office.

Abbreviations: *rh*, rhodopsin; Nrl, neural retina leucine zipper; NRE, Nrl response element; Crx, cone rod homeobox; *exorh*, exo-rhodopsin; PIPE, pineal expression-promoting element; EGFP, enhanced GFP; dpf, days postfertilization; hpf, hours postfertilization.

Data deposition: The sequences reported in this paper have been deposited in the GenBank database (accession nos. AB079551 and AB079552).

*Y.A. and H.M. contributed equally to this work.

†Present address: Department of Molecular and Cellular Biology, Harvard University, Cambridge, MA 02138.

‡To whom correspondence should be addressed. E-mail: sfukada@mail.ecc.u-tokyo.ac.jp.

www.pnas.org/cgi/doi/10.1073/pnas.232444199

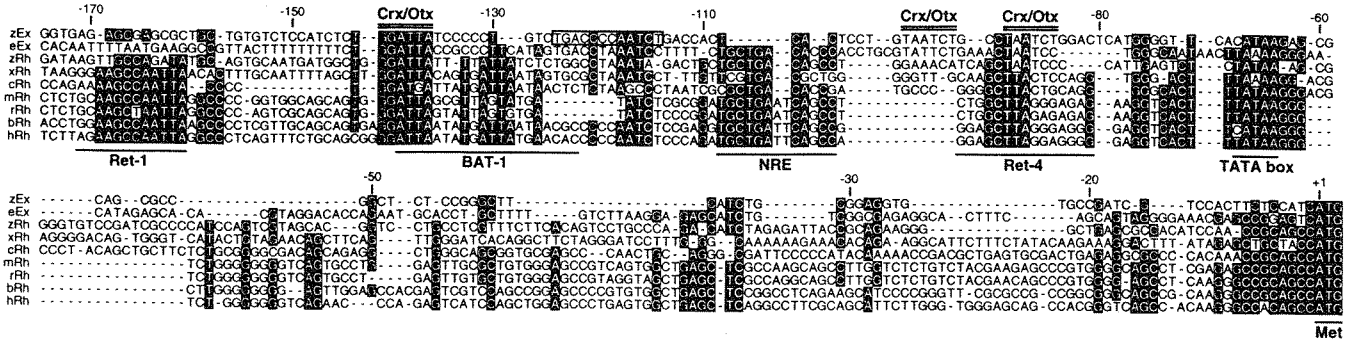

Fig. 1. The proximal promoter sequences of *exorh* and *rh* genes of vertebrates. The upstream sequence of the zebrafish *exorh* (zEx) was aligned with those of *rh* genes of the zebrafish (zRh), *Xenopus* (xRh), chicken (cRh), mouse (mRh), rat (rRh), bovine (bRh), and human (hRh). The upstream sequence of the European eel *exorh* (eEx) was determined in the present study and included in the alignment. Nucleotides conserved among at least six sequences are shown with white characters on black backgrounds. Horizontal lines indicate TATA box, ATG initiation codon, and conserved *cis*-elements identified previously in the *rh* promoters. Potential Crx/Otx-binding sites found in the zebrafish *exorh* promoter are double-lined. The PIPE sequence in the zebrafish *exorh* gene is boxed. The nucleotide numbers are relative to the translation initiation site of the zebrafish *exorh* gene. Accession numbers of the sequences obtained from GenBank are U23808 (xRh), M98497 (cRh), M55171 (mRh), U22180 (rRh), and U49742 (hRh). The bRh sequence was obtained from the original paper (17).

both pineal and retinal genes. It should be stressed, however, that the transcriptional regulation operated by Crx/Otx is inadequate to explain the mechanism segregating the pineal- and retina-specific gene expression. As yet unidentified transcription factor(s) and *cis*-acting element(s) should strictly determine pineal-specific gene expression, most probably in combination with the Crx/Otx-dependent regulation.

We previously demonstrated that the zebrafish has two distinct rhodopsin genes that are highly similar in coding sequence to each other (74% identical) but show unique tissue distributions (32). One is the canonical *rh* gene expressed only in the retina and the other is exo-rhodopsin (*exorh*) gene expressed specifically in the pineal gland. A phylogenetic analysis indicated that *rh* and *exorh* genes were produced by gene duplication that occurred early in the ray-finned fish lineage (32). Such a close kinship between the two genes, together with their specificities in tissue distribution, prompted us to investigate the evolutionary scenario of tissue-specific promoters. Because the proximal promoter sequences of *rh* genes are highly conserved among vertebrates including the zebrafish (33), we expected that the zebrafish *exorh* promoter sequence should provide an invaluable information about the mechanism segregating the pineal- and retina-specific gene expression. The zebrafish is an excellent animal model suitable for an *in vivo* promoter analysis with an (E)GFP reporter gene, because of its feasibility of transgenesis and transparency of embryos and larvae (34, 35). Taking into account these advantages, the present study undertook the isolation and *in vivo* analyses of the zebrafish *exorh* promoter, and we identified a previously uncharacterized *cis*-acting element mediating the pineal-specific gene expression. We named it pineal expression-promoting element (PIPE).

Materials and Methods

Isolation of 5′-Flanking Regions of the Zebrafish *exorh*, Zebrafish *rh*, and European Eel *exorh* Genes. A 1,076-bp region upstream from the ATG initiation codon of the zebrafish *exorh* gene (GenBank accession no. AB079551) was obtained by three rounds of PCR-based genome walking with the LA PCR *in vitro* Cloning Kit (Takara Shuzo, Kyoto). Subsequent PCR with zebrafish genome and a pair of primers (5′-GCTCA GCTGG CAGTA CTACC-3′ and 5′-GCAGC TTCTT GTGCT GCACC-3′) amplified a genomic fragment containing a 1,055-bp upstream region together with a short coding sequence of the zebrafish *exorh* gene. The amplified product was then subcloned into pCR2.1-TOPO vector (Invitrogen). Six clones were obtained from three independent amplification reactions and sequenced to confirm the sequence with no PCR error. In a similar manner, a 238-bp region upstream from the ATG initiation codon of the European eel *exorh* gene (GenBank accession no. AB079552) was obtained from the eel genomic DNA by using the LA PCR *in vitro* Cloning Kit and sequenced. On the other hand, screening of λ-Fix II zebrafish genomic library resulted in isolation of a 10.5-kbp fragment containing a 4,558-bp sequence upstream of the *rh* coding region.

Microinjection and Generation of Germ-Line Transgenic Zebrafish. Multiple DNA constructs were generated for microinjection (see *Results* and *Supporting Methods*, which is published as supporting information on the PNAS web site, www.pnas.org). They were prepared with the Plasmid Midi Kit (Qiagen, Chatsworth, CA). Rh(−1084), Rh(−1084)/PIPE, and PIPE-Rh(−1084) were treated with *Sac*I, and the other constructs were treated with *Eco*RI for linearization of each plasmid (cut at a unique site located upstream of the promoter). The linearized DNA was purified by phenol-chloroform extraction and subsequently by chloroform extraction and precipitated with ethanol. The purified DNA was dissolved at a final concentration of 25 ng/μl either in distilled water containing 0.05% phenol red (for transient expression assay) or in 0.1 M KCl/0.05% phenol red solution (for production of transgenic fish). Each DNA construct was microinjected into one-cell-stage embryos of WT zebrafish by using Transjector 5246 and Micromanipulator 5171 (Eppendorf). F_0 founder fish were identified by PCR analysis of the genomic DNA pool of 2- to 3-day-old F_1 embryos with primers specific for the enhanced GFP (EGFP) coding sequence. We established three, four, three, one, and three independent transgenic lines of the zebrafish with DNA constructs Ex(−1055), Ex(−301), Ex(−147), Rh(−1084), and Rh(−1084)/PIPE, respectively.

Results

Characterization of the 5′-Flanking Region of the Zebrafish *exorh* Gene. We isolated a 1.1-kbp genomic DNA fragment upstream of the coding region of the zebrafish *exorh* gene (Fig. 5, which is published as supporting information on the PNAS web site). The putative promoter sequence contained five copies of TA-ATCC/T sequence, a potential binding site of Crx/Otx (22, 24) that contributes to the pineal gene expression (25, 29–31). When the sequence in the proximal promoter region (−175 to −1 having three potential sites for Crx/Otx-binding) was aligned with those of the *rh* promoters from various vertebrates (Fig. 1), we found a single conserved site for Crx/Otx-binding at position

DEVELOPMENTAL

−142 to −137 (inverted form). Another site (−90 to −85) was conserved in the fish *rh* and *exorh* genes, and the third site (−99 to −94) was found only in the zebrafish *exorh* gene (Fig. 1). A TATA-like sequence in the zebrafish *exorh* promoter was aligned with TATA box conserved among *rh* genes. On the other hand, Nrl response element (NRE) that is present in many *rh* genes (Fig. 1) and is important for retinal gene expression was not found in the zebrafish *exorh* promoter (Fig. 1 and Fig. 5).

A 1,055-bp Fragment Upstream of the *exorh*-Coding Region Directs Pineal-Specific Gene Expression. To investigate whether the 1.1-kbp upstream region of the zebrafish *exorh* promoter is sufficient to direct pineal-specific gene expression, we generated a reporter construct Ex(−1055) by ligating EGFP gene to the 1,055-bp fragment upstream from the *exorh* translation initiation site (Fig. 2*A*) and established three lines of the transgenic zebrafish having this construct. The transgenic larvae from every line at 7 days postfertilization (dpf) showed EGFP fluorescence signals in the pineal gland with no detectable signal in the other tissues (Fig. 2 *B* and *C*). Each of the EGFP-positive pineal cells displayed highly differentiated morphology with an outer segment-like extrusion (Fig. 2*D*), a structure characteristic of the (pineal) photoreceptor cell (36). No EGFP signal was detectable within another type of the pineal neurons that project their axons outside the pineal gland (37), and this pineal projection neuron never emitted EGFP signals throughout maturation (data not shown). On the other hand, strong EGFP signals were sustained in the photoreceptor-like pineal cells of matured transgenic fish (6 months old; Fig. 2*E*), indicating that the 1,055-bp fragment upstream from the *exorh* translation initiation site is sufficient to maintain pineal-specific gene expression in the zebrafish.

Developmental change in EGFP expression pattern was examined in Ex(−1055) transgenic embryos at earlier stages. The EGFP-positive cell in the pineal gland was first detected at around 26 hours postfertilization (hpf; Fig. 2 *F* and *G*), which is consistent with the previous study showing the differentiation of the pineal photoreceptor cells at a similar timing (38). Intensity of the pineal EGFP fluorescence signals became stronger at 43 hpf (Fig. 2 *H* and *I*). Although weak fluorescence signals were observed in the ventral retina at 43 hpf (Fig. 2 *H* and *I*), the retinal signals disappeared by 7 dpf (Fig. 2 *J* and *K*) and were not observed at any later stages. These results indicated that the 1,055-bp region of the *exorh* promoter should be a good target for investigating the regulatory mechanism of pineal-specific gene expression.

The 147-bp Proximal Region of the Zebrafish *exorh* Promoter Is Sufficient for Pineal-Specific Gene Expression. To localize *cis*-acting DNA element(s) required for the pineal-specific gene expression, we generated two reporter constructs, Ex(−301) and Ex(−147), by ligating EGFP gene to 301-bp and 147-bp fragments of the *exorh* promoter, respectively (see Fig. 6*A*, which is published as supporting information on the PNAS web site). Then, the transgenic zebrafish were established for Ex(−301) and Ex(−147), respectively. Both of the constructs drove the pineal-specific EGFP expression in the transgenic animals (Fig. 6 *D–G*), and the EGFP-positive cells in these Ex(−301) and Ex(−147) transgenic larvae showed morphological features of the pineal photoreceptor cell (data not shown). The number of the EGFP-positive cells within each pineal gland of these larvae was also indistinguishable from that of Ex(−1055) transgenic larvae. These results demonstrate that the short promoter region of *exorh* gene (−147 to −1) retains the DNA element(s) essential for the pineal cell-specific gene expression. Among these larvae, the intensity of the pineal fluorescence signal tended to decrease as the promoter region of the transgene became shorter (Fig. 6 *C*, *E*, and *G*), although the signal intensity varied slightly among individuals from different lines that were produced with the same construct. The length-dependent change in signal intensity suggests that the region between −1055 and −148 contributes to enhancement of *exorh* gene expression because of the two putative Crx/Otx-binding sites (Fig. 5) and/or unknown elements in this region.

Internal Deletion and Mutational Analyses Revealed a Positive Regulatory Element in the *exorh* Promoter. We focused on identification of the pineal-specific *cis*-acting element(s) presumably present in the short upstream region (−147 to −1) of *exorh* gene. A series of systematic deletion constructs (Exdel-1 to Exdel-8) was generated by introducing consecutive 11-bp internal deletions (del-1 to del-8) into the promoter region of Ex(−147) construct (Fig. 3*A*). These deletions cover the 88-bp region (−147 to −60) of the *exorh* proximal promoter without any overlap nor gap between the neighbors. Embryos microinjected with each construct were raised to 5 dpf, and we scored the percentage of the larvae expressing EGFP fluorescence signals in the pineal gland. In this transient expression assay, the parental construct Ex(−147) induced the pineal EGFP expression in 40% of 166 larvae examined (Fig. 3*A*), and six of the eight deletion constructs showed lower percentages (3–23%). Among these, Exdel-8 (23%) lacks the TATA-like sequence (Fig. 3*A*), and Exdel-1 (11%), Exdel-5 (3%) and Exdel-6 (9%) carry a deletion of a potential Crx/Otx-binding site (Fig. 3*A*), an element that is important for the gene expression in the pineal gland as well as in the retina (25, 29–31). Notably, the promoter activities were significantly reduced in Exdel-2 (7%) and Exdel-3 (14%), of which the deleted sequences in tandem (see Fig. 3*B*) showed no homology with any known regulatory element, and it is most probable that the 22-bp region (from −136 to −115) contains a positive regulatory element(s) indispensable for pineal-specific gene expression.

To define the element(s), the parental construct Ex(−147) was mutated in the 22-bp region to generate another series of constructs (Exmut-1 to Exmut-7), in each of which consecutive 3–4 nucleotides were systematically mutated (Fig. 3*B*). Every construct was microinjected into the zebrafish embryos for the transient expression assay at 5 dpf, and we observed strikingly reduced promoter activities in the four constructs, Exmut-4 to Exmut-7 (Fig. 3*B*) that have mutations at the 12-bp cluster (−126 to −115) covering del-3 region together with an end of del-2 sequence. On the other hand, mutations at positions covering most of del-2 region (−136 to −127) had less effect on the promoter function (Fig. 3*B*, Exmut-1, -2, and -3). These results of the transient expression assay altogether demonstrate that the pineal(-specific) expression of *exorh* gene highly depends on the 12-bp DNA sequence TGACCCCAATCT (−126 to −115), which we termed PIPE in this study.

PIPE Can Direct Gene Expression in Pineal Photoreceptor Cells. PIPE may govern directly the pineal-specific gene expression in cooperation with Crx/Otx-binding sites or, alternatively, enhance the promoter activity without contributing to the tissue-specific regulation. Considering these possibilities, we examined the effect of ectopic placement of PIPE on expression of a gene regulated by the *rh* promoter that structurally resembles the *exorh* promoter (Fig. 1) but probably drives retina-specific gene expression in the zebrafish (32). As a control parental construct, we produced a reporter Rh(−1084), in which 1,084 bps upstream of the zebrafish *rh* coding region were fused to the EGFP gene (Fig. 4*A*), and it was used to generate transgenic fish. Rh(−1084) transgenic larvae displayed strong EGFP fluorescence signals exclusively in the eyes, and no detectable signal was observed in the pineal gland (Fig. 4 *C* and *D*). A detailed examination of tissue sections prepared from the transgenic larvae revealed localization of EGFP expression in the rod photoreceptor cells (data not shown), consistent with the previous study that used a

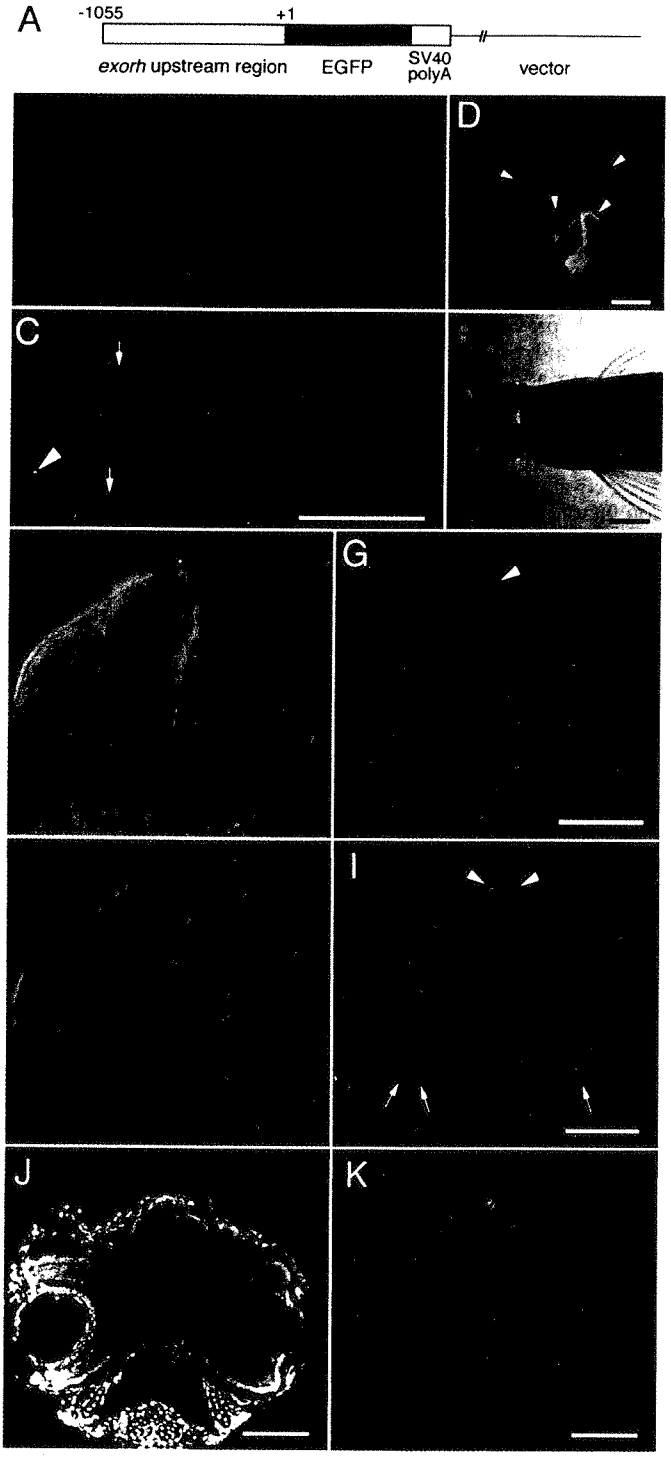

Fig. 2. Pineal-specific EGFP expression in Ex(−1055) transgenic zebrafish. (*A*) Schematic representation of Ex(−1055) construct in a linearized form used for microinjection. (*B*) Dorsolateral views (bright field image) of a WT larva (upper) and Ex(−1055) transgenic larva (lower) at 7 dpf. (*C*) Fluorescent image of *B*. The transgene-dependent fluorescence signal was observed specifically in the pineal gland of Ex(−1055) transgenic larva (arrowhead), and autofluorescence signals observed in transgenic and WT fish are marked by arrows. (*D*) High-magnification confocal image (dorsal view) of EGFP-positive pineal cells of 7-dpf-larva, with anterior to the left. The outer segment-like extrusion is indicated by each arrowhead. (*E*) Dorsal view of Ex(−1055) transgenic adult fish illuminated with both tungsten lamp and blue light. EGFP fluorescence signals were observed only in the pineal gland throughout its life. (*F–I*) Frontal views (dorsal up) of living transgenic embryos observed at 28 hpf (*F* and *G*) or 43 hpf (*H* and *I*) by using Nomarski optics (*F* and *H*) or fluorescence microscopy (*G* and *I*). Arrowheads in *G* and *I* indicate EGFP-positive cells in the pineal gland, and arrows in *I* point to EGFP-positive cells in the retina. The embryos in *G* and *I* were photographed under the same exposure conditions. (*J*) 4′,6-diamidino-2-phenylindole staining of a 10-μm-thick cross-section of the head of Ex(−1055) transgenic larva at 7 dpf. (*K*) EGFP fluorescent image of *J*. [Bars = 1 mm (*B* and *C*), 10 μm (*D*), 2 mm (*E*), and 100 μm (*F–K*).] For a clear demonstration, pigmentation of the embryos and larvae was reduced by treatment with 0.003% 1-phenyl-2-thiourea (Nacalai Tesque, Kyoto).

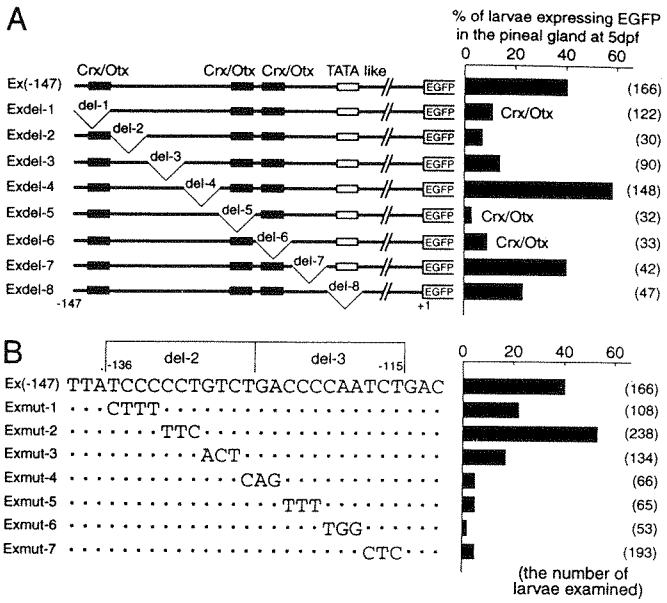

Fig. 3. Effects of internal deletions (*A*) and site-directed mutations (*B*) in the *exorh* promoter sequence. (*Right*) Bar graphs indicate the percentage of larvae that expressed EGFP fluorescence signals in the pineal gland at 5 dpf, and the number of larvae examined at 5 dpf is shown in parentheses. (*A Left*) The parental construct Ex(−147) and its deletion mutants (Exdel-1 to Exdel-8) are schematically depicted. Black and white boxes indicate the positions of three putative Crx/Otx-binding sites and the TATA-like sequence, respectively. (*B Left*) The partial nucleotide sequences of the parental construct Ex(−147) and its seven mutant constructs, Exmut-1 to Exmut-7, with dots representing unaltered nucleotides. Numbers at the top indicate the positions of nucleotides relative to the translation initiation site.

1.2-kbp fragment of the zebrafish *rh* promoter (33). Then, the parental construct Rh(−1084) was modified to carry an ectopic PIPE sequence by introducing four nucleotide substitutions and one nucleotide insertion (Fig. 4*B*) to a region that is aligned with PIPE in the *exorh* promoter (Fig. 1). Three independent lines of transgenic zebrafish were established with this chimeric construct Rh(−1084)/PIPE, and all of the transgenic larvae (at 7 dpf) exhibited EGFP fluorescence signals in the pineal gland in addition to those in the eyes (Fig. 4 *E* and *F*), with no detectable signal in the other tissues. The expression pattern of EGFP signals in the pineal gland was indistinguishable from those observed in Ex(−1055), Ex(−301), and Ex(−147) transgenic larvae. The *rh* promoter acquired the ability to drive ectopic gene expression in the pineal gland by virtue of the mutational change of only several nucleotides, supporting the idea that newly created PIPE is functional as a *cis*-acting DNA element that induces pineal-specific gene expression. No significant difference was observed in retinal fluorescence signals between Rh(−1084) and Rh(−1084)/PIPE transgenic animals, and this eliminates a negative regulatory role of PIPE for retinal gene expression.

Finally, we asked whether the above mutations introduced into Rh(−1084) might have disrupted an unknown DNA element(s)

DEVELOPMENTAL BIOLOGY

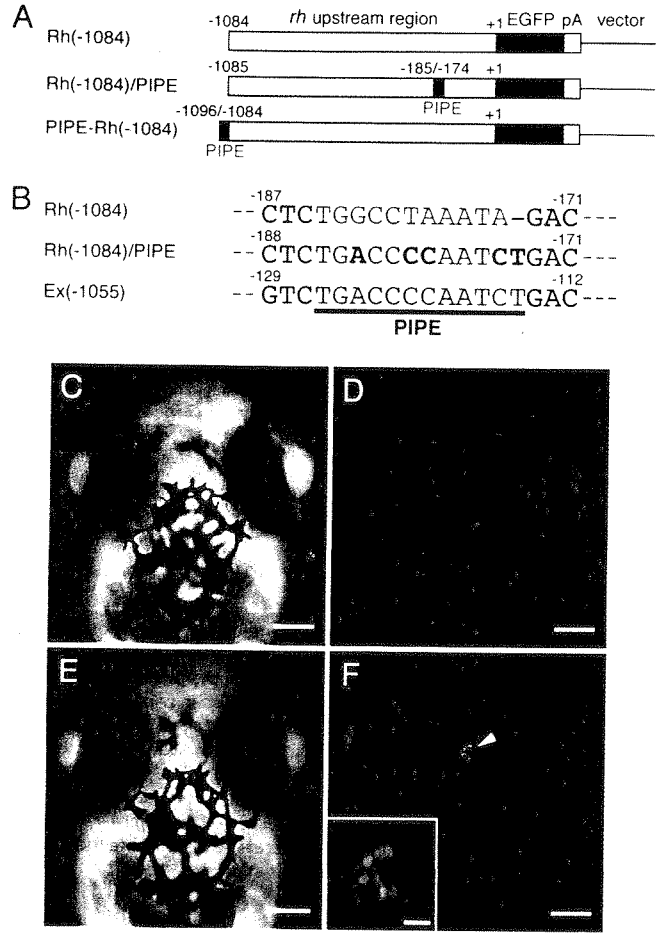

Fig. 4. Ectopic gene expression in the pineal gland driven by the zebrafish *rh* chimeric promoter carrying the PIPE sequence. (*A*) Schematic representation of the constructs, Rh(−1084), Rh(−1084)/PIPE, and PIPE-Rh(−1084). (*B*) Comparison of PIPE and nearby sequence in Ex(−1055) with those in the corresponding region of Rh(−1084) or Rh(−1084)/PIPE. Bold characters in Rh(−1084)/PIPE represent five nucleotides (four substitutions and a single insertion) modified from Rh(−1084) to create an ectopic PIPE sequence. (*C–F*) Dorsal views (anterior up) of Rh(−1084) (*C* and *D*) and Rh(−1084)/PIPE (*E* and *F*) transgenic larvae at 7 dpf. Nomarski (*C* and *E*) and fluorescent (*D* and *F*) images were taken at the same focal plane without moving the larvae. EGFP fluorescence signals in the pineal gland of Rh(−1084)/PIPE transgenic larva are marked by an arrowhead (*F*). (*F Inset*) High-magnification image of the EGFP-positive pineal structure. The larvae in *C–F* were not treated with 1-phenyl-2-thiourea, so that strong EGFP fluorescence signals in the pigmented eyes (*D* and *F*) are only visible through the pupil. [Bars = 100 μm (*C–F*), 20 μm (*F Inset*).]

responsible for pineal-specific repression of the *rh* gene expression. To demonstrate the positive regulatory role of PIPE more directly, we generated an additional chimeric construct PIPE-Rh(−1084), which has one copy of PIPE upstream of Rh(−1084) construct (Fig. 4*A*). In transient expression assay, ≈60% of larvae injected with PIPE-Rh(−1084) expressed EGFP fluorescence signals both in the pineal gland and in the retina at 5 dpf. Control injection of the parental construct Rh(−1084) induced no detectable expression of EGFP signals in the pineal gland at 5 dpf. Together, these results demonstrate that PIPE can direct gene expression in the pineal gland. We concluded that PIPE is the major contributor to the pineal-specific gene expression mediated by the zebrafish *exorh* promoter.

Discussion

In the present study, we accomplished detailed analyses of the *exorh* promoter without assistance of *in vitro* assay, by taking advantage of zebrafish transgenesis technology. This may represent an excellent example of zebrafish transgenesis to delineate a *cis*-acting DNA element *in vivo*, and the identification of PIPE corroborates the prominent aspect of the strategy (39). We used the rapidity of the transient expression assay for scanning the *exorh* promoter region (Fig. 3) while we established multiple transgenic lines to prove eventually the crucial role of PIPE in the pineal-specific gene expression (Fig. 4).

Our systematic deletion analysis revealed that, just like regulation of the *rh* promoter, the pineal-specific activity of the *exorh* promoter required the putative Crx/Otx-binding sites to be present in the proximal region (Fig. 3*A*). This finding is consistent with previous studies on several genes expressed in the pineal gland of the rat, mouse, chicken, and zebrafish (25, 29–31). In addition to the Crx/Otx-binding sites, our analysis identified PIPE as a major contributor to the pineal-specific gene expression, suggesting strongly that the pineal-specific expression of the zebrafish *exorh* gene is mediated by a combination of those *cis*-acting elements and presumably by multiple transcription factors. Such a mode of transcriptional regulation operated by multiple *cis*-elements and transcription factors is generally seen in a variety of tissue-specific promoters including the *rh* promoter, which contains a number of evolutionarily conserved *cis*-acting elements such as BAT-1, Ret-4, and NRE (16, 17, 20, 21). Indeed, *rh* gene is transactivated cooperatively by Crx and Nrl proteins through these sites (22). We speculate that the Crx/Otx-binding site would provide a basis for photoreceptor cell (cell type)-specific expression in both the retina and pineal gland, whereas NRE and PIPE would serve for determination of tissue-specificity, i.e., expression in the retina and pineal gland, respectively.

It is possible that PIPE also plays a role in transcriptional regulation of other genes expressed in the zebrafish pineal gland. For example, we found a 12-bp DNA sequence (TGACCCCTCTCT) similar to PIPE in the proximal promoter region of the zebrafish *floating head*, an important gene that is expressed from early stages in the pineal gland and is required for differentiation of most pineal neurons (37). On the other hand, PIPE or PIPE-related sequence is not found in a 2.1-kbp fragment upstream of the chicken pineal-specific gene, pinopsin (12, 40), and PIPE may be present at a more distal region or downstream of the translation initiation site. Further sequence analysis of pineal-specific genes in other vertebrates as well as in the zebrafish should help to evaluate the general role of PIPE in pineal-specific gene expression.

PIPE is most likely recognized by the transcription factor(s) expressed specifically in the pineal gland, but none of the pineal-specific transcription factors has been identified yet. One noticeable feature of PIPE is a CCAAT motif (Fig. 5), a binding site for many transcription factors such as CBF/NF-Y, CTF/NF1, and C/EBP (41). Thus, it is possible that PIPE serves as a functional CCAAT box for the pineal-specific expression. This idea is, however, at odds with our sequence analysis of the *exorh* promoter of the European eel, *Anguilla anguilla*, in which a CCAAT motif is not found at the equivalent site (Fig. 1). The consensus sequence between the zebrafish PIPE and the PIPE-like element in the eel *exorh* is TGACCNNAATCN. The conserved nine nucleotides rather than the CCAAT motif might be essential for binding of a common transcription factor(s), although it remains to be determined whether the PIPE-like element in the eel *exorh* promoter serves for pineal-specific expression.

We previously suggested that teleost *exorh* and *rh* genes were produced from an ancestral gene by gene duplication that occurred in the ray-finned fish lineage before the teleost radiation (32). It is conceivable that the ancestral gene was expressed in both the retina and pineal gland, and that the two descendent genes, *rh* and *exorh* genes, became segregated from one another

with respect to the localization and function. This possibility is consistent with the duplication-degeneration-complementation (DDC) model (42), which predicts that complementary nonfunctionalization of the *cis*-acting elements can produce the spatio-temporal partitioning of the ancestral functions between the descendents. The present study showed complementary absence of the *cis*-elements, PIPE and NRE, in the proximal promoters of the zebrafish *rh* and *exorh* genes, respectively, as predicted by the DDC model. This model leads to the speculation that the promoter region of the common ancestor of *rh* and *exorh* genes formerly contained both PIPE and NRE. Subsequent loss of a functional PIPE in the *rh* promoter could restrict the *rh* gene expression to the retina, whereas loss of NRE might lead to the pineal-specific expression of *exorh* gene. Consistently, a sequence comparison revealed significant homology in nucleotide sequence between PIPE and the equivalent site in the zebrafish *rh* promoter (Fig. 1), and experimentally we showed that only several nucleotide changes within the site of the *rh* promoter induced the pineal expression (Fig. 4). Interestingly, the eel *exorh* promoter has a sequence highly similar to NRE at a site corresponding to that of *rh* NRE (Fig. 1), although no NRE-like sequence is found in the zebrafish *exorh* promoter. These observations seem to support the idea that a functional NRE was originally present in the ancestral *exorh* promoter and then lost in the Euteleost lineage after the divergence between the Anguilliformes and the Euteleostei. Further study of the molecular basis for similarity and difference between the pineal and retinal gene expression could provide an important insight into the evolution of the vertebrate photoreceptive organs.

We thank Dr. K. Kawakami (National Institute of Genetics) for helpful advice about maintenance of fish. We thank Dr. H. Okamoto (Brain Science Institute, RIKEN) for providing the zebrafish strain Michigan and the zebrafish genomic library. We are grateful to Dr. David R. Hyde (University of Notre Dame) for his kind gifts of antibodies to the zebrafish opsins. We also thank Dr. T. Okano for helpful comments and discussion and K. Imazato for assistance with fish maintenance. This work was supported in part by Grants-in-Aid from the Japanese Ministry of Education, Science, Sports, and Culture.

1. Pu, G. A. & Dowling, J. E. (1981) *J. Neurophysiol.* **46,** 1018–1038.
2. Cole, W. C. & Youson, J. H. (1982) *Am. J. Anat.* **165,** 131–163.
3. Tamotsu, S. & Morita, Y. (1986) *J. Comp. Physiol. A* **159,** 1–5.
4. Collin, J. P., Voisin, P., Falcón, J., Faure, J. P., Brisson, P. & Defaye, J. R. (1989) *Arch. Histol. Cytol.* **52,** 441–449.
5. Shedpure, M. & Pati, A. K. (1995) *Indian J. Exp. Biol.* **33,** 625–640.
6. Falcón, J. (1999) *Prog. Neurobiol.* **58,** 121–162.
7. Meissl, H. (1997) *Biol. Cell* **89,** 549–554.
8. Kusmic, C. & Gualtieri, P. (2000) *Micron* **31,** 183–200.
9. Mirshahi, M., Faure, J. P., Brisson, P., Falcón, J., Guerlotte, J. & Collin, J. P. (1984) *Biol. Cell* **52,** 195–198.
10. Vigh-Teichmann, I. & Vigh, B. (1990) *J. Pineal Res.* **8,** 323–333.
11. Korf, H. W., White, B. H., Schaad, N. C. & Klein, D. C. (1992) *Brain Res.* **595,** 57–66.
12. Okano, T., Yoshizawa, T. & Fukada, Y. (1994) *Nature* **372,** 94–97.
13. Yoshikawa, T., Yashiro, Y., Oishi, T., Kokame, K. & Fukada, Y. (1994) *Zool. Sci.* **11,** 675–680.
14. Livesey, F. J. & Cepko, C. L. (2001) *Nat. Rev. Neurosci.* **2,** 109–118.
15. Morabito, M. A., Yu, X. & Barnstable, C. J. (1991) *J. Biol. Chem.* **266,** 9667–9672.
16. DesJardin, L. E. & Hauswirth, W. W. (1996) *Invest. Ophthalmol. Visual Sci.* **37,** 154–165.
17. Chen, S. & Zack, D. J. (1996) *J. Biol. Chem.* **271,** 28549–28557.
18. Swaroop, A., Xu, J., Pawar, H., Jackson, A., Skolnick, C. & Agarwal, N. (1992) *Proc. Natl. Acad. Sci. USA* **89,** 266–270.
19. Liu, Q., Ji, X., Breitman, M. L., Hitchcock, P. F. & Swaroop, A. (1996) *Oncogene* **12,** 207–211.
20. Kumar, R., Chen, S., Scheurer, D., Wang, Q. L., Duh, E., Sung, C. H., Rehemtulla, A., Swaroop, A., Adler, R. & Zack, D. J. (1996) *J. Biol. Chem.* **271,** 29612–29618.
21. Rehemtulla, A., Warwar, R., Kumar, R., Ji, X., Zack, D. J. & Swaroop, A. (1996) *Proc. Natl. Acad. Sci. USA* **93,** 191–195.
22. Chen, S., Wang, Q. L., Nie, Z., Sun, H., Lennon, G., Copeland, N. G., Gilbert, D. J., Jenkins, N. A. & Zack, D. J. (1997) *Neuron* **19,** 1017–1030.
23. Freund, C. L., Gregory-Evans, C. Y., Furukawa, T., Papaioannou, M., Looser, J., Ploder, L., Bellingham, J., Ng, D., Herbrick, J. S., Duncan, A., *et al.* (1997) *Cell* **91,** 543–553.
24. Furukawa, T., Morrow, E. M. & Cepko, C. L. (1997) *Cell* **91,** 531–541.
25. Furukawa, T., Morrow, E. M., Li, T., Davis, F. C. & Cepko, C. L. (1999) *Nat. Genet.* **23,** 466–470.
26. Mathers, P. H., Grinberg, A., Mahon, K. A. & Jamrich, M. (1997) *Nature* **387,** 603–607.
27. Martinez, J. A. & Barnstable, C. J. (1998) *Biochem. Biophys. Res. Commun.* **250,** 175–180.
28. Kimura, A., Singh, D., Wawrousek, E. F., Kikuchi, M., Nakamura, M. & Shinohara, T. (2000) *J. Biol. Chem.* **275,** 1152–1160.
29. Li, X., Chen, S., Wang, Q., Zack, D. J., Snyder, S. H. & Borjigin, J. (1998) *Proc. Natl. Acad. Sci. USA* **95,** 1876–1881.
30. Bernard, M., Dinet, V. & Voisin, P. (2001) *J. Neurochem.* **79,** 248–257.
31. Gamse, J. T., Shen, Y. C., Thisse, C., Thisse, B., Raymond, P. A., Halpern, M. E. & Liang, J. O. (2002) *Nat. Genet.* **30,** 117–121.
32. Mano, H., Kojima, D. & Fukada, Y. (1999) *Mol. Brain Res.* **73,** 110–118.
33. Kennedy, B. N., Vihtelic, T. S., Checkley, L., Vaughan, K. T. & Hyde, D. R. (2001) *J. Biol. Chem.* **276,** 14037–14043.
34. Higashijima, S., Okamoto, H., Ueno, N., Hotta, Y. & Eguchi, G. (1997) *Dev. Biol.* **192,** 289–299.
35. Long, Q., Meng, A., Wang, H., Jessen, J. R., Farrell, M. J. & Lin, S. (1997) *Development (Cambridge, U.K.)* **124,** 4105–4111.
36. Kusmic, C., Barsanti, L., Passarelli, V. & Gualtieri, P. (1993) *Micron* **24,** 279–286.
37. Masai, I., Heisenberg, C. P., Barth, K. A., Macdonald, R., Adamek, S. & Wilson, S. W. (1997) *Neuron* **18,** 43–57.
38. Heisenberg, C. P., Brand, M., Jiang, Y. J., Warga, R. M., Beuchle, D., van Eeden, F. J. M., Furutani-Seiki, M., Granato, M., Haffter, P., Hammerschmidt, M., *et al.* (1996) *Development (Cambridge, U.K.)* **123,** 191–203.
39. Meng, A., Tang, H., Ong, B. A., Farrell, M. J. & Lin, S. (1997) *Proc. Natl. Acad. Sci. USA* **94,** 6267–6272.
40. Takanaka, Y., Okano, T., Yamamoto, K. & Fukada, Y. (2002) *J. Neurosci.* **22,** 4357–4363.
41. Maity, S. N. & de Crombrugghe, B. (1998) *Trends Biochem. Sci.* **23,** 174–178.
42. Force, A., Lynch, M., Pickett, F. B., Amores, A., Yan, Y. L. & Postlethwait, J. (1999) *Genetics* **151,** 1531–1545.